Materials Horizons: From Nature to Nanomaterials

Zeba Khanam
Neelam Gogoi
Divesh Narayan Srivastava *Editors*

# 2D Nanomaterials for Energy and Environmental Sustainability

Springer

# Materials Horizons: From Nature to Nanomaterials

**Series Editor**

Vijay Kumar Thakur, School of Aerospace, Transport and Manufacturing, Cranfield University, Cranfield, UK

Materials are an indispensable part of human civilization since the inception of life on earth. With the passage of time, innumerable new materials have been explored as well as developed and the search for new innovative materials continues briskly. Keeping in mind the immense perspectives of various classes of materials, this series aims at providing a comprehensive collection of works across the breadth of materials research at cutting-edge interface of materials science with physics, chemistry, biology and engineering.

This series covers a galaxy of materials ranging from natural materials to nanomaterials. Some of the topics include but not limited to: biological materials, biomimetic materials, ceramics, composites, coatings, functional materials, glasses, inorganic materials, inorganic-organic hybrids, metals, membranes, magnetic materials, manufacturing of materials, nanomaterials, organic materials and pigments to name a few. The series provides most timely and comprehensive information on advanced synthesis, processing, characterization, manufacturing and applications in a broad range of interdisciplinary fields in science, engineering and technology.

This series accepts both authored and edited works, including textbooks, monographs, reference works, and professional books. The books in this series will provide a deep insight into the state-of-art of Materials Horizons and serve students, academic, government and industrial scientists involved in all aspects of materials research.

More information about this series at https://link.springer.com/bookseries/16122

Zeba Khanam · Neelam Gogoi ·
Divesh Narayan Srivastava
Editors

# 2D Nanomaterials for Energy and Environmental Sustainability

Springer

*Editors*
Zeba Khanam
School of Materials Science
and Engineering,
Harbin Institute of Technology
Shenzhen, Guangdong, China

Neelam Gogoi
School of Life and Environmental Sciences
School of Chemistry
University of Sydney
Sydney, NSW, Australia

Divesh Narayan Srivastava
Analytical and Environmental Science
Division and CIF
CSIR-Central Salt and Marine Chemicals
Research Institute
Bhavnagar, Gujarat, India

ISSN 2524-5384 ISSN 2524-5392 (electronic)
Materials Horizons: From Nature to Nanomaterials
ISBN 978-981-16-8537-8 ISBN 978-981-16-8538-5 (eBook)
https://doi.org/10.1007/978-981-16-8538-5

# Preface

Two-dimensional (2D) nanomaterials are attracting tremendous research interest ever since the advent of graphene hit the headlines. Inspired by the astonishing physical, optical, and electronic properties of graphene, other thin-layered 2D nanomaterials have been discovered. These include transition metal dichalcogenides (TMDs), transition metal oxides (TMOs), transition metal halides (TMHs), transition metal carbides/carbonitrides/nitrides (MXenes), elemental 2D analogs (silicene, germanene, phosphorene, tellurene, etc.), layered double hydroxides (LDHs), 2D metal–organic frameworks (MOF), covalent organic frameworks (COF), 2D polypeptoid, 2D metallenes, and many more. Interestingly, the library of 2D nanomaterials expanding enormously has featured more than 150 exotic members so far. The advancement in 2D nanomaterials has shown very significant contributions toward a sustainable future. This has driven us to manifest the dynamic applications of 2D nanomaterials in energy storage/conversion and environmental remediation.

This book *2D Nanomaterials for Energy and Environmental Sustainability* aims to shift the paradigm from fundamental studies on 2D nanomaterials to more application-oriented studies. With a collection of 12 chapters written by 38 experts in the field, it covers the wide spectrum of 2D nanomaterials in the field of energy and environment. It brings together recent breakthroughs and overpowering innovations of 2D nanomaterials engaged in an extended range of fields, such as energy storage/conversion, photocatalytic degradation and adsorption of pollutants, desalination and membrane filtration, detection and sensing, drug delivery, and nanoencapsulated fertilizers. This book is aimed to highlight a balanced approach toward 2D nanomaterials by presenting a comprehensive account of potential advantages and associated risks/shortcomings. The authors have provided an informative outlook for the future prospects of 2D nanomaterials to offer a way forward.

Chapter 1 introduces the latest trends on top-down and bottom-up synthesis approaches and properties followed by chapters covering critical status and progress in energy and environmental applications. Chapters 2 and 3 briefly outline the recent advancements of 2D nanomaterials in energy conversion and storage devices with substantial emphasis centered on solar cells, water splitting, piezo-thermoelectric devices and supercapacitors fabrication, along with properties and their mechanism

studies. Moving toward environmental applications, Chap. 4 discusses the state-of-the art advances in 2D nanomaterials-based photocatalytic systems for degrading organic dyes and antibiotics. Further, the 2D nanomaterials-based adsorbents are sequentially presented in Chap. 5, highlighting recent developments in the adsorption of organic dye pollutants, heavy metal ions, and toxic gases. Then, various types of functional membrane-based water treatment technologies including desalination and membrane filtration are presented in Chap. 6. We then expand our discussion on the 2D nanomaterials-related detection of toxic gases, water pollutants, and other biological contaminants in environment in Chaps. 7 and 8. Each chapter has covered the key aspects, viz., preparation methods, analytical techniques followed by mechanistic studies relevant to curb environmental issues. Additionally, an overview on drug delivery applications is presented mainly focusing on the newly emerged 2D mesoporous silica nanomaterial in Chap. 9. Seeing the current agriculture scenario, we also included Chap. 10 on 2D nanomaterials-based agro-formulations as nano-fertilizers and nano-pesticides for nutrient delivery, pest detection, drought resistance, etc. In spite of largely proven track record, biological/ecological risk assessment of 2D nanomaterials is another important issue that should be taken into consideration. Hence, we provided Chap. 11 to shed some light on the fate and toxicity risks of 2D nanomaterials on the environment and human health. This book ends with Chap. 12 addressing the unresolved challenges and promising future research directions of 2D nanomaterials in the field of energy and environment. This chapter also covers a special section on the latest patented research/products or potential nanodevices/gadgets/appliances that could make way to the market. It concludes that massive efforts are still needed to gain the commercial success of these exciting materials.

This book is a timely contribution to a research area of eminent significance. It overviews the current scenarios of targeted applications and provides an impetus toward the fast development of this highly interdisciplinary research field that involves material science, chemistry, physics, environmental science, life sciences, and many others. The editors and contributing authors believe that this book will be beneficial for researchers from diversified fields to recognize the emerging trends and to identify persistent knowledge gaps on 2D nanomaterials for sustainable energy and environment.

Shenzhen, China — Zeba Khanam
Sydney, Australia — Neelam Gogoi
Bhavnagar, India — Divesh Narayan Srivastava

# Contents


1 **An Introduction to the Wonder 2D Nanomaterials: Synthetic Approaches and Fundamental Properties** . . . . . 1
Amit K. Rana and Amreen A. Hussain

2 **Emerging 2D Nanomaterial Composites for Efficient Energy Conversion: Insight into the Evolutionary Perspective of Devices** . . . . . 25
Amreen A. Hussain and Amit K. Rana

3 **Next-Generation 2D Nanomaterial Composites Electrodes for Electrochemical Energy Storage** . . . . . 47
Harish Mudila, Parteek Prasher, Anil Kumar, M. G. H. Zaidi, Mousamee Sharma, and Amit Verma

4 **Novel 2D Nanomaterial Composites Photocatalysts: Application in Degradation of Water Contaminants** . . . . . 75
Mohd Saquib Tanweer and Masood Alam

5 **Advanced 2D Nanomaterial Composites: Applications in Adsorption of Water Pollutants and Toxic Gases** . . . . . 97
Mohd Saquib Tanweer, Harshvardhan Chauhan, and Masood Alam

6 **Progress in 2D Nanomaterial Composites Membranes for Water Purification and Desalination** . . . . . 125
Savan K. Raj and Vaibhav Kulshrestha

7 **Advancements in 2D Nanomaterial Composites-Based Electrochemical Sensors for Environmental Contaminants** . . . . . 149
Zeba Khanam, Sameer Ahmad, Mohd Saquib Tanweer, Weqar Ahmad Siddiqi, and Masood Alam

**8 Trending 2D Nanomaterial Composites in Detection and Sensing of Biological Contaminants** ..... 173
Jayanta Sarmah Boruah, Sristi Majumdar, Ankita Deb, Jahnabi Gogoi, and Devasish Chowdhury

**9 Newly Emerged 2D Mesoporous Silica Nanoparticles: Role in Target-Setting Biomedicines** ..... 197
Prateek Srivastava, Sumit Kumar Hira, and Partha Pratim Manna

**10 Futuristic 2D Nanomaterial Composites Agro-Formulations for Sustainable Agriculture** ..... 223
Poonam Gogoi Konwar

**11 Fate of 2D Nanomaterials and Their Toxic Effects on the Environment and Human Health** ..... 243
Achyut Konwar, Jayanta Sarmah Boruah, Kabyashree Phukan, and Sazzadur Rahman

**12 Prospective on 2D Nanomaterials for Energy and Environment: Challenges, Commercial Aspect, and the Future Research Endeavor** ..... 267
Zeba Khanam, Neelam Gogoi, and Divesh Narayan Srivastava

# About the Editors

**Dr. Zeba Khanam** is currently working as a postdoctoral researcher at School of Materials Science and Engineering, Harbin Institute of Technology, Shenzhen, China. She obtained her Ph.D. in Environmental sciences from G. B. Pant University of Agriculture and Technology, Pantnagar, India. Her research work encompasses a broad spectrum of energy and environmental applications including electrochemical energy storage materials, flexible electrodes, polymer electrolytes, anticorrosive coatings, electrochemical sensing, and water quality assessment. She authored 11 scientific articles published in leading international journals, 5 popular articles in national magazines and 5 book chapters. She has presented her work at numerous national/international conferences including the most prestigious RSC FD-173 event. She is a recipient of national/international fellowships and recently received NESA Junior Scientist-2020 award from National Environmental Science Academy (NESA), India. She is serving as a referee for reputed journals of Springer, Elsevier, Wiley, and T&F, and holds the membership of scientific societies namely, RSC-London, NESA-India, and ISCA-India.

**Dr. Neelam Gogoi** is a postdoctoral research associate at School of Life and Environmental Sciences and a research affiliate at School of Chemistry, University of Sydney. Before that, she worked at Chinese Academy of Sciences. She obtained her Ph.D. in Chemistry from University of Gauhati, India. Her research areas include genetic nano-engineering in plants, polymer chemistry, and carbon nanomaterials for sensors, drug delivery, and gene delivery systems. She published 14 research articles in American Chemical Society, Royal Society of Chemistry, and Elsevier along with 2 chapters. She received Nature travel grant to present at GRC, Massachusetts. DST, Government of India, sponsored her work to present at Royal Society of Chemistry, London. She is a recipient of RSC Nanoscale Best Poster Award, Dr. Shanti Nath Ghosh Memorial Award for Best Oral Talk, and many more. Dr. Neelam is currently in the editorial board of JENR, Medwin Publishers.

**Dr. Divesh Narayan Srivastava** currently holds the position of the senior principal scientist at CSIR-CSMCRI, India, and a professor, AcSIR. He graduated from BHU,

India, in 1999, followed by spent few years at Bar-Ilan University, Israel, and IIT Bombay, India, as a postdoctoral fellow. His current research interest includes electrochemical sensors and electrocatalysis. He has 98 research papers, 3 book chapters and 4 patents in his credit and developed technologies such as “Plastic chip electrodes” and “Tailored Potentiostat”. He is associate fellow of Gujarat Science Academy and is a recognized member of several other national/international scientific and administrative organizations.

# Chapter 1
# An Introduction to the Wonder 2D Nanomaterials: Synthetic Approaches and Fundamental Properties


**Amit K. Rana and Amreen A. Hussain**

## 1 Introduction

Nanomaterials have been attracting the scientific world because of their unusual physiochemical characteristics due to their high aspect ratio, strange surface morphology, unique surface chemistry, and quantum-size effect, as compared to their bulk counterparts [1]. Based on their unique properties, they can be applied in a wide range of multifunctional application. In the last few decades, a large number of research works are published in the field of nanomaterials with a progressing span of about 30,000 publications per year. Dimensionality is one of the key factors to manipulate the nanomaterial properties. It is to be noted that the properties of nanomaterials are mostly attributed to their unique nanostructure and composition. Moreover, in terms of dimensions or confinement of electrons, nanomaterials have been categorized as zero (0D-), one (1D-), and two (2D-) nanostructures. For instance, the 0D nanomaterials (such as spherical nanoparticles and quantum dots) confine electrons in all three dimensions in the nanometre range. Similarly, with 1D and 2D structures, the electrons are confined in either one or two dimensions (2D) in the nanometre range [1]. In this chapter, we are interested to discuss different types of 2D nanomaterials along with their synthetic approaches, properties, and material characterizations.

In 2004, Novoselov and co-workers exfoliated a single-atom-thick layer of graphite using a mechanical cleavage method where the carbon atoms are arranged in a 2D hexagonal structure, which led to the discovery of Nobel Prize-winning

A. K. Rana (✉)
Department of Materials Science and Engineering, Ulsan National Institute of Science and Technology (UNIST), Ulsan 44919, South Korea
e-mail: aramitrana4@gmail.com

A. A. Hussain
Facilitation Centre for Industrial Plasma Technologies (FCIPT), Institute for Plasma Research (IPR), Gandhinagar 382428, Gujarat, India
e-mail: amreenhussain8888@gmail.com



Z. Khanam et al. (eds.), *2D Nanomaterials for Energy and Environmental Sustainability*,
Materials Horizons: From Nature to Nanomaterials,
https://doi.org/10.1007/978-981-16-8538-5_1

graphene [2]. With the discovery of graphene, the scientific community has received a lot of attention to exploring the other potential 2D nanostructures. Therefore, after years of hard work, the scientists working in the field of 2D nanomaterials have found novel ways to synthesize 2D nanomaterials such as mechanical cleavage, ion-intercalation, liquid exfoliation, chemical vapour deposition (CVD), plasma-enhanced chemical vapour deposition (PECVD), hydrothermal syntheses [3–6]. For the synthesis of 2D nanomaterials, a large variety of materials are explored: from metals to semiconductors to insulators and even to superconductors which show remarkable properties with better performance than graphene. Based on the electron confinement in single-layered 2D nanomaterials, they show outstanding electronic and transport properties. In addition, the nanomaterials have a high surface area, owing to the exposure of edge sites, and flexibility in atomic level, high thermal endurance which made them suitable candidates for diverse applications such as in nano-electronics, optoelectronics, medical, civil fields and in space applications [5–7].

## *1.1 Type of 2D Nanomaterials*

As already highlighted, graphene is known as a wonder nanomaterial consisting of crystalline carbon film and exhibits various unprecedented properties, such as ultrahigh carrier mobility (~10,000 $cm^2\ V^{-1}\ s^{-1}$), quantum hall effect, high specific surface area (2630 $m^2\ g^{-1}$), optical transparency (~97.7%), and excellent thermal conductivity (3000–5000 $W\text{-}m^{-1}\ K^{-1}$) [2]. Inspired by the unexpected properties of graphene, the quest to explore other ultrathin 2D nanomaterials begins. Efforts are made by the researchers to exploit new 2D nanomaterials that possess similar features to that of graphene, yet capable of versatile properties. Among the family of new 2D materials originates the transition metal dichalcogenides (TMDs; e.g. $MoS_2$, $NbSe_2$, $TaS_2$, $WS_2$, $MoSe_2$, $WSe_2$, etc.), hexagonal boron nitride (h-BN), carbon nitride (CN), transition metal oxides, layered perovskites, metal–organic frameworks, black phosphorus (BP), and MXenes [7–11], as schematically presented in Fig. 1.

***Transition metal dichalcogenides (TMDs)***: TMD monolayers are semiconductor materials with atomically thin layers with a general representation of $MX_2$; where M is a transition metal (Mo, W, Te, etc.), and X is a chalcogen atom (X = S, Se, Te, etc.). In a typical structure of $MX_2$, one layer of M atoms is sandwich between two separate layers of X atoms to form X–M–X structure [10]. With this atomic arrangement, the crystal structure forms a honeycomb, hexagonal lattice. Usually, the M–X bonds (intralayer) between the transition metal and chalcogen atoms are known to be covalent bonds, whereas the individual $MX_2$ layers are bonded together by van der Waals (vdW) (interlayer) forces which are considered as weak bonds. Moreover, the TMDs can form metal coordination such as trigonal prismatic or octahedral. This coordination of metals and also the order of staking between the monolayers describe the phase of TMD materials. Some most common phases are

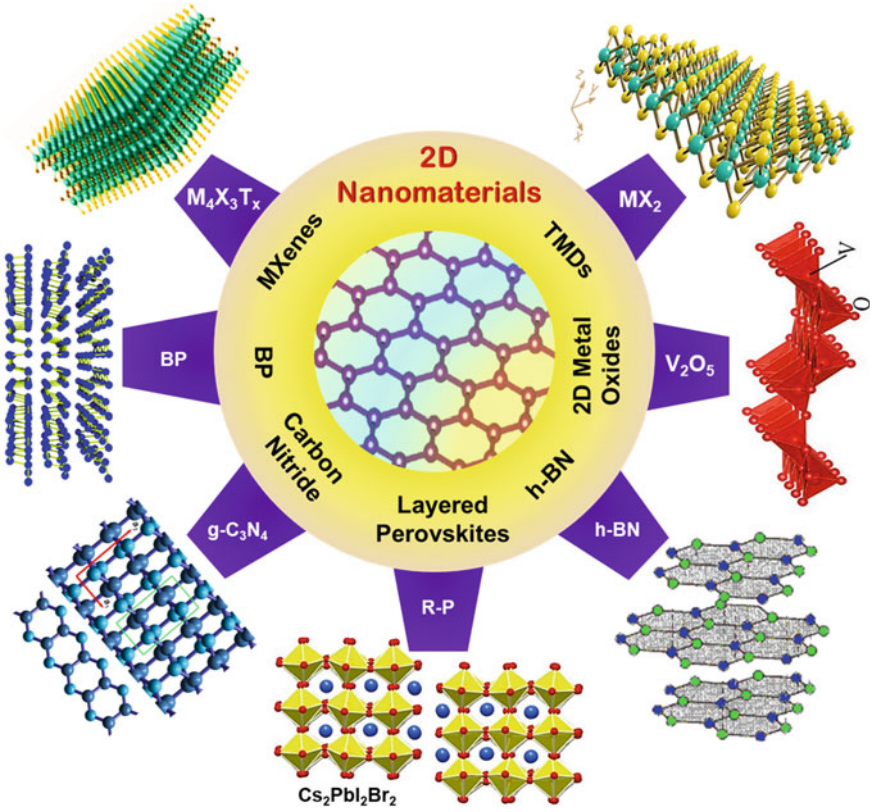


**Fig. 1** Schematic illustration of different kinds of typical ultrathin 2D nanomaterials, such as graphene, h-BN, TMDs, MXenes, TMOs (2D metal oxides), layered perovskite, and BP (phosphorene)

1T, 2H, or 3R, where T, H, and R stand for tetragonal, hexagonal, and rhombohedral, while 1, 2, and 3 denote the number of X–M–X sandwiches per unit cell.

***Hexagonal boron nitride (h-BN)***: h-BN is a layered material that has a similar structure to graphite, which in turn has similar properties like graphite. The crystal arrangement of h-BN consists of alternate boron and nitrogen atoms which is bonded with $sp^2$ hybridization forming an atomic-level thick layer [11, 12]. Usually, the bond length among two consecutive boron and nitrogen atoms is 0.144 nm. h-BN exhibits covalent bonding within the plane. Irrespective of this, its interplane bonding is relatively weak due to vdW forces. In h-BN, the spacing between two successive layers is 0.334 nm which is analogous to graphene (0.333 nm). Thus, h-BN displays advantages for efficient electronic and optical applications.

***Carbon nitride (CN)***: Graphitic carbon nitride (general formula g-$C_3N_4$) is one of the hardest and most stable compounds belonging to the library of 2D nanomaterials.

The fundamental structure of $C_3N_4$ forms a polymeric stacked structure which is more like graphite containing $sp^2$ hybridized carbon and nitrogen atoms [13]. It consists of tris-triazine-based patterns where the carbon to nitrogen ratio is typically ¾ with a small amount of hydrogen. Because of the presence of nitrogen (lone pair) and π-conjugation system with carbon $p_z$-orbital, the $C_3N_4$ shows promising electronic properties. There are mainly two known structures of $C_3N_4$, one is based on heptazine, and the other is poly-triazine imide units based on which the reaction conditions, reactivities, and the associated properties can vary.

***Transition metal oxides***: The transition metal oxides from their bulk state can be transformed into atomically thin nanosheets, thus placing their stand as 2D nanomaterials [14]. It is already known that the bulk metal oxides can show unique combination of both physical and chemical properties with earth abundance. However, the 2D nanosheets of metal oxides provide even more unprecedented features such as larger surface area, improved active sites, and interplanar charge transport. There are various metal oxides found in nature, and to name a few are $MoO_3$, $TiO_2$, ZnO, $Co_3O_4$, $V_2O_5$, etc. Every 2D metal oxides have different crystal structures which will be discussed in detail in the succeeding sections of the chapter.

***Layered perovskites***: The dimensionality of the 3D perovskite structure when reduced to layered 2D form enables very interesting properties for diverse applications. In simple terms, the 2D perovskite resembles the slice cut from the 3D perovskite lattice. Different from the 3D perovskite with $ABX_3$ structure (where a larger cation (A) simply fills the voids between $BX_6$ octahedra), and in 2D perovskite, some larger cations are introduced into the structure with acts as spacers [15]. These spacers help to isolate the inorganic octahedra to form quantum well superlattices. Furthermore, these extra spacing cations induce asymmetric lattice structure, thereby providing an additional degree of freedom. Thus, the structural slicing along a definite crystallographic plane forms a layered material that is coupled by weak vdW interactions. The empirical formula of 2D perovskites is $L_2MX_4$, where L is the large monovalent organic cation/spacer, M the metal cation, and X the anion. Few examples of 2D-layered perovskites are $Cs_2PbI_2Br_2$, $(BA)_2(MA)_2Pb_3I_{10}$, etc.

***Metal–Organic frameworks***: Metal–organic frameworks also form 2D structures which are considered as an attractive alternate crystalline porous material [16, 17]. It basically consists of metal bridging nodes and multi-podal organic ligands that are bonded together. This type of bonding usually forms through basic coordination chemistry. In general, the metal node is coupled to the organic ligand by a coordination bond; however, the layers of the metal–organic framework are linked by weak vdW forces.

***Elemental 2D nanomaterials***: Elemental 2D nanomaterials are attracting great attention with the experimental demonstrations of borophene nanosheets belonging to the group III. Boron forms almost 16 number of allotropes through complex B–B bonds, out of which only three forms are thermodynamically stable (α-rhombohedral, β-rhombohedral, γ-orthorhombic, and γ-tetragonal) [18]. These allotropes consist of the icosahedral $B_{12}$ units as the building blocks. Notable structure among the

borophene is the $B_{36}$, which has a bowl-shaped cluster with a periodic hexagonal holes arrangement forming a triangular lattice. The hexagonal arrangements of atoms can be visualized as graphene-like nanosheets [18, 19].

Another interesting 2D nanomaterials are silicene, germanene, and stanene belonging to the group IV elements [19]. Silicene is derived from silicon which comprises a buckled sheet and can host non-trivial electronic states, spin-polarized edges, and a tunable bandgap that allows for application in quantum information. Similarly, germanene is also a buckled monolayer of germanium that forms a nearly flat honeycomb nanosheets [18]. Germanene shows strong spin–orbit coupling for topological insulator properties. Stanene, on the other hand, is derived from tin (α-Sn). Stanene is epitaxially grown on various substrates; however, its structure is not well-defined [18, 19].

From the group V elements, phosphorene or black phosphorus (BP) is an allotrope of phosphorous which is known to be thermodynamically stable at room temperature (RT). It also emerges as one of the novel 2D semiconducting materials which has similar properties and colour of graphite. Typically, BP has an orthorhombic crystal structure, closely analogous to graphene. In the crystal arrangement, the phosphorous atoms are organized in a honeycomb lattice with puckered double layers. BP monolayer has $sp^3$ hybridization where one phosphorous atom is covalently bonded to three other adjacent phosphorous atoms having a bond length of 2.18 Å [20]. In addition, it has one lone pair of electrons, thus forming a quadrangular pyramid structure. The adjacent layers of phosphorous atoms interact by weak vdW interactions where the distance between two layers is about 0.5 nm. Similarly, arsenene also belongs to group V that has a single buckled honeycomb 2D layer of arsenic. Arsenene has an indirect bandgap of 2.49 eV and a high charge carrier mobility. Another 2D structures are antimonene and bismuthene which are extracted buckled honeycomb network of antimony and bismuth [19]. Antimonene has high carrier mobility and excellent thermal conductivity. Bismuthene is extensively used in topological insulators through the reduction of bismuth [ref]. Notably, various structures and properties of BP-like puckered structures (α-phase) of arsenene, antimonene, and bismuthene have been predicted [18–20]. However, fabrication of monolayer α-phase is challenging mainly due of the lack of layered allotropes.

***MXenes***: With the expansion of the family of 2D nanomaterials, the derivatives of transition metals using carbides, carbonitrides, and nitrides lead to the discovery of MAX phases where M stands for transition metal (Ti, Zr, Cr, etc.), A is an element from A-group mainly IIIA, IVA (Ga, Pb, Al, etc.), and X is either carbon or nitrogen. By introducing selective etching of the A element from the MAX phases, MXenes are created. MXenes are considered as layered solids linked by strong metallic, ionic, and covalent bonds. Having a layered hexagonal structure, they belong to space group $P6_3/mmc$ symmetry. MXenes have a general formula $M_{n+1}AX_n$, with $n = 1$–3, and thereby, the MXene sheets consist of 3, 5, or 7 atomic layers constructing $M_2X$, $M_3X_2$, and $M_4X_3$, respectively [9]. Some examples of MXenes are $Ti_2C$, $Ti_3C_2$, $Mo_2Ga_2C$, $Nb_4C_3$, etc.

## 2 Synthesis of 2D Nanomaterials

The 2D nanomaterials possess both similarities and differences in their fundamental crystalline features compared to their 3D counterparts. Therefore, to maintain their unique structural/crystalline features and simultaneously retaining their outstanding properties, atomically thin 2D nanomaterials have become the forefront in condensed matter physics, materials science, and nanotechnology. In literature, there are numerous methods available for the synthesis of 2D nanomaterials. However, before addressing the individual experimental techniques, it is worth mentioning that the nanoscale synthesis methods are broadly categoried into two types: bottom-up approach and top-down approach (Fig. 2) [21].

### *2.1 Bottom-Up Approach*

The bottom-up approach is also referred as the gathering-up method in which the 2D nanomaterials can be synthesized from atomic or molecular precursors in the form of nanoparticles or nanocrystals that are allowed to grow in size after undergoing certain chemical reactions. The nanoscale particles thus self-assembled into larger complex substances or can be supplemented to any substrate of interest [21, 22]. The bottom-up approach is mainly desired for achieving controlled size, shape, composition, sequential stacking arrangement, and stable chemical structure. There are various synthetic methods used to prepare 2D nanomaterials using the bottom-up approach such as hydrothermal or solvo-thermal method, wet chemical synthesis, CVD, PECVD, organic ligand-assisted synthesis, interface-assisted synthesis, and template-assisted synthesis [23, 24]. Here, we have discussed the most regularly used techniques.

*Hydrothermal method*: This is one of the most common and widely used synthesis methods of 2D nanomaterials. It is cleared from the name itself that this technique deals with water (hydro) and heat (thermal). This means that this method is somewhat analogous to wet thermal synthesis. Although there are few additional requirements in the hydrothermal method which are the high temperature and pressure. Typically, the hydrothermal reaction is carried out inside an autoclave (vessel) with a Teflon liner. At first, the precursor materials are mixed thoroughly in an appropriate concentration and then transferred to the autoclave vessel. The autoclave vessel is designed in such a manner so that it can easily work under high-pressure conditions. Finally, the precursor-filled vessel is placed in a heating furnace, setting a specific temperature and time for the reaction to start till completion. Here, the solvents serve as the catalyst to initiate the reaction and help the growth of nanostructures [25]. This technique has several benefits such as high product yield, controlled size/shape, high-quality crystals, and most importantly, the low-cost instrumentation with environment-friendly synthesis. Yin et al. have presented a novel hydrothermal strategy to synthesize

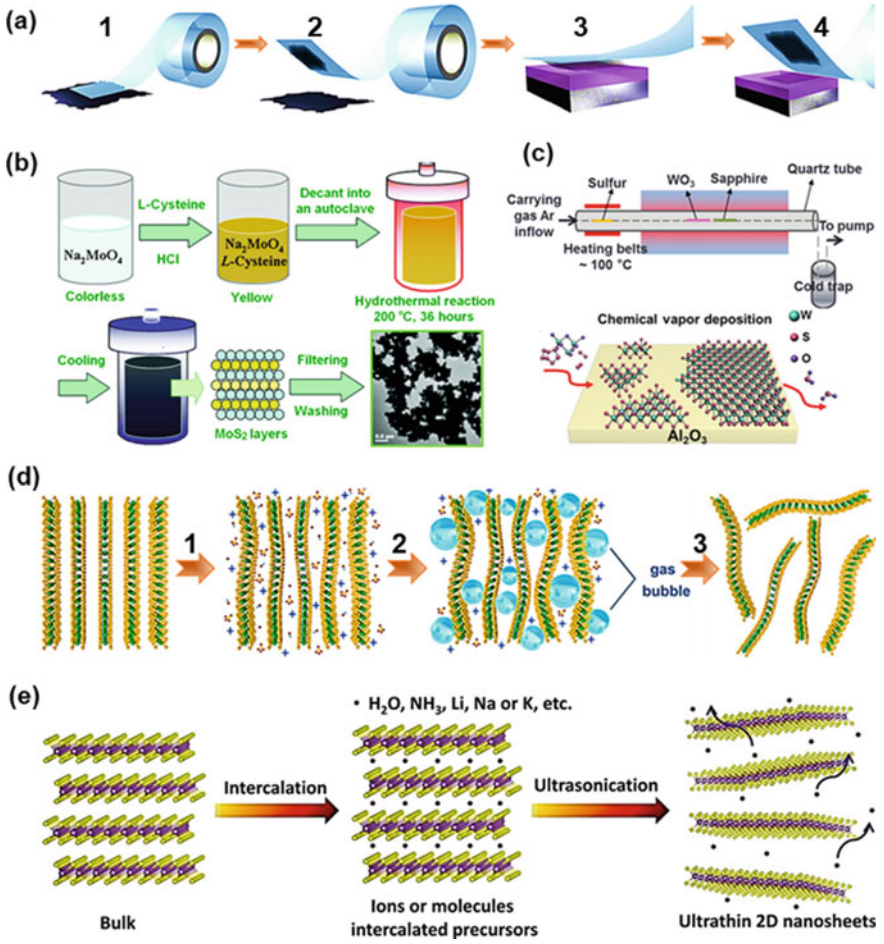


**Fig. 2** Different synthesis techniques for the growth of 2D nanomaterials: top-down and bottom-up approaches. **a** Mechanical cleavage method (1) press the adhesive tape against the 2D crystals, (2) few layers are attached to the tape, (3) the tape with crystals is pressed against a surface, (4) upon peeling, the bottom layer left on the substrate, **b** hydrothermal method, **c** CVD technique, **d** sonication derived exfoliation via (1) the addition of exfoliating/stabilizing agents, (2) sonication, and (3) exfoliated 2D nanosheets. **e** Ion-intercalation method. Reprinted with copyright permission from [5–8, 10]

$MoSe_2$ nanosheets [26]. This synthetic approach provides the synergistic regulation of both crystal phase (1T) and disorder engineering. In addition, one modified approach using the hydrothermal technique is reported by Dai et al., where graphene-like $MoSe_2$ nanosheets are synthesized under the synergy of graphene and polyvinylpyrrolidone [27]. Moreover, Alam et al. have synthesized metal oxide-based 2D nanomaterials using Bi-$TiO_2$ nanotube/graphene nanocomposites through simple hydrothermal synthesis [28]. Similarly, various 2D nanosheets of metal oxides such

as $Ga_2O_3$, $ZnGa_2O_4$, and $MnGa_2O_4$ are prepared by hydrothermal synthesis [29]. These nanosheets exhibit a triangular/hexagonal configuration with ultrathin thickness. In addition, Peng et al. demonstrated the use of a modified hydrothermal route using some basic etching agent to synthesize 2D MXene ($Ti_3C_2$) [30]. They have also extended their route to other MXene such as $Nb_2C$. Subsequently, to boost the material yield of MXenes, Han et al. have adopted a facile hydrothermal-assisted intercalation approach to form 2D $Ti_3C_2T_x$ and achieved 74% yield which was conventionally limited to 20% [31]. Hydrothermal synthesis is also used to prepare 2D nanosheets of boron nitride. Xie et al. reported the hydrothermal exfoliation method where the bulk h-BN undergoes expansion with the insertion of $Li^+$ and then exfoliated into ultrathin 2D nanosheets [32]. Catalyst-free g-$C_3N_4$ is also prepared by the low-cost hydrothermal approach [33].

*Chemical vapour deposition (CVD) method*: As the name suggests, CVD is a gas phase deposition method for the preparation of thin films over any desired substrate. Here, the precursors (volatile or viscous liquids) are injected into the vacuumed sealed reaction chamber in the form of vapours/gases and are allowed to go through some specific chemical reactions at a specific ambient temperature. Consequently, the placed substrates get coated when the reaction products of the precursors are assembled onto it [23, 34]. There are various synthesis parameters to take care of while performing the deposition such as process temperature, pressure, substrate temperature, and gas mixture composition. Therefore, simply controlling these parameters, it is possible to synthesize good quality thin films with high purity. This technique has some special advantages: for instance, low film porosity, high purity, and outstanding stability at air ambient comprehensively adopted in industries. Based on the CVD method, numerous 2D nanomaterials are synthesized for targeted applications. McCreary et al. reported the synthesis of large-area monolayers of $WS_2$ using CVD [35]. Likewise, Dankert et al. have worked on the fabrication of all CVD-based heterostructures with h-BN/graphene/h-BN configuration for developing high-performance Hall sensors [36]. As one kind of CVD technique, the researchers have also explored the PECVD technique to grow CN films using methane ($CH_4$) and $N_2$ gases [37]. Again, adopting an in-situ CVD approach, large-area 2D BP is grown with an average area of $> 3\ \mu m^2$ and about four layers of thickness [38]. A similar effort has been done by other groups to grow TMDs ($WS_2$) atomic layer on h-BN film by CVD technique [39].

*Interface-assisted synthesis*: Basically, an interface is referred as any flat or curved space (more precisely can be known as any phase boundary) between two dissimilar materials. Likewise, the interface formed between air and matter or between vacuum and matter is called the surface. Typically, the thickness of any interface ranges from angstrom (Å) to nanometres to few micrometres. Therefore, once the ratio of area to thickness in any interface is high enough, it is called a 2D interface. In the field of materials science, this 2D interface is highly active for multiple reactions as compared to the bulk phase. Some common interfaces that are involved in chemical reactions include the air/liquid, liquid/liquid, solid/liquid, and vacuum/solid interfaces. These types of 2D interfaces provide space to the precursors to gather and

induce the growth process or nucleation in a confined 2D space. This confined reaction in 2D space plays an important role in controlling the material properties of the final product [40]. Therefore, as one kind of bottom-up approach, there are various interface-assisted synthetic approaches reported in the literature for the development of 2D nanomaterials. Considering the synthesis of graphene (a star material in the field of materials science), the gas/solid or the vacuum/solid interface is a popular strategy that can be done using CVD. In CVD, a selective solid substrate is kept in a vacuumed/air chamber, and the gases of interest (say $CH_4$ for graphene) are inserted into the chamber which is allowed to react on the substrate. Pollard et al. confirmed the growth of graphene on a Ni film (Ni is used as a catalyst) deposited on the $SiO_2$/Si substrate using CVD [41]. Similarly, using CVD with a vapour/solid interface, h-BN is also synthesized by Shi et al. [42]. Interfacial synthesis strategies towards the preparation of TMDs have also been explored. Transition metal selenides such as $TiSe_2$, $NbSe_2$, and $TaSe_2$ are synthesized by surfactant lamellar templating which acts as efficient 2D catalysts. These 2D structures feature the thickness from single sheets to tens of nanometres [43]. Other noble 2D metal oxides such as $SnO_2$, CuO, and $In_2O_3$ are developed using surfactants. For the growth of 2D metal oxides using bottom-up approach from molecular precursors, Sun et al. have addressed the surfactant self-assembly, where the surfactants serve as the agents for structure design and help to confine the growth along the desired 2D direction [44]. In addition, an interesting 2D metal–oxide framework nanosheets are demonstrated by Nishihara and co-workers. At the air/water interface, they have tried to synthesize a single-layer nickel bis(dithiolene) nanosheets under atmospheric pressure [45]. Moreover, with regards to the other 2D nanomaterials such as MXenes, CN, and BP, the current synthesis methods are primly focused on the physical and chemical exfoliation of their bulk structures. Thus, the growth of single- to few-layered structures through the interface-assisted synthesis is still under progressive development.

## *2.2 Top-Down Method*

In contrast to the bottom-up approach, the top-down approach is more complex and requires sophistication. The top-down approach is also referred as the destructive method where the nanostructures are formed by removing the building blocks from the matter or cutting/sizing the solid crystal planes [21]. Particularly considering the synthesis of 2D nanomaterials, the top-down approach involves the breaking of interlayer spacing of a 3D matter to prepare atomically thin layers. Again, the top-down method is grouped into various types such as exfoliation method, chemical etching, sputtering, nano-lithography, and laser ablation. Here, we have discussed some of the widely used techniques:

*Exfoliation method*: The exfoliation method is categorized into two types: chemical exfoliation and physical exfoliation. Chemical exfoliation is resulted from the thinning of a layered crystal down to atomic-level layers through appropriate chemical

routes involving intercalants [46] to form 2D-layered structures. A large number of intercalants are used for chemical exfoliation such as acids/bases ($HSO_4^-$, $SO_2^{2-}$, and KOH), inorganic salts ($Li^+$, $Na^+$), oxidizing agents (hydrogen peroxide and hydroxyl radicals), and functional molecules ($NH^+$, pyrene sulfonic acid). Diazonium salts are effectively used to chemically exfoliate the semiconducting bulk $MoS_2$ in the 2H phase [47]. Similarly, some other bulk chalcogenides such as $Bi_2S_3$ and $Sb_2S_3$ are also exfoliated into 2D nanosheets using this chemistry [48, 49]. On the other hand, one report addresses that with aryldiazonium modification, it is possible to exfoliate bulk BP without undergoing any pre-treatment and passivation of the surface to form 2D nanosheets which can be applied in field-effect transistors (FET) [50]. Composites of graphene oxide/manganese phosphate are also realized by the chemical exfoliation process through Hummer's method as reported by Yuan et al. [51]. The liquid exfoliation method is also explored by many researchers for the synthesis of 2D metal oxides. This process is associated with gentle cutting of the bulk interlayers where different organic cations such as TBA and ammonium ions are used as the intercalant agents [52]. Chemical exfoliation of MAX phases into 2D MXenes is also highlighted by the research community. Khazaei et al. have utilized a series of first-principle calculations based on DFT and studied the exfoliation energies, forces, bond strengths, and electronic structures of the MAX phase. Based on their DFT calculations, around 37 MAX phases are proposed for successful exfoliation into 2D MXenes such as $Ti_3C_2$, $Ti_4C_3$, $Zr_2C$, $Hf_2C$, $V_3C_2$, $V_4C_3$, $Mo_2C$, and so on [53]. From the above-mentioned examples, now it is clear that with chemical exfoliation the chemical structure of 2D nanomaterials can be tuned through some appropriate reactions. During the chemical exfoliation process, sometimes the 2D nanomaterials suffer from loss of their inherent properties causing rapid degradation.

Physical exfoliation, on the other hand, can preserve the important properties of exfoliated 2D nanomaterials without experiencing much degradation. Physical exfoliation also offers large-scale production suitable for all practical applications. This type of exfoliation is mainly achieved through some external driving forces such as sonication, wet/dry ball milling, shear mixing, using some supercritical fluids, polar/non-polar solvents, and stabilizers. Considering the simplest case of ultrasonication, it has been reported by Kim et al. that any layered bulk material such as graphene, $MoS_2$, and h-BN can be exfoliated by controlling the temperature in an ultrasonic bath [54]. The as-exfoliated 2D materials, for instance, h-BN display an alternating charge distribution with a strong polarity across the boron and nitrogen termination edges. However, $MoS_2$ and $MoSe_2$ provide moderate polarity, where the surface has a negative charge with the sulphur atoms and counter-charges inside the molybdenum atoms. With ultrasonication, the 2D nanomaterials often suffer from the introduction of undesired defects. Therefore, the use of supercritical fluid is another approach to physical exfoliation [55]. As one of the most common supercritical fluids, $CO_2$ presents a solvent-like behaviour which can dissolve non-polar chemical species. Using $CO_2$, thick nanosheets of more than ten layers can be formed [56]. A molecular dynamics study is conducted for stabilizing MXene ($Ti_2CO_2$) structures using supercritical $CO_2$ as reported by Khaledialidusti et al. [57]. In addition, ball milling is also one type of physical exfoliation technique which is used to prepare

MXenes ($Ti_2C_2T_x$). After ball grinding, the $Ti_3AlC_2$ size is found to be uniform and can be tuned from 4.488 to 1.454 μm, with a well-defined 2D nanosheets structure [58]. Similarly, g-$C_3N_4$ powders are also synthesized by ball milling from amorphous carbon at high temperatures [59]. Graphene, TMDs, and h-BN synthesis with solvent-stabilizer exfoliation is also addressed using PVA-assisted shear-exfoliation and using chloroform/acetonitrile and IPA/water [60].

*Sputtering*: Sputtering is a comprehensively used industrial-based technique that provides large-scale high purity production of diverse materials maintaining high quality and controllability. With this technique, it is possible to use any kind of substrate and even applicable to insulating material deposition. In general, sputtering is performed under a vacuum with a target material to be sputtered. Generally, an inert gas (or a reactive gas) is used as a carrier gas to initiate the plasma glow upon applied bias. The ionized gases are then accelerated to the target material in the presence of an electric field and thus bombards the target surface with high kinetic energy, thereby ejection of the target atoms. Those target atoms are then self-assembled or accumulated on the substrates to form the smooth and uniform coating [61]. Various 2D nanomaterials are synthesized by sputtering. Rigi et al. have demonstrated a RF magnetron sputtering method to produce $MoS_2$ layers [62]. For the experiment molybdenum target was used under sulphur environment using an in-situ effusion cell. A highly pure 2H-$MoS_2$ phase is obtained using RF magnetron sputtering. Likewise, thin $MoSe_2$ interlayer is prepared by sputtering and selenization process by pressure variation and applied for efficient Cu(In, Ga)$Se_2$ solar cell (PCE = 10.8%) [63]. Moreover, high-quality boron nitride (BN) films are also deposited by magnetron sputtering as addressed by Sutter et al. [64]. Here, the boron is sputtered under $N_2$ and Ar environment, and the thickness of the deposited film is carefully controlled. Ensuring effective substrate temperature, two atomic layers of BN are successfully deposited by magnetron sputtering. Li et al. have reported an ionized magnetron sputtering method to deposit amorphous CN [65]. High purity graphite is used as the sputtering target with an inductively coupled plasma assembly between the target and the substrate under Ar/$N_2$ mixture gases. Within the $N_2$ to C ratio of 0.3–0.4, hardness up to 16–17 GPa is achieved. Moreover, Wang et al. using magnetron sputtering tried to deposit MXene with molybdenum carbide ($Mo_2C$) structure to be applicable in solid-state Q-switched pulsed laser generation [66]. The overall summary of the different synthetic approaches for the preparation of 2D nanomaterials including their advantages and challenges is tabulated in Table 1.

## 3 Properties and Characterizations of 2D Nanomaterials

The 2D nanomaterials based on their unique structures and wide range of synthetic approaches emerge as one of the novel classes of nanoscale materials. With the unique structural constructions of various 2D nanomaterials, they show interesting

**Table 1** Summary of various synthesis techniques to grow 2D nanomaterials with their achievements and challenges

| Synthetic methods | | 2D nanomaterials | Achievements | Challenges | References |
|---|---|---|---|---|---|
| Bottom-up | Hydrothermal/solvo-thermal method | TMDs: $MoSe_2$, $MoS_2$<br>Oxides: $Ga_2O_3$, $ZnGa_2O_4$, $MnGa_2O_4$<br>MXenes: $Ti_3C_2$, $Ti_3C_2T_x$<br>CN: g-$C_3N_4$ | • Easy processing<br>• High product yield<br>• Controlled size/shape<br>• Tunable morphology<br>• Low cost and eco-friendly | • Thickness control<br>• Long synthesis duration<br>• Repeatability<br>• Not scalable | [20–32] |
| | CVD, PECVD | TMDs: $WS_2$<br>h-BN<br>BP | • High purity<br>• Large-area coverage on any substrate<br>• Pin-hole free film<br>• Excellent stability<br>• High scalability | • Defect control<br>• High temperature<br>• High-cost sophisticated vacuum technique | [33–39] |
| | Interface-assisted synthesis | TMDs: $TiSe_2$, $NbSe_2$, $TaSe_2$<br>Oxides: $SnO_2$, CuO, and $In_2O_3$ | • Composition and design function<br>• Controlled size/shape<br>• Tunable morphology | • Small crystallites<br>• Thickness control<br>• Low-yield<br>• Inert atmosphere | [40–45] |
| Top-down | Exfoliation: Physical and chemical | TMDs: $MoS_2$, $Nb_2S_3$, $Sb_2S_3$<br>BP, silicene<br>MXenes: $Ti_3C_2$, $Ti_4C_3$, $Zr_2C$, $Hf_2C$, $V_3C_2$, $V_4C_3$, $Mo_2C$<br>CN: g-$C_3N_4$ | • High purity<br>• High porosity<br>• Uniform growth<br>• Wafer scalable | • Small crystallites<br>• Thickness control<br>• Low-yield<br>• Not scalable | [46–59] |
| | Sputtering | TMDs: $MoSe_2$, $MoS_2$<br>h-BN<br>MXenes: $Mo_2C$ | • High purity<br>• Large-area coverage on any substrate<br>• Pin-hole free film<br>• Excellent stability<br>• High scalability | • Defect control<br>• Comparatively high-cost technique | [60–66] |


**Fig. 3** Different properties of 2D nanomaterials with their corresponding unique characteristic features

properties like unprecedented optical or photonic properties and tunable morphological features. In addition, the 2D nanomaterials also offer unique electrical transport properties based on their dimensional restrictions. Moreover, the thermal, mechanical, and magnetic properties are also explored for some targeted applications with high stability (Fig. 3). Therefore, concerning the new synthesis approaches and vibrant properties, the 2D nanomaterials are realized in various applications related to material sciences such as in energy conversion (solar cells, water electrolysis, photocatalysis, thermoelectric devices, etc.) and energy storage devices (supercapacitors, batteries, etc.) [4–11]. In this section, we will elaborate on the individual properties shown by various 2D nanomaterials.

## *3.1 Structural Properties*

Geim and Novoselov won the Nobel Prize in 2004 for the invention of graphene which is an important class of 2D nanomaterial [2]. Graphene holds a hexagonal structure with $sp^2$ hybridized carbon atoms. The structure has alternate single and double bonds (i.e. a conjugated structure) with p-orbital overlapping and electron delocalization. Because of this structural arrangement, graphene holds a very stable crystalline form and offers unique properties such as high surface area, outstanding catalytic features, high optical transparency, and so on. Graphene has shown its potential as a promising candidate for diverse applications, for instance, in optoelectronics, supercapacitors, drug delivery, biosensors, and image sensors. Regardless of consuming numerous advantages and applications, graphene has some shortcomings too. For example,

the material is insoluble and infusible in nature. Therefore, for full utilization of graphene, some structural modifications are always required such as modifications in the basal plane, edges, and surface functionalization.

Now, expanding the portfolio of 2D nanomaterials from graphene, currently other new 2D materials such as TMDs, h-BN, g-$C_3N_4$, MXenes, and black phosphorous are in the forefront [4–10]. The sandwiched structured TMDs with X–M–X structure exhibit semiconducting properties with a tuneable bandgap which makes them a suitable candidate for optoelectronic devices [9]. Moreover, based on its unique layered structures, it is also used as an efficient catalyst material for applications in electrochemical cells [11]. $SnS_2$ belongs to the class of TMDs which crystallize in hexagonal $CdI_2$ lattice structure. It shows n-type semiconducting characteristics and is known to have a wide bandgap (2.03–2.4 eV) [67]. Its strong anisotropy makes it possible for its use in efficient holographic recording systems. Moreover, other TMDs such as $MoS_2$, $MoSe_2$, $WS_2$, and $TaS_2$ have out-of-plane mirror symmetry and in-plane inversion symmetry, owing to which they show complementary characteristics to that of graphene [9]. Also, in some cases, even these TMDs surpass the performance of graphene. The main uniqueness of these TMDs is their strong spin–orbit interaction. The most studied $MoS_2$ is a semiconductor with a 2H phase and tuneable bandgap from 1.2 to 1.9 eV. In addition, the $MoS_2$ monolayers have in-plane Young's modulus of 200–300 GPa. Another special parameter is its high mobility (> 190 $cm^2\ V^{-1}\ s^{-1}$), high on/off current ratio ($10^8$), and polarization properties. As such, $MoS_2$ shows potential applications in several fields such as nano-electronics, solar cells, chemosensing, energy storage, and catalysis [9, 68]. Tran et al. recently announced a new member of the MXene family: $V_4C_3T_x$ which is prepared by means of chemical exfoliation of the MAX phase ($V_4AlC_3$) using aqueous hydrofluoric acid [69]. The successfully exfoliated MXene $V_4C_3T_x$ is confirmed from the SEM morphology and STEM characterizations. In parallel, Rosen's group has addressed the synthesis of quaternary MAX solution with $(Nb_{2/3}Sc_{1/3})_2AlC$ structure. They have selectively etched both Al and Sc atoms to produce $Nb_{1.33}CT_x$ MXene, which is confirmed from XRD, XPS, and STEM [70]. Likewise, h-BN also belongs to the family of 2D nanomaterials which has a noteworthy structural resemblance to graphene. The 2D h-BN comprises both armchair and zigzag edge-terminated structures, where the layers are coupled to one another by the relatively weak vdW forces. The h-BN offers a high surface area and improved stability [12]. Silva et al. have demonstrated the synthesis of nanostructured BN through thermal CVD at 1150 °C. For this, iron compound ($FeS/Fe_2O_3$) is used as the catalyst on $Al_2O_3$ nanostructures [71].

## *3.2 Optical and Photonic Properties*

As already highlighted, the 2D nanomaterials provide diverse properties suitable for a broad spectrum of applications. One important property is the optical/photonic response of the 2D nanomaterials. The optical characteristics of materials are mostly

determined by the electronic band structure. The precise engineering of the electronic bands in 2D nanomaterials yields useful optical properties. It is well known that every 2D nanostructured material shows different optical bandgaps based on their individual structure–property relationship. The layered 2D halide perovskites show unprecedented optical properties with a tunable bandgap suitable for optoelectronic applications such as photodetectors, solar cells, and light-emitting diodes. [72]. $MA_3Bi_2I_9$, $Cs_2PbI_2Cl_2$, and $(BA)_2(MA)_2Pb_3I_{10}$ have a 2D-layered structure with bandgaps ranging from 1.5 to 1.9 eV. As one of the typical layered perovskite derivatives, these are used in solar cells and photodetectors [73]. Moreover, some 2D nanomaterials have large electronic bandgaps such as TMDs, h-BN, and MXenes. In particular, significant changes occur in the optical properties of TMDs due to the existence of indirect-to-direct bandgap transition. This depends on varying the thicknesses of $MoS_2$ layers. Monolayered $MoS_2$ with an energy bandgap of 1.8 eV can detect green light, whereas a triple-layered $MoS_2$ with a bandgap of 1.35 eV responds towards red light [74]. Moreover, h-BN and BP are also being investigated extensively for their photonic and optoelectronic properties. Brar et al. have demonstrated the surface phonon–plasmon–polariton modes in a heterostructure based on graphene and h-BN. They have shown experimentally that the plasmon mode of graphene is split into two modes which display anti-crossing behaviour near the energy of h-BN optical phonon at 1370 $cm^{-1}$ [75]. Preparation of g-$C_3N_4$ nanosheets incorporating plasmonic silver as an efficient photocatalyst is also explored for enhanced visible-light photocatalysis experiments. Deng et al. have studied the improved photocatalytic activity of plasmonic Ag and $N_2$ doped graphene QDs which are co-decorated on g-$C_3N_4$ nanosheets [76]. The experimental findings reveal an improved photocatalytic activity with 92.8% removal efficacy under white light and NIR irradiation. Plasmonic photodetection of MXenes is also reported based on its atomically thin layers. Velusamy et al. have reported $Mo_2CT_x$ MXene thin films which are successfully deposited on paper substrates. The as-fabricated photodetectors with this MXene structure exhibit extended photoresponse within 400–800 nm along with a high responsivity of 9 $AW^{-1}$ and detectivity of $5 \times 10^{11}$ Jones. It also exhibits reproducible photo-switching featured at a wavelength of 660 nm [77]. Moreover, a photodetector based on black phosphorous is also reported by Engel et al. for high-speed imaging [78]. Here, a multi-layered BP is capable of acquiring high contrast in the visible and infrared region of the electromagnetic spectrum showing its applicability for broadband optical detection.

## *3.3 Electrical Properties*

Electronic/electrical property is influenced by the presence of localized or delocalized transport of electrons in a solid material. Based on the electronic properties of various materials, the economy of numerous industries has improved by adopting state-of-the-art fabrication technologies. For the case of 2D nanomaterials, the electrons or holes are restricted to occupy the quantized energy levels in one spatial dimension.

Based on this, various important electronic properties are arising related to the energy level, transport, and phonon scattering and excitation in 2D nanomaterials.

Numerous heterostructures have been designed based on graphene for bandgap engineering such as graphene/h-BN, graphene/ZnO, and graphene/$MoS_2$ [79, 80]. In general, TMDs hold a vast range of electronic properties, from semi-metals to semiconductors to insulators. Xiong et al. reported the lithium intercalation in $MoS_2$ [81]. Because of Li insertion into the interlayer spacing, the electrical conductivity enhanced 200 times. Likewise, electrical transport in various TMDs has been investigated such as in 2H-$NbS_2$, -$NbSe_2$, -$TaS_2$, and $TaSe_2$, respectively. Here, to investigate the carrier scattering mechanisms, the charge density wave (CDW) system is used. Based on this, the measurements of the resistivity and the Hall coefficient of 2H-TMDs are carried out between 4.2 and 300 K [82]. The resistivity of 2H–$NbS_2$ displays no CDW transition. On contrary, 2H–$TaSe_2$ shows the highest CDW transition and along with several anomalous features. The electrical properties of MXene structure $Ti_3C_2T_x$ monolayers are investigated by Miranda et al. [83]. They have demonstrated the metallic nature of MXene with a high free carrier density of $8 \pm 3 \times 10^{21}$ $cm^{-3}$ and high mobility of $0.7 \pm 0.2$ $cm^2$ $V^{-1}$ $s^{-1}$. Based on the electrical performance of MXenes, they have been successfully utilized as promising candidates for energy storage applications, for example, in Na, Li, K ion batteries, supercapacitors, and fuel cells. As a 2D equivalent of graphene, the electrical properties of h-BN are also studied both individually and by forming heterostructure of graphene and h-BN [84]. In general, h-BN is considered as an insulator with a wide bandgap; however, forming the heterostructure with graphene (graphene/h-BN) for transistor application, the electron mobility and the drain current switching ratios are as high as 573 $cm^2$ $V^{-1}$ $s^{-1}$ and $-2 \times 10^{11}$ $cm^{-2}$ [85]. Moreover, the electrical properties of sputter-deposited CN thin films are also studied by Broitman et al. [86]. They have reported that by increasing the $N_2$ content during sputtering, the resistivity decreases from $4 \times 10^{-2}$ Ω-cm to $4 \times 10^{-3}$ Ω-cm. The electrical conductivity of BP has been measured by Keyes et al. [87]. They observed p-type conductivity under low temperatures. The electron and hole mobilities at room temperature are reported to be 350 and 220 $cm^2$ $V^{-1}$ $s^{-1}$, respectively.

### *3.4 Thermal Properties*

Thermal property management is an essential subject for designing robust electronic devices. 2D nanomaterials based on the thermoelectric effects can directly convert heat into electricity for harnessing waste heat. For this, mainly the Seebeck effect is used to modulate the conversion of heat into voltage [88]. Numerous studies were performed to achieve appreciable Seebeck coefficients. For instance, Hippalgaonkar et al. and Hewitt et al. have reported the Seebeck coefficients of $MoS_2$ and $Sb_2Te_3$ to be 8.5 mW-$m^{-1}$ $K^{-1}$ and 371 μW-$m^{-1}$ $K^{-1}$, respectively [89, 90]. In addition, among all the TMDs, $WS_2$ based on the Boltzmann transport equation provides the highest thermal conductivity of 142 $Wm^{-1}$ $K^{-1}$ followed by $MoS_2$ and $MoSe_2$ with

103 and 54 $Wm^{-1}$ $K^{-1}$ [91]. It has been addressed that the heterostructures of 2D nanomaterials provide an ideal platform to study interfacial heat transport. The interface thermal conductance of $MoS_2$ on Au substrate is as high as 221 MW-$m^{-2}$ $K^{-1}$ [92]. Moreover, polymeric carbon nitride (PCN) is investigated for thermoelectric performance using molecular dynamic simulations. It is found that PCN has a high figure-of-merit, ZT ($ZT = S^2\sigma T/\kappa$, where S is the Seebeck coefficient, σ is the electronic conductivity, T is the absolute temperature, and κ is the thermal conductivity) of 0.52 at 300 K which contributes to n-type thermoelectric group materials [93]. Heterojunction devices based on graphene/h-BN also offer a high thermoelectric power factor of 10.35 W-$m^{-2}$ $K^{-1}$ [94]. Introduction of MXene ($Ti_3C_2T_x$) into $(Bi, Sb)_2Te_3$ matrix also provides improved thermoelectric performance with ZT of 1.3 within 300–475 K towards high thermoelectric conversion efficiency [95].

## *3.5 Mechanical and Magnetic Properties*

Mechanical properties of 2D nanomaterials play an important role in various applications. Some mechanical properties include the fracture strengths, Young's modulus, elasticity, etc. [96]. One of the ways to control the mechanical properties of 2D nanomaterials is based on defect engineering, which helps to enhance the toughness of classical materials from metals to semiconductors to insulators [97].

Magnetic properties of 2D nanomaterials are of utmost importance which can find interest in applications related to electric motors, computers, and medical diagnosis. For example, ferromagnetism is considered as one of the intrinsic properties of atomically thin layered 2D materials at room temperature [98]. This property has also shown a broader prospect for nano-device design. In particular, for spintronic applications, the intrinsic magnetic orders in ultrathin 2D nanomaterials have been extensively studied [99]. Sanikop et al. have tried to tailor the magnetically active sites of $MoS_2$ nanosheets for spintronic applications [100]. For this, defect-density controlled 2H phase of $MoS_2$ nanosheets is prepared at 500–900 °C which shows a ferromagnetic-like transition at 120 K. Likewise, Du et al. have elaborated the first-principle prediction of metal-free magnetism in g-$C_3N_4$ [101]. The ferromagnetic ground state displayed by the g-$C_4N_3$ also possesses an intrinsic half-metallicity. Kumar et al. have demonstrated the intrinsic ferromagnetism in $Mn_2NT_x$, $Ti_2NO_x$, and $Cr_2NO_x$, MXene structures [102]. High magnetic moments, high Curie temperature (1877 K), and robust ferromagnetism are found in these MXenes for spintronic applications. Furthermore, in the heterostructure of $Ni(OH)_2$ and h-BN, a larger magnetic moment with ferromagnetic coupling is found [40]. Furthermore, ferromagnetic 2D nanomaterials with superior electronic and optical properties are used for the construction of compact magnetic, magneto-electronic, and magneto-optical devices. Table 2 provides an overview of all the unique properties of various 2D nanomaterials.

**Table 2** Summary of different properties of various 2D nanomaterials

| 2D material | Properties | | | | | | | References |
|---|---|---|---|---|---|---|---|---|
| | Structural | Optical | Electrical | Thermal | Mechanical | | Magnetic | |
| | Phase; Thickness (Å) | $E_g$ (eV) | Mobility ($cm^2 V^{-1} s^{-1}$) | Thermal conductivity ($Wm^{-1} K^{-1}$) | Young's modulus (GPa) | Fracture strength (GPa) | | |
| g-$C_3N_4$ | Hexagonal, rhombic; 3.35 | 0.98–3.34 | $3 \times 10^5$ | 7.6 | 822 | 45.4(Z), 31.4(A) | Ferromagnetic metal | [59, 76, 86, 93] |
| $MoS_2$ | 2H, 1T, 3R, 1T'; 6.04 | 1.2–1.9 (2H) | > 190 | 103 | 219(Z), 222(A) | 16.9(Z), 7.3(A) | RT ferromagnetic | [8, 89, 92, 99] |
| $WS_2$ | 2H, 1T; 0.608 | 1–2 (2H) | 140 | 142 | 240(Z), 244(A) | 19.9(Z), 29.9(A) | Ferromagnetic, anti-ferromagnetic, and metallic | [35, 39, 91] |
| $MoSe_2$ | 2H, 1T; 0.637 | 1.1–1.55 | 121 | 54 | 175(Z), 178(A) | – | Anti-ferromagnetic | [26, 27, 63] |
| $MoTe_2$ | 2H, 1T'; 0.691 | < 1 (2H), 60 m (1T') | 4000 | 0.35 | 205 | – | Diamagnetic and paramagnetic | [8, 96] |
| $WSe_2$ | 2H, 1T; 0.641 | 1.4–1.6 | 66 | 3.935 | 194(Z), 196(A) | 15.0(Z), 24.7(A) | Ferromagnetic upon doping and creating defects in $WSe_2$ | [8, 96] |

(continued)

**Table 2** (continued)

| 2D material | Properties | | | | | | | References |
|---|---|---|---|---|---|---|---|---|
| | Structural | Optical | Electrical | Thermal | Mechanical | | Magnetic | |
| | Phase; Thickness (Å) | $E_g$ (eV) | Mobility ($cm^2 V^{-1} s^{-1}$) | Thermal conductivity ($Wm^{-1} K^{-1}$) | Young's modulus (GPa) | Fracture strength (GPa) | | |
| $WTe_2$ | 1T'; 0.691 | 55 m | 74 | 3 | 135(Z), 137(A) | 9.30(Z), 18.7(A) | RT ferromagnetic upon doping | [8, 96] |
| h-BN | Hexagonal; 3.34 | 5–6 | 573 | 10.35 | 865 | 70.5 | RT ferromagnetic upon doping | [40, 85, 94, 96] |
| BP | Cubic, rhombohedral; 5.55 | 0.3–2.3 | 350–220 | 40 | 166(Z), 44(A) | 18(Z), 8(A) | Non-magnetic, but shows ferromagnetic upon doping and creating defects in BP | [87, 96] |
| Silicene | $(\sqrt{3} \times \sqrt{3})R30^o$; 4.20 | 1.55 m | $2.5 \times 10^5$ | 5.4 | 82.2 | 12.5 | Ferromagnetic upon doping and creating defects silicene | [18, 19, 96] |
| Bismuthene | Hexagonal; 4.94 | 0.5 | $5.7 \times 10^6$ | 1.3 | 26.1 | 25.5 | Ferromagnetic upon doping | [18, 19, 96] |
| $Ti_3C_2$ | Hexagonal; 3 | 3 | 2.6 | 11.57 | 80–100 | – | RT Ferromagnetic | [9, 30] |

***$E_g$*** bandgap, *A* armchair, *Z* zigzag, *RT* room temperature

## 4 Future Aspects and Conclusions

This chapter offers an overview of the fundamentals of 2D nanomaterials including their structure, types, synthesis, and properties. It is now well established that 2D nanomaterials are the special class of materials which open up a new avenue of diverse applications including energy conversion, storage, and in the environment and biomedical fields. We have mainly highlighted the 2D nanomaterials based on TMDs ($MoS_2$, $WSe_2$, $MoSe_2$, etc.), BP, g-$C_3N_4$, h-BN, MXenes, 2D metal oxides, and layered perovskites. The 2D nanomaterials can be synthesized from various routes, among which we have discussed in detail the bottom-up and top-down approaches. Finally, numerous interesting properties including structural, optical, electrical, mechanical, thermal, and magnetic properties are elaborated with examples of 2D nanomaterials. Based on the special properties of 2D nanomaterials, significant applications are highlighted related to energy conversion technologies suitable for energy harvesting and energy storage devices. However, the commercialization of 2D nanomaterials is still in the progressing stage of technology.

With the intervening time, nanotechnology has been revolutionized by the use of 2D nanomaterials. 2D nanomaterials cover a number of important topics in basic and applied sciences making a novel class of materials with a promising future. 2D nanomaterials with high surface area, high electronic and excellent optical properties will be very useful in the near future for nano-electronic applications to be utilized in lithium-ion batteries, image sensors, biosensors, solar cells, supercapacitors, and catalysts. However, it is noteworthy that the cost of 2D nanomaterials is relatively higher, but as technologies will reach the maturing phase, the use of 2D nanomaterials will nurture, thus enabling the higher demand for targeted applications with lower prices that may start to establish themselves in the marketplace. It is anticipated that the contents summarized in this chapter can afford an important reference and guideline for further systematic studies on 2D nanomaterials.

**Acknowledgements** This study is financially supported by the Department of Science and Technology (DST), Government of India, under the Inspire Faculty Award (DST/INSPIRE/04/2018/001721).

## References

1. Jitendra NT, Rajanish NT, Kwang SK (2012) Zero-dimensional, one-dimensional, two-dimensional, and three-dimensional nanostructured materials for advanced electrochemical energy devices. Prog Mater Sci 57:724–803
2. Novoselov KS, Geim AK, Morozov SV et al (2004) Electric field effect in atomically thin carbon films. Science 306:666–669
3. Huang X, Zeng ZY, Zhang H (2013) Metal dichalcogenide nanosheets: Preparation, properties and applications. Chem Soc Rev 42:1934–1946
4. Cai Z, Liu B, Zou X et al (2018) Chemical vapor deposition growth and applications of two-dimensional materials and their heterostructures. Chem Rev 118:6091–6133

5. Han Y, Ge Y, Chao Y et al (2018) Recent progress in 2D materials for flexible supercapacitors. J Energy Chem 27:57–72
6. Novoselov KS, Neto AHC (2012) Two-dimensional crystals-based heterostructures: materials with tailored properties. Phys Scr T146:014006
7. Liu N, Kim P, Kim JH et al (2014) Large-area atomically thin $MoS_2$ nanosheets prepared using electrochemical exfoliation. ACS Nano 8:6902–6910
8. Zhang Y, Zhang Y, Ji Q et al (2013) Controlled growth of high-quality monolayer WS2 layers on sapphire and imaging its grain boundary. ACS Nano 7:8963–8971
9. Naguib M, Mochalin VN, Barsoum MW et al (2014) 25th anniversary article: MXenes: a new family of two-dimensional materials. Adv Mater 26:992–1005
10. Guo X, Wang Y, Wu F et al (2015) A colorimetric method of analysis for trace amounts of hydrogen peroxide with the use of the nano-properties of molybdenum disulfide. Analyst 140:1119–1126
11. Lin Y, Williams TV, Connell JW (2010) Soluble, exfoliated hexagonal boron nitride nanosheets. J Phys Chem Lett 1:277–283
12. Zhi C, Bando Y, Tang C et al (2009) Large-scale fabrication of boron nitride nanosheets and their utilization in polymeric composites with improved thermal and mechanical properties. Adv Mater 21:2889–2893
13. Zhao Z, Sun Y, Dong F (2015) Graphitic carbon nitride based nanocomposites: a review. Nanoscale 7:15–37
14. Osada M, Sasaki T (2009) Exfoliated oxide nanosheets: new solution to nanoelectronics. J Mater Chem 19:2503–2511
15. El-Ballouli A, Bakr OM, Mohammed OF (2020) Structurally tunable two-dimensional layered perovskites: from confinement and enhanced charge transport to prolonged hot carrier cooling dynamics. J Phys Chem Lett 11:5705–5718
16. Rodenas T, Luz I, Prieto G et al (2015) Metal-organic framework nanosheets in polymer composite materials for gas separation. Nat Mater 14:48–55
17. Peng Y, Li Y, Ban Y et al (2014) Metal-organic framework nanosheets as building blocks for molecular sieving membranes. Science 346:1356–1359
18. Bhimanapati GR, Zhong L, Vincent M et al (2015) Recent advances in two-dimensional materials beyond graphene. ACS Nano 9:11509–11539
19. Xiangkai K, Qiangchun L, Changlin Z et al (2017) Elemental two-dimensional nanosheets beyond graphene. Chem Soc Rev 46:2127–2157
20. Liu H, Du Y, Deng Y et al (2015) Semiconducting black phosphorus: synthesis, transport properties and electronic applications. Chem Soc Rev 44:2732–2743
21. Iqbal P, Preece JA, Mendes PM (2012) Nanotechnology: the "top-down" and "bottom-up" approaches. Supramol Chem Mol Nanomater. https://doi.org/10.1002/9780470661345.smc195
22. Xiao X, Wang H, Urbankowski P et al (2018) Topochemical synthesis of 2D materials. Chem Soc Rev 47:8744–8765
23. Jiang J, Li N, Zou J et al (2019) Synergistic additive-mediated CVD growth and chemical modification of 2D materials. Chem Soc Rev 48:4639–4654
24. Han ZJ, Murdock AT, Seo DH et al (2018) Recent progress in plasma-assisted synthesis and modification of 2D materials. 2D Mater 5:032002
25. Feng S, Xu R (2001) New materials in hydrothermal synthesis. Acc Chem Res 34:239–247
26. Yin Y, Zhang Y, Gao T (2017) Synergistic phase and disorder engineering in 1T-nanosheets for enhanced hydrogen-evolution reaction. Adv Mater 29:1700311
27. Dai C, Zhou Z, Tian C et al (2017) Large-scale synthesis of graphene-like $MoSe_2$ nanosheets for efficient hydrogen evolution reaction. J Phys Chem C 121:1974–1981
28. Alam U, Fleisch M, Kretschmer I et al (2017) One-step hydrothermal synthesis of Bi-$TiO_2$ nanotube/graphene composites: an efficient photocatalyst for spectacular degradation of organic pollutants under visible light irradiation. Appl Catal B 218:758–769
29. Yang W, Li J, Zhang X et al (2019) Hydrothermal approach to spinel-type 2D metal oxide nanosheets. Inorg Chem 58:549–556

30. Peng C, Wei P, Chen X et al (2018) A hydrothermal etching route to synthesis of 2D MXene ($Ti_3C_2$, $Nb_2C$): enhanced exfoliation and improved adsorption performance. Ceram Int 44:18886–18893
31. Han F, Luo S, Xie L et al (2019) Boosting the yield of MXene 2D Sheets via a facile hydrothermal-assisted intercalation. ACS Appl Mater Interfaces 11:8443–8452
32. Xie B, Li C, Chen J et al (2020) Exfoliated 2D hexagonal boron nitride nanosheet stabilized stearic acid as composite phase change materials for thermal energy storage. Sol Energy 204:624–634
33. Zhang P, Li X, Shao C et al (2015) Hydrothermal synthesis of carbon-rich graphitic carbon nitride nanosheets for photoredox catalysis. J Mater Chem A 3:3281–3284
34. Zhang Y, Zhang L, Zhou C (2013) Review of chemical vapor deposition of graphene and related applications. Acc Chem Res 46:2329–2339
35. McCreary KM, Hanbicki AT, Jernigan GG et al (2016) Synthesis of large-area $WS_2$ monolayers with exceptional photoluminescence. Sci Rep 6:19159
36. Dankert A, Karpiak B, Saroj P (2017) Dash hall sensors batch-fabricated on all-CVD h-BN/graphene/h-BN heterostructures. Sci Rep 7:15231
37. Khanis NH, Ritikos R, Azlinda S et al (2017) Investigations on the Role of $N_2$:($N_2$ + $CH_4$) ratio on the growth of hydrophobic nanostructured hydrogenated carbon nitride thin films by plasma enhanced chemical vapor deposition at low temperature. Mater 10:102
38. Smith JB, Hagaman D, Ji H-F (2016) Growth of 2D black phosphorus film from chemical vapor deposition. Nanotechnology 27:215602.
39. Okada M, Sawazaki T, Watanabe K et al (2014) Direct chemical vapor deposition growth of $WS_2$ atomic layers on hexagonal boron nitride. ACS Nano 8:8273–8277
40. Dong R, Zhang T, Feng X et al (2018) Interface-assisted synthesis of 2D materials: trend and challenges. Chem Rev 118:6189–6235
41. Pollard AJ, Nair RR, Sabki SN et al (2009) Formation of monolayer graphene by annealing sacrificial nickel thin films. J Phys Chem C 113:16565–16567
42. Shi Y, Hamsen C, Jia X et al (2010) Synthesis of new-layer hexagonal boron nitride thin film by chemical vapor deposition. Nano Lett 10:4134–4139
43. Brent JR, Savjani N, O'Brien P (2017) Synthetic approaches to two-dimensional transition metal dichalcogenide nanosheets. Prog Mater Sci 89:411–478
44. Sun Z, Liao T, Dou Y et al (2014) Generalized self-assembly of scalable two-dimensional transition metal oxide nanosheets. Nat Commun 5:3813
45. Kusamoto T, Nishihar H (2019) Zero-, one- and two-dimensional bis(dithiolato)metal complexes with unique physical and chemical properties. Coord Chem Rev 380:419–439
46. Le T-H, Oh Y, Kim H et al (2020) Exfoliation of 2D materials for energy and environmental applications. Chem Eur J 26:6360–6401
47. Lee H, Bak S, An S-J et al (2017) Highly efficient thin-film transistor via cross linking of 1T edge functional 2H molybdenum disulfides. ACS Nano 11:12832–12839
48. Dhar N, Syed N, Mohiuddin M et al (2018) Exfoliation behavior of van der waals strings: Case study of $Bi_2S_3$. ACS Appl Mater Interfaces 10:42603–42611
49. Li DO, Gilliam MS, Chu XS (2019) Covalent chemical functionalization of semiconducting layered chalcogenide nanosheets. Mol Syst Des Eng 4:962
50. Ryder CR, Wood JD, Wells SA (2016) Covalent functionalization and passivation of exfoliated black phosphorus via aryl diazonium chemistry. Nat Chem 8:597–602
51. Yuan R, Yuan J, Wu Y (2018) Graphene oxide-monohydrated manganese phosphate composites: preparation via modified Hummers method. Colloids Surf A 547:56–63
52. Zhang Q, Mei L, Cao X (2020) Intercalation and exfoliation chemistries of transition metal dichalcogenides. J Mater Chem A 8:15417–15444
53. Khazaei M, Ranjbar A, Esfarjani K (2018) Insights into exfoliation possibility of MAX phases to MXenes. Phys Chem Chem Phys 20:8579–8592
54. Kim J, Kwon S, Cho D-H (2015) Direct exfoliation and dispersion of two-dimensional materials in pure water via temperature control. Nat Commun 6:8294

55. Sun Z, Fan Q, Zhang M (2019) Supercritical fluid-facilitated exfoliation and processing of 2D materials. Adv Sci 6:1901084
56. Sasikala SP, Poulin P, Aymonier C (2016) Prospects of supercritical fluids in realizing graphene-based functional materials. Adv Mater 28:2663
57. Khaledialidusti R, Mahdaviab E, Barnoush A (2019) Stabilization of 2D graphene, functionalized graphene, and $Ti_2CO_2$ (MXene) in super-critical $CO_2$: a molecular dynamics study. Phys Chem Chem Phys 21:12968–12976
58. Huang S, Mochalin VN (2019) Hydrolysis of 2D transition-metal carbides (MXenes) in colloidal solutions. Inorg Chem 58:1958–1966
59. Zhen F, Yu-Xian L (2003) Carbon nitride compounds synthesized by thermal annealing amorphous nanostructured graphite under the flow of $NH_3$ gas. Chin Phys Lett 20:1540–1543
60. Khanam Z, Liu J, Song S (2020) Flexible graphene paper electrode prepared via polyvinyl alcohol-assisted shear-exfoliation for all-solid-state polymer supercapacitor application. Electrochim Acta 363:137208
61. Kelly PJ, Arnell RD (2000) Magnetron sputtering: a review of recent developments and applications. Vacuum 56:159–172
62. Rigi VJC, Jayaraj MK, Saji KJ (2020) Envisaging radio frequency magnetron sputtering as an efficient method for large scale deposition of homogeneous two-dimensional $MoS_2$. Appl Surf Sci 529:147158
63. Lin W-T, Chan S-H, Tseng S-Z (2014) Manipulation of $MoSe_2$ films on CuIn(Ga)Se2 solar cells during rapid thermal process, Int J Photoenergy 253285
64. Sutter P, Lahiri J, Zahl P (2013) Scalable synthesis of uniform few-layer hexagonal boron nitride dielectric films. Nano Lett 13:276–281
65. Li D, Lopez S, Chung YW et al (1995) Ionized magnetron sputter deposition of amorphous carbon nitride thin films. J Vac Sci Technol A 13:1063
66. Wang J, Liu S, Wang Y et al (2020) Magnetron-sputtering deposited molybdenum carbide MXene thin films as a saturable absorber for passively Q-switched lasers. J Mater Chem C 8:1608–1613
67. Ye G, Gong Y, Lei S et al (2017) Synthesis of large-scale atomic-layer $SnS_2$ through chemical vapor deposition. Nano Res 10:2386–2394
68. Bazaka K, Levchenko I, Wei J et al (2019) $MoS_2$–based nanostructures: synthesis and applications in medicine. J Phys D: Appl Phys 52:183001
69. Tran MH, Schafer T, Shahraei A et al (2018) Adding a new member to the MXene family: synthesis, structure, and electrocatalytic activity for the hydrogen evolution reaction of $V_4C_3T_x$. ACS Appl Energy Mater 1:3908–3914
70. Lu J, Thore A, Meshkian R et al (2017) Theoretical and experimental exploration of a novel in-plane chemically ordered $(Cr_{2/3}M_{1/3})_2AlC$ i-MAX Phase with M = Sc and Y. Cryst Growth Des 17:5704–5711
71. Silva WH, Ribeiro H, Ferreira TH et al (2017) Synthesis of boron nitride nanostructures from catalyst of iron compounds via thermal chemical vapour deposition technique. Phys E 89:177–182
72. Mao L, Stoumpos CC, Kanatzidis MG (2019) Two-dimensional hybrid halide perovskites: principles and promises. J Am Chem Soc 141:1171–1190
73. Blancon J-C, Even J, Stoumpos CC et al (2020) Semiconductor physics of organic–inorganic 2D halide perovskites. Nat Nanotechnol 15:969–985
74. Lopez-Sanchez O, Lembke D, Kayci M et al (2013) Ultrasensitive photodetectors based on monolayer $MoS_2$. Nat Nanotechnol 8:497–501
75. Brar VW, Jang MS, Sherrott M et al (2014) Hybrid surface-phonon-plasmon polariton modes in graphene/monolayer h-BN heterostructures. Nano Lett 14:3876–3880
76. Deng Y, Tang L, Feng C et al (2017) Construction of plasmonic Ag and nitrogen-doped graphene quantum dots codecorated ultrathin graphitic carbon nitride nanosheet composites with enhanced photocatalytic activity: full spectrum response ability and mechanism insight. ACS Appl Mater Interfaces 9:42816–42828

77. Velusamy DB, El-Demellawi JK, El-Zohry AM et al (2019) MXenes for plasmonic photodetection. Adv Mater 31:1807658
78. Engel M, Steiner M, Avouris P (2014) Black phosphorus photodetector for multispectral, high-resolution imaging. Nano Lett 14:6414–6417
79. Sutter P, Cortes R, Lahiri J et al (2012) Interface formation in monolayer graphene-boron nitride heterostructures. Nano Lett 12:4869–4874
80. Wang S, Tian H, Ren C et al (2018) Electronic and optical properties of heterostructures based on transition metal dichalcogenides and graphene-like zinc oxide. Sci Rep 8:12009
81. Xiong F, Wang H, Liu X et al (2015) Li intercalation in $MoS_2$: in situ observation of its dynamics and tuning optical and electrical properties. Nano Lett 15:6777–6784
82. Liu Y, Shao DF, Li LJ et al (2016) Nature of charge density waves and superconductivity in $1T-TaSe_{2-x}Te_x$. Phys Rev B 94:045131
83. Miranda A, Halim J, Lorke A et al (2017) Rendering $Ti_3C_2T_x$ (MXene) monolayers visible. Mater Res Lett 5:322–328
84. Wang J, Ma F, Liang W et al (2017) Electrical properties and applications of graphene, hexagonal boron nitride (h-BN) and graphene/h-BN heterostructures. Mater Today Phys 2:6–34
85. Wang X, Hossain M, Wei Z et al (2019) Growth of two-dimensional materials on hexagonal boron nitride (h-BN). Nanotechnology 30:034003
86. Broitman E, Hellgren N, Neidhardt J et al (2002) Electrical properties of carbon nitride thin films: role of morphology and hydrogen content. J Electron Mater 31:L11–L15
87. Keyes RW (1953) The electrical properties of black phosphorus. Phys Rev 92:580
88. Li D, Gong Y, Chen Y et al (2020) Recent progress of two-dimensional thermoelectric materials. Nano-Micro Lett 12:36
89. Hippalgaonkar K, Wang Y, Ye Y et al (2017) High thermoelectric power factor in two-dimensional crystals of $MoS_2$. Phys Rev B 95:115407
90. Hewitt CA, Li Q, Xu J et al (2017) Ultrafast digital printing toward 4D shape changing materials. Adv Mater 29:1605390
91. Gu X, Yang R (2014) Phonon transport in single-layer transition metal dichalcogenides: a first-principles study. Appl Phys Lett 105:131903
92. Ding Z, Pei Q-X, Jiang J-W et al (2016) Interfacial thermal conductance in graphene/$MoS_2$ heterostructure. Carbon 96:888–896
93. Ding Z, An M, Mo S et al (2014) Unexpectedly high cross-plane thermoelectric performance of layered carbon nitrides. J Mater Chem A 7:2114
94. Duan J, Wang X, Lai X et al (2016) High thermoelectric power factor in graphene/hBN devices. PNAS 113:14272–14276
95. Lu X, Zhang Q, Liao J (2020) High-efficiency thermoelectric power generation enabled by homogeneous incorporation of MXene in (Bi, $Sb_)2T_e3$ Matrix. Adv Energy Mater 10:1902986
96. Liu B, Zhou K (2019) Recent progress on graphene-analogous 2D nanomaterials: properties, modeling and applications. Prog Mater Sci 100:99e169
97. Deji A, Christopher JB, Scott BJ et al (2017) A review on mechanics and mechanical properties of 2D material-graphene and beyond. Extreme Mech Lett 13:42–77
98. Miao N, Xu B, Zhu L et al (2018) 2D Intrinsic ferromagnets from van der Waals antiferromagnets. J Am Chem Soc 140:2417–2420
99. Miller JL (2017) Ferromagnetism found in two-dimensional materials. Phys Today 70:16
100. Sanikop R, Sudakar C (2020) Tailoring magnetically active defect sites in $MoS_2$ nanosheets for spintronics applications. ACS Appl Nano Mater 3:576–587
101. Du A, Sanvito S, Smith SC (2012) First-principles prediction of metal-free magnetism and intrinsic half-metallicity in graphitic carbon nitride. Phys Rev Lett 108:197207
102. Kumar H, Frey NC, Dong L et al (2017) Tunable magnetism and transport properties in nitride MXenes. ACS Nano 11:7648–7655

# Chapter 2
# Emerging 2D Nanomaterial Composites for Efficient Energy Conversion: Insight into the Evolutionary Perspective of Devices


**Amreen A. Hussain and Amit K. Rana**

## 1 Introduction

Over the span of time, today's world is confronted with two major predicaments: one is the rapidly growing climatic change and other is the exhaustion of fossil fuels. One of the gentlest and yet effective suggestion for generating the world's energy prerequisites comes from the renewable energy conversion. The rapid growth in the renewable energy conversion technologies has spread its horizon during the past decades thereby providing a clean and sustainable alternative to improve the associated energy and environmental issues. The concern begins due to the burning of fossil fuels and nuclear energy relating to carbon waste, radioactive waste, and high accidental risks [1, 2].

Commonly, the energy conversion system/device is a continuous cycle of reuse and reform where, mainly three processes such as the energy generation, energy conversion and energy storage should collaborate to facilitate the targeted applications. Harnessing energy directly from sunlight is one option to fulfill the need for clean energy which simultaneously have a negligible effect on the environment. It is well known that solar energy can be utilized in photovoltaic applications such as the solar cells, to generate electricity through photoelectric effect or photochemical effect [3–5]. Additionally, solar energy can also be effective in splitting water to produce hydrogen fuel [6–8]. Therefore, direct transformation of solar energy into electricity or chemical fuels is an efficient technology to addressing the intermittency

A. A. Hussain (✉)
Facilitation Centre for Industrial Plasma Technologies (FCIPT), Institute for Plasma Research (IPR), Gandhinagar 382428, Gujarat, India
e-mail: amreenhussain8888@gmail.com

A. K. Rana
Department of Material Sciences and Engineering, Ulsan National Institute of Science and Technology (UNIST), Ulsan 44919, South Korea
e-mail: aramitrana4@gmail.com



Z. Khanam et al. (eds.), *2D Nanomaterials for Energy and Environmental Sustainability*,
Materials Horizons: From Nature to Nanomaterials,
https://doi.org/10.1007/978-981-16-8538-5_2

in renewable energy sources. Likewise, the other energy conversion application is related to the thermoelectric heating/cooling devices that transform electric energy into thermal energy and vice versa [9, 10].

Concerning to efficient energy conversion, one of the key components required relies in the design and development of novel advanced materials which are affordable. Recently, going from first to third generation of materials, the emergence of two-dimensional (2D) materials have placed themselves as a strong candidate for energy conversion and storage [11, 12]. In common terms, the 2D material structures are referred as nanosheets or layered thin films which are derived by their atomically thin thicknesses and extremely larger lateral dimensions. There are numerous materials from where the nanosheets or layered thin films can be exfoliated to form 2D nanomaterials ranging from insulators to semiconductors to superconductors. In recent times, various configurations of 2D materials or layered structures are explored with higher surface areas suitable for various environmental applications such as catalytic, adsorption-related, water splitting, and solar cell applications [12–15]. The transition metal dichalcogenides (TMDs) such as $MoSe_2$, $SnS_2$, $MoS_2$, and $WSe_2$ are highlighted as a major compound for hydrogen generation catalysts owing to their robustness and scalability [16]. Moreover, specific to optoelectronics and water-splitting applications, the layered perovskite structures are also realized for instance $MA_3Bi_2I_9$, $Cs_2PbI_2Cl_2$, $La_{1-x}Sr_xCoO_{3-\delta}$, etc. [17, 18]. Apart from these, 2D metal oxides and metal–organic frameworks have also proven their applicability in effective energy conversion [19, 20].

According to the citation databases (Google Scholar, Web of Science, SciFinder), the research on energy conversion using 2D nanomaterials has grown tremendously. Since 2010 till date, over one million journal publications have addressed to efficient energy conversion through solar cells, water splitting, oxygen reduction/hydrogen evolution (electrocatalysis), piezoelectricity, and thermoelectricity. This chapter thus focuses on the emerging importance of 2D nanomaterials for energy conversion. The sections in this chapter will explore the robustness of the 2D nanomaterials for solar conversion and catalytic activities and also focus on the possibility for long-term stability based on their structure–property relationship. Importantly, the strategic approaches reported till date will be discussed concerning to the various energy conversion devices such that the 2D nanomaterials might be used as a building block for production of competent and robust energy conversion technologies. Finally, an outlook on offering the fundamental scientific opportunities/challenges for investigating and understanding the intrinsic effects of 2D nanomaterials for proficient energy conversion devices will be highlighted.

## 2 Two-Dimensional Nanomaterials: Fundamental Properties for Energy Conversion

A comprehensive introduction to 2D nanomaterials becomes necessary in order to search for their potential applicability for energy conversion. The discoveries related to both material diversity and new technologies to fulfill the increasing energy demands have served to categorize the key scientific information and landmarks to the researchers which might have a significant effect in a global level. Commonly, the dimensionality spectrum of solid materials, for instances zero-dimension (0D), one-dimension (1D), two-dimension (2D), and three-dimension (3D) is known to have different density of states (DOS) (mainly associated with the number of electrons present) which play an important influence on the intrinsic properties of materials [21]. Among these low-dimensional materials, the 2D nanostructures emerge as a promising candidate for efficient energy conversion where it can be synthetically grown by exfoliating the bulk solids into nanosheets bounded by van der waal's forces (vdW) [22]. Historically, the 2D nanomaterials are announced with the discovery of graphene which are derived from atomically thin carbon materials [23]. Graphene possesses remarkable chemical and electronic properties which brings new innovations in diverse applications materials world. Following the same quest, the library of 2D nanomaterials grows exponentially every year where the researchers have stimulated the hunt for new 2D nanomaterials such as TMDs, layered perovskites, elemental 2D nanomaterials (black phosphorous, silicene, germenene bismuthine, arsenene etc.), hexagonal boron nitride (h-BN), carbon nitrides, and MXenes for diverse applications, as presented in Fig. 1 [18, 19, 21, 24–29]. All these 2D nanoma-

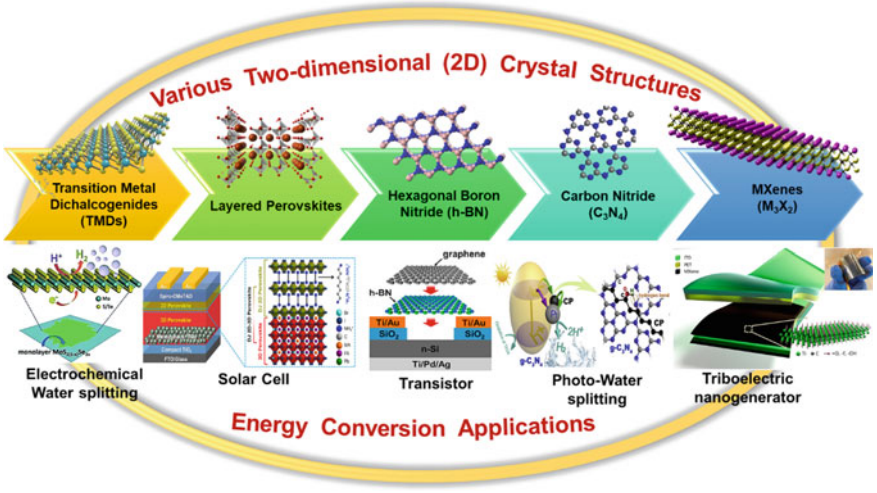


**Fig. 1** Library of 2D nanomaterials with their corresponding crystal structures and potential applications. Reproduced with permission [25–29]

terials show unique characteristics based on their structure–function-property relationships. Specifically, unlike other bulk materials, 2D materials have a unique crystal lattice which is analogous to an exposed crystal geometry in the form of nanowires, nano-pores, nanotubes, nano-sheets, etc., that exposed various active sites for the targeted reaction/activities to take place. It is important to highlight that graphene, being a zero bandgap material experiences difficulty in electronic devices.

At par, it is well-established that various features differentiate the 2D nanostructures with respect to conventional bulk materials. In addition, they are significantly relevant for the development of novel energy conversion technologies.

***Structural and optical properties***: Recently, the chalcogenides represent the most studied 2D nanomaterials [16]. TMDs belongs to the semiconductor group which has tunable bandgap and interesting electrical properties making them suitable for nano-electronic devices. For example, monolayers of $MoSe_2$ have moderate direct bandgaps and very fast electronic responses suitable for energy conversion [24]. However, the direct realization of single 2D nanomaterials for targeted application is limited due to the ineffective separation of charge carriers (electrons and holes) in $MoSe_2$ monolayers. This is because atomically thin TMDs display insufficient surface scattering as compared to other ultrathin metal counterparts. Typically, from an atomic arrangement perspective, the TMDs structure consist of sandwich layers of transition metals and chalcogens which are coupled by weak van der waals forces whereas the intralayer between the atoms has strong covalent character. This structural arrangement of TMDs makes its bulk crystal highly stable under different environmental conditions. Additionally, the crystal structure is also stable under illumination conditions. The absorption coefficients and bandgap energies of these 2D TMDs have made them attractive candidates for energy conversion technologies in photovoltaics and photo-electrochemical systems. For example, monocrystalline $WSe_2$ demonstrated in achieving solar power conversion efficiency of 17% [30]. Moreover, wafer-scale monolayers of $WSe_2$ photocatalysts have accorded for direct solar-driven hydrogen production via effective water splitting [31]. Likewise, hexagonal boron nitride (h-BN) is another material which shows strong deep ultraviolet absorption and high emission efficiency that originates from the strong light-matter interaction of 2D materials [24]. Likewise, as a new family of transition metal carbides, MXene phases ($Ti_2CF_2$) offer maximum absorption coefficient in the infrared region [16]. Furthermore, 2D perovskite structures such as $MA_3Bi_2I_9$ and $Cs_3Bi_2I_9$, also emerge as a potential candidate in improving the photovoltaic energy conversion with high stability [17, 32]. Recently, elemental 2D nanomaterials are attracting great attention. For instance, the experimental demonstrations of group III element, borophene; group IV elements, silicene, germanene, stanine; and group V elements, black phosphorous (BP), bismuthine, arsenene (group V) show that based on their individual structure, can host non-trivial electronic states, spin-polarized edges and a tunable bandgap that allows for application in energy conversion systems [33]. Few layers of BP with a layer dependent direct bandgap and large tunability are shown to be promising in IR detectors and emitters, which also provides a new insight into the light-matter interaction in anisotropic materials [34].

***Electronic properties***: The electronic properties of TMDs hinge on the crystal phase that leads to a range of electronic characteristics, including metallic, semi-metallic, semiconducting, and superconducting features, for different TMDs [24, 33]. Group V-B and VI-B metals constructing the 2D TMDs are widely studied being the ability to form stable compounds with excellent electronic structures. The semiconducting TMDs, for instance $MoS_2$, $WS_2$, and $WSe_2$, have been highlighted as efficient electronic device materials because of their comparatively high charge carrier motilities and appreciable bandgaps, which enable large switching ratios in field effect transistors (FETs) [33, 35]. At room temperature (RT) the TMDs ($MoS_2$) have electron carrier mobility of about 200 $cm^2\ V^{-1}\ s^{-1}$ with bandgaps of 1–2 eV in the visible range. It is worth mentioning that this high carrier mobility is comparative to the silicon technology [36]. Therefore, based on these unique electronic characteristics the 2D TMDs represent an attractive platform for energy conversion and for elementary studies related to light-matter interactions, optoelectronics, and nano-photonics. In parallel, group V TMDs, specifically $TaS_2$ and $NbSe_2$, were explored which have shown their strong potential in electronic phenomena such as in superconductors and charge density waves [24]. The electronic properties of MXenes based on a detailed study of their density of states, however, show metallic character thereby improving their conductivity [26]. Moreover, the electronic properties of h-BN can be easily modulated by external pressure. It is found that along with the increase in the hydrostatic pressure, the electrons in the basal planes transfer to the inter-plane [33]. From the group V elemental group, arsenene has a single buckled honeycomb 2D layer of arsenic. Arsenene has an indirect bandgap of 2.49 eV and a high charge carrier mobility. Another 2D structures are antimonene and bismuthene which are extracted buckled honeycomb network of antimony and bismuth [37]. Antimonene also exhibit high carrier mobility and excellent thermal conductivity.

***Catalytic properties***: The bulk TMDs are historically studied in the catalysis community. Based on this, the recently renewed interest in 2D TMDs has revitalized the exploration of this class of materials for catalysis in efficient energy conversions including some biological and chemical sensor devices. One of the important applications in energy conversion is electrocatalysis. 2D TMDs such as $MoS_2$, $MoSe_2$, $WS_2$, and $NbS_2$ have demonstrated their realization as excellent electrocatalyst where these are extensively investigated for hydrogen evolution reaction (HER) for hydrogen production [38]. In general, the catalyst reactivity mainly relies on the physico-chemical properties of the catalyst surface and the interface between the electrode and electrolyte. Therefore, to achieve effective catalytic activity, the catalysts should be efficient in lowering the energy barriers and thereby improving the rate of surface electron charge transfer. To fulfill this prime need for catalytic activity, the 2D nanomaterials are currently one of the most up-to-date materials in the research field. MXene-based materials are identified as efficient electrocatalyst particularly in hydrogen evolution [39]. In addition, 2D metal oxides and hydroxides such as $Pd_5O_4$, $MnO_2$, and $TiO_2$ show very diverse catalytic properties due to their capability of adopting different binding configurations [19]. Moreover, the elemental 2D nanomaterials like BP also offer unprecedented catalytic properties owing to its

large specific surface area with more active sites and high theoretical capacity as Li/Na-ion batteries anode for both electrocatalyst and novel electrode material [33].

***Thermal properties***: Thermoelectric materials with high figure of merits (ZT) that have the capability to convert the wasted heat directly into electricity, remains a challenge. However, with the discovery of 2D nanomaterials, this challenge is addressed to certain extent [40]. Particularly, 2D TMDs such as $MoS_2$, $MoSe_2$, $WS_2$, and $WSe_2$ are identified as ideal materials which can harvest waste heat with efficiencies about 7–8%. The TMDs show high Seebeck coefficients, for instance, $MoS_2$ gives $\alpha^2\sigma = 8.5$ mW $m^{-1}$ $K^{-2}$ with low cross-plane thermal conductivity. The thermal conductivities of $WTe_2$ and $MoS_2$ are reported to be 3 and 59 $Wm^{-1}$ $K^{-1}$, respectively [41]. For the construction of energy conversion devices, the interfacial contact between the metal and the 2D nanomaterials also play an important role. Therefore, the management of interfacial thermal resistance between the metal side and edge side (TMDs) is extremely essential. TMDs, such as $MoS_2$, based on their higher interfacial energy coupling show better interface contact due to which the internal thermal conductance increases to 68.6 mW $m^{-2}$ $K^{-1}$ [42]. On the contrary, h-BN is electrically insulating but can offer high thermal conductivity. This feature of h-BN makes it an interesting candidate for thermal management where it is required to have electrical insulation [43]. Heterostructures based on 2D graphene and transition metal oxides also show high thermal conductivity with $\alpha^2\sigma = 2500$ $\mu Wm^{-1}$ $K^{-2}$ at room temperature [40, 41].

## 3 Why Two-Dimensional Nanomaterials for New Energy Conversion Technologies?

The 2D nanomaterials, specifically the TMDs, 2D perovskites and other metal oxide-based materials have a restricted role in a fossil fuel-dominated energy scenario. However, their position is progressively stirring to a new energy scenario largely based on the use of renewable energy. 2D TMDs heterostructures, MXene, metal oxide is the current widely used anode materials in commercialized storage devices such as supercapacitors [44]. Moreover, the TMDs also supports as the efficient electrocatalysis for applications in fuel cells, mainly to produce hydrogen [45]. Normally, all these processes are associated with energy conversion and energy storage that can be transferred into a solar energy-based future energy scenario. However, the main drawback that is faced with these materials is their performance which is below the requirement with respect to the fossil energy-based society. This is because the energy requirement demands the use of not only cell phone, laptops, and cars but also power stations, long-distance transport, lighting, and heating need to be powered.

Therefore, the future energy situation must be the driving force for existing activities in 2D nanomaterial research for energy conversion applications. There lie many reasons for choosing 2D nanomaterials: as it is cost effective, stable, earth abundant, and environmentally friendly. Also, the heterostructures of 2D nanomaterials are

foreseen to have a special role in the future energy scenario that the classical single counterpart cannot have.

While comparing with conventional energy conversion materials, the 2D nanomaterials possess unique size- and surface-dependent properties such as morphology, electrical, optical, and mechanical properties that allow a step forward in enhancing energy conversion and storage performance. Derived from them are the various nanostructures in the form of quantum dots, nanotubes, nanofibers, nanoribbon, nanocages, etc. The most common advantages of these new nanomaterials are their low dimension, specific morphology, and electronic properties. The nano-dimension with precise morphology enables tunable physical and chemical properties such as high electro-conductivity, good thermal conductivity, and outstanding mechanical properties. An interesting characteristic of these 2D materials is the possibility of tailoring their electronic structure by introducing heteroatoms and heterostructures, to adapt their physical property by controlling their pore structure, and to change their chemical property by introducing functional groups onto the surface. In this way, it is possible to introduce a level of control in the characteristics of these materials that is not possible in other systems.

Another significant feature of the 2D materials is the possibility of its infusion in designing the state-of-the-art hybrid or composite heterostructures [46]. An interesting example is found where TMDs and perovskite oxides heterostructures are developed to improve the energy conversion systems for producing fuels [47]. A recent study also addresses the first principles calculations to determine the bandgap energies of porous h-BN. The bandgap engineering is performed using carbon doping which is able to absorb the visible light. This resulted in the matching of conduction and valence band with the potentials of both hydrogen and oxygen evolution reactions [48]. From a similar concept, semi-hydrogenated BN emerge as a novel 2D metal-free photocatalyst for effective water splitting under visible light [49]. Again, the 2D layered perovskites such as $(CH_3NH_3)_3Bi_2I_9$, $Cs_2PbI_2Cl_2$, $Cs_3Bi_2I_9$ can serve as photosensitizers or can be used to facilitate charge transport between different semiconductor materials for achieving remarkable solar power conversion efficiency of 27% [17, 18, 32, 50]. In parallel, the advantages of 2D nanomaterials in photo-electrochemical applications are diverse [51]. 2D layered nanomaterials can:

(1) Transfer electrons into the semiconducting material to serve as a photosensitizer that helps in extending the optical absorption range.
(2) Effectively separate the photoexcited electrons and holes in the photoactive semiconducting materials.
(3) Conduct excess heat away during the catalytic reaction.
(4) Serve as a template and heat sink for stabilizing small catalysts due to which larger specific surface area can convert more reactant molecules.
(5) Improve the overall lifetime by reducing the amount of active catalyst by decreasing its weight.

Therefore, this kind of 2D layered nanomaterials such as TMDs, layered perovskites, h-BN, $C_3N_4$, MXenes, metal oxides nanosheets, and black phosphorous which are derived from their basic 3D bulk crystalline blocks may have great potential for efficient energy conversion applications.

# 4 Energy Conversion Systems Using Two-Dimensional Materials

## *4.1 Solar Cells*

One of the important sources of sustainable energy conversion is the solar cell devices which works on the principle of photovoltaic effect thereby directly converting the incident optical signals (sunlight) into electricity (Fig. 2a). As already known that the crystalline silicon-based solar cells have been ruling the ever-expanding global photovoltaic market with about 95% market share. Reaching the theoretical Shockley-Queisser (S-Q) limit of 33%, silicon solar cells achieved its highest power conversion efficiency (PCE) of 26.6% [52].

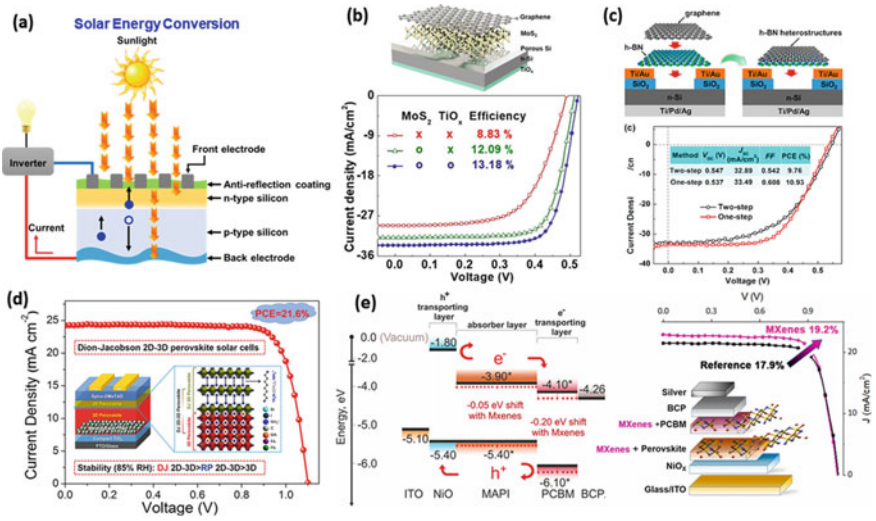


**Fig. 2** **a** Schematic representation showing the working of a solar photovoltaic device. **b** $MoS_2$/graphene/porous Si-based photovoltaic device. Reproduced with permission [65], Copyright 2020, Elsevier. **c** h-BN interface on graphene/Si schottky junction for improving solar cell efficiency. Reproduced with permission [29], Copyright 2016, Elsevier. **d** 2D-3D perovskite for improved solar cell stability and efficiency of 21.6%. Reproduced with permission [25], Copyright 2020, Elsevier. **e** MXene/$NiO_x$ for inverted-type solar energy conversion. Reproduced with permission [68], Copyright 2021, Elsevier

In the past decade, solar cell with organic–inorganic lead halide perovskites ($CH_3NH_3PbI_3$) have outperformed all other thin film photovoltaics in terms of PCE, with the highest laboratory record standing at around 25% which is placed in the NREL chart [52–54]. With the utilization of lead halide perovskites, the record efficiency solar cells have been increasing with an unprecedented speed. For efficient photovoltaic conversion, the photoactive materials must show high absorption coefficients ($\approx 10^5$ $cm^{-1}$), high charge carrier mobility, low trap density, tunable bandgap (typically from 1.17 to 2.24 eV) [55]. The merits will be manifold if the photoactive materials are cost effective and have easy processing/fabrication. A perovskite-based device holds the most potential as a top cell for a two-terminal tandem solar cell with silicon as its bottom cell. Sahli et al. have demonstrated an approach of co-evaporating and spin coating to prepare the perovskite on crystalline-Si pyramids, which yielded an efficiency of 25.2% [56]. Likewise, an oxford photovoltaic device has been highlighted by Snaith's group that has reported a record PCE for two-terminal tandem cell up to 28% [57].

Even though the perovskite/Si tandem cells have achieved great success, there remains a major challenge in the production of the less-toxic, high-quality, and stable perovskite absorbers. Two-dimensional layered perovskite structures have emerged as a possible solution to address this issue [18]. Unlike the conventional bulk lead halide perovskites, the 2D layered perovskites are constructed with additional larger organic cations which are introduced as spacers. This isolates the inorganic metal halide octahedral layers to form quantum well super lattices. Emerging novel derivatives of 2D layered perovskites pave new prospects for versatile energy conversion applications. M. G. Kanatzidis's group reported the perovskite compound based on $Cs_2PbI_2Cl_2$, which displays extremely high ambient and thermal stability [58]. Also, their high density and high atomic number elements also render it as a decent candidate for ultraviolet radiation detector applications.

Progress on the nanostructured metal oxides are found to have appreciable performances in solar cells. Gold (Au) nano-mesh sandwiched between two molybdenum trioxide ($MoO_3$) layers ($MoO_3$/Au/$MoO_3$) is fabricated using mild thermal evaporation, which emerge as an excellent electrode material to be utilized in semi-transparent solar cells. Here, the ultrathin Au nano-mesh affords the high conductivity and better transparency along with the $MoO_3$ layer acting as an antireflection layer thereby significantly minimizing the optical loss. Based on this, the PCE of semi-transparent solar cells is increased to 18.3%. From the similar grounds, the semi-transparent perovskite layers are utilized in a stacked configuration to form a heterojunction with silicon solar cell which yielded PCE of 27.0% [50]. Till date, this is one of the highest reported value for tandem solar cells.

With the discovery of the exfoliated flakes derived from various bulk organic and inorganic materials, hold the fundamental basis to understand their unique and tunable optical and electronic properties [59]. Concerning to the ever-growing interest in the TMDs, the first principle density functional theory calculations exclusively accords that the band structure of TMDs change dramatically upon exfoliation to lower dimension owning to strong quantum confinement effects [60]. Particularly, the bulk TMDs is converted from an indirect bandgap semiconductor to direct bandgap

semiconductor when thinned to a monolayer. Due to strong light-matter interactions within the monolayers, resulted in superior light harvesting characteristics compared with their bulk counterparts suitable for energy conversion. For instance, a single monolayer of $MoS_2$ with 0.6 nm thickness is projected to generate a maximum photocurrent of 4.7 mA $cm^{-2}$ with a PCE of 1.3% under simulated irradiance [61]. The additional benefits of ultrathin 2D TMDs rely on the inertness of chalcogenide surface, which does not hamper the defect related recombination processes at the atomic layer heterojunctions. Moreover, the 2D TMD layers do not suffer from anisotropic electronic properties. A novel method has been freshly executed by using ultrathin $Bi_2Te_3$ as a supporting material in electron transport layer and based on which the solar cell conversion efficiency reached up to 19.46% and stable over 1100 h under 1 Sun irradiance [62].

It is worth mentioning that the first demonstration of single or monolayers is based on lateral p-n junctions [63]. In the intervening time, various p-n junctions have been addressed using two TMDs layers. To present some examples, a photoactive $WSe_2/MoS_2$ p-n heterojunction has been established which are mechanically exfoliated from bulk. The photovoltaic performances as characterized by the J-V curves upon illumination under white light offer a clear photovoltaic effect with a PCE reaching 10% [64]. Similarly, employing a layer-controlled $MoS_2$ in a heterojunction of graphene/Si demonstrated the photovoltaic performance of 13.18% with a long-term stability for 30 days [65]. Very recently, 2D hexagonal boron nitride is used for surface passivation to enhance the photovoltaic performance of $MoS_2/WSe_2$ solar cells with 74% improvement in conversion efficiency [66]. Moreover, an interface engineering approach is performed on graphene/Si schottky junction solar cells with the introduction of h-BN thereby achieving a maximum efficiency of 10.93% [29]. Another study is conducted with graphitic carbon nitride which acts as a booster in improving the solar cell efficiency to 70% employing a binary composite of g-$C_3N_4$/ZnO NR [67]. Subsequently MXene based on $Ti_3C_2T_x$ is prepared to engineer the p-i-n perovskite solar cell with an improved power conversion efficiency of 19.2% [68]. In addition, the elemental 2D nanomaterials like black phosphorous (BP) has also proven its potential as a hole selective layer in improving the perovskite solar cell efficiency by 16.4% [69].

## *4.2 Electrochemical Water Splitting*

Water electrolysis is a viable technology to decompose water into chemical fuels, especially hydrogen, either using electricity (potential) or solar light which can be efficiently used in a fuel cell for power generation [28]. Based on this technology, hydrogen is now considered as a green energy carrier. However, to generate hydrogen, some key factors must be addressed: properly choosing the materials for catalytic activity, designing the catalysts, and engineering the water-splitting devices [47].

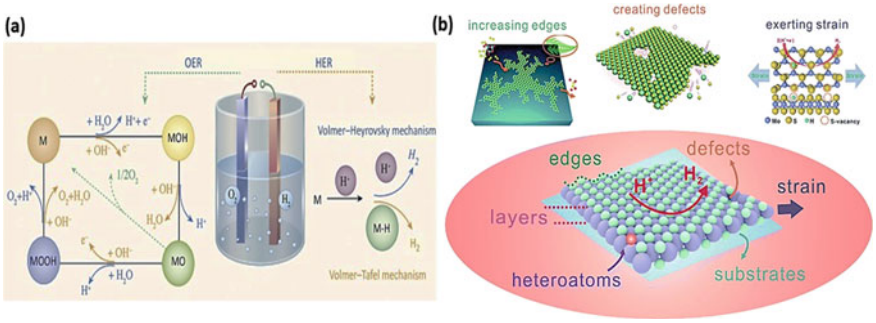


**Fig. 3** **a** Schematic representation showing the electrochemical reactions for evolution of hydrogen and oxygen gas. Reproduced with permission [70], Copyright 2019, Elsevier. **b** Engineering of 2D nanomaterials with respect to defects, strain, increasing edges and doping. Reproduced with permission [28], Copyright 2017, Royal Society of Chemistry

Extensive investigations on TMDs have been highlighted for electrocatalytic production of hydrogen. Progressive efforts have been made by the scientific community where the hydrogen generation efficiency is promoted using 2D TMDs. This approach resulted in the minimal use of precious Pt-based catalysts which effectively reduces the cost. Significant amount of both computational and experimental studies is conducted to understand the underlying reaction mechanisms and the reaction steps involved in such energy conversion systems. Two major reactions that are associated with water electrolysis are the oxygen evolution reaction (OER) and the hydrogen evolution reaction (HER). For electrolytic cells, the OER and HER occur at the cathode and anode surfaces, thus creating $H_2$ and $O_2$ gas, respectively. Among these, HER ($2H^+ + 2e^- \rightarrow H_2$) is a complex multiple-step electrochemical process, which takes place on the electrode surface containing catalysts to generate pure hydrogen which can be supplied to fuel cells. Mainly, three reaction steps have been anticipated for HER in an acidic solution (Fig. 3a) [70, 71]:

Discharge reaction (Volmer):

$$H_3O^+ + e^- \rightarrow H_{ads} + H_2O \tag{1}$$

Electrochemical desorption reaction (Heyrovsky):

$$H_{ads} + e^- + H^+ \rightarrow H_2 \tag{2}$$

Combination reaction (Tafel):

$$H_{ads} + H_{ads} \rightarrow H_2 \tag{3}$$

As mentioned in the three reactions, chemical adsorption and desorption of hydrogen atoms on the electrode surface are the competitive processes. Here the prime requirement is to have a good HER catalyst that must form an adequately

strong bond with the adsorbed hydrogen. This will promote the proton-coupled electron-transfer process. In addition, to ensure the facile release of hydrogen gas, the bonds should also be weak enough. Thus, these electrochemical reactions serve an important role in energy conversion and energy storage systems [71].

The typical electrochemical water splitting is performed in an electrolyser system consisting of three components: a cathode, an electrolyte which act as ionic conductor, and an anode. The water decomposition by means of electrochemical reactions in an electrolyser is composed of two half-cell reactions: HER on the cathode and OER on the anode. However, in this system, it is required to have an input energy to accelerate the two half-cell reaction with the application of an external voltage. This extra energy comes in the form of a potential difference between the electrodes and can be calculated using the Gibbs free energy ($\Delta G^0 = 237.2$ kJ $mol^{-1}$) is often referred as the overpotential ($\eta$). In order to split water a high activation energy is required and simultaneously the issues related to the low conductivity of water are minimized by the utilization of effective electrocatalyst along with the addition of salts, acids, or bases to improve the water conductivity. Moreover, electrochemical measurements are carried out in a three-electrode system, where a suitable reference electrode (RE) is applied according to the nature of the electrolyte solution to check the proper value of overpotential. The overpotential is reported with reference to the reversible hydrogen electrode (RHE), normal hydrogen electrode (NHE), and standard hydrogen electrode (SHE). These three terms are used interchangeably in the literature, but they are particularly different. For instance, the NHE is constructed by immersing a platinum electrode into a solution of one normal concentration for protons and bubbling pure hydrogen gas through the solution at 1 atmospheric pressure. The limitation with NHE is that it is not reversible, and its potential changes with time due to which its use is restricted. Similarly, the SHE also composed of Pt dipped in acidic solution and hydrogen gas at 100 kPa. The absolute potential of SHE is $4.44 \pm 0.02$ V at 25 °C but its potential is considered as zero in order to serve as the reference. Unlike NHE, SHE is reversible, however the ideal 1 M protons never exists because of which SHE is an ideal model and cannot be made. When expressing the potentials of redox half reactions, without otherwise stated, the potentials are by default referenced to SHE (vs. SHE). On the other hand, the RHE conversion from the practically applied RE in most published literature and is widely accepted based on the simplified theoretical Nernst equation or the extension of SHE. The only difference between the definition of RHE and that of SHE is that RHE does not require the proton effective concentration to be unity. This characteristic brings out the pH dependence of RHE potential [70, 71].

The HER mechanism usually proceeds via the Volmer-Tafel-Heyrovsky steps, where the different pH value leads to different reactants and products in each step. As already mentioned, in HER, the electrochemical reduction of proton is mediated by an appropriate catalyst for which the most commonly used catalyst is based on platinum (Pt). However, Pt is very expensive which leads to the search for alternative catalyst materials with highest possible activity. TMDs are considered as a strong candidate for electrocatalyst material and various efforts have been made to engineer the TMDs such as creating edges, defects, and strain as illustrated in Fig. 3b. Liu et al.

have systematically optimized various TMDs (with $MX_2$ structure) catalysts such as $MoS_2$, $NbS_2$, and $TaS_2$ for efficient hydrogen evolution [72]. They proposed that highly basal plane active $MX_2$ sites are favorable for HER activity. Likewise, Swesi et al. have reported another catalyst with textured $NiSe_2$ film for water splitting with an energy efficiency of 83% at high current density [73]. Very recently, Kwon et al. have addressed the synthesis of Se-rich $MoSe_2$ nanosheets for improved electrocatalytic performance [74]. They have reported the best HER activity with low overpotential of 0.13 V and a Tafel slope of 46 mV $dec^{-1}$ at 10 mA $cm^{-2}$. Furthermore, the heterostructures of $MoSe_2$ and perovskite oxide with $La_{0.5}Sr_{0.5}CoO_{3-\delta}$ highlight as a superior bifunctional electrocatalyst for stable water electrolysis over 1000 h [75]. Efficient catalysts for anodic OER have been realized where prime importance is given to perovskite oxides with $ABO_3$ structure. Liu et al. have prepared hierarchical mesoporous $La_{1-x}Sr_xCoO_{3-\delta}$ and presented its improved OER activity in a lithium oxygen battery [76]. Again, with the same perovskite oxide structure, Mefford et al. have reported a strategy where the OER can be enhanced by exploiting the oxygen vacancy defect [77].

In addition to TMDs, elemental 2D materials, layered metal oxides, oxyhalides, and layered double hydroxides are being actively investigated for their potential application to photo-electrochemical water splitting. It is known that numerous metal oxides such as $TiO_2$, $Fe_2O_3$, ZnO, $SnO_2$, and $WO_3$ have been extensively used as photocatalyst for solar water splitting [78]. Yao et al. have shown the feasibility of constructing a porous hybrid structure containing $Fe_2O_3$ nanothorn/$TiO_2$ nanosheet photoanodes that exhibited high PEC activity under visible light [79]. He et al. synthesized the heterostructure of carbon nitride and h-BN nanosheets (CN/BN) using an annealing mixture of h-BN and urea. The CN/BN heterostructure exhibited enhanced photocatalytic productions of $H_2$ and $H_2O_2$ of 2.4 and 59.8 μmol $h^{-1}$, respectively [80]. Additionally, few layers of phosphorene (or BP) also emerge as a promising candidate for HER activity. Lu et al. have investigated the edges, defects, strain, and metal doping on BP, and a linear relationship is highlighted between the lowest occupied state and hydrogen adsorption energy [81].

### *4.3 Piezo- and Thermoelectric Devices*

It has been discovered that many of the 2D nanomaterials such as TMDs and transition metal oxides, and h-BN show piezoelectric properties unlike their bulk counterparts [82]. As one of the energy conversion system, the piezoelectric devices basically convert mechanical energy (in the form of pressure, sound wave, or force) into electricity (Fig. 4a). Piezoelectricity may also be used to generate charge carriers or construct relays in an electronic circuit. Moreover, various research work exploits piezoelectric nanomaterials as piezo-phototronic facilitators for light emission including some prototype devices such as transistors, photodiodes, and sensors [83].

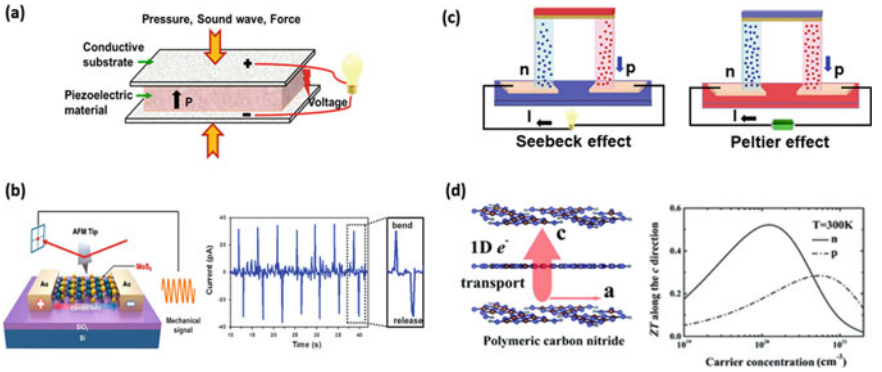


**Fig. 4** **a** Schematic representation of a piezoelectric device. **b** Piezoelectric behavior of $MoS_2$ using lateral piezo-response force microscopy and output the nanogenerator response. Reproduced with permission [87], Copyright 2016, Elsevier. **c** Thermoelectric effects: Seebeck and Peltier effects. **d** Thermoelectric performance of layered carbon nitride with high ZT. Reproduced with permission [97], Copyright 2018, Royal Society of Chemistry

Piezoelectricity is a property of electric polarization triggered by macroscopic strains, that couples the mechanical and electrical behaviors to promote competent mechanical-to-electrical energy conversion. Currently, the most prominent piezoelectric crystals should have non-centrosymmetric structure which are identified in hexagonal boron nitride (h-BN) and the broad family of TMDs. Li et al. demonstrated the non-centrosymmetric structure of h-BN using optical second-harmonic generation, thus validating the existence of h-BN piezoelectricity [84]. Likewise, the experimental evidence for the generation of piezoelectric fields in monolayer h-BN is reported with a piezoelectric coefficient of $2.91 \times 10^{-10}$ $cm^{-1}$ which is comparable to bulk ZnO [85]. Blonsky et al. adopted the first principle calculation to uncover the presence of in-plane piezoelectricity in TMDs such as $MoSe_2$, $MoS_2$, $WS_2$, $NbSe_2$ [86]. The 2D piezoelectric materials play an important role in energy harvesting devices which have the capability in future wireless nano-systems without any external power source including environmental monitors, implantable medical sensors, and personal electronics. A flexible piezoelectric nanogenerator based on CVD grown $MoS_2$ was highlighted by Kim et al. for scavenging the mechanical energy for low power consuming devices and realizing self-powered electronics (Fig. 4b) [87]. Motivated by the work, Lee et al. established a monolayer $WSe_2$ piezoelectric nanogenerator, which gives a peak voltage of 45 mV under a strain of 0.39% [88]. Piezo-phototronic devices are also developed where the principle is based on the piezo-polarized charges to tune the charge carrier generation, separation, diffusion, and recombination processes. The strategy of this novel device has been also proved in the monolayer $MoS_2$ photodetectors [89].

The existing status of thermoelectric has been marked from its debut by Mahan in 1998 [90]. Ever since, by means of thermoelectricity the energy conversion technologies have been progressively growing. Thermoelectric is considered as a direct energy

conversion technology by the transport of electrons in solids [91]. Based on this thermoelectric phenomenon in solids, various advancements in realizing devices with high thermal endurance are explored which finds applications in harsh environments including space applications.

The predominant thermoelectric effects are the Seebeck effect and Peltier effect (Fig. 4c) [92]. In solids (specially, semiconductors), the elementary charge carriers (electrons) are known to reside under thermal equilibrium. Along with this, the electrons also carry heat and entropy from the fundamentals of thermodynamics. These electrons can therefore flow from hot side to a cooler side wherever there is a temperature gradient. Because of this, arises the correlation between thermal and electronic phenomena, which is now called as the thermoelectric effects. The Seebeck effect is based on the existence of a voltage proportional to a temperature gradient ($V = S\Delta T$), where, $S$ is the Seebeck coefficient (also referred as thermoelectric power or thermos-power). Whereas, the Peltier effect is a phenomenon that where the heat absorption or emission is induced at the junctions which leads to the applied current ($Q = \Pi\ I$), where $\Pi$ is the Peltier coefficient. With the help of these two effects, it is possible to convert heat into electrical energy and vice versa. Such type of energy conversion technology leads to the discovery of various thermoelectric generators/coolers.

The commonly adopted approach to harvest the waste heat into electricity is based on Seebeck effect. In general, the thermoelectric devices are characterized by the figure-of-merit (denoted as $ZT$) given by [93]:

$$ZT = \frac{T\alpha^2}{\frac{K_l}{\mu ne} + LT} \tag{4}$$

where $\alpha$, $K_l$, $n$, $\mu$, $e$, and $T$ are the Seebeck coefficient, lattice thermal conductivity, carrier density, carrier mobility, elementary electronic charge, and absolute temperature. L is the Lorentz number given as $2.44 \times 10^{-8}$ W Ω $K^{-2}$. Equation (4) is mainly used to predict the discrepancies between the theoretical and experimental measurements. During 1990s, the best $ZT$ is achieved for $Bi_2Te_3$ alloy with value 1.0 at 300 K. After that, progressive research efforts based on novel 2D nanomaterials and their interfacial engineering to reduce lattice thermal conductivity and to improve the carrier mobility leads to the improvement in $ZT$ value to 3.0 [94, 95]. With these progresses, recently the heterostructures of 2D nanomaterials based on graphene and TMDs are addressed that show improved thermoelectric performances. Liang et al. have reported that the thermionic energy conversion using graphene/$MoSe_2$ or graphene/$WSe_2$ are two ideal configurations having the ability to harvest the waste heat at 400 K with 7–8% efficiency [40]. Kim et al. have developed a stretchable thermoelectric generator using a nanocomposite of TMDs and single-walled carbon nanotubes (SWCNT). The thermoelectric power factor with $WS_2$/SWCNT was reported to be 46 μW/$K^2$m [96]. Also, they have shown that the thermoelectric properties were preserved within the range of 290–330 K. It has been addressed that

**Table 1** Summary of different 2D nanomaterials in energy conversion systems

| Application | 2D nanomaterial and its role | Performance description |
|---|---|---|
| Solar cell | 2D perovskites as light harvesting and passivation layer | Light harvester: PCE = 12.51%, Stable for 2250 h [58]<br>Passivation layer: PCE = 21.6% [25] |
| | TMDs as hole transport layer ($MoS_2$, $WS_2$) and p-n heterojunction ($WSe_2/MoS_2$) | PCE = 17% [24]<br>PCE = 10% [64] |
| | MXene ($Ti_3C_2T_x$) as electron transport layer | PCE = 19.2% [68] |
| | h-BN fusion in Si/graphene Schottky junction | PCE = 10.93% [29] |
| | BP as hole transport layer with perovskite | PCE = 16.4% [69] |
| Electrochemical water splitting | Textured $NiSe_2$ Film (bifunctional electrocatalyst) | OER:<br>$\eta = 0.14$ V, Tafel slope = 48.7 mV $dec^{-1}$<br>HER:<br>$\eta = 170$ mV, Tafel slope = 107 mV $dec^{-1}$<br>[73] |
| | Se rich $MoSe_2$ nanosheet (Transition from the 2H to the 1T′ phase) | HER:<br>$\eta = 130$ mV, Tafel slope = 46 mV $dec^{-1}$<br>[74] |
| | $MoSe_2/La_{0.5}Sr_{0.5}CoO_3$ (TMD, Perovskite heterostructure) | OER:<br>$\eta = 0.29$ V, Tafel slope = 77 mV $dec^{-1}$<br>HER:<br>$\eta = 0.20$ V, Tafel slope = 34 mV $dec^{-1}$<br>(1000 h stability at 100 mA $cm^{-2}$)<br>[75] |
| | L- BP(Co)<br>L-BP<br>S-BP | HER:<br>$\eta = 194$ mV, Tafel slope = 47 mV $dec^{-1}$<br>$\eta = 355$ mV, Tafel slope = 91 mV $dec^{-1}$<br>$\eta = 299$ mV, Tafel slope = 85 mV $dec^{-1}$<br>[81] |
| Piezo-electronic device | h-BN | Piezoelectric coefficient:<br>291 pC $m^{-1}$ [85] |
| | 2H-$MoSe_2$ | 383 pC $m^{-1}$ [86] |
| | 2H $WS_2$ | 243 pC $m^{-1}$ [86] |
| | 2H $NbSe_2$ | 222 pC $m^{-1}$ [86] |

(continued)

**Table 1** (continued)

| Application | 2D nanomaterial and its role | Performance description |
|---|---|---|
| | 2H $TaS_2$ | 267 pC $m^{-1}$ [86] |
| | BP | 240 pC $m^{-1}$ [86] |
| | ZnO (Planar) | 266 pC $m^{-1}$ [86] |
| Thermoelectric device | $MoS_2$ | Thermal conductance: 221 mW $m^{-2}$ $K^{-1}$ [41] |
| | $WS_2$/SWCNT | 46 μW $m^{-2}$ $K^{-1}$ [96] |
| | Graphene/h-BN | 10.35 W $m^{-2}$ $K^{-1}$ [98] |
| | CN | ZT: 0.52 at 300 K [97] |
| | MXene | ZT: 1.3 at 300–475 K [99] |

*PCE* power conversion efficiency (solar), $\eta$ overpotential, *ZT* thermal figure of merit

the heterostructures of 2D nanomaterials provide an ideal platform to study the interfacial heat transport. The interface thermal conductance of $MoS_2$ on Au substrate is as high as 221 mW $m^{-2}$ $K^{-1}$ [41]. Moreover, polymeric carbon nitride (PCN) is investigated for thermoelectric performance using molecular dynamic simulations. It is found that PCN has high ZT of 0.52 at 300 K which contributes to n-type thermoelectric group materials (Fig. 4d) [97]. Heterojunction devices based on graphene/h-BN also offer high thermoelectric power factor of 10.35 $Wm^{-2}$ $K^{-1}$ [98]. Introduction of MXene ($Ti_3C_2T_x$) into $(Bi, Sb)_2Te_3$ matrix also provides improved thermoelectric performance with ZT of 1.3 within 300–475 K toward high thermoelectric conversion efficiency [99] (Table 1).

## 5 Conclusions and Outlook

This chapter offers an overview of the energy conversion technologies/systems specifically relating to 2D nanomaterials. The 2D nanomaterials have had a significant role in energy conversion technologies suitable for energy harvesting and energy storage devices. However, the commercialization of 2D nanomaterials is still in the progressing stage technology. Starting from the small-scale production of 2D nanomaterials by the small start-up companies, the industrialization will soon push an advancement towards a wide range of possibilities for on-field application of such 2D nanomaterials in energy conversion systems/devices. Our motive is to deliver an up-to-date view research progress with a balanced experimental perspective on 2D devices for energy conversion. It is anticipated that the contents summarized in this chapter can afford an important reference and guideline for further systematic studies on 2D nanomaterials.

We have focused on the specific material properties of 2D nanomaterials based on TMDs, layered perovskite structures and inorganic semiconductor oxides relevant for energy conversion systems or devices. Particularly, how the 2D nanomaterials can have a significant impact on the energy generation system is highlighted. Moreover, an elaborated discussion on the energy conversion devices is presented. First the progress of 2D nanomaterials in the field of solar cell devices is addressed. Second, the influence of 2D nanomaterials on improving the electrochemical activity for water splitting is discussed in detail. Finally, the direct influence of the piezo and thermal property management and dissipation related to the applications of 2D semiconductors have been discussed including the thermoelectric effects.

**Acknowledgements** This study is financially supported by the Department of Science and Technology (DST), Government of India under the Inspire Faculty Award (DST/INSPIRE/04/2018/001721).

## References

1. Gernaat DEHJ, Boer HS, Daioglou V et al (2021) Climate change impacts on renewable energy supply. Nat Clim Change 11:119–125
2. Shayegh S, Sanchez DL (2021) Impact of market design on cost-effectiveness of renewable portfolio standards. Renew Sustain Energy Rev 136:110397
3. Fonash SJ (1981) Solar cell device physics. Academic Press Inc., London
4. Gong J, Li C, Wasielewski MR (2019) Advances in solar energy conversion. Chem Soc Rev 48:1862–1864
5. Pagliaro M, Meneguzzo F (2019) Digital management of solar energy En route to energy self-sufficiency. Global Chall 3:1800105
6. He Y, Hamann T, Wang D (2019) Thin film photoelectrodes for solar water splitting. Chem Soc Rev 48:2182–2215
7. Lee DK, Choi K-S (2018) Enhancing long-term photostability of $BiVO_4$ photoanodes for solar water splitting by tuning electrolyte composition. Nat Energy 3:53–60
8. Lee DK, Lee DL, Lumley MA et al (2019) Progress on ternary oxide-based photoanodes for use in photoelectrochemical cells for solar water splitting. Chem Soc Rev 48:2126–2157
9. Patil DS, Arakerimath RR, Walke PV (2018) Thermoelectric materials and heat exchangers for power generation—a review. Renew Sustain Energy Rev 95:1–22
10. May AF, Sales BC (2021) Twisting the thermoelectric potential. Nat Mater 20:451–452
11. Xue Y, Zhang Q, Wang W et al (2017) Opening two-dimensional materials for energy conversion and storage: a concept. Adv Energy Mater 7:1602684
12. Tao H, Fan Q, Ma T et al (2020) Two-dimensional materials for energy conversion and storage. Prog Mater Sci 111:100637.
13. Chen M, Guan R, Yang S (2018) Hybrids of Fullerenes and 2D Nanomaterials. Adv Sci 6:1800941
14. Zhang H, Cheng HM, Ye P (2018) 2D nanomaterials: beyond graphene and transition metal dichalcogenides. Chem Soc Rev 47:6009–6012
15. Das S, Pandey D, Thomas J et al (2019) The role of graphene and other 2D materials in solar photovoltaics. Adv Mater 31:1802722
16. Hu Z, Wu Z, Han C et al (2018) Two-dimensional transition metal dichalcogenides: interface and defect engineering. Chem Soc Rev 47:3100–3128

17. Hussain AA, Rana AK, Ranjan M (2019) Air-stable lead-free hybrid perovskite employing self-powered photodetection with an electron/hole-conductor-free device geometry. Nanoscale 11:1217–1227
18. Zheng K, Pullerits T (2019) Two dimensions are better for perovskites. J Phys Chem Lett 10:5881–5885
19. Browne MP, Sofer Z, Pumera M et al (2019) Layered and two dimensional metal oxides for electrochemical energy conversion. Energy Environ Sci 12:41–58
20. Calbo J, Golomb MJ, Walsh A (2019) Redox-active metal-organic frameworks for energy conversion and storage. J Mater Chem A 7:16571–16597
21. Fang J, Zhou Z, Xiao M et al (2019) Recent advances in low-dimensional semiconductor nanomaterials and their applications in high-performance photodetectors. InfoMat 2:1–27
22. Novoselov KS, Mishchenko A, Carvalho A et al (2016) 2D materials and van der waals heterostructures. Science 353:aac9439
23. Singh V, Joung D, Zhai L et al (2011) Graphene based materials: past, present and future. Prog Mater Sci 56:1178–1271
24. Khan K, Tareen AK, Aslam M et al (2020) Recent developments in emerging two-dimensional materials and their applications. J Mater Chem C 8:387–440
25. Jiang X, Zhang J, Ahmad S (2020) Dion-Jacobson 2D-3D perovskite solar cells with improved efficiency and stability. Nano Energy 75:104892
26. Dong Y, Mallineni SSK, Kathleen M et al (2018) Metallic MXenes: a new family of materials for flexible triboelectric nanogenerators. Nano Energy 44:103–110
27. Li H, Lee H-Y, Park G-S et al (2018) Conjugated polyene-functionalized graphitic carbon nitride with enhanced photocatalytic water-splitting efficiency. Carbon 129:637–645
28. Chen Y, Yang K, Jiang B et al (2017) Emerging two-dimensional nanomaterials for electrochemical hydrogen evolution. J Mater Chem A 5:8187–8208
29. Meng J-H, Liu X, Zhang X-W et al (2016) Interface engineering for highly efficient graphene-on-silicon schottky junction solar cells by introducing a hexagonal boron nitride interlayer. Nano Energy 28:44–50
30. Yu X, Sivula K (2017) Layered 2D semiconducting transition metal dichalcogenides for solar energy conversion. Curr Opin Electrochem 2:97–103
31. Wang Y, Zhao S, Wang Y et al (2018) Wafer-scale synthesis of monolayer $WSe_2$: a multi-functional photocatalyst for efficient overall pure water splitting. Nano Energy 51:54–60
32. Hussain AA (2020) Constructing caesium-based lead-free perovskite photodetector enabling self-powered operation with extended spectral response. ACS Appl Mater Interfaces 12:46317–46329
33. Xiangkai K, Qiangchun L, Changlin Z et al (2017) Elemental two-dimensional nanosheets beyond graphene. Chem Soc Rev 46:2127–2157
34. Zhang G, Huang S, Wang F et al (2020) The optical conductivity of few-layer black phosphorous by infrared spectroscopy. Nat Commun 11:1847
35. Sebastian A, Pendurthi R, Choudhury TH et al (2021) Benchmarking monolayer $MoS_2$ and $WS_2$ field-effect transistors. Nat Commun 12:693
36. Kappera R, Voiry D, Yalcin SE et al (2014) Phase-engineered low-resistance contacts for ultrathin $MoS_2$ transistors. Nat Mater 13:1128
37. Pumera M, Sofer Z (2017) 2D Monoelemental arsenene, antimonene, and bismuthene: beyond black phosphorus. Adv Mater 29:1605299
38. Fu Q, Han J, Wang X et al (2021) 2D transition metal dichalcogenides: design, modulation, and challenges in electrocatalysis. Adv Mater 33:1907818
39. Kang Z, Khan MA, Gong Y et al (2021) Recent progress of MXenes and MXene-based nanomaterials for the electrocatalytic hydrogen evolution reaction. J Mater Chem A 9:6089–6108
40. Liang S-J, Liu B, Hu W et al (2017) Thermionic energy conversion based on graphene van der Waals heterostructures. Sci Rep 7:46211
41. Zhao Y, Cai Y, Zhang L et al (2020) Thermal transport in 2D semiconductors-considerations for device applications. Adv Funct Mater 30:1903929

42. Yuan P, Li C, Xu S et al (2017) Interfacial thermal conductance between few to tens of layered-$MoS_2$ and c-Si: effect of $MoS_2$ thickness. Acta Mater 122:152–165
43. Bhimanapati GR, Lin Z, Meunier V et al (2015) Recent advances in two-dimensional materials beyond graphene. ACS Nano 9:11509–11539
44. Yu P, Fu W, Zeng Q et al (2017) Controllable synthesis of atomically thin type-II weyl semimetal $WTe_2$ nanosheets: an advanced electrode material for all-solid-state flexible supercapacitors. Adv Mater 29:1701909
45. Zhu CR, Gao D, Ding J et al (2018) TMD-based highly efficient electrocatalysts developed by combined computational and experimental approaches. Chem Soc Rev 47:4332–4356
46. Liu Y, Weiss NO, Duan X et al (2016) Van der Waals heterostructures and devices. Nat Rev 1:16042
47. Wang F, Shifa TA, Zhan X et al (2015) Recent advanced in transition-metal dichalcogenide based nanomaterials for water splitting. Nanoscale 7:19764–19788
48. Wan Q, Wei F, Ma Z et al (2019) Novel porous boron nitride nanosheet with carbon doping: potential metal-free photocatalyst for visible-light-driven overall water splitting. Adv Theory Simul 2:1800174
49. Li X, Zhao J, Yang J (2013) Semihydrogenated BN sheet: a promising visible-light driven photocatalyst for water splitting. Sci Rep 3:1858
50. Wang Z, Zhu X, Zuo S et al (2020) 27%-efficiency four-terminal perovskite /silicon tandem solar cells by sandwiched gold nanomesh. Adv Funct Mater 30:1908298
51. Hill JW, Hill CM (2019) Directly mapping photoelectrochemical behaviour within individual transition metal dichalcogenide nanosheets. Nano Lett 19:5710–5716
52. Yoshikawa K, Kawasaki H, Yoshida W et al (2017) Silicon heterojunction solar cell with interdigitated back contacts for a photoconversion efficiency over 26%. Nat Energy 2:17032
53. NREL Chart (2020) https://www.nrel.gov/pv/cell-efficiency.html
54. Li H, Zhang W (2020) Perovskite tandem solar cells: from fundamentals to commercial deployment. Chem Rev 120:9835–9950
55. Huang J, Yuan Y, Shao Y (2017) Understanding the physical properties of hybrid perovskites for photovoltaic applications. Nat Rev Mater 2:17042
56. Sahli F, Werner J, Kamino BA (2018) Fully textured monolithic perovskite/silicon tandem solar cells with 25.2% power conversion efficiency. Nat Mater 17:820–826
57. Oxford Photovoltaic Sets World Record for Perovskite Solar Cell (2018) https://www.oxfordpv.com/news/oxford-pv-sets-world-record-perovskite-solar-cell
58. Li J, Yu Q, He Y et al (2018) $Cs_2PbI_2Cl_2$, All-inorganic two-dimensional Ruddlesden-Popper mixed halide perovskite with optoelectronic response. J Am Chem Soc 140:1085–11090
59. Niu W, Eiden A, Prakash GV et al (2014) Exfoliation of self-assembled 2D organic-inorganic perovskite semiconductors. Appl Phys Lett 104:171111
60. An S-J, Kim YH, Lee C et al (2018) Exfoliation of transition metal dichalcogenides by a high-power femtosecond laser. Sci Rep 8:12957
61. Shanmugam M, Bansal T, Durcan CA et al (2012) Molybdenum disulphide/titanium dioxide nanocomposite-poly 3-hexylthiophene bulk heterojunction solar cell. Appl Phys Lett 100:153901
62. Tsikritzis D et al (2020) A two-fold engineering approach based on $Bi_2Te_3$ flakes towards efficient and stable inverted perovskite solar cells. Mater Adv 1:450–462
63. Lim JY, Kim M, Jeong Y et al (2018) Van der Waals junction field effect transistors with both n- and p-channel transition metal dichalcogenides. NPJ 2D Mater Appl 2:37
64. Cho A-J, Song M-K, Kang D-W et al (2018) Two-dimensional $WSe_2/MoS_2$ p-n heterojunction-based transparent photovoltaic cell and its performance enhancement by fluoropolymer passivation. ACS Appl Mater Interfaces 10:35972–35977
65. Jang CW, Shin DH, Ko JS et al (2020) Performance enhancement of graphene/porous Si solar cells by employing layer-controlled $MoS_2$. Appl Surf Sci 532:147460
66. Cho A-J, Kwon J-Y (2019) Hexagonal boron nitride for surface passivation of two-dimensional van der Waals heterojunction solar cells. ACS Appl Mater Interfaces 11:39765–39771

67. Chetia TR, Ansari MS, Qureshi M (2016) Graphitic carbon nitride as a photovoltaic booster in quantum dot sensitized solar cells: a synergistic approach for enhanced charge separation and injection. J Mater Chem A 4:5528–5541
68. Saranin D, Pescetelli S, Pazniak A et al (2021) Transition metal carbides (MXenes) for efficient NiO-based inverted perovskite solar cells. Nano Energy 82:105771
69. Batmunkh M, Bat-Erdene M, Shapter JG (2017) Black phosphorous: synthesis and application for solar cells. Adv Energy Mater 8:1701832
70. Yang W, Wang Z, Zhang W et al (2019) Electronic-structure tuning of water-splitting nanocatalysts. Trends Chem 1:259–271
71. Jiao Y, Zheng Y, Jaroniec M et al (2015) Design of electrocatalysts for oxygen-and hydrogen-involving energy conversion reactions. Chem Soc Rev 44:2060–2086
72. Liu Y, Wu J, Hackenberg KP et al (2017) Self-optimizing, highly surface-active layered metal dichalcogenide catalysts for hydrogen evolution. Nat Energy 2:17127
73. Swesi AT, Masud J, Wipula PR et al (2017) Textured $NiSe_2$ film: bifunctional electrocatalyst for full water splitting at remarkably low overpotential with high energy efficiency. Sci Rep 7:2401
74. Kwon IS, Kwak IH, Debela TT et al (2020) Se-rich $MoSe_2$ nanosheets and their superior electrocatalytic performance for hydrogen evolution reaction. ACS Nano 14:6295–6304
75. Oh NK, Kim C, Lee J et al (2019) In-situ local phase-transitioned $MoSe_2$ in $La_{0.5}Sr_{0.5}CoO_{3-\delta}$ heterostructure and stable overall water electrolysis over 1000 hours. Nat Commun 10:1723
76. Liu G, Chen H, Xia L et al (2015) Hierarchical mesoporous/microporous perovskite $La_{0.5}Sr_{0.5}CoO_{3-x}$ nanotubes:a bifunctional catalyst with enhanced activity and cycle stability for rechargeable lithium oxygen batteries. ACS Appl Mater Interfaces 7:22478–22486
77. Mefford JT, Rong X, Abakumov AM et al (2016) Water electrolysis on $La_{1-x}Sr_xCoO_{3-x}$ perovskite electrocatalysts. Nat Commun 7:11053
78. Faraji M, Yousefi M, Yousefzadeh S et al (2019) Two dimensional materials in semiconductor photoelectrocatalytic systems for water splitting. Energy Environ Sci 12:59–95
79. Yao H, Liu L, Fu W et al (2017) $Fe_2O_3$ nanothorns sensitized two-dimensional $TiO_2$ nanosheets for highly efficient solar energy conversion. Flat Chem 3:1–7
80. He Z, Kim C, Lin L et al (2017) Formation of heterostructures via direct growth CN on h-BN porous nanosheets for metal-free photocatalysis. Nano Energy 42:58–68
81. Lu J, Zhang X, Liu D et al (2019) Modulation of phosphorene for optimal hydrogen evolution reaction. ACS Appl Mater Interfaces 11:37787–37795
82. Duerloo K-AN, Ong MT, Reed EJ (2012) Intrinsic piezoelectricity in two-dimensional materials. J Phys Chem Lett 3:2871–2876
83. Wang ZL (2007) Nanopiezotronics. Adv Mater 19:889–892
84. Li Y, Rao Y, Mak KF et al (2013) Probing symmetry properties of few-layer $MoS_2$ and h-BN by optical second-harmonic generation. Nano Lett 13:3329–3333
85. Ares P, Cea T, Holwill M et al (2019) Piezoelectricity in monolayer hexagonal boron nitride. Adv Mater 9:1905504
86. Blonsky MN, Zhuang HL, Singh AK et al (2015) Ab Initio prediction of piezoelectricity in two-dimensional materials. ACS Nano 9:9885–9891
87. Kim SK, Bhatia R, Kim T-H et al (2016) Directional dependent piezoelectric effect in CVD grown monolayer $MoS_2$ for flexible piezoelectric nanogenerators. Nano Energy 22:483–489
88. Lee JH, Park JY, Cho EB et al (2017) Reliable piezoelectricity in bilayer $WSe_2$ for piezoelectric nanogenerators. Adv Mater 29:1606667
89. Wu W, Wang L, Yu R et al (2016) Piezophototronic effect in single-atomic-layer $MoS_2$ for strain-gated flexible optoelectronics. Adv Mater 28:8463
90. Bartkowiak M, Mahan GD (1998) Boundary effects in thin film thermoelectrics. MRS Online Proc Libr 545:265
91. Dubi Y, Ventra MD (2009) Thermoelectric effects in nanoscale junction. Nano Lett 9:97–101
92. Goldsmid HJ (2017) The Seebeck and Peltier effects. Morgan and Claypool Publishers
93. Hicks LD, Dresselhaus MS (1993) Effect of quantum-well structures on the thermoelectric figure of merit. Phys Rev B 47:12727–12731

94. Dresselhaus MS et al (2007) New directions for low-dimensional thermoelectric materials. Adv Mater 19:1043–1053
95. Zebarjadi M, Esfarjani K, Dresselhaus M et al (2012) Perspectives on thermoelectrics: from fundamentals to device applications. Energy Environ Sci 5:5147–5162
96. Kim JY, Oh JY, Lee TI (2019) Multi-dimensional nanocomposites for stretchable thermoelectric applications. Appl Phys Lett 114:043902.
97. Ding Z, An M, Mo S et al (2018) Unexpectedly high cross-plane thermoelectric performance of layered carbon nitrides. J Mater Chem A 7:2114–2121
98. Duan J, Wang X, Lai X et al (2016) High thermoelectric power factor in graphene/hBN devices. PNAS 113:14272–14276
99. Lu X, Zhang Q, Liao J et al (2019) High-efficiency thermoelectric power generation enabled by homogeneous incorporation of MXene in (Bi, $Sb_)2T_e3$ matrix. Adv Energy Mater 10:1902986

# Chapter 3
# Next-Generation 2D Nanomaterial Composites Electrodes for Electrochemical Energy Storage


**Harish Mudila, Parteek Prasher, Anil Kumar, M. G. H. Zaidi, Mousamee Sharma, and Amit Verma**

## 1 Introduction

The sustainable energy sources like solar energy, wind/tidal energy, etc., have an immense potential to meetup with the energy requirement of current and future generations. However, owing to their intermittent energy supply these non-conventional resources are required with energy storage/backup to meet the challenging and endless energy demand. The intermittent energy supply can cost loss of billions of dollars annually, thereby making the requirement of efficient electrical energy storage devices (EESD) very critical. Also, the stored energy should be able to use whenever and wherever needed [1, 2]. EESDs that find their immense application in

H. Mudila (✉) · A. Kumar
Department of Chemistry, Lovely Professional University, Phagwara 144411, Punjab, India
e-mail: harismudila@gmail.com

A. Kumar
e-mail: rsanil.nit@gmail.com

H. Mudila · M. G. H. Zaidi
Department of Chemistry, G. B. Pant University of Agriculture and Technology, Pantnagar 263145, Uttarakhand, India
e-mail: mgh_zaidi@yahoo.com

P. Prasher
Department of Chemistry, UPES, Dehradun 248007, Uttarakhand, India
e-mail: parteekchemistry@gmail.com

M. Sharma
Department of Chemistry, Uttaranchal University, Dehradun 248007, Uttarakhand, India
e-mail: mousmee.sharma90@gmail.com

A. Verma
Department of Biochemistry, Sardarkrushinagar Dantiwada Agricultural University, Palanpur 385506, Gujarat, India
e-mail: amibiochem19@gmail.com



Z. Khanam et al. (eds.), *2D Nanomaterials for Energy and Environmental Sustainability*,
Materials Horizons: From Nature to Nanomaterials,
https://doi.org/10.1007/978-981-16-8538-5_3

energy storage include various sorts of electrochemical capacitors, primary batteries (Alkaline Leclanché cell, Li-$MnO_2$ etc.), secondary batteries (Li-ion, Na-ion, etc.) etc., where an electrochemical conversion of redox chemical reaction to electrical energy takes place. A variety of electrode materials of different dimensions has been proposed for high-performing EESDs. These electrode materials are required to have properties such as high power density which can be achieved with rapid ion/electron transport. Maximum charge storage capacity is required for achieving this high energy density which can't be supplied by conventional electrode materials due to their limited sites available for ion intercalation and small surface to volume ratio, a major hindrance in high charge storage capacity [2]. These conventional materials also suffer from drop in capacity because of the generation of redox inactive levels and disintegration of materials caused by continuous electrode contraction and expansion due to reversible intercalation of ions [3]. In this quest for a material with higher energy and power densities and extended cyclability, 2D nanomaterials have become a promising contender for EESDs owing to their explicit mechanical, electrical, chemical, and optical properties. In this regard, graphene has find its unambiguous position, but other 2D nanomaterials for instance, transition metal compounds (TMOs, TMDs, TMNs, etc.), conducting polymers, boron nitride, black phosphorous, etc., have also been explored. Studies show that atomic-thin layer arrangements and extended surface area of most of the 2D nanomaterial generate a slit shaped ion diffusion channels thereby allowing them for ultra-fast charge carrier mobility and greater energy transfer efficiency. This ultra-fast charge carrier mobility of 2D nanomaterials depends on numerous factors such as polarity of charge carrier, number of layers, localized states, defects present, and various other physical factors. Most of the 2D nanomaterials are bestowed with high redox properties and excellent performance but carries certain limitations, such as (i) consumption of excess of electrolytes causing irreversible capacity during first cycle by forming a solid-electrolyte interface, (ii) electrolytic decomposition due to parasitic reactions resulted due to numerous active sites. These suicidal factors limit the performance of 2D nanomaterials which can be regulated by various modifications, for instance, collective layer formation of different 2D nanomaterials, etc. However, in-depth knowledge and detailed studies are required to understand the associated problems and to generate the possible solutions. Therefore, it is important to figure out the specific properties of 2D nanomaterials, factors affecting them and how these factors can be modified to alleviate the associated challenges.

This chapter brings a detailed insight on the superiority of 2D nanomaterials over other dimensional materials, their properties, and the factors affecting their performance. A highlight on the application of 2D nanomaterials for their use in EESDs by considering the various aspect of energy, power, and cyclability is also included. This chapter reviews the mechanism involved in the charging of EESDs along with the detailed advantages and disadvantages associated with the variety of 2D nanomaterials-based electrodes. A focus on the current and probable future challenges to introduce such hetero-structured 2D nanomaterials as the material of future EESDs is also addressed.

## 2 Mechanism of Charge-Storage in EESDs

Electrochemical capacitors, also designated as ultracapacitor or supercapacitors, are typically classified into electric double layer capacitors (EDLCs) and pseudocapacitors based on their potential to store electrochemical energy [3]. Each class of the supercapacitors is characterized by its specific charge storage mechanism (non-faradaic and faradaic mechanisms for EDLCs and pseudocapacitors, respectively) (Fig. 2).

### *2.1 EDLCs (Electric Double-Layer Capacitors)*

EDLCs is an electrochemical capacitor which generally involves carbonaceous material (activated carbon, carbon nanotubes (CNTs), graphene, etc.) as electrodes. In EDLCs, a reversible and infinite cyclable process is carried on, where electric double layers are formed next to the electrode and electrolyte junction, which store charge physiochemically by charge–discharge mechanism with porous electrode materials (Fig. 1a, b) [1, 2]. The EDLCs have extraordinary power density but low energy density (but higher as compared to early capacitors), hence, an augmentation in electric double layer capacitance is required in order to develop the applications related to energy storage. EDLCs don't undergo any specific chemical mechanism/change and the charges are distributed on the surface of electrode via physical processes only. The mechanism of generation of electrical energy in EDLCs is similar to the conventional capacitor. In EDLCs, the process of adsorption and desorption of the electrolyte ions (chemisorption) through the electric double layer on the porous electrode material generates the charge–discharge process, while dielectric way of storing charge is followed in conventional capacitors. The pore size of the electrode material significantly effects the movement of ions and hence the charge–discharge mechanism. Greater is the specific accessible surface area ($m^2/g$), higher is the capacitance of the electrode material employed. However, micropores (< 2 nm) of narrower size prevent the process of adsorption by sieving the electrolytic ions, while mesopores (2 nm $\leq$ pore size < 50 nm) alter this effect and enhance the capacitance [4, 5]. During applied voltage, ions diffuse into the oppositely charge electrodes (through ion permeable separator), the instant charge accumulation at the junction of each electrode and electrolyte generates two electric double layers. A large surface area at a small distance/thickness (0.1 nm) is generated in the interface between electrolyte and electrodes due to highly porous structure thereby generating high capacitance. The capacitance of a conventional capacitor can be determined by the distance between the electrodes, while in a supercapacitor it is determined by the electrical double layer generated in the interface between electrolyte and electrodes [6] (Fig. 2).

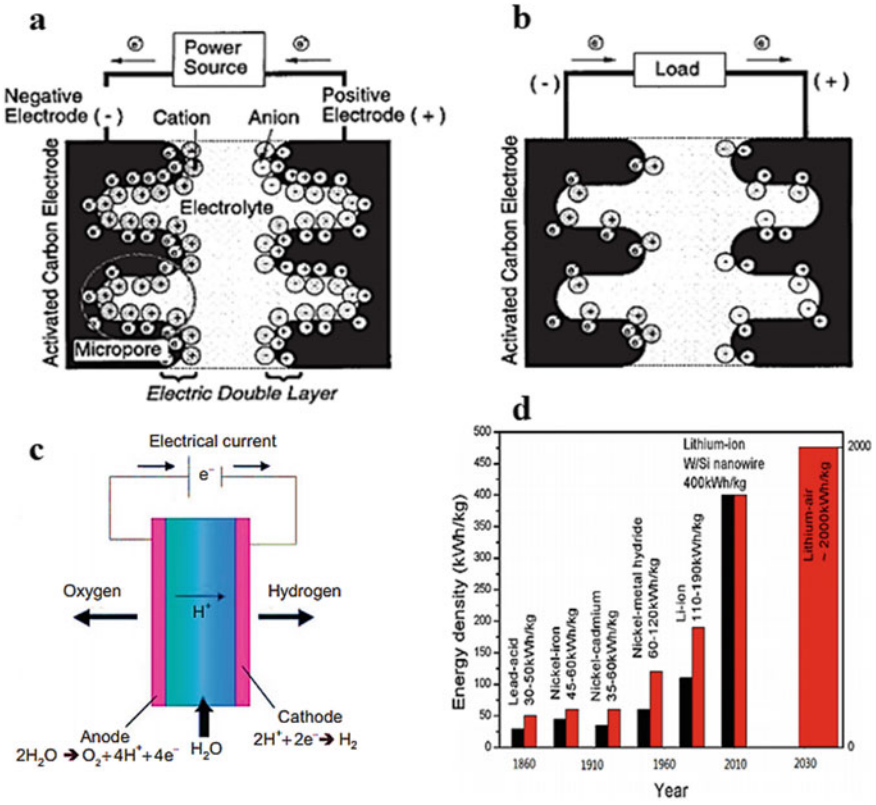


**Fig. 1** Electric double layer capacitor: **a** charge state, **b** discharge state, **c** schematic representation of fuel cell, **d** evolution of LIBs-based stationary energy storage (reproduce with permission [2, 6, 10])

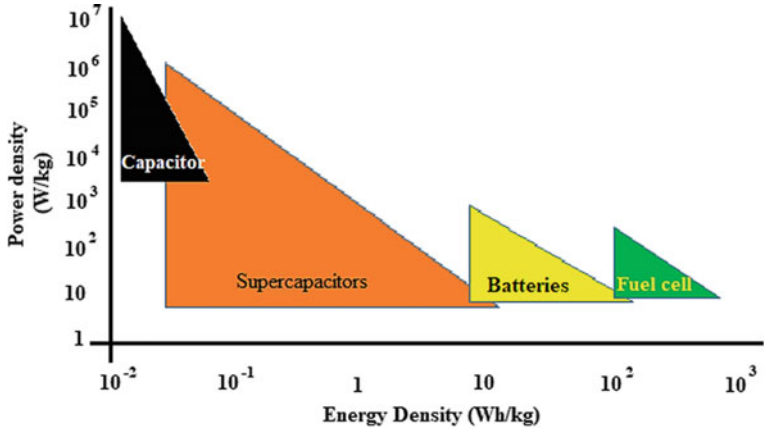


**Fig. 2** Comparison of energy and power densities of various EESDs

## 2.2 Pseudocapacitors

It is also termed as faradic supercapacitor which stores electrochemical energy not only on the concept of EDLCs but also on the redox mechanism. A pseudocapacitance is developed on the surface and bulk of the electrode material by the process of insertion (intercalation) or surface redox reaction (electrosorption) [7]. This reversible and rapid redox reaction passes the charge carriers through the double layer resulting in the passage of faradic current through the pseudocapacitor [8]. When compared to EDLCs, pseudocapacitors have comparatively low power density and cyclability owing to the slower faradic processes, but their energy density, specific/volumetric energies, and capacitance value are much higher [8, 9]. Also, the condition of having two oxidation states in a particular studied potential window can be considered as one of the most distinguishing property of pseudocapacitor materials. In general, pseudocapacitors involve three types of faradic (redox) processes; reversible adsorption, redox reaction (in transition metal oxide), and reversal electrochemical doping-de-doping (in CPs) [8, 10, 11]. Mostly, metal oxides (TMO), conducting polymers, etc., are used as electrode material for pseudocapacitors.

## 2.3 Fuel Cells

These are unique energy sources with potential applications which can run a simple computer or even large power station. As compared to the conventional energy system these fuel cells convert chemical energy to electrical energy with greater efficiency and zero hazardous emission. The phenomenon behind fuel cell is similar to batteries (conversion of chemical energy to electrical) but without need of recharging. In fuel cells (for instance, $H_2$–$O_2$) oxidation of fuel (of $H_2$, HOR) takes place at anode and reduction (of $O_2$, ORR) occurs at cathode, while in reverse process $H_2O$ undergoes $H_2$ and $O_2$ evolution, i.e., HER and OER at cathode and anode, respectively (Fig. 1c).

$$\text{At Anode (HOR)}: 2H_2 \rightarrow 4H^+4e^- \tag{1}$$

$$\text{At Cathode (ORR)}: O_2 + 4e^- + 4H^+ \rightarrow 2H_2O \tag{2}$$

In recent times, Polymer Electrolyte Membrane Fuel Cells (PEMFC) have emerged as an efficient and ecofriendly clean source of energy, which are coated with catalyst layers over the electrodes. Numerous 2D catalysts such as $RuO_2$, $IrO_2$, FeCoNi, and graphene have shown their ability to enhance the performance of fuel cells [12–14]. For an electro-catalyst to be used in HER or HOR, etc., processes high specific surface area, high catalytic activity, low energy barrier, appreciable electrical conduction and stability is essential. Pt is successfully replaced via N-doped CNT and graphene, for the ORR in fuel cells [15, 16]. GO and graphene membrane are established as a capable membrane material for microbial, alkaline, fuel cells

[17, 18]. Transition metal macrocyclic complexes also show their explicit position in PEMFC for ORR [19].

### *2.4 Batteries*

These are the electrochemical cells where energy is generated via redox reaction occurring at the junction of electrode and electrolyte. Batteries offer superior energy density compared to any type of capacitors, while the energy is stored chemically resulting in more storage of energy. However, the power density and life cycle of these batteries as compared to supercapacitor is very low. With time electrochemical cell develops irregularities across the surface of the electrode which decreases its storage capacity and also the heat produced by the system limits its performance. A variety of battery systems are introduced to meet the energy demand which includes lead acid batteries (specific energy of 60–75 Wh/L), alkaline batteries (specific energy of 160 Wh/L), Ni–Fe battery (specific energy of 30 Wh/L), metal-air batteries, Nickel-metal hydride battery, Li-based batteries (energy density of 150–200 Wh/kg), etc. (Fig. 1d) [6, 7, 10]. A variety of 2D nanomaterials are considered over the decade for understanding their application in battery technology. In this field, graphene and its analogue, MXenes, monoelemental form (P, Si, Ge, etc.), metal oxide, chalcogenides and hydroxide, etc., have gained significant results with a major focus on in Li-based batteries [20]. Although these battery systems are vastly modified from their initial stages, still some major hindrances (high polarization, huge capacity loss, poor reversibility and low electrochemical performance) have limited their applications in high energy density and high-performance systems [20, 21]. Therefore, an extensive and judicious research is required in this direction.

## 3 Various EESDs Electrodes Based on 2D Nanomaterials and Their Composites

2D nanomaterials are the material of current and future generation for applications related to various sectors, mainly in energy production and storage. A variety of 2D nanomaterials such as graphene, transition metal dichalcogenides (TMDs), transition metal oxides (TMOs), transition metal oxides (TMHs), transitional metal carbides (TMCs), various CPs and material such as boron nitride, black phosphorous, etc., [22] are being employed due to their specific characteristic, which strongly effect the performance of the active material to be used for EESD applications [23–25]. The section below details the characteristics of different 2D nanomaterials used in EESDs.

## 3.1 Graphene

Graphene has been the most investigated 2D nanomaterial since its discovery. Graphene is established as the strongest material present in the nature, where high Young's modulus, high surface to volume ratio, rapid reaction kinetics and low mass are the key factors for establishing this material effective for all its applications. Graphene monolayer ($sp^2$ hybridized, honeycomb) with extraordinary mechanical strength, flexibility, toughness, chemical stability, enhanced conductivity, etc., has paved its role in the arena of transparent and flexible electronic devices and sensors [26, 27]. Researchers have reported very high specific capacitance for graphene-based supercapacitors while the resistance of graphene is lower than silver [28]. Graphene-based supercapacitors are in great demand due to factors like great cyclability (minimum performance loss), high galvanic charge–discharge (GCD) rate, great power density, no issue of short circuit, etc. Although graphene is being employed from some last decades only, a lot of advancement is achieved with supercapacitor based on graphene as an active material. Hydrogen annealed nanoporous graphene, carbon nanodots converted to graphene, porous graphene-based carbons, etc., are found to have high energy and power density [29, 30]. Similarly, graphene-based hybrid material with judicious combinations of carbon dots, transition metals composites ($NiCo_2S_4$, $V_2O_5$, etc.), and other doping are observed to have similar results [31, 32]. Graphene along with CP is also one of the major research areas for generating potential supercapacitor materials. CPs like PAni, PPy, etc., are witnessed to enhance the electrochemical performance of graphene-based composites [33, 34]. Figure 3 represents the CV curves of the graphene/CP nanocomposite electrode-based supercapacitor. The superior properties of as-prepared electrode, viz., ideal and uniform pore size, along with excellent ion accessibility supports superior performance of device. Therefore, graphene alone or in hybrid form is being extensively employed in the field of energy such as EESD, photovoltaic cells, optoelectronics, and Li-ion batteries.

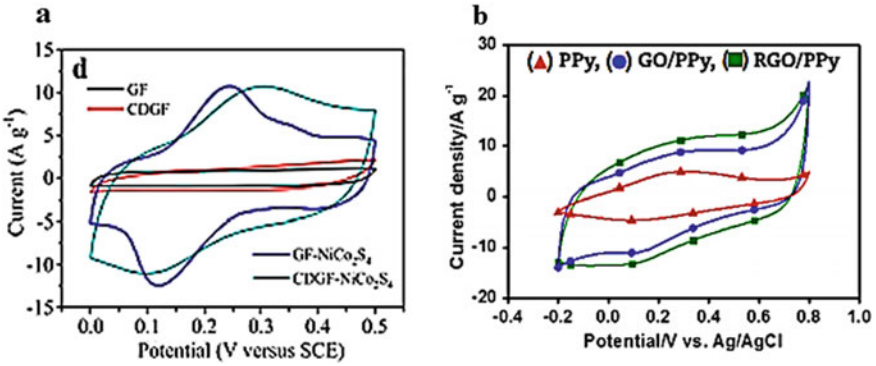


**Fig. 3** **a** CV curves of G (Graphene), CDG, G-$NiCo_2S_4$ and CDG-$NiCo_2S_4$ electrodes at a scan rate of 5 mV/s; **b** CV curve of PPY, GO/PPY and rGO/PPY (reproduce with permission [31, 33])

### 3.2 *Transitional Metal Dichalcogenides (TMDs)*

Though graphene is most prevalent material to be used in EESD, but lack of a considerable bandgap in graphene generates a quest for finding other 2D nanomaterials with semiconducting properties to be employed for energy storage. A variety of 2D transition metal compounds possess the potential to substitute graphene as a perfect candidate for EESDs (Fig. 4). In this regard, 2D TMDs (bandgap of 0 to ~ 2 eV) are emerging as a contender to effectively replace the graphene from various applications. The general formula for TMDs is $MX_2$, where M suggests the presence of a transition metal (most common are W, Mo, Re, Ta, etc.) while X is a chalcogen (gr. 16 family including, S, Se, and Te). A variety of TMDs (viz. $MoS_2$, $WS_2$ etc.) is being used for various applications including EESDs [35].

The structure of TMDs plays a significant role in generating their specific properties. TMDs exist in two common structural phases which are characterized by trigonal prismatic (1T, metallic phase), octahedral/hexagonal coordination (2H, semiconductive phase), or rhombohedral (3R, semiconductive phase) structure. These are resulted due to different coordination spheres of the transition metal atoms, while the ideal phase of the TMD monolayer depends on the number of d-electron present in the metal. TMDs of gr. VI (chalcogens of Mo, W, etc.) exhibit a direct bandgap range of 1–2 eV showing their semiconductive nature. The thin layered TMDs readily provide catalytic sites for redox reaction to generate their electrochemical activity which is independent on the analyte used. The interface between electrolyte and electrode (along with catalyst) marks the position of electrolytic reaction where the performance of catalyst is found to be critical [36]. Similarly, the catalytic edges also play crucial role in electrochemical activities of TMDs. Wang et al. explained that the active sites of $MoS_2$ are positioned at the edge planes which provide a significant enhancement in the electrochemical performances [37]. A high anisotropic behavior with an exceptional crystal structure is demonstrated by 2D TMDs. These

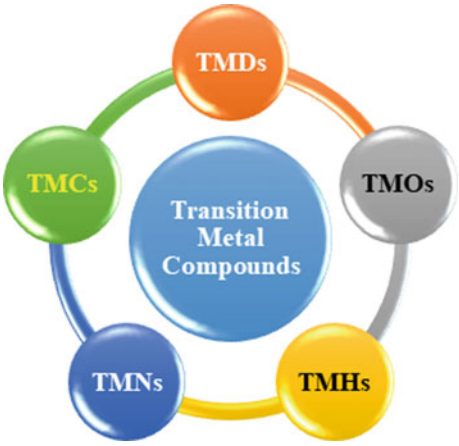


**Fig. 4** Types of transition metal compounds employed for EESDs

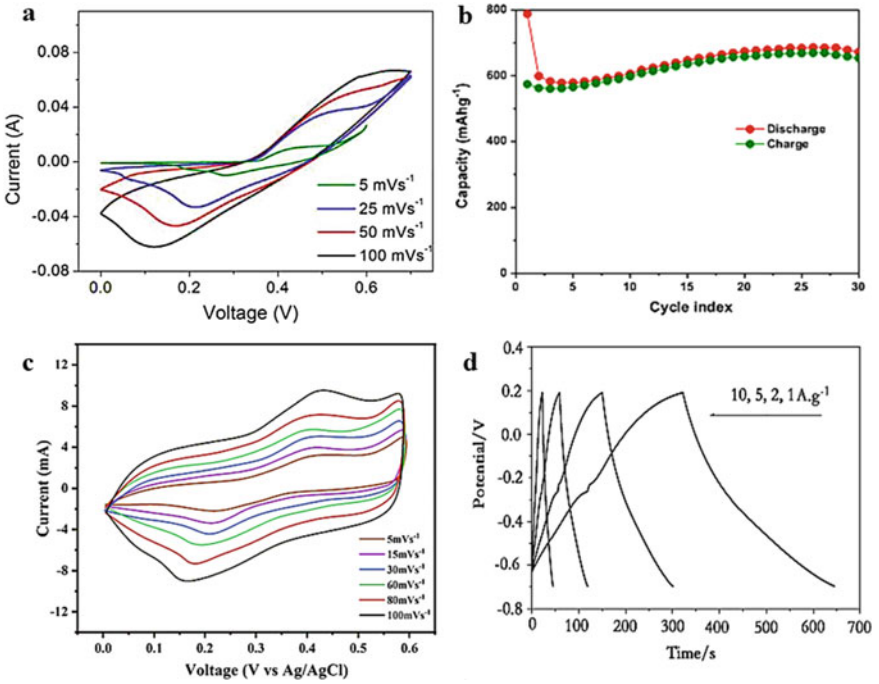


**Fig. 5** CV of $MoS_2$/Graphene nanocomposite (**a**); Charge–discharge cycling of $MoO_2$ electrode (**b**); CV profile of the $Ni(OH)_2$ (**c**); Charge–discharge curve of TiN electrode (**d**) (reproduce with permission [38, 59, 74, 82])

TMDs can be easily tuned up via variety of methodologies (alloying, intercalation, reduction in dimensions, heterostructured formation) as to be used in EESDs. A variety of combinations of TMDs with other 2D nanomaterials are studied for their electrochemical behavior so as to generate hybrid composites having superior electrochemical output, performance, and stability (Fig. 5a). Hybrid composite of $MoS_2$ (with graphene, $MnO_2$, ZnO, poly(ethyleneimine)-modified graphene oxide, PEI-GO/activated-carbon, etc.) [38–41], and $WS_2$ (with AC, $W_2C$, etc.) are the most studied TMDs as electrode material for EESDs [42, 43].

## *3.3 Layered Post-transition Metal Chalcogenides (PTMCs)*

PTMCs also entail layered 2D structure like TMDs, which generate explicit properties (higher photo-responsivities, great mobility, in-plane anisotropy, etc.) in the electrodes generated through them. The compounds have semiconductive characteristics with appreciable band gap (1–3 eV) which ranges from UV region to the near-infrared region [44, 45]. These PTMCs follow the general formula of MX,

where M is Ga and In, while X represents chalcogens (like S, Se, and Te). Unlike TMDs which have X–M–X type of motif, PTMCs theme layer composed of X–M–M–X type of arrangement, exception being GaTe. These PTMCs found their explicit application in the field of Li-ion and Na-ion batteries (LIB and SIB), electrocatalysis, transistors, photodetectors, optoelectronics, EESDs, sensors, etc. [44, 46]. Owing to the presence of weak Van der Waals interactions between the deposits/layers, a few layered 2D PTMCs can be isolated which helped the material to endure against a heavy strain and undergo a change in its structure [47]. PTMCs of Ga and In are the most studied composite materials. These materials are employed as anode in LIBs and SIBs to produce high energy density batteries [48–50].

### *3.4 Transition Metal Oxides (TMOs)*

TMOs owing to their extraordinary properties such as stability, great gravimetric capacities tunable redox potential are of great interest to be employed for EESDs [51]. A variety of TMOs are studied for EESDs including $MnO_2$ (polymorphs), $MoO_3$, $V_2O_5$, sodium metal oxides ($Na_xMO_2$), $TiO_2$, $NiMn_2O_4$, iron oxides, $RuO_2$, $ZrO_2$, cobalt oxide, copper oxide, etc. [52, 53]. Most of the metal oxides undergo basically three different alkali cation storage mechanisms, viz., insertion/intercalation, alloying, and conversion. However, process *Insertion* generates a little volume variation, where there is no deterioration of the original crystal organization. It allows reasonable cyclability and hence excellent capacity retention but this mechanism is restricted to generate high-power devices in spite of high power density [52, 53]. *Alloying*: a mechanism that presents a rapid method for Li and Na storage capacities, but extensive volume variation decreases the cyclability of these electrodes (of Si, Sn, Ge, Zn, etc.), also drying up of cell can take place due to decomposition of electrolyte owing to introduction of fresh layers of electrode to the used electrolyte. These issues can be partially overcome by using metal oxides, which however generates the problem of agglomeration of elemental particle thus enhance capacitive degradation on discharging. *Conversion*: TMO's negative electrode are generally used in LIBs and SIBs, the conversion of TMO to $TM^0$ or to Li/Na oxides permits electron conduction thus generating great cyclability, less volume variation [51, 54, 55]. $MnO_2$, $MoO_3$, $V_2O_5$, $RuO_2$, $Fe_2O_3$, etc., have been majorly studied for their electrochemical behavior (CV, CD, etc. Fig. 5b), most of these TMOs prove their supremacy with outstanding specific capacitance, high capacitive retention, and high energy densities [56–63]. TMOs with other 2D nanomaterials generate high end hybrid electrode material to be used as a component for EESDs. TMOs such as $MoO_3$ and $TiO_2$ with graphene have been majorly studied and are found to exhibit high energy and power density [64, 65]. Few other reported composites of $ZrO_2$ and $RuO_2$ with carbonaceous material are observed to have appreciable specific capacitance and retention [9, 66].

## 3.5 Transition Metal Hydroxides (TMHs)

Likewise, other 2D nanomaterial THMs are also employed for EESDs, with certain properties, viz. abundance, cost effective, greater surface area, fast electron and charge transfer, high and easy tunable composition, etc. [67]. Similar to TMOs, these TMHs are compatible with range of electrolytes and are chemically stable and environmentally benign. Also, they have higher theoretical capacitance as compared to graphene. Generally, TMHs are featured with wide energy bandgaps, thus endowing low electronic conductivities, which results in reduced redox reversibility consequently restricting their application in high-rate measurements. This is where tunablity of TMHs generates a solution for the mentioned drawback through complete utilization of all the accessible sites. Additionally, the multiple oxidation states and redox reactions make these TMHs a promising contender for EES [67–70]. Generally, TMHs can be studied as layered single metal hydroxides (LSHs) and layered double metal hydroxides (LDHs). Nanoparticles of β-$Ni(OH)_2$, $Fe(OH)_3$, $Co(OH)_2$, etc., are synthesized via a variety of procedure (hydrothermal, ultra-sonication method, etc.), which when subjected to electrochemical studies (Fig. 5c shows CV profile of $Ni(OH)_2$) generate high energy and power density with great cyclability [72–74].

## 3.6 Transition Metal Nitrides (TMNs)

Similar to other 2D materials, TMNs are also employed as a potential candidate to be used in EESDs which have a great charge–discharge character (Fig. 5d). In TMNs, the metal entails interstitial sites which are covered by nitrogen atoms to generate cubic, hexagonal closed packing (hcp) and simple hexagonal structures. These TMNs have metallic, covalent, and ionic characteristics which endow specific properties, viz., high volume to surface area, appreciable electrical conductivity, comprehensive catalytic properties, great volumetric energy density, etc., which has drawn significant research attention toward TMNs [75, 76]. But, a few drawbacks like restricted number of active sites (leading to low ionic kinetics), low durability and brittleness restrict their electrochemical performance. These shortcomings can be easily tuned via various synthetic approaches and modification in morphology, which eventually leads to even dispersity (prevent agglomeration), generates higher specific surface with numerous active sites, and facilitates high ionic kinetics, thus improves the electronic conductivity [77, 78].

## 3.7 Transition Metal Carbides (TMCs)

TMCs ($M_{n+1}X_n$, same for TMNs) are generally fabricated by incorporating atoms of carbon into the interstitial sites/locants (radius ratio 0.491–0.576) of transition metals

[76]. TMCs owing to their specific and unique properties is fascinating research community to employ them in variety of applications [79, 80]. The characteristics such as significant chemical and thermal stability (high melting point), high electrical conductivity (due to low electrical resistivity), corrosion resistance are the major reason behind their explicit use [76, 81]. Likewise, other combination of transition metal with non-metals, TMCs also exhibit covalent bond, ionic bond, and metallic bond, which impart characteristics such as toleration to stress (during lithiation and delithiation), chemical stability excellent electronic properties (Table 1).

### *3.8 Conducting Polymers (CPs) Composites*

CPs based on their nanostructure can be classified into 1D, 2D and 3D nanostructures. All of these nanostructures find their exceptional application in the field of EESDs. 2D CPs are of boundless length but are ultrathin materials possessing spatially confined structure generated via in-plane interactions [87]. The CPs demonstrate similar electrochemical and electrical properties as of metals and semiconductors; however, CPs comprise of decent specific capacitance but does associate with a few limitations like low cyclability and swelling in electrolytes [88]. Some of the unique features of 2D CPs such as tunable surface morphology, high porosity, more active sites, manageable thickness, synthesis ease and variety of processibility, and low cost give CPs a superiority over other 2D nanomaterials [89]. Techniques such as layer by layer, spin coating, sonication, electrochemical polymerization are the most common and fruitful method for generation of ultrathin, porous, large surfaced, 2D CPs [90]. PANI, PPY, and various other CPs that are being employed for EESDs applications. These CPs are subjected to various electrochemical studies like CV, GCD, etc., to establish them as potential 2D electrode materials. Generally, these CPs offered a low electrical conductivity which limits their excessive use in energy storage and conversion. However, many a times with specific polymerization technique, modified physical factors, use of specific electrolytes, and doping-dedoping conditions can help in improving the conductivity. Owing to the merits mentioned earlier numerous efforts have been carried to fabricate novel 2D CP nanocomposites with high specific capacitance, energy and power densities with fast charging characteristics [58]. Band gap theory established on quantum theory and molecular orbital theory provides the explanation why materials conduct charge, however band gap doesn't generate the clear picture in case of CPs, though the theory of conjugation, present the accurate condition of conduction of charge in these CPs by the delocalization of electronic states, and mobility of charge carriers. Yet a drawback is present with most of the CPs is that they are devoid of intrinsic charge carrier and thus need the condition of doping (p/n-type) which generates the polarons, bipolarons, and solitons in the CP chain that act as charge carriers [91]. The inbuilt limitations of these CPs can be astounded by judiciously modifying them with other heterogeneous material thus enhancing their conductivity, stability, cyclability, etc. To improve the electrochemical properties, hybrid electrode materials are being

**Table 1** Transition metal compounds, their types and EESDs related data

| Species | Specific capacitance | Power density | Energy density | Cyclic retention | References |
|---|---|---|---|---|---|
| *Transitional metal dichalcogenides (TMDs)* | | | | | |
| $MoS_2$ | 128 F/g | 50 W/Kg | 6.15 Wh/kg | 80% after 4 × $10^3$ cycles | [37] |
| $WS_2$ | 170 mAh/g | 1134.4 W/kg | 132.7 Wh/kg | 100% after 100 cycles | [42] |
| $WS_2$/AC | 47.2 F/g | 224.9 W/kg | 132.7 Wh/kg | | [42] |
| $MoS_2$/ZnO | 42 F/g | – | – | – | [40] |
| $MoS_2$/PEI/GO | 153.9 F/g | 4500 W/kg | 19.3 Wh/kg | 96% after 6.8 × $10^3$ cycles | [41] |
| $MoS_2$/PEI-GO/AC | 42.9 F/g | | | 93.1% after 8 × $10^3$ cycles | [41] |
| $W_2C/WS_2$ | 1040 mAh/g | | | 50% after 100 cycles | [43] |
| $MoSe_2$ | 1287 mAh/g | 50 W/kg | 6.15 Wh/kg | 100% after 100 cycles | [44] |
| *Transition metal oxides (TMOs)* | | | | | |
| $ZrO_2$/GO | 300 F/g | 59.40 W/kg | – | – | [9] |
| $MnO_2$ | 459.0 F/g | – | – | 94.8% after 3 × $10^3$ cycles | [56] |
| α-$MnO_2$ | 535 F/g | – | – | 80% after 3 × $10^3$ cycles | [57] |
| α-$MoO_3$ | 1249.2 F/g | – | – | 85% after 5 × $10^3$ cycles | [58] |
| $MoO_3$ | 600 mAh/g | – | | 86% after 30 cycles | [59] |
| $V_2O_5$ | 350 F/g | – | 48.6 Wh/kg | 75% | [60] |
| $RuO_2$ | 192 F/g | 1·5 kW/kg | 41·6 Wh/kg | 95% | [61] |
| α-$Fe_2O_3$ | 138 F/g | – | – | 89% after 500 cycles | [62] |
| α-$MoO_3$/graphene | 483 F/g | 2.67 kW/kg | 12.35 Wh/kg | 100% after 5 × $10^3$ cycles | [63] |
| $Li_4Ti_5O_{12}$ | 173 mAh/g | | – | – | [64] |
| Ru/$RuO_2$/AC | 1460 F/g | – | – | 94% after 1 × $10^4$ cycles | [66] |
| *Transition metal hydroxides (TMHs)* | | | | | |
| β-$Ni(OH)_2$ | 404 F/g | – | – | 85.37% | [71] |

(continued)

**Table 1** (continued)

| Species | Specific capacitance | Power density | Energy density | Cyclic retention | References |
|---|---|---|---|---|---|
| β-Ni(OH)/CNT | 724 F/g | | – | 92.10% | [71] |
| $Fe(OH)_2$ | 1066 F/g | 1.27 kW/kg | 104 Wh/kg | 91% after 1 × $10^4$ cycles | [72] |
| $Co(OH)_2$ | 3.4 C/$cm^2$ | – | – | 91% after 1.4 × $10^3$ cycles | [73] |
| Ni-Co/MWCNT | 502 F/g | – | 69 Wh/kg | 80% after 5 × $10^3$ cycles | [74] |
| *Transition metal nitrides (TMNs)* | | | | | |
| Ni/Co–$Co_2N$ | 361.93 C/g | 9.85 kW/kg | 20.4 Wh/kg | 82.4% after 5 × $10^3$ cycles | [77] |
| P/MoN | 400 mF/$cm^2$ | – | – | – | [78] |
| NbN/NC | 143 mAh/g | – | – | 100% after 2 × $10^3$ cycles | [79] |
| $Ni_3N$ | 593 mAh/g | – | – | 81% | [80] |
| VN | 64.2 F/g | 512.3 W/kg | 109.3 Wh/kg | – | [81] |
| TiN | 407 F/g | – | – | 90.2% after 2 × $10^4$ cycles | [82] |
| TiN | 53.66 mF/$cm^2$ | – | – | 97% after 1 × $10^4$ cycles | [83] |
| *Transition metal carbides (TMCs)* | | | | | |
| $Ti_3C_2$ | 447 F/g | – | – | – | [84] |
| $Ti_2C$ | 248 F/g | – | – | – | [85] |
| $Nb_2C$ | 354 mAh/g | – | – | 63.6% after 800 cycles | [85] |
| $Mo_2C$ | 218 F/g | – | – | 94.7% after 1 × $10^4$ cycles | [86] |
| $Mo_2C$/AC | – | 9028.8 W/kg | 23.5 Wh/kg | 99% after 5 × $10^3$ cycles | [86] |

explored thus combining energy storage through electrostatic attraction and faradic reaction. Numerous carbonaceous composites such as metal oxide/carbon [92] and conducting polymer/carbon composites [93] had been developed in this regard (Table 2).

**Table 2** EESDs data for CPs and hybrid material polymer

| CPss | Additive | Specific capacitance | Energy density | Power density | References |
|---|---|---|---|---|---|
| PIND | – | 24.48 F/g | 1 Wh/kg | 36.00 W/kg | [94] |
| PIND | Graphene | 389.17 F/g | 13.51 Wh/kg | 511.95 W/kg | [94] |
| PPY | GO | 526.33 F/g | – | 731.19 W/Kg | [95] |
| PANI | – | 772 F/g | – | – | [58] |
| PANI | Graphene | 909 F/g | – | – | [58] |
| PANI | SWCNTs | 128 ± 5 mAh/g | 320 mWh/g | 8,000 mW/g | [96] |
| PPY | – | 245 F/g | – | – | [97] |
| PPY | Cu–TCPP | 500 F/g | 0.29 mWh/cm$^3$ | 270 mW/cm$^3$ | [97] |
| PPY | Graphene | 137 F/cm$^3$ | 4.8 mWh/cm$^3$ | 645.1 mW/cm$^3$ | [98] |
| PPY | Carbon black | 366 F/g | – | – | [99] |
| PTH | – | 3.5 F/g | 0.7 Wh/kg | – | [100] |
| PTH | GO | 16.39 F/g | 2.28 Wh/kg | – | [100] |
| PTH | Graphite | 28.68 F/g | 3.98 Wh/kg | – | [100] |

## *3.9 Carbonitrides (CN)*

Generally, the composite of CN is employed as protective covering and finds its application in the field of diffusion barrier layers; CNs have excellent electrical conductivity, thermal and mechanical stability with great corrosion resistance [101]. Due to the condition such as disintegration of crystalline structure, lithiation/delithiation, poor specific capacity, and cyclability, CN finds somewhat lower application in LIBs. However, certain modifications in the structure can overcome these specific issues; Angamuthu et al., synthesized CN ($C_3N_4$) in varying temperature (500 and 600 °C by direct heating melamine (10 g, $C_3N_6H_6$), the CN synthesized at 600 °C displays an excellent initial charge–discharge capacity (2221/1986 mAh/g), while after 300 cycles a reversible charge capacity of 1701 mAh/g was produced [102]. A graphite/$C_3N_4$ material over $ZnCo_2O_4$ was fabricated via hydrothermal method, the as prepared composite material was found to have the extended surface area, enhanced electroactive sites and was chemically stable. The hybrid composite at 4 A/g current density was observed to have a specific capacity of 157 mAh/g, while a capacity retention of 90% was obtained even after 2500 cycles. The device was able to display an energy density of 39 Wh/kg with a power density of 1478 W/kg [103].

### 3.10 Hexagonal-Boron Nitride (h-BN)

Isostructural to graphene also known as "white graphene", h-BN consists of $sp^2$ hybridized alternate presence of boron and nitrogen atoms, where the different layers are held together via Van der Waals force of attraction. Owing to their specific characteristics of having distinctive structure and semiconductive nature, h-BN (nanotubes) found their specific use in the field of EESDs [104]. Study claims that h-BN has chemical inertness and poor electronic conductivity (band gap 5.9 eV) [105], though tuning of h-BN via certain physical and chemical modification can help them to be used in energy conversion and storage. Studies suggest that doping (with heteroatoms) and grafting (functional groups) can minimize the band gap of h-BN in a range of 0.3–3.1 eV, thus, modifying its surface, electrical, and optical characteristics.

Attribute to nested assembly, h-BN/rGO composite material enhances the specific capacity (179.5 mAh/g) and stability of Lithium Titanium oxide (LTO, $Li_4Ti_5O_{12}$), the specific capacity of rGO/LTO (161.6 mAh/g) and h-BnN/LTO was way below than the h-BN/rGO/LTO composite material. The nested assembly permits facile Li-ion diffusion, better electron transport and thus enhanced lithium ion storage [106]. Functionalized h-BN (OH, O and LiO) in LIBs was used by Zhang et al., through a reaction between h-BN and LiOH (molten) which leads to exfoliation and functionalization of h-BN. The agglomerated Fh-BN was able to charge/discharge reversibly and exhibit a specific capacity of 400 mAh/g at 0.01 V with appreciable cyclability [107]. BN (along with $MOS_2$ and $WS_2$), a 2D layered material, was used as fixers for the compounds of S and sulfide and the effect of immobilization through the repeated charge/discharge processes was studied, BN/S/C composite at a current density of 100 mA/g was observed to display a very high capacity of 532 mAh/g while a 94.3% columbic efficiency was generated after 300 continuous cycles at ~ 1.15 V [108].

### 3.11 Phosphorene (Black Phosphorous)

Phosphorene (allotrope of phosphorus) is 2D in nature where the different layers are held along with weak Van der Waals bonds. Phosphorene resembles graphene in many of its properties; therefore, it is employed in various arenas of electronics (nano and opto), energy conversion/storage, sensors, and infrastructure [109, 110]. The electrocatalytic effect of 2D phosphorene over iodide ions in 1 M $H_2SO_4$ and 0.5 M KI undergoes redox reactions. This generates a high specific discharge capacity of 3181.5 F/g with a specific energy density is 203.7 Wh/kg, while specific energy remains 36.6 Wh/Kg even after 1000 charge–discharge processes [111]. Few layered phosphorene hybridized along with layers of graphene generates a 2D hybrid electrode material. The conductive graphene layers act as the pathway for charge transport which further generate a buffer space where the anisotropically expanded phosphorene layer can be accommodated. This hybrid 2D material displays a very high

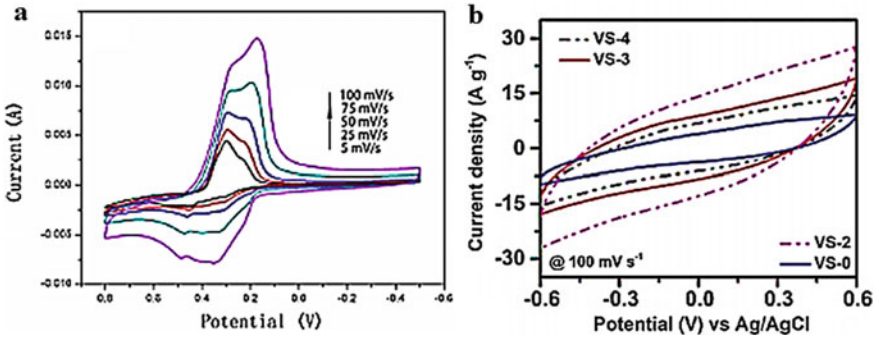


**Fig. 6** CV curve of Phosphorene (**a**); CV curves of VS/Sb (reproduce with permission (**b**) [112, 117]

specific capacity of 2440 mA/g at a current density of 0.05 A/g with a substantial capacity retention of 83% after 100 cycles in the potential window of 0 to 1.5 V [112] (Fig. 6a).

## *3.12 Antimonene*

Isostructural to Phosphorene, Antimonene isolated (epitaxial growth, solution-phase synthesis, mechanical and liquid-phase exfoliation) from its layered allotrope is an emerging 2D nanomaterial to be employed for electrochemical applications, solar cells, electrocatalysis. Properties like thermodynamic, air and environmental stability, lamellar structure (gap of 3.73 Å), tunable band gap (0–2.28 eV), appreciable electrical conductivity ($1.6 \times 10^4$ S/m) and rapid ion diffusion are associated with Antimonene [113]. However, its strong binding energy, fast interlayer ionic transport, small layer distance, etc., restrict its application in EESDs [114]. A number of research carried out in recent times have suggested that Antimonene is a material of high specific capacitance (597–1578 F/g), good cyclability, and appreciable energy and power densities [115, 116]. Antimonene electrodes are modified to enhance their performance by reducing its limitations (Fig. 6b). The 2D fillers such as MXenes, TMCs, graphene are also employed for this purpose [116–118].

## *3.13 Xenes*

Likewise, other 2D Xene materials (X = Si, Ge, Sn, etc.) owing to their mechanical flexibility, distorted atomic layer, high surface/volume ratio, and higher electron mobility are anticipated to have potential to be used in EDLCs and LIBs [119–121]. Silicene, Stanene, and Germanene are graphene equivalent, having similar electronic

properties as of graphene and can be successfully synthesized over metallic and ceramic substrates by molecular beam-epitaxy deposition method, solid-state reaction method, etc. (as can't be exfoliated from bulk material). However, production of high-quality freestanding silicene is still a great task to researchers. Also, violent volume alterations and unstable solid electrolyte interface limit the application of use of Group IVA elements. Studies suggest that the defect present in Xenes is responsible for its enhanced quantum capacitance [122, 123]. Various reports significantly establish high theoretical capacitance (4200, 1625, and 994 mAh/g), electrical performance and long cyclabilty of Xenes (Si, Ge, Sn), and establish them as significant materials to be used for EESDs [124, 125].

## 4 Factors Affecting 2D Materials Performance

Various parameters such as temperature, defects, and doping have deep effect on the performance of any electrode. The judicious variation in these parameters can result in an improved extraordinary electrode material which can be used efficiently in the field of EESDs [125].

### *4.1 Effect of Temperature*

Temperature is a critical aspect for energy storage material as it can significantly augment or limit the application of various EESDs. Mudila et al. studied the effect of reduced temperature ($10 \pm 1$ °C) on the electrochemical performance of PPY/GO nanocomposite, CV studies in 1 M KOH (at 0.2–0.001 V/s) rendered a specific conductivity of 526.33 F/g with 731.19 W/Kg of power density, while a high capacitive retention (96%) after 500 cycles rate was observed [95]. $Co_3O_4$/rGO nanocomposites (anode) prepared through microwave irradiation method (at 100 °C) for LIBs demonstrate good electrochemical performance, an initial charge/discharge capacity of 47 and 42.7 mAh/g at 500 mA/g, while a 100% coulombic efficiency after 50 cycles was gained [126]. Gel electrolytes of fumed silica and fumed silica/$TiO_2$ characterized by CV and EIS show the increased anodic peak currents (at 30 °C for fumed silica and 40 °C for fumed silica/$TiO_2$) and redox capacities with increasing temperature [127]. PAN co-MMA (Polyacrylonitrile/methyl methacrylate) copolymer nanofibers synthesized by electrospinning technique were further converted to carbon nanofibers on heating at varying temperature (1000, 1800, and 2200 °C). These prepared carbon nanofibers were studied for their application in LIBs. It was observed that with an increasing temperature the specific capacitance was decreased (254, 238 and 105 mAh/g for 1000, 1800, and 2200 °C). However, an improved microstructure and surface area (~60 $m^2$/g) were determined at 2000 °C which could be attributed to the distribution of pore in fibers along with a low electrolyte wetting, also at 1000 °C, a high capacitance (238 mAh/g) was retrieved after 500 cycles [128].

## 4.2 Effect of Dopant

Doping of electrochemical active material with variety of dopants tune their performance multifold and a variety of dopants are used in energy conversion/storage sector for the above-mentioned purpose. Graphene doped with hetero atom (N-doped) give a few layer nanocomposite with density of ~ 2.1 mg/cm$^3$ which delivers a specific capacitance of 484 F/g in 1 M KOH [129]. Co-doped $Ni(OH)_2$ enhances the specific capacitance of TMH to 1500 F/g at current density of 10 A/g, which falls to 1560 F/g after 100 discharge/charge cycles [130]. Co-doped cobalt oxide was tuned to have appreciable pore size and surface area which helped in generating synergistic effect of ordered nanopores (which enables osmotic solution flux and diffusive solute transport) and small nanoparticles (paving channel for electron transportation and ion diffusion), that generate a specific capacitance of 902.3 F/g at 2 A/g with better cyclability [131]. $Li_2MoO_3$ doped by cation (Zn, Mg, Cr, and La) generate materials with good structural stability and electrical conductivities. Undoped $Li_2MoO_3$ gives the lowest specific capacity of 246.87 mAh/g while the highest specific capacity was generated by Cr doped $Li_2MoO_3$ ($Li_2Mo_{0.96}Cr_{0.04}O_3$). La-doped $Li_2MoO_3$ displays a specific capacity of 149.89 mAh/g after 50th cycle at current density of 34 mA/g [132].

## 4.3 Effect of Defect

Though 2D nanomaterial is presented significantly by many researchers to be employed in the direction of energy conversion/storage, but the performance of EESDs can be optimized considerably through the introduction of certain defects in electroactive materials. These introduced imperfections expose the unsaturated sites which play a crucial role in electrochemical reactions. Defects/imperfections generate novel functionality in electrode which enhances ion diffusion by generating new active sites. Also, the surface energy is evolved which enhances the electrochemical phase revolution. [133–135].

Structurally defective and non-defective graphene were allowed to adsorb Mg over their surface. Mg energy storage capacity was enhanced with increasing the defect concentration or altering the organization of available carbon rings of graphene. High availability of Mg enhances the electrochemical energy storage specific capacity to 1042 mAh/g (25% di-vacancy defects) [136]. $Mg_xFe_2–xB_2O_5$ and $MgVBO_4$ (metal borate) with high specific capacities of 186 and 360 mAh/g, respectively, were synthesized. At higher temperature (200–500 °C) by thermal oxidation Mg can be removed from the lattice, the diffusion of Mg through interstitial channels thus with Mg mobility in the sites enhances the capacity [137]. Introduction of certain cationic defects (of Li, Si and P) into the surface of $TiS_2$ through using a thermal annealing

method was carried by Liu et al. showed that the presence of cationic defects efficiently increases cyclability and reaction rate of the electrodes. The presence of phosphorus impurities generates highest 63.56% of retention after 450 cycles which was much higher (35.13%) than $TiS_2$ electrode alone. Thus, Ti vacancy defect were found to be advantageous in generating interlayer spacing, weakening of strain, generating perfect interstitial sites for cationic doping [138]. n-type Ag particle were doped to CdSe via electronic tuning to cover certain imperfections where these defects cover were found to behave as charge trappers. The densities of the charge trapping defects in the material were found to be in the range of $1018-1020\ cm^3$ [139].

## 5 Conclusion

Various EESDs in different forms offer a potential alternative to meet the present and future energy/power demands. Though different types of materials are present which render high power density, comes with great charge-recharge cyclability and also have specific capability to work in extreme physical condition of temperatures, etc. These capabilities increase the efficiency of the end-product and eventually condensing the expenses and being environmental friendliness. In this direction, 2D nanomaterials (graphene, TMDs, MXenes, etc.) have presented themselves significantly to be employed in the direction of energy conversion/storage. 2D nanomaterials are present with certain unique properties which help them to show their marked performance in the area of energy storage and conversion. Tuning the nanostructures via doping with certain heteroatoms and functional group generates micro/nano pores which modify the electronic and surface properties of these 2D nanomaterials. But, many of the inherent deficits limit the ultimate use of these 2D nanomaterials in physical devices due to the issues such as low conductivity (compared to other nanostructures), limited electroactive sites (limited electrochemical performance), poor reversibility high cost, reduced oxidation resistance. Though continuous and efficient research approaches have produced many significant nanomaterials of 2D nature which however fulfill the energy demand of current time, a continuous and scalable effort along with noble modifications in the morphology is required to achieve high-quality, powerful and economical 2D nanomaterial for enormous future energy demands.

## References

1. Funabashi T (2016) Integration of distributed energy resources in power systems: introduction 1–14
2. Shiraishi S (2003) Carbon alloys. Electric Double Layer Capacitors 447–457
3. Patrice S, Thierry B, Frédéric F (2017) Supercapacitors based on carbon or pseudocapacitive materials. Electrochem Double-Layer Capacitors (EDLC). https://doi.org/10.1002/9781119007333

4. Jinyue Y (2015) Handbook of clean energy systems. Electrochem Supercapacitors Energy Storage Convers 1–25
5. Okonkwo PC, Collins E and Okonkwo E (2017) Application of biopolymer composites in super capacitor. In: Biopolymer composites in electronics, pp 487–503
6. Diouf B, Pode R (2015) Potential of lithium-ion batteries in renewable energy. Renew Energy 76:375–380. https://doi.org/10.1016/j.renene.2014.11.058
7. Zhang C, He D, Ma J, Tang W, Waite TD (2018) Faradaic reactions in capacitive deionization (CDI)—problems and possibilities: a review. Water Res 128:314–330
8. Viswanathan B (2017) Supercapacitors. Energy Sources 315–328
9. Mudila H, Prasher P, Kumar M, Kumar A, Zaidi MGH, and Kumar A (2019) Critical analysis of polyindole and its composites in supercapacitor application. Mater Renew Sustain Energy 8(2)
10. Zaghib K, Mauger A, and Julien CM (2015) Rechargeable lithium batteries for energy storage in smart grids. Rechargeable Lithium Batteries 319–351
11. Zhou L, Li C, Liu X, Zhu Y, Wu Y, and van Ree T (2018). Metal oxides in supercapacitors. Metal Oxides Energy Technol 169–203
12. Khan K, Tareen AK, Aslam M, Zhang Y, Wang R, Ouyang Z, Gou Z, Zhang H (2019) Recent advances in two-dimensional materials and their nanocomposites in sustainable energy conversion applications. Nanoscale. https://doi.org/10.1039/c9nr05919a
13. Tsai FT, Deng YT, Pao CW, Chen JL, Lee JF, La KT, Liaw WF (2020) HER/OER mechanistic study of FeCoNi-based electrocatalyst for alkaline water splitting. J Mater Chem A. https://doi.org/10.1039/d0ta01877e
14. Page MP, Sahoo M, Holmes SM (2019) Single layer 2D crystals for electrochemical applications of ion exchange membranes and hydrogen evolution catalysts. Adv Mater Interfaces 1–24:1801838
15. Yang L, Shui J, Du L, Shao Y, Liu J, Dai L, Hu Z (2019) Carbon-based metal-free ORR electrocatalysts for fuel cells: past, present, and future. Adv Mater. https://doi.org/10.1002/adma.201804799
16. Qu L, Liu Y, Baek JB, Dai L (2010) Nitrogen-doped graphene as efficient metal-free electrocatalyst for oxygen reduction in fuel cells. ACS Nano 4(3):1321–1326
17. Farooqui UR, Ahmad AL, Hamid NA (2018) Graphene oxide: a promising membrane material for fuel cells. Renew Sustain Energy Rev 82:714–733. https://doi.org/10.1016/j.rsr.2017.09.081
18. Su H, Hu YH (2020) Recent advances in graphene-based materials for fuel cell applications. Energy Sci Eng. https://doi.org/10.1002/ese3.833
19. Liu Y, Yue X, Li K, Qiao J, Wilkinson DP, Zhang J (2016) PEM fuel cell electrocatalysts based on transition metal macrocyclic compounds. Coord Chem Rev 315:153–177. https://doi.org/10.1016/j.ccr.2016.02.002
20. Rojaee R, Shahbazian-Yassar R (2020) Two dimensional materials to address the Li-based battery challenges. ACS Nano. https://doi.org/10.1021/acsnano.9b08396
21. Gogotsi Y, Penner RM (2018) Energy storage in nanomaterials—capacitive, pseudocapacitive, or battery-like? ACS Nano 12(3):2081–2083. https://doi.org/10.1021/acsnano.8b01914
22. Lee G (2016) Structure, morphology, and electrochemical properties of transition metal oxide, hydroxide, and phosphate nanomaterials for energy storage. Dissertation, Duke University. Retrieved from https://hdl.handle.net/10161/12161
23. Barpuzary D, Kim K, Park MJ (2019) Two-dimensional conducting polymers: synthesis and charge transport. J Polym Sci, Part B: Polym Phys 57(18):1169–1176
24. Shavanova K, Bakakina Y, Burkova I, Shtepliuk I, Viter R, Ubelis A, Beni V, Starodub N, Yakimova R, Khranovskyy V (2016) Application of 2D non-graphene materials and 2D oxide nanostructures for biosensing technology. Sensors 16(2):223
25. Hynek DJ, Pondick JV, Cha JJ (2019) The development of 2D materials for electrochemical energy applications: a mechanistic approach. APL Mater 7(3)
26. Kim JH, Jeong JH, Kim N, Joshi R, Lee GH (2018) Mechanical properties of two-dimensional materials and their applications. J Phys D: Appl Phys 52:083001

27. Mudila H, Joshi V, Rana S, Zaidi MGH, Sarfaraz A (2014) Enhanced electrocapacitive performance and high-power density of polypyrrole/graphene oxide nanocomposites prepared at reduced temperature. Carbon Letters 15(3):171–179
28. Lin Z, McCreary A, Briggs N, Subramanian S, Zhang K, Sun Y, Li X, Borys NJ, Yuan H, Fullerton-Shirey SK, Chernikov A, Zhao H, McDonnell S, Lindenberg AM, Xiao K, LeRoy BJ, Drndić M, Hwang JCM, Park J, Chhowalla M, Schaak RE, Javey A, Hersam MC, Robinson J, Terrones M (2016) 2D materials advances: from large scale synthesis and controlled heterostructures to improved characterization techniques, defects and applications. 2D Mater 3(4)
29. You X, Feng Q, Yang J, Huang K, Hu J, Dong S (2019) Preparation of high concentration graphene dispersion with low boiling point solvents. J Nanopart Res 21:19
30. Xiong S, Shi Y, Chu J, Gong M, Wu B, Wang X (2014) Preparation of high-performance covalently bonded polyaniline nanorods/graphene supercapacitor electrode materials using interfacial copolymerization approach. Electrochim Acta 127:139–145
31. Xu L, Wang H, Gao J, Jin X (2019) Electrochemical performance enhancement of flexible graphene supercapacitor electrodes by carbon dots modification and $NiCo_2S_4$ electrodeposition. J Alloys Compounds 809:151802
32. Yang H, Kannappan S, Pandian AS, Jang JH, Lee YS, Lu W (2017) Graphene supercapacitor with both high power and energy density. Nanotechnology 28(44):445401
33. Chang HH, Chang CK, Tsai YC, Liao CS (2012) Electrochemically synthesized graphene/polypyrrole composites and their use in supercapacitor. Carbon 50(6):2331–2336
34. Gupta S, Price C (2016) Investigating graphene/conducting polymer hybrid layered composites as pseudocapacitors: interplay of heterogeneous electron transfer, electric double layers and mechanical stability. Compos B Eng 105:46–59
35. Manzeli S, Ovchinnikov D, Pasquier D, Yazyev OV, Kis A (2017) 2D transition metal dichalcogenides. Nat Rev Mater 2(8):17033
36. Naumis GG (2020) Electronic properties of two-dimensional materials. In: Synthesis modelling and characterization of 2D materials and their heterostructures, pp 77–109
37. Wang H, Tsai C, Kong D, Chan K, Abild-Pedersen F, Nørskov J, Cui Y (2015) Transition-metal doped edge sites in vertically aligned $MoS_2$ catalysts for enhanced hydrogen evolution. Nano Res 8:566–575
38. Paravannoor A, Babu A (2018) $MoS_2$/graphene nanocomposites for efficient electrochemical energy storage—a novel strategy based on electrolyte formulation. Surf Interfaces. https://doi.org/10.1016/j.surfin.2018.11.006
39. Liao X, Zhao Y, Wang J, Yang W, Xu L, Tian X, Shuang Y, Owusu KA, Yan M, Mai L (2018) $MoS_2/MnO_2$ heterostructured nanodevices for electrochemical energy storage. Nano Res 11:2083–2092
40. Ali S, Khan T, Khan M, Zulfiqar Khan R, Hussain S (2019) Morphological structural and energy storage based study of $MoS_2$/ZnO nanocomposite. Mater Res Exp https://doi.org/10.1088/2053-1591/ab5bc1
41. Liu MC, Xu Y, Hu YX, Yang QQ, Kong LB, Liu W, Niu W, Chueh YL (2018) Electrostatically charged $MoS_2$/graphene oxide hybrid composites for excellently electrochemical energy storage devices. ACS Appl Mater Interfaces. https://doi.org/10.1021/acsami.8b09085
42. Liu MC, Zhang H, Hu YX, Lu C, Li J, Xu YG, Kong LB (2019) Special layer structure WS2 nanoflakes as high performances sodium ion storage materials. Sustain Energy Fuels. https://doi.org/10.1039/c9se00047j
43. Nguyen TP, Kim IT (2020) W2C/WS2 alloy nanoflowers as anode materials for lithium-ion storage. Nanomaterials 10(7):1336
44. Hu S, Jiang Q, Ding S, Liu Y, Wu Z, Huang Z, Zhou T, Guo Z, Hu J (2018) Construction of hierarchical $MoSe_2$ hollow structures and its effect on electrochemical energy storage and conversion. ACS Appl Mater Interfaces 10(30):25483–25492
45. Luxa J, Wang Y, Sofer Z, Pumera M (2016) Layered post-transition-metal dichalcogenides (X−M−M−X) and their properties. Chem Eur J 22(52):18810–18816

46. Woods-Robinson R, Han Y, Zhang H, Ablekim T, Khan I, Persson KA, Zakutayev A (2020) Wide band gap chalcogenide semiconductors. Chem Rev. https://doi.org/10.1021/acs.chemrev.9b00600
47. Chua CK, Sofer Z, Lim CS, Pumera M (2014) Inherent electrochemistry of layered post-transition metal halides: the unexpected effect of potential cycling of PbI2. Chem Eur J 21(7):3073–3078
48. Wang C, Yang S, Cai H, Ataca C, Chen H, Zhang X, Xu J, Chen B, Wu K, Zhang H, Liu L, Li J, Grossman JC, Tongay S, Liu Q (2016) Enhancing light emission efficiency without color change in post-transition metal chalcogenides. Nanoscale 8(11):5820–5825
49. Tan SM, Chua CK, Sedmidubský D, Sofer Z, Pumera M (2016) Electrochemistry of layered GaSe and GeS: applications to ORR, OER and HER. Phys Chem Chem Phys 18(3):1699–1711
50. Sun X, Chang Y, Mu C, Nie A, Wang B, Xiang J, Zhai K, Wen F, Liu Z (2019) Two-dimensional layered materials InSe nanoflakes/carbon nanotubes composite for flexible all-solid-state supercapacitors. J Mater Sci. https://doi.org/10.1007/s10853-019-04151-x
51. Yuan Y, Yang M, Liu L, Xia J, Yan H, Liu J, Wen J, Zhang Y, Wang X (2020) The electrochemical storage mechanism of an $In_2S_3$/C nanofiber anode for high-performance Li-ion and Na-ion batteries. Nanoscale 12(39):20337–20346
52. Fang S, Bresser D, Passerini S (2019) Transition metal oxide anodes for electrochemical energy storage in lithium- and sodium-ion batteries. Adv Energy Mater 1902485
53. Chen Z, Belharouak I, Sun Y-K, Amine K (2012) Titanium-based anode materials for safe lithium-ion batteries. Adv Func Mater 23(8):959–969
54. Nava-Avendaño J, Morales-García A, Ponrouch A, Rousse G, Frontera C, Senguttuvan P, Tarascon J, Arroyo-de Dompablo ME, Palacín MR (2015) Taking steps forward in understanding the electrochemical behavior of $Na_2Ti_3O_7$. J Mater Chem A 3(44):22280–22286
55. Armand M, Axmann P, Bresser D, Copley M, Edström K, Ekberg C, Guyomard D, Lestriez B, Novak P, Petranikova M, Porcher W, Trabesinger S, Wohlfahrt-Mehrens M, Zhang H (2020) Lithium-ion batteries—current state of the art and anticipated developments. J Power Sour 479:228708
56. Shen M, Wang Y, Zhang Y (2020) Neatly arranged mesoporous $MnO_2$ nanotubes with oxygen vacancies for electrochemical energy storage. Dalton Trans 49:17552–17558
57. Yin B, Zhang S, Jiang H, Qu F, Wu X (2015) Phase-controlled synthesis of polymorphic MnO2 structures for electrochemical energy storage. J Mater Chem A 3(10):5722–5729
58. Deokate RJ, Kate R, Shinde NM, Mane RS (2021) Energy storage potential of sprayed α-$MoO_3$ thin films. New J Chem. https://doi.org/10.1039/d0nj03910a
59. Sen UK, Mitra S (2014) Synthesis of molybdenum oxides and their electrochemical properties against Li. Energy Procedia 54:740–747
60. Xie JD, Li HY, Wu TY, Chang JK, Gandomi YA (2018) Electrochemical energy storage of nanocrystalline vanadium oxide thin films prepared from various plating solutions for supercapacitors. Electrochim Acta 273:257–263
61. Deshmukh PR, Pusawale SN, Bulakhe RN, Lokhande CD (2013) Supercapacitive performance of hydrous ruthenium oxide ($RuO_2 \cdot nH_2O$) thin films synthesized by chemical route at low temperature. Bull Mater Sci 36(7):1171–1176
62. Xie K, Li J, Lai Y, Lu W, Zhang Z, Liu Y, Zhou L, Huang H (2011) Highly ordered iron oxide nanotube arrays as electrodes for electrochemical energy storage. Electrochem Commun 13(6):657–660
63. Nagaraju P, Arivanandhan M, Alsalme A, Alghamdi A, Jayavel R (2020) Enhanced electrochemical performance of α-$MoO_3$/graphene nanocomposites prepared by an in situ microwave irradiation technique for energy storage applications. RSC Adv 10(38):22836–22847
64. Kim H, Oh M, Son W, Kim T, Park S (2006) Novel synthesis method and electrochemical characteristics of lithium titanium oxide as anode material for high power device. In: 2006 IEEE 8th international conference on properties & applications of dielectric materials, Bali, 464–467
65. Zheng P, Liu T, Su Y, Zhang L, Guo S (2016) $TiO_2$ nanotubes wrapped with reduced graphene oxide as a high-performance anode material for lithium-ion batteries. Sci Rep 6:36580

66. Hossain MN, Chen S, Chen A (2018) Fabrication and electrochemical study of ruthenium-ruthenium oxide/activated carbon nanocomposites for enhanced energy storage. J Alloy Compd 751:138–147
67. Wan L, Wang P (2020) Recent progress on self-supported two-dimensional transition metal hydroxides nanosheets for electrochemical energy storage and conversion. Int J Hydrogen Energy. https://doi.org/10.1016/j.ijhydene.2020.12.061
68. Tan HT, Sun W, Wang L, Yan Q (2015) 2D transition metal oxides/hydroxides for energy-storage applications. ChemNanoMat 2(7):562–577
69. Guan M, Wang Q, Zhang X, Bao J, Gong X, Liu Y (2020) Two-dimensional transition metal oxide and hydroxide-based hierarchical architectures for advanced supercapacitor materials. Front Chem 8
70. Lu Z, Wu X, Jiang M, Wang J, Liu J, Lei X, Sun X (2014) Transition metal oxides/hydroxides nanoarrays for aqueous electrochemical energy storage systems. Sci China Mater 57(1):59–69
71. Salunkhe RR, Jang K, Lee S, Yu S, Ahn H (2012) Binary metal hydroxide nanorods and multi-walled carbon nanotube composites for electrochemical energy storage applications. J Mater Chem 22(40):21630
72. Owusu K, Qu L, Li J, Wang Z, Zhao K, Yang C, Hercule KM, Lin C, Shi C, Wei Q, Zhou L, Mai L (2017) Low-crystalline iron oxide hydroxide nanoparticle anode for high-performance supercapacitors. Nat Commun 8:14264
73. Santos CS, deOliveira RD, Marchesi LFQP, Pessôa CA (2018) Electrodeposited cobalt hydroxide in expanded carbon graphite electrode obtained from exhausted batteries applied as energy storage device. Arab J Chem. https://doi.org/10.1016/j.arabjc.2018.11.017
74. Shakir I, Ammar Almutairi Z, Saad Shar S, Nafady A (2020) Nickel hydroxide nanoparticles and their hybrids with carbon nanotubes for electrochemical energy storage applications. Results Phys 103117
75. Wang H, Jianmin LJ, Li K, Lin Y, Chen J, Gao L, Nicolosi V, Xiao X, Lee JM (2021) Transition metal nitrides for electrochemical energy applications. Chem Soc Rev. https://doi.org/10.1039/D0CS00415D
76. Zhang C, Ma Y, Zhang X, Abdolhosseinzadeh S, Sheng H, Lan W, Pakdel A, Heier J, Nüesch F (2019) Two-Dimensional Transition Metal Carbides and Nitrides (MXenes): synthesis, properties, and electrochemical energy storage applications. Energy Environ Mater https://doi.org/10.1002/eem2.12058
77. Liu X, Zang W, Guan C, Zhang L, Qian Y, Elshahawy AM, Zhao D, Pennycook SJ, Wang J (2018) Ni-doped cobalt-cobalt nitride heterostructure arrays for high poer supercapacitors. ACS Energy Lett. https://doi.org/10.1021/acsenergylett.8b01393
78. Dubal DP, Abdel-Azeim S, Chodankar NR, Han YK (2019) Molybdenum nitride nanocrystals anchored on phosphorus-incorporated carbon fabric as a negative electrode for high-performance asymmetric pseudocapacitor. iScience 16:50–62
79. Lee J, Kim S, Park JH, Jo C, Chun J, Sung YE, Lim E, Lee J (2020) Small−strain niobium nitride anode with ordered mesopores for ultra−stable potassium−ion batteries. J Mater Chem A. https://doi.org/10.1039/c9ta11663j
80. Balogun MS, Zeng Y, Qiu W, Luo Y, Onasanya A, Olaniyi TK, Tong Y (2016) Three-dimensional nickel nitride ($Ni_3N$) nanosheets: free standing and flexible electrodes for lithium ion batteries and supercapacitors. J Mater Chem A 4(25):9844–9849
81. Liu W, Zhang W, Kang L, Kong L (2019) Vanadium nitride nanoparticles as anode material for lithium ion hybrid capacitor applications. J Wuhan Univ Technol-Mat Sci Edit 34:1274–1278
82. Tang S, Cheng Q, Zhao J, Liang J, Liu C, Lan Q, Cao YC, Liu J (2017) Preparation of Titanium nitride nanomaterials for electrode and application in energy storage. Results Phys 7:1198–1201
83. Ansari SA, Khan NA, Hasan Z, Shaikh AA, Ferdousi FK, Barai HR, Lopa NS, Rahman MM (2020) Electrochemical synthesis of titanium nitride nanoparticles onto titanium foil for electrochemical supercapacitors with ultrafast charge/discharge. Sustain Energy Fuels. https://doi.org/10.1039/d0se00049c

84. Syamsai R, Kollu P, Kwan Jeong S, Grace AN (2017) Synthesis and properties of 2D-titanium carbide MXene sheets towards electrochemical energy storage applications. Ceram Int 43(16):13119–13126
85. Zhao J, Wen J, Bai L, Xiao J, Zheng R, Shan X, li L, Gao H, Zhang X (2019) One-step synthesis of few-layer niobium carbide MXene as promising anode material for high-rate lithium ion batteries. Dalton Trans https://doi.org/10.1039/c9dt03260f
86. Zhang WB, Ma XJ, Kong LB, Liu MC, Luo YC, Kang L (2016) Intermetallic molybdenum carbide for pseudocapacitive electrode material. J Electrochem Soc 163(10):A2441–A2446
87. Mudila H, Rana S, Zaidi MGH, Alam S (2014) Polyindole/graphene oxide nanocomposites: the novel material for electrochemical energy storage. Fullerenes Nanotubes Carbon Nanostruct 23(1):20–26
88. Zhai Y, Dou Y, Zhao D, Fulvio PF, Mayes RT, Dai S (2011) Carbon materials for chemical capacitive energy storage. Adv Mater 23(42):4828–4850
89. Xiao P, Xu Y (2018) Recent progress in two-dimensional polymers for energy storage and conversion: design, synthesis, and applications. J Mater Chem A. https://doi.org/10.1039/c8ta02820f
90. Barpuzary D, Kim K, Park MJ (2019) Two-dimensional conducting polymers: synthesis and charge transport. J Polym Sci Part B: Polym Phys. https://doi.org/10.1002/polb.24777
91. Ramachandran R, Wang F (2017) Electrochemical capacitor performance: influence of aqueous electrolytes. In: Supercapacitors—theoretical and practical solutions. Lionginas Liudvinavičius, IntechOpen
92. Shinde PV, Singh MK (2019) Synthesis, characterization, and properties of graphene analogs of 2D material. Fundam Sens Appl 2D Mater 91–143
93. Wang Z, Hu T, Liang R, and Wei M (2020) Application of zero-dimensional nanomaterials in biosensing. Front Chem 8
94. Kumar A, Kumar A, Mudila H, Awasthi, K, Kumar V (2020) Synthesis and thermal analysis of polyaniline (PANI). J Phys Conf Ser 1531:012108
95. Gao B, Li X, Ding K, Huang C, Li Q, Chu PK, Huo K (2018) Recent progress of nanostructured transition metal nitrides for advanced electrochemical energy storage. J Mater Chem A 7:14–37
96. Flouda P, Quinn AH, Patel A, Loufakis D, Lagoudas DC, Lutkenhaus J (2020) Branched aramid nanofiber-polyaniline electrodes for structural energy storage. Nanoscale. https://doi.org/10.1039/d0nr04573j
97. Yao H, Zhang F, Zhang G, Luo H, Liu L, Shen M, Yang Y (2018) A novel two-dimensional coordination polymer-polypyrrole hybrid material as a high-performance electrode for flexible supercapacitor. Chem Eng J 334:2547–2557
98. Qin J, Zhou F, Xiao H, Ren R, Wu ZS (2018) Mesoporous polypyrrole-based graphene nanosheets anchoring redox polyoxometalate for all-solid-state micro-supercapacitors with enhanced volumetric capacitance. Sci China Mater 61:233–242
99. Yang C, Liu P, Wang T (2011) Well-defined core−shell carbon black/polypyrrole nanocomposites for electrochemical energy storage. ACS Appl Mater Interfaces 3(4):1109–1114
100. Azimi M, Abbaspour M, Fazli A, Pourabbas B (2018) Investigation on electrochemical properties of polythiophene nanocomposite with graphite derivatives as supercapacitor material on breath figure-decorated PMMA electrode. J Electr Mater 47:2093–2102
101. Sharma M, Gaur A (2020) Designing of carbon nitride supported $ZnCo_2O_4$ hybrid electrode for high-performance energy storage applications. Sci Rep 10:2035
102. Zhang H, Yan J, Zhang X, Tang S (2006) Properties of titanium carbonitride matrix cermets. Int J Refract Metal Hard Mater 24(3):236–239
103. Angamuthu G, Jayabal E, Rengarajan V (2020) Electrochemical performance evaluation of carbon nitride synthesized at different temperatures as an anode material for lithium-ion batteries. Ionics 26:3863–3873
104. Chen X, Gao XP, Zhang H, Zhou Z, Hu WK, Pan GL, Zhu HY, Yan TY, Song DY (2005) Preparation and electrochemical hydrogen storage of boron nitride nanotubes. J Phys Chem B 109(23):11525–11529

105. Han R, Liu F, Wang X, Huang M, Li W, Yamauchi Y, Sun X, Huang Z (2020) Functionalised hexagonal boron nitride for energy conversion and storage. J Mater Chem A. https://doi.org/10.1039/d0ta05008c
106. Ergen O (2020) Hexagonal boron nitride incorporation to achieve high performance Li4Ti5O12 electrodes. AIP Adv 10(4):045040
107. Zhang F, Németh K, Bareño J, Dogan F, Bloom ID, Shaw LL (2016) Experimental and theoretical investigations of functionalized boron nitride as electrode materials for Li-ion batteries. RSC Adv 6(33):27901–27914
108. Zhang K, Lee TH, Cha JH, Varma RS, Choi JW, Jang HW, Shokouhimehr M (2019) Two-dimensional boron nitride as a sulfur fixer for high performance rechargeable aluminum-sulfur batteries. Sci Rep 9(1)
109. Khandelwal A, Mani K, Karigerasi MH, Lahiri I (2017) Phosphorene—the two-dimensional black phosphorous: properties, synthesis and applications. Mater Sci Eng, B 221:17–34
110. Tao Y, Huang T, Ding C, Yu F, Tan D, Wang F, Xie Q, Yao S (2019) Few-layer phosphorene: an emerging electrode material for electrochemical energy storage. Appl Mater Today 15:18–33
111. Sun J, Lee HW, Pasta M, Yuan H, Zheng G, Sun Y, Li Y, Yi YA (2015) Phosphorene–graphene hybrid material as a high-capacity anode for sodium-ion batteries. Nat Nanotech 10:980–985
112. Zu L, Gao X, Lian H, Li C, Liang Q, Liang Y, Cui X, Liu Y, Wang X, Cui X (2019) Electrochemical prepared phosphorene as a cathode for supercapacitors. J Alloy Compd 770:26–34
113. Xiao Q, Hu C, Wu H, Ren Y, Li X, Yang Q, Dun G, Huang Z, Peng Y, Yan F, Wang Q, Zhang H (2019) Antimonene-based flexible photodetector. Nanoscale Horiz. https://doi.org/10.1039/C9NH00445A
114. Martínez-Periñán E, Down MP, Gibaja C, Lorenzo E, Zamora F, Banks CE (2017) Antimonene: a novel 2D nanomaterial for supercapacitor applications. Adv Energy Mater 8(11):1702606
115. Mohamed IM, Vigneshwaran JSA, Mani D, Arivanandhan M, Jose SP, Ramasamy J (2020) Antimonene nanosheets with enhanced electrochemical performance for energy storage applications. Dalton Trans. https://doi.org/10.1039/d0dt01753a
116. Yu J, Zhou J, Yao P, Xie H, Zhang M, Ji M, Liu H, Liu Q, Zhu C, Xu J (2019) Antimonene engineered highly deformable freestanding electrode with extraordinarily improved energy storage performance. Adv Energy Mater 1902462
117. Singal S, Joshi A, Singh G, Sharma RK (2020) Dual approach of antimonene hybridization and hierarchical structuration to expose more active sites for improved charge storage characteristics of VS4. J Power Sour 475:228669
118. Gupta T, Elibol K, Hummel S, Stöger-Pollach M, Mangler C, Habler G, Meyer JC, Eder D, Bayer BC (2021) Resolving few-layer antimonene/graphene heterostructures. npj 2D Mater Appl 5:53
119. Xu Q, Yang G, Fan X, Zheng WT (2019) Adsorption of metal atoms on silicene: stability and quantum capacitance of silicene-based electrode materials. Phys Chem Chem Phys. https://doi.org/10.1039/C8CP05982A
120. Xu Q, Si X, She W, Yang G, Fan X, Zheng W (2020) First-principle calculation of optimizing performance of germanene-based supercapacitors by vacancies and metal atoms. J Phys Chem C. https://doi.org/10.1021/acs.jpcc.0c00354
121. Pielnhofer F, Menshchikova TV, Rusinov IP, Zeugner A, Yu Sklyadneva I, Heid R, Bohnen K, Golub P, Baranov AI, Chulkov E, Pfitzner A, Ruck M, Isaeva A (2017) Designing 3D topological insulators by 2D-Xene (X = Ge, Sn) sheet functionalization in GaGeTe-type structures. J Mater Chem C 5(19):4752–4762
122. Momeni MJ, Mousavi-Khoshdel M, Leisegang T (2020) Exploring the performance of pristine and defective silicene and silicene-like XSi3 (X= Al, B, C, N, P) sheets as supercapacitor electrodes: a density functional theory calculation of quantum capacitance. Physica E: Low-Dimensional Syst Nanostruct 114290
123. Liu J, Yang Y, Lyu P, Nachtigall P, Xu Y (2018) Few-layer silicene nanosheets with superior lithium-storage properties. Adv Mater 30(26):1800838

124. Liu D, Liu ZJ, Li X, Xie W, Wang Q, Liu Q, Fu Y, He D (2017) Group IVA element (Si, Ge, Sn)-based alloying/dealloying anodes as negative electrodes for full-cell lithium-ion batteries. Small 13(45):1702000
125. Badwal SP, Giddey SS, Munnings C, Bhatt AI, Hollenkamp AF (2014) Emerging electrochemical energy conversion and storage technologies. Front Chem 2:79
126. Mussa Y, Ahmed F, Abuhimd H, Arsalan M, Alsharaeh E (2019) Enhanced electrochemical performance at high temperature of cobalt oxide/reduced graphene oxide nanocomposites and its application in lithium-ion batteries. Sci Rep 9:44
127. Gencten M, Dönmez KB, Şahin Y (2016) Investigation of the temperature effect on electrochemical behaviors of $TiO_2$ for gel type valve regulated lead-acid batteries. Anadolu Univ J Sci Technol A—Appl Sci Eng 17(5):882–894
128. Gupta A, Gurunathan P, Ramesha K, Singh M, Dhakate SR (2019) Effect of heat treatment temperature on energy storage performance of PAN co-MMA based carbon nanofibers as freestanding lithium ion batteries anode. Energy Storage. https://doi.org/10.1002/est2.89
129. Zhao Y, Hu C, Hu Y, Cheng H, Shi G, Qu L (2012) A versatile, ultralight, nitrogen-doped graphene framework. Angew Chem 124(45):11533–11537
130. Lee G, Varanasi CV, Liu J (2015) Effects of morphology and chemical doping on electrochemical properties of metal hydroxides in pseudocapacitors. Nanoscale 7(7):3181–3188
131. Deng X, Zhang H, Zhang J, Lei D, Peng Y (2020) Synergistic effect of hierarchical nanopores in Co-doped cobalt oxide 3D flowers for electrochemical energy storage. RSC Adv 10(71):43825–43833
132. Teng R, Yu HT, Guo CF, Wang XD, Qiao YJ, Xie Y, Yi TF (2020) Effect of cation doping on the electrochemical properties of $Li_2MoO_3$ as a promising cathode material for lithium-ion battery. Ionics 26:4413–4422
133. Liu H, Lei W, Tong Z, Li X, Wu Z, Jia Q, Zhang S, Zhang H (2020) Defect engineering of 2D materials for electrochemical energy storage. Adv Mater Interf 2000494
134. Zhang Y, Tao L, Xie C, Wang D, Zou Y, Chen R, Wang Y, Jia C, Wang S (2020) Defect engineering on electrode materials for rechargeable batteries. Adv Mater 1905923
135. Mohanty D, Hockaday E, Li J, Hensley DK, Daniel C, Wood DL (2016) Effect of electrode manufacturing defects on electrochemical performance of lithium-ion batteries: cognizance of the battery failure sources. J Power Sources 312:70–79
136. Er D, Detsi E, Kumar H, Shenoy VB (2016) Defective graphene and graphene allotropes as high-capacity anode materials for Mg Ion batteries. ACS Energy Lett 1(3):638–645
137. Bo SH, Grey CP, Khalifah PG (2015) Defect-tolerant diffusion channels for Mg2+ ions in ribbon-type borates: structural insights into potential battery cathodes $MgVBO_4$ and $MgxFe_2$–$xB_2O_5$. Chem Mater 27(13):4630–4639
138. Liu T, Zhang X, Xia M, Yu H, Peng N, Jiang C, Shui M, Xie Y, Yi TF, Shu J (2019) Functional cation defects engineering in $TiS_2$ for high-stability anode. Nano Energy 104295
139. Almeida AJ, Sahu A, Riedinger A, Norris DJ, Brandt MS, Stutzmann M, Pereira RN (2016) Charge trapping defects in CdSe nanocrystal quantum dots. J Phys Chem C 120(25):13763–13770

# Chapter 4
# Novel 2D Nanomaterial Composites Photocatalysts: Application in Degradation of Water Contaminants


**Mohd Saquib Tanweer and Masood Alam**

## 1 Introduction

The ubiquitous presence of residuals of organic contaminants such as toxic dyes and pharmaceuticals in wastewaters significantly poses an extreme damage to both flora and fauna including human health. Manufacturing industries related to textile, paper, bleaching, and leather tanning generate and discharge untreated dye effluents into water sources resulting in water pollution due to their recalcitrance nature. It gives the water an unpalatable color, reduces sunlight penetration and makes aquatic lives more resilient due to photochemical and biological threats. Besides, the pharmaceutical industries and hospitals are primarily accountable for the production and discharge of untreated antibiotic residues into natural water bodies. Tetracycline is the most widely used antibiotics in humans, veterinary and aquaculture medicine [1]. When environmental bacteria encounters with tetracycline residues, they develop changes in genes that make them resistant to stronger antibiotics, resulting in pathogenic strains. Several researchers have recently shown that these harmful contaminants can have detrimental effects on the aquatic environment, even at very minute levels [2]. Table 1 shows the classification of dyes based on their chemical structure and Table 2 shows possible impact of dyes and antibiotics on living systems in aquatic environment. Hence, the development of environmental remediation technologies to eliminate these toxic contaminants is on priority. Several technologies have recently been developed by the researchers to remediate the environmental pollution [3–6]. Among these technologies, photocatalysis has emerged as a very promising and eco-friendly technique for water purification [7]. Photocatalysis is a phenomenon

M. S. Tanweer · M. Alam (✉)
Environmental Science Research Lab, Department of Applied Sciences and Humanities, Faculty of Engineering and Technology, Jamia Millia Islamia, New Delhi 110025, India
e-mail: malam@jmi.ac.in

M. S. Tanweer
e-mail: saquibtanweer701@gmail.com



Z. Khanam et al. (eds.), *2D Nanomaterials for Energy and Environmental Sustainability*,
Materials Horizons: From Nature to Nanomaterials,
https://doi.org/10.1007/978-981-16-8538-5_4

**Table 1** Classification of dyes on the basis of chemical structure adapted from [16]

| Class | Chromospheres | Example |
|---|---|---|
| Azo dyes | 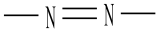 | 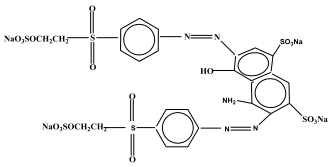 Reactive Black 5 |
| Anthraquinone dyes | 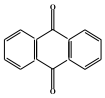 | 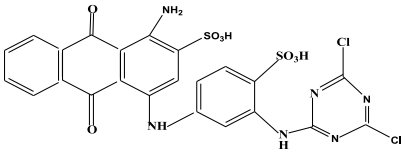 Reactive Blue 4 |
| Indigoid dyes | 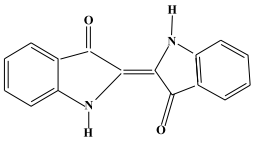 | 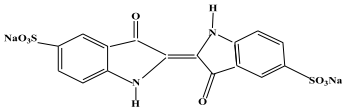 Acid blue 71 |
| Nitroso dyes | 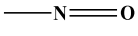 | 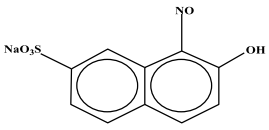 Acid green 1 |
| Nitro dyes | 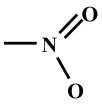 | 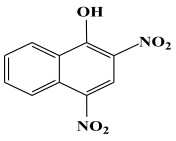 Acid Yellow 24 |
| Triarylmethane dyes | 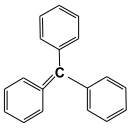 | 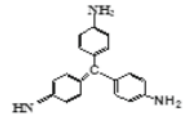 Basic Red 9 |

**Table 2** Impact on living system by residues of dyes and antibiotics in the aquatic environment

| Model contaminants | Impact on living system | References |
|---|---|---|
| Reactive dyes | Skin allergy | [22, 23] |
| Disperse blue 106 and 124 | Skin allergy | [24] |
| Orange II | Carcinogenic | [25] |
| Rose Bengal | Cytotoxic, cytostatic, genotoxic and mutagenic | [26, 27] |
| Eriochrome black T | Carcinogenic | [28] |
| Indigo carmine | Damaging the aquatic life | [29] |
| Malachite green | Carcinogenic effects in immune and reproductive system | [30] |
| Methyl violet | • Reduces photosynthesis reactions of aquatic plants<br>• Respiratory tracks injury, diarrhea, pain, vomiting, headache and dizziness<br>• Mutagenic and carcinogenic | [31–33] |
| Rhodamine B | Carcinogenic, neurotoxicity and chronic toxicity | [34] |
| Brilliant blue-R | Irritation to the skin, eyes, respiratory system | [35] |
| Crystal violet | Mitotic poisoning | [36] |
| Basic fuchsin | Severe eye, skin, gastrointestinal and respiratory tract irritation | [37] |
| Penicillin | Nephritis, eosinophilia, and haemolytic anaemia, impaired platelet aggregation | [38] |
| Chloramphenicol | Pancytopenia | [38] |
| Erythromycin | Headache, ototoxicity (deafness), ventricular arrhythmias | [38] |
| Ampicillin | Diarrhoea | [38] |
| β-Lactams | Drug fever, drug rash | [38] |
| Ciprofloxacin | Neuroexcitatory symptoms, tendon rupture | [39] |
| Levofloxacin | Genotoxicity | [40] |
| Gentamicin | Nephrotoxic | [41] |

which occurs when any light source interacts with the surface of any semiconductor materials, called photocatalysts. Generally, it is a two-step process. First, the process of oxidation takes place after the formation of photogenerated holes, and then finally, the process of reduction occurs after the generation of photogenerated electrons. Photocatalysts are responsible for capturing solar energy to degrade contaminants thus, making photocatalysis an economically viable treatment approach. The desire for innovative and robust photocatalysts led to the exploitation of nanomaterials that are now being used in every field of science and technology due to their excellent physicochemical properties. Till date, numerous types of nanomaterial photocatalysts such as CdS [7], ZnO [8], $TiO_2$ [8], and 2D nanomaterials [9, 10] have been developed and utilized to remediate the polluted water under UV irradiation, visible light and

sunlight. Among the nanomaterial photocatalysts, 2D nanomaterial photocatalysts based on MXene, TMDs and phosphorene are regarded as highly effective for the degradation of dyes and antibiotics, due to their exceptional physical and chemical properties.

With increasing interests in applications of 2D nanomaterial-based photocatalysts, we have focused to write an overview of the recent progress of 2D nanomaterial photocatalysts in eliminating the environmental pollution. This chapter discusses various types of water contaminants such as dyes and antibiotics and their impact on living systems including humans. The synthesis and properties of 2D nanomaterial-based catalysts are briefly discussed. The role of nanomaterial photocatalysts in the photocatalytic degradation of organic contaminants is also elaborated followed by a conclusion and future perspectives of the 2D nanomaterial-based photocatalysts.

## 2 Impact of Organic Contaminants on Living Systems

The term "contamination" in environmental chemistry is a synonym to pollution, where the primary focus is the damage done to living organisms and environment on a wide scale. Water contaminants may be suspended and dissolved chemicals (dye and antibiotic residues) or biologicals (pathogenic bacteria, virus, invasive species) in nature. In this chapter, we have briefly discussed organic contaminants in particular, organic dyes and antibiotics and their impact on living systems.

### *2.1 Organic Dyes*

Dyes are chemical compounds that are commonly used to color a variety of goods, including textile, leather, paper, rubber, plastics, etc. Unfortunately, the dye wastes enter the aqueous environment through the effluent and become a major source of water pollution due to its recalcitrant and non-biodegradable nature [11]. Presence of dye residues blocks the penetration of sunlight needed beneath water by aquatic lives for normal functioning of life-saving processes like respiration and photosynthesis [12]. Globally, $7 \times 10^5$ tonnes of organic dyes are produced annually, out of which more than 15–20% is discharged into aqueous environment [13]. Dyes can be classified according to structure, color and their application purposes (Table 1). On the other hand, dyes could also be categorized based on their dissolution of their particle charge in solution, namely, cationic (all basic dyes), anionic (direct, acid and reactive dyes) and non-ionic (dispersed dyes). Cationic dyes have high color strength and are visible even in minute concentrations [14, 15]. Dyes are very toxic and carcinogenic in nature. The presence of dyes in aquatic ecosystems can significantly affect photosynthesis reactions causing oxygen deficiency due to reduced penetration of sunlight; thereby affecting the viability of aquatic flora and fauna. Sardar et al. [13] reported

that dyes could also be teratogenic and mutagenic to various types of microbiological species and fishes.

Azo dyes can be anaerobically reduced to produce very toxic aromatic amines by the intestinal microflora and are proven to be a potential carcinogenic, and mutagenic in humans [17, 18]. In addition, it may also cause significant harms to humans, in the form of renal malfunction and sexual, liver, brain and central nervous system dysfunction [19]. Anthraquinone-containing dyes are the most resistant to degradation and its color persists in effluents for a longer time [20]. As reactive dyes are highly soluble in water, it is difficult to remove them from the effluent, thus causing serious harms to the environment [21]. Some reactive dyes form complexes with metals such as Cu, Cr, Co and Ni. When these metal-complexed dyes degrade, toxic heavy metals get free from the dyes and finally end up in the food chain leading to biomagnification. The use of different dyes has created a great concern because of their toxicity and adverse effects on the living systems (Table 2). Therefore, 2D nanomaterial-based photocatalysts are required for photocatalytic degradation of dyes from different types of wastewaters.

## *2.2 Antibiotics*

Selman Waksman coined the term Antibiotic in 1942. He described antibiotic as a substance produced by a microorganism that is antagonistic to the growth of other microorganisms. After the discovery of first antibiotic, viz., Penicillin by Alexander Fleming in 1928, a decent progress resulted in controlling a large variety of bacterial diseases [42]. A study reveals that approximately 90% of the antibiotics excreted by animals enter into the water sources directly or indirectly. A data published in year 2013 by World Health Organization states that out of the total antibiotic's consumption of two lakh tons per year, 80% of it is consumed for veterinary use alone. It thus recognizes animal husbandry as the primary cause for developing antibacterial resistance. It is further estimated that by the year 2050, the diseases caused by multi-resistant bacteria can engulf about 10 million people per year worldwide [43]. Besides toxicity, the antibiotics have an advantage to control infectious diseases. It is, therefore, an important factor for the abuse of antibiotics. Rise in the consumption of antibiotics causes more resistance by bacteria and therefore, more harm. The inoculation of antibiotics in aqueous media is largely because of intensive farming throughout the world as food sector is considered the fastest growing industry. As a result of it, sewage and water treatment plants contain an abundant quantity of antibiotics of pharmaceutical origin [44]. Different types of antibiotics, namely, Fluoroquinolones, sulphamethoxazole, lincomycin, trimethoprim, sulphonamides and beta-lactams have been found in hospital effluents in large quantities with 35,500 ng/L detection rate [45]. Other sources of antibiotics include veterinary, pharmaceutical plants, animal excreta, dairies, municipal wastes, animal husbandry and poultry industries [46]. The antibiotic pollution not only disturbs microbial populations but also badly effects human lives (Table 2). Since, there is an

antagonistic effect of antibiotics, a long-term exposure even of very low concentration could alter drinking water, food and other consumer goods. Triclosan is an antimicrobial agent that is largely present in soaps and clothes causing reproductive problems and muscle weakness. About 75% of US population is exposed to triclosan or other antibiotics through consumer goods [47]. Tetracycline causes gastrointestinal effects like vomiting, nausea and diarrhea. It changes the normal intestinal flora that stops coliform organisms. Vaginal candidiasis is also reported due to unintended uptake of tetracycline. The patients with pre-developed hepatic insufficiency are likely to face liver toxicity [48]. In sewage treatment plants, antibiotics are only partly removed. During the water treatment process, antibiotics pass through the sewage plant and end up in the aqueous environment. Therefore, there is an urgent need for the complete removal of antibiotics residues from sewage water effluents. Previous studies show that 2D nanomaterial-based photocatalysts could be a better option to remediate the environment [49, 50].

## 3 Preparation and Properties of 2D Nanomaterial-Based Photocatalysts

Photocatalysis has received great attention as an exciting and promising replacement for conventional water purification technologies to remove waterborne contaminants. 2D nanomaterial-based photocatalysts have shown great potential in photocatalysis field because of their unique optical, electronic and physicochemical properties. In the past decade, graphene-based photocatalysts were the most extensively studied 2D nanomaterial-based photocatalysts. The rapid development of graphene-based photocatalysts motivated many researchers in exploring their potential in 2D nanomaterial-based photocatalysts for photocatalysis applications. Generally, two types of synthetic strategies are reported, namely (a) in situ growth and (b) ex situ assembly method. In case of in situ growth, low dimensional nanomaterial is either directly grown on the surface of the 2D materials (template) or the 2D materials are developed in the presence of low dimensional nanomaterials. While in ex situ assembly method, nanomaterials are pre-synthesized with defined compositions, shape and size then mixed with 2D nanomaterials through covalent or non-covalent interactions. In situ methods, which include one-step in-situ calcination [51], hydrothermal [52, 53] or solvothermal methods [54] are employed to synthesize 2D nanomaterial-based photocatalysts. Shen et al. [54] synthesized $CeO_2$/$Ti_3C_2$-MXene hybrids by in-situ growth of cube-like $CeO_2$ onto 2D ultrathin $Ti_3C_2$-MXene nanosheets via simple hydrothermal route. The close contact between in situ grown $CeO_2$ and 2D $Ti_3C_2$-MXene nanosheets generated a built-in electric field which induces Schottky junction favoring the charge transfer from $CeO_2$ to 2D $Ti_3C_2$-MXene nanosheets. It enhanced the separation efficiency and subsequently increased the photocatalytic activity. Novel flower-like $WS_2$/$Bi_2O_2CO_3$ photocatalysts were developed via one-pot hydrothermal approach [53]. Flower-like heterojunctions

showed synergistic effects between the enhanced separation efficiency of photo-induced charge carriers and a high specific surface area (SSA) thereby, improving the photocatalytic degradation activity. 2D TMDs-based photocatalysts possess various properties such as quantum confinement effect with rearranged energy levels, large SSA and the variation of the electronic band structure which are considered appropriate for the activation of the photocatalytic process. The introduction of ZnO during synthesis of $ZnO/MoS_2$ photocatalyst results in an increase of photocatalytic properties because of the enhanced interfacial charge transfer and absorption strength in UV region, large SSA and favorable in-plane carrier transport [55]. The photocatalytic properties of 2D TMDs-based photocatalysts can be enhanced by loading of TMDs as co-catalysts on semiconductors/metal-semiconductors which produce junctions and a greater number of interfaces. Bahadur et al. [56] successfully improved the photocatalytic properties of $Ag_3PO_4/MoS_2$ after loading of $MoS_2$ as co-catalyst in comparison to pristine $Ag_3PO_4$ nanoparticles. It has been reported that about 97.6% MB dyes were degraded by $Ag_3PO_4/MoS_2$ within 15 min in the presence of visible light illumination. Authors have reported that the rate of photocatalytic degradation of MB using $Ag_3PO_4/MoS_2$ could further be enhanced. The photocatalytic enhancement resulted due to interfacial energy band (conduction band (CB) and valence band (VB)) alignment between $MoS_2$ sheets, and $Ag_3PO_4$ nanoparticles, increased electron–hole pair separation, uniform distribution of $Ag_3PO_4$ nanoparticles (5.4 nm) and large SSA of $MoS_2$. 2D MXene-based photocatalysts have recently drawn the attention of several researchers due to their exceptional electrical conductivity, large SSA, tunable band gap and hydrophilic behavior. In 2D MXene-based photocatalysts, MXenes are used as a substrate to support one or more catalyst materials to gain higher photocatalytic property. Improvement in Schottky barriers with different composition of MXenes heterostructures are efficient and unambiguous ways to accelerate the photocatalytic activity. Shahzad et al. [57] demonstrated a facile hydrothermal treatment strategy to produce a hybrid photocatalyst based on $Ti_3C_2T_x$ (MXene) nanoflakes $TiO_2$/MXene. The photocatalytic property of $TiO_2$/MXene was significantly enhanced due to construction of a Schottky barrier between interfaces of $TiO_2$-MXene.

## 4 Application of 2D Nanomaterial Photocatalysts in Water and Wastewater Treatment

### *4.1 Mechanism of Photocatalytic Degradation*

In the photodegradation of organic contaminants such as organic dyes and antibiotics, both electrons and holes play a pivotal part. The first step in the photocatalytic degradation is the segregation of electrons and holes. Photogenerated electrons captured by oxygen molecules to produce superoxide radicals ($\cdot O_2^-$) make

them capable of taking part in photocatalytic degradation process. In the meantime, photogenerated holes are bonded with surficial hydroxyl groups or adsorbed water molecules to readily produce hydroxyl radicals (·OH), which are oxidative in nature and participate in degradation of environmental contaminants. Therefore, it can be said that the engagement of photogenerated electrons holes and radicals like superoxides and hydroxides are solely responsible for photocatalytic degradation of environmental contaminants. Meenakshi et al. [58] developed a novel 2D/2D heterojunction of Z-scheme Chitosan@g-$C_3N_4$/MXene (CS@g-$C_3N_4$/MX) hybrid composite via one-pot hydrothermal reaction. The construction of the heterojunction increases the separation of photogenerated charge carriers which facilitates charge transmission-bridge along Z-scheme heterojunction resulting in increased photodegradation of organic contaminants (MB and RhB). The process of charge separation and its transmission is shown in Fig. 1a. The inclusion of chitosan (CS) in between g-$C_3N_4$ (PS-II) and MXene (PS-I) leads to the formation of photogenerated electrons and holes, which hinder the recombination of electron and hole pairs. This substantially increases the photocatalytic degradation rate of MB (99.1%) and RhB (98.5%). A possible Z-scheme photocatalytic mechanism has been proposed for the Chitosan@g-$C_3N_4$/MXene heterojunction. The main reaction steps are depicted as follows:

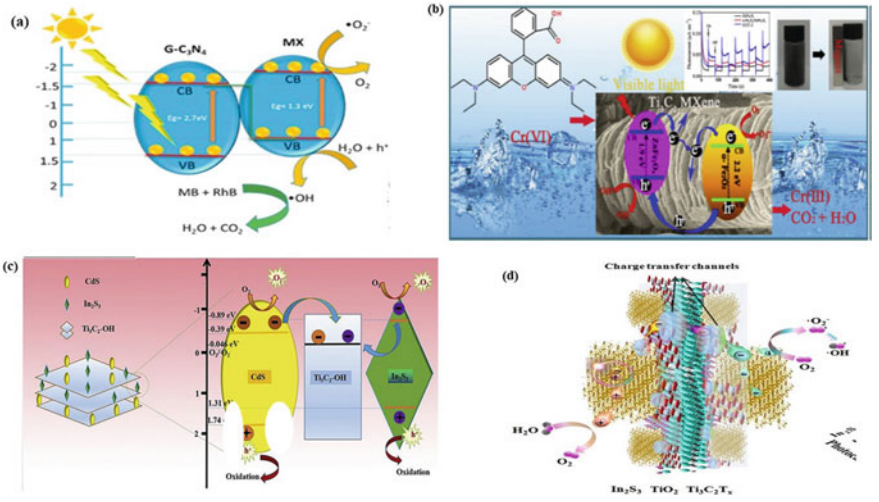


**Fig. 1** **a** Schematic illustration of the possible separation of charge carriers during the photocatalytic degradation of MB and RhB in the Vis/Chitosan@g-$C_3N_4$/MXene hybrid composite system. Reprinted with permission from [58]. Copyright 2018, Elsevier; **b** schematic mechanism of magnetic α-$Fe_2O_3$/$ZnFe_2O_4$@$Ti_3C_2$ MXene photocatalyst. Reprinted with permission from [63]. Copyright 2019, Elsevier; **c** photocatalytic mechanisms of the $Ti_3C_2$–OH/$In_2S_3$/CdS composites, Reprinted with permission from [66]. Copyright 2019, Elsevier; and **d** proposed mechanism for pollutant degradation in the InTi-16 system under visible light illumination, Reprinted with permission from [65]. Copyright 2018, Elsevier

$$\mathrm{CS@g\text{-}C_3N_4/MX} \overset{h\nu}{\rightarrow} \left(\mathrm{h^+ + e^-}\right)\mathrm{CS@g\text{-}C_3N_4/MX}$$

$$\mathrm{H_2O + e^- + h^+ \rightarrow 2 \cdot OH}$$

$$\mathrm{H_2O_2 \rightarrow \cdot OH + \cdot OH}$$

$$\mathrm{H_2O_2 + \cdot OH \rightarrow \cdot OOH + H_2O}$$

$$\mathrm{CS@g\text{ - }C_3N_4/MX + dyes \rightarrow OH + \cdot O_2^-}$$

$$\mathrm{MB + RhB + (\cdot OH + \cdot O_2 \text{ and } H_2O_2) \rightarrow H_2O + CO_2 + Intermediates}$$

In another investigation, Wu et al. [51] developed a highly photoactive Z-type heterojunction catalyst with a graphene layer embedded $TiO_2$/g-$C_3N_4$ (GTOCN) photocatalyst via one-step in-situ calcination of $Ti_3C_2$. In between graphene, $TiO_2$ and g-$C_3N_4$, solid phase interaction occurs to segregate photogenerated electrons and holes. The aggregation of g-$C_3N_4$ electrons with high reduction capability and $TiO_2$ holes with high oxidation activity occur. Organic contaminants such as tetracycline (TC) and ciprofloxacin (CIP), bisphenol A (BPA) and rhodamine B (RhB) have shown tremendously high degradation rate under visible light irradiation. The as-prepared GTOCN photocatalyst presented substantial enhancement due to visible light absorption and photogenerated charge carrier segregation. The single-electron O-vacancy of GTOCN photocatalyst generated at a modest calcination temperature is the foremost accountability for enhancing its photocatalytic activity and contaminant degradation stability.

## *4.2 MXenes-Based Photocatalysts*

MXenes are among the latest addition to the family of 2D transition metal carbides, nitrides and/ or carbonitrides with the general formula $M_{n+1}X_nT_x$, where M is an early transition metal (e.g., Ti, Zr, V, Nb, Ta, or Mo), X is carbon and/or nitrogen, and $T_x$ denotes the surficial functional groups of MXene. Over the past decade, more than 20 varieties of MXene materials have been synthesized in laboratory, including $Ti_3C_2$, TiNbC, $Ti_2C$, $V_2C$, $Nb_4C_3$ and $Mo_2C$ [59–75]. 2D MXenes photocatalysts proved to be a model material for the photocatalytic degradation process because of their excellent electronic and optical properties along with excellent surface functionality [59–77].

***Degradation of organic dyes***: Gogotsi et al. [61] investigated the photocatalytic properties of $Ti_3C_2T_x$ for the degradation of cationic methylene blue (MB) and anionic acid blue 80 (AB80). The presence of surficial functional groups like –OH

and –F makes MXene negatively charged in water, thus enabling cationic methylene blue to be adsorbed more favorably than anionic acid blue 80. Therefore, MB can be firmly bound with $Ti_3C_2T_x$, while AB80 suffered to adsorb. Within 5 h, MB was degraded by 81% under UV irradiation, while only 18% of MB degraded in the dark. In the same manner, within 5 h, 62% of AB80 was degraded under UV irradiation, whereas no degradation took place in the dark, even after 24 h. The formation of titanium tetrahydroxide and titanium dioxide triggers the photocatalytic effect on the surface of MXene under UV irradiation. The intimate contact of MXene to dissolved $O_2$ in water for a long period facilitates MXene's surface to oxidize to form $TiO_2$. As a result, MB degradation is enhanced in the dark and speeding up photodegradation under UV illumination. In another study, $TiO_2/Ti_3C_2$ photocatalysts were successfully synthesized and efficiently used to degrade MB under UV irradiation. This can be mainly attributed to hole-electron segregation of the $TiO_2/Ti_3C_2$ composite under UV light [62]. Zhang et al. [63] ultrasonically fabricated $\alpha$-$Fe_2O_3/ZnFe_2O_4@Ti_3C_2$ MXene photocatalyst through a simple self-assembly method. The well distributed and incorporated $Fe_2O_3$ nanoparticles on the surface of MXene can effectively use visible light, resulting in successfully photocatalytic degradation of rhodamine B (RhB) and Cr(VI) adsorption. It is mainly due to properties like high charge-transfer rate, numerous heterostructure interfaces, high conductivity and charge separation efficiency. Figure 1b displays the possible photocatalytic mechanism of $\alpha$-$Fe_2O_3/ZnFe_2O_4@Ti_3C_2$ MXene.

Undoubtedly, metal sulfides such as CdS, ZnS and $In_2S_3$ (Indium sulfide) perform a critical role in the application of photocatalytic degradation [64–66]. To gain super-efficient photocatalysis of metal sulfides, visible-light-driven ternary $Ti_3C_2$–OH/$ln_2S_3$/CdS composites were constructed by Pan and coworkers [66] using hydrothermal method. $Ti_3C_2$–OH/$ln_2S_3$/CdS composites with 4-weight percentage of $Ti_3C_2$–OH are in spherical shape; have larger surface area thus providing more active sites for better degradation of selected contaminants. In addition, excellent electrical property of $Ti_3C_2$–OH and close contact between $Ti_3C_2$–OH, $ln_2S_3$ and CdS boost the degradation performance of $Ti_3C_2$–OH/$ln_2S_3$/CdS composites. Figure 1c illustrates the photocatalytic mechanisms of $Ti_3C_2$–OH/$In_2S_3$/CdS composites. To check the photocatalytic performance of another ternary mesoporous catalyst, $In_2S_3$/anatase$TiO_2@Ti_3C_2T_x$ [65] composites were investigated by degrading methyl orange and tetracycline hydrochloride. The degradation reaction constant of hybrid photocatalyst (InTi-16: $Ti_3C_2T_x$ content 16 mg) possessed higher activity than bare $In_2S_3$ and $Ti_3C_2T_x$. For this quasi-core–shell photocatalyst framework, MXene and derived $TiO_2$ served as unique and novel methods for the embedment of $In_2S_3$. MXene's surface and its edge paved with plentiful asymmetrical $In_2S_3$. The Schottky barrier formed between $In_2S_3$, $TiO_2$ and $Ti_3C_2T_x$ facilitates multiple channels for the migration of photoinduced electrons (Fig. 1d). Upon exposure to visible light, the electrons of $In_2S_3$ are excited and transferred to $TiO_2$ along the heterojunction. In addition, the Schottky barrier between $TiO_2$ and $Ti_3C_2T_x$ enhanced the charge segregation and migration and inhibited the back diffusion of electrons.

***Degradation of antibiotics***: $Ti_3C_2$-MXene is recognized as a promising noble-metal-free co-catalyst to produce effective photocatalysts for the degradation of pharmaceutical contaminants. For instance, on ultrathin $Ti_3C_2$-MXene nanosheets cube-like $CeO_2$ has been grown to form $CeO_2/Ti_3C_2$-MXene hybrids [52] by a facile hydrothermal method. The $CeO_2/Ti_3C_2$-MXene hybrid with the optimum weight percentage of $Ti_3C_2$-MXene showed efficient photocatalytic degradation of tetracycline and $CO_2$ reduction under sunlight illumination. The photocatalytic degradation by hybrid material is greater than bare $CeO_2$. The photocatalytic degradation of hybrid material increased due to Schottky junction in between $CeO_2$ and $Ti_3C_2$-MXene that was triggered by built-in electric field. It leads to transfer of photoinduced electrons from $CeO_2$ to $Ti_3C_2$-MXene, thus causing the separation between electrons and holes. Shen et al. [67] developed ternary MXene-based Z-scheme composite, namely, $CdS@Ti_3C_2@TiO_2$ nanohybrids through a simple calcination method followed by hydrothermal method. The as-prepared nanostructure was employed for efficient degradation of sulfachloropyridazine, methylene blue, rhodamine B and phenol under visible light illumination. The $CdS@Ti_3C_2@TiO_2$ nanohybrids with 2:1 ratio showed 100% degradation for selected model contaminants under visible light irradiation. The increased photocatalytic degradation of organic contaminants is due to "sink" effect of MXene together with well-defined band gap of $CdS@Ti_3C_2@TiO_2$ nanohybrids. The photogenerated charge electron and hole pairs in the Z-scheme type photocatalyst are segregated in efficient manner which successively produce free radicals such as $\cdot O_2^-$ and ·OH that play pivotal roles in oxidizing the organic contaminants. Various 2D MXene-based photocatalysts used in degradation are listed in Table 3.

## *4.3 TMDs-Based Photocatalysts*

Transition metal dichalcogenides (TMDs) are comprised of hexagonal metal atom (M) layers sandwiched between the layers of chalcogen (S, Se and Te) with a general formula $MX_2$. TMDs possess various properties associated with their compositional formulation. Among TMDs, $MoS_2$ and $WS_2$ are the most widely used for photocatalytic degradation due to their robust nature and easy availability of raw materials [53–55, 78–80].

***Degradation of organic dyes***: Generally, TMDs are used as co-catalysts embedded on semiconductors to form junctions between them, thereby, facilitating charge transport of the photogenerated charge carriers such as electrons and holes. Yu et al. [79] have successfully developed flower-like $MoS_2/BiVO_4$ composite by two-step approach. The coupling of $MoS_2$ with $BiVO_4$ significantly enhanced the photocatalytic performance of MB (94.2%) degradation compared with bare $MoS_2$ and $BiVO_4$ in the presence of visible light irradiation. This can be attributed to a special charge-transfer mechanism. Since, the conduction band (CB) and valence band (VB) of $BiVO_4$ lie below the energy bands of $MoS_2$, the migration of excited photogenerated electrons

**Table 3** 2D nanomaterial-based photocatalysts for degradation of contaminants

| 2D nanomaterial photocatalyst | Target contaminants | Removal capacity | Morphology | References |
|---|---|---|---|---|
| *MXenes* | | | | |
| a-$Fe_2O_3/Ti_3C_2$ | Rhodamine B | 98% | Nanosheets/nanosheets | [68] |
| $CeO_2/Ti_3C_2$-MXene | Tetracycline | 80.2% | Cubic/nanosheets | [52] |
| g-$C_3N_4/Ti_3C_2$ | Ciprofloxacin | – | Nanosheets/nanosheets | [69] |
| MXene-$Co_3O_4$ | Methylene blue and Rhodamine B | 128.91 mg/g (MB), 47.076 mg/g (RhB) | Nanosheets/cubic particle | [70] |
| Sm-doped g-$C_3N_4/Ti_3C_2$ MXene | Ciprofloxacin | More than 99% | Hollow porous seaweed/nanosheets | [71] |
| $CuFe_2O_4$/MXene | Sulfamethazine | 59.4% | Nanoparticles/nanosheets | [72] |
| (001)$TiO_2/Ti_3C_2$ | Methyl orange | 97.4% | Nanosheets/nanosheets | [73] |
| $Bi_3TaO_7/Ti_3C_2$ | Methylene blue | 99% | Nanoparticles/nanosheets | [74] |
| $Ti_3C_2$-Bi/BiOCl | Ciprofloxacin | 89% | Nanosheets/microspheres | [75] |
| $Ti_3C_2$/g-$C_3N_4$ | Diclofenac | 100% | Nanosheets/nanosheets | [76] |
| $TiO_2/Ti_3C_2$ | Rhodamine B | 95% | Nanorods/nanoparticles | [77] |
| *TMDs* | | | | |
| $MoS_2/TiO_2$ | Rhodamine B | 98.2% | Nanosheets/nanofibers | [78] |
| $MoS_2/BiVO_4$ | Methylene blue | 94.2% | Nanoflower | [79] |
| $MoS_2/Bi_2WO_6$ | Methylene blue | 82% | Core–shell heterostructure | [80] |
| $WS_2/Bi_2O_2CO_3$ | Lanasol Red 5B | 91% | Nanoflower | [53] |
| $WS_2/Bi_2O_2CO_3$ | Ciprofloxacin | 95% | Nanoflower | [53] |
| $WSe_2$/RGO | Rhodamine B | – | Nanosheets/nanosheets | [54] |
| ZnO/$MoS_2$ | Tetracycline | – | Nanosheets | [55] |
| ZnO/$MoS_2$ | Methylene blue, Rhodamine B | More than 90% for both | Nanosheets | [55] |

take place to CB of $BiVO_4$ and holes to VB of $MoS_2$. Thus, photocatalysis reactions occur. In addition, the segregation of photogenerated charge carriers enhances the photocatalytic degradation reactions. Xiao et al. [81] have fabricated a novel 2D/2D heterostructure composite, namely, 1T/2H $MoSe_2$/pg-$C_3N_4$ with Z-scheme heterojunction in two steps. First, 1T/2H $MoSe_2$ is developed in an orderly manner using $NaBH_4$-assisted hydrothermal method. Second, 1T/2H $MoSe_2$ with different weight percentage gets embedded as co-catalyst on proton g-$C_3N_4$to produce final product through solvothermal strategy. The coupling of 1T/2H $MoSe_2$ (1 wt%) with proton g-$C_3N_4$ significantly improved the photocatalytic degradation of tetracycline and rhodamine B degradation under solar light irradiation, which is more than pristine

1T/2H $MoSe_2$ and proton g-$C_3N_4$. This is because of a narrow band gap, surplus active sites, excellent photocurrent response and conductivity of 1T/2H $MoSe_2$/pg-$C_3N_4$. Figure 2a illustrates the synthesis and Z-scheme photocatalytic mechanism of 1T/2H $MoSe_2$/pg-$C_3N_4$. A 2D photocatalyst phosphorene/$MoS_2$ hybrid was developed by liquid exfoliation procedure. The as-prepared nanocomposites were employed for the photocatalytic decomposition of Congo red (CR), Methylene blue (MB) and Methyl orange (MO) dyes in the presence of UV illumination. The results indicated that the synthesized photocatalysts have a very high photocatalytic efficiency at a very low concentration (0.58 ppm). This can be attributed mainly to an increase in energy band gap, large specific surface area, interfacial charge transfer and spatial separation [82].

***Degradation of antibiotics***: TMDs are another type of 2D nanomaterials that are often employed to degrade antibiotics (Table 3). For example, NiS and $MoS_2$ nanosheet co-modified graphitic $C_3N_4$ (NiS/$MoS_2$/g-$C_3N_4$ hybrids) ternary heterostructures were synthesized through hydrothermal method followed by ultrasound method (Fig. 2b). The NiS/$MoS_2$/g-$C_3N_4$ hybrids were applied to photodegrade antibiotics like ciprofloxacin and tetracycline hydrochloride under the visible light. After 2 h visible light irradiation, the optimum photodegradation rate of the NiS/$MoS_2$/g-$C_3N_4$ hybrids exceeds approximately 96%, which is 2.1 times greater than that of bare g-$C_3N_4$ for tetracycline hydrochloride degradation. The higher rate of photocatalytic

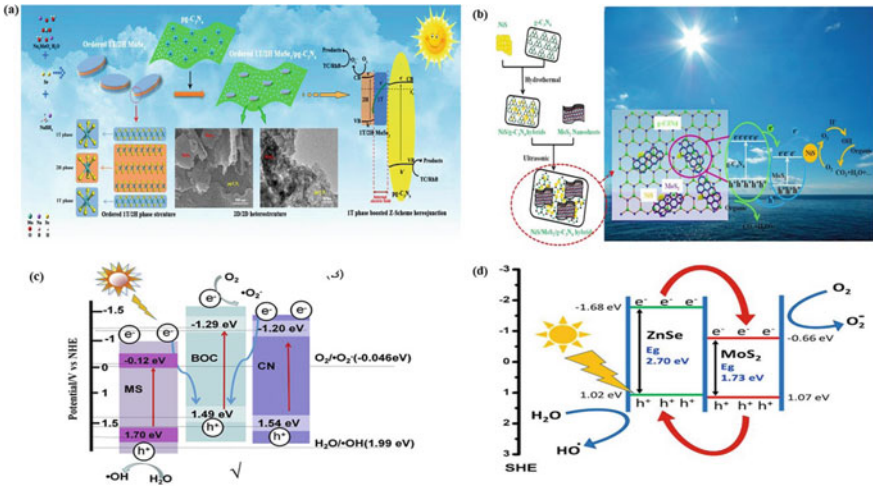


**Fig. 2** **a** Illustrates the synthesis and Z-scheme photocatalytic mechanism of 1T/2H $MoSe_2$/pg-$C_3N_4$. Reprinted with permission from [81]. Copyright 2020, Elsevier; **b** displays the photocatalytic degradation mechanism of NiS/$MoS_2$/g-$C_3N_4$ hybrids. Reprinted with permission from [83]. Copyright 2018, Elsevier; **c** the possible steps of the photocatalytic process and the charge-transfer mechanism in the CN/MS/BOC composite. Reprinted with permission from [84]. Copyright 2020, Elsevier; and **d** schematic illustration of alignment of the energy level of 3:1 $MoS_2$/ZnSe nanocomposite. Reprinted with permission from [85]. Copyright ***Catalysts*** 2020, MDPI

degradation is mainly attributed to enhanced visible light harness and charge separation efficiency. Figure 2b displays the photocatalytic degradation mechanism of NiS/$MoS_2$/g-$C_3N_4$ hybrids [83]. Very recently, dual Z-scheme ternary heterojunction photocatalysts, namely, g-$C_3N_4$/$MoS_2$/$Bi_{24}O_{31}Cl_{10}$ (CN/MS/BOC) composite were developed by Wang et al. [84] via impregnation-calcination method. The as-prepared CN/MS/BOC composite exhibited a superb and durable photocatalytic performance in the decontamination of tetracycline under the visible light. The photocatalytic degradation rate of CN/MS/BOC was 97.5% for tetracycline after 50 min under visible light irradiation, which was 5.38, 1.96 and 2.51 times more than that that of BOC, CN/BOC and MS/BOC catalysts, respectively. The high rate of photocatalytic degradation is due to enhanced optical absorption, increase in separation, transportation of the electron–hole pairs and robust redox competence resulting from the dual Z-scheme heterostructure of CN/MS/BOC. The possible steps of the photocatalytic process and the charge-transfer mechanism in the CN/MS/BOC composite are shown in Fig. 2c. In another study, photocatalytic activity of $MoS_2$/ZnSe heterostructures [85] was investigated to degrade levofloxacin under visible light irradiation. $MoS_2$/ZnSe nanocomposites were synthesized by a facile ultrasonication method. The results showed that the degradation activity of $MoS_2$/ZnSe nanocomposites was 73.2% for levofloxacin, whereas bare $MoS_2$ and ZnSe degraded levofloxacin only about 29 and 17.1%, respectively, in 2 h under visible light. The synergistic interaction between $MoS_2$ and ZnSe produces superoxide and hydroxide radicals subsequently accounting for levofloxacin degradation in the $MoS_2$/ZnSe process (Fig. 2d). Various TMDs-based photocatalysts used in degradation are listed in Table 3.

### *4.4 Phosphorene-Based Photocatalysts*

Phosphorene is a new family member of 2D nanomaterials. It has characteristic properties like extraordinary carrier mobility, excellent optical and better absorption in the range of ultraviolet along with a tunable bandgap that depends on the number of layers. Additionally, phosphorene materials are remarkably anisotropic due to the presence of two different P-P bond lengths [86]. Because of these characteristics phosphorene has fascinated significant attention in a variety of fields such as electronic, optical, and sensing [87, 88]. Like graphene, phosphorene exhibits much higher surface-to-volume ratio due to its "puckered" lattice structure [89]. The above-mentioned properties can make a material to be a potential photocatalyst.

***Degradation of organic dyes***: The photocatalytic activity of phosphorene can be enhanced by improving interfacial charge relocation and segregation of the photoinduced charges. Farbod and coworkers developed few-layered black phosphorus (FL-BP) nanosheets by exfoliation of bulk black phosphorus in an organic solvent such as N-Methyl-2-Pyrrolidone (NMP) using ultrasonication. FL-BP exhibited direct band gap and high stability in NMP which was chosen as a suitable solvent to prevent oxidation of black phosphorus. Author investigated the photocatalytic performance

of FL-BP to reduce dyes such as Congo red, methylene blue and methyl orange under UV light irradiation. It has been reported that small amount of FL-BP (4.5 mg/L) is enough to degrade the model dyes [90]. The same author has designed a 2D semiconductor hybrid, namely, phosphorene/$MoS_2$ to enhance their photocatalytic activity [82]. In this investigation, phosphorene/$MoS_2$ was prepared by liquid-phase exfoliation method and its photocatalytic activity in degradation of Congo red, methylene blue and methyl orange dyes under UV radiation was checked. Upon UV light irradiation, model dyes and phosphorene/$MoS_2$ photocatalyst start to generate electrons and holes in CB and VB of hybrid semiconductors. The photoinduced electrons and holes react with NMP to produce free radicals such as $\cdot CH_3^+$, $\cdot O_2^-$ and $H^+$ ions (Fig. 3a). Further, these free radicals start to decompose model dyes and convert them into harmless species. Additionally, photoinduced electrons and holes segregate in lower energy levels, inhibit recombination rate and increase their lifetime, consequently further enhancing degradation efficiency of phosphorene/$MoS_2$ photocatalyst. Semiconductor like ZnO was coupled with black phosphorus for pollutant degradation. For example, Liu et al. [91] developed the black phosphorus nanosheets-ZnO nanohybrid (BPNs-ZnO nanohybrid) through a facile one-step co-precipitation method. BPNs-ZnO nanohybrid showed excellent photocatalytic degradation for methylene blue (dye) and ciprofloxacin (antibiotic) under visible light illumination. The BPNs-ZnO nanohybrid exhibited better photocatalytic degradation in comparison to bare BPNs,

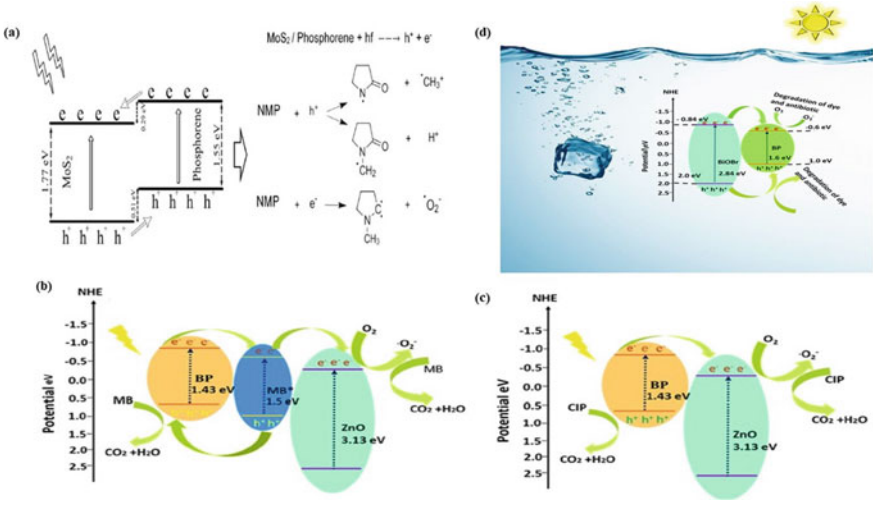


**Fig. 3** **a** Schematic illustration for the band structure of phosphorene/$MoS_2$ 2D system and the proposed mechanism of electron-holes generation and producing free radicals by NMP. Reprinted with permission from [82]. Copyright 2021, Elsevier; **b, c** illustrates the proposed mechanisms for degradation of MB and CIP by BPNs-ZnO nanohybrid. Reprinted with permission from [91]. Copyright 2019, Elsevier; and **d** schematic representation of photocatalytic performance of BPNs-BiOBr photocatalysts. Reprinted with permission from [96]. Copyright 2021, Elsevier

ZnO and the bulk black phosphorus. Data showed that recombination rate of photoinduced charge carriers is effectively suppressed, and segregation of charge carriers occurs by BPNs-ZnO nanohybrid. This causes photocatalytic degradation of selected pollutants. Further, photodegradation efficiency of BPNs-ZnO can be attributed to large specific surface area of composites, enhanced optical adsorption of visible light for BPNs-ZnO nanohybrid and suitable band gap between BPNs and ZnO. Figure 3b, c illustrate the proposed mechanisms for the degradation of MB and CIP by BPNs-ZnO nanohybrid. Shen et al. [92] prepared a double phosphorus-based semiconductor composite BP/RP (black phosphorus/red phosphorus) and chose rhodamine B (RhB) as the target contaminant to evaluate its photocatalytic efficiency. The results revealed that BP/RP heterojunction exhibited the efficient degradation for RhB (89%) in 30 min under visible light illumination. Whereas after increasing reaction time to 120 min, the RhB removal enhanced and the maximum amount of RhB (97%) degraded. The results also revealed that in the first 30 min illumination, the BP/RP (89%) heterostructure photocatalyst showed higher catalytic degradation rate than CdS (32%) for RhB removal. Another advantage of using phosphorus as a photocatalyst over CdS is that phosphorus does not release toxic metals during photocatalysis reaction. The BP/RP heterostructure showed more absorption of visible light leading to segregation of photoinduced charge carriers. Consequently, photocatalytic activity of BP/RP nanocomposites was increased.

***Degradation of antibiotics***: For the first time, silver nanoparticle was loaded on black phosphorus to prepare AgNPs@BP with more active sites using ultrasonication followed by centrifugation [93]. The photocatalytic efficiency of AgNPs@BP was investigated to degrade norfloxacin in wastewater under near infrared (NIR) light illumination. The resulting data revealed that 85% of model pollutants quickly got photo-catalytically degraded. The increased photocatalytic efficiency of AgNPs@BP nanocomposite can be attributed to the sensitization of black phosphorus nanosheets by completely harvesting of NIR light and high electron–hole segregation capability. Interestingly, AgNPs@BP exhibited no reduction in photocatalytic activity even after five cycles of pollutant degradation. Bismuth oxyhalide (BiOX) is a common catalytic material and finds a special position in the field of photocatalysis due to its eco-friendly nature, compatible energy band and non-toxic properties [75, 94, 95]. To solve the problem of capturing the full spectrum of solar light, Li et al. [96] developed black phosphorus nanosheets/BiOBr (BPNs-BiOBr) nanocomposites through one-step co-precipitation technique. BPNs-BiOBr photocatalysts presented a remarkable photocatalytic performance toward methyl orange and ciprofloxacin degradation under visible light illumination (Fig. 3d). The nanocomposites displayed better degradation capability as compared to pure BPNs and BiOBr. The type I BPNs-BiOBr nanocomposites (with 15 ml of BPNs dispersion) exhibited higher BET surface area than BiOBr indicating that there were more active sites on BPNs-BiOBr. The photostability of black phosphorus nanosheets (BPN) was enhanced by passivation effect of poly dimethyldiallyl ammonium chloride (PPDA). The enhanced photocatalytic efficiency of BPNs-BiOBr photocatalysts was mainly derived due to

the Type-I bandgap configuration, the increased light absorption and the huge surface area.

## 5 Conclusions and Future Outlooks

The chapter summarizes the progress of 2D MXene-based photocatalysts, TMDs-based photocatalysts and phosphorene-based photocatalysts for their application in degradation of dyes and antibiotics. Types of common water pollutants such as organic dyes and pharmaceutical residues and their effect on living systems are briefly studied. Moreover, the application of MXene, TMDs and phosphorene as photocatalysts in the photocatalytic field and degradation of water-borne organic contaminants is systematically studied. Though more than 20 forms of MXene nanomaterials have been discovered, yet only a few of them, such as $Ti_3C_2$, TiNbC, $Nb_2C$, $Nb_4C_3$, $Mo_2C$, $Ti_2C$ and $V_2C$ are commonly used as photocatalyst nanomaterials. Therefore, theoretical study must be implemented for the efficient designing of MXene-based photocatalysts. This approach will help to identify possible structural behavior and deep insights of photocatalytic reaction at micro level. Doping and surface functionalization of 2D nanomaterial-based photocatalysts affect its electronic and optoelectronics properties, thus enhancing photocatalytic performance. As so far, fundamental theoretical investigations can be done. 2D nanomaterial-based photocatalysts must be low cost. Additionally, it is also important to understand the effect of 2D nanomaterial photocatalysts on energy and the environment. The 2D nanomaterial-based photocatalysts which are discussed in this chapter are efficient photocatalytic semiconductors. However, there are several challenges that still exit to produce nanocatalyst with long-term stability. A robust and detailed assessment of ecotoxicity and life cycle study of these nanomaterials is needed to be conducted. The 2D/2D heterostructures show higher stability and intimate interfaces that facilitate photogenerated charge migration and segregation. As the synergistic effects of 2D/2D heterostructures are presently less studied, new designs of 2D/2D heterostructures with exceptional photocatalytic activity must be studied. All in all, many opportunities remain awaited for researchers to explore possibilities of new insight into 2D nanomaterials in various fields in the near future.

**Acknowledgements** One of the authors, Tanweer S. M. thankful to the University Grants Commission (UGC) for the Non-NET Fellowship.

## References

1. Gao P, Mao D, Luo Y et al (2012) Occurrence of sulfonamide and tetracycline-resistant bacteria and resistance genes in aquaculture environment. Water Res. https://doi.org/10.1016/j.watres.2012.02.004

2. Bilal M, Mehmood S, Rasheed T, Iqbal HMN (2020) Antibiotics traces in the aquatic environment: persistence and adverse environmental impact. Curr Opin Environ Sci Heal. https://doi.org/10.1016/j.coesh.2019.11.005
3. Al S, Tanweer MS, Alam M (2020) Kinetic, isothermal, thermodynamic and adsorption studies on Mentha piperita using ICP-OES. Surf Interfaces. https://doi.org/10.1016/j.surfin.2020.100516
4. Wang J, Zhuan R (2020) Degradation of antibiotics by advanced oxidation processes: an overview. Sci Total Environ. https://doi.org/10.1016/j.scitotenv.2019.135023
5. Ahmad R, Ansari K (2020) Polyacrylamide-grafted actinidia deliciosa peels powder (PGADP) for the sequestration of crystal violet dye: isotherms, kinetics and thermodynamic studies. Appl Water Sci. https://doi.org/10.1007/s13201-020-01263-7
6. Ahmad R, Ansari K (2021) Comparative study for adsorption of congo red and methylene blue dye on chitosan modified hybrid nanocomposite. Process Biochem 108:90–102. https://doi.org/10.1016/j.procbio.2021.05.013
7. Athar MS, Danish M, Muneer M (2021) Fabrication of visible light-responsive dual Z-Scheme ($\alpha$-$Fe_2O_3$/CdS/g-$C_3N_4$) ternary nanocomposites for enhanced photocatalytic performance and adsorption study in aqueous suspension. J Environ Chem Eng 9:105754. https://doi.org/10.1016/j.jece.2021.105754
8. Elmolla ES, Chaudhuri M (2010) Photocatalytic degradation of amoxicillin, ampicillin and cloxacillin antibiotics in aqueous solution using UV/$TiO_2$ and UV/$H_2O_2$/$TiO_2$ photocatalysis. Desalination. https://doi.org/10.1016/j.desal.2009.11.003
9. Zhang Z, Huang J, Zhang M et al (2015) Ultrathin hexagonal $SnS_2$ nanosheets coupled with g-$C_3N_4$ nanosheets as 2D/2D heterojunction photocatalysts toward high photocatalytic activity. Appl Catal B Environ. https://doi.org/10.1016/j.apcatb.2014.08.013
10. Lu Q, Yu Y, Ma Q et al (2016) 2D transition-metal-dichalcogenide-nanosheet-based composites for photocatalytic and electrocatalytic hydrogen evolution reactions. Adv Mater. https://doi.org/10.1002/adma.201503270
11. Katheresan V, Kansedo J, Lau SY (2018) Efficiency of various recent wastewater dye removal methods: a review. J Environ Chem Eng. https://doi.org/10.1016/j.jece.2018.06.060
12. Wong YC, Szeto YS, Cheung WH, McKay G (2004) Adsorption of acid dyes on chitosan—equilibrium isotherm analyses. Process Biochem. https://doi.org/10.1016/S0032-9592(03)00152-3
13. Sardar M, Manna M, Maharana M, Sen S (2021) Remediation of dyes from industrial wastewater using low-cost adsorbents. Springer, Cham, pp 377–403. https://doi.org/10.1007/978-3-030-47400-3_15
14. Clarke EA, Anliker R (1980) Organic dyes and pigments. In: Handbook of environmental chemistry
15. Moawed EA, Kiwaan HA, Elshazly MM (2017) Application of polyurethane@salvadora persica composite for detection and removal of acidic and basic dyes from wastewater. J Taiwan Inst Chem Eng. https://doi.org/10.1016/j.jtice.2017.07.028
16. Yagub MT, Sen TK, Afroze S, Ang HM (2014) Dye and its removal from aqueous solution by adsorption: a review. Adv Colloid Interface Sci. https://doi.org/10.1016/j.cis.2014.04.002
17. Chen X, Deng Q, Lin S et al (2017) A new approach for risk assessment of aggregate dermal exposure to banned azo dyes in textiles. Regul Toxicol Pharmacol. https://doi.org/10.1016/j.yrtph.2017.10.022
18. Brüschweiler BJ, Merlot C (2017) Azo dyes in clothing textiles can be cleaved into a series of mutagenic aromatic amines which are not regulated yet. Regul Toxicol Pharmacol. https://doi.org/10.1016/j.yrtph.2017.06.012
19. Kadirvelu K, Kavipriya M, Karthika C et al (2003) Utilization of various agricultural wastes for activated carbon preparation and application for the removal of dyes and metal ions from aqueous solutions. Bioresour Technol. https://doi.org/10.1016/S0960-8524(02)00201-8
20. Li HH, Wang YT, Wang Y et al (2019) Bacterial degradation of anthraquinone dyes. J Zhejiang Univ Sci B https://doi.org/10.1631/jzus.B1900165

21. Lambert SJ, Davy AJ (2011) Water quality as a threat to aquatic plants: Discriminating between the effects of nitrate, phosphate, boron and heavy metals on charophytes. New Phytol. https://doi.org/10.1111/j.1469-8137.2010.03543.x
22. Hatch KL (1984) Chemicals and textiles: part I: dermatological problems related to fiber content and dyes. Text Res J. https://doi.org/10.1177/004051758405401005
23. Hatch KL, Maibach HI (1985) Textile dye dermatitis: a review. J Am Acad Dermatol. https://doi.org/10.1016/S0190-9622(85)70137-5
24. Pratt M, Taraska V (2000) Disperse blue dyes 106 and 124 are common causes of textile dermatitis and should serve as screening allergens for this condition. Am J Contact Dermat. https://doi.org/10.1016/S1046-199X(00)90030-7
25. Kousha M, Daneshvar E, Sohrabi MS et al (2012) Adsorption of acid orange II dye by raw and chemically modified brown macroalga Stoechospermum marginatum. Chem Eng J. https://doi.org/10.1016/j.cej.2012.03.057
26. Chequer FMD, de Venâncio VP, de Bianchi MLP, Antunes LMG (2012) Genotoxic and mutagenic effects of erythrosine B, a xanthene food dye, on HepG2 cells. Food Chem Toxicol. https://doi.org/10.1016/j.fct.2012.07.042
27. Ritchie EE, Princz JI, Robidoux PY, Scroggins RP (2013) Ecotoxicity of xanthene dyes and a non-chlorinated bisphenol in soil. Chemosphere. https://doi.org/10.1016/j.chemosphere.2012.10.096
28. San NO, Celebioglu A, Tümtaş Y et al (2014) Reusable bacteria immobilized electrospun nanofibrous webs for decolorization of methylene blue dye in wastewater treatment. RSC Adv. https://doi.org/10.1039/c4ra04250f
29. Othman I, Mohamed RM, Ibrahem FM (2007) Study of photocatalytic oxidation of indigo carmine dye on Mn-supported $TiO_2$. J Photochem Photobiol A Chem. https://doi.org/10.1016/j.jphotochem.2007.01.010
30. Srivastava S, Sinha R, Roy D (2004) Toxicological effects of malachite green. Aquat Toxicol. https://doi.org/10.1016/j.aquatox.2003.09.008
31. Hameed BH (2008) Equilibrium and kinetic studies of methyl violet sorption by agricultural waste. J Hazard Mater. https://doi.org/10.1016/j.jhazmat.2007.10.010
32. Ofomaja AE (2008) Kinetic study and sorption mechanism of methylene blue and methyl violet onto mansonia (Mansonia altissima) wood sawdust. Chem Eng J. https://doi.org/10.1016/j.cej.2007.12.019
33. Crini G (2006) Non-conventional low-cost adsorbents for dye removal: a review. Bioresour Technol. https://doi.org/10.1016/j.biortech.2005.05.001
34. Khan TA, Sharma S, Ali I (2011) Adsorption of rhodamine B dye from aqueous solution onto acid activated mango (Magnifera indica) leaf powder: equilibrium, kinetic and thermodynamic studies. J Toxicol Environ Heal Sci. https://doi.org/10.5897/JTEHS.9000003
35. Pearce CI, Lloyd JR, Guthrie JT (2003) The removal of colour from textile wastewater using whole bacterial cells: a review. Dye Pigment. https://doi.org/10.1016/S0143-7208(03)00064-0
36. Kumar R, Ahmad R (2011) Biosorption of hazardous crystal violet dye from aqueous solution onto treated ginger waste (TGW). Desalination. https://doi.org/10.1016/j.desal.2010.07.040
37. Gupta VK, Mittal A, Gajbe V, Mittal J (2008) Adsorption of basic fuchsin using waste materials-bottom ash and deoiled soya-as adsorbents. J Colloid Interface Sci. https://doi.org/10.1016/j.jcis.2007.09.091
38. Cunha BA (2001) Antibiotic side effects. Med Clin North Am. https://doi.org/10.1016/S0025-7125(05)70309-6
39. Schluter G (1987) Ciprofloxacin: review of potential toxicologic effects. Am J Med
40. El-Maraghy CM, El-Borady OM, El-Naem OA (2020) Effective removal of levofloxacin from pharmaceutical wastewater using synthesized zinc oxid, graphen oxid nanoparticles compared with their combination. Sci Rep. https://doi.org/10.1038/s41598-020-61742-4
41. Kümmerer K (2009) Antibiotics in the aquatic environment—a review—Part I. Chemosphere. https://doi.org/10.1016/j.chemosphere.2008.11.086
42. Calvete MJF, Piccirillo G, Vinagreiro CS, Pereira MM (2019) Hybrid materials for heterogeneous photocatalytic degradation of antibiotics. Coord Chem Rev. https://doi.org/10.1016/j.ccr.2019.05.004

43. Jorgensen SE, Halling-Sorensen B (2000) Editorial: drugs in the environment. Chemosphere. https://doi.org/10.1016/S0045-6535(99)00438-5
44. Rizzo L, Manaia C, Merlin C et al (2013) Urban wastewater treatment plants as hotspots for antibiotic resistant bacteria and genes spread into the environment: a review. Sci Total Environ. https://doi.org/10.1016/j.scitotenv.2013.01.032
45. Kumar M, Jaiswal S, Sodhi KK et al (2019) Antibiotics bioremediation: perspectives on its ecotoxicity and resistance. Environ Int. https://doi.org/10.1016/j.envint.2018.12.065
46. Pruden A, Joakim Larsson DG, Amézquita A et al (2013) Management options for reducing the release of antibiotics and antibiotic resistance genes to the environment. Environ Health Perspect. https://doi.org/10.1289/ehp.1206446
47. Calafat AM, Ye X, Wong LY et al (2008) Urinary concentrations of triclosan in the U.S. population: 2003–2004. Environ Health Perspect. https://doi.org/10.1289/ehp.10768
48. Katzung (2012) Basic and clinical pharmacology, 12th edn. Critical Care Quarterly
49. Zhou C, Lai C, Xu P et al (2018) Rational design of carbon-doped carbon nitride/$Bi_{12}O_{17}Cl_2$ composites: a promising candidate photocatalyst for boosting visible-light-driven photocatalytic degradation of tetracycline. ACS Sustain Chem Eng. https://doi.org/10.1021/acssuschemeng.8b00782
50. Cao S, Zhang Y, He N et al (2020) Metal-free 2D/2D heterojunction of covalent triazine-based frameworks/graphitic carbon nitride with enhanced interfacial charge separation for highly efficient photocatalytic elimination of antibiotic pollutants. J Hazard Mater. https://doi.org/10.1016/j.jhazmat.2020.122204
51. Wu Z, Liang Y, Yuan X et al (2020) MXene $Ti_3C_2$ derived Z–scheme photocatalyst of graphene layers anchored $TiO_2$/g–$C_3N_4$ for visible light photocatalytic degradation of refractory organic pollutants. Chem Eng J. https://doi.org/10.1016/j.cej.2020.124921
52. Shen J, Shen J, Zhang W et al (2019) Built-in electric field induced $CeO_2$/$Ti_3C_2$-MXene Schottky-junction for coupled photocatalytic tetracycline degradation and $CO_2$ reduction. Ceram Int. https://doi.org/10.1016/j.ceramint.2019.08.123
53. Li L, Cai J, Yan Y et al (2019) Flower-like direct Z-scheme $WS_2$/$Bi_2O_2CO_3$ photocatalyst with enhanced photocatalytic activity. J Alloys Compd. https://doi.org/10.1016/j.jallcom.2019.151872
54. Yu B, Zheng B, Wang X et al (2017) Enhanced photocatalytic properties of graphene modified few-layered $WSe_2$ nanosheets. Appl Surf Sci. https://doi.org/10.1016/j.apsusc.2016.12.015
55. Islam SE, Hang DR, Chen CH, Sharma KH (2018) Facile and cost-efficient synthesis of quasi-0D/2D ZnO/$MoS_2$ nanocomposites for highly enhanced visible-light-driven photocatalytic degradation of organic pollutants and antibiotics. Chem A Eur J. https://doi.org/10.1002/chem.201801397
56. Sharma M, Mohapatra PK, Bahadur D (2017) Improved photocatalytic degradation of organic dye using $Ag_3PO_4$/$MoS_2$ nanocomposite. Front Mater Sci. https://doi.org/10.1007/s11706-017-0404-x
57. Shahzad A, Rasool K, Nawaz M et al (2018) Heterostructural $TiO_2$/$Ti_3C_2T_x$ (MXene) for photocatalytic degradation of antiepileptic drug carbamazepine. Chem Eng J. https://doi.org/10.1016/j.cej.2018.05.148
58. Vigneshwaran S, Karthikeyan P, Park CM, Meenakshi S (2020) Boosted insights of novel accordion-like (2D/2D) hybrid photocatalyst for the removal of cationic dyes: mechanistic and degradation pathways. J Environ Manage. https://doi.org/10.1016/j.jenvman.2020.111125
59. Sinopoli A, Othman Z, Rasool K, Mahmoud KA (2019) Electrocatalytic/photocatalytic properties and aqueous media applications of 2D transition metal carbides (MXenes). Curr Opin Solid State Mater Sci. https://doi.org/10.1016/j.cossms.2019.06.004
60. Guan G, Ye E, You M, Li Z (2020) Hybridized 2D nanomaterials toward highly efficient photocatalysis for degrading pollutants: current status and future perspectives. Small. https://doi.org/10.1002/smll.201907087
61. Mashtalir O, Cook KM, Mochalin VN et al (2014) Dye adsorption and decomposition on two-dimensional titanium carbide in aqueous media. J Mater Chem A. https://doi.org/10.1039/c4ta02638a

62. Gao Y, Wang L, Zhou A et al (2015) Hydrothermal synthesis of $TiO_2/Ti_3C_2$ nanocomposites with enhanced photocatalytic activity. Mater Lett. https://doi.org/10.1016/j.matlet.2015.02.135
63. Zhang H, Li M, Zhu C et al (2020) Preparation of magnetic α-$Fe_2O_3$/$ZnFe_2O_4$@$Ti_3C_2$ MXene with excellent photocatalytic performance. Ceram Int. https://doi.org/10.1016/j.ceramint.2019.08.236
64. Xie X, Zhang N, Tang ZR et al (2018) $Ti_3C_2T_x$ MXene as a Janus cocatalyst for concurrent promoted photoactivity and inhibited photocorrosion. Appl Catal B Environ. https://doi.org/10.1016/j.apcatb.2018.05.070
65. Wang H, Wu Y, Xiao T et al (2018) Formation of quasi-core-shell $In_2S_3$/anatase $TiO_2$@metallic $Ti_3C_2T_x$ hybrids with favorable charge transfer channels for excellent visible-light-photocatalytic performance. Appl Catal B Environ. https://doi.org/10.1016/j.apcatb.2018.04.012
66. Fang H, Pan Y, Yin M et al (2019) Facile synthesis of ternary $Ti_3C_2$–OH/$ln_2S_3$/CdS composite with efficient adsorption and photocatalytic performance towards organic dyes. J Solid State Chem. https://doi.org/10.1016/j.jssc.2019.120981
67. Liu Q, Tan X, Wang S et al (2019) MXene as a non-metal charge mediator in 2D layered CdS@$Ti_3C_2$@$TiO_2$ composites with superior Z-scheme visible light-driven photocatalytic activity. Environ Sci Nano. https://doi.org/10.1039/c9en00567f
68. Zhang H, Li M, Cao J et al (2018) 2D a-$Fe_2O_3$ doped $Ti_3C_2$ MXene composite with enhanced visible light photocatalytic activity for degradation of rhodamine B. Ceram Int. https://doi.org/10.1016/j.ceramint.2018.07.262
69. Liu N, Lu N, Su Y et al (2019) Fabrication of g-$C_3N_4/Ti_3C_2$ composite and its visible-light photocatalytic capability for ciprofloxacin degradation. Sep Purif Technol. https://doi.org/10.1016/j.seppur.2018.10.027
70. Luo S, Wang R, Yin J et al (2019) Preparation and dye degradation performances of self-assembled MXene-$Co_3O_4$ nanocomposites synthesized via solvothermal approach. ACS Omega. https://doi.org/10.1021/acsomega.9b00231
71. Yu M, Liang H, Zhan R et al (2020) Sm-doped g-$C_3N_4/Ti_3C_2$ MXene heterojunction for visible-light photocatalytic degradation of ciprofloxacin. Chinese Chem Lett. https://doi.org/10.1016/j.cclet.2020.11.069
72. Cao Y, Fang Y, Lei X et al (2020) Fabrication of novel $CuFe_2O_4$/MXene hierarchical heterostructures for enhanced photocatalytic degradation of sulfonamides under visible light. J Hazard Mater. https://doi.org/10.1016/j.jhazmat.2020.122021
73. Peng C, Yang X, Li Y et al (2016) Hybrids of two-dimensional $Ti_3C_2$ and $TiO_2$ exposing 001 facets toward enhanced photocatalytic activity. ACS Appl Mater Interfaces. https://doi.org/10.1021/acsami.5b11973
74. Li K, Lu X, Zhang Y et al (2020) $Bi_3TaO_7/Ti_3C_2$ heterojunctions for enhanced photocatalytic removal of water-borne contaminants. Environ Res. https://doi.org/10.1016/j.envres.2020.109409
75. Wu S, Su Y, Zhu Y et al (2020) In-situ growing Bi/BiOCl microspheres on $Ti_3C_2$ nanosheets for upgrading visible-light-driven photocatalytic activity. Appl Surf Sci. https://doi.org/10.1016/j.apsusc.2020.146339
76. He J, Yang J, Jiang F et al (2020) Photo-assisted peroxymonosulfate activation via 2D/2D heterostructure of $Ti_3C_2$/g-$C_3N_4$ for degradation of diclofenac. Chemosphere. https://doi.org/10.1016/j.chemosphere.2020.127339
77. My Tran N, Thanh Hoai Ta Q, Noh JS (2021) Unusual synthesis of safflower-shaped $TiO_2/Ti_3C_2$ heterostructures initiated from two-dimensional $Ti_3C_2$ MXene. Appl Surf Sci. https://doi.org/10.1016/j.apsusc.2020.148023
78. Zhang J, Huang L, Lu Z et al (2016) Crystal face regulating $MoS_2/TiO_2$(001) heterostructure for high photocatalytic activity. J Alloys Compd. https://doi.org/10.1016/j.jallcom.2016.07.263
79. Li H, Yu K, Lei X et al (2015) Hydrothermal synthesis of novel $MoS_2/BiVO_4$ hetero-nanoflowers with enhanced photocatalytic activity and a mechanism investigation. J Phys Chem C. https://doi.org/10.1021/acs.jpcc.5b06729

80. Zhang J, Huang L, Jin H et al (2017) Constructing two-dimension $MoS_2/Bi_2WO_6$ core-shell heterostructure as carriers transfer channel for enhancing photocatalytic activity. Mater Res Bull. https://doi.org/10.1016/j.materresbull.2016.09.013
81. Wang Y, Xiao X, Chen J et al (2020) 1T phase boosted $MoSe_2$/pg-$C_3N_4$ with Z-scheme heterojunction for enhanced photocatalytic degradation of contaminants. Appl Surf Sci. https://doi.org/10.1016/j.apsusc.2020.145341
82. Farbod M, Taheri R, Kosarian A (2021) Preparation, characterization and photocatalytic performance of phosphorene/$MoS_2$ as a 2D hybrid semiconductor. Mater Sci Semicond Process. https://doi.org/10.1016/j.mssp.2020.105562
83. Lu X, Wang Y, Zhang X et al (2018) NiS and $MoS_2$ nanosheet co-modified graphitic $C_3N_4$ ternary heterostructure for high efficient visible light photodegradation of antibiotic. J Hazard Mater. https://doi.org/10.1016/j.jhazmat.2017.07.004
84. Kang J, Jin C, Li Z et al (2020) Dual Z-scheme $MoS_2$/g-$C_3N_4/Bi_{24}O_{31}Cl_{10}$ ternary heterojunction photocatalysts for enhanced visible-light photodegradation of antibiotic. J Alloys Compd. https://doi.org/10.1016/j.jallcom.2020.153975
85. Sitara E, Ehsan MF, Nasir H et al (2020) Synthesis, characterization and photocatalytic activity of MoS2/ZnSe heterostructures for the degradation of levofloxacin. Catalysts. https://doi.org/10.3390/catal10121380
86. Pacchioni G (2019) Cutting phosphorene nanoribbons. Nat Rev Mater https://doi.org/10.1038/s41578-019-0114-3
87. Kaewmaraya T, Ngamwongwan L, Moontragoon P et al (2021) Novel green phosphorene as a superior chemical gas sensing material. J Hazard Mater. https://doi.org/10.1016/j.jhazmat.2020.123340
88. Kovalska E, Luxa J, Melle-Franco M et al (2020) Single-step synthesis of platinoid-decorated phosphorene: perspectives for catalysis, gas sensing, and energy storage. ACS Appl Mater Interfaces. https://doi.org/10.1021/acsami.0c15525
89. Yang A, Wang D, Wang X et al (2018) Recent advances in phosphorene as a sensing material. Nano Today. https://doi.org/10.1016/j.nantod.2018.04.001
90. Taheri R, Farbod M (2020) Superb photocatalytic performance of single/few layer phosphorene prepared via sonication method. Phys E Low-Dimensional Syst Nanostruct. https://doi.org/10.1016/j.physe.2020.114009
91. Li S, Wang P, Wang R et al (2019) One-step co-precipitation method to construct black phosphorus nanosheets/ZnO nanohybrid for enhanced visible light photocatalytic activity. Appl Surf Sci 497:143682. https://doi.org/10.1016/j.apsusc.2019.143682
92. Shen Z, Sun S, Wang W et al (2015) A black-red phosphorus heterostructure for efficient visible-light-driven photocatalysis. J Mater Chem A. https://doi.org/10.1039/c4ta06871h
93. Chen P, Guo Z, Cui K et al (2020) Photo-induced degradation of norfloxacin by nanosilver modified two-dimensional black phosphorus. Solid State Sci. https://doi.org/10.1016/j.solidstatesciences.2020.106188
94. Huang Q, Liu Y, Cai T, Xia X (2019) Simultaneous removal of heavy metal ions and organic pollutant by BiOBr/$Ti_3C_2$ nanocomposite. J Photochem Photobiol A Chem. https://doi.org/10.1016/j.jphotochem.2019.02.026
95. Wang C, Shen J, Chen R et al (2020) Self-assembled BiOCl/$Ti_3C_2T_x$ composites with efficient photo-induced charge separation activity for photocatalytic degradation of p-nitrophenol. Appl Surf Sci. https://doi.org/10.1016/j.apsusc.2020.146175
96. Li S, Wang P, Zhao H et al (2021) Fabrication of black phosphorus nanosheets/BiOBr visible light photocatalysts via the co-precipitation method. Colloids Surfaces A Physicochem Eng Asp. https://doi.org/10.1016/j.colsurfa.2020.125967

# Chapter 5
# Advanced 2D Nanomaterial Composites: Applications in Adsorption of Water Pollutants and Toxic Gases


**Mohd Saquib Tanweer, Harshvardhan Chauhan, and Masood Alam**

## Abbreviations

| | |
|---|---|
| Au NPs | Gold nanoparticles |
| BPNs/ZnO | Black phosphorus nanosheets/ZnO |
| $CeO_2$–$MoS_2$ | Cerium-doped molybdenum disulphide |
| $CH_4N_2S$ | Thiourea |
| CNFs | Carbon nano fibers |
| CR | Congo red |
| EY | Eosin Y |
| FA | Fuchsin acid |
| HCl | Hydrochloric acid |
| MB | Methylene blue |
| MG | Malachite green |
| MNP-PN-TNT | Magnetic nanoparticle-Phosphorene-Titanium nano tubes |
| MO | Methyl orange |
| $MoS_2$/CuS NCs | Molybdenum disulfide/copper(II)sulphide nanosheet composites |
| $MoS_2$/GQD | Molybdenum disulfide/graphene quantum dot nanocomposite |
| $MoS_2$@2DMMT | Molybdenum disulfide-montmorillonite |

M. S. Tanweer (✉) · H. Chauhan · M. Alam
Environmental Science Research Lab, Department of Applied Sciences and Humanities, Faculty of Engineering and Technology, Jamia Millia Islamia, New Delhi 110025, India
e-mail: saquibtanweer701@gmail.com

H. Chauhan
e-mail: chauhanhvsc@gmail.com

M. Alam
e-mail: malam@jmi.ac.in



Z. Khanam et al. (eds.), *2D Nanomaterials for Energy and Environmental Sustainability*,
Materials Horizons: From Nature to Nanomaterials,
https://doi.org/10.1007/978-981-16-8538-5_5

| | |
|---|---|
| $MoS_2$-g-PDMA | Molybdenum disulfide-grafted-poly(diethyl (4-vinylbenzyl) phosphonate-co-maleic anhydride) |
| $MoS_2$-rGO hybrid | Molybdenum disulphide-reduced graphene oxide |
| MX@ $Fe_3O_4$ | MXene decorated with $Fe_3O_4$ |
| MXene-COOH@(PEI/PAA)n | Carboxyl modified MXene@(polyethylene polyimide/poly (acrylic acid) |
| MXene/LDH | MXene/Layered double metal hydroxide |
| NaF | Sodium fluoride |
| NMP | N-methyl-2-pyrrolidone |
| NR | Neutral red |
| RhB | Rhodamine B |
| RhB 6G | Rhodamine 6G |
| RSM | Response surface methodology |
| ST | Safranine T |
| $Ti_3C_2$–$SO_3H$ | Sulfonic groups functionalized titanium carbide |
| $Ti_3C_2T_x$-PDOPA | MXene-Levodopa composite |
| TNT | Titanium nano tubes |
| TPAOH | Tetrapropylammonium hydroxide |
| $WO_3$–BPNs | Tungsten trioxide-black phosphorus composites |
| $WS_2$ | Tungsten disulfide |
| $WSe_2$ | Tungsten diselenide |
| $ZnIn_2S_4$/protonated g-$C_3N_4$ | Zinc indium sulfide/protonated graphitic carbon nitride |

## 1 Introduction

Over increasing pace of industrialization, uncontrolled growth of human population and vast expansion of urban areas have become principal factors to produce hazardous wastes. It poses serious toxicological impact on health of living systems including humans and different ecosystems resulting in huge negative effect on the global economic development [1, 2]. The environmental pollutants that are chiefly encountered are water pollutants and air pollutants. The water pollutants include pharmaceutical residues (namely antibiotics, analgesic, anti-inflammatory drugs and steroid hormones), heavy metal ions (namely chromium (Cr), mercury (Hg), lead (Pb), cadmium (Cd), arsenic (As) and their salts), organics (namely textile dyes, agricultural herbicides and pesticides, detergents surfactants, and oil) and bio-toxins (namely bacteria, fungi, and virus). And the air pollutants include different types of toxic gases specifically oxides of sulfur ($SO_x$), oxides of nitrogen ($NO_x$) and oxides of carbon (namely CO, $CO_2$). These pollutants may cause several diseases in humans, for instance, kidney damage and skeletal damage caused due to Cd exposure, lung and kidney damage, neurological and psychological disorder caused due to Hg exposure, headache, irritability, abdominal pain and neurological disorder caused due to

Pb poisoning gastrointestinal problems, disturbances to cardiovascular systems and even death can occur due to As poisoning; while Cr exposure may cause mutagenic and carcinogenic effects [3, 4].

Several physiochemical and biological treatment methods such as precipitation [5], advanced oxidation [6], ion exchange [7], membrane filtration [8], adsorption [9] and aerobic/anaerobic digestion [10] are developed to eliminate and reduce environmental pollutants. Among these, adsorption is regarded as one of the most effective conventional methods due to its simplicity of design, ease of operation, efficient and low cost [11]. So far, various nanomaterials are developed as adsorbents for environmental remediation, such as activated carbon [12], clay [13], silica [14], zeolites [15], polymers [16] and metal–organic frameworks (MOFs) [17].

After the discovery of single-layered graphene in 2004, numerous two-dimensional (2D) nanomaterials such as MXenes, phosphorene, transition metal dichalcogenides (TMDs), hexagonal boron nitride (h-BN), silicene and germanene have garnered a lot of attention from scientific community because of their astonishing physicochemical properties [18]. MXenes are a new and rapidly rising family of 2D transition-metal carbides, nitrides and carbonitrides that are analogous to graphene. More than 30 types of MXenes compositions are reported so far with and dozens more are being developed by computational methods. Ti-based MXenes such as $Ti_3C_2T_x$, and $Ti_2CT_x$ are the most commonly used adsorbents in environmental remediation [19, 20]. The existence of functional groups like oxygen, hydroxyl, fluorine, chlorine on the surface of MXenes allows sites for direct ion exchange, although it also eliminates certain cations and organic molecules [21–23]. The most widely studied among TMDs is $MoS_2$ because of their robustness and abundant availability of raw materials [24]. Numerous types of 2D TMDs nanocomposites are developed and used as nanoadsorbents for water treatment and toxic gas adsorption because of their remarkable properties such as large specific surface area (SSA), tunable band gaps, excellent chemical resistance and thermal stability [25, 26]. Besides them, 2D Phosphorene, a mono- or few-layered material is arising as a star material at 2D platform in nanotechnology field. In the context of environmental remediation, a tremendous amount of resources is spent to explore the adsorption properties of bulk black phosphorus and 2D phosphorene either by theoretical calculation or experimental measurements [27, 28]. 2D nanomaterial composites are found to be the most privileged adsorbents to remove water and toxic air pollutants because of their hydrophilic behavior. They have several reactive surficial functional sites which make them good candidates for removing pollutants from the environment. Recent studies proved that these composites exhibited excellent adsorption capacities when compared with traditional adsorbents.

This chapter provides an overview on the preparation and properties of 2D nanomaterials composites. The use of 2D nanomaterial composites as an adsorbent for toxic gases, heavy metals ions (HMI) and dye removal is also discussed, alongwith the mechanism of the adsorption process. The chapter finally concludes with the future prospects and challenges of 2D nanomaterial composites.

## 2 Preparation and Properties of 2D Nanocomposites-Based Adsorbents

2D nanomaterial composites have been primarily synthesized through two methods, (a) top-down method such as mechanical exfoliation and liquid exfoliation, (b) bottom-up method such as hydrothermal method, self-assembly method and solvothermal method (Fig. 1a). Under top-down method, mechanical exfoliation is a basic and useful method to fabricate dense 2D-layered inorganic sheets or composites by splitting the weak van der Waals forces (VWFs) between two adjacent layers in layered bulk materials. This method is facile, fast and low cost to produce large sized and high quality 2D nanosheets or composites but with extremely low yield. As an example, polyaniline@$MoS_2$-based organic–inorganic nanohybrid composite was prepared using mechanical exfoliation followed by a facile in-situ oxidative polymerization. Firstly, bulk $MoS_2$ was exfoliated using simple mechanical ball milling method and then it was dispersed in 1M HCl by ultra-sonication. Subsequently, aniline monomer was added followed by potassium persulphate as an oxidant to initiate the polymerization under stirring, forming polyaniline@$MoS_2$ composites. The result showed that the polyaniline deposited as a flat sheet with irregular structure (Fig. 1b). The final product was used as an adsorbent to sequestrate CR dye from aqueous solutions [29]. Zhang and co-workers [30] also used exfoliation method to synthesize MXene@$Fe_3O_4$ composites to remove MB dye. Liquid exfoliation method can be exploited to produce 2D composites on a larger scale for wide

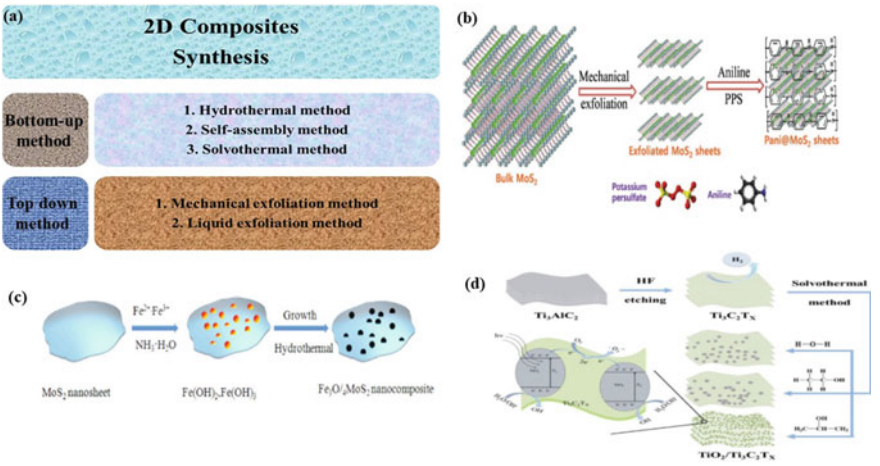


**Fig. 1** **a** Schematic representation of synthesis of 2D nanomaterial composites; **b** schematic diagram of the $MoS_2$ exfoliation and its Pani@$MoS_2$ composite synthesis process. Reprinted with permission from [29]. Copyright 2018 Royal Society of Chemistry; **c** schematic procedure for the synthesis of $Fe_3O_4/MoS_2$ nanocomposites. Reprinted with permission from [33]. Copyright 2015 Elsevier B.V.; **d** schematic illustration of the synthesis process of the $TiO_2/Ti_3C_2T_x$ composites. Reprinted with permission from [45]. Copyright 2020 Elsevier B. V.

applications. This method can be categorized into four different forms: (i) oxidation, (ii) intercalation, (iii) ion exchange and (iv) ultrasonic cleavage. Liu et al. [31] prepared 2D $MoS_2$/carbon composites using liquid-phase shear exfoliation method followed by annealing. 2D $MoS_2$/carbon composites were effective in the removal of MB dye with a maximum adsorption capacity of 272 mg $g^{-1}$. In another study, $MoS_2$/g-$C_3N_4$ composites were fabricated using liquid exfoliation method assisted by sonication, suitable for hydrogen generation [32]. The main advantage of top-down approach is that almost none or very less requirement of any chemicals. The disadvantages include low yield, broad size distribution (10–100 nm) and more defects in composites.

In bottom-up methods, hydrothermal technique is generally used to fabricate 2D composites for environmental applications. This technique is especially suitable to produce good quality 2D nanocomposites with a better-controlled composition. For example, Jia and co-workers [33] synthesized $Fe_3O_4$/$MoS_2$ nanocomposites via a facile hydrothermal technique in a water–ethanol system. The prepared nanocomposite displayed excellent performance in water treatment processes. $MoS_2$ is dispersed in ethanol–water (1:1) and ultrasonicated followed by the addition of ferric and ferrous salts aqueous solution. The solution was then doped with ammonia followed by heating in Teflon-lined stainless-steel autoclave at 100 °C (Fig. 1c). This method was extensively used to synthesize various types of 2D nanocomposites such as $CeO_2$–$MoS_2$ [34], $MoS_2$@2DMMT [35], $MoS_2$@Kaolin [36], $MoS_2$/graphene quantum dot [37], magnetic titanium nanotubes coated phosphorene [4], $MoS_2$/CuS [25], $Bi_2S_3$/$MoS_2$ [38] and phytic acid (PA)-MXene composites [39].

Self-assembly method is a type of interfacial modification technique, employed to synthesize different composite materials. It is a simple process, requiring mild preparation condition and different types of forces such as electrostatic interaction, coordination bond, hydrogen bond, hydrophobic interaction, π-π stacking [40]. Jiao et al. [41] synthesized MXene-COOH@$(PEI/PAA)_n$ core–shell nanocomposites via layer-by-layer self-assembled method to achieve increased adsorption capacities. The electronic force from $–NH_3^+$ of polyethylene polyimide and hydrogen bond from $COO^-$ groups of polyacrylic acid helped to form MXene-COOH@$(PEI/PAA)_n$ nanocomposites. In another study, 2D/2D ultrathin $ZnIn_2S_4$/protonated g-$C_3N_4$ composites were synthesized via electrostatic self-assembly technique [42]. Very recently, MXene-based nanocomposites are developed by Jiao et al. using self-assembly method for water purification [43]. Solvothermal method is somewhat similar to hydrothermal method. The solvent used in hydrothermal method is water while in solvothermal method solvent is other than water [44]. A group of researchers have successfully developed $TiO_2$/MXene composites via in-situ solvothermal method. Firstly, $Ti_3AlC_2$ was etched by HF to obtain $Ti_3C_2T_x$ which was then mixed with different organic solvents. The solution was transferred to a Teflon-lined stainless-steel hydrothermal reaction kettle and placed in an oven at 200 °C to obtain the final product (Fig. 1d) [45]. The solvothermal method is employed to produce various 2D nanocomposites such as MXene-$Co_3O_4$ [46], $MoS_2$/$C_3N_4$ [47], $MoS_2$/$ZnIn_2S_4$ [48], 2D $MoS_2$-2D PbS [49]. These have been efficiently used to remediate the environment.

2D nanomaterial composites with limited thickness and larger SSA show unique structural, physical and chemical properties compared with the conventional adsorbents. These properties make 2D nanomaterial composites more competitive in fabricating novel adsorbent. The last decade has observed more successful efforts for the application of 2D-based adsorbents in environmental remediation. This field is explored using a variety of 2D nanomaterial composites, including MXene-based composites, TMDs-based composites and phosphorene-based composites. Due to specific structural properties of these materials, different modification strategies are carried out to take advantages of their adsorptive behavior. The surface functionalization of MXenes leads to changes in its physical properties and consequently enhances its adsorption behavior toward certain species. Yang et al. [50] synthesized $Ti_3C_2T_x$-PDOPA composites for efficient Cu(II) removal through surface functionalization of $Ti_3C_2T_x$ using an amino acid i.e., levodopa (DOPA) as a modification agent under alkaline conditions. The main purpose to use DOPA was to introduce carboxyl groups (- COOH) on the outer surface of $Ti_3C_2T_x$ which enhances the adsorption capacity and selectivity toward adsorption of Cu(II). A lack of separation and poor dispersibility of composites dramatically reduces its adsorption property and restricts the application of 2D nanomaterial composites. In order to enhance the adsorption property, Zhang et al. [30] introduced an in-situ growth approach to successfully synthesize 2D MXene/$Fe_3O_4$ composites. The $Fe_3O_4$ NPs cover and disperse uniformly on the surface of MXene. It can effectively increase the SSA and active functional groups enhancing the adsorption capacity of nanocomposites for MB removal. It has been found that 2D MXene/$Fe_3O_4$ nanocomposites show an excellent superparamagnetic property which can be quickly obtained from the heterogeneous environment using an external magnetic field. Similarly, $MoS_2$/$Fe_3O_4$ nanocomposites showed a strong dispersion and magnetic separation property in water remediation [33]. Among TMDs, $MoS_2$-based nanocomposites exhibited some fascinating properties including peculiar 2D structure, richness in sulfur, excellent mechanical flexibility, huge SSA and exceptional chemical and thermal stability. Tong et al. [51] first time reported $MoS_2$/$CeO_2$ nanocomposites capable of specific adsorption of Pb(II) ions with an adsorption capacity of 333 mg $g^{-1}$ at pH 2.0. The properties of $MoS_2$/$CeO_2$ nanocomposites like richness in sulfur content, broad spacing between layers, strong soft–soft interactions between sulfur and lead species and low ion-exchange interaction play a critical role in effective removal of Pb(II) ions. Lin and co-workers showed that the presence of titanium nanotubes and magnetite nanoparticles should contribute to improved adsorption property due to the presence of large amount of hydroxides on the resultant nanocomposites [4].

## 3 Applications of 2D Nanomaterials in Adsorption Processes

Various types of 2D nanomaterials are recently being extensively used for the purification of water. The primary reason lies in their extraordinary behavior due to unique properties, which are very distinct from their counterparts. Different 2D nanomaterial composites used as adsorbents for the sequestration of heavy metal ions and dyes from aqueous environments are listed in Table 1.

### *3.1 Adsorption Mechanism*

The adsorption of heavy metal ions on the surfaces of 2D nanomaterial composites can be explained by various mechanisms. For instance, the mechanism for the removal of Pb(II) and Cu(II) ions using Mxene/alginate nanocomposites involve ion exchange and chemical coordination processes [52]. After adsorption of Pb(II) and Cu(II), Na 1 s peak disappears, and Pb 4d and Pb 4f (or Cu 2p) peaks emerge implying that an ion-exchange mechanism is involved in the adsorption process. The chemical coordination process between metal ions and composites occurs after the adsorption of Pb(II) (or Cu (II)) ions onto the surface and is identified by the shifting of carboxylated peaks from 1410 to 1386 and 1398 $cm^{-1}$ (Fig. 2a).

The adsorption mechanism of Pb(II) ions on $MoS_2$@Kaolin nanocomposites is explained in Fig. 2b [36]. The adsorption of lead ions onto $MoS_2$@Kaolin composites occurs due to the attachment of Pb(II) ions with S atoms on the surface of composites under oxidation conditions forming an insoluble compound β-$Pb_3O_2SO_4$, which is effectively eliminated from the solution. The adsorption of Cu(II) onto $MoS_2$@2DMMT hydrogel nanocomposites occurs mainly due to the reaction between Cu(II) and functional groups such as carboxyl, hydroxyl and amidogen on the surface of composites [35]. As confirmed by XPS and EDS, ion exchange occurs between $MoS_2$@2DMMT and Cu(II) resulting in enhanced adsorption of Pb(II).

Dye sorption on composites is mainly caused by the interaction between dye molecules and different functional groups present on the surface of the nanocomposites. Figure 2c presents the proposed mechanism of MB adsorption onto MXene@$Fe_3O_4$ [30]. As presented in Eqs. (1) and (2), $MB^+$ molecules probably bond with hydroxyl groups on the surface of MXene to ionize $H^+$ (Eq. 1), forming monodentate complex through the M–O–H$\cdots$N bond.

$$\text{TiOH} \leftrightarrows \text{Ti-O}^- + \text{H}^+ \tag{1}$$

$$\text{Ti-O}^- + \text{MB}^+ \leftrightarrows \text{TiO}^- \text{MB} \tag{2}$$

**Table 1** Different 2D nanocomposites-based adsorbents for adsorption of heavy metal ions and dyes

| 2D nanomaterial composites | Surface area ($m^2/g$) | Target pollutant | Sorption capacity ($Q_{max}$ mg $g^{-1}$)/efficiency (%) | Isotherms/kinetics | References |
|---|---|---|---|---|---|
| MNP-PN-TNT | NA | Cr(VI) | 35 mg $g^{-1}$ | Pseudo-second-order | [4] |
| alk-MXene/LDH | NA | Ni(II) | 222.717 mg $g^{-1}$ | Redlich-peterson/pseudo-second-order | [11] |
| $MoS_2$/CuS | 106.27 | RhB, MB, MO, and RhB 6G | 273.23, 432.68, 98.78, and 211.18 mg $g^{-1}$ | Langmuir/pseudo-second-order | [25] |
| Pani@$MoS_2$ nanocomposite | 50 | CR | 70.921 mg $g^{-1}$ | Langmuir/pseudo-second-order | [29] |
| MXene@$Fe_3O_4$ | NA | MB | 11.68 mg $g^{-1}$ or 94% for MB, 17% for MO and 5% for RhB | Langmuir | [30] |
| $Fe_3O_4$/$MoS_2$ nanocomposites | 72.0727 | RhB | 71 mg $g^{-1}$ | NA | [33] |
| $CeO_2$-$MoS_2$ | NA | Cr(VI) | 99.6% | NA | [34] |
| $MoS_2$@2DMMT | NA | Pb(II) | 65.75 mg $g^{-1}$ | Langmuir/pseudo-second-order | [35] |
| $MoS_2$@Kaolin | 14.56 | Pb(II) | 280.39 mg $g^{-1}$ | Langmuir/pseudo-second-order | [36] |
| $MoS_2$/GQD | 151.4 | RhB, MB and MO | 285, 210, and 140 mg $g^{-1}$ | NA | [37] |
| MXene-COOH@(PEI/PAA)n | NA | MB | 81.9672 mg $g^{-1}$ | Langmuir/pseudo-second-order | [41] |
| MXene-COOH@(PEI/PAA)n | NA | ST | 35.5999 mg $g^{-1}$ | Pseudo-second-order | [41] |
| MXene-COOH@(PEI/PAA)n | NA | NR | 46.1255 mg $g^{-1}$ | Pseudo-second-order | [41] |
| MXene-$Co_3O_4$ | NA | MB and RhB | 136.24 and 47.687 mg $g^{-1}$ | Pseudo-first-order/pseudo-second order Pseudo-second-order | [46] |
| $Ti_3C_2T_X$-PDOPA | NA | Cu(II) | 65.126 mg $g^{-1}$ | Freundlich/pseudo-first-order | [50] |
| Mxene/alginate composites | NA | Pb(II) and Cu(II) | 382.7 and 87.6 mg $g^{-1}$ | Langmuir/pseudo-second-order | [52] |

(continued)

**Table 1** (continued)

| 2D nanomaterial composites | Surface area ($m^2/g$) | Target pollutant | Sorption capacity ($Q_{max}$ mg $g^{-1}$)/efficiency (%) | Isotherms/kinetics | References |
|---|---|---|---|---|---|
| 2D-MX@$Fe_3O_4$ | NA | MB | 9.85 mg $g^{-1}$ at 55 °C, 3.95 mg $g^{-1}$ at 40 °C and 1.71 mg $g^{-1}$ at 25 °C | Freundlich (40 and 55 °C) Langmuir (25 °C) | [66] |
| $Ti_3C_2$–$SO_3H$ | NA | MB | 111.11 mg $g^{-1}$ | Langmuir/pseudo-first-order | [68] |
| Iron doped phosphorene | 1594 $Å^2$ | As(III) | NA | NA | [77] |
| $MoS_2/Fe_3O_4$ | NA | Pb(II) and Hg(II) | 263.6 and 428.9 mg $g^{-1}$ | Langmuir/pseudo-second-order | [81] |
| $Ti_3C_2T_x$/PmPD | 55.93 | Cr(VI) | 540.47 mg $g^{-1}$ | Redlich-Peterson/pseudo-second-order | [82] |
| $MoS_2$-rGO hybrid | 102.8 | Pb(II) and Ni(II) | 322 and 294 mg $g^{-1}$ | Langmuir | [83] |
| BiOCl/$WS_2$ | NA | Cr(VI) | 94.9% | Pseudo-second-order | [84] |
| BiOCl/$WS_2$ | NA | MG | 98.4% | Pseudo-first order/pseudo-second-order | [84] |
| $WO_3$–BPNs | 10.50 | RhB | 19.8% | First order reaction | [85] |
| Phosphorene/$MoS_2$ | NA | CR, MB and MO | NA | NA | [86] |
| BPNs/ZnO | 27.36 | MB | 96% | Langmuir–Hinshelwood pseudo-first order | [87] |

*NA* Not available

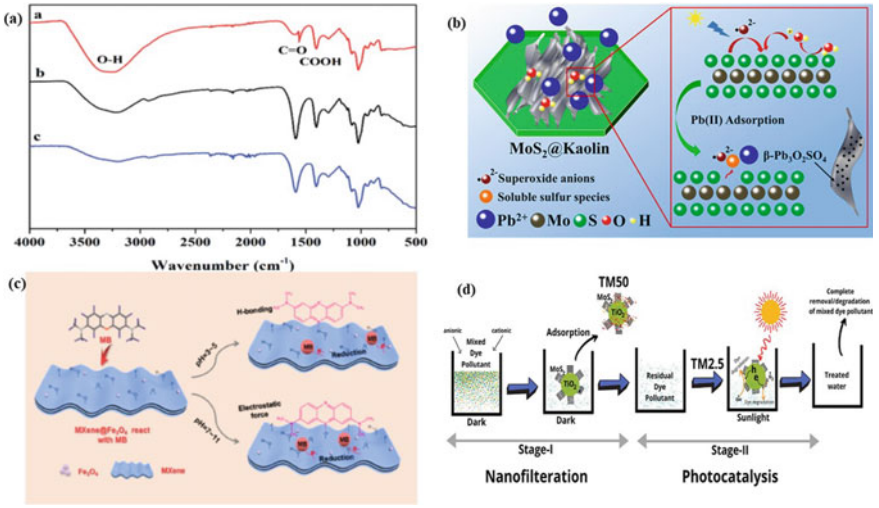


**Fig. 2** FT-IR spectra of **a** MXene/alginate composite, **b** Mxene/alginate composite loaded Pb(II) and **c** Mxene/alginate composite loaded Cu(II). Reprinted with permission from [52]. Copyright 2019 RSC Advances; **b** schematic view of the adsorption mechanism of Pb(II) on $MoS_2$@Kaolin. Reprinted with permission from [36]. Copyright 2020 Elsevier B.V.; **c** proposed mechanism for the adsorption of MB on the surface of MXene@$Fe_3O_4$. Reprinted with permission from [30]. Copyright 2019 ACS Applied Materials and Interfaces; **d** schematic illustration of two-stage rapid-adsorption and photocatalysis-based dye pollutant removal. Reprinted with permission from [53]. Copyright 2021 Elsevier B.V.

The electrostatic adsorption of MB facilitates MXene-MB complexation, whereas the complex formation is hampered by the electrostatic repulsion between MB + and positive charges on the surface of MXene@$Fe_3O_4$ composites. As a result, MB adsorption is primarily dependent on the interactions between Ti site and OH group present on MXene@$Fe_3O_4$. There are also dipole–dipole interactions between N of MB and Ti–OH groups, forming OH···N bonds. Cai et al. [39] explained that the adsorption of MB and RhB onto phytic acid (PA)-MXene composites with an increase in the adsorption capacity as the temperature increased. In acidic conditions, MB was adsorbed onto composites via electrostatic attraction. While adsorption potential of RhB is unaffected by the changes in pH since it is a neutral dye. Similar results are reported by Ansari et al. [29] in their studies to remove CR from aqueous solutions using polyaniline@$MoS_2$-based composites. The removal of cationic dye MB using 2D $MoS_2/TiO_2$ (TM) nanocomposite occurs via two-stage integrated adsorption and photocatalytic decomposition processes [53]. In stage-I, namely adsorption stage, anionic (RhB, MO) and cationic (MB, CV), dye molecules are adsorbed onto TM surface due to electrostatic interactions between dye molecules and TM composites. In stage-II, namely photocatalytic stage, the photocatalytic degradation of dyes takes place under sunlight illumination, possibly due to photo charge career transfer from $TiO_2$. Figure 2d presents the proposed adsorption/photocatalytic mechanism for the dye on 2D $MoS_2/TiO_2$ (TM) nanocomposites.

## 3.2 MXenes-Based Composites

2D MXenes have the general formula $M_{n+1}X_nT_x$ ($n$ = 1–3), where "M" denotes an early transition metal (mostly Sc, Ti, V, Cr, Mo, W, Nb, Ta, Ti, Zr, Hf), "X" represents carbon (C) and/or nitrogen (N) and "T" stands for surficial functional groups, such as oxygen (–O), hydroxyl (–OH), fluorine (–F) and chlorine (–Cl), which are bonded with the outer layers of early transition metal where "x" stands for number of surficial functional groups [54–57]. Typically, MXenes can be developed from their precursor MAX phases by a chemical etching process [11, 21, 58]**.** The term "MAX" has the general formula $M_{n+1}AX_n$ ($n$ = 1, 2, or 3), where "M" is a transition metal element (primarily Ti, V, Cr, Y, Zr, Nb, Mo, Hf, Ta and W), "A" element is from groups IIIA (Al, Ga, In and Tl), IVA (Si, Ge, Sn, Pb), VA (P, As, S and Bi), VIA(S), "X" is carbon and/or nitrogen element [55, 59]. Due to the extraordinary properties such as significant high SSA, availability of abundant –OH sites, biocompatible nature, ease of surface functionalization, hydrophilicity and high conductivity, 2D MXenes have drawn the considerable attention of several researchers to utilize them in environmental remediation [54, 60]. Recently, MXenes-based nanocomposites have risen to a prominence as compared to other adsorbent materials in the field of water purification, for instance, adsorption, membranes and capacitive deionization [61–63]. The unique combination of properties of MXenes including in situ reduction plus adsorption makes MXenes a distinct material and opens a new door for the remediation of water pollutants.

**Adsorption of HMIs**: MXenes-based nanocomposites are shown to be superior adsorbents for the removal of heavy metals. For instance, $Ti_3C_2T_x$-based films prepared via Coulombic assembly process followed by vacuum-assisted filtration were exploited for the removal of Cr(VI), Ag(I), Au(III) and Pd(II) from water. The reduced graphene oxides (rGO) were inserted in between the layers of $Ti_3C_2T_x$-MXene to mitigate the restacking of $Ti_3C_2T_x$ nanosheets thus enabling an interaction between $Ti_3C_2T_x$ and HMIs in aqueous systems. The surface hydroxylation of $Ti_3C_2T_x$ was done by using HCl to increase the number of hydroxyl groups on $Ti_3C_2T_x$ resulting in higher wettability and adsorption capacity. The maximum adsorption capacities of Cr(VI), Ag(I), Au(III) and Pd(II) on $Ti_3C_2T_x$-based films were 84, 890, 1241 and 1172 mg $g^{-1}$, respectively [64]. A novel 2D $Ti_3C_2T_x$ MXene nanosheet having 57 $m^2$ $g^{-1}$ SSA was developed via intercalation followed by exfoliation process in 10% HF solution. It showed an excellent Cr(VI) adsorption capacity of 250 mg $g^{-1}$ (pH 5 and at room temperature) because of its larger SSA, well dispersibility in water, and reductivity. Especially, after purification of the effluent, Cr(VI) content reached as low as 5 ppb, which is lower than the drinking water standard set by the World Health Organization (0.05 ppm). At the same time, this kind of 2D $Ti_3C_2T_x$ MXene nanosheets can reduce Cr(VI) to Cr(III) and simultaneously adsorb the less toxic Cr(III). Additionally, the experimental data suggests that this reductive 2D $Ti_3C_2T_x$ MXene nanosheet can also be used to remove strong oxidant agents, including $K_3[Fe(CN)_6]$, $KMnO_4$ and $NaAuCl_4$. This substantially widens the practical applications of 2D

$Ti_3C_2Tx$ MXene nanosheets in water and wastewater treatment [21]. Another 2D-layered alk-MXene material ($Ti_3C_2(OH/ONa)_xF_{2-x}$) was prepared through chemical exfoliation followed by alkalization intercalation method using 5% sodium hydroxide solution. It strongly captured Pb(II) from water with a maximum sorption capacity of 140 mg $g^{-1}$ at pH 6.5, even under the presence of competing cations (Ca(II)/Mg(II)) at high concentrations. Figure 3a shows a schematic illustration of the synthesis and applications of $Ti_3C_2(OH/ONa)_xF_{2-x}$ nanocomposite. The results revealed that Pb(II) loaded $Ti_3C_2(OH/ONa)_xF_2$-x could be regenerated with an efficiency of 95.2% using 0.1% $HNO_3$ and 5% $Ca(NO_3)_2$ solution. The preferential adsorption of Pb(II) was due to low hydration energy (−1425 kJ $mol^{-1}$) as compared to Ca(II) (1505 kJ $mol^{-1}$) and Mg (II) (−1830 kJ $mol^{-1}$) [65]. In another method, a 2D/2D (alk-MXene/LDH) nanocomposite was successfully synthesized using a cautious and facile hydrothermal method and mechanical self-assembly method to remove carcinogenic Ni(II) from wastewater treatment systems (Fig. 3b) [11]. It showed an ultra-high adsorption capacity (222.717 mg $g^{-1}$) under a broad range of pH conditions (pH = 5–13) and best fitted with Redlich Peterson isotherm followed by multi-molecular layer adsorption i.e., Freundlich isotherm model ($R^2 = 0.99202$) and effectively suited with pseudo-second-order kinetic models ($R^2 = 0.99992$). The far more remarkable thing is that the alk-MXene/LDH nanocomposite possessed a good adsorbent capacity of more than 85.32% in eight successive sorption–desorption cycles.

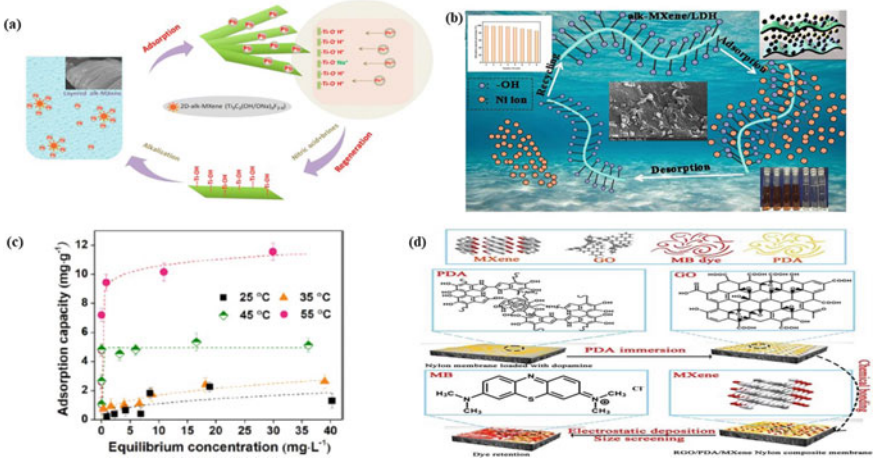


**Fig. 3** **a** Schematic illustration of synthesis and application of $Ti_3C_2(OH/ONa)_xF_{2x}$ composite. Reprinted with permission from [65]. Copyright 2014 JACS; **b** schematic illustration of adsorption and desorption of alk-MXene/LDH nanocomposite. Reprinted with permission from [11]. Copyright 2020 Elsevier B.V.; **c** Adsorption capacity of MXene@$Fe_3O_4$ for MB at different temperatures. Reprinted with permission from [30]. Copyright 2019 ACS Applied Materials and Interfaces; **d** schematic diagram of membrane dye removal process. Reprinted with permission from [67]. Copyright 2020 Elsevier B.V.

**Adsorption of Dyes**: The adsorptive performance of MXenes toward MB dye removal can be substantially enhanced by increasing the number of functional groups via in situ growth approach. The interlayer spacing of 2D-$Ti_3C_2T_x$ MXene was increased by functionalization with magnetic $Fe_3O_4$ nanoparticles that led to the formation of final product, MXene@$Fe_3O_4$ [30]. MB adsorption onto the MXene@$Fe_3O_4$ was found to be 11.68 mg $g^{-1}$ at 55 °C as calculated from the Langmuir isotherm model. Adsorption mechanism between MB and MXene@$Fe_3O_4$ is primarily because of the presence of Ti site and hydroxyl group of MXene@$Fe_3O_4$ nanocomposites. The reusability tests demonstrated that MXene@$Fe_3O_4$ nanocomposites could be reused for five times and the retained adsorption capacity exceeded upto 77%. In another report, a 2D-MX@$Fe_3O_4$ was synthesized by a two-step exfoliation of $Ti_3AlC_2$ MAX-phase ceramic (as bulk), including HF etching followed by intercalation by TPAOH [66]. It exhibited good adsorption capacity toward MB (cationic dyes) at various temperatures i.e., 9.85 mg $g^{-1}$ at 55 °C which decreased to 3.95 mg $g^{-1}$ at 40 °C and 1.71 mg $g^{-1}$ at 25 °C (Fig. 3c). The high removal rate of MB (about 91.93%) at higher temperature is primarily because of the intimate interaction of surficial Ti–OH group of 2D-MX@$Fe_3O_4$, as well as the availability of the unsaturated nitrogen heteroatoms in the MB, which additionally facilitates MB adsorption process. Langmuir (at high temperature) and Freundlich (at low temperature) models were chosen to suit the isotherm experimental data. The mechanism of MB on 2D-MX@$Fe_3O_4$ involved hydrogen bonding accompanying with electrostatic interaction at 55 °C, while electrostatic interactions at 25 °C. The RGO/PDA/MXene composite membrane exhibited excellent dye molecule separation performance (over 96%) against MB, MO, MR, CR and EB and oil–water separation [67]. Figure 3d represents a schematic diagram of the membrane dye removal process. It may be attributed to hydrophilicity behavior by MXenes surface and regular straight-rigid channels of RGO/PDA/MXene composite material. The structure and separation efficiency of RGO/PDA/MXene composite was significantly influenced by varying the MXene ratio. More specifically, RPM/PDA/MXene composite membrane was found to be extremely stable which could be operated for a longer time. The introduction of sulfonic group improved the adsorption capacity of MXenes ($Ti_3C_2$–$SO_3H$) toward MB (111.11 mg $g^{-1}$ within 70 min). The main binding mechanism between $Ti_3C_2$–$SO_3H$ and MB was predicted to be electrostatic interaction in an alkaline environment, showing monolayer coverage [68].

## *3.3 TMDs-Based Composites*

Transition metal dichalcogenides (TMDs) have the general formula $MX_2$, where "M" is a transition metal (such as Mo, W, V, Nb, Ta, Ti, Zr, Hf, Tc, and Re), "X" is a chalcogen element of group 16 (such as S, Se and Te). The unit layer of TMDs is in the form of X–M–X, in which one center atom layer of transition metal (M) is placed between two chalcogen's atom layers (X). Various types of TMDs nanocomposites

were synthesized and exploited for the removal of water pollutants due to chalcogen's strong affinity toward heavy metal ions and organic dyes.

**Adsorption of HMIs**: TMDs nanocomposites are frequently used as a potential competent adsorbent for the elimination of several divalent cations including Pb(II), Co(II), Hg(II) and Cd(II). For example, flower-like $WSe_2$ and $WS_2$ microspheres were prepared by a simple and scalable approach i.e., solvothermal method, and used to sequestrate As(V), As(III), Cd(II), Pb(II) and Hg(II) from water. They showed an extremely high adsorption capacities for Pb(II): 288 and 386 mg $g^{-1}$ for the $WSe_2$ and $WS_2$, respectively, and for Hg(II): 1512 and 1954 mg $g^{-1}$ for the $WSe_2$ and $WS_2$, respectively. The excellent adsorption abilities of $WSe_2$ and $WS_2$ microspheres toward Pb(II) and Hg(II) are due to their structural rigidity and the abundance of chalcogen's ligands with an instinctive reactivity to soft heavy metal ions [69]. Among TMDs, $MoS_2$ exhibited some fascinating properties such as a peculiar 2D structure, rich in sulfur, excellent mechanical flexibility, huge SSA and exceptional chemical and thermal stability. A novel super adsorbent, 2D $MoS_2$, containing less than five S−Mo−S layers and huge sulfur-rich surface area was synthesized via exfoliation method for the removal of Hg(II) metal ions in water. The authors reported that Hg(II) adsorption onto 2D $MoS_2$ was mainly relied on the temperature (maximum adsorption capacity: 518.135 mg $g^{-1}$ at 20 °C, and 584.795 mg $g^{-1}$ at 35 °C). This might be due to more availability of sulfur atoms on the surface of 2D $MoS_2$ [70]. $MoS_2$@Kaolin nanocomposites were synthesized by a simple one-step hydrothermal method to adsorb Pb(II) from the aqueous solution. It showed maximum adsorption capacity of 280.39 mg $g^{-1}$ at pH 4 that followed the Langmuir isotherm model for pseudo-second-order kinetic model. In addition, $MoS_2$@Kaolin nanocomposites showed an excellent regeneration properties with more than 77% adsorption capacity even after five cycles [36]. Figure 4a illustrates the adsorption of Pb(II) using $MoS_2/CeO_2$ nanocomposites [51]. The superior selectivity of the $MoS_2/CeO_2$ nanocomposites toward Pb(II) could be attributed to the strong soft–soft interactions between Pb and S of $MoS_2$ surface. Figure 4b presents schematic illustration of preparation and application of a novel ternary nanocomposite ($MoS_2$@PDA@PAM) to sequestrate Cu(II) ions [71]. The result suggested that the addition of PAM to $MoS_2$ increased the adsorption capability by 2.5 folds against Cu(II). Freundlich models and pseudo-second order were chosen to suit the isotherm and kinetic experimental data. The adsorption mechanism of Cu(II) on $MoS_2$@PDA@PAM involved an electrostatic interaction and/or a chemical chelation between Cu (II) ions and -$NH_2$ of $MoS_2$@PDA@PAM nanocomposites. Another novel material, $MoS_2$-g-PDMA exhibits an excellent adsorption capacities of 448.4 and 171.2 mg $g^{-1}$ toward U(VI) and Eu(III), respectively, as obtained from the Langmuir model. The high adsorption capacity is mainly because of the existence of a large number of phosphates, carboxyl and sulfur groups on the $MoS_2$-g-PDMA. The equilibrium adsorption data closely followed the pseudo-second-order kinetic model which means that the adsorption process was controlled by chemical sorption [72]. Further studies suggested that the cation selectivity of $MoS_2$ followed the order Pb(II) > Cu(II) ≫ Cd(II) > Zn(II), Ni(II) > Mg(II), K(I), Ca(II) [73]. The regeneration experiments showed that the 2D

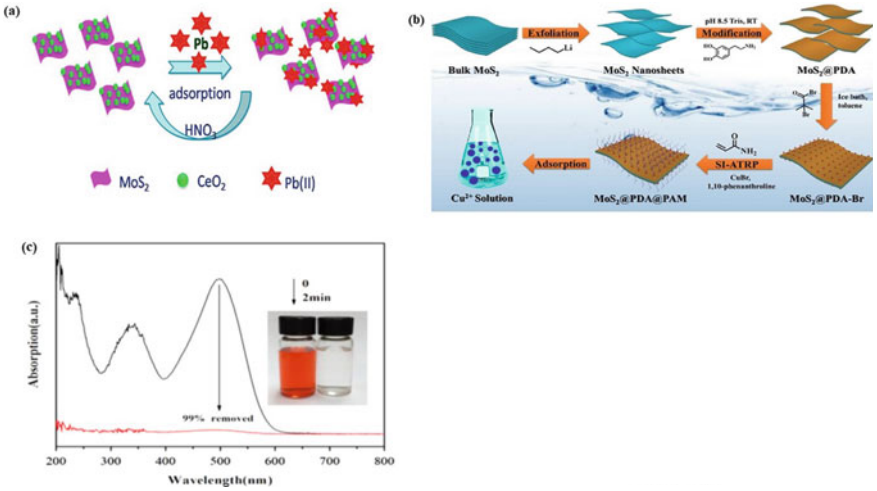


**Fig. 4** **a** Schematic illustration of the application of $MoS_2/CeO_2$ nanocomposites. Reprinted with permission from [67]. Copyright 2020 Elsevier B.V.; **b** schematic illustration of preparation and application of $MoS_2$@PDA@PAM nanocomposites. Reprinted with permission from [71]. Copyright 2018 Elsevier B.V.; **c** the adsorption spectra of Congo red aqueous solution of $Fe_3O_4/MoS_2$ nanocomposites. Reprinted with permission from [33]. Copyright 2015 Elsevier B.V.

$MoS_2$ nanosheets could be reused from two to five adsorption cycles with 85–95% lead removal.

**Adsorption of Dyes**: Like as heavy metal ion adsorption, the organic dye adsorption on $MoS_2$ also solely depends on SSA. Therefore, it is utmost important to increase the SSA of $MoS_2$ by tuning its surface to achieve more exposed sites for a better adsorption of pollutants. For example, $MoS_2$ microspheres based on different sulfur sources such as $Na_2S$, $C_2H_5NS$, $CH_4N_2S$ and $(NH_4)_2S$ were investigated for the sequestration of anionic dye RhB [74]. The mesoporous $MoS_2$–$CH_4N_2S$ microsphere showed the highest adsorption capacity (136.99 mg $g^{-1}$ at 293.15 K, 1 atm) with a BET SSA of 72.0 $m^2$ $g^{-1}$. This could be attributed to a significant degree of puckering and pore structure. Furthermore, the synthesized mesoporous $MoS_2$/GQD with a pore size of 8.6 nm and SSA of 151.4 $m^2$ $g^{-1}$ demonstrated an excellent selective adsorption capacity and ultrafast adsorption for RhB dye within 2 s under ultrasound assistant [37]. The $MoS_2$/GQD showed a high adsorption performance for RhB dye (285 mg $g^{-1}$). It also exhibited a high cycling adsorption stability for RhB removal with more than 98% reclaim ratio. A highly active sites containing ultrathin-layered $MoS_2$ nanoflowers were synthesized through hydrothermal method and used as an efficient adsorbent to sequestrate RhB from wastewater [75]. The $MoS_2$ nanoflowers were polycrystalline in nature, comprised of irregular and non-uniform nanoflowers that looked like "sponges" with a smooth surface (BET SSA ($S_{BET}$): 71.7 $m^2$ $g^{-1}$, average pore diameter: 280.7 Å). The adsorption kinetic data of $MoS_2$ nanoflowers for RhB fitted with Langmuir isotherm model with a maximum

adsorption capacity of 365 mg $g^{-1}$. The possible adsorption mechanism of $MoS_2$ nanoflowers to remove RhB includes electrostatic attraction, π-π conjugated effect and van der Waals force. The regeneration capability of $MoS_2$ nanoflowers seems to be excellent, as their results indicated the elimination of RhB even after six cycles and it was approximately 85%. A study reported the maximum adsorption capacity of 71 mg $g^{-1}$ for CR and adsorption equilibrium in only 2 min using superparamagnetic $Fe_3O_4$ nanoparticles (average size: 10–15 nm) anchored to $MoS_2$ nanosheets (Fig. 4c) [33].

### *3.4 Phosphorene-Based Composites*

Phosphorene is one of the most rapidly emerging 2D nanomaterials which finds wide applications due to its desirable properties such as puckered hexagonal layered structure, adjustable band gap, high SSA, abundance, high carrier mobility and high dispersion capability [28, 76]. Several theoretical studies are done on phosphorene nanocomposites in order to remediate heavy metal ions and dyes, however, experimental approaches are still very less due to their associated stability problems.

**Adsorption of HMIs**: Novel phosphorene composite, MNP-PN-TNT adsorbents are prepared via hydrothermal process to remove Cr(VI) from synthetic water in acidic environments. Adsorption capacity of MNP-PN-TNT was found to be 35 mg $g^{-1}$ at 50 ppm initial Cr(VI) concentration and 318 K temperature. The possible adsorption mechanism of Cr(VI) on MNP-PN-TNT might be due to the displacement of surface hydroxyl groups (Fig. 5a). The regeneration test showed that the adsorption capacity of MNP-PN-TNT for Cr(VI) was 6 mg $g^{-1}$ even after three cycles [4]. The iron-incorporated phosphorene nanoadsorbents were studied for the removal of arsenic from water using density functional theory (DFT) calculations [77]. The obtained results suggested that As(III) uptake incurred as a consequence of strong inner-sphere surface complex formation in between the As(III) and Fe-doped phosphorene nanoadsorbents from the aqueous system at 25 °C. Adatom doping scheme showed a better adsorption behavior than substitutional doping in water. The effect of $H_2O$ studies showed that arsenic adsorption onto the nanocomposite remains stable under acidic to neutral condition (Fig. 5b). As(III) adsorption onto Fe-doped phosphorene nanocomposite attributed to permanent electrostatics, polarization and charge-transfer stabilizing effects. Further, it was reported that this nanocomposite can also be used to remove As(III) and As(V) directly and concurrently, without a pre-oxidation step to transform As(III) to As(V). The mutual interaction and permanency between trivalent arsenic and pristine with metal (Ni and Cu)-doped phosphorene using DFT were further explored [78]. The purpose of using dopants (Ni and Cu) was to create adsorption sites on the phosphorene nanoadsorbents, which consequently allowed the inner-sphere surface complexation of As(III) onto the chosen nanoadsorbents. The DFT study showed that metallic dopants significantly enhanced the interaction and adsorption stability between phosphorene and As(III) as compared to

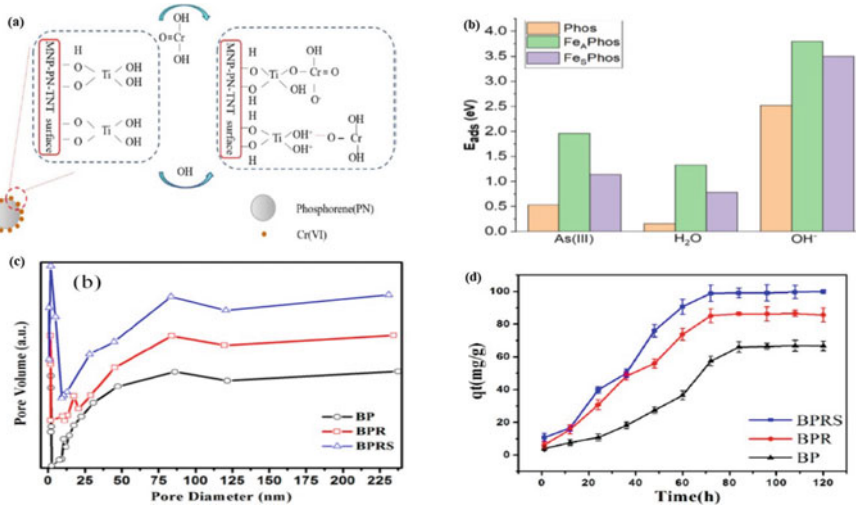


**Fig. 5** **a** Schematic illustration of the Cr(VI) removal mechanism with MNP-PN-TNT. Reprinted with permission from [4]. Copyright 2019 Elsevier B.V.; **b** comparative of adsorption energies ($E_{ads}$) of As(III) versus $H_2O$ versus $OH^-$ anions. Reprinted with permission from [77]. Copyright 2020 Elsevier B.V.; **c** pore size distributions of BP, BPR, and BPRS. Reprinted with permission from [80]. Copyright 2020 sustainability, MDPI; **d** MB dye removal as function of time. Reprinted with permission from [80]. Copyright 2020 sustainability, MDPI

the intrinsic phosphorene. The adsorption process of As(III) on single-layer phosphorene and graphene was elucidated as a function of temperature, pH and concentration [79]. The results revealed that As(III) adsorption was more favorable for phosphorene under acidic conditions having the maximum adsorption capacity of 4.83 mg $g^{-1}$, which was found to be higher than graphene (1.33 mg $g^{-1}$) under similar conditions. The thermal dynamic analysis suggested that As(III) adsorption on phosphorene was a non-spontaneous, irreversible reaction with chemisorption.

**Adsorption of Dyes**: 2D black phosphorus (BP), black phosphorene (BPR) and sulfonated BPR (BPRS) comparatively studied as adsorbents for the adsorptive removal of MB dyes from water [80]. The SSA of BP, BPR and BPRS was calculated to be 6.78, 6.92 and 7.72 $m^2$ $g^{-1}$, respectively (Fig. 5c). BPRS provided more number of free active sites for MB adsorption, thus exhibited a higher adsorption capacity which was 140.85 mg $g^{-1}$(it was 84.03 mg $g^{-1}$ for BP and 91.74 mg $g^{-1}$ for BPR). Figure 5d presents the removal of MB dye as a function of time. The study suggested that adsorption mechanisms included electrostatic interaction, hydrophobic interaction, intraparticle diffusion, chemical adsorption, sulfonic acid functional group-guided adsorption and wrinkle-induced adsorption. As revealed by the desorption study, the as-prepared BP-based adsorbents could not be reused. MB has a tendency to attach with adsorbents due to the presence of hydrogen bonds between them which resulted in a lesser chance for MB to diffuse through the adsorbents.

### 3.5 *Adsorption of Toxic Gases and Volatile Organic Compounds*

The burning of fossil fuels indisputably emits and increases the concentration of $CO_2$ in the atmosphere causing global warming and greenhouse effects. 2D nanomaterials with high surface-to-volume ratio such as zeolites, MOFs, functionalized GO, MXenes, and TMDs features as a potential solid adsorbents. To date, various 2D nanomaterial composites are theoretically and experimentally studied to remove toxic gaseous contaminants [88].

MXenes-based nanocomposites are theoretically investigated for $CO_2$ abatement, storage and activation [89]. The studies revealed that $M_2C$ (MXene carbides) compounds enable to capture $CO_2$ within a range of 2.34–8.25 mol $CO_2$ per kilogram even at high temperatures and low partial pressures. Furthermore, different findings indicated that the high value of adsorption energies (about 3.69 eV), bent structures and activation verified by high charge transfer from MXene to $CO_2$ confirmed the conversion of $CO_2$ molecules to strongly anionic $CO_2^{\delta-}$ species with δ-Bader values ranging between −0.90 and −2.86e [90]. The theoretical investigations using DFT demonstrated that bare 2D-$M_2N$ MXenes even without surficial functional groups could efficiently uptake $CO_2$ (2.32–7.96 mol $CO_2$ $Kg^{-1}$) even at low partial pressures of $CO_2$ and elevated temperatures [91]. $M_2C$, $M_2N$ MXenes show higher adsorption energies values accompanied by $CO_2$ activation, supported by the bent structures, appearance of a strongly anionic $CO_2^{\delta-}$ adsorbed species, and high charge transfer from MXenes to $CO_2$. Therefore, these studies suggest that MXenes can act as a potential material for the capture, storage and activation of $CO_2$. It was found that a change in the composition does not significantly affect MXenes' properties, while the functionalization of pristine MXenes can lead to change in the electronic properties [92]. In a theoretical study, the improvement of the selectivity of MXenes through O-functionalization; O-MXenes or $M_2CO_2$ was proposed for the adsorption of small gas molecules such as $H_2$, $H_2O$, CO, $CO_2$, $N_2$, NO, $NO_2$, $NH_3$, $H_2S$ and $SO_2$. The results depicted that the adsorption of small gas molecules on MXenes occurred predominantly by the chemisorption process. Pristine MXenes seem to be very reactive and thus suitable for catalytic process with a low selectivity toward these gas molecules. Among these gases, only $NH_3$ gets adsorbed on MXenes. In this case, functionalization of MXenes reduces its reactivity, whereas selectivity is enhanced for gas sensing and separation. $Mo_2CO_2$ and $V_2CO_2$ strongly adsorb NO molecules as compared to others, while $Nb_2CO_2$ and $Ti_2CO_2$ prefer $NH_3$ [93]. Recently, the gas adsorption behavior of S-functionalized $M_2N$ (M = Ti, V) MXenes i.e., $Ti_2NS_2$ and $V_2NS_2$ were considered as model nanomaterials to theoretically examine the inorganic gases including $CH_4$, CO, $CO_2$, $NH_3$, NO, $NO_2$, $H_2S$, and $SO_2$ by DFT. Among all these gases only nitric oxide (NO), and nitrogen dioxide ($NO_2$) showed exceptional sensitivity toward S-terminated nitride MXenes because of appreciable amount of charge transfer from NO, and $NO_2$ gas molecules to $Ti_2NS_2$ (adsorption energy, $E_B$, of −0.406 eV) and $V_2NS_2$ (adsorption energy of −0.208 eV), respectively [94]. A non-functionalized MXene having a general formula 2D $M_2C$ (M

= Ti, Zr, Hf, V, Nb, Ta, Cr, Mo, and W) was developed, isolated and investigated using first-principle simulations for $CO_2$ abatement. The high adsorption energies (−3.69 eV) of $M_2C$ and effective adsorption of $CO_2$ at a very low $CO_2$ partial pressure and high temperatures suggested that the 2D $M_2C$ MXenes can be a potential material for $CO_2$ capture, and its storage was followed by activation [90].

TMDs may be considered for tackling the air pollution through the sensing and adsorption of toxic gases. To date, several studies are done to adsorb toxic gases like CO, $SO_x$, $H_2S$, $NO_x$ on TMDs. For instance, first-principles calculations by DFT are systematically implemented to investigate the adsorption of gas molecules, including CO and NO on metal-(Au, Pt, Pd, or Ni) doped $MoS_2$ monolayer [95]. The adsorptive removal of CO and NO on a metal-doped $MoS_2$ monolayer is exothermic i.e., chemisorption. It may be due to a higher adsorption energy value (larger than 0.9 eV for CO and NO) and the short distance between the adsorbed CO or NO and the metal-doped $MoS_2$. In case of CO adsorption, the transport properties of Pt-, Pd-, or Ni-doped $MoS_2$ monolayer change due to the charge transfer. However, in case of NO, the transport properties of metal-doped $MoS_2$ monolayer changed due to the alteration in band gap and charge transfer [95]. Apart from this, several other TMDs including Pt/Au-decorated $WSe_2$ monolayer [96], $Al_2O_3$-doped $MoS_2$ [97], Au nanoparticles on monolayer $MoS_2$ [98], Rh-doped $MoSe_2$ [99] are also investigated against CO adsorption. The incorporation of Cu nanoparticles into $MoS_2$ nanosheets greatly enhanced its adsorption capability for $CO_2$ uptake [100]. $SnO_2$-doped $MoS_2$ [26] and $Bi_2S_3/MoS_2$ [38] are theoretically investigated for $CO_2$ reduction process, while N-doped $TiO_2/WSe_2$ nanocomposite for $SO_x$ [101], and $MoS_2$-g-$C_3N_4$ nanocomposite for NO [102] using DFT. $CO_2$ adsorption on $MoS_2$ monolayers was found to drastically increase in the presence of an external applied electric field, which is mainly attributed to a decrease in C–S bond length, an increase in adsorption energy accompanied by high charge transfer [103]. However, in the absence of an applied electric field, the interaction between $CO_2$ and $MoS_2$ monolayers is very week due to van der Waals forces between them. Monolayer $MoS_2$ sheets are also studied for the adsorption of polyatomic species such as $O_3$ and $SO_x$ ($SO_2$ and $SO_3$) with respect to charge transfer, adsorption energy, band structures and charge density differences by using first-principles calculations [104]. The weak van der Waals (vdWs) interactions between polyatomic gas molecules and $MoS_2$ sheets confirmed the physisorption. It thus formed the most stable configurations which were energetically favored. It subsequently elongated oxygen–oxygen (O –O) and sulfur-oxygen (S–O) bonds of the gas molecules. Electronic band structure calculations confirmed the alteration in $MoS_2$ sheets after the adsorption of selected gas molecules. Charge density difference studies showed that $O_3$, $SO_2$ and $SO_3$ molecules served as charge acceptor from $MoS_2$. Another novel gas adsorbent, Ni-doped $MoS_2$ monolayer (Ni-$MoS_2$) was projected for the adsorption of $SO_2$ and $H_2S$ molecules [105]. The molecules of $SO_2$ and $H_2S$ may be strongly chemisorbed on Ni-$MoS_2$ with apparent charge transfer and strong adsorption energy which made Ni-$MoS_2$ a potential candidate as a $SO_2$ and $H_2S$ capturer. Besides these 2D TMDs, some other types of TMDs; Rh-doped $MoSe_2$ (Rh-$MoSe_2$) monolayer for CO, NO, $NO_2$ and $SO_2$ [99], Pd-doped $MoSe_2$ (Pd-$MoSe_2$) monolayer for NO, $NO_2$, $SO_2$ and $H_2S$ [106],

N-doped $TiO_2/WSe_2$ nanocomposite for $SO_x$ [101], Pd, Ag, and Au, Pt-doped monolayer $WSe_2$ for $CO_2$, $NO_2$ and $SO_2$ [107], $MoS_2$-g-$C_3N_4$ nanocomposites for NO [102] were widely studied. Elemental 2D nanomaterials such as silicene, germanene and phosphorene reported to have a better adsorption capacity for gas contaminants. Theoritical study revealed that $NO_2$ molecules can be strongly physisorbed on 2D monolayer phosphorene ($E_B = -0.50$ eV), while gas molecules with low adsorption energies (CO ($E_B = -0.31$), $H_2$ ($E_B = -0.13$), $H_2O$ ($E_B = -0.14$), $NH_3$ ($E_B = -0.18$), NO ($E_B = -0.32$), and $O_2$ ($E_B = -0.27$)) are weakly physiosorbed [108]. Based on the charge transfer study, NO, $NO_2$ and $O_2$ gas molecules act as acceptor, and the electronic and magnetic properties of 2D phosphorene change significantly after the adsorption of NO, $NO_2$ and $O_2$ molecules, together with strong binding energy which indicated that 2D phosphorene can be a potential molecular sensor. Another DFT study indicated that Li-decorated phosphorene was favorable for $CO_2$ molecules adsorption because of a high value of adsorption energy ($E_{ads}$) of 0.376 eV [27]. And Al-decorated phosphorene proved to be more competent to adsorb $NO_2$ and $SO_2$ due to the large adsorption energies of 3.951 and 3.608 eV, respectively. In addition, Pt-decorated phosphorene turned out to be efficient for $NO_2$ and $SO_2$ dissociations because of the low energy barriers of acidic gases and exothermic reaction process. The adsorption energy values as calculated form DFT seem to indicate that Pt-, Al- and Ni-decorated phosphorene exhibited the maximal adsorption behavior toward $H_2S$, HCN and $NH_3$, respectively [109]. Very recently, red phosphorene nanosheets (P-NS) are used to adsorb the toxic cigarette vapors such as acrolein (causing lung cancer), acrylamide (causing neurological disorders) and nicotine (affecting central nervous system). The adsorption behavior of P-NS at two different sites (top and middle site) computed by first-principles calculations. The value of Bader charge transfer ($Q$) and energy gap variation enunciated that the middle site of P-NS has astonishing adsorption tendency due to a high transmission of electron and larger energy gap variation [110].

In addition to inorganic toxic gases adsorption, the volatile organic compounds (VOCs) can also be sensed and removed using 2D nanomaterial composites. $Ti_3C_2T_x$ MXene with properties like low electrical noise and strong signal are synthesized to detect VOCs gases such as acetone, ethanol, propanal and ammonia in a concentration range of 50–100 ppb at 25 °C [111]. On the surface of $Ti_3C_2T_x$ MXene, the terminal hydroxyl groups were solely responsible for capturing the targeted contaminants. Furthermore, the study suggested that $Ti_3C_2T_x$ MXene showed intrinsically ultra-high signal-to-noise ratio (SNR) due to its high metallic conductivity, and the functionalized surfaces made it a suitable material for high sensitive gas-sensing applications. S-doped MXene(S–$Ti_3C_2T_x$) showed an astonishing response for different VOCs such as ethanol, hexane, hexyl acetate and toluene. The binding mechanism and the unique selectivity of toluene by both undoped and S-doped MXene are theoretically studied by DFT [112]. 2D $MoS_2$ nanoflakes were utilized in detecting oxygen-based VOCs such as acetone, ethanol and 2-propanol at room temperature. DFT calculations demonstrated that Au nanoparticles functionalization enhanced the adsorption performance of $MoS_2$ nanoflakes toward acetone by more than two

folds (i.e., 31.6%) [113]. In another study, the adsorption enthalpies ($\Delta H_{ad}$) of non-polar VOCs including 1,4-dioxane, benzene, cyclohexane and polar VOCs including acetone, acetonitrile, nitromethane, and tetrachloromethane on black phosphorus were experimentally determined using inverse gas chromatography technique [114]. The properties like anisotropic and deformed layers of black phosphorus exhibited an affinity enhancement to polar VOCs (e.g., HCN) due to dipole–dipole interactions and molecule-surface attachment.

## 4 Conclusions, Challenges and Future Prospects

2D nanomaterial composites have emerged as excellent adsorbent materials for the environmental remediation. However, there are many challenges and stubborn problems that must be thoroughly studied and experimentally verified in the laboratory in order to completely leverage their physicochemical properties. The low yield and massive cost of MXenes synthesis are two of the biggest problems faced by the research community. In near future, it is expected that the ease of design, low cost and efficient production of MXenes on a larger scale will be advantageous for further advancement of research to a new doorway to widen their applications. Furthermore, it is found that many MXenes compositions are only theoretically studied using DFT for water treatment and toxic gases' adsorption. To validate the outcomes of these theoretical calculations, systematic experiments and strategies of efficient systems must be designed and proved. In case of TMDs, $MoS_2$ is widely exploited for water purification because of its high adsorption capacity, but pollution blocks its active sites thereby reducing its adsorption capacity. It needs to be resolved by creating more free active surficial sites. The research work on 2D phosphorene is still in its infancy for environment remediation as compared to other 2D nanomaterials. More studies are needed to focus on the development of different types of phosphorene nanocomposites with hydrophilic nature, super adsorption behavior for applications in water purification in real environmental conditions.

**Acknowledgements** One of the authors, Tanweer S. M. is thankful to the University Grants Commission (UGC) for the Non-NET Fellowship.

## References

1. Yu M-H (2005) Environmental toxicology: biological and health effects of pollutants. Water Research
2. Jasper JT, Yang Y, Hoffmann MR (2017) Toxic byproduct formation during electrochemical treatment of latrine wastewater. Environ Sci Technol. https://doi.org/10.1021/acs.est.7b01002
3. Ghangrekar MM, Chatterjee P (2018) Water pollutants classification and its effects on environment. In: Carbon nanostructures. Springer International Publishing, pp 11–26. https://doi.org/10.1007/978-3-319-95603-9_2

4. Jung LY, Chen JJ, Cao WZ, Persson KM, Ouyang T, Zhang L, Xie X, Liu F, Li J, Chang CT (2019) Novel materials for Cr(VI)adsorption by magnetic titanium nanotubes coated phosphorene. J Mol Liq. https://doi.org/10.1016/j.molliq.2019.04.103
5. Fathi A, Mohamed T, Claude G, Maurin G, Mohamed BA (2006) Effect of a magnetic water treatment on homogeneous and heterogeneous precipitation of calcium carbonate. Water Res. https://doi.org/10.1016/j.watres.2006.03.013
6. Andreozzi R, Caprio V, Insola A, Marotta R (1999) Advanced oxidation processes (AOP) for water purification and recovery. Catal Today. https://doi.org/10.1016/S0920-5861(99)00102-9
7. Abdulgader HA, Kochkodan V, Hilal N (2013) Hybrid ion exchange—pressure driven membrane processes in water treatment: a review. Sep Purif Technol. https://doi.org/10.1016/j.seppur.2013.05.052
8. Rosman N, Salleh WNW, Mohamed MA, Jaafar J, Ismail AF, Harun Z (2018) Hybrid membrane filtration-advanced oxidation processes for removal of pharmaceutical residue. J Colloid Interface Sci. https://doi.org/10.1016/j.jcis.2018.07.118
9. Ali S, Tanweer MS, Alam M (2020) Kinetic, isothermal, thermodynamic and adsorption studies on Mentha piperita using ICP-OES. Surf Interfaces. https://doi.org/10.1016/j.surfin.2020.100516
10. Jiménez AM, Borja R, Martín A (2003) Aerobic-anaerobic biodegradation of beet molasses alcoholic fermentation wastewater. Process Biochem. https://doi.org/10.1016/S0032-9592(02)00325-4
11. Feng X, Y, Zongxue, Long R, Li X, Shao L, Zeng H, Zeng G, Zuo Y (2020) Self-assembling 2D/2D (MXene/LDH) materials achieve ultra-high adsorption of heavy metals Ni2+ through terminal group modification. Sep Purif Technol. https://doi.org/10.1016/j.seppur.2020.117525
12. Ma Y, Zhao J, Yang BL (2006) Removal of H2S in waste gases by an activated carbon bioreactor. Int Biodeterior Biodegradation. https://doi.org/10.1016/j.ibiod.2005.10.010
13. Uddin MK (2017) A review on the adsorption of heavy metals by clay minerals, with special focus on the past decade. Chem Eng J. https://doi.org/10.1016/j.cej.2016.09.029
14. Anghel D, Lascu A, Epuran C, Fratilescu I, Ianasi C, Birdeanu M, Fagadar-Cosma E (2020) Hybrid materials based on silica matrices impregnated with pt-porphyrin or ptnps destined for Co2 gas detection or for wastewaters color removal. Int J Mol Sci. https://doi.org/10.3390/ijms21124262
15. Yan Z, Tang S, Zhou X, L, Yang, Xiao X, Chen H, Qin Y, Sun W (2019) All-silica zeolites screening for capture of toxic gases from molecular simulation. Chin J Chem Eng. https://doi.org/10.1016/j.cjche.2018.02.025
16. Ahmad R, Ansari K (2020) Polyacrylamide-grafted Actinidia deliciosa peels powder (PGADP) for the sequestration of crystal violet dye: isotherms, kinetics and thermodynamic studies. Appl Water Sci. https://doi.org/10.1007/s13201-020-01263-7
17. Li J, Wang H, Yuan X, Zhang J, Chew JW (2020) Metal-organic framework membranes for wastewater treatment and water regeneration. Coord Chem Rev. https://doi.org/10.1016/j.ccr.2019.213116
18. Rajapakse M, Karki B, Abu UO, Pishgar S, Rajib Khan Musa Md, Shah Riyadh SM, Yu M, Sumanasekera G, Jasinski JB (2021) Intercalation as a versatile tool for fabrication, property tuning, and phase transitions in 2D materials. npj 2D materials and applications. Nat Res https://doi.org/10.1038/s41699-021-00211-6
19. Naguib M, Kurtoglu M, Presser V, Jun L, Niu J, Heon M, Hultman L, Gogotsi Y, Barsoum MW (2011) Two-dimensional nanocrystals produced by exfoliation of Ti 3AlC 2. Adv Mater. https://doi.org/10.1002/adma.201102306
20. Rasool K, Pandey RP, Abdul Rasheed P, Buczek S, Gogotsi Y, Mahmoud KA (2019) Water treatment and environmental remediation applications of two-dimensional metal carbides (MXenes). Mater Today. https://doi.org/10.1016/j.mattod.2019.05.017
21. Ying Y, Liu Y, Wang X, Mao Y, Cao W, Pan H, Peng X (2015) Two-dimensional titanium carbide for efficiently reductive removal of highly toxic chromium(VI) from water. ACS Appl Mater Interfaces. https://doi.org/10.1021/am5074722

22. Shahzad A, Rasool K, Miran W, Nawaz M, Jang J, Mahmoud KA, Lee DS (2017) Two-dimensional $Ti_3C_2Tx$ MXene nanosheets for efficient copper removal from water. ACS Sustain Chem Eng. https://doi.org/10.1021/acssuschemeng.7b02695
23. Zou G, Guo J, Peng Q, Zhou A, Zhang Q, Liu B (2015) Synthesis of urchin-like rutile titania carbon nanocomposites by iron-facilitated phase transformation of MXene for environmental remediation. J Mater Chem A. https://doi.org/10.1039/c5ta07343j
24. Manzeli S, Ovchinnikov D, Pasquier D, Yazyev OV, Kis A (2017) 2D transition metal dichalcogenides. Nat Rev Mater. https://doi.org/10.1038/natrevmats.2017.33
25. Tian C, Xiang X, Juwei W, Li B, Cai C, Khan B, Chen H, Yuan Y, Xiaotao Z (2018) Facile synthesis of MoS2/CuS nanosheet composites as an efficient and ultrafast adsorbent for water-soluble dyes. J Chem Eng Data. https://doi.org/10.1021/acs.jced.8b00593
26. Hu X, Yang H, Gao M, Tian H, Li Y, Liang Z, Jian X (2019) Insights into the photoassisted electrocatalytic reduction of $CO_2$ over a two-dimensional $MoS_2$ nanostructure loaded on $SnO_2$ nanoparticles. ChemElectroChem. https://doi.org/10.1002/celc.201900632
27. Kuang A, Kuang M, Yuan H, Wang G, Chen H, Yang X (2017) Acidic gases ($CO_2$, $NO_2$ and $SO_2$) capture and dissociation on metal decorated phosphorene. Appl Surf Sci. https://doi.org/10.1016/j.apsusc.2017.03.135
28. Zhang HP, Hou Jl, Wang Y, Tang PP, Zhang YP, Lin XY, Liu C, Tang Y (2017) Adsorption behavior of 2, 3, 7, 8-tetrachlorodibenzo-p-dioxin on pristine and doped black phosphorene: a DFT study. Chemosphere. https://doi.org/10.1016/j.chemosphere.2017.06.120
29. Kumar R, Ansari SA, Barakat MA, Aljaafari A, Cho MH (2018) A polyaniline@$MoS_2$-based organic-inorganic nanohybrid for the removal of Congo red: adsorption kinetic, thermodynamic and isotherm studies. New J Chem. https://doi.org/10.1039/c8nj02803f
30. Zhang P, Xiang M, Liu H, Yang C, Deng S (2019) Novel two-dimensional magnetic titanium carbide for methylene blue removal over a wide pH range: insight into removal performance and mechanism. ACS Appl Mater Interfaces. https://doi.org/10.1021/acsami.9b04222
31. Li Y, Yin X, Huang X, Tian J, Wu W, Liu X (2019) The novel and facile preparation of 2DMoS2@C composites for dye adsorption application. Appl Surf Sci 495:143626. https://doi.org/10.1016/j.apsusc.2019.143626
32. Yuan YJ, Shen Z, Wu S, Su Y, Pei L, Ji Z, Ding M et al (2019) Liquid exfoliation of g-C3N4 nanosheets to construct 2D-2D MoS2/g-C3N4 photocatalyst for enhanced photocatalytic H2 production activity. Appl Catal B: Environ 246:120–128. https://doi.org/10.1016/j.apcatb.2019.01.043
33. Song HJ, You S, Jia XH, Yang J (2015) $MoS_2$ nanosheets decorated with magnetic $Fe_3O_4$ nanoparticles and their ultrafast adsorption for wastewater treatment. Ceram Int. https://doi.org/10.1016/j.ceramint.2015.08.023
34. Wang H, Wen F, Li X, Gan X, Yang Y, Chen P, Zhang Y (2016) Cerium-doped MoS2 nanostructures: efficient visible photocatalysis for Cr(VI) removal. Sep Purif Technol. https://doi.org/10.1016/j.seppur.2016.06.049
35. Wang W, Wen T, Bai H, Zhao Y, Ni J, Yang L, Xia L, Song S (2020) Adsorption toward Cu(II) and inhibitory effect on bacterial growth occurring on molybdenum disulfide-montmorillonite hydrogel surface. Chemosphere. https://doi.org/10.1016/j.chemosphere.2020.126025
36. Yuan W, Kuang J, Mingming Y, Huang Z, Zou Z, Zhu L (2020) Facile preparation of MoS2@Kaolin composite by one-step hydrothermal method for efficient removal of Pb(II). J Hazard Mater. https://doi.org/10.1016/j.jhazmat.2020.124261
37. Wang C, Jin J, Sun Y, Yao J, Zhao G, Liu Y (2017) In-situ synthesis and ultrasound enhanced adsorption properties of MoS2/graphene quantum dot nanocomposite. Chem Eng J. https://doi.org/10.1016/j.cej.2017.06.163
38. Kim R, Kim J, Do JY, Seo MW, Kang M (2019) Carbon dioxide photoreduction on the Bi2S3/MoS2 catalyst. Catalysts. https://doi.org/10.3390/catal9120998
39. Cai C, Wang R, Liu S, Yan X, Zhang L, Wang M, Tong Q, Jiao T (2020) Synthesis of self-assembled phytic acid-MXene nanocomposites via a facile hydrothermal approach with elevated dye adsorption capacities. Colloid Surf A: Phys Eng Aspects 589:124468. https://doi.org/10.1016/j.colsurfa.2020.124468

40. Borges J, Mano JF (2021) Chemical reviews, and undefined 2014. Molecular interactions driving the layer-by-layer assembly of multilayers. ACS Publications. https://pubs.acs.org/doi/full/10.1021/cr400531v?casa_token=0k__Cfv_QAAAAAAA:IAor3sx6Xr2dzR3KUCzx55UYXxxD7SyYD_QgZCqPe_w8IWCORK-XxSARo3S-Cl7ZMPHhU4_pIw8i31TN. Accessed May 4
41. Li K, Zou G, Jiao T, Xing R, Zhang L, Zhou J, Zhang Q, Peng Q (2018) Self-assembled MXene-based nanocomposites via layer-by-layer strategy for elevated adsorption capacities. Colloids Surf, A. https://doi.org/10.1016/j.colsurfa.2018.05.044
42. Yang H, Cao R, Sun P, Yin J, Zhang S, Xu X (2019) Constructing electrostatic self-assembled 2D/2D ultra-thin $ZnIn_2S_4$/protonated g-$C_3N_4$ heterojunctions for excellent photocatalytic performance under visible light. Appl Catal B: Environ 256:117862. https://doi.org/10.1016/j.apcatb.2019.117862
43. Yin J, Ge B, Jiao T, Qin Z, Yu M, Zhang L, Zhang Q, Peng Q (2021) Self-assembled sandwich-like MXene-derived composites as highly efficient and sustainable catalysts for wastewater treatment. Langmuir 37:1267–1278. https://doi.org/10.1021/acs.langmuir.0c03297
44. Saxena V, Shukla I, Pandey LM (2019) Hydroxyapatite: an inorganic ceramic for biomedical applications. In: Mater Biomed Eng: Nanobiomat Tissue Eng 205–249. https://doi.org/10.1016/B978-0-12-816909-4.00008-7
45. Chen J, Zheng H, Zhao Y, Que M, Wang W, Lei X (2020) Morphology and photocatalytic activity of $TiO_2$/MXene composites by in-situ solvothermal method. Ceram Int 46:20088–20096. https://doi.org/10.1016/j.ceramint.2020.05.083
46. Luo S, Wang R, Yin J, Jiao T, Chen K, Zou G, Zhang L, Zhou J, Zhang L, Peng Q (2019) Preparation and dye degradation performances of self-assembled MXene-$Co_3O_4$ nanocomposites synthesized via solvothermal approach. ACS Omega. https://doi.org/10.1021/acsomega.9b00231
47. Yan J, Chen Z, Ji H, Liu Z, Wang X, Xu Y, She X et al (2016) Construction of a 2D graphene-like $MoS_2/C_3N_4$ heterojunction with enhanced visible-light photocatalytic activity and photoelectrochemical activity. Chem-A Eur J 22:4764–4773. https://doi.org/10.1002/chem.201503660
48. Liu C, Chai B, Wang C, Yan J, Ren Z (2018) Solvothermal fabrication of $MoS_2$ anchored on $ZnIn_2S_4$ microspheres with boosted photocatalytic hydrogen evolution activity. Int J Hydr Energy 43:6977–6986. https://doi.org/10.1016/j.ijhydene.2018.02.116
49. Li M, Zhang Q, Ruan H, Wang X, Liu Y, Lu Z, Hai J (2019) An in-situ growth approach to 2D MoS2–2D PbS heterojunction composites with improved photocatalytic activity. J Solid State Chem 270:98–103. https://doi.org/10.1016/j.jssc.2018.11.008
50. Gan D, Huang Q, Dou J, Huang H, Chen J, Liu M, Wen Y, Yang Z, Zhang X, Wei Y (2020) Bioinspired functionalization of MXenes ($Ti_3C_2TX$) with amino acids for efficient removal of heavy metal ions. Appl Surf Sci. https://doi.org/10.1016/j.apsusc.2019.144603
51. Tong S, Deng H, Wang L, Huang T, Liu S, Wang J (2018) Multi-functional nanohybrid of ultrathin molybdenum disulfide nanosheets decorated with cerium oxide nanoparticles for preferential uptake of lead (II) ions. Chem Eng J. https://doi.org/10.1016/j.cej.2017.10.056
52. Dong Y, Sang D, He C, Sheng X, Lei L (2019) Mxene/alginate composites for lead and copper ion removal from aqueous solutions. RSC Adv. https://doi.org/10.1039/c9ra05251h
53. Chandrabose G, Dey A, Singh Gaur S, Pitchaimuthu S, Jagadeesan H, St John Braithwaite N, Selvaraj V, Kumar V, Krishnamurthy S (2021) Removal and degradation of mixed dye pollutants by integrated adsorption-photocatalysis technique using 2-D $MoS_2/TiO_2$ nanocomposite. Chemosphere 279:130467. https://doi.org/10.1016/j.chemosphere.2021.130467
54. Anasori B, Lukatskaya MR, Gogotsi Y (2017) 2D metal carbides and nitrides (MXenes) for energy storage. Nat Rev Mater. https://doi.org/10.1038/natrevmats.2016.98
55. Gogotsi Y, Anasori B (2019) The rise of MXenes. ACS Nano. https://doi.org/10.1021/acsnano.9b06394
56. Lei JC, Zhang X, Zhou Z (2015) Recent advances in MXene: preparation, properties, and applications. Front Phys. https://doi.org/10.1007/s11467-015-0493-x

57. Sun W, Shah SA, Chen Y, Tan Z, Gao H, Habib T, Radovic M, Green MJ (2017) Electrochemical etching of $Ti_2AlC$ to $Ti_2CT$: X (MXene) in low-concentration hydrochloric acid solution. J Mater Chem A. https://doi.org/10.1039/c7ta05574a
58. Shahzad A, Nawaz M, Moztahida M, Jang J, Tahir K, Kim J, Lim Y, Vassiliadis VS, Woo SH, Lee DS (2019) $Ti_3C2Tx$ MXene core-shell spheres for ultrahigh removal of mercuric ions. Chem Eng J. https://doi.org/10.1016/j.cej.2019.02.160
59. 2D Metal Carbides and Nitrides (MXenes) (2019) 2D metal carbides and nitrides (MXenes). https://doi.org/10.1007/978-3-030-19026-2
60. Szuplewska A, Kulpińska D, Dybko A, Chudy M, Jastrzębska AM, Olszyna A, Brzózka Z (2020) Future applications of MXenes in biotechnology, nanomedicine, and sensors. Trends Biotechnol. https://doi.org/10.1016/j.tibtech.2019.09.001
61. Huang Q, Liu Y, Cai T, Xia X (2019) Simultaneous removal of heavy metal ions and organic pollutant by BiOBr/$Ti_3C_2$ nanocomposite. J Photochem Photobiol A. https://doi.org/10.1016/j.jphotochem.2019.02.026
62. Ren CE, Hatzell KB, Alhabeb M, Ling Z, Mahmoud KA, Gogotsi Y (2015) Charge- and size-selective ion sieving through $Ti_3C_2Tx$ MXene membranes. J Phys Chem Lett. https://doi.org/10.1021/acs.jpclett.5b01895
63. Chen B, Feng A, Deng R, Liu K, Yun Y, Song L (2020) MXene as a cation-selective cathode material for asymmetric capacitive deionization. ACS Appl Mater Interfaces. https://doi.org/10.1021/acsami.9b19684
64. Xie X, Chen C, Zhang N, Tang ZR, Jiang J, Yi Jun X (2019) Microstructure and surface control of MXene films for water purification. Nat Sustain. https://doi.org/10.1038/s41893-019-0373-4
65. Peng Q, Guo J, Zhang Q, Xiang J, Liu B, Zhou A, Liu R, Tian Y (2014) Unique lead adsorption behavior of activated hydroxyl group in two-dimensional titanium carbide. J Am Chem Soc. https://doi.org/10.1021/ja500506k
66. Zhu Z, Xiang M, Shan L, He T, Zhang P (2019) Effect of temperature on methylene blue removal with novel 2D-Magnetism titanium carbide. J Solid State Chem. https://doi.org/10.1016/j.jssc.2019.120989
67. Feng X, Yu Z, Long R, Sun Y, Wang M, Li X, Zeng G (2020) Polydopamine intimate contacted two-dimensional/two-dimensional ultrathin nylon basement membrane supported RGO/PDA/MXene composite material for oil-water separation and dye removal. Separ Purif Technol 247:116945. https://doi.org/10.1016/j.seppur.2020.116945
68. Lei Y, Cui Y, Huang Q, Dou J, Gan D, Deng F, Liu M, Li X, Zhang X, Wei Y (2019) Facile preparation of sulfonic groups functionalized Mxenes for efficient removal of methylene blue. Ceram Int. https://doi.org/10.1016/j.ceramint.2019.05.331
69. Li W, Chen D, Xia F, Tan JZY, Song J, Song WG, Caruso RA (2016) Flowerlike WSe2 and WS2 microspheres: one-pot synthesis, formation mechanism and application in heavy metal ion sequestration. Chem Commun. https://doi.org/10.1039/c6cc00577b
70. Jia F, Wang Q, Jishan W, Li Y, Song S (2017) Two-dimensional molybdenum disulfide as a superb adsorbent for removing Hg2+ from water. ACS Sustain Chem Eng. https://doi.org/10.1021/acssuschemeng.7b01880
71. Huang Q, Zhao J, Liu M, Li M, Ruan J, Li Q, Tian J, Zhu X, Zhang X, Wei Y (2018) Synthesis of polyacrylamide immobilized molybdenum disulfide ($MoS_2$@PDA@PAM) composites via mussel-inspired chemistry and surface-initiated atom transfer radical polymerization for removal of copper (II) ions. J Taiwan Inst Chem Eng 86:174–184. https://doi.org/10.1016/j.jtice.2017.12.027
72. Yang S, Hua M, Shen L, Han X, Meiyun X, Kuang L, Hua D (2018) Phosphonate and carboxylic acid co-functionalized $MoS_2$ sheets for efficient sorption of uranium and europium: multiple groups for broad-spectrum adsorption. J Hazard Mater. https://doi.org/10.1016/j.jhazmat.2018.05.005
73. Wang Z, Qingsong T, Sim A, Julie Y, Duan Y, Poon S, Liu B et al (2020) Superselective removal of lead from water by two-dimensional $MoS_2$ nanosheets and layer-stacked membranes. Environ Sci Technol. https://doi.org/10.1021/acs.est.0c02651

74. Li Z, Meng X, Zhang Z (2019) Equilibrium and kinetic modelling of adsorption of Rhodamine B on MoS2. Mater Res Bull. https://doi.org/10.1016/j.materresbull.2018.11.012
75. Xiao X, Wang Y, Cui B, Zhang X, Zhang D, Xingyou X (2020) Preparation of MoS2 nanoflowers with rich active sites as an efficient adsorbent for aqueous organic dyes. New J Chem. https://doi.org/10.1039/d0nj00129e
76. Li L, Yijun Y, Ye GJ, Ge Q, Xuedong O, Hua W, Feng D, Chen XH, Zhang Y (2014) Black phosphorus field-effect transistors. Nat Nanotechnol. https://doi.org/10.1038/nnano.2014.35
77. Cortés-Arriagada D, Ortega DE (2020) Removal of arsenic from water using iron-doped phosphorene nanoadsorbents: a theoretical DFT study with solvent effects. J Mol Liq. https://doi.org/10.1016/j.molliq.2020.112958
78. Ortega DE, Cortés-Arriagada D (2020) Exploring the nature of interaction and stability between water-soluble arsenic pollutants and metal-phosphorene hybrids: a density functional theory study. J Phys Chem A. https://doi.org/10.1021/acs.jpca.0c00532
79. Po CO, Lin YJ, Cao WZ, Chang CT (2017) Arsenic removal with phosphorene and adsorption in solution. Mater Lett. https://doi.org/10.1016/j.matlet.2017.01.030
80. Wang J, Zhang Z, He D, Yang H, Jin D, Qu J, Zhang Y (2020) Comparative study on the adsorption capacities of the three black phosphorus-based materials for methylene blue in water. Sustainability 12:8335. https://doi.org/10.3390/SU12208335
81. Wang Z, Zhang J, Wen T, Liu X, Wang Y, Yang H, Sun J, Feng J, Dong S, Sun J (2020) Highly effective remediation of Pb(II) and Hg(II) contaminated wastewater and soil by flower-like magnetic MoS2 nanohybrid. Sci Total Environ. https://doi.org/10.1016/j.scitotenv.2019.134341
82. Jin L, Chai L, Yang W, Wang H, Zhang L (2020) Two-dimensional titanium carbides ($Ti_3C_2Tx$) functionalized by poly(m-phenylenediamine) for efficient adsorption and reduction of hexavalent chromium. Int J Environ Res Public Health. https://doi.org/10.3390/ijerph17010167
83. Aghagoli M, Shemirani F (2017) Hybrid nanosheets composed of molybdenum disulfide and reduced graphene oxide for enhanced solid phase extraction of Pb(II) and Ni(II). Microchimica Acta
84. Ashraf W, Bansal S, Singh V, Barman S, Khanuja M (2020) BiOCl/WS2hybrid nanosheet (2D/2D) heterojunctions for visible-light-driven photocatalytic degradation of organic/inorganic water pollutants. RSC Adv. https://doi.org/10.1039/d0ra02916e
85. Wang Q, Li B, Zhang P, Zhang W, Xiaoru H, Li X (2020) 2D black phosphorus and tungsten trioxide heterojunction for enhancing photocatalytic performance in visible light. RSC Adv. https://doi.org/10.1039/d0ra05230b
86. Farbod M, Taheri R, Kosarian A (2020) Preparation, characterization and photocatalytic performance of phosphorene/$MoS_2$ as a 2D hybrid semiconductor. Mater Sci Semicond Proces Pergamon. https://doi.org/10.1016/j.mssp.2020.105562
87. Li S, Wang P, Wang R, Liu Y, Jing R, Li Z, Meng Z, Liu Y, Zhang Q (2019) One-step co-precipitation method to construct black phosphorus nanosheets/ZnO nanohybrid for enhanced visible light photocatalytic activity. Appl Surf Sci 497:143682. https://doi.org/10.1016/j.apsusc.2019.143682
88. Kemp KC, Seema H, Saleh M, Le NH, Mahesh K, Chandra V, Kim KS (2013) Environmental applications using graphene composites: water remediation and gas adsorption. Nanoscale. https://doi.org/10.1039/c3nr33708a
89. Liu F, Liu X, Sun L, Li R-X, Yin C, Wu B (2021) MXene-supported stable adsorbents for superior $CO_2$ capture. J Mater Chem A. https://doi.org/10.1039/D1TA01403J
90. Morales-García Á, Fernández-Fernández A, Viñes F, Illas F (2018) CO2 abatement using two-dimensional MXene carbides. J Mater Chem A. https://doi.org/10.1039/c7ta11379j
91. Morales-Salvador R, Morales-García Á, Viñes F, Illas F (2018) Two-dimensional nitrides as highly efficient potential candidates for $CO_2$ capture and activation. Phys Chem Chem Phys. https://doi.org/10.1039/c8cp02746c
92. Khazaei M, Ranjbar A, Arai M, Sasaki T, Yunoki S (2017) Electronic properties and applications of MXenes: a theoretical review. J Mater Chem C. https://doi.org/10.1039/c7tc00140a

93. Junkaew A, Arróyave R (2018) Enhancement of the selectivity of MXenes (M2C, M = Ti, V, Nb, Mo) via oxygen-functionalization: promising materials for gas-sensing and -separation. Phys Chem Chem Phys. https://doi.org/10.1039/c7cp08622a
94. Naqvi SR, Shukla V, Jena NK, Luo W, Ahuja R (2020) Exploring two-dimensional M2NS2 (M = Ti, V) MXenes based gas sensors for air pollutants. Appl Mater Today. https://doi.org/10.1016/j.apmt.2020.100574
95. Ma D, Weiwei J, Li T, Zhang X, He C, Ma B, Zhansheng L, Yang Z (2016) The adsorption of CO and NO on the $MoS_2$ monolayer doped with Au, Pt, Pd, or Ni: a first-principles study. Appl Surf Sci. https://doi.org/10.1016/j.apsusc.2016.04.171
96. Lu X, Guo L, Wang P, Cui M, Kanghong D, Peng W (2020) Theoretical investigation of the adsorption of gas molecules on $WSe_2$ monolayers decorated with Pt, Au nanoclusters. Appl Surf Sci. https://doi.org/10.1016/j.apsusc.2020.145860
97. Li Z, He J, Wang H, Wang B, Ma X (2015) Enhanced methanation stability of nano-sized $MoS_2$ catalysts by adding $Al_2O_3$. Front Chem Sci Eng. https://doi.org/10.1007/s11705-014-1446-6
98. Almeida K, Peña P, Rawal TB, Coley WC, Akhavi AA, Wurch M, Yamaguchi K, Le D, Rahman TS, Bartels L (2019) A single layer of $MoS_2$ activates gold for room temperature CO oxidation on an inert silica substrate. J Phys Chem C. https://doi.org/10.1021/acs.jpcc.8b12325
99. Cui H, Zhang G, Zhang X, Tang J (2019) Rh-doped $MoSe_2$ as a toxic gas scavenger: a first-principles study. Nanoscale Adv. https://doi.org/10.1039/c8na00233a
100. Shi G, Luo Y, Ba X, Zhang X, Zhou J, Ying Y (2017) Copper nanoparticle interspersed $MoS_2$ nanoflowers with enhanced efficiency for $CO_2$ electrochemical reduction to fuel. Dalton Trans. https://doi.org/10.1039/c6dt04381j
101. Abbasi A, Sardroodi JJ (2017) A novel strategy for SOx removal by N-doped $TiO_2/WSe_2$ nanocomposite as a highly efficient molecule sensor investigated by van der Waals corrected DFT. Comput Theor Chem. https://doi.org/10.1016/j.comptc.2017.05.020
102. Wen MQ, Xiong T, Zang ZG, Wei W, Tang XS, Dong F (2016) Synthesis of $MoS_2$/g-$C_3N_4$ nanocomposites with enhanced visible-light photocatalytic activity for the removal of nitric oxide (NO). Opt Express. https://doi.org/10.1364/oe.24.010205
103. Sun Q, Qin G, Ma Y, Wang W, Li P, Aijun D, Li Z (2017) Electric field controlled $CO_2$ capture and $CO_2/N_2$ separation on $MoS_2$ monolayers. Nanoscale. https://doi.org/10.1039/c6nr07001a
104. Abbasi A, Sardroodi JJ (2019) Adsorption of $O_3$, $SO_2$ and $SO_3$ gas molecules on $MoS_2$ monolayers: a computational investigation. Appl Surf Sci. https://doi.org/10.1016/j.apsusc.2018.11.039
105. Wei H, Gui Y, Kang J, Wang W, Tang C (2018) A DFT study on the adsorption of $H_2S$ and $So_2$ on Ni doped $MoS_2$ monolayer. Nanomaterials. https://doi.org/10.3390/nano8090646
106. Ma S, Liancun S, Jin L, Jinsheng S, Jin Y (2019) A first-principles insight into Pd-doped $MoSe_2$ monolayer: a toxic gas scavenger. Phys Lett Sect A: Gener Atom Solid State Phys. https://doi.org/10.1016/j.physleta.2019.125868
107. Ni J, Wang W, Quintana M, Jia F, Song S (2020) Adsorption of small gas molecules on strained monolayer $WSe_2$ doped with Pd, Ag, Au, and Pt: a computational investigation. Appl Surf Sci. https://doi.org/10.1016/j.apsusc.2020.145911
108. Cai Y, Ke Q, Zhang G, Zhang YW (2015) Energetics, charge transfer, and magnetism of small molecules physisorbed on phosphorene. J Phys Chem C. https://doi.org/10.1021/jp510863p
109. Kuang A, Ran Y, Peng B, Kuang M, Wang G, Yuan H, Tian C, Chen H (2019) Adsorption and decomposition of metal decorated phosphorene toward $H_2S$, HCN and $NH_3$ molecules. Appl Surf Sci. https://doi.org/10.1016/j.apsusc.2018.12.131
110. Bhuvaneswari R, Nagarajan V, Chandiramouli R (2020) Toxicants in cigarette smoke adsorbed on red phosphorene nanosheet: a first-principles insight. Chem Phys. https://doi.org/10.1016/j.chemphys.2019.110604
111. Kim SJ, Koh HJ, Ren CE, Kwon O, Maleski K, Cho SY, Anasori B et al (2018) Metallic $Ti_3C_2Tx$ MXene gas sensors with ultrahigh signal-to-noise ratio. ACS Nano. https://doi.org/10.1021/acsnano.7b07460

112. Shuvo SN, Gomez AMU, Mishra A, Chen WY, Dongare AM, Stanciu LA (2020) Sulfur-doped titanium carbide MXenes for room-temperature gas sensing. ACS Sensors. https://doi.org/10.1021/acssensors.0c01287
113. Chen WY, Yen CC, Xue S, Wang H, Stanciu LA (2019) Surface functionalization of layered molybdenum disulfide for the selective detection of volatile organic compounds at room temperature. ACS Appl Mater Interfaces. https://doi.org/10.1021/acsami.9b13827
114. Lazar P, Otyepková E, Pykal M, Čépe K, Otyepka M (2018) Role of the puckered anisotropic surface in the surface and adsorption properties of black phosphorus. Nanoscale. https://doi.org/10.1039/c8nr00329g

# Chapter 6
# Progress in 2D Nanomaterial Composites Membranes for Water Purification and Desalination


**Savan K. Raj and Vaibhav Kulshrestha**

## 1 Introduction

Water is the most crucial part of living life, and its supply has become progressively intense. It is abundant in nature, but only some of its portion is available and suitable for human life [1]. Many regions in the world do not have the facility to make the water clean and safe. As of today, rapid expansion in population and industrialization causes increases in demand for high-quality water [2]. According to the World Water Council report, approximately 4 billion people will live in water shortage areas by 2030 [3]. The water resource prices will simultaneously increase as the water resources are restricted, which automatically gives rise to the operating cost in many of the water-consuming industries [4]. After this, the other parameter is the quality of water used for drinking, which should be pollutant-free. Water pollution is a severe risk of water consumption. It happens when any unwanted material is entered or diffused in water and makes the water unsafe for drinking, agriculture, or industrial consumption [5, 6]. Such polluted water is not suitable for plants and aquatic and land animals. So, removing pollutants from the water is a must for all the uses, as mentioned earlier. The potable groundwater contains several hazardous contaminants like a viruses, heavy metals, bacteria, and other toxic materials, affecting the environment and human health [7–10]. The poor quality of water and scarcity of functioning water resources is another major problem to resolve. High attentiveness should be given to the conservation of water resources to meet the increasing demand for freshwater. In the prospect of this, better technology for water purification and desalination is required. Recently, renewable and cost-efficient membrane

S. K. Raj · V. Kulshrestha (✉)
CSIR-Central Salt and Marine Chemicals Research Institute, Gijubhai Badheka Marg, Bhavnagar 364002, Gujarat, India
e-mail: vaibhavphy@gmail.com

S. K. Raj
e-mail: savankraj@gmail.com



Z. Khanam et al. (eds.), *2D Nanomaterials for Energy and Environmental Sustainability*,
Materials Horizons: From Nature to Nanomaterials,
https://doi.org/10.1007/978-981-16-8538-5_6

science for water purification applications is a highly attractive area for research [11, 12]. Such membrane technologies have advantages over other technologies like low power consumption, operated at low cost, need no chemical additives or thermal energy, or any regeneration of used media. These membranes, with various physical and porous aspects, can successfully desalinate the water [13]. The alteration in physicochemical properties (like pore size, surface charge, hydrophilicity, etc.) will enhance its working efficiency. At present, commercial membrane technologies like microfiltration (MF), ultrafiltration (UF), nanofiltration (NF), and reverse osmosis (RO) are assessable. Generally, the MF membranes are used to remove the suspended solids and bacteria. The UF membranes typically remove colloids and viruses. The organic matter and bulky cations can be removed using NF membranes [14, 15]. The preparation of ultrapure water, desalination, and water reuse can be done using RO membranes. Water desalination technologies (like adsorption, reduction, oxidation, membranes, and filtration) can be enhanced dramatically using two-dimensional nanomaterials (2D materials) [16]. Immobilization of 2D nanomaterials on or within the membrane matrix is a promising approach. There will be an improvement in the overall performance by improving separation performance, mechanical and thermal stability. Even though a simple fabrication technique for the preparation of 2D material membranes has gained a lot of attention in the scientific community, understanding suitable methods for fabrication and mechanism is still a challenge. At present, these 2D based membranes can be prepared in two forms, that is, pristine and modified membranes. Generally, the pristine nanosheets contain monolayers or a few layers of a 2D material with uniformly distributed nanopores, like graphene-based, metal–organic framework (MOFs), MXenes, transition metal dichalcogenides (TMDCs), and hexagonal boron nitride nanosheets (hBN). Even though outstanding separation efficiency can be achieved using pristine membranes, but fabrication on a large scale and pore-controlled nanosheets of such 2D material membranes is still challenging. Our objective is to review the basic concepts of 2D material-based membranes, methods of fabrication, and application in water desalination.

## 2 Different Synthesis Techniques for 2D Material-Based Membranes

Membrane filtration process can be classified into different categories including microfiltration (MF), ultrafiltration (UF), nanofiltration (NF), gas separation, reverse osmosis (RO), dialysis, and electrodialysis (ED) based on their pore size (Table 1) [17]. As per International Organization for Standardization (ISO), 2D nanomaterials can be divided into two categories: nanostructured materials and nano-objects, for the synthesis of 2D material-based membranes [18].

There are different techniques available for the synthesis of 2D material-based membranes; the brief description is given below.

**Table 1** Classification of various types of membrane filtration process [17]

| Technique | Pore size | Driving force | Average permeability $L/m^2h$ bar |
|---|---|---|---|
| Microfiltration | 0.05–10 μm | 1–3 bar | 500 |
| Ultrafiltration | 0.001–0.05 μm | 2–5 bar | 150 |
| Nanofiltration | < 2.0 nm | 5–15 bar | 0–20 |
| Reserve osmosis | < 1 nm | 15–75 bar | 5–10 |
| Gas separation | < 0.5–1 nm | – | – |
| Membrane distillation | 0.5–2 nm | – | – |
| Electrodialysis | MW < 200 Da | Electrical potential, 1–2 V/cell | – |

## *2.1 Drop-Casting*

One of the most straightforward process to fabricate the 2D material membranes is drop-casting. The colloidal solution of that 2D material is drop cast onto the substrate on the surface of silica or paper, followed by drying at room temperature. The freestanding membrane is then peeled off from the underlying substrate. Due to enormous surface tension and low vapor pressure, water is not an ideal choice for drop-casting. Some other polar solvents like alcohol or organic solvents like toluene, hexane, and halogenated solvents can be superior choices for nanoparticles with hydrophobic capping ligands [19]. Due to its ease of performing and preparation of thin film on a small substrate, this technique was favored by many researchers. However, the main disadvantage of this strategy is that the evaporation rates within the substrate or the concentration gradient in the fluid phase can lead to the variation in the internal structure and the thickness of the membrane [20].

## *2.2 Vacuum Filtration*

For the large scale synthesis of the self-standing membrane, the most common and uncomplicated way is vacuum filtration (Fig. 1a). In this process, there is no change in the physicochemical properties of 2D nanomaterial because the interaction is mostly van der Waal, hydrogen, or electrostatic repulsion but cannot be the covalent bonding [21]. The vacuum filtration method can be used to prepare composite membranes with the homogeneous distribution of nanomaterials. Some 2D materials like GO, when used in the membrane, bear good hydrophobic properties. The papery membrane can be prepared using a vacuum filtration method, but the thickness of the membrane mostly depends on the material suspension volume introduced into the system (Fig. 2) [22]. 2D material membrane can be prepared by depositing specific material on the polymeric membrane, followed by the determination of the surface wettability and roughness [21, 22].

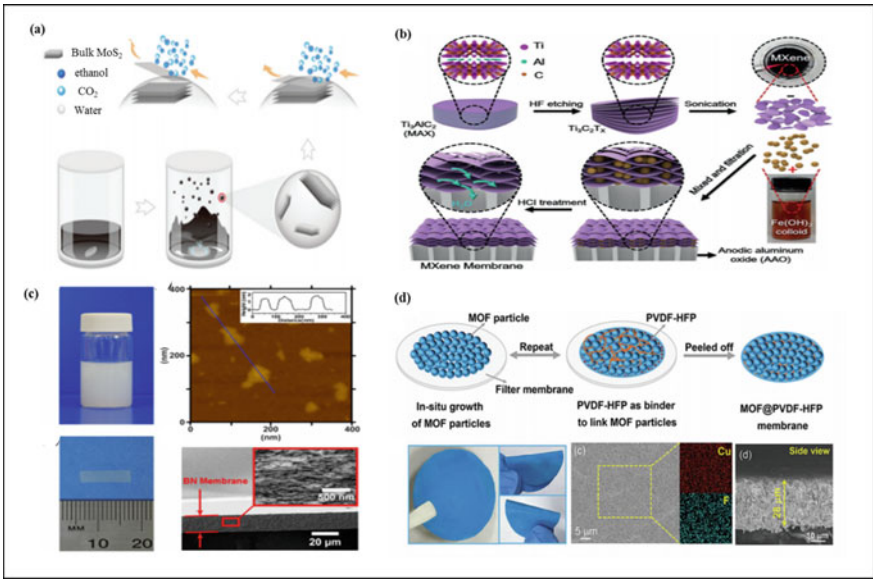


**Fig. 1** **a** Systematic procedure to fabricate $MoS_2$ nanosheets from layered bulk using vacuum filtration method [42], **b** Systematic presentation of synthesis of a 2D $Ti_3C_2T_x$ lamellar membrane nanosheets on AAO [50], **c** Freestanding BN-laminated membrane, the photograph shows the colloidal solution of few layered BN sheets. A freestanding BN membrane with size of 15 mm × 4 mm. Cross-sectional SEM image of a BN membrane, with the inset showing the lamellar structure. AFM image showing the few layered BN nanosheets [44]. **d** Systematic method to fabricate MOF membranes @ PVDF-HFV. The cross section SEM image of the membrane [57]

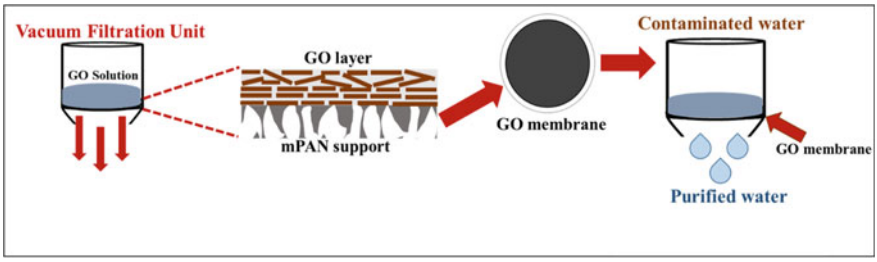


**Fig. 2** A schematic diagram demonstrating membrane-based desalination assembly [32]

## *2.3 Spin Coating*

Another method for film deposition is spin coating, used in numerous industries like thin-film coating technologies and microelectronics industries. This technique provides many advantages such as thickness control of the film, high uniformity film deposition, easy and fast process, and low-cost equipment [23]. Although some of drawbacks like the shape and size of the substrate are a significant concern when

talking about the industrial-scale implementation of this technique. Currently, this technique has been used widely for the preparation of high-quality 2D material membrane. These 2D materials can be deposited on the substrate directly or dispersed in the membrane solution and then deposited on the opaque substrate (like glass or any other polymeric support) to fabricate uniform and thin films [24]. In this process, the nanomaterial suspension is dropped using dropper, and then, the substrate is spinned at various speeds as per requirement until the uniformity is achieved. The fabricated membrane is then obtained by applying etchants corresponding to multiple substrates. The obtained membrane is lastly cleaned and dried at a moderate temperature. The fabricated thin film with dense layers of 2D sheets is expected in this method.

## *2.4 Langmuir–Blodgett (LB)*

At present, Langmuir–Blodgett (LB) is broadly used method for 2D material-based membranes preparation. For example, GO sheets have been considered to have amphiphilic nature because of $sp^3$ hybridized carbon atom, further bonded with oxygen-containing functional groups [25]. The thickness and staking layers of the sheets can be controlled using this method. For the formation of GO membranes using this method, trough must be washed and carefully rinsed with chloroform and then filled with deionized water. The GO solution was very slowly delivered onto the water surface at constant speed using a glass syringe to a total volume by using tensiometer (surface pressure measurement). The monolayer of the material is deposited by submerging the substrate vertically into the trough and slowly (2 mm $min^{-1}$) bring it up [26]. Among the above techniques, the most frequently used is vacuum filtration [27]. Moreover, issues like requirement of large volume of liquid, alignment, and scalability are also significant concerns. Some potential problems can also be observed in dip-coating, drop-casting, or layer-by-layer assembly methods. Thus, it is a major challenge to produce the 2D material-based membranes using stable and robust processing techniques. Mostly, the ideal membrane used in filtration process has a defect-free, thin, and dense structure; besides, the porous structure will enhance the mechanical strength and permeability in the membrane. Therefore, attention is required to fabricate these kind of membranes by cost-effective and straightforward synthesis techniques [28, 29]. Many approaches are going on to develop 2D material-based membrane on extensive scale application, which includes the methods using a conventional rotogravure printer. A small amount of material was deposited on the printer plate and outspread using a doctor blade. Afterward, the rubber-coated roller pressed the substrate onto the printing sheet, and the liquid film was transported to the substrate from the printing plate. The fabricated membranes contain good stacking layers of nanosheets and exhibit high rejection rate of small organic particles and water permeability compared to conventional membranes used for nanofiltration [30].

## 3 Various 2D Nanomaterials Based Membranes

### *3.1 Graphene Membranes*

Graphene, a trendy carbon-based 2D material, is currently being examined for different water purification applications. This 2D sheet material has hexagonally arranged $sp^2$ carbon atoms [31, 32]. The layer is several atomic thick with excellent mechanical strength, microscopic pores, and is impermeable to helium [33]. The desired pore size can be created by utilizing different techniques like electron beam irradiation, oxidation, ions bombarding, doping, and chemical etching [34–36]. Theoretical studies suggest that regular size distribution of pore size can lead to forming a novel 2D material for RO membrane. Recent study concludes that salt rejection is feasible though graphene membranes having pore diameters up to 5.5 Å [37]. Graphene sheets need to be produced on a large scale to get popularity in the membrane market. The antifouling properties and scaling factors are some other severe matters which need serious attention. Only then, it will be viable to operate these membranes at a higher flux, which ultimately reduces the operational and capital cost. Graphene is more economical and has far better characteristic properties than CNTs and having an enormous theoretical specific surface area of around 2600 $m^2g^{-1}$ [38]. Additionally, graphene at ambient temperature shows high electrical conductivity of about 7200 S $m^{-1}$ [39]. All these outstanding qualities make graphene a promising nanomaterial for water desalination.

### *3.2 Transition Metal Dichalcogenides (TMDCs) Membranes*

TMDCs can be synthesize in both nanosheets and laminar membrane structures. These 2D TMDCs nanosheets can be manufactured via mechanical cleavage and chemical vapor deposition (CVD) methods. This is not reasonable for the functional application as the eventual outcome has low yield and other drawbacks as well, as uncontrolled development of sheets and layers [40]. At present, a couple of studies have been reported on separation using TMDC-based membranes, the reason being the low aspect ratio of the nanosheets (exfoliated) that make this challenging to form defect-free membranes [41–43]. Some new highlights of these TMDCs membranes provide diverse surface chemistries, but excluding various advantages over these materials, some disadvantages like low yield and uncontrollable growth of sheet size and number are still a hindrance to overcome.

### 3.3 Hexagonal Boron Nitride (hBN) Membranes

Recently, hBN membranes were fabricated from the colloidal solution of BN nanosheets through one-step functionalization and exfoliation [44]. These BN membranes were prepared through the vacuum filtration method (Fig. 1c). Similar to other 2D nanomaterial-based membranes, the solution of BN is dispersed through an anodisc filter membrane having a diameter and pore size, 25 mm and 0.02 μm, respectively. The fabricated membranes, after drying, peeled off from the filter. White translucent membrane is obtained and further detached using a razor blade into any shape and size. The thickness of the fabricated membrane was 10–25 μm. These BN nanosheets are well aligned and forming a laminar structure. Apart from this, hBN membranes can be combined with nafion for the fabrication of composite membranes via eco-friendly and water-phase exfoliation methods (nafion-assisted). Nafion and BN nanocomposite membranes can be fabricated; as nafion has amphiphilic nature, it can provide support via hydrophilic or hydrophobic interaction and hydrogen bonding [45]. Even though sufficient studies are reported on these 2D material-based laminar membranes, but other 2D materials like MOFs, layer double hydroxides (LDHs), and graphene are still needed for the fabrication of membranes efficiently to attain the current demand for the separation application [46, 47]. These materials are successfully examined theoretically for the separation membranes but are yet to be explored experimentally because of few fabrication and engineering issues.

### 3.4 MXene Membranes

MXene, class of another 2D materials, fascinates the research community due to its unique and exciting properties. Above all MXenes, $Ti_3C_2Tx$ is the most used MXene until now for different applications. $Ti_3C_2Tx$ is synthesized using $Ti_3C_2T_2$ by HF etching technique (Fig. 1b). Tx is the termination group in $Ti_3C_2Tx$, where T denotes O, OH, or F groups, while x represents the number of terminating groups [48, 49]. $Ti_3C_2Tx$ has been broadly utilized in lithium-ion batteries, supercapacitor fabrication, oxygen evolution reaction (OER), adsorption of heavy metal ions, and recently in nanofiltration membranes for water desalination [50]. Only a few studies are reported on MXenes membrane for separation of gas and water distillation. The chemistry behind the MXenes and TMDC-based membranes is the same and can be fabricated the same as the GO-based membranes. MXene membranes showed flexibility and good mechanical strength. $Ti_3C_2Tx$ membrane with controlled thickness was fabricated, using PVDF as support [51]. These membrane was fabricated via the filtration method and used further for molecules and ions separation application. The hydrophilic surface of $Ti_3C_2Tx$ membranes makes these 2D materials suitable for the separation application and used for investigating antibacterial and bio-fouling properties by altering the membrane layers in a colloidal solution of MXene [50]. $Ti_3C_2T_x$ membrane shows excellent water permeability (1000 $Lm^{-2}\ h^{-1}\ bar^{-1}$) and rejection

capability (up to 90%) for various molecules that have size < 2.5 nm. The stability of these membranes can be improved by the incorporation of other 2D materials via a suitable cross-linking agent [51]. These membranes show good performance, although some of their properties still need to be enhanced to achieve excellent water diffusion, separation capability, and mechanical strength under severe conditions for the nanofiltration application [52]. The need for the self-supported membrane is still there with incredible mechanical strength via improvement in ongoing fabrication techniques or little modification in these methods to improve the properties of the membranes.

### *3.5 Metal Organic Frameworks (MOFs) Membranes*

MOF, another class of advanced 2D material, is used to fabricate laminar membranes. MOFs can be exfoliated into thin sheets, just like other 2D material (Fig. 1d). In addition to this, MOFs possess high oxygen content and high pore density in comparison with other 2D materials, hence promising materials for the membranes fabrication [53]. Highly porous MOF is incorporated to the polymer matrix to increase the separation capability. Only a few reports have been published on MOF based membranes because of strenuous synthesis. These parameters restrict MOF exploration in the membrane field. In terms of mechanical properties, MOFs have relatively low elastic modulus (~ 7 GPa) in comparison with monolayer graphene (~ 1000 GPa) and GO (~ 207 GPa) [54]. In another report, MOF membranes have been fabricated via hot drop-casting technique; the substrate used was porous ceramic to enhance the mechanical strength of the laminated MOF membranes [55]. Many approaches were made to fabricate the MOF membranes via top-down methods [56, 57]. This method involves wet ball-milling of 2D MOF sheets under ultrasonication using appropriate solvent followed by the addition of required chemical substance for the successive applications. In this process, due to external forces like solvent intercalation and ultrasonication, the internal forces like van der Waals are demolished [58, 59]. In spite of all these studies for the development of MOF membranes, only a few have been utilized for industrial and analytical applications. The prime reason being is difficulty in quality control when these are produced on a large scale. To utilize such membranes on an industrial level, these hurdles must be overcome.

### *3.6 Zeolite Membranes*

Zeolite, another class of 2D material, is having a porous structure and is broadly studied for various applications related to separation and water purification. The overall performance of the porous membrane fabricated using zeolite is depends upon the pore structure, crystal shape, and size [60, 61]. In recent years, the precisely crystal growth of the 2D zeolite layer and fabrication of freestanding laminar

membranes with superior mechanical strength and flexibility is still a tough job for the researchers. The fabrication method for the zeolite membranes is quite similar to the MOF and GO membranes. The preparation of 2D zeolite membrane depends upon many factors like thickness uniformity in zeolite nanosheets, high aspect ratio, the stability of the colloidal solution, and contaminant-free colloidal solution. Apart from this, the growth in deposition techniques for the transfer of 2D nanomaterial to the porous substrate is also necessary [62]. Different approaches have been made to make the dispersed zeolite nanosheets suspension by utilizing exfoliation techniques, but during the process, the structure and the morphology of the nanosheets are destructed. Due to such issues, so far, only a few studies have been reported regarding the fabrication of the pristine zeolite membranes for the separation-based application. In recent research, 2D zeolite nanosheets were fabricated on the silicon wafer via Langmuir–Blodgett method by Tsapatsis et al. [63]. These nanosheets were then calcined at 500 °C, and the size of these nanosheets was ~ 3 mm. Additionally, in another work, zeolite nanosheets were prepared to have a thickness of ~ 3.5 nm using the same method as above [64]. Apart from these attempts, the fabrication of these such membranes at a large scale is still a hurdle. Although, the fundamental focus should be on nanostructured membranes, having required orientation, grain boundaries, well-designed interfaces, and stability under multi-component composition. Apart from this, modification in fabrication processes is still necessary to meet the requirement for high yield large-scale production. Parameters such as high cost and low yields of 2D zeolites are matter of concern in terms of large-scale production. Such high-quality materials are significantly needed for the separation and purification-based applications with excellent permeability and selectivity. Therefore, to fulfil the requirement, 2D zeolite nanosheets are incorporated with a suitable polymer matrix (Fig. 3).

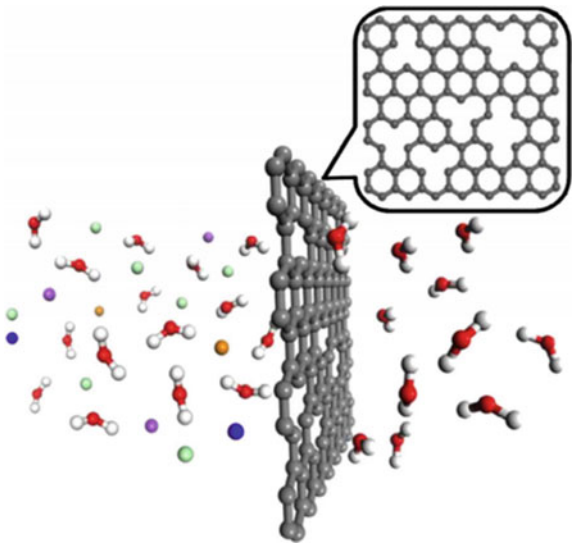

**Fig. 3** Graphene nanosheet for the removal of large hydrated ions [32]

## 4 Proposed Mechanism for Water Desalination Using 2D Material-Based Membranes

It is very important to recognize the diffusion process of water molecules or any solvent for designing the membranes for desalination. The transportation of water is generally based on the solution diffused model.

$$J_w = A(\Delta P - \Delta \pi_m) \tag{1}$$

where $J_W$ and $A$ represent water flux and permeability coefficient, respectively. $\Delta P$ and $\Delta \pi_m$ represent the applied hydraulic pressure and osmotic pressure difference (both side, feed, and permeate). In reverse osmosis (RO), the water movement is driven by hydraulic pressure, which drives the flow of water in RO, while in forward osmosis (FO), water flow is caused by osmotic pressure. Thus, increment in external pressure in RO mode on the feed solution, or raising the drawn solution concentration in FO mode both can accelerate the diffusion process across the membrane. The flux of solute can be modeled by Fick's law, given as

$$J_s = B\Delta c_m \tag{2}$$

where $J_s$ is the solute flux, $B$ is solute permeability coefficient, and $\Delta c_m$ is the solute concentration difference across the membrane. According to Fick's law, regardless of FO or RO operation, increasing the concentration of feed solution accelerates solvent diffusion across membranes.

The solute/solvent permeability is affected by the coefficients A and B. The commercial membranes can be modified by tailoring these coefficients by changing the polyamide layer's thickness. Generally, the polyamide layer reduction can increase the water diffusion, but the salt refusal rate will be affected (lower down). Therefore, controlling the thickness compactness and the chemistry of the layers affects the desalination performance [65]. The mechanism is identical for the 2D materials, and instead of dense layers, the nanosheets promote mass transportation. The filtration of ions can be attained by drilling nanopores on the surface of the sheets or by creating nanochannels in stacked membranes. Mainly two principal mechanisms are proposed for the desalination via 2D material membranes, i.e., size exclusion and Donnan electrostatic exclusion. Size exclusion concludes the permeation of smaller ions while blocking the hydrated ions. The second mechanism principle concludes the blockage of hydrated ions using an electrically charged surface [66, 67]. Nevertheless, in stacked and nanoporous membranes, this effect promotes selective transportation. For this instance, ions are blocked either on the pore edges or on the nanosheets' line edges through electrostatic surface charges. In stacked membranes, as the interlayer distance increases, the values of $J_w$ and $J_s$ also increase. Despite this, $J_w$ and $J_s$ are directly proportional to the pore size in the case of nanoporous membranes. One can achieve the ideal selectivity ($J_s$), permeability

($J_w$), and mass transfer by altering the pore size and the interlayer spacing of the stacked nanosheets. Additionally, the surface chemistry and polarity are crucial in altering the salt rejection performance of nanopores and nanosheets.

## 5 2D Nanomaterial-Based Membranes in Water Purification and Desalination

Problems related to the water across the globe is the most crucial issue [1]. The research community is trying to resolve this issue by developing suitable technologies to use saline water for different purposes at affordable values. Utilizing the nanotechnology in desalination membranes will elevate this approach to resolve the water catastrophe. Fouling decreases membrane life and increases operational cost; thus, most of the research operates to fabricate membranes with antifouling properties [68, 69]. To date, researchers made considerable efforts to resolve these limitations by incorporation of new materials like carbon nanomaterials, zeolites, silica, and other inorganic material in membranes [70–72]. Although synthesis technique and properties of these materials play an essential role in membrane processing. Recently, research based on 2D materials in membrane for ionic and molecular separation has increased immensely [73, 74]. Therefore, this chapter mainly focus on nanoporous and laminated membranes for desalination applications.

In the list of 2D materials, GO is one of the most utilized nanomaterials for different separation and purification applications. Some studies have also shown graphene as a filler material in composite membranes to enhance its barrier properties. The addition of graphene as a filler in the composite membrane can change the membranes' structure by altering the polymer filler interfaces. Till now, many mechanisms using molecular dynamics have been proposed to define the layer-by-layer and porous structure of graphene-based materials [37]. Graphene oxide (GO) flakes generally have two regions, i.e., oxidized (functionalized) and nonoxidized (pristine). The similar functional groups were repelled by formers, and this increases the interlayer spacing between the flakes. The oxides surface promotes strong bonding between the polymers and the graphene flakes. Although, the cluster formation of flakes within the membranes during the synthesis is still a hurdle to resolve. In some reports, the graphene and its derivatives are modified to the unique porous structure that enhances membrane properties (Fig. 4). Thus, nanosheets with highly dense nanochannels and interedge spaces are preferred to fabricate graphene membranes to upgrade water diffusion. The size of the interlayer can be variate by using different sized intercalating agents. In a computational study, Grossman et al. examined a high-performance single-layered graphene to separate out NaCl from the water and conclude the relationship between flux and pore area [37]. The hydrophobic pores with a small area cause low pressure and effectively reject more salts due to direct size exclusion, whereas large volumes of ions and deficiency of hydrogen bonds cause high energy hurdle to the ionic passage. Outstanding properties like the monolayer thickness of sheets with high mechanical stability and chemical inertness have

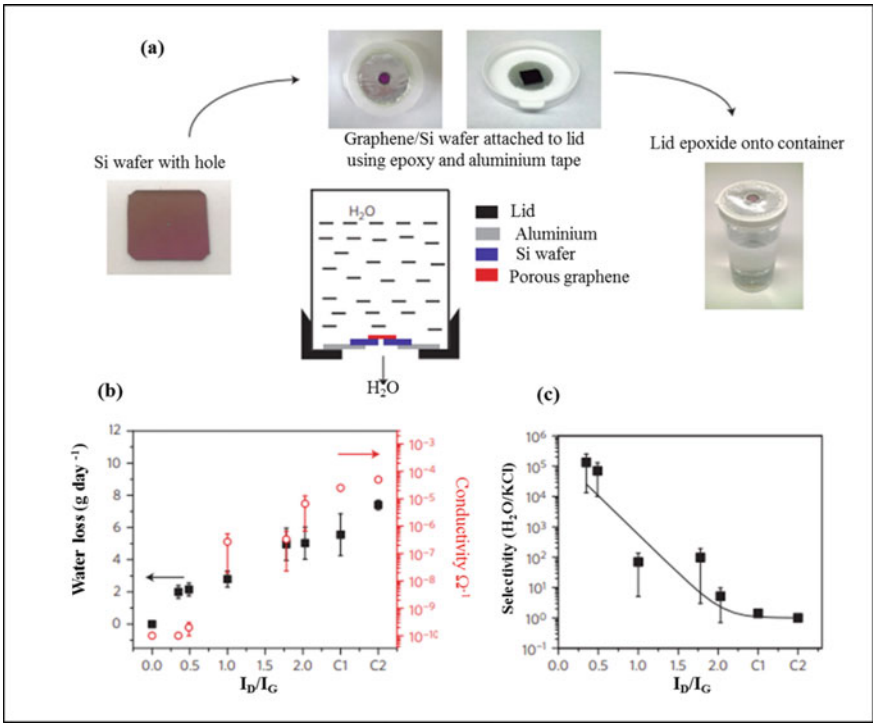


**Fig. 4** Graphene membrane (porous) preparation. **a** Graphene membrane loaded on a silicon substrate. SiN membrane caped on a vial filled with distilled water after that rotate the vial upside down and put in an oven at 40 °C. **b** Water loss and ionic conductivity after 24 h. **c** Water/salt selectivity versus $I_D/I_G$ showing exceptionally large selectivity for a less etching time [79]

inspired the researchers to drill holes in the graphene nanosheets to grow more nanopores to fabricate nanoporous graphene membranes. In theoretical studies, the nanoporous graphene has shown ultrafast high water permeance and chokes the movement of species larger than surface pores [75]. Obtaining the required porous membrane having controlled pore size distribution within the graphene layers is still a crucial parameter to resolve for the scientific community. Consider this; many perforation techniques are proposed to create pores in the graphene nanosheets like electron beam ablation, ion beam ablation, ultraviolet-induced oxidative etching, and various other etching techniques [76–79]. Well-distributed pores can be drilled in graphene monolayer by using the electron beam irradiation technique. Still, this technique is limited to a certain area of membranes, and the size of the pore is in the range of 3.5–100 nm, which is unfit for successive sieving separation. Scalability and pore size can be effectively improved by the oxidative etching route. However, from the practical point of view, the pore size distribution density still requires improvement. Thus, enhancement in these techniques to produce high density and uniformly

distributed pores improves the existing performance, which enables the energy-efficient filtration and separation processes. In another investigation (Fig. 4a–c), Mahurin et al. demonstrated that nanoporous single-layer graphene as nanofiltration membrane could be utilized in desalination [79]. In another reported study, the author has produced porous monolayer graphene using atmospheric pressure chemical vapor deposition (APCVD) on catalyst made up of copper for the desalination applications [80]. The graphene was transferred onto the microchip (silicon nitride) with 70% yield by utilizing polymer transfer technique, followed by oxygen plasma method to fabricate nanoporous graphene. Oxygen plasma is the most suitable method to produce the nanoporous monolayer graphene carrying the desire pore size and chemical properties with exceptional precision. The fabricated membranes show excellent salt rejection (100%) for many metal ions ($K^+$, $Na^+$, $Li^+$, and Cl) with rapid transportation of water [79].

Computational studies propose that nanoporous graphene can exhibit high permitivity and selectivity exceeding to those of existing state-of-the-art membranes by orders of magnitude. Moreover, experimentally, such membranes are strenuous to manufacture on an industrial scale. This is due to numerous engineering barriers to develop controlled-subnanometer pores using ion bombardment and selective etching. In computational studies, nanoporous graphene has shown high permeance and selectivity although these membranes are experimentally challenging to fabricate on a large scale. As the nature of the technique used is very random, such pores with high density and uniformity are very difficult to achieve to fulfill the industrial applications. In comparison with nanoporous monolayer graphene, GO is a more suitable material for water desalination applications [81–83]. It can be easily used as laminated sheets and can be incorporated with other materials to form composites. Due to the availability of oxygen-containing groups on the basal plane and the edges of GO, it shows fascinating properties in filtration and separation application [84, 85]. These GO sheets having nanochannels work as a strainer, which removes all the molecules of large size by blocking them, and the resultant membrane showed excellent separation properties. Moreover, carbon atoms in GO are generally bonded to oxygen atoms in the form of carboxyl, hydroxyl, and epoxy groups. Due to these groups, an amorphous region is created, which tends to form nanocrinkles and compositional defects in the GO nanosheets' basal plane. These defects and winkles are the prime reason for water transportation when GO sheets are mustered in membranes. The functional groups (oxygen containing) present on the GO surface act as reactive handles to different surface enhance reactions that can fabricate GO-based membranes with escalated the separation capabilities. Till now, GO-based membranes have been investigated widely from both experimental and theoretical approaches for the separation of ions and molecules [82–85]. Although, some factors such as controlling the d-spacing, permeability, fouling properties, and stability are still needed to be explored for the total utilization of these laminar sheets in the desalination technology. In the reported study, the GO membranes have been demonstrated to have a thickness in few microns. This membrane has shown good permeance of water vapor. It blocks other liquids and gases under the dry state as the nanocapillaries formed due to the empty interlayer space between the nonoxidized regions in GO sheets [23].

The transportation of water vapor was quite rapid. Although, hydration of the GO sheets will increase the d-space in the membrane after water immersion and allow the permeation of the small-sized molecules and ions (< 0.45 nm) while choking other molecules having bigger sizes than 0.45 nm. Another study demonstrated the permeation of the selective ions through GO membranes [86]. The investigators conclude that the sodium salts penetrate from the membranes very freely, but the membrane partially blocked other heavy metal salts (Fig. 5a–d). The fabricated membrane was able to block copper salts and other organic pollutants. Generally, the metal salts penetrate through nanocapillaries present in the GO membrane, but in heavy metal salts, the collaboration between them and the membrane blocks the diffusion. The mechanism was suggested by Nair et al. (Fig. 6a–d), and as per the study, the distance between the layers is responsible for the flow of water in the membrane, and frictionless flow of water was due to the high capillary pressure [23]. Thus, ions can easily pass through the membranes' channels in their hydrated form when the distance is large. Hence, the species having a larger size cannot penetrate, while little ones can proceed through the capillaries easily. Although, fascinating permeable properties

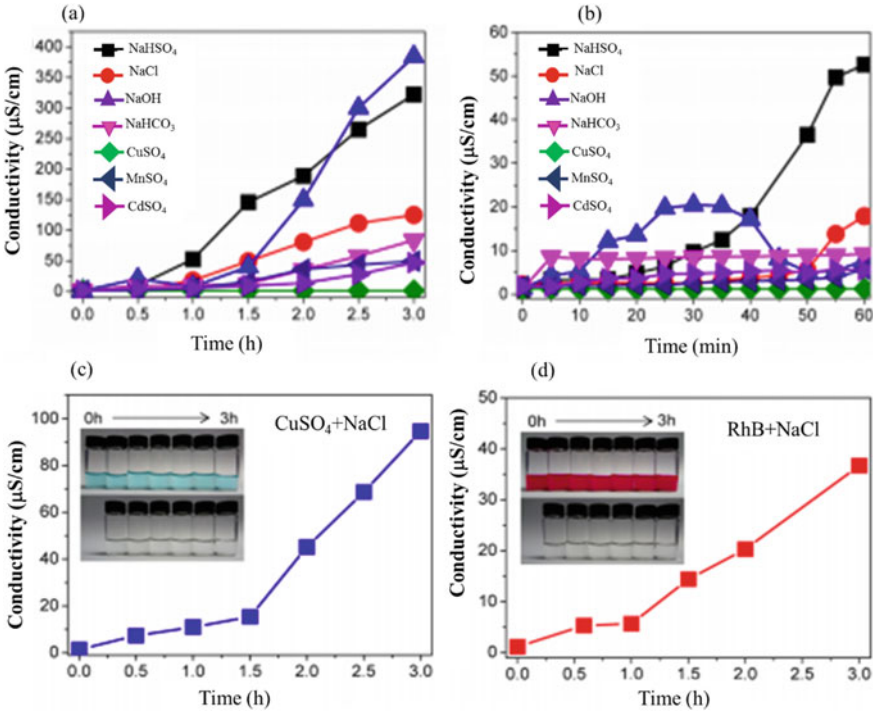


**Fig. 5** **a** Conductivity variation with time for different salts. **b** The plot shows salt transport process through GO membrane. **c** Diffusion process with respect to the mixture (NaCl + $CuSO_4$) through GO membrane. Insert photograph reveals the feed solution and penetrate. **d** Same procedure for of NaCl and RB mixture [86]

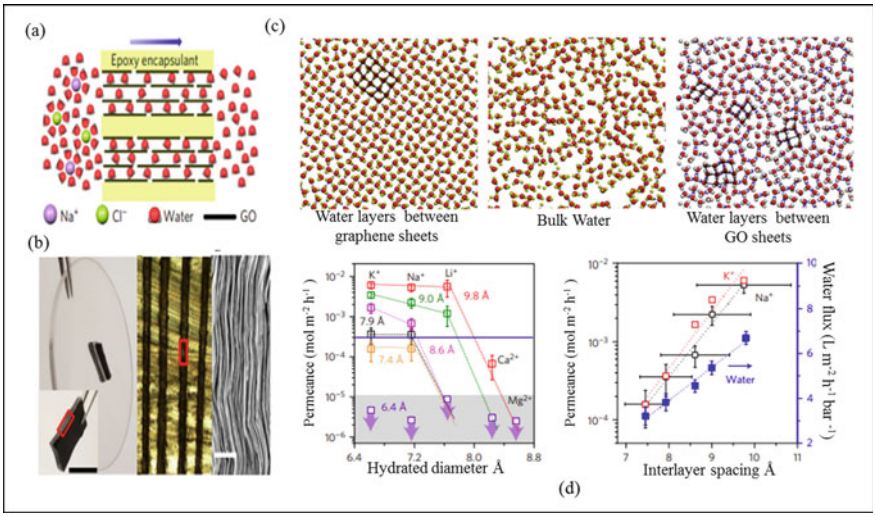


**Fig. 6** **a** Schematic illustrating the direction of ion/water permeation along graphene planes. **b** Photograph of a PCGO membrane glued into a rectangular slot within a plastic disk of 5 cm in diameter. Scanning electron microscopy image at 1 μm [29]. **c** Images showing the alignment of water layer between graphene sheets, the image of bulk water, and water layers between the GO sheets [89]. **d** Permeation rates through PCGO membranes with different interlayer distances and hydrated diameter (color coded). The salts used were KCl, NaCl, LiCl, $CaCl_2$, and $MgCl_2$ [29]

were reported, which was independent of the size of the species tested. In the reported study, ions follow the fashion, i.e., Na > Mn > Cd, but actual size trend follows Mn > Cd > Cu > Na. Additionally, the investigation also includes the resistance separation properties and the filtration of sodium salts from the copper salts and other organic particles by utilizing GO membranes. This study demonstrated the ion permeation from the GO membrane just by managing the d-spacing using physical confinement. The study revealed that the membrane had d-spacing in the range of 9.8–6.4 Å, which provides accuracy and tunability in ion sieving, smaller than hydrated ions in diameter [86]. The GO laminates have been cut into rectangular strips of 4mmX10mm under humid conditions for 1–2 weeks. The interlayer d-spacing was switch to 6.4–9.8 Å as the humidity increases from 0–100%. The membrane was soaked in water and the d-spacing noted was 13.7 ± 0.3 Å. The membranes were stacked up together using epoxy to meet the required cross section area (1 mm). The above-staked laminates of GO were mentioned as physically confined GO membranes (PCGO) as it restricts the laminates' swelling on humid exposure. Eventually, the membrane was successfully fabricated, having a limited swelling ratio, and utilized for the effective NaCl separation. In a recent investigation done by Chen et al., they demonstrated the selective ion rejection by GO membranes just by improving the interlayer spacing of the membranes by utilizing cations like $K^+$, $Na^+$, $Ca^{2+}$, $Li^+$ and $Mg^{2+}$ themselves [87]. The required interlayer spacing can be managed as precisely as 1.0 Å. This membrane can be directed by one type of cation that can eliminate the other cations

having a larger radius and that can be sheltered with larger spacing between the interlayers.

Implementing first-principle calculations, authors have revealed that the noncovalent cation interactions between the aromatic rings of GO and the hydrated cations present in solution are the reason behind unpredicted behavior. However, considerable progress for GO-based membranes has been achieved for water filtration and desalination applications. Even so, some good topics like the interlayer spacing, the pore dimensions, modification chemistry, and the number of layers in graphene still need more attention. As the pore size increases larger than 0.8 nm, graphene derived membranes show more water flux than CNT membranes as the center cause higher velocity [88]. Several efforts were made to alter the interlayer spacing. Reports suggest that the interlayer spacing can be widened by inserting large nanomaterials or cross-linking large and firm molecules to increase the permeability [87–89]. RGO membranes are highly impenetrable for most liquids, gases, and many inorganic chemicals. The interlayers are very small, so the task to reduce the interlayer spacing while maintaining the separation process constant and excluding the small ions when immersed in the aqueous solution is quite challenging. These issues become a barrier when the process is done on a large scale to separate selective ions of a particular size from the bulk ion solution. Additionally, swelling of GO in the presence of an aqueous solution is still a hurdle to overcome [89]. About TMDCs, only a few investigations have been reported of filtration using these materials [90–92]. TMDC membranes have shown high rejection (> 80%) of large organic impurities; still, ionic rejection properties and nanocapillary behavior in TMDCs layers need serious attention for full utilization of these membranes in filtration and desalination applications. In recent work, Bissett et al. prepared the $MoS_2$ membrane with excellent ionic sieving up to 99% for all the cationic components ($Na^+$, $K^+$, $Ca^{2+}$, and $Mg^{2+}$) present in seawater [16]. The water flux maintained was significantly five times greater in comparison with those reported GO-based membranes. The fabricated functionalized $MoS_2$ membranes exhibited high mechanical stability with no swelling in 6 months immersed in water. The ion rejection capability of this membrane remained the same for 6 months. This membrane's stability was exposed using different organic solvents, but the performance remained the same for the membrane and was desirable for the filtration applications. Besides this, only a few studies are reported regarding MXenes, TMDCs, and other LDH membranes for the desalination application [90–92]. Recently, a freestanding membrane was fabricated using 2D MXene ($Ti_3C_2T_x$) by Gogotsi et al. on PVDF support using the vacuum filtration method [51]. This membrane was used to separate the selective ions ($Li^+$, $Na^+$, $K^+$, $Mg^{2+}$, and $Ca^{2+}$) and heavy metal ions ($Ni^{2+}$ and $Al^{3+}$) from the water; also in the same investigation, the membrane shows excellent separation for the methylene blue dye (Fig. 7a–d). This fabricated MXenes membrane showed an acceptable water flux of 37.4 L $m^{-2}$ $h^{-1}$ $bar^{-1}$. The metal ions carrying a high charge and smaller hydration radius than the interlayer spacing of $Ti_3C_2T_x$ show slower penetration than the cations having a single charge. Lamellar membranes using a stack of 2D MXenes nanosheets have been fabricated by Ding et al. and demonstrated the separation of different molecules (> 2.5 nm) with a 90% rejection rate with outstanding water

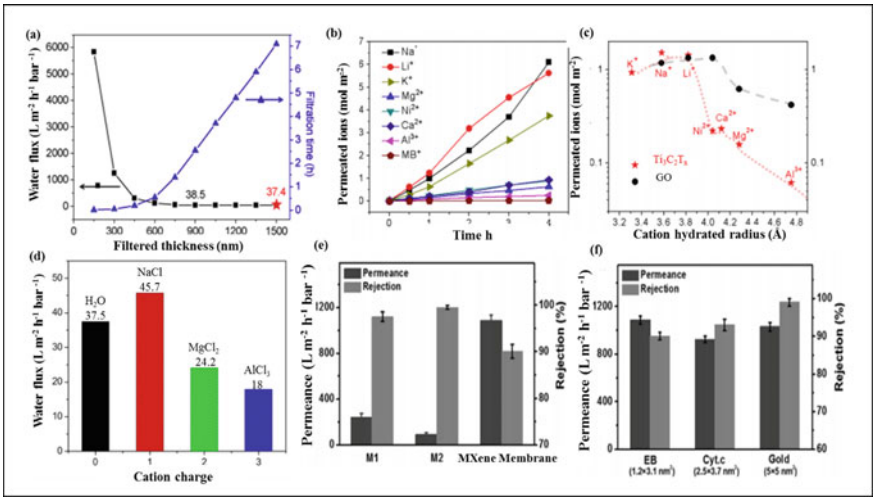


**Fig. 7** Water flux through $Ti_3C_2T_x$ membranes. **a** Water flux when thicknesses is varying. **b** Number of cations diffused through the MXene membranes versus time plot. **c** The diffusion rates of different cations versus their hydration radii plot [51]. **d** Flux of water salt solutions versus cation's charge plot; and **e**, **f** performance of the various MXene membranes for the separation of ethylene blue (EB) molecules and other various molecules with different sizes [50]

permeability of 1000 L $m^{-2}$ $h^{-1}$ $bar^{-1}$ and was better than the previous reports (Fig. 7e, f) [50]. Moreover, the performance of separation can be enhanced by incorporating MXenes with other 2D materials using appropriate cross-linking agents for the fabrication of composite nanostructures. Just as GO laminar membranes, the $Ti_3C_2T_x$ membranes also have hydrophilic nature and have intergalleries that promote water flow. Zongli Xie et al., fabricated a 2D lamellar composite MXene membrane (MXMA) fabricated on microporous nylon substrate by vacuum filtration. Fabricated membranes have structurally well-defined nanochannels (~ 0.49 nm) and have swelling resistance and mechanical strength. The MXMA membrane showed magnificent desalination with large flux and salt rejection [93]. Yan Yang et al. fabricate a composite MXene membrane embedded with polyamide layer using in-situ polymerization with outstanding water permeability of 2.53 $Lm^{-2}$ $h^{-1}$ $bar^{-1}$ and high NaCl rejection (98.5%) [94].

Furthermore, 2D zeolite sheets can be used as a surface enhancer to prepare composite membranes for water desalination [95]. The different loading of zeolite enhances the hydrophilicity of the membranes and structural and thermomechanical properties. Zeolites reduced the undesirable voids of the membranes. Huanting et al. have fabricated ultrathin graphene membrane (subatomic pores) on a porous ceramic substrate using carbonization [96]. The fabricated membrane shows water flux of $49.8 \pm 1.5$–$472.3 \pm 14.2$ $Lm^{-2}$ $h^{-1}$ with 99.99% NaCl rejection at various temperatures (20–70 °C). The flux reported was remarkably higher than the previous reports. Kaisong et al., prepare nanocomposite membrane using functionalized molybdenum

disulfide (O-$MoS_2$). High oxidation of $MoS_2$ increases the hydrophilicity and electronegativity of the membrane. Accordingly, the rejection of $Na_2SO_4$ was 97.9%, including excellent antifouling properties [97]. Jinyu Lia et al. have investigated the ion separation efficiency by hBN membrane by implementing molecular dynamics molecular. The simulation promotes the fact of using hBN as a promising candidate in membranes for desalination [98]. On the other hand, the synthesis of MOF membranes has some severe limitations like grain boundary defects and intercrystalline cracks. A study was reported in which MOF membrane was fabricated by using plant polyphenol tannic acid as an interlayer to overcome this hurdle. The membrane showed a good water permeation of 3.6 L $m^{-2}$ $h^{-1}$ $bar^{-1}$ along with the rejection of NaCl and $Na_2SO_4$ up to 64.7 and 92.2%, respectively, and demonstrating great potential toward efficient water desalination [99].

The comparison study of different 2D material membrane is given in Table 2. Satisfying efforts have been made to enhance the aseptic properties, increase diffusion, and also enhance the mechanical properties for desalination applications. Mostly their work is dedicated to graphene-based materials, while other 2D materials are limitedly touched. Due to hydrophilic groups present at the basal plane of the GO sheets,

**Table 2** 2D material-based membranes for different water purification applications

| Membranes type | Fabrication technique | Types of feed/conc | Permeability (L $m^{-2}$ $h^{-1}$ $bar^{-1}$) | Rejection (%) | References |
|---|---|---|---|---|---|
| Porous grapheme monolayer | Oxygen plasma etching | KCl (1 M) | 250 | 100 | [79] |
| Base-refluxing reduced GO/PVDF | Vacuum filtration | MB (0.02 mM)<br>$Na_2SO_4$ (20 mM)<br>NaCl (20 mM) | 21.8<br>3.3<br>– | 99.2<br>20<br>40 | [100] |
| PAH cross-linked GO/PAN | Layer by layer | Sucrose (1 M) | 2.1–5.8 | 99 | [101] |
| $MoS_2$ membranes | Vacuum filtration | EB (15 μM) | 245 | 89 | [53] |
| NSC-$WS_2$ membranes | Vacuum filtration | EB (15 μM) | 704 | 82 | [54] |
| MXene membranes | Vacuum filtration | NaCl<br>$MgCl_2$<br>$AlCl_3$ | 45.7<br>24.2<br>18.3 | –<br>–<br>– | [64]<br>–<br>– |
| $Ti_3C_2T_x$ MXene nanosheet membrane | Vacuum filtration | EB (15 μM) | 1084 | 90 | [63] |
| GO15$WS_2$/Nylon | Vacuum filtration | $[Fe(CN)_6]^{3-}$ | 178.1 | 64.3 | [102] |
| GO-SWCNT/AAO | Vacuum filtration | Rhodamine blue | 710 | 97.4 | [103] |
| GO/FLG/deoxycholate membrane | Spray coating | NaCl | – | 85 | [104] |
| rNPGO | Vacuum filtration | $Na_2SO_4$ | 39.93 | 99 | [105] |

these GO-based fabricated membranes show excellent permeability and antifouling properties. Pore size adjustment and altering the nanochannels by modification and installation of oxygen-rich groups, narrow pore size distributed membranes can be created. Incorporation of such 2D materials in membrane fabrication increases the selectivity and decreases hydrophobicity on the membranes' surface, enhances the pore density, and reduces the cost of production. Oxygen functional groups in abundance result in the hydrophilic nature of GO and make the membrane swell in the aqueous or humid environments due to the water absorption, which can decrease the overall required performance of the membrane. GO membranes have natural tendency to swell in the aqueous phase due to water absorption by GO nanochannels, which ultimately increases the size of interlayer spacing.

Apart from the chemical stability, mechanical stability is vital when the membranes are fabricated on a large scale at various high-pressure conditions. Recently, many other 2D material membranes beyond graphene, such as MXene and TMDCs, have shown better performance in different water purification applications.

## 6 Challenges Associated with 2D Nanomaterial-Based Membranes

Several technical challenges listed below are still need overcome to utilize such membranes at large scale.

- Membrane fouling reduction.
- Flux increment is needed.
- Pressure drop and accordingly energy consumption reduction.
- Membrane performance should be accurately simulated and modeled.
- Achieve uniform pore-size distribution.
- Enhance chemical and mechanical stability of the membranes.
- Selectively of the membrane should be improved.

Fouling in membranes is a very technical problem. It is generally the deposition of material accumulated on the membrane. Fouling causes a decrease in flux due to the pore-clogging. Thus, membranes must be cleaned at regular intervals of times. Another hurdle is performance modeling, which interrupts membranes' formation on a large scale and not enough to predict the performance at the industrial level. The membranes depend on the quality of the particular source of water used for the experiments. Up to now, only laboratory-scale experiments are performed with these 2D material-based membranes. Recent reports are dedicated to the growth of solvent-resistant nanostructured membranes, but the extensive installation of the nanostructured membrane units is not economically viable. Generally, the water industry utilizes conservative methods to process and resist new techniques with rules and regulation. However, in most cases, 2D nanomaterial-based membranes need an entirely different maintenance structure.

## 7 Conclusion

This chapter is mainly focused on various characteristics of the 2D material-based membranes and classifications of water desalination application with possible challenges. The discussed 2D nanomaterials are promising candidates for membranes fabrication. Selectivity and scalability are the core limitations of these type of membranes. Improving the selectivity can enhance the quality of separation of water. The other prime characteristic of the membrane is its durability and mechanical strength. Furthermore, to explore the broad application, some serious efforts should be made to enhance membrane design. Therefore, MOF and GO-based composite materials utilize a high surface area and can be modified using various functionalities.

## References

1. Castro-Muñoz R (2020) Breakthroughs on tailoring pervaporation membranes for water desalination: a review. Water Res 116428
2. Motoshita M, Ono Y, Pfister S, Boulay AM, Berger M, Nansai K, Tahara K, Itsubo N, Inaba A (2018) Consistent characterisation factors at midpoint and endpoint relevant to agricultural water scarcity arising from freshwater consumption. Int J Life Cycle Assess 23(12):2276–2287
3. Bouman BA (2007) Water management in irrigated rice: coping with water scarcity. Int Rice Res Inst
4. Yu H, He Y, Xiao G, Fan Y, Ma J, Gao Y, Hou R, Yin X, Wang Y, Mei X (2020) The roles of oxygen-containing functional groups in modulating water purification performance of graphene oxide-based membrane. Chem Eng J 389:124375
5. Du T, Kang S, Zhang J, Davies WJ (2015) Deficit irrigation and sustainable water-resource strategies in agriculture for China's food security. J Exp Bot 66(8):2253–2269
6. Vatanpour V, Khadem SS, Dehqan A, Al-Naqshabandi MA, Ganjali MR, Hassani SS, Rashid MR, Saeb MR, Dizge N (2021) Efficient removal of dyes and proteins by nitrogen-doped porous graphene blended polyethersulfone nanocomposite membranes. Chemosphere 263:127892
7. Calderon RL (2000) The epidemiology of chemical contaminants of drinking water. Food Chem Toxicol 1(38):S13-20
8. Bove F, Shim Y, Zeitz P (2002) Drinking water contaminants and adverse pregnancy outcomes: a review. Environ Health Perspect 110(suppl 1):61–74
9. Raj SK, Yadav V, Bhadu GR, Patidar R, Kumar M, Kulshrestha V (2020) Synthesis of highly fluorescent and water soluble graphene quantum dots for detection of heavy metal ions in aqueous media. Environ Sci Pollut Res 13:1–7
10. Raj SK, Rajput A, Gupta H, Patidar R, Kulshrestha V (2019) Selective recognition of $Fe^{3+}$ and $Cr^{3+}$ in aqueous medium via fluorescence quenching of graphene quantum dots. J Dispersion Sci Technol 40(2):250–255
11. Gahlot S, Sharma PP, Gupta H, Kulshrestha V, Jha PK (2014) Preparation of graphene oxide nano-composite ion-exchange membranes for desalination application. RSC Adv 4(47):24662–24670
12. Rasch F, Postica V, Schütt F, Mishra YK, Nia AS, Lohe MR, Feng X, Adelung R, Lupan O (2020) Highly selective and ultra-low power consumption metal oxide based hydrogen gas sensor employing graphene oxide as molecular sieve. Sens Actuat Chem 320:128363
13. Vishak PM (2016) Nanostructured polymer membranes: applications, state-of-the-art, new challenges and opportunities. In: Nanostructured polymer membranes: applications, pp 1–25
14. Wang Z, Wang Z, Lin S, Jin H, Gao S, Zhu Y, Jin J (2018) Nanoparticle-templated nanofiltration membranes for ultrahigh performance desalination. Nat Commun 9(1):1–9

15. Hilal N, Al-Zoubi H, Darwish NA, Mohamma AW, Arabi MA (2004) A comprehensive review of nanofiltration membranes: treatment, pretreatment, modelling, and atomic force microscopy. Desalination 170(3):281–308
16. Hirunpinyopas W, Prestat E, Worrall SD, Haigh SJ, Dryfe RA, Bissett MA (2017) Desalination and nanofiltration through functionalized laminar $MoS_2$ membranes. ACS Nano 11(11):11082–11090
17. Younssi SA, Breida M, Achiou B (2018) Alumina membranes for desalination and Water treatment. InTech 2018
18. ISO T. 80004-1: nanotechnologies-vocabulary—Part 1: core terms. 2007. International Standards Organization, Geneva, 2007
19. Huang H, Ying Y, Peng X (2014) Graphene oxide nanosheet: an emerging star material for novel separation membranes. J Mater Chem A. 2(34):13772–13782
20. Sun P, Zheng F, Zhu M, Song Z, Wang K, Zhong M, Wu D, Little RB, Xu Z, Zhu H (2014) Selective trans-membrane transport of alkali and alkaline earth cations through graphene oxide membranes based on cation$-\pi$ interactions. ACS Nano 8(1):850–859
21. Huang H, Mao Y, Ying Y, Liu Y, Sun L, Peng X (2013) Salt concentration, pH and pressure controlled separation of small molecules through lamellar graphene oxide membranes. Chem Commun 49(53):5963–5965
22. Liu S, Hu K, Cerruti M, Barthelat F (2020) Ultra-stiff graphene oxide paper prepared by directed-flow vacuum filtration. Carbon 1(158):426–434
23. Nair RR, Wu HA, Jayaram PN, Grigorieva IV, Geim AK (2012) Unimpeded permeation of water through helium-leak–tight graphene-based membranes. Science 335(6067):442–444
24. Pham VH, Cuong TV, Hur SH, Shin EW, Kim JS, Chung JS, Kim EJ (2010) Fast and simple fabrication of a large transparent chemically-converted graphene film by spray-coating. Carbon 48(7):1945–1951
25. Zheng QB, Shi LF, Yang JH (2012) Langmuir-Blodgett assembly of ultra-large graphene oxide films for transparent electrodes. Trans Nonferrous Metals Soc China 22(10):2504–2511
26. Cote LJ, Kim J, Zhang Z, Sun C, Huang J (2010) Tunable assembly of graphene oxide surfactant sheets: wrinkles, overlaps and impacts on thin film properties. Soft Matter 6(24):6096–6101
27. Xu C, Wu X, Zhu J, Wang X (2008) Synthesis of amphiphilic graphite oxide. Carbon (New York, NY). 46(2):386–389
28. Wei N, Peng X, Xu Z (2014) Understanding water permeation in graphene oxide membranes. ACS Appl Mater Interfaces 6(8):5877–5883
29. Abraham J, Vasu KS, Williams CD, Gopinadhan K, Su Y, Cherian CT, Dix J, Prestat E, Haigh SJ, Grigorieva IV, Carbone P (2017) Tunable sieving of ions using graphene oxide membranes. Nat Nanotechnol 12(6):546
30. Ng LY, Mohammad AW, Leo CP, Hilal N (2013) Polymeric membranes incorporated with metal/metal oxide nanoparticles: a comprehensive review. Desalination 2(308):15–33
31. Homaeigohar S, Elbahri M (2017) Graphene membranes for water desalination. NPG Asia Mater 9(8):e427
32. Teow YH, Mohammad AW (2019) New generation nanomaterials for water desalination: a review. Desalination 1(451):2–17
33. Lee C, Wei X, Kysar JW, Hone J (2008) Measurement of the elastic properties and intrinsic strength of monolayer graphene. Science 321(5887):385–388
34. Hashimoto A, Suenaga K, Gloter A, Urita K, Iijima S (2004) Direct evidence for atomic defects in graphene layers. Nature 430(7002):870–873
35. Thomas M, Corry B, Hilder TA (2014) What have we learnt about the mechanisms of rapid water transport, ion rejection and selectivity in nanopores from molecular simulation? Small 10(8):1453–1465
36. Garaj S, Hubbard W, Reina A, Kong J, Branton D, Golovchenko JA (2010) Graphene as a subnanometre trans-electrode membrane. Nature 467(7312):190–193
37. Cohen-Tanugi D, Grossman JC (2012) Water desalination across nanoporous graphene. Nano Lett 12(7):3602–3608

38. Daer S, Kharraz J, Giwa A, Hasan SW (2015) Recent applications of nanomaterials in water desalination: a critical review and future opportunities. Desalination 1(367):37–48
39. Stoller MD, Park S, Zhu Y, An J, Ruoff RS (2008) Graphene-based ultracapacitors. Nano Lett 8(10):3498–3502
40. Sun L, Huang H, Peng X (2013) Laminar $MoS_2$ membranes for molecule separation. Chem Commun 49(91):10718–10720
41. Sun L, Ying Y, Huang H, Song Z, Mao Y, Xu Z, Peng X (2014) Ultrafast molecule separation through layered $WS_2$ nanosheet membranes. ACS Nano 8(6):6304–6311
42. Qi Y, Wang N, Xu Q, Li H, Zhou P, Lu X, Zhao G (2015) A green route to fabricate MoS 2 nanosheets in water–ethanol–$CO_2$. Chem Commun 51(31):6726–6729
43. Shen Y, Wang H, Zhang X, Zhang Y (2016) $MoS_2$ nanosheets functionalized composite mixed matrix membrane for enhanced $CO_2$ capture via surface drop-coating method. ACS Appl Mater Interfaces 8(35):23371–23378
44. Qin S, Liu D, Wang G, Portehault D, Garvey CJ, Gogotsi Y, Lei W, Chen Y (2017) High and stable ionic conductivity in 2D nanofluidic ion channels between boron nitride layers. J Am Chem Soc 139(18):6314–6320
45. Jia W, Tang B, Wu P (2017) Novel composite proton exchange membrane with connected long-range ionic nanochannels constructed via exfoliated nafion–boron nitride nanocomposite. ACS Appl Mater Interfaces 9(17):14791–14800
46. Kou J, Zhou X, Lu H, Wu F, Fan J (2014) Graphyne as the membrane for water desalination. Nanoscale 6(3):1865–1870
47. Kou J, Zhou X, Chen Y, Lu H, Wu F, Fan J (2013) Water permeation through single-layer graphyne membrane. J Chem Phys 139(6):064705
48. Naguib M, Mochalin VN, Barsoum MW, Gogotsi Y (2014) 25th anniversary article: MXenes: a new family of two-dimensional materials. Adv Mater 26(7):992–1005
49. Anasori B, Lukatskaya MR, Gogotsi Y (2017) 2D metal carbides and nitrides (MXenes) for energy storage. Nat Rev Mater 2(2):1–7
50. Ding L, Wei Y, Wang Y, Chen H, Caro J, Wang H (2017) A two-dimensional lamellar membrane: MXene nanosheet stacks. Angew Chem Int Ed 56(7):1825–1829
51. Ren CE, Hatzell KB, Alhabeb M, Ling Z, Mahmoud KA, Gogotsi Y (2015) Charge-and size-selective ion sieving through $Ti_3C_2T_x$ MXene membranes. J Phys Chem Lett 6(20):4026–4031
52. Ihsanullah I (2020) Potential of MXenes in water desalination: current status and perspectives. Nano-Micro Letters 12(1):1–20
53. Adatoz E, Avci AK, Keskin S (2015) Opportunities and challenges of MOF-based membranes in gas separations. Sep Purif Technol 25(152):207–237
54. Wang X, Chi C, Zhang K, Qian Y, Gupta KM, Kang Z, Jiang J, Zhao D (2017) Reversed thermo-switchable molecular sieving membranes composed of two-dimensional metal-organic nanosheets for gas separation. Nat Commun 8(1):1
55. Peng Y, Li Y, Ban Y, Yang W (2017) Two-dimensional metal–organic framework nanosheets for membrane-based gas separation. Angew Chem Int Ed 56(33):9757–9761
56. Cheetham AK, Rao CN, Feller RK (2006) Structural diversity and chemical trends in hybrid inorganic–organic framework materials. Chem Commun 46:4780–4795
57. He Y, Chang Z, Wu S, Qiao Y, Bai S, Jiang K, He P, Zhou H (2018) Simultaneously inhibiting lithium dendrites growth and polysulfides shuttle by a flexible MOF-based membrane in Li–S batteries. Adv Energy Mater 8(34):1802130
58. Amo-Ochoa P, Welte L, González-Prieto R, Miguel PJ, Gómez-García CJ, Mateo-Martí E, Delgado S, Gómez-Herrero J, Zamora F (2010) Single layers of a multifunctional laminar Cu (I, II) coordination polymer. Chem Commun 46(19):3262–3264
59. Junggeburth SC, Diehl L, Werner S, Duppel V, Sigle W, Lotsch BV (2013) Ultrathin 2D coordination polymer nanosheets by surfactant-mediated synthesis. J Am Chem Soc 135(16):6157–6164
60. Agrawal KV, Topuz B, Pham TC, Nguyen TH, Sauer N, Rangnekar N, Zhang H, Narasimharao K, Basahel SN, Francis LF, Macosko CW (2015) Oriented MFI membranes by gel-less secondary growth of sub-100 nm MFI-nanosheet seed layers. Adv Mater 27(21):3243–3249

61. Rangnekar N, Shete M, Agrawal KV, Topuz B, Kumar P, Guo Q, Ismail I, Alyoubi A, Basahel S, Narasimharao K, Macosko CW (2015) 2D zeolite coatings: langmuir-Schaefer deposition of 3 nm thick MFI zeolite nanosheets. Angew Chem Int Ed 54(22):6571–6575
62. Liu G, Jin W, Xu N (2016) Two-dimensional-material membranes: a new family of high-performance separation membranes. Angew Chem Int Ed 55(43):13384–13397
63. Jeon MY, Kim D, Kumar P, Lee PS, Rangnekar N, Bai P, Shete M, Elyassi B, Lee HS, Narasimharao K, Basahel SN (2017) Ultra-selective high-flux membranes from directly synthesized zeolite nanosheets. Nature 543(7647):690–694
64. Varoon K, Zhang X, Elyassi B, Brewer DD, Gettel M, Kumar S, Lee JA, Maheshwari S, Mittal A, Sung CY, Cococcioni M (2011) Dispersible exfoliated zeolite nanosheets and their application as a selective membrane. Science 334(6052):72–75
65. Werber JR, Deshmukh A, Elimelech M (2016) The critical need for increased selectivity, not increased water permeability, for desalination membranes. Environ Sci Technol Lett 3(4):112–120
66. You Y, Sahajwalla V, Yoshimura M, Joshi RK (2016) Graphene and graphene oxide for desalination. Nanoscale 8(1):117–119
67. Safaei J, Xiong P, Wang G (2020) Progress and prospects of two-dimensional materials for membrane-based water desalination. Mater Today Adv 8:100108
68. Simeonidis K, Mourdikoudis S, Kaprara E, Mitrakas M, Polavarapu L (2016) Inorganic engineered nanoparticles in drinking water treatment: a critical review. Environ Sci: Water Res Technol 2(1):43–70
69. Jhaveri JH, Murthy ZV (2016) A comprehensive review on anti-fouling nanocomposite membranes for pressure driven membrane separation processes. Desalination 1(379):137–154
70. Lee B, Baek Y, Lee M, Jeong DH, Lee HH, Yoon J, Kim YH (2015) A carbon nanotube wall membrane for water treatment. Nat Commun 6(1):1–7
71. Hegab HM, Zou L (2015) Graphene oxide-assisted membranes: fabrication and potential applications in desalination and water purification. J Membr Sci 15(484):95–106
72. Lee A, Elam JW, Darling SB (2016) Membrane materials for water purification: design, development, and application. Environ Sci: Water Res Technol 2(1):17–42
73. Liu P, Hou J, Zhang Y, Li L, Lu X, Tang Z (2020) Two-dimensional material membranes for critical separations. Inorg Chem Front 7(13):2560–2581
74. Ying Y, Yang Y, Ying W, Peng X (2016) Two-dimensional materials for novel liquid separation membranes. Nanotechnology 27(33):332001
75. Sun C, Wen B, Bai B (2015) Recent advances in nanoporous graphene membrane for gas separation and water purification. Sci Bull 60(21):1807–1823
76. Zhao Y, Xie Y, Liu Z, Wang X, Chai Y, Yan F (2014) Two-dimensional material membranes: an emerging platform for controllable mass transport applications. Small 10(22):4521–4542
77. Celebi K, Buchheim J, Wyss RM, Droudian A, Gasser P, Shorubalko I, Kye JI, Lee C, Park HG (2014) Ultimate permeation across atomically thin porous graphene. Science 344(6181):289–292
78. Liu G, Jin W, Xu N (2015) Graphene-based membranes. Chem Soc Rev 44(15):5016–5030
79. Surwade SP, Smirnov SN, Vlassiouk IV, Unocic RR, Veith GM, Dai S, Mahurin SM (2015) Water desalination using nanoporous single-layer graphene. Nat Nanotechnol 10(5):459–464
80. Liu L, Zhou H, Cheng R, Chen Y, Lin YC, Qu Y, Bai J, Ivanov IA, Liu G, Huang Y, Duan X (2012) A systematic study of atmospheric pressure chemical vapor deposition growth of large-area monolayer graphene. J Mater Chem 22(4):1498–1503
81. Zhang Y, Chung TS (2017) Graphene oxide membranes for nanofiltration. Curr Opin Chem Eng 1(16):9–15
82. Joshi RK, Alwarappan S, Yoshimura M, Sahajwalla V, Nishina Y (2015) Graphene oxide: the new membrane material. Appl Mater Today 1(1):1–2
83. Goh PS, Ismail AF (2015) Graphene-based nanomaterial: the state-of-the-art material for cutting edge desalination technology. Desalination 15(356):115–128
84. Raj SK, Sharma J, Kulshrestha V (2021) Facile synthesis of reusable graphene oxide composite magnetic beads for removal of arsenic (III). SPE Polymers 1–12

85. Dreyer DR, Todd AD, Bielawski CW (2014) Harnessing the chemistry of graphene oxide. Chem Soc Rev 43(15):5288–5301
86. Sun P, Zhu M, Wang K, Zhong M, Wei J, Wu D, Xu Z, Zhu H (2013) Selective ion penetration of graphene oxide membranes. ACS Nano 7(1):428–437
87. Chen L, Shi G, Shen J, Peng B, Zhang B, Wang Y, Bian F, Wang J, Li D, Qian Z, Xu G (2017) Ion sieving in graphene oxide membranes via cationic control of interlayer spacing. Nature 550(7676):380–383
88. Suk ME, Aluru NR (2010) Water transport through ultrathin graphene. J Phys Chem Lett 1(10):1590–1594
89. Zheng S, Tu Q, Urban JJ, Li S, Mi B (2017) Swelling of graphene oxide membranes in aqueous solution: characterization of interlayer spacing and insight into water transport mechanisms. ACS Nano 11(6):6440–6450
90. Dai L, Huang K, Xia Y, Xu Z (2020) Two-dimensional material separation membranes for renewable energy purification, storage, and conversion. Green Energy Environ 6(2):193–211
91. Kim WG, Nair S (2013) Membranes from nanoporous 1D and 2D materials: a review of opportunities, developments, and challenges. Chem Eng Sci 18(104):908–924
92. Dervin S, Dionysiou DD, Pillai SC (2016) 2D nanostructures for water purification: graphene and beyond. Nanoscale 8(33):15115–15131
93. Ding M, Xu H, Chen W, Yang G, Kong Q, Ng D, Lin T, Xie Z (2020) 2D laminar maleic acid-crosslinked MXene membrane with tunable nanochannels for efficient and stable pervaporation desalination. J Memb Sci 600:117871
94. Wang X, Li Q, Zhang J, Huang H, Wu S, Yang Y (2020) Novel thin-film reverse osmosis membrane with MXene Ti3C2Tx embedded in polyamide to enhance the water flux, anti-fouling and chlorine resistance for water desalination. J Memb Sci 603:118036
95. Jamshaid F, Dilshad MR, Islam A, Khan RU, Ahmad A, Adrees M, Haider B (2020) Synthesis, characterization and desalination study of polyvinyl chloride-co-vinyl acetate/cellulose acetate membranes integrated with surface modified zeolites. Microporous Mesoporous Mater 309:110579
96. Chen X, Zhu YB, Yu H, Liu JZ, Easton CD, Wang Z, Hu Y, Xie Z, Wu HA, Zhang X, Li D (2020) Ultrafast water evaporation through graphene membranes with subnanometer pores for desalination. J Memb Sci 118934
97. Yang S, Jiang Q, Zhang K (2020) Few-layers 2D O–$MoS_2$ TFN nanofiltration membranes for future desalination. J Memb Sci 604:118052
98. Liu L, Liu Y, Qi Y, Song M, Jiang L, Fu G, Li J (2020) Hexagonal boron nitride with nanoslits as a membrane for water desalination: a molecular dynamics investigation. Separ Purif Technol 251:117409
99. Xu Y, Xiao Y, Zhang W, Lin H, Shen L, Li R, Jiao Y, Liao BQ (2021) Plant polyphenol intermediated metal-organic framework (MOF) membranes for efficient desalination. J Memb Sci 618:118726
100. Han Y, Xu Z, Gao C (2013) Ultrathin graphene nanofiltration membrane for water purification. Adv Func Mater 23(29):3693–3700
101. Hu M, Mi B (2014) Layer-by-layer assembly of graphene oxide membranes via electrostatic interaction. J Membr Sci 1(469):80–87
102. Cheng P, Chen Y, Gu YH, Yan X, Lang WZ (2019) Hybrid 2D $WS_2$/GO nanofiltration membranes for finely molecular sieving. J Memb Sci 591:117308
103. Gao SJ, Qin H, Liu P, Jin J (2015) SWCNT-intercalated GO ultrathin films for ultrafast separation of molecules. J Mater Chem A 3(12):6649–6654
104. Morelos-Gomez A, Cruz-Silva R, Muramatsu H, Ortiz-Medina J, Araki T, Fukuyo T, Tejima S, Takeuchi K, Hayashi T, Terrones M, Endo M (2017) Effective NaCl and dye rejection of hybrid graphene oxide/graphene layered membranes. Nat Nanotechnol 12(11):1083
105. Li Y, Zhao W, Weyland M, Yuan S, Xia Y, Liu H, Jian M, Yang J, Easton CD, Selomulya C, Zhang X (2019) Thermally reduced nanoporous graphene oxide membrane for desalination. Environ Sci Technol 53(14):8314–8323

# Chapter 7
# Advancements in 2D Nanomaterial Composites-Based Electrochemical Sensors for Environmental Contaminants


**Zeba Khanam, Sameer Ahmad, Mohd Saquib Tanweer, Weqar Ahmad Siddiqi, and Masood Alam**

## 1 Introduction

The booming technologies are providing great comfort in livings but with a consequence of a distressful environment. Rapid urbanization and population explosion have stretched the use of natural resources to the maximum, rendering severe environmental hazards. Owing to industrial, agricultural, and other anthropogenic activities, every year over million tons of contaminants including toxic gases, heavy metals, organic compounds, and other harmful wastes, etc., are being released into the environment. The undesirable interaction of these pollutants with the air/water brought unhealthy changes in the innate physiochemical properties of the ecosystem [1–8]. New chemicals are constantly being produced; hence, the research efforts should be

Zeba Khanam, Sameer Ahmad and Mohd Saquib Tanweer are first co-authors.

Z. Khanam (✉)
School of Materials Science and Engineering, Harbin Institute of Technology, Shenzhen 518055, China
e-mail: zbkhnm@gmail.com

S. Ahmad (✉) · W. A. Siddiqi
Department of Applied Sciences and Humanities, Faculty of Engineering and Technology, Jamia Millia Islamia, New Delhi 110025, India
e-mail: ahmad.sameer68@yahoo.com

W. A. Siddiqi
e-mail: wsiddiqui@jmi.ac.in

M. S. Tanweer (✉) · M. Alam
Environmental Science Research Lab, Department of Applied Sciences and Humanities, Faculty of Engineering and Technology, Jamia Millia Islamia, New Delhi 110025, India
e-mail: saquibtanweer701@gmail.com

M. Alam
e-mail: malam@jmi.ac.in



Z. Khanam et al. (eds.), *2D Nanomaterials for Energy and Environmental Sustainability*,
Materials Horizons: From Nature to Nanomaterials,
https://doi.org/10.1007/978-981-16-8538-5_7

directed to curtail the release of such chemicals to avoid any risk to the environment and the life forms. It is highly demandable to regulate, monitor, and evaluate the dynamics of the emerging contaminants for the safety of human health and the environment and aiding sustainable growth on the earth.

The conventional techniques (such as mass spectrometry, optical methods, and high-performance liquid chromatography) are unable to quantify trace levels of contaminants and are complex, time-consuming, and relatively expensive. Besides, the lack of monitoring standards and efficient regulatory programs has further crippled the environmental protection management system. On this account, advanced electrochemical sensing techniques are acknowledged for the efficient monitoring and detection of pollutants at trace levels. Electrochemical sensing methods hold the attributes of fast response, high accuracy and precision, superior sensitivity, good selectivity, short analysis time, reproducibility, stability, cost-effectiveness, simplicity, and easy data readout [1–15]. Nevertheless, the sensor's performance directly relies upon the active sensing electrode material. The sensing materials may act as, or be responsible for, the recognition/sensing element and signal amplification [9–15]. In trends, 2D nanomaterials are receiving great attention as sensing material because of their unique quantum size effect, tunable surface properties, enhanced mass transport, sufficient conductivity, and redox activity. The electronic properties arising from the electrons/holes confinement make 2D nanostructures very sensitive to external perturbations and matter [9–15]. On exposure to the target analyte, 2D nanomaterials-based sensing electrode induce a fast change in current, potential, impedance, or any other parameter that can be recorded and analyzed. The detection mechanism mainly involves the binding of the target analyte to the surface of 2D nanomaterial electrode through physical/chemical interactions, viz. absorption, charge transfer, intercalation, and shifts in permittivity and lattice vibrations [15]. To date, various 2D nanomaterials including transition metal compounds (TMDs, TMOs, TMHs), MXenes (transition metal carbides/nitrides/carbonitrides), 2D organic frameworks (MOF, COF), phosphorene, etc., have been extensively explored to develop high-performance electrochemical sensors for detecting toxic gases [5, 16], heavy metals [15, 17], and other organic contaminants [9, 17], etc., and a lot of research is still in progress.

This chapter summarizes the recent advances of 2D nanomaterials in electrochemical sensing applications particularly emphasizing on detection of toxic gases and water pollutants along with a brief presentation of the underlying principle and performance of different electrochemical sensors.

## 2 Advanced Electrochemical Sensing Techniques

Typically, a sensor is composed of (a) the receptor that recognizes the target analyte (e.g., pollutant), and (b) the transducer which converts and produces a quantifiable sensing signal. The receptor, being the crucial component, accounts for the specificity, affinity, response time, and lifespan of the sensor. In general, the receptor binds

to a specific analyte in a given environment and the transducer amplifies the sensing signal proportional to analyte concentration which can be measured and analyzed [3, 18–20]. Based on different signal transduction mechanisms, the sensing event could be a change in current, potential, amplitude, conductivity, fluorescence, or luminescence activity. Sensors could be designated according to the detection principles—for instance, electrochemical, optical, thermal, piezoelectric, field-effect transistor sensors, etc. [3, 9, 13–15, 18–20]. Herein, our focus is on the electrochemical sensors as they dominate much of the current literature.

Electrochemical sensing of pollutants typically relies on active electrodes that are able to produce a quantifiable electrical signal in response to the electrochemical adsorption or reaction with target analytes. The presence of pollutants is detected and recorded in the form of a measurable sensing signal induced by a change of current, resistance, capacitance, or potential [1, 3, 10, 13]. Different modes of electrochemical techniques can be employed for the pollutant's detection

- *Potentiometry*: Potentiometric sensors analyze the chemical activity of the targeted ions under thermal equilibrium conditions by measuring the difference in electrical potential. The possible analytes are redox-inert species [9, 10, 18–20].
- *Voltammetry*: Voltammetric sensors monitor the relative concentrations of the target analyte by measuring the change in current arising due to the electron transfer under applied potential. Cyclic voltammetry is a fingerprint technique to identify the presence of targeted analytes through a redox reaction. Numerous other voltammetric methods could enhance the selectivity and sensitivity, like square-wave voltammetry (SWV), normal pulse voltammetry (NPV), anodic stripping voltammetry (ASV), cathodic stripping voltammetry (CSV), and differential pulse voltammetry (DPV). Among these, ASV or CSV are widely known for trace metals analysis, involving the electrochemical accumulation of analyte at the electrode surface, followed by its oxidation in a linear sweep or pulsed reverse scan. Voltammetry methods can detect specific redox analytes giving information about the reversible reactions and the nature of the analyte present [9, 10, 18–20].
- *Amperometry*: Like voltammetric sensors, amperometric sensors measure the magnitude of current as a function of analyte concentration at a fixed potential. The response times, dynamic ranges, and sensitivities are similar to potentiometric sensors and can only detect redox-active species like voltammetric sensors. It is worth noting that any perturbation or disturbance causes no effect on the sensor performance [9, 10, 18–21].
- *Impedance*: Impedimetric sensors determine the current response by applying a small sinusoidal AC voltage. Impedance methods are quite powerful as they are capable of characterizing physicochemical processes of widely differing time constants, sampling electron transfer at high frequency and mass transfer at low frequency. It does not require voltage scanning which is time-consuming and may degrade the electrochemical interface during wide potential sweeps. In addition, impedance sensing is largely insensitive to environmental disturbance, which is often problematic for other sensors [5, 9, 10, 18–22].

## 3 Fabrication of 2D Nanocomposites-Electrochemical Sensing Platforms/Electrodes

Tremendous research interest has been stimulated among the scientific community to develop novel, facile, cost-effective, portable, miniaturized 2D nanomaterial composite electrodes for precise and rapid electrochemical detection of environmental contaminants. The fine structural and compositional tuning of 2D nanomaterials can improve their electrochemical and electrical characteristics, enabling efficient signal transduction after an analyte binding event. Recent studies demonstrated that creating heteroatoms, metal or chemical doping, hybridizing/compositing with other nanomaterials or polymers, and integrating with biological entities such as enzyme/nucleic acid/protein immobilization can effectively tune the bandgap of resulting 2D nanomaterials composite and thereby enhancing the strength and selectivity of the sensing element–analyte interactions [3, 7, 9, 15, 17, 23, 24]. Up to now, several methods such as wet chemical, hydrothermal, solvothermal, co-precipitation, sol–gel, chemical oxidative polymerization, micro-emulsion, layer-by-layer assembly, pyrolysis, and ultrasonic/high-shear/supercritical-assisted dispersion have been reported to prepare such 2D nanomaterial-based composites [3, 7, 9, 12–17, 23, 24]. The prepared 2D nanocomposites are then usually drop-casted over the glassy carbon electrodes (GCE) or screen-printed electrodes (SPE) or interdigitated electrodes (IDE). Alternatively, 2D nanomaterials composites dispersion can be coated over flexible substrates (such as carbon paper, cellulose paper, fiber, cloth) by means of inkjet printing, pencil drawing, painting, spin coating, dip-coating, spray coating, drop-casting, electrophoretic deposition, electrospinning, and rolled-up technologies. Most recently, the template-free self-standing flexible electrodes are in high demand which can be directly fabricated as thin films or hydrogel/aerogel membranes by simple solution casting [3, 7, 9, 12–17, 23–26]. The related studies are summarized in Table 1.

The major key factors of a 2D nanocomposite electrode impacting the electrochemical sensor performance are:

- *Specific surface area*: 2D nanomaterials electrodes with large surface area ensure sufficient material–analyte interactions, beneficial to realize high sensitivity even at extremely low concentrations of the analyte [9, 15].
- *Electrical conductivity*: 2D nanomaterials exhibit a range of electrically conductive behaviors including metallic, semimetallic, semi-conductive, and insulating behavior. In addition, they have direct and indirect bandgaps ranging from ultraviolet to infrared, and throughout the visible spectrum. In 2D nanomaterials, the confinement of charge transport is in the 2D plane which may instigate considerable change in the electrical conductivity upon analyte binding [9, 15].
- *Electrochemical activity*: The intrinsic electrochemical properties of 2D nanomaterials are advantageous for electrochemical sensing applications. The intriguing confined nanospaces between adjacent 2D layers interfaces can accelerate many electrochemical reactions such as faradic, capacitive, electron mobility, current density, and mass transport [9, 15].

**Table 1** Summary of various 2D nanocomposite-based electrochemical sensors for detection of toxic gases/VOCs, heavy metals, and other water pollutants

| 2D nanomaterials-based sensing platform | Fabrication method | Air/water contaminants | Sensing techniques | References |
|---|---|---|---|---|
| *TMDs* | | | | |
| $MoS_2/C_3N_4$ aerogel @IDE | Thermal decomposition and freeze drying | $NO_2$ gas | Electrochemical, I–V | [27] |
| $MoS_2/MoO_3$ @GCE | Hydrothermal | $NH_3$ gas | Electrochemical, I–V | [37] |
| $MoS_2/WO_3$ @GCE | Probe-sonication | $NH_3$ gas | Electrochemical, I–V | [38] |
| 1T $WS_2$ @IDE | Exfoliation | Methanol vapor | Impedance | [39] |
| $MoS_2$-Au hybrid @IDE | Simple solution mixing | Acetone vapor | Electrochemical sensing | [40] |
| $MoS_2$/rGO @GCE | Hydrothermal | Pb(II) ions | SWASV | [41] |
| DNA1–QD–PDDA–$MoS_2$ @GCE | Multi-step immobilization | Hg(II) ions | Electrochemiluminescence | [42] |
| $MoS_2$-DMF @GCE | Sonication | Cd(II) ions | SWASV | [43] |
| $MoSe_2/MoO_3$ @GCE | Hydrothermal | Nitrite ions | Amperometry | [44] |
| *MXenes* | | | | |
| MXene($V_2C$)/PANI @IDE | In-situ polymerization | $NH_3$ gas | Integrated self-powered electrochemical sensing | [49] |
| MXene/PU core–sheath fibers (template-free) | Wet spinning of PU, spray coating of MXene over PU fibers | Acetone vapor | Amperometry | [50] |
| MXene ($Ti_3C_2T_x$) @IDE | MXene etching and drop-casting over IDE | Ethanol vapor | Impedance | [51] |
| MXene-bismuth @PET microgrid assembly | Solution mixing, micromilling | Pb(II), Cd(II) and Zn(II) ions | SWASV | [52] |
| MXene-bismuth @GCE | Sonication | Pb(II) and Cd(II) ions | SWASV | [53] |

(continued)

**Table 1** (continued)

| 2D nanomaterials-based sensing platform | Fabrication method | Air/water contaminants | Sensing techniques | References |
|---|---|---|---|---|
| $Ti_3C_2T_x/BiVO_4$ @ITO | $BiVO_4$ electrodeposition over ITO followed by spin coating of $Ti_3C_2T_x$ | Hg(II) ions | Photoelectrochemical sensing | [54] |
| $Ti_3C_2T_x$/Nafion @GCE | Sonication | Bromate ions | DPV | [55] |
| Au@CQDs-MXene @GCE | One-pot green synthesis | Nitrite ions | DPV | [56] |
| Pt@$Ti_3C_2T_x$ @GCE | Sonication | Bisphenol A | DPV | [57] |
| *MOFs* | | | | |
| Cu-BTC (MOF-199) @Cu | Electrochemical synthesis of a thin film of MOF over Cu plate | Ethanol and methanol vapors | Capacitive sensing | [63] |
| PANI-cobalt zeolitic benzimidazolate MOF | Chemical oxidative polymerization | $H_2$ gas | Chronoamperometry | [64] |
| Silica-coated-CuBTC MOF-PAN-graphene @Cr | Polymerization | $NH_3$ gas | Electrochemical, I–V | [65] |
| CDMOF-2 pellet | Solution mixing | $CO_2$ | Impedance | [66] |
| Ni-MOF-74 @IDE | Sonication and thermal reflux | $NO_2$ gas | Impedance | [67] |
| MOF-derived $Co_3V_2O_8$ | Solvothermal, screen-printing over solid electrolyte | $NO_2$ gas | Electrochemical, I–V | [68] |
| UiO-66-$NH_2$MOF-PANI @GCE | Hydrothermal, sonication | Cd(II) ions | DPSV | [70] |
| Polypyrrole-MOF film free-standing | Interfacial polymerization | Cd(II) ions | SWASV | [71] |
| DNA immobilized-AgPtNPs/MIL-101(Fe) MOF @GCE | Hydrothermal, solution mixing | Pb(II) ions | DPV | [69] |
| Zn-MOF/GO @GCE | Solvothermal | As(III) ions | DPASV | [72] |

(continued)

**Table 1** (continued)

| 2D nanomaterials-based sensing platform | Fabrication method | Air/water contaminants | Sensing techniques | References |
|---|---|---|---|---|
| Zirconium-porphyrin-MOF-525 | Solvothermal | Nitrite ions | Amperometry | [73] |
| *Phosphorene (BP)* | | | | |
| BP @IDE | CVD | Methanol vapor | Impedance | [83] |
| Platinoid-BP @IDE | Electrochemical synthesis | Methanol vapor | Impedance | [84] |
| BP @IDE | Exfoliation | $NO_2$ $NH_3$ and $H_2$ gas | Amperometry | [85] |
| Polyethyleneimine-BP @GCE | One step electrostatic adsorption method | Cu(II) ions | Amperometry | [87] |
| Porous Gr-BP @GCE | Sonication, pyrolysis | Bisphenol-A | DPV | [88] |
| BP quantum dots-ZnO @GCE | Sonication, hydrothermal | $H_2O_2$ | Amperometry | [89] |
| Hexamethylenediamine (HA)-coated AuNPs-BP | Sonication, seed-induced growth | Polychlorinated biphenyl (PCB77) | DPV | [90] |

- *Surface defects or functionalization*: The rich surface chemistry could effectively enhance the selectivity and sensitivity of the targeted species. Integration with other recognition components (e.g., metallic nanoparticles, metal oxides, and enzymes) could provide more active sites to further improve the sensing performance of a device. It can influence the electron or photon movement and interfacial charge transfer between sensing material and analyte [9, 15].

There lies a co-relationship between the electrical conductivity, active sites, electrochemical activity, and surface defects/functionalization. The high electrical conductivity and abundant active sites can considerably improve electrochemical activity. An increase in the degree of structural disorders usually improves the number of active sites which can enhance the electron scattering, beneficial for sensing applications [9, 15].

## 4 2D Nanocomposites-Based Electrochemical Sensors for Toxic Gases and Water Pollutants

As a result of anthropogenic and natural activities, many toxic gases, such as carbonous (CO and $CO_2$), sulfurous ($H_2S$ and SOx), and nitrogenous ($NH_3$, NO, $N_2O$, $N_2O_4$, etc.) or their by-products and volatile organic compounds (VOCs) such as ethanol, methanol, acetone, benzene, are deteriorating the air quality. Even a low concentration exposure to these hazardous gases and VOCs can cause fatal respiratory nuisance and turn lethal to life forms. The detection of such harmful gases and VOCs is crucial for efficient air quality monitoring, industrial process management as well as effective emissions control [5, 6, 9, 16, 21–27]. On the other hand, there is a high need to regulate the discharge of inorganic/organic chemicals and heavy metals into aqueous systems. They mainly include nitrites, pesticides, dyes, lead, arsenic, mercury, etc., which not only pollutes surface water but groundwater as well. Many chronic diseases and billion deaths are reported due to the intake of contaminated water [1–4, 7, 9–15, 28–31]. Over the decade, electrochemical sensors have made significant advances in the field of environmental monitoring. As mentioned above, the sensor performance depends on the sensing material. Therefore, various 2D nanocomposites have been explored as an active sensing material for the electrochemical detection of a range of analytes. The broad chemical diversity of 2D nanomaterials provides a great deal of surface structure tunability for specific host–analyte interactions [9]. So far, numerous 2D nanocomposite electrochemical sensing devices have been developed for the detection of toxic gases and water pollutants, a few of which are reviewed here. Substantial progress is toward integrated electrochemical sensors like electrochemiluminescence (ECL) and photoelectrochemical (PEC) sensors. In ECL sensing, electrochemical reactions by electron transfer trigger chemiluminescence, which is then recorded and analyzed. While PEC sensors involve photon-electricity conversion through charge separation and subsequent charge transfer after absorption of photons during illumination

where light energy is an excitation source and electrical signals were recorded [32]. Some recently developed 2D nanocomposites-based ECL and PEC sensors are also included herein. This section has mainly addressed the 2D TMDs, MXenes, MOFs, and phosphorene-based electrochemical sensing devices for detecting toxic gases and water contaminants.

## *4.1 TMDs/TMOs-Based Sensors*

2D transition metal compounds (TMDs, TMOs, TMHs) have diverse structural and electronic behaviors (semi-conductors, conductors, or insulators), allowing them to be incorporated into different analytical devices. Benefitted with the atomically thin layer structure, high surface-to-volume ratio, tunable bandgaps, and fast electron transfer kinetics, render these materials as promising candidates for detecting gases, VOCs, heavy metal ions, etc. The charge transport can be easily modulated through surface engineering of TMDs, providing abundant host–analyte active sites along with thermal and chemical stability [7, 9–11, 33–36].

### 4.1.1 Detection of Toxic Gases

Various 2D transition metal compounds and their composites or heterostructures are successfully applied for sensing toxic gases, such as $MoS_2/C_3N_4$ [27], $MoS_2/MoO_3$ [37], $MoS_2/WO_3$ [38], and 1T $WS_2$ [39]. A recent study reported the preparation of heterostructure of $MoS_2/MoO_3$ via hydrothermal process that was efficiently employed for selective electrochemical sensing of $NH_3$ under highly humid conditions. Figure 1a, b displays the change in corresponding resistance of as-prepared $MoS_2/MoO_3$ based sensor on exposure to different reducing gases (hydrogen sulfide, formaldehyde, methanol, ethanol, and acetone) and oxidizing gases (NO and $NO_2$) at relative humidity (RH) of 40% and 60%, respectively. It was found that the sensor exhibited superior sensitivity and selectivity toward $NH_3$ (down to 1 ppm) as compared to others. It is believed that the selectivity behavior is mainly governed by operating temperature, concentration, and the lowest unoccupied molecular orbital (LUMO) energy of adsorbed gas. And it is probably due to the matched LUMO energy of $NH_3$ with that of electronic energy of adsorbed oxygen on the sensor surface at ambient temperature which enhances their interaction, thereby enhancing the selectivity of the sensor toward $NH_3$ [37]. The authors conducted another study with $MoS_2/WO_3$ composite, prepared by a facile probe-sonication method, for the detection of $NH_3$. The composite sensor exhibited p-type semiconducting behavior with better selectivity and sensitivity toward $NH_3$ (down to 1 ppm) and excellent response-recovery features in contrast to individual $MoS_2$ (p-type) and $WO_3$ (n-type) counterparts at an operating temperature of 200 °C. As shown in Fig. 1c, the composite sensor displayed an increased resistance response toward $NH_3$ as compared to different reducing gases. This is mainly due to the creation of n-p

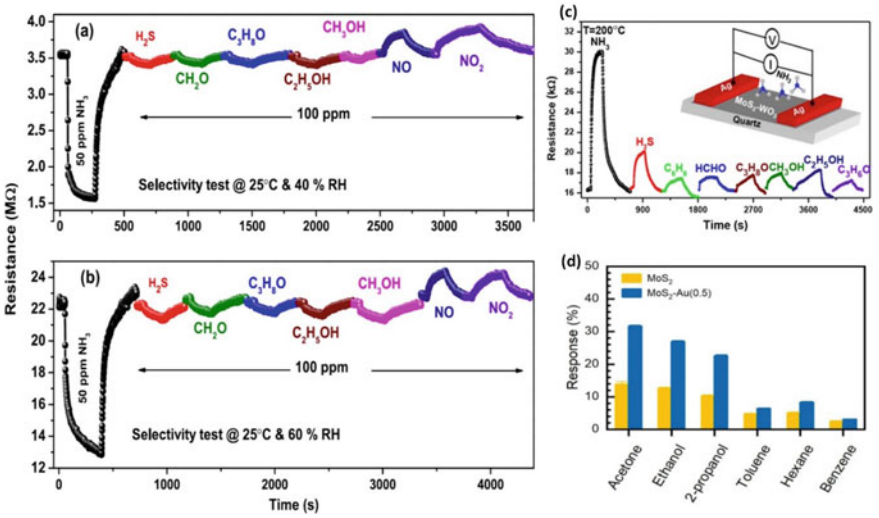


**Fig. 1** Selectivity behavior of the $MoS_2/MoO_3$ sensor toward $NH_3$ and other analytes at room temperature and **a** RH = 40% and **b** RH = 60%. Reprinted with permission from [37] Copyright 2021 American Chemical Society. **c** Selective response of the $MoS_2/WO_3$ composite-based sensor toward $NH_3$ (50 ppm) at 200 °C compared to other reducing gases (100 ppm). Reprinted with permission from [38] Copyright 2021 American Chemical Society. **d** Corresponding response bar chart showing the selectivity of $MoS_2$ sensors is significantly enhanced by the adequate decoration of AuNPs. Reprinted with permission from [40] Copyright 2019 American Chemical Society

heterojunction which formed a depletion layer at the interface through the interdiffusion of the majority carriers. The width of the depletion layer reduces on exposure to $NH_3$ where the oxygen ions interacted with the adsorbed gas molecules releasing the trapped electron back to the conduction band, thus reflected an increased resistance [38]. Another study reports the incorporation of gold nanoparticles (AuNPs) on 2D $MoS_2$ nanoflakes through simple solution mixing to form $MoS_2$-Au hybrid electrochemical sensor for detection of VOCs including acetone, ethanol, and 2-propanol at room temperature. Results indicated that the developed sensor was highly sensitive to oxygen-containing VOCs delivering an improved response (131%), particularly for acetone as compared to bare $MoS_2$ (Fig. 1d). The proposed mechanism suggested that its due to the electro-donating effect of AuNPs that caused an increase in electron density on the $MoS_2$-Au channel. On exposure to a high concentration of oxygen species, the channel traps more electrons and increased the adsorption energy of oxygen ions which in turn makes Au-decorated $MoS_2$ more responsive and selective toward oxygen-containing VOCs [40]. These studies indicate that among transition metal compounds $MoS_2$-based sensors are promising in electrochemical sensing of toxic gases.

### 4.1.2 Detection of Water Pollutants

TMDs exhibit a strong binding affinity toward heavy metals due to their numerous intrinsic chalcogen atoms. Many studies have been carried out to detect the heavy metal ions (HMIs) using 2D TMDs nanocomposites-based electrochemical sensors. The detection relies heavily on electrode modification materials that can enhance sensor sensitivity. For instance, a sensitive and anti-interference electrochemical sensing interface based on flower-like $MoS_2$/rGO composite modified GCE ($MoS_2$/rGO-GCE) was developed to detect Pb(II) using square wave anodic stripping voltammetry (SWASV). A low detection limit (LOD) of 0.005 μM and high sensitivity of 50.80 μA $\mu M^{-1}$ evince the excellent Pb(II) detecting performance of the $MoS_2$/rGO-GCE sensor. This is due to the superb adsorption capacity and electrical conductivity of the $MoS_2$/rGO nanocomposite where the redox reaction of Pb(II) occurs directly on the surface (Fig. 2a) [41]. In another study, quantum dots (QD)-functionalized $MoS_2$-composite and DNA/gold nanoparticles/glucose oxidase ($DNA_2$–AuNP–GOD) conjugates were prepared and immobilized onto the GCE surface, constructing a novel electrochemiluminescence (ECL) biosensor for detecting Hg(II) ions in water samples. Under optimized experimental conditions, the ECL biosensor demonstrated a linearity range between $1.0 \times 10^{-12}$ and $1.0 \times 10^{-6}$ M

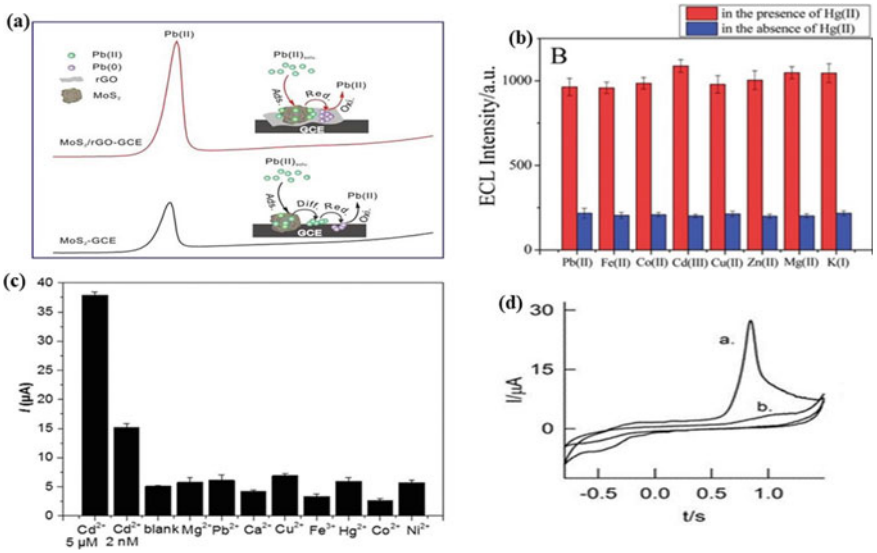


**Fig. 2** **a** Redox reaction of Pb(II) on the surface of $MoS_2$/rGO nanocomposite sensor. Reprinted with permission from [41] Copyright 2019 Elsevier B.V. **b** The effects of different species on the ECL intensity of Hg(II) at the biosensor. Reprinted with permission from [42] Copyright 2019 RSC. **c** Selectivity investigation of the proposed sensor for Cd(II) detection. Reprinted with permission from [43] Copyright 2018 Elsevier B.V. **d** CV of $MoSe_2$-$MoO_3$ modified GCE (curve a) and GCE (curve b) in 50 μM $NO_2^-$ containing 0.1 M pH 4.75 acetate buffer at a scan rate of 50 $mVs^{-1}$. Reprinted with permission from [44] Copyright 2019 Wiley Analytical Science

with LOD of $1.0 \times 10^{-13}$ M of Hg(II) ions. The detection mechanism involved the glucose oxidation that was marked by the production of $H_2O_2$ which in turn enhanced the ECL property of QDs and facilitated signal amplification selectively for Hg(II). The experimental results (Fig. 2b) suggested that the ECL biosensor possessed good stability and selectivity for Hg(II) compared to other heavy metals [42]. Yet another study reported the surface functionalization of $MoS_2$ in N, N-dimethyl formamide (DMF) using sonication to construct an electrochemical sensor for Cd(II) detection. The sensor showed a LOD of 0.2 nM and a linear range from 2 nM to 20 μM under optimized conditions. The strong binding energy between Cd(II) and oxygen donor atom of DMF-functionalized $MoS_2$ contributes to higher sensitivity and selectivity toward Cd(II) as compared to other analytes, as shown in Fig. 2c [43]. A recent study reported the single-step hydrothermal preparation of $MoSe_2/MoO_3$ heterostructure to design a highly sensitive electrochemical sensor for amperometric detection of nitrite in real water samples collected from industrial areas. The sensor displayed high electrocatalytic activity as revealed with CV curves (Fig. 2d). It showed a well-defined oxidation peak for $MoSe_2$-$MoO_3$ modified GCE (curve a), due to conversion of $NO_2^-$ to $NO_3^-$, in contrast to bare GCE (curve b). Under optimal amperometric i-t conditions, the sensor demonstrated good stability, reproducibility (<3 s), high sensitivity (10.84 A $M^{-1}$ $cm^{-2}$), and LOD (0.1 μM) in a linear range of 2.5–80 μM for nitrite with negligible effect toward the interfering ions that coexist in water bodies. The high surface area from 1T phase $MoSe_2$ and α phase $MoO_3$ accredited the superior performance of the sensor [44].

## *4.2 MXenes-Based Sensors*

Bestowed with rich surface functional groups, high conductivity, tunable bandgap, large aspect ratio, good hydrophilicity, and mechanical flexibility, MXenes are widely under consideration to design electrochemical sensors for the detection of environmental contaminants including toxic gases, VOCs, HMIs, and other inorganic or organic contaminants [32, 45–48].

### 4.2.1 Detection of Toxic Gases

Few studies related to MXenes and their composites have been reported for electrochemical detection of toxic gases and VOCs. Recently, an integrated self-powered electrochemical sensory system based on MXene($V_2C$)/PANI composite was developed for $NH_3$ detection (Fig. 3a). The sensor displayed an astonishing sensing response (14.9%), good stability, and fast response time (9 s) toward $NH_3$ at 1 ppm concentration. The suggested mechanism is related to the creation of a depletion region due to p-n heterojunctions interactions that widen when the $NH_3$ molecules adsorbed on the N–H group of PANI and thus amplified the resistance signals [49]. Yet another study reported a wearable sensor based on MXene/polyurethane (PU)

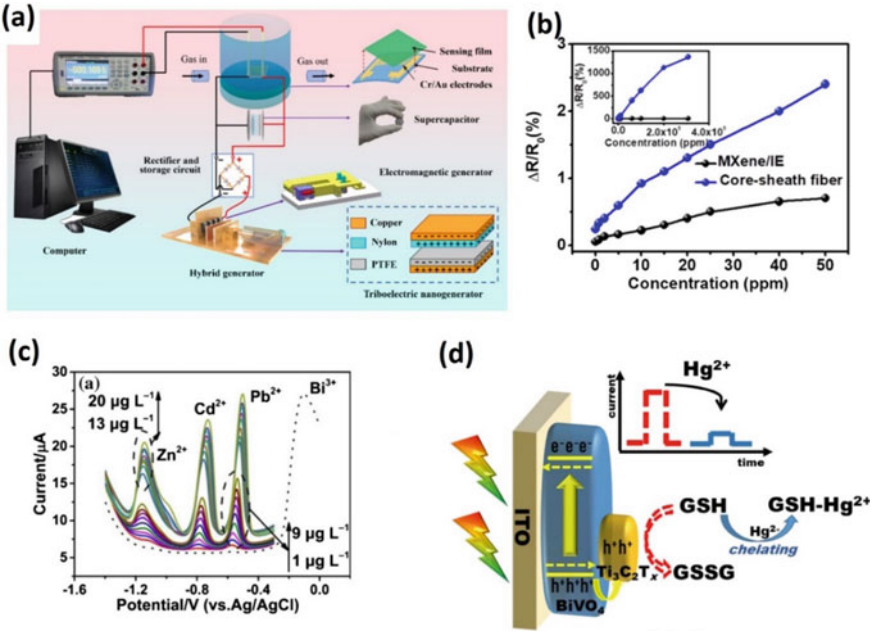


**Fig. 3** **a** Schematic of the PANI/MXene gas sensor driven by self-powered device for $NH_3$ sensing in an ultra-low concentration. Reprinted with permission from [49] Copyright 2021 Elsevier B.V. **b** Sensing response of MXene/PU core–sheath fiber under different concentrations of acetone in contrast to MXene/IE sensor. Reprinted with permission from [50] Copyright 2021 Elsevier B.V. **c** SWASV analysis for simultaneous detection of Pb(II), Cd(II), and Zn(II) in wide detection range. Reprinted with permission from [52] Copyright 2019 Springer. **d** A photoelectrochemical sensing platform based on the Schottky heterojunction between 2D $Ti_3C_2T_x$ MXene and $BiVO_4$ was constructed for sensitive determination of Hg(II). Reprinted with permission from [54] Copyright 2020 Elsevier B.V

core–sheath fibers that were prepared by spray coating of MXenes over PU fibers for the detection of VOCs using the amperometry method. As seen in Fig. 3b, the MXenes/PU core–sheath fibers-based sensor showed high sensitivity toward acetone (down to 50 ppm) across a wide sensing range (up to saturated vapor) and high signal-to-noise ratio, contrary to the MXene/IDE-based sensor. It is believed that the swelling-induced stretching of MXenes due to acetone interaction with PU and the simultaneous charge transfer due to acetone adsorption onto MXene through H-bonding synergistically contributed to change in resistance and lead to high sensitivity response toward acetone [50]. Another study proposed a virtual sensor array (VSA) fabricated by depositing a thin film of MXene ($Ti_3C_2T_x$) over IDE for precise and selective detection of VOCs using the electrochemical impedance method. VSA exhibited a unique fingerprint for each VOC and showed a selective response toward ethanol. The possible detection mechanism involved the interaction of VOCs with surface functional groups/defects of MXenes that increased the interlayer spacing,

thereby resulted in a change in impedance with a highly sensitive response toward ethanol [51].

### 4.2.2 Detection of Water Pollutants

MXenes nanocomposites have also been employed for the detection of varied water pollutants. For instance, a study reported a microgrid electrochemical sensor based on MXene-bismuth nanocomposite for the simultaneous detection of HMIs using SWASV. The Bi(III) were accumulated on delaminated $Ti_3C_2$ surface through electrostatic attraction, and subsequently, ultrasmall bismuth nanorods were in-situ grown at hybridization matrix which was then integrated to microgrid assembly via mechanical milling. The microgrid sensor exhibited high sensitivities for Pb(II), Cd(II), and Zn(II) with LOD of 0.2, 0.4, and 0.5 $\mu g\ L^{-1}$, respectively, in a linear range from 1 to 20 $\mu g\ L^{-1}$ under optimum conditions (Fig. 3c). The uniformly dispersed Bi nanorods and the microgrid structure facilitated the hemispherical diffusion and improved the cathodic accumulation of HMIs, thereby enhanced the sensing performance [52]. Similar studies were reported for the quantification of Pb(II) and Cd(II) ions in water using MXene-Bi nanocomposite sensor. At optimized conditions, as-prepared nano-sensor simultaneously detected Pb(II) and Cd(II) with LOD of 10.8 nM and 12.4 nM, respectively, using SWASV. The excellent sensing properties toward model pollutants are due to high surface area and quick transfer of electrons [53]. Another study reported the designing of an integrated photoelectrochemical (PEC) sensor using $BiVO_4/Ti_3C_2T_x$ composite for the selective detection of Hg(II) ions from the water (Fig. 3d). Coating of $BiVO_4$ over $Ti_3C_2T_x$ facilitated the charge transfer of the photo-generated carriers and abated the charge recombination. The photocurrent was boosted along with the addition of a hole scavenger (reduced glutathione-GSH). However, the chelation of GSH with Hg(II) considerably decreased the photocurrent by retaining the photo-generated holes. Consequently, the sensor displayed a high sensing and selective response toward Hg(II) with LOD of 1 pM in a linear range from 1 pM to 2 nM. Moreover, the PEC sensor also showed acceptable accuracy and repeatability in real sample water [54]. Besides HMIs, MXenes were also investigated for several other inorganic/organic contaminants. For instance, a $Nafion/Ti_3C_2T_x$ modified GCE displayed excellent selective electrocatalytic reduction capacity toward bromate ($BrO_3^-$) ions in drinking water among other interfering ions with LOD of 41 nM using DPV [55]. Next, an Au-carbon quantum dots immobilized MXene nanocomposite (Au@CQDs-MXene)-based electrochemical sensor was developed to detect nitrite ions in water. At optimized conditions, the sensor displayed with LOD of 0.078 μM in linear detection range from 1 to 3200 μM [56]. In another study, $Pt@Ti_3C_2T_x$ was employed for electrocatalytic reduction and detection of Bisphenol A using DPV which showed a fast response with LOD of 32 nM and good stability [57].

## *4.3 Metal–Organic Frameworks-Based Sensors*

Metal–organic frameworks (MOFs) are porous coordination polymers (CPs) that are constructed by the metal-based inorganic linkage and organic ligands bonded through a chemical bond. In recent years, 2D MOFs have been extensively studied as a promising material to fabricate electrochemical sensors for the removal of environmental contaminants, due to their notable properties such as high surface area, porosity, excellent electrochemical activity, and controllable structure [16, 23, 25, 58–62].

### 4.3.1 Detection of Toxic Gases

The potential of MOFs and their composites have been explored for electrochemical detection of gases and VOCs. For instance, a capacitive sensor was fabricated by growing a thin film of Cu-BTC (MOF-199) on a Cu substrate to quantify VOCs. It displayed the high selectivity and sensitivity toward ethanol and methanol vapors with LOD of 130.0 ppm and 39.1 ppm, respectively [63]. Recently, polyaniline (PANI)-cobalt zeolitic benzimidazolate MOF composite has been synthesized by chemical oxidative polymerization for electrochemical sensing of $H_2$ gas. The electrocatalytic capability of the PANI-MOF sensing composite was tested with hydrogen evolution reaction using chronoamperometry. It exhibited higher sensing efficiency, and a high catalytic rate constant with fast response time accredited to increased electron density at the interface [64]. In a recent study, a new electrochemical sensory material based on a ternary composite of silica-coated-CuBTC MOF-PAN-graphene was proposed for the detection of $NH_3$ gas. It showed high selectivity and sensitivity with LOD for of 0.6 ppm due to synergetic effects of the materials [65]. In another study, a cyclodextrin-based MOF (CDMOF-2) was reported to detect $CO_2$ gas using the impedance method. The reduction in ionic conductivity by 500-folds was observed due to the loss of –OH base ions that help in catalytic deprotonation of the methanolic medium. The sensitivity was affected by the reaction rate related to carboxylation, and it is relatively high at a low concentration of $CO_2$ [66]. Another study reported a Ni-MOF-74 modified IDE sensor for impedimetric detection of $NO_2$ gas. The sensor showed a sharp decline in impedance magnitude within 4 h of exposure to $NO_2$ gas, indicating its superior sensing response [67]. In another report, a novel solid-state electrochemical sensor was developed based on MOF-derived $Co_3V_2O_8$ for the detection of $NO_2$ gas (Fig. 4a). The sensor showed a high sensing response (78.2 mV/decade) toward $NO_2$ in a detection range of 50–500 ppm at 575 °C. It also exhibited long-term stability, reproducibility, and anti-interference ability toward other gases such as $CH_4$, $CO_2$, $O_2$, NO, and CO. The mixed potential mechanism justified the enhanced sensitivity and selectivity of the sensor [68].

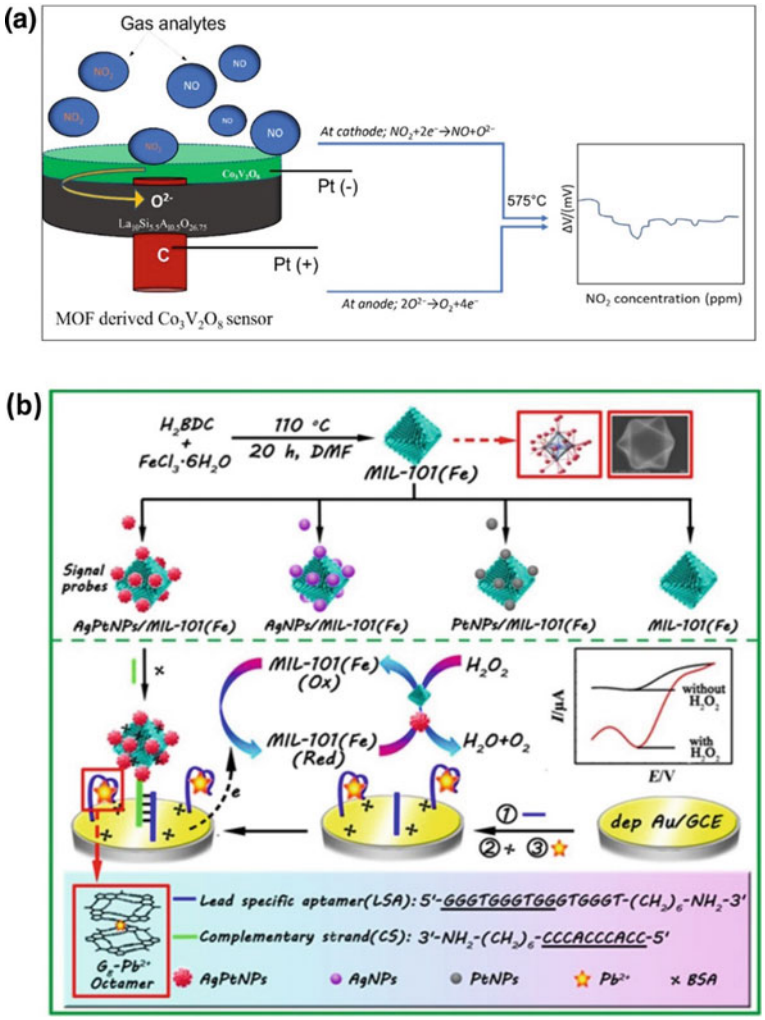


**Fig. 4** **a** Schematic diagram of $NO_2$ detection by $Co_3V_2O_8$ MOF sensor [68]; **b** schematic illustration of the electrochemical aptamer sensor for detection of Pb(II) ion. Reprinted with permission from [69] Copyright 2017 Elsevier B.V

### 4.3.2 Detection of Water Pollutants

Various MOF-nanocomposite-based electrochemical sensors have been developed for the detection of HMIs in water. For instance, a conductive polyaniline (PANI) polymer-UiO-66-$NH_2$ MOF composite (UiO-66-$NH_2$-PANI)-based sensor was fabricated for electrochemical detection of Cd(II) using DPSV. It demonstrated excellent repeatability with a LOD of 0.3 $\mu g\ L^{-1}$. The sensing mechanism was attributed to the fast diffusion of electrons/ions in the matrix due to the chelation between

Cd(II) and the amine groups of composite [70]. In a recent report, interfacial polymerization was adopted to prepare a free-standing polypyrrole-MOF hybrid film for electrochemical detection of Cd(II) using SWASV. It exhibited excellent selectivity and sensitivity with a LOD of 0.29 $\mu g\ L^{-1}$, which is significantly below the standard value for Cd(II) in drinking water [71]. Yet another study reported the fabrication of a lead (Pb)-specific-aptamer (LSA) enzyme-free electrochemical sensor based on AgPtNPs/MIL-101(Fe)-MOF which acted as sensing probes and signal enhancer. The DNA immobilized AgPtNPs/MIL-101(Fe)-MOF exhibited redox activity along with the superior electrocatalytic activity. In the presence of Pb(II) ions, the LSA grabbed the signal through a DNA hybridization reaction and the signal amplified with electrocatalysis of AgPtNPs/MIL-101(Fe) which promoted the electron transfer at the interface (Fig. 4b). In consequence, the sensor anticipated excellent Pb(II) specificity and stability with LOD of 0.032 pM in a wide detection range from 0.1 pM to 100 nM [69]. In another study, a simple solvothermal method was used to prepare Zn-MOF/GO composite modified GCE for electrochemical sensing of As(III) using DPASV. The sensor showed a high response with LOD of 0.06 ppb in the detection range of 0.2–25 ppb ($\mu g\ L^{-1}$) and good reproducibility [72]. Another study reported the preparation of thin-film zirconium-porphyrin MOF (MOF-525) by solvothermal method for amperometric detection of nitrite. The high sensing response with LOD of 2.1 $\mu M$ was due to the electrocatalytic oxidation of nitrite which contributed to fast charge transfer at the sensing surface [73].

## *4.4 Phosphorene and Other 2D Elemental Nanomaterial-Based Sensors*

2D mono-elements (such as phosphorene, arsenene, silicene, etc.) are emerging as outstanding materials for widespread applications [74–76]. Among them, phosphorene (black phosphorus) is gaining significant interest in sensing applications owing to its remarkable characteristics including ultrahigh surface–aspect ratio, anisotropic electric conductance, high electrochemical activity, tunable direct bandgap, and excellent carrier mobility [10, 77–82].

### 4.4.1 Detection of Toxic Gases

An impedimetric sensor based on layered black phosphorus (BP) modified IDE (BP@IDE) was developed for selective quantification of methanol vapor, showing LOD of 28 ppm (Fig. 5a). On exposure to methanol vapor, it exhibited a high impedance response, while the capacitance decreased at the BP@IDE interface, suggesting its superior selectivity and sensitivity [83]. In another study, an electrochemically synthesized platinoid-decorated few-layer phosphorene was employed

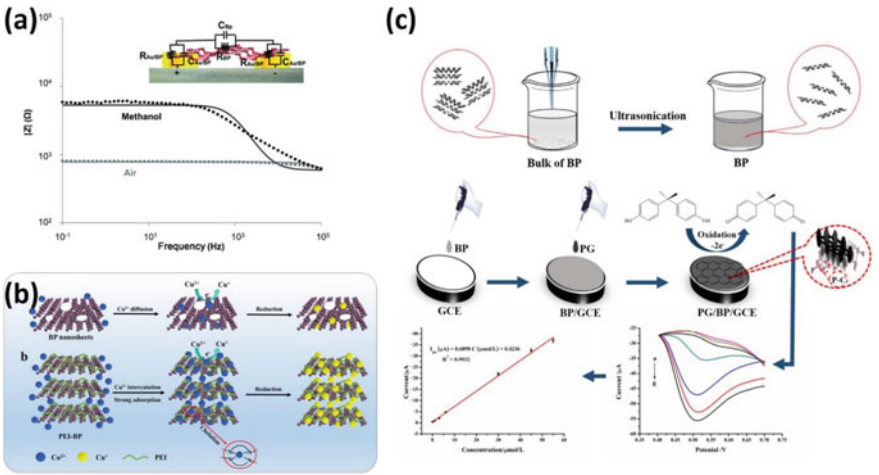


**Fig. 5** **a** Impedance module for layered BP@IDE in the absence (air) and the presence of 1140 ppm methanol vapor (experimental (••••) and simulated (—) data) and equivalent electrical circuit model (inset). Reprinted with permission from [83] Copyright 2015 Wiley. **b** Schematic illustration for sensing mechanism of PEI-BP composite, compared to BP for reduction of Cu(II). Reprinted with permission from [87] Copyright 2019 Elsevier. **c** Schematic illustration of graphene-BP nanocomposite modified GCE fabrication for electrochemical sensing of BPA at different concentrations. Reprinted with permission from [88] Copyright 2019 Elsevier B.V

for the detection of methanol vapor using impedance measurements. The high selectivity and sensitivity were attributed to change in local carrier concentration at electrode due to the adsorption of gas molecules on phosphorene which induced variation in impedance sensing signals [84]. Another study reported the gas sensing properties of exfoliated BP. The BP modified IDE was tested for sensing of oxidizing gases ($NO_2$, $CO_2$) and reducing ($NH_3$, $H_2$, CO) gases using a volt–amperometric method at room temperature. The sensor showed high selectivity and p-type sensitivity toward $NO_2$ and $NH_3$ with LOD of 20 ppb and 10 ppm, respectively. Also, a steady sensing response was recorded for $H_2$; however, no signals were observed for CO and $CO_2$. The mechanism was justified based on the structural morphology of BP and the binding energies of the adsorbed gas molecules [85]. Apart from this, other 2D elemental materials are at the evolutionary stage and very few reports are available on gas sensing applications. One of the recent studies is based on a few-layered arsenene modified IDE sensing interface employed for impedimetric detection of VOCs (methanol, ethanol, chloroform diethyl ether, acetonitrile, tetrahydrofuran, acetone, hexane, dichloromethane). Compared to others, a notable phase shift in resonance frequency was analyzed for methanol, suggesting ultrahigh sensitivity and selectivity [86].

### 4.4.2 Detection of Water Pollutants

Recently, a polyethyleneimine PEI-BP composite was synthesized via the single-step electrostatic adsorption method and deposited over GCE for its application in electrochemical sensing of Cu(II) using amperometry. The sensor achieved a fast response (1.5 s) and high sensitivity with a LOD of 0.02 μM in a wide detection range of 0.25–177 μM, which is much below permissible limits for Cu(II) according to EPA drinking water standards. The superior performance was explained due to the synergistic effect of BP and PEI which enhanced the intercalation and adsorption of Cu(II) (Fig. 5b). PEI acted as an agent to specifically capture Cu(II) for BP and improved its electrochemical reduction while providing stability to BP. The presence of abundant N atoms favored PEI Cu(II)-PEI chelation which increased the reaction sites and eventually resulted in a high reduction current. The sensing efficiency of nanocomposite was also tested in real water samples by fabricating a flexible PEI-BP modified SPE and successfully employing it for selective detection of (II) in river water [87]. In another study, porous graphene functionalized BP nanocomposite (Gr-BP) was prepared for electrochemical detection of bisphenol-A (BPA) in plastic water bottle samples using DPV (Fig. 5c). The sensing involved the diffusion-controlled electrochemical oxidation of BPA, where the trace levels are quantified in a wide detection range of $4 \times 10^{-8} \sim 5 \times 10^{-5}$ mol $L^{-1}$ with LOD of 7.8 $\times 10^{-9}$ mol $L^{-1}$ along with good response time and stability [88]. Further, a recent study reported the fabrication of BP quantum dots doped ZnO modified GCE sensing platform for detection of $H_2O_2$ in tap water samples using amperometry. The high sensitivity of 195.4 μA $mM^{-1}$ cm was delivered by the sensor in linear range from 5 μmol $L^{-1}$ to 0.05 mmol $L^{-1}$ along with excellent response and repeatability [89]. Next, a novel aptamer sensor based on hexamethylenediamine (HA)-coated AuNPs-BP nanocomposite was developed for electrochemical detection of polychlorinated biphenyl (PCB77) in tap water samples using DPV. It exhibited excellent sensitivity of 391.1 μA $cm^{-2}$ and LOD of 33 pg $L^{-1}$ with high reproducible efficiency [90].

## 5 Conclusions

Conclusively, the advancements in electrochemical sensors based on 2D nanomaterials composites (mainly TMDs, MXene, MOF, and phosphorene) have been discussed in the context of their significance toward combating environmental pollution. The fascinating physicochemical properties of 2D nanomaterials, such as unique morphological structure, large specific surface area, tunable bandgap, and good mechanical stability, encouraged lots of research toward designing active sensing platforms for the detection of toxic gases and water pollutants. Several fabrication strategies to achieve superior sensing performance using 2D nanomaterials have been highlighted in this chapter, such as the creation of heterostructure, hybridization with other materials, compositing with polymers, or immobilization with enzymes.

In addition, the fundamental principles in electrochemical detection such as potentiometry, voltammetry, amperometry, and impedance have been briefly described. The chapter has overviewed the research studies from the past decade on developing novel, reliable, efficient 2D nanocomposites-recognition element/sensory systems which act as or are responsible for signal amplification or transduction. The experimental results of detection limit, selectivity, stability, and reproducibility for different 2D nanocomposite-based electrochemical sensing devices toward a diverse range of contaminants, particularly, toxic gases, VOCs, heavy metals, nitrites, etc., have been summarized. It is seen that the progress in the fabrication strategies and integrated device designing has largely advanced the development of 2D nanocomposites-based electrochemical sensors with desired strong interfacial interactions. From the survey, it is ascertained that the inherent 2D basal plane ensures rich-active sites for host–analyte interactions as well as shortens the ion diffusion paths which effectively facilitates the charge transfer processes and consequently enhances the sensing response. Nevertheless, 2D nanocomposites-based electrochemical sensors are still far behind real applications and need tremendous research effort to develop sensing devices for real-time onsite monitoring of air/water contaminants as a future perspective.

## References

1. Gan X, Zhao H (2019) Understanding signal amplification strategies of nanostructured electrochemical sensors for environmental pollutants. Curr Opin Electrochem 17:56–64
2. Ramachandran R, Chen TW, Chen SM, Baskar T, Kannan R, Elumalai P et al (2019) A review of the advanced developments of electrochemical sensors for the detection of toxic and bioactive molecules. Inorg Chem Front 6(12):3418–3439
3. Khanam Z, Gupta S, Verma A (2020) Endophytic fungi-based biosensors for environmental contaminants—a perspective. S Afr J Bot 134:401–406
4. Kanoun O, Lazarević-Pašti T, Pašti I, Nasraoui S, Talbi M, Brahem A et al (2021) A review of nanocomposite-modified electrochemical sensors for water quality monitoring. Sensors 21(12):4131
5. Balasubramani V, Chandraleka S, Rao TS, Sasikumar R, Kuppusamy MR, Sridhar TM (2020) Recent advances in electrochemical impedance spectroscopy based toxic gas sensors using semiconducting metal oxides. J Electrochem Soc 167(3):037572
6. Dhall S, Mehta BR, Tyagi AK, Sood K (2021) A review on environmental gas sensor: materials and technologies. Sens Int 100116
7. Su S, Chen S, Fan C (2018) Recent advances in two-dimensional nanomaterials-based electrochemical sensors for environmental analysis. Green Energy Environ 3(2):97–106
8. Ho CK, Robinson A, Miller DR, Davis MJ (2005) Overview of sensors and needs for environmental monitoring. Sensors 5(1):4–37
9. Meng Z, Stolz RM, Mendecki L, Mirica KA (2019) Electrically-transduced chemical sensors based on two-dimensional nanomaterials. Chem Rev 119(1):478–598
10. Tyagi D, Wang H, Huang W, Hu L, Tang Y, Guo Z et al (2020) Recent advances in two-dimensional-material-based sensing technology toward health and environmental monitoring applications. Nanoscale 12(6):3535–3559
11. Su S, Chao J, Pan D, Wang L, Fan C (2015) Electrochemical sensors using two-dimensional layered nanomaterials. Electroanalysis 27(5):1062–1072
12. Lee CW, Suh JM, Jang HW (2019) Chemical sensors based on two-dimensional (2D) materials for selective detection of ions and molecules in liquid. Front Chem 7:708

13. Zeng M, Chen M, Huang D, Lei S, Zhang X, Wang L, Cheng Z (2020) Engineered two-dimensional nanomaterials: an emerging paradigm for water purification and monitoring. Mater Horiz
14. Tan C, Cao X, Wu XJ, He Q, Yang J, Zhang X et al (2017) Recent advances in ultrathin two-dimensional nanomaterials. Chem Rev 117(9):6225–6331
15. Gan X, Zhao H, Schirhagl R, Quan X (2018) Two-dimensional nanomaterial-based sensors for heavy metal ions. Microchim Acta 185(10):1–30
16. Mashao G, Modibane KD, Mdluli SB, Iwuoha EI, Hato MJ, Makgopa K, Molapo KM (2019) Polyaniline-cobalt benzimidazolate zeolitic metal-organic framework composite material for electrochemical hydrogen gas sensing. Electrocatalysis 10(4):406–419
17. Fethi A (2020) Novel materials for electrochemical sensing platforms. Sens Int 100035
18. Eggins BR (2002) Chemical sensors and biosensors. Wiley, Chichester
19. Wilson JS (2005) Sensor technology handbook. Elsevier, Amsterdam/Boston
20. Grieshaber D, MacKenzie R, Vörös J, Reimhult E (2008) Electrochemical biosensors—sensor principles and architectures. Sensors 8:1400–1458
21. Xiong L, Compton RG (2014) Amperometric gas detection: a review. Int J Electrochem Sci 9(12):7152–7181
22. Suni II (2008) Impedance methods for electrochemical sensors using nanomaterials. TrAC Trends Anal Chem 27(7):604–611
23. Liu CS, Li J, Pang H (2020) Metal-organic framework-based materials as an emerging platform for advanced electrochemical sensing. Coord Chem Rev 410:213222
24. Liu F, Chu X, Dong Y, Zhang W, Sun W, Shen L (2013) Acetone gas sensors based on graphene-$ZnFe_2O_4$ composite prepared by solvothermal method. Sens Actuators B 188:469–474
25. Chuang CH, Kung CW (2020) Metal–organic frameworks toward electrochemical sensors: challenges and opportunities. Electroanalysis 32(9):1885–1895
26. Tai H, Duan Z, Wang Y, Wang S, Jiang Y (2020) Paper-based sensors for gas, humidity, and strain detections: a review. ACS Appl Mater Interfaces 12(28):31037–31053. https://doi.org/10.1021/acsami.0c06435
27. Ikram M, Lv H, Liu Z, Khan M, Liu L, Raziq F et al (2020) Rational design of $MoS_2/C_3N_4$ hybrid aerogel with abundant exposed edges for highly sensitive $NO_2$ detection at room temperature. Chem Mater 32(17):7215–7225. https://doi.org/10.1021/acs.chemmater.0c01468
28. Khanam Z, Singh V (2014) Groundwater quality assessment near polluted canal area in Kichha town, Uttarakhand, India. Int J Recent Sci Res 5(2):362–368
29. Khanam Z, Singh V (2012) Groundwater pollution: a threat to the last hope on the blue planet. In: Singh V et al (eds) Climate change and hydrosphere. Biotech Books, pp 59–72. ISBN 9788176222570
30. Khanam Z, Singh V (2014) Nanotechnology for remediation of contaminated groundwater. In: Singh V et al (eds) Environment, agriculture and sustainable development. S.K. Book Agency, pp 192–205. ISBN 9789383158171
31. Khanam Z, Singh V, Zaidi MGH (2016) Recent trends in nanocomposites towards sustainable environment. In: Trivedi PC (ed) Bio-exploitation for sustainable agriculture. Avishkar Publishers, Distributors, pp 107–145. ISBN 9788179105399
32. Wu X, Ma P, Sun Y, Du F, Song D, Xu G (2021) Application of MXene in electrochemical sensors: a review. Electroanalysis
33. Li BL, Wang J, Zou HL, Garaj S, Lim CT, Xie J et al (2016) Low-dimensional transition metal dichalcogenide nanostructures based sensors. Adv Funct Mater 26(39):7034–7056
34. Sinha A, Tan B, Huang Y, Zhao H, Dang X, Chen J, Jain R (2018) $MoS_2$ nanostructures for electrochemical sensing of multidisciplinary targets: a review. TrAC Trends Anal Chem 102:75–90
35. Jiang F, Zhao WS, Zhang J (2020) Mini-review: recent progress in the development of $MoSe_2$ based chemical sensors and biosensors. Microelectron Eng 225:111279
36. Ping J, Fan Z, Sindoro M, Ying Y, Zhang H (2017) Recent advances in sensing applications of two-dimensional transition metal dichalcogenide nanosheets and their composites. Adv Funct Mater 27(19):1605817

37. Singh S, Deb J, Sarkar U, Sharma S (2021) $MoS_2/MoO_3$ nanocomposite for selective $NH_3$ detection in a humid environment. ACS Sustain Chem Eng 9:7328–7340. https://doi.org/10.1021/ACSSUSCHEMENG.1C01527
38. Singh S, Deb J, Sarkar U, Sharma S (2021) $MoS_2/WO_3$ nanosheets for detection of ammonia. ACS Appl Nano Mater 4:2594–2605. https://doi.org/10.1021/ACSANM.0C03239
39. Mayorga-Martinez CC, Ambrosi A, Eng AYS, Sofer Z, Pumera M (2015) Metallic 1T-$WS_2$ for selective impedimetric vapor sensing. Adv Funct Mater 25(35):5611–5616. https://doi.org/10.1002/adfm.201502223
40. Chen WY, Yen C-C, Xue S, Wang H, Stanciu LA (2019) Surface functionalization of layered molybdenum disulfide for the selective detection of volatile organic compounds at room temperature. ACS Appl Mater Interfaces 11:34135–34143. https://doi.org/10.1021/ACSAMI.9B13827
41. Sun YF, Sun JH, Wang J, Pi ZX, Wang LC, Yang M, Huang XJ (2019) Sensitive and anti-interference stripping voltammetry analysis of Pb(II) in water using flower-like $MoS_2$/rGO composite with ultra-thin nanosheets. Anal Chim Acta 1063:64–74. https://doi.org/10.1016/J.ACA.2019.03.008
42. He Z-J, Kang T-F, Lu L-P, Cheng S-Y (2020) An electrochemiluminescence sensor based on CdSe@CdS-functionalized $MoS_2$ and a GOD-labeled DNA probe for the sensitive detection of Hg(II). Anal Methods 12:491–498. https://doi.org/10.1039/C9AY02524C
43. Gan X, Zhao H, Wong KY, Lei DY, Zhang Y, Quan X (2018) Covalent functionalization of $MoS_2$ nanosheets synthesized by liquid phase exfoliation to construct electrochemical sensors for Cd(II) detection. Talanta 182:38–48. https://doi.org/10.1016/J.TALANTA.2018.01.059
44. Vishnu N, Badhulika S (2019) Single step synthesis of $MoSe_2$–$MoO_3$ heterostructure for highly sensitive amperometric detection of nitrite in water samples of industrial areas. Electroanalysis 31:2410–2416. https://doi.org/10.1002/ELAN.201900310
45. Gui JC, Han L, Cao WY (2021) Lamellar MXene: a novel 2D nanomaterial for electrochemical sensors. J Appl Electrochem 1–14
46. Qin R, Shan G, Hu M, Huang W (2021) Two-dimensional transition metal carbides and/or nitrides (MXenes) and their applications in sensors. Mater Today Phys 100527
47. Sinha A, Zhao H, Huang Y, Lu X, Chen J, Jain R (2018) MXene: an emerging material for sensing and biosensing. TrAC Trends Anal Chem 105:424–435
48. Pei Y, Zhang X, Hui Z, Zhou J, Huang X, Sun G, Huang W (2021) $Ti_3C_2T_x$ MXene for sensing applications: recent progress, design principles, and future perspectives. ACS Nano 15(3):3996–4017
49. Wang X, Zhang D, Zhang H, Gong L, Yang Y, Zhao W, Yu S, Yin Y, Sun D (2021) In situ polymerized polyaniline/MXene ($V_2C$) as building blocks of supercapacitor and ammonia sensor self-powered by electromagnetic-triboelectric hybrid generator. Nano Energy 88:106242. https://doi.org/10.1016/J.NANOEN.2021.106242
50. Tang Y, Xu Y, Yang J, Song Y, Yin F, Yuan W (2021) Stretchable and wearable conductometric VOC sensors based on microstructured MXene/polyurethane core-sheath fibers. Sens Actuators B Chem 346:130500
51. Li D, Liu G, Zhang Q, Qu M, Fu YQ, Liu Q, Xie J (2021) Virtual sensor array based on MXene for selective detections of VOCs. Sens Actuators B Chem 331:129414
52. Zhu X, Liu B, Li L, Wu L, Chen S, Huang L, Yang J et al (2019) A micromilled microgrid sensor with delaminated MXene-bismuth nanocomposite assembly for simultaneous electrochemical detection of lead(II), cadmium(II) and zinc(II). Microchim Acta 186(12):186, 1–7. https://doi.org/10.1007/S00604-019-3837-3
53. He Y, Ma L, Zhou L, Liu G, Jiang Y, Gao J (2020) Preparation and application of bismuth/MXene nano-composite as electrochemical sensor for heavy metal ions detection. Nanomaterials 10:866. https://doi.org/10.3390/NANO10050866
54. Jiang Q, Wang H, Wei X, Wu Y, Gu W, Hu L, Zhu C (2020) Efficient $BiVO_4$ photoanode decorated with $Ti_3C_2T_x$ MXene for enhanced photoelectrochemical sensing of Hg(II) ion. Anal Chim Acta 1119:11–17. https://doi.org/10.1016/J.ACA.2020.04.049

55. Rasheed PA, Pandey RP, Rasool K, Mahmoud KA (2018) Ultra-sensitive electrocatalytic detection of bromate in drinking water based on Nafion/$Ti_3C_2T_x$ (MXene) modified glassy carbon electrode. Sens Actuators B Chem 265:652–659. https://doi.org/10.1016/J.SNB.2018.03.103
56. Feng X, Han G, Cai J, Wang X (2022) Au@Carbon quantum Dots-MXene nanocomposite as an electrochemical sensor for sensitive detection of nitrite. J Colloid Interface Sci 607:1313–1322. https://doi.org/10.1016/J.JCIS.2021.09.036
57. Rasheed PA, Pandey RP, Jabbar KA, Mahmoud KA (2021) Platinum nanoparticles/$Ti_3C_2T_x$ (MXene) composite for the effectual electrochemical sensing of bisphenol A in aqueous media. J Electroanal Chem 880:114934. https://doi.org/10.1016/J.JELECHEM.2020.114934
58. Liu L, Zhou Y, Liu S, Xu M (2018) The applications of metal-organic frameworks in electrochemical sensors. ChemElectroChem 5(1):6–19
59. Ahmad S, Ansari A, Siddiqi WA, Akram MK (2019) Nanoporous metal-organic-framework. In: Metal-organic framework composites II. Materials Research Foundation LLC, vol 58, pp 107–139. https://doi.org/10.21741/9781644900437-6
60. Ma T, Li H, Ma JG, Cheng P (2020) Application of MOF-based materials in electrochemical sensing. Dalton Trans 49(47):17121–17129
61. Gonçalves JM, Rocha DP, Silva MNT, Martins PR, Nossol E, Angnes L, Rout CS, Munoz RAA (2021) Feasible strategies to promote the sensing performances of spinel $MCo_2O_4$ (M = Ni, Fe, Mn, Cu and Zn) based electrochemical sensors: a review. J Mater Chem C 9:7852–7887. https://doi.org/10.1039/d1tc01550h
62. Gonçalves JM, Martins PR, Rocha DP, Matias TA, Julião MS, Munoz RA, Angnes L (2021) Recent trends and perspectives in electrochemical sensors based on MOF-derived materials. J Mater Chem C 9(28):8718–8745
63. Hosseini MS, Zeinali S, Sheikhi MH (2016) Fabrication of capacitive sensor based on Cu-BTC (MOF-199) nanoporous film for detection of ethanol and methanol vapors. Sens Actuators B Chem 230:9–16
64. Mashao G, Modibane KD, Mdluli SB, Iwuoha EI, Hato MJ, Makgopa K, Molapo KM (2019) Polyaniline-cobalt benzimidazolate zeolitic metal-organic framework composite material for electrochemical hydrogen gas sensing. Electrocatalysis 10:406–419. https://doi.org/10.1007/s12678-019-00529-2
65. Bhardwaj SK, Mohanta GC, Sharma AL, Kim KH, Deep A (2018) A three-phase copper MOF-graphene-polyaniline composite for effective sensing of ammonia. Anal Chim Acta 1043:89–97. https://doi.org/10.1016/j.aca.2018.09.003
66. Gassensmith JJ, Kim JY, Holcroft JM, Farha OK, Stoddart JF, Hupp JT, Jeong NC (2014) A metal–organic framework-based material for electrochemical sensing of carbon dioxide. J Am Chem Soc 136:8277–8282. https://doi.org/10.1021/ja5006465
67. Henkelis SE, Percival SJ, Small LJ, Rademacher DX, Nenoff TM (2021) Continuous MOF membrane-based sensors via functionalization of interdigitated electrodes. Membranes 11(3):176
68. Li C, Meng W, Xu X, Zhuang X, Wen Y, Wang L, He Z, Dai L (2020) High performance solid electrolyte-based $NO_2$ sensor based on $Co_3V_2O_8$ derived from metal-organic framework. Sens Actuators B Chem 302:127173. https://doi.org/10.1016/j.snb.2019.127173
69. Xu W, Zhou X, Gao J, Xue S, Zhao J (2017) Label-free and enzyme-free strategy for sensitive electrochemical lead aptasensor by using metal-organic frameworks loaded with AgPt nanoparticles as signal probes and electrocatalytic enhancers. Electrochim Acta 251:25–31. https://doi.org/10.1016/j.electacta.2017.08.046
70. Wang Y, Wang L, Huang W, Zhang T, Hu X, Perman JA, Ma S (2017) A metal–organic framework and conducting polymer based electrochemical sensor for high performance cadmium ion detection. J Mater Chem A 5(18):8385–8393. https://doi.org/10.1039/C7TA01066D
71. Li Y, Cai Y, Shao K, Chen Y, Wang D (2021) A free-standing poly-MOF film fabricated by post-modification and interfacial polymerization: a novel platform for $Cd^{2+}$ electrochemical sensors. Microporous Mesoporous Mater 111200
72. Baghayeri M, Ghanei-Motlagh M, Tayebee R, Fayazi M, Narenji F (2020) Application of graphene/zinc-based metal-organic framework nanocomposite for electrochemical sensing of As(III) in water resources. Anal Chim Acta 1099. https://doi.org/10.1016/j.aca.2019.11.045

73. Kung CW, Chang TH, Chou LY, Hupp JT, Farha OK, Ho KC (2015) Porphyrin-based metal-organic framework thin films for electrochemical nitrite detection. Electrochem Commun 58:51–56. https://doi.org/10.1016/j.elecom.2015.06.003
74. Kong X, Liu Q, Zhang C, Peng Z, Chen Q (2017) Elemental two-dimensional nanosheets beyond graphene. Chem Soc Rev 46(8):2127–2157
75. Nasir MZM, Pumera M (2019) Emerging mono-elemental 2D nanomaterials for electrochemical sensing applications: from borophene to bismuthene. TrAC Trends Anal Chem 121:115696
76. Glavin NR, Rao R, Varshney V, Bianco E, Apte A, Roy A et al (2020) Emerging applications of elemental 2D materials. Adv Mater 32(7):1904302
77. Tapia MA, Gusmão R, Serrano N, Sofer Z, Ariño C, Díaz-Cruz JM et al (2021) Phosphorene and other layered pnictogens as a new source of 2D materials for electrochemical sensors. TrAC Trends Anal Chem 139. https://doi.org/10.1016/j.trac.2021.116249
78. Yang A, Wang D, Wang X, Zhang D, Koratkar N, Rong M (2018) Recent advances in phosphorene as a sensing material. Nano Today 20:13–32
79. Donarelli M, Ottaviano L (2018) 2D materials for gas sensing applications: a review on graphene oxide, $MoS_2$, $WS_2$ and phosphorene. Sensors 18(11):3638
80. Wang L, Sofer Z, Pumera M (2015) Voltammetry of layered black phosphorus: electrochemistry of multilayer phosphorene. ChemElectroChem 2(3):324–327
81. Li Q, Wu JT, Liu Y, Qi XM, Jin HG, Yang C et al (2021) Recent advances in black phosphorus-based electrochemical sensors: a review. Anal Chim Acta 338480
82. Irshad R, Tahir K, Li B, Sher Z, Ali J, Nazir S (2018) A revival of 2D materials, phosphorene: its application as sensors. J Ind Eng Chem 64:60–69
83. Mayorga-Martinez CC, Sofer Z, Pumera M (2015) Layered black phosphorus as a selective vapor sensor. Angew Chem Int Ed 54(48):14317–14320
84. Kovalska E, Luxa J, Melle-Franco M, Wu B, Marek I, Roy PK et al (2020) Single-step synthesis of platinoid-decorated phosphorene: perspectives for catalysis, gas sensing, and energy storage. ACS Appl Mater Interfaces 12(45):50516–50526
85. Donarelli M, Ottaviano L, Giancaterini L, Fioravanti G, Perrozzi F, Cantalini C (2016) Exfoliated black phosphorus gas sensing properties at room temperature. 2D Mater 3(2):025002
86. Beladi-Mousavi SM, Pourrahimi AM, Sofer Z, Pumera M (2019) Atomically thin 2D-arsenene by liquid-phased exfoliation: toward selective vapor sensing. Adv Funct Mater 29(5):1807004
87. Li Y, Shi Z, Zhang C, Wu X, Liu L, Guo C, Li CM (2021) Highly stable branched cationic polymer-functionalized black phosphorus electrochemical sensor for fast and direct ultratrace detection of copper ion. J Colloid Interface Sci
88. Cai J, Sun B, Li W, Gou X, Gou Y, Li D, Hu F (2019) Novel nanomaterial of porous graphene functionalized black phosphorus as electrochemical sensor platform for bisphenol A detection. J Electroanal Chem 835:1–9. https://doi.org/10.1016/j.jelechem.2019.01.003
89. Ding H, Zhang L, Tang Z, Dong Y, Chu X (2018) Black phosphorus quantum dots doped ZnO nanoparticles as efficient electrode materials for sensitive hydrogen peroxide detection. J Electroanal Chem 824:161–168. https://doi.org/10.1016/j.jelechem.2018.07.055
90. Liang S, Wu L, Liu H, Li J, Chen M, Zhang M (2019) Organic molecular passivation of phosphorene: an aptamer-based biosensing platform. Biosens Bioelectron 126:30–35. https://doi.org/10.1016/j.bios.2018.10.037

# Chapter 8
# Trending 2D Nanomaterial Composites in Detection and Sensing of Biological Contaminants


**Jayanta Sarmah Boruah, Sristi Majumdar, Ankita Deb, Jahnabi Gogoi, and Devasish Chowdhury**

## 1 Introduction

Nanomaterials are small-sized materials that typically have at least one dimension ranging from sub-nanometers to hundred nanometers. The materials in nanometer-scale differ in their physical and chemical properties significantly from those of bulk counterparts of the same composition due to an increase in surface area, tunable mechanical, electrical, and optical phenomena. With the evolution of facile, low-cost, efficient, and innovative synthetic protocols for the synthesis of nanomaterial and advanced characterization techniques, nanomaterials in diverse applications have attracted immense attention among the scientific community. As such, the range of applications of nanomaterials has broadened to biomedical, electronics, chemical processes, building materials, catalysis, etc. Particle size is an important aspect of nanomaterials, and with the difference in sizes, the properties and the function of the nanomaterials also vary. In 2D nanomaterials, the electron confinement is restricted to only one dimension resulting in a quantum well or plane. Ever since the first isolation

All the Authors contributed equally.

J. S. Boruah · S. Majumdar · A. Deb · J. Gogoi · D. Chowdhury (✉)
Material Nanochemistry Laboratory, Physical Sciences Division, Institute of Advanced Study in Science and Technology, Paschim Boragaon, Garchuk, Guwahati 781035, India
e-mail: devasish@iasst.gov.in

J. S. Boruah
e-mail: chem.jayanta2013@gmail.com

S. Majumdar
e-mail: me.sristi18@gmail.com

A. Deb
e-mail: anksdb26@gmail.com

J. Gogoi
e-mail: gjahnabi@gmail.com



Z. Khanam et al. (eds.), *2D Nanomaterials for Energy and Environmental Sustainability*, Materials Horizons: From Nature to Nanomaterials,
https://doi.org/10.1007/978-981-16-8538-5_8

of graphene in 2004 [1], an increasing addition into the library of 2D nanomaterials has been observed, which includes materials such as transition metal dichalcogenides (TMDs) [2], hexagonal boron nitride [3], 2D metal oxides/sulfides [4, 5], transition metal carbides, nitrides, carbonitrides (MXenes) [6–8], graphitic carbon nitride [9], black phosphorus [10], layered double hydroxides (LDHs) [11], silicene [12], and so on. The overall types, significant properties, and their use in different areas can be represented in Fig. 1.

2D nanomaterials have a high surface-to-volume ratio compared to other nanomaterials with dense active surface sites in a large area, making them a very suitable material for various biosensing applications. Moreover, through surface functionalization and the introduction of defects, 2D materials can be made as desired for selective and sensitive detection of different analytes [13]. The active surface binding sites in a sensor material increase with the increase in surface area that results in enhanced interaction between the sensor and analyte. This, in turn, contributes to a greater modulation in the electrical properties of the material system, creating a sensitive method with a lowered limit of detection (LOD) [14]. The surface area per gram (SAPG) of a material is the deciding factor for the LOD of a nanomaterial system. Monolayer graphene was reported to have the highest SAPG value of 2630 $m^2/g$ among the nanomaterials [15]. Also, for 2D nanomaterials, as the number

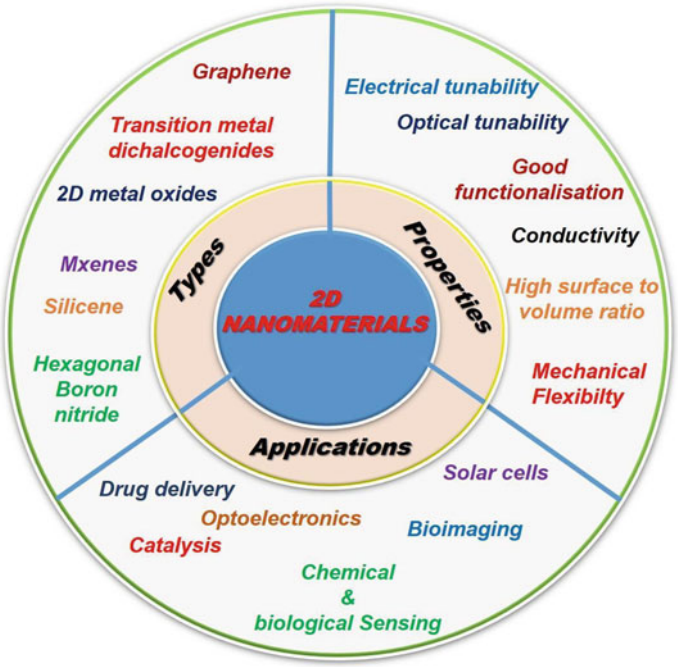


**Fig. 1** A representative view depicting the types, properties, and various applications of 2D nanomaterials. *Source* "Author"

of layers decreases, the SAPG value increases while going from bulk to a few layers [16]. Therefore, 2D nanomaterials are proven to be an excellent candidate for sensing and identification of wide-ranged chemical as well as biological analytes.

Biological contaminants are a category of toxins including bacteria, viruses, fungus, protozoa, and insects that can cause serious health hazards and environmental issues by affecting food, air, water, and soil. These contaminants cause various diseases like molds and pollens that can cause allergies to significant human populations. It is noted that foodborne illness is primarily driven by contaminants like pathogenic microorganisms. Aflatoxins, one of the cancer-causing mycotoxins (fungal toxins), are related to agricultural grain contamination leading to serious fatalities. These molecules can be devastating when they get into the body of other organisms [17]. The degradation of air quality due to such biological toxins is also alarming. The growth and spreading of such contaminants are primarily affected by temperature, relative humidity, sources of nutrients, and air motion. Identifying such biological contaminants and their source, which is causing a particular human disease, is very difficult and hence their prevention [18]. Therefore, attempts are being made to detect or sense them by utilizing various external systems made up of organic or inorganic substances. The involvement of nanostructures has demonstrated paramount importance for the detection and sensing of such microscopic toxins. Among them, 2D nanomaterials are considered as superior platforms to perform such critical detections due to their unique physicochemical properties attributed to their ultrathin layers. Some of the 2D nanomaterials mentioned above are directly or indirectly linked with the detection and sensing of biological contaminants. Most of them have also been involved in environmental pollutants sensing (like toxic gases and heavy metals) [19]. Here, in this chapter, we have discussed the use of different 2D nanomaterial and their composites that have been studied and reported for the sensing and detection of different biological contaminants.

## 2 Different Types of Sensors

Typically, as illustrated above, sensors are platforms that can collect a physical, chemical, or biological change, and a measurable signal is used for identification. Basically, it is a material with some affinity for a particular analyte of interest owing to the presence of some binding sites on it. In the case of a biosensor, a biological component is combined with a physicochemical detector to find the presence of different biomolecules like proteins, DNA, aptamer, amino acid, and microbial toxin by the base material showing significant changes like color, conductivity, fluorescence behavior depending on the properties of the target. Biosensors are always associated with an enzyme or an antibody, or even microbial components. On the other hand, chemosensors can detect chemical compounds which are also very much selective to the functionality of those analytes. Nanomaterials and their composites are well known for their capability to work as both biosensors and chemosensors. Sensors can be categorized based on the transducer or the detector element

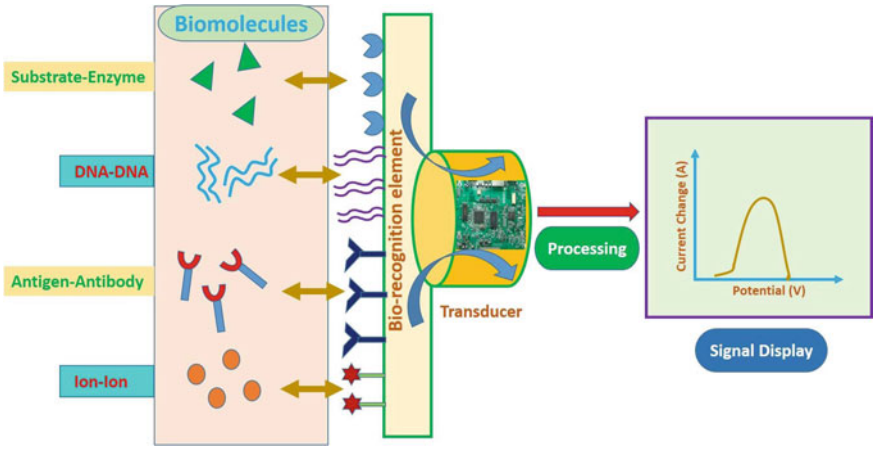


**Fig. 2** A typical biosensor with its components and basic principle. *Source* "Author"

like (a) electrochemical, (b) optical, (c) calorimetric, (d) piezoelectric, (e) microbial biosensor, (f) enzyme biosensor [20, 21].

In principle, the biological/chemical part of the sensor interacts with the specific analyte generating a signal that can be studied using the transducer element. For a biosensor, the essential components are a bio-recognition site, transducer component, and electronic system, which consists of a signal amplifier, processor, and display. Membrane, enzyme, antibody/antigen, receptor, protein, intact cells, tissue, or whole organ can be used as bio-recognition sites. A schematic of a typical biosensor with its sensing principle is shown in Fig. 2.

The mechanism for some important types of sensors is discussed below.

## *2.1 Fluorescence-Based Sensors*

The fluorescent sensing techniques are developed and appreciated over the last few decades as a highly sensitive and selective technique for the use as an ideal biosensor. However, various working strategies can be observed for the detection of various analytes. Different molecules exhibit fluorescence in their natural state, and certain modifications can cause minor to major changes in their fluorescence intensity. This property is utilized to develop simple fluorescence-based biosensors. However, various fluorescent labels are used for the detection of non-fluorescent analytes. Fluorescent labels are strategically attached to the analyte via any reactive group such as carboxyl, sulfhydryl, hydroxyl, or amino groups that assists in forming a chemical linkage. Aptabeacon is one of the most commonly used formats among fluorescence aptasensors [22]. The hairpin-like structure at the end of aptabeacons is labeled with a quencher and a fluorophore. Attachment of the target molecule with

the aptamer disrupts the initial confirmation of the Forster resonance energy transfer (FRET) pair, causing a turn-on fluorescence signal. The fluorescent label must be selectively excitable without exciting the other components in the system and must be able to generate a clear, demonstrable signal. Certain examples of different types of fluorescence labels are organic dyes, nanomaterials as fluorophores, and quenchers.

## 2.2 Field-Effect Transistor (FET)-Based Sensors

Field-effect transistors (FET) are mainly used as chemosensors [23]. The system consists of parts like source and drain electrodes, a channel, an insulating gate oxide, and a gate electrode [24]. The channel is composed of a semiconducting material sensitive to the target analytes. It is operated by monitoring the change in current in the channel before and after the adsorption of target molecules [23]. When the current flows through the channel, it is called the drain current, $I_{DS}$. $I_{DS}$ can be modulated by an electric field perpendicular to the semiconductor resulting from the voltage ($V_{GS}$) applied. The $I_{DS}$ is given by

$$I = \frac{C_i \mu W}{L}\left[(V_{GS} - V_{th}) - \frac{1}{2}V_{DS}\right]V_{DS}$$

where $C_i$ is the capacitance of the gate insulator per unit area,
$\mu$ is the charge carrier mobility in the channel,
$W/L$ is the width-to-length ratio of the channel,
$V_{GS}$ and $V_{DS}$ are the applied gate-source and drain-source voltage, and
$V_{th}$ is the threshold voltage required on the gate to create charge carriers.

When $V_{DS} << (V_{GS} - V_{th})$, it signifies a linear region and, when $V_{DS} > (V_{GS} - V_{th})$, it denotes a saturation region. At low drain-source voltages, the $I_{DS}$ current is proportional to $V_{DS}$ (at constant $V_{GS}$) following Ohm's law. FET sensors are known to operate in the linear range of $I_{DS}$. Besides this, the bandgap is another important parameter to consider for the performance of a sensor [23]. In the FET-based sensors, the type of semiconductor (p-type/n-type), the morphology of the sensing materials, and reactivity of the analyte (reducing/oxidizing) will control the electrical conductivity [25, 26]. FET-based sensors have attracted attention because of the varied features like miniaturization, parallel sensing, high sensitivity, and selectivity. One notable advantage is that FET sensor platforms can work in both gas and liquid environments, making the detection for a wide range of analytes, including gases, ions, and biomolecules easier [23, 25]. For example, 2D $MoS_2$ was integrated into a FET device to detect NO by exhibiting n-type dopant behavior [23]. Because of the flexibility of modulating the charge carrier mobility by controlling the gate voltage, FET devices are used to increase the sensitivity compared with other device architectures. However, the integration of materials into FET devices requires

advanced techniques such as lithography and a high degree of control over material morphology.

## 2.3 Colorimetric Sensors

Colorimetric sensors are a class of optical sensors that change color under the influence of external stimuli (temperature, pH, radiation, etc.). Colorimetric sensors are extensively used for the sensing of protein, DNA, pathogens, heavy metal ions, toxic gases, and organic compounds. It is used to sense biological contaminants, particularly on-site detection compared to plate colony counting method, polymerase chain reaction (PCR), and ELISA [27–29]. Mainly, colorimetric detection of bacteria involves enzymatic assay and glucose metabolism but has some limitations associated with enzymatic instability. Hence, the incorporation of diverse nanomaterials comes into the picture. Metal nanoparticles have unique optical properties like surface plasmon leading to a noticeable change in the color by aggregation or surface chemical reaction [30, 31]. With various surface modification using DNA, RNA, and antibodies, they perform a rapid and sensitive colorimetric response to target bacteria. Typically, conjugation of pathogen-specific receptors like antibodies or DNA aptamers on the surface of nanomaterials can detect bacteria via sandwich-type colorimetric assay procedures [32].

## 2.4 Electrochemical Sensors

Electrochemical sensors are designed for rapid, sensitive, and reliable recognition of the presence of pathogens [33]. There are basically three common electrochemical methods for pathogen detection: voltammetric, potentiometric, and impedance spectroscopy. Voltammetry method of detection captures the change in the potential that is applied as a function of time to the electrode–solution interface and measures the current in the process [34]. In potentiometric methods, the pathogens are detected by the change that occurs in current/potential when the electrode is kept at a fixed potential/current with respect to the reference electrode. In impedimetric methods, the sensor detects the change in impedance as a function of frequency with applied potential. Here, the biological recognition factors such as nucleic acids, aptamers, antibodies, bacteriophages are immobilized onto the sensing surface through adsorption, entrapment, or covalent linkage methods [35]. Two kinds of strategies come into play while sensing pathogens. In one case, the bare electrodes or modified electrodes with the bio-receptors are subjected to changes in current or potential when they encounter some targeted or untargeted analyte. In the other case, the metabolites secreted by the pathogens are detected [36].

## 3 Preparation of 2D Nanocomposite-Based Sensors

2D nanomaterials are well known for their sensing ability toward different toxic gases, hazardous chemicals, pathogenic microbes, and many bioactive molecules. The high surface area-to-volume ratios and multiple reaction sites on 2D nanomaterials are the leading factors to fabricate chemical and biosensors with high performance. 2D nanomaterials that are being used for the sensing of biological contaminants are graphene family, transition metal dichalcogenides, Mxenes, and their composites and phosphorene family [37, 38].

Graphene is advantageous as a sensing platform because different bioreceptor ligands can be integrated densely onto the surface through non-covalent, covalent, π–π, and electrostatic interaction [39]. But graphene facilitates interactions with blood serum components when these sensors are used for real-time application creating limitations [40]. As reduced graphene oxide (rGO) is more conducting than graphene itself, rGO is extensively used to fabricate electrochemical labels. In general, an electrochemical sensing layer is fabricated using a thermal reducing agent to deposit rGO on nanocellulose paper or using electrophoretic deposition of rGO/polyethylenimine (PEI) on gold electrode or rGO coated on gold nanoparticles (AuNPs) is used.

Another 2D nanomaterial that is being used is transition metal dichalcogenides. The most widely used transition metal dichalcogenides (TMD) are $MoSe_2$ and $MoS_2$. 2D nanomaterial $MoSe_2$ and $MoS_2$ are synthesized by a hydrothermal process at 200–220 °C. $MoS_2$ can also be obtained by electrodeposition on a gold electrode or in-situ prepared with AuNPs to form $MoS_2$-AuNPs nanocomposite, which can be subsequently deposited on the electrode. $MoS_2$ can also be fabricated via a simple ultrasound exfoliation method.

MXenes are another unique 2D nanomaterial having layered morphology that includes early transition metal carbides, nitrides, and carbonitrides. MXenes, in general, are prepared by exfoliation of $Ti_3AlC_2$ in 40–50% hydrogen fluoride (HF) at room temperature for 2 h.

Two-dimensional-layered semiconductor material known for its unique single-layer feature is phosphorene. Black phosphorene (BP) nanosheets can be prepared by mechanical exfoliation. BP can also be prepared by sonochemical exfoliation with in-situ reduction of BP on $HAuCl_4$ to form BP-Au nanocomposite.

In the following section, the use of 2D nanomaterials in the detection and sensing of biological contaminants is described in detail. What strikes out in these examples is that the mostly utilized technique in the fabrication of detection and sensing system for biological contaminants is electrochemical sensing platform. This could be due to the large surface area of 2D nanomaterials which can be modified to tune the conductivity to felicitate electron transfer between electrochemical species and the underlying electrode surface.

# 4 2D Nanomaterials for Detection and Sensing of Biological Contaminants

## *4.1 Nanomaterials from Graphene Family and Their Composites*

Nanomaterials derived from carbon and other sources serve a better purpose owing to their high surface area as compared to their traditional adsorbent counterparts, such as activated charcoal [41]. Out of the various nanomaterials, graphene and its composites have been widely used for the same. Graphene has sparked great interest for an exceptionally large surface area, high thermal, and electron mobility. In graphene, carbon atoms are hexagonally arranged in $sp^2$ bonded aromatic structures [42, 43]. It is obtained by exfoliation of graphite which contains a stack of sheets with an interlayer spacing of 3.34 Å between them [44]. Micromechanical exfoliation of the graphite into single-layer graphene sheets by ultrasonication in organic solvents [45] and chemical vapor deposition (CVD) method for large-scale production were some of the many ways for the synthesis of graphene [46]. Currently, the most studied graphene nanomaterials are graphene oxide (GO) and reduced graphene oxide (rGO) [47]. GO possesses abundant oxygen-containing functional groups providing scope for further modification, whereas rGO is obtained by removing these oxygen functionalities through reduction routes [48]. Each atom of the single layer of graphene has maximum exposure to the environment, thereby having the highest surface area (2630 $m^2\ g^{-1}$) among all the nanomaterials [49]. As such, graphene, GO, rGO, and their composites can be effectively used for wide-ranged applications, particularly in the biomedical field [50]. Graphene and its nanocomposite materials have bacterial inactivation properties [51]. Graphene nanocomposites of polymer and metal/metal oxides are found to be the most promising in disinfecting microbial contamination in water treatments [52]. Traditionally, nanocomposite systems were employed to kill bacterial cells or to inhibit cell division. Although graphene and graphene-based composite materials are used by many researchers as sensing platforms, their use in sensing and detection of biological contaminants is limited. Mostly, electrochemical sensors designed from graphene and graphene-based nanocomposites are reported for the detection of biological toxins. A few examples are discussed below.

*Electrochemical sensors*: Burrs et al. [53] illustrated the electrochemical biosensing of *Escherichia coli*, a pathogenic bacterium using a graphene paper functionalized with platinum nano-cauliflower. The paper is conductive with a high electroactive surface area of 0.2970.13 $cm^2$ which has a LOD of 4 CFU $mL^{-1}$ and a response time of 12 min for *E. coli O157:H7*. Another work on detecting a uropathogenic bacteria *E. coli UTI89* in aqueous and serum samples was reported by Jijie et al. using gold electrodes modified with rGO/polyethyleneimine (PEI) [54]. The selectivity was induced by changing the electrode surface covalently with anti-fimbrial *E. coli* antibodies and additional modification with pyrene-polyethylene glycol moieties. The LOD obtained was 10 CFU $mL^{-1}$. Fei et al. explored the detection of a food

pathogen *Salmonella pullorum* (*S. pullorum*) by the electrochemical immunoassay with gold nanoparticles coated graphene oxide (rGO/AuNPs) and the immunomagnetic beads (IMB). Using differential pulse voltammetry (DPV), LOD was found 89 CFU $mL^{-1}$ [55]. A fast, selective, and ultrasensitive detection of *Staphylococcus aureus* (*S. aureus*) was reported by Hernández et al. using a potentiometric biosensor based on chemically modified graphene and aptamers [56].

## *4.2 Transition Metal Dichalcogenides and Their Composites*

The lack of an intrinsic bandgap in pure graphene and limited chemical modification has prompted the scientific community to search for other 2D nanomaterials with semiconducting properties. Transition metal dichalcogenides (TMCs) are a group of inorganic materials of the general formula, $MX_2$, where M is a transition metal typically from groups 4–10, and X stands for chalcogen series (such as S, Se, and Te) [57]. The structure of TMCs is like that of sandwiches wherein X–M–X is stacked together by the covalent bonding of trilayers and monolayers along the crystallographic *c*-axis (0, 0, 1) [58]. They have mainly three structural polytypes; 2H (hexagonal symmetry), 3R (rhombohedral symmetry), and 1T (tetragonal symmetry) [58, 59]. The symmetry of $MX_2$ can either be trigonal prismatic ($D_{3h}$) or anti-prismatic ($D_{3d}$) with a coordination number 6 [60]. The bandgap ranges from 0 to 2 eV for semimetal and semiconductor structures depending on the number of layers, the presence or lack of doping atoms, and elemental composition [56, 61]. The underlying van der Waals interactions between the layers make TMCs a unique material for interlayer diffusion susceptible to high charge mobility [58, 62]. The preparation of TMD monolayers requires mechanical exfoliation by ultrasonication, electrochemical exfoliation, hydrothermal method, CVD, etc. The exfoliation process results in a higher degree of monolayers with high aspect ratios and a greater number of monolayers in a polymer matrix [58, 63].

The high specific surface area, along with the possibility of surface treatment, makes TMCs monolayer a suitable choice for designing different polymer composites [64, 65]. Among the different TMCs, the group VI TMCs, $MoS_2$, and $MoSe_2$ show excellent physicochemical properties and biocompatibility [66, 67]. There are several reports of TMCs-based nanocomposites acting as electrochemical biosensors for sensing various biological contaminants. Most of the detection techniques use the strategy of fabricating aptamer-based-electrosensors because of the lack of cross-reactivity, thereby high specificity toward the target analyte giving instant response in the electrochemical signal. Following are some examples of detection of microbial toxins by TMCs based on electrochemical techniques.

*Electrochemical sensors*: Among many bacterial toxins, *Salmonella paratyphi* is the food-borne pathogen that causes paratyphoid A fever [68]. Mishra et al. designed a $MoSe_2$-modified aptasensor to detect the *Salmonella* bacteria [69], where an aptamer functionalized with amine, and specific to the bacteria was incorporated onto $MoSe_2$

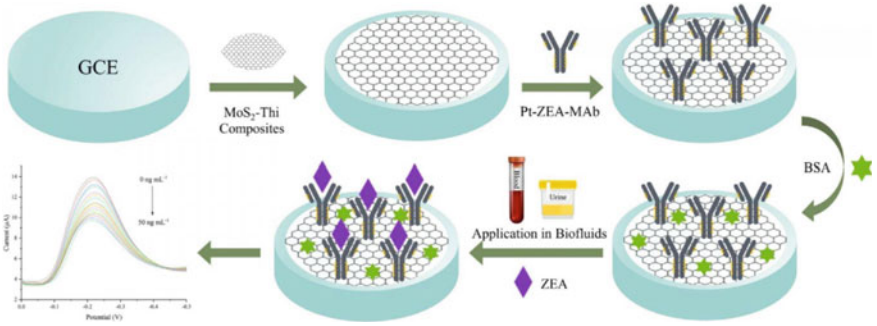


**Fig. 3** Illustration of the electrochemical immunosensor for detection of ZEA in biofluids based on $MoS_2$-Thi nanocomposites. Reproduced with permission from Ref. [74]

nanobroom-modified fluorine-doped tin oxide by cross-linking with glutaraldehyde. The study showed good linearity of detection ranging from $10^{-2}$ to $10^{-10}$ CFU/mL with a low LOD of $1 \times 10^{-10}$ CFU $mL^{-1}$. Considering the detection of fungal toxins, the most toxic aflatoxin, AFB1 [70], was detected by building an electrochemical aptasensor based on tetrahedral DNA nanostructures (TDNs), immobilized on macroporous $MoS_2$-AuNPs hybrids [71]. This hybrid was able to increase the immobilization amount of TDNs, thereby also facilitating the mobility of electrons. The aptasensor showed a LOD of 0.01 fg $mL^{-1}$. The system could detect AFB1 in grain products such as wheat powder and rice samples.

Wang et al. fabricated a methylene blue (MB)-modified OTA (Ochratoxin A, mycotoxin causing nephrotoxicity) aptamer on the $MoS_2$ nanosheet/AuNP ($MoS_2$-AuNP) nanocomposite that is surrounded by gold electrode via host–guest recognition of β-cyclodextrin (β-CD) [72, 73]. The aptasensor possesses satisfactory results with detection ranging from 0.1 to 50 nmol $L^{-1}$ and sensitivity (LOD) of 0.06 nmol $L^{-1}$. Another mycotoxin produced by *Fusarium*, zearalenone (ZEA), was detected by Jiang et al. by constructing an electrochemical immunosensor based on thin-layer $MoS_2$ and thionin ($MoS_2$-Thi) composites (as shown in Fig. 3) that were used as electrochemical probes [74]. The $MoS_2$-Thi-based immunosensor showed a linear range of 0.01–50 ng $mL^{-1}$, low LOD (0.005 ng $mL^{-1}$ ZEA) carried out in both urine and plasma.

Microcystins (MCs), a group of algal toxins, are associated with multiple health issues, and their toxicity is evaluated from the Microcystin-LR (MC-LR) content. Pang et al. constructed an enzyme-free electrochemical immunosensor for detecting MC-LR using $MoS_2$ nanosheets/BSA-stabilized gold nanocluster ($MoS_2$/AuNCs) nanocomposites and Au core/Pt shell nanoparticles (Au@PtNPs) [75]. The immunosensor exhibits LOD of 0.3 ng $L^{-1}$ for MC-LR in various water samples.

### *4.3 Mxene Family*

Another unique two-dimensional nanomaterial of layered morphology consists of MXenes that include early transition metal carbides, nitrides, and carbonitrides. MXenes are obtained from layered hexagonal MAX phases having a general formula, $M_{n+1}AX_n$, where M is an early transition metal, A denotes elements of Group 13 and 14 of the periodic table, and X is either carbon or nitrogen [76]. The multilayer structured MAX phase is composed of alternating layers of M and A consisting of a strong mixed metallic-covalent (M–X) bond and weak M–A bond [76, 77]. Modulation of layer A from the MAX phase emerges from highly stabilized closed packed $M_{n+1}X_nT_x$ nanosheets, termed MXene [78]. Here, T stands for surface terminating groups of etched MXenes such as –O, –F, –OH produced due to chemical etching. As predicted by DFT calculations, the surface termination is the controller of surface activating properties. The monolayer of MXene is said to be metallic with high electron density [62].

Titanium carbide ($Ti_3C_2$) is the most explored Mxene. It is prepared by exfoliation of $Ti_3AlC_2$ in 50% hydrogen fluoride (HF) at room temperature for 2 h. The aqueous HF solution acts as an etching agent to remove the Al layer, followed by adding a surface termination group to the exfoliated layers to finally form $Ti_3C_2(OH)_2$ and/or $Ti_3C_2F_2$ [79]. Interestingly, one study showed higher antibacterial activity toward both gram-negative (*Escherichia coli*) and gram-positive (*Bacillus subtilis*) compared to that of graphene [80].

The non-toxic degradation by-products ($CO_2$, $N_2$) of MXenes make them suitable for environmental remediation applications [81]. The metallic character, tuneable conductivity, and variety of functional groups make MXene an interesting 2D nanomaterial for sensing applications. Their added advantage of hydrophilicity, biocompatibility, compared, and ease of functionalization with high intercalation capacity [82] in comparison with the other 2D materials help in designing a sensor system to be utilized at a commercial scale.

Although several works of MXenes as sensors have been used for the detection of biomarkers, gases, and other environmental contaminants [83], the sensing of biological contaminants/microbial toxins is not well-explored yet.

*Electrochemical sensing*: One report has found that MXene is used as an electrochemical immunosensor to detect gliotoxin, the most toxic mycotoxin produced by *Aspergillus fumigatus* [85]. The biosensor was prepared by incorporating tetrahedral DNA nanostructure (TDN) onto the surface of MXene nanosheets [84] (Fig. 4). The presence of Ti on the MXene nanosheets provides an easy method for assembly via a strong interaction between titanium and phosphate groups of TDNs, thereby eliminating the requirement of complex chemical modification of TDNs generally required for the immobilization of TDNs onto the electrode. The use of MXenes in designing the sensor has helped enhance the sensitivity with the added benefit of providing an ample surface area to incorporate a larger amount of TDN onto the electrode.

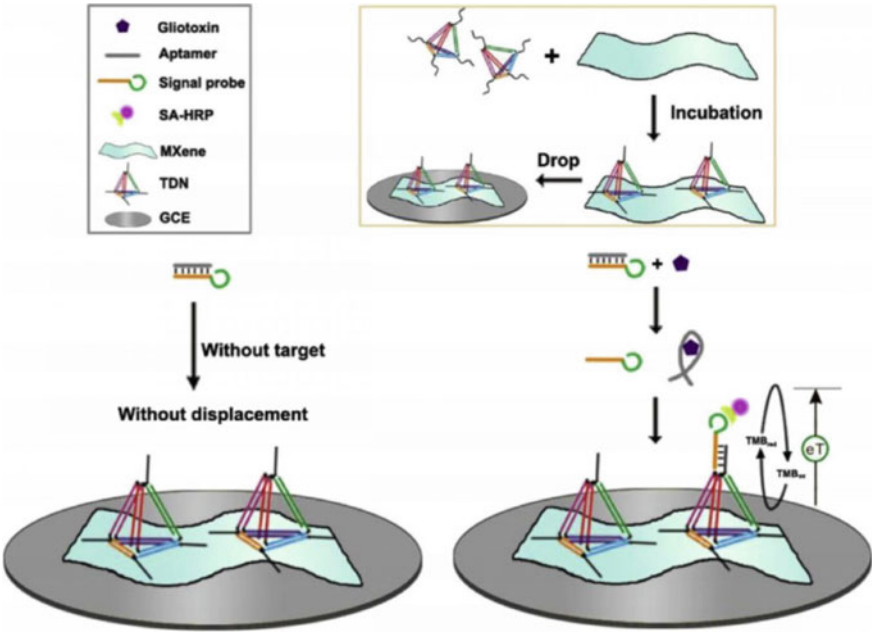


**Fig. 4** Schematic representation of the TDN/MXene-based electrochemical sensors to detect gliotoxin. Reproduced with permission from Ref. [84]

The biosensor exhibited a broad detection range to gliotoxin concentrations (5 pM–10 nM) with a LOD of 5 pM. Such fabrication of MXene-based E-DNA biosensor will open avenues for its applicability in detecting other biological contaminants.

## *4.4 Phosphorene Family*

Phosphorene is another 2D layered semiconductor material and known for its unique single-layer feature. It was first synthesized from black phosphorus using a scotch tape-based micro-cleavage [86]. The resulting 2D material is layered dependent, having a hinge-like structure, giving anisotropy in its structure, and behaves as a quasi-one-dimensional excitonic nature that contrasts to those found in other 2D nanomaterials [86–88]. 2D phosphorene, composed of $sp^3$ hybridized phosphorus atoms, represents layered orthorhombic crystal structure with space group $C_{mca}$ [89]. It forms a honeycomb lattice structure with non-planarity in the form of structural ridges [90].

The phosphorene monolayer reveals a tunable direct bandgap of the layers modulating in the order of 1.51 eV for a single layer to 0.59 eV for a five-layer system [91]. This advantageous feature of phosphorene leads to high drain current modulation up to $10^5$ and charge mobility (~1000 $cm^2\ V^{-1}\ s^{-1}$) [92]. The stacking of multiple 2D

phosphorene is due to van der Waals interactions which form multilayers with an interlayer distance of 5.5 Å [93].

The combination of the features like narrow bandgap, anisotropic electrical conductance, and reactive edge structure makes 2D phosphorene suitable for an application in electrically transduced sensing technologies [94]. Moreover, due to its puckered honeycomb structure, it has high chemical adsorption energy offering plentiful adsorption sites for interaction with analytes [94, 95]. The introduction of structural ripples and dopants on the surface of black phosphorus (BP) helps in improving sensitivity and charge transfer toward analytes [96].

Two-dimensional phosphorene has been used as electrochemical sensors for the detection of gases, volatile compounds, different ions, and biomolecules [97]. However, a few reports were found for electrochemical sensing biological contaminants which are mentioned below.

*Electrochemical sensors*: A simple voltammetric method was reported for the sensing of ochratoxin A (OTA) in food samples [98]. OTA is a fungal contaminant and is categorized as Group 2B carcinogen by the International Agency for Research on Cancer (IARC) [99]. It is known to be highly stable throughout the food chain, imposing a threat to human beings. In this work, Xiang et al. fabricated a nanosensor using BP nanosheets and functionalized it with $Ag^+$ ions and employed the sensor to a voltammetric analysis of OTA in food samples using DPV [98]. The detection of OTA by an electrochemical sensing platform has a disadvantage of a strong fouling effect on electrodes from the oxidation products of OTA [100]. However, functionalized BP as an electro-sensor showed good stability, electrocatalytic ability, and strong anti-fouling property toward OTA oxidation. The BP nanosensor can selectively detect OTA in a linear way ranging from 0.3 to 10 μg/mL with a LOD of 0.18 μg/mL through an irreversible electrochemical response with an adsorption-controlled process.

The easy functionalization and biocompatibility made this two-dimensional material a promising transducer with an improved biosensor performance. This has prompted the researchers to develop a unified apta-sensing system to detect okadaic acid (OA, $C_{44}H_{68}O_{13}$), a marine toxin produced by several species of *dinoflagellates* known to accumulate in both sponges and shellfish, causing seafood poisonings. Ramalingam et al. fabricated an electrochemical microfluidic biochip for detecting OA by using a screen-printed carbon electrode (SPCE) [101] (Fig. 5). The SPCE was designed with phosphorene-gold nanocomposite on which an OA specific to an aptamer was immobilized and potassium ferro-ferricyanide was used as a redox indicator.

Phosphorene when paired with AuNPs significantly enhanced the electrochemical response and proved to be effective in creating the aptamer specific to OA without flaking and displaying a LOD of 8 pmol $L^{-1}$. The electrochemical aptasensor has excellent selectivity as it did not show any cross-reactivity with other types of food toxins and is employed to detect OA in fresh mussel extracts. The results suggest that the microfluidic electrochemical aptasensor can be applied as a POC device for an on-field assay.

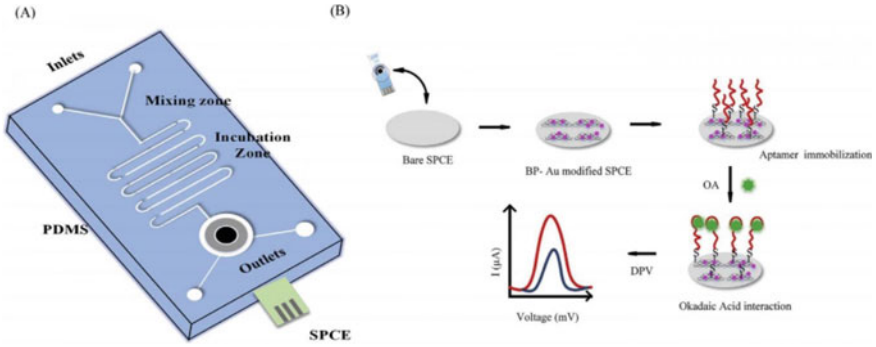


**Fig. 5** **a** Graphical representation of the microfluidic chip to detect okadaic acid. **b** Schematic view of the sensing process. Reproduced with permission from Ref. [101]

From all the work discussed above for the categories of 2D nanomaterials, it was found that most of the reports are based on electrochemical sensing. A summary of the 2D nanomaterial-based electrochemical sensors is tabulated, mentioning the type of contaminant, the sensor element, and the respective LOD values (Table 1).

## 5 Other 2D Nanomaterials with Future Prospects in Sensing of Biological Contaminants

The newer members of 2D nanomaterial; germanene and silicene family, boron nitride and borophene family, tin, antimony, bismuth, tellurium family are still in the nascent stage of the study. Different computational methods can be utilized to study sensing through density-functional theory (DFT) which is a computational quantum mechanical modeling method to investigate the electronic structure in atoms or molecules. The ab initio DFT calculations (from first principles) predict the material behavior following quantum mechanics avoiding the use of fundamental material properties. Some theoretical functions are applied to the systems of interest to see the properties. For instance, non-equilibrium Green's function was recently employed to study the anisotropic gas (CO, NO, $NO_2$ and $NH_3$) sensing properties of borophene [102]. Although DFT-based studies have been reported for them, they need to be supported by experiments to get correlated data. These newer 2D nanomaterials are discussed in detail below.

**Table 1** 2D nanomaterial-based electrochemical sensors

| Detection technique | Biological contaminant | 2D nanomaterial/nanocomposite | LOD | References |
|---|---|---|---|---|
| *Electrochemical sensors* | *Escherichia coli* | Graphene paper functionalized with platinum nano-cauliflower | 4 CFU $mL^{-1}$ | [53] |
| *Electrochemical sensors* | *Escherichia coli* | rGO/PEI | 10 CFU $mL^{-1}$ | [54] |
| *Electrochemical sensors* | *Salmonella pullorum* | rGO/AuNPs | 89 CFU $mL^{-1}$ | [55] |
| *Electrochemical sensors* | *Staphylococcus aureus* | Graphene | 1 CFU $mL^{-1}$ | [56] |
| *Electrochemical sensors* | *Salmonella paratyphi* | $MoSe_2$ | $1 \times 10^{-10}$ CFU $mL^{-1}$ | [69] |
| *Electrochemical sensors* | Aflatoxin, AFB1 | $MoS_2$-AuNPs | 0.01 fg $mL^{-1}$ | [71] |
| *Electrochemical sensors* | Ochratoxin A | $MoS_2$-AuNP | 0.06 nmol $L^{-1}$ | [73] |
| *Electrochemical sensors* | Zearalenone | MoS2-Thi | 0.005 ng $mL^{-1}$ | [74] |
| *Electrochemical sensors* | Microcystins | $MoS_2$/AuNCs and Au@PtNPs | 0.3 ng $L^{-1}$ | [75] |
| *Electrochemical sensors* | Ochratoxin A | BP nanosheets | 0.18 μg/mL | [99] |
| *Electrochemical sensors* | Okadaic acid | Phosphorene-gold nanocomposite | 8 pmol $L^{-1}$ | [102] |
| *Electrochemical sensors* | Gliotoxin | MXene nanosheets | 5 pM | [86] |

## *5.1 Silicene and Germanene Family*

Silicene, an allotrope of silicon, is a 2D nanomaterial with a hexagonal honeycomb structure like graphene. The stronger coupling between layers in silicene compared to multilayered graphene contributes to its non-flatted structure. The hybridization in silicene is $sp^2$-$sp^3$ mixed hybridization [103]. In recent years, elemental sheets of silicon (silicene) and germanium (germanene) are emerging as strong candidates in the realm of 2D nanomaterials [104]. The greater binding affinity of common contaminants than that for graphene is based on their hybridization. Moreover, both the silicene and germanene with their buckled honeycomb structures possess higher reactivity than graphene, showing sensitivity to various pollutants [105]. The silicene synthesis has already been successfully carried out on different metal substrates [92], while germanene was made on Pt (111) surface. The report of the multilayer germanene exfoliated on $SiO_2$/Si surface is well-established [106]. As of now, no

such sensors (fluorescent, FET, electrochemical, colorimetric) have been developed except for some density-functional theory (DFT)-based systems as discussed below.

Silicene and germanene have been investigated so far to detect toxic gases like $H_2S$, $CO_2$, $SO_2$ by incorporating defects into them, with the help of DFT [92, 107]. Theoretical studies suggest that doping with B, Al, N, and P could produce effective silicene over pristine one in terms of sensing. Another theoretical research on these two systems revealed that biomolecules like DNA nucleobase, amino acid, and heterocyclic molecules could be efficiently adsorbed. This suggests that they have tremendous potential to work for other sensing materials [108]. However, this field remains unexplored, with no report of the use of silicene and germanene in detecting biological contaminants.

## *5.2 Boron Nitride and Borophene Family*

Boron nitride (BN), with layered hexagonal microstructure, has recently received a lot of attention owing to its unique properties like thermal stability, increased mechanical strength, and oxidation resistance [109]. The C–C bonds in BN nanomaterials (BNN) present a partial ionic character, and BNN has high electronegativity. This, in turn, results in enhanced optical, electronic, and mechanical properties [110]. The excellent biocompatibility of BNN has grasped the attention of scientists for their possible application in the biological field [111]. Balmain in 1842, first demonstrated the synthesis of BN [112]. Monodispersed 2D BNN can be synthesized via modified solid-state metathesis reaction [113, 114].

However, BNN has played a significant role in the detection of biological contaminants. Yang et al. in 2019, synthesized graphene oxide and BN 2D nanomembrane for the effective removal of antibiotics from water [115]. Chao et al. showed the adsorption capacity of hexagonal BN (g-BN) for fluoroquinolone antibiotic gatifloxacin (GTF) to be more than 90% [116]. Adsorption efficiency of g-BN increases with higher temperature, indicating that adsorption is exothermic. The primary removal mechanism was determined to be electrostatic interaction as the adsorption of GTF is inversely proportional to the ionic strength. BN nanosheets were synthesized to demonstrate their efficiency for the pre-concentration of chlortetracycline hydrochloride (CTC), tetracycline (TC), norfloxacin (NOR), and ciprofloxacin (CIP) [117]. More aromatic rings in CTC and TC resulted in their higher sorption by BN nanosheets. Recently, Zhi et al. demonstrated the immobilization of proteins in BN nanotubes via electrostatic interactions and $\pi-\pi$ interactions [118]. Lin et al. also demonstrated that BN nanosheets in water displayed excellent affinity toward proteins with an adsorption capacity of 312 mg/g at room temperature [119]. But the 2D BN nanomaterial is yet to be explored in the biosensor field.

Borophene is a new generation super material discovered in 2015 and the lightest material to date [120]. It is a 2D boron nanosheet first fabricated on argentum (Ag) substrate [121]. Many researchers have claimed their potential applications due to

their excellent properties. Borophene has been used to develop sensors for formaldehyde [122], ethanol [123], and hydrogen cyanide [124]. Density-functional theory (DFT) and non-equilibrium Green's function (NEGF) methods were used to study the electronic properties of borophene. The adsorption of ethanol molecules on the surface of edge-hydrogenated 2D borophene caused an increment in the current passing through it. In addition to this borophene, fullerene was also used as NO and CO sensors [125].

However, the use of borophene in the detection and removal of biological contaminants were still to be explored. By determining the electron sensitivity and energy of borophene to the purine and pyrimidine bases (A, T, G, and C), researchers have found that borophene attached to different bases has different conductivities generating different electrical signals [126]. In addition, the sensitivity of borophene to different bases was also measured (A > G > C > T). Hence, borophene nanosheets could be the future material for biosensor devices [127].

## *5.3 Tin, Antimony, Bismuth, Tellurium Family*

Another member of the 2D family, stanene, is formed from tin (Sn) hexagonal lattice in buckled arrangement [128]. The first successful formation of stanene was achieved in 2015 on a $Bi_2Te_3$ substrate [129]. Its persistent room temperature conductivity is another exciting property that could be explored further [130]. The stability of stanene comes from low-buckling originating from σ-π bonding [131]. It shows $sp^2$-$sp^3$ hybridization. Recently, stanene with monolayers and a few layers were successfully synthesized on $Bi_2Te_3$ (111), InSb (001), Au (111), and Sb (111) substrates [130, 132]. From its discovery, it has been employed in application in gas sensing purposes ($SO_2$, $H_2S$, $NO_2$, $O_3$) only through DFT [133]. The use of stanene as a sensor for biological contaminants is yet to be explored.

Antimonene and bismuthene are also 2D layer materials of group V elements of Sb and Bi. Antimonene was first experimentally synthesized in 2016 [134]. Antimonene monolayer sheets consisting of $sp^3$ hybridized antimony atoms possess a honeycomb-like structure, unlike flat graphene. The stability comes from the puckered atoms, held together by weak van der Waals forces. This material has significant properties with good electrical conductivity (1.63104 $Sm^{-1}$), tuneable bandgap (2.28 eV), and so on [135]. Although there are few reports of toxic gas and reagents (like acetone, dimethyl ether, and ethyl methyl ether) sensing by different forms of antimonene [79, 136, 137], no application related to biological sensors has been reported to date. Similarly, bismuthene has been limited to use only in voltammetric detection of ions and sensing of toxic gases [138–140]. Sensing study for biological contaminants by antimonene and bismuthene is still unexplored.

Tellurene, a highly anisotropic 2D nanostructure of tellurium (Te), has the most stable α-phase for a few-layer tellurene and the tetragonal β-phase for a monolayer tellurene [141]. It has a direct bandgap of nearly 0.33 eV in bulk and an indirect

monolayer bandgap of 0.92 eV [142]. Tellurene monolayer has been employed theoretically to act as a chemosensor for various toxic gases, solvents [143, 144] and as a biosensor for DNA/RNA nucleobases and amino acids [145]. However, it is yet to be explored to apply experimentally in actual samples.

From the above discussion, it is noted that these recently developed 2D nanomaterials are primarily involved in chemosensing and biosensing for toxic gases and other bioactive molecules using computational study (like DFT). The properties and bandgap tunability of such 2D nanomaterials give a probable scope to develop sensors for biological contaminants.

## 6 Conclusion

Biological contaminants are considered prime contributors to environmental pollution as well as hazards to human health. Therefore, it is essential to find out ways to eradicate such contaminants. Several 2D nanomaterials were effective in the sensing of biological toxins contaminated in soil, water, air, food, etc. However, it was found that primarily electrochemical sensors were used to serve the purpose as they offer several advantages like easy miniaturization and operation, high sensitivity, reproducibility, and suitable on-site analysis. Besides, most of the 2D nanomaterial systems consist of electron-rich sites that aid in designing of these sensors. Modifying such systems with aptamer, DNA, RNA, antibody is another strategy to enhance their sensing properties toward microbial toxins. Bandgap tunability is one of the functional advantages of 2D nanomaterials, and it can be achieved by attaching metal nanoparticles with 2D nanostructures. Functional groups available on the surface of such materials are also a leading factor for a selective and efficient sensing. Among different 2D nanomaterials, graphene has been explored to a great extent. Transition metal dichalcogenides-based platforms are used for the detection of many food-borne pathogens and fungal toxins. It is interesting to note that composites of graphene or other 2D nanomaterials are more promising in terms of their microbial decontamination capacity, specifically in water. This is usually accomplished with the help of metal and metal oxide. There is no report on the use of newer 2D nanomaterials, viz. borophene, stanene, antimonene, and bismuthene as sensors for biological contaminants. Hence, there is a promising scope to develop sensors for biological contaminants using these novel 2D nanomaterials.

## References

1. Xu M, Liang T, Shi M, Chen H (2013) Graphene-like two-dimensional materials. Chem Rev 113:3766–3798
2. Huang X, Zeng Z, Zhang H (2013) Metal dichalcogenide nanosheets: preparation, properties and applications. Chem Soc Rev 42:1934–1946

3. Weng Q, Wang X, Wang X, Bando Y, Golberg D (2016) Functionalized hexagonal boron nitride nanomaterials: emerging properties and applications. Chem Soc Rev 45:3989–4012
4. Ma R, Sasaki T (2015) Two-dimensional oxide and hydroxide nanosheets: controllable high-quality exfoliation, molecular assembly, and exploration of functionality. Acc Chem Res 48:136–143
5. Du Y, Yin Z, Zhu J, Huang X et al (2012) A general method for the large-scale synthesis of uniform ultrathin metal sulphide nanocrystals. Nat Commun 3:1177
6. Naguib M, Mochalin VN, Barsoum MW, Gogotsi Y (2014) 25th anniversary article: MXenes: a new family of two-dimensional materials. Adv Mater 26:992–1005
7. Anasori B, Lukatskaya MR, Gogotsi Y (2017) 2D metal carbides and nitrides (MXenes) for energy storage. Nat Rev Mater 2:16098
8. Hong Ng VM, Huang H, Zhou K et al (2017) Recent progress in layered transition metal carbides and/or nitrides (MXenes) and their composites: synthesis and applications. J Mater Chem A 5:3039–3068
9. Zhang J, Chen Y, Wang X (2015) Two-dimensional covalent carbon nitride nanosheets: synthesis, functionalization and applications. Energy Environ Sci 8:3092–3108
10. Eswaraiah V, Zeng Q, Long Y, Liu Z (2016) Black phosphorus nanosheets: synthesis, characterization and applications. Small 12:3480–3502
11. Wang Q, O'Hare D (2012) Recent advances in the synthesis and application of layered double hydroxide (LDH) nanosheets. Chem Rev 112:4124–4155
12. Lalmi B, Oughaddou H, Enriquez H et al (2010) Epitaxial growth of a silicene sheet. Appl Phys Lett 97:223109
13. Lin Z, Carvalho BR, Kahn E et al (2016) Defect engineering of two-dimensional transition metal dichalcogenides. 2D Mater 3:022002
14. Varghese S, Singh K, Swaminathan S, Varghese S, Mittal V (2015) Two-dimensional materials for sensing: graphene and beyond. Electronics 4:651–687
15. Bonaccorso F, Colombo L, Yu G et al (2015) Graphene related two-dimensional crystals and hybrid systems for energy conversion and storage. Science 347:1246501
16. Liu G, Robertson AW, Li MMJ, Kuo WCH et al (2017) $MoS_2$ monolayer catalyst doped with isolated Co atoms for the hydrodeoxygenation reaction. Nat Chem 9:810–816
17. Dorner B, Rummel A (2015) Preface biological toxins-ancient molecules posing a current threat. Toxins 7:5320–5321
18. Seltzer JM (1994) Biological contaminants. J Allergy Clin Immunol 94(2):318–326
19. Hussain T, Kaewmaraya T, Chakraborty T, Ahuja R (2016) Defect and substitution-induced silicene sensor to probe toxic gases. J Phys Chem C 120:25256–25262
20. Heineman WR, Jensen WB (2006) Leland C. Clark Jr. (1918–2005). Biosens Bioelectron 21:1403–1404
21. Cavalcanti A, Shirinzadeh B, Zhang M, Kretly LC (2008) Nanorobot hardware architecture for medical defense. Sensors 8:2932–2958. https://doi.org/10.3390/s8052932
22. Yamamoto R, Kumar PK (2000) Molecular beacon aptamer fluoresces in the presence of tat protein of HIV-1. Genes Cells 5:389–396
23. Li H, Yin Z, He Q, Li H, Huang X, Lu G, Fam DW, Tok AI, Zhang Q, Zhang H (2012) Fabrication of single- and multilayer $MoS_2$ film-based field-effect transistors for sensing NO at room temperature. Small 8:63–67
24. Cervenka J, Budi A, Dontschuk N, Stacey A, Tadich A, Rietwyk KJ et al (2015) Graphene field effect transistor as a probe of electronic structure and charge transfer at organic molecule–graphene interfaces. Nanoscale 7:1471–1478
25. Yoshizumi T, Miyahara Y (2017) Field-effect transistors for gas sensing. In: Different types of field-effect transistors—theory and applications. IntechOpen
26. Stine R, Mulvaney SP, Robinson JT, Tamanaha CR, Sheehan PE (2013) Fabrication, optimization, and use of graphene field effect. Sensors Anal Chem 85:509–521
27. Brooks B, Devenish J, Lutze-Wallace C, Milnes D, Robertson R, Berlie-Surujballi G (2004) Evaluation of a monoclonal antibody-based enzyme-linked immunosorbent assay for detection of *Campylobacter fetus* in bovine preputial washing and vaginal mucus samples. Vet Microbiol 103:77–84

28. Heo J, Hua SZ (2009) An overview of recent strategies in pathogen sensing. Sensors 9:4483–4502
29. Zhu L, He J, Cao X, Huang K, Luo Y, Xu W (2016) Development of a double-antibody sandwich ELISA for rapid detection of *Bacillus cereus* in food. Sci Rep 6:16092
30. Halas NJ, Lal S, Chang WS, Link S, Nordlander P (2011) Plasmons in strongly coupled metallic nanostructures. Chem Rev 111:3913–3961
31. Jain PK, Huang X, El-Sayed IH, El-Sayed MA (2008) Noble metals on the nanoscale: optical and photothermal properties and some applications in imaging, sensing, biology, and medicine. Acc Chem Res 41:1578–1586
32. Chen J, Andler SM, Goddard JM, Nugen SR, Rotello VM (2017) Integrating recognition elements with nanomaterials for bacteria sensing. Chem Soc Rev 46:1272–1283
33. Lermo A, Campoy S, Barbe J et al (2007) In situ DNA amplification with magnetic primers for the electrochemical detection of food pathogens. Biosens Bioelectron 22:2010–2017
34. Monzo J, Insua I, Trillo FF et al (2015) Fundamentals, achievements and challenges in the electrochemical sensing of pathogens. Analyst 140:7116–7128
35. Lazcka O, Del Campo FJ, Munoz FX (2007) Pathogen detection: a perspective of traditional methods and biosensors. Biosens Bioelectron 22:1205–1217
36. Wang Y, Ye Z, Ying Y (2012) New trends in impedimetric biosensors for the detection of foodborne pathogenic bacteria. Sensors 12:3449–3471
37. Choi JH, Lee J, Byeon M, Hong TE, Park H, Lee CY (2020) Graphene-based gas sensors with high sensitivity and minimal sensor-to-sensor variation. ACS Appl Nano Mater 3:2257–2265
38. Lee E, Yoon YS, Kim DJ (2018) Two-dimensional transition metal dichalcogenides and metal oxide hybrids for gas sensing. ACS Sens 3(10):2045–2060
39. Peña-Bahamonde J, Nguyen HN, Fanourakis SK, Rodrigues DF (2018) Recent advances in graphene-based biosensor technology with applications in life sciences. J Nanobiotechnol 16:75
40. Amiri M, Bezaatpour A, Jafari H et al (2018) Electrochemical methodologies for the detection of pathogens. ACS Sens 3:1069–1086
41. Brady-Estevez AS, Kang S, Elimelech M (2008) A single-walled carbon-nanotube filter for removal of viral and bacterial pathogens. Small 4:481–484
42. Novoselov K, Geim A, Morozov S et al (2004) Electric field effect in atomically thin carbon films. Science 306:666–669
43. Geim AK, Novoselov KS (2007) The rise of graphene. Nat Mater 6:183–191
44. Kang SH, Fang TH, Hong ZH (2013) Electrical and mechanical properties of graphene oxide on flexible substrate. J Phys Chem Solids 74:1783–1793
45. Geim AK (2009) Graphene: status and prospects. Science 324:1530–1534
46. Bae S, Kim H, Lee Y, Xu X, Park JS et al (2010) Roll-to-roll production of 30-inch graphene films for transparent electrodes. Nat Nanotechnol 5:574–578
47. He K, Chen G, Zeng G et al (2017) Stability, transport and ecosystem effects of graphene in water and soil environments. Nanoscale 9:5370–5388
48. Dreyer DR, Park S, Bielawski CW, Ruoff RS (2010) The chemistry of graphene oxide. Chem Soc Rev 39:228–240
49. Perreault F, Faria AF, Elimelech M (2015) Environmental applications of graphene-based nanomaterials. Chem Soc Rev 44:5861–5896
50. Zhang Y, Nayak TR, Hong H, Cai W (2012) Graphene: a versatile nanoplatform for biomedical applications. Nanoscale 4:3833–3842
51. Upadhyayula VKK, Deng S, Mitchell MC, Smith GB (2009) Application of carbon nanotube technology for removal of contaminants in drinking water: a review. Sci Total Environ 408:1–13
52. Guo J, Wang R, Tjiu WW, Pan J, Liu T (2012) Synthesis of Fe nanoparticles @graphene composites for environmental applications. J Hazard Mater 225–226:63–73
53. Burrs SL, Bhargava M, Sidhu R, Lewis JK et al (2016) A paper based graphene-nano cauliflower hybrid composite for point of care biosensing. Biosens Bioelectron 85:479–487

54. Jijie R, Kahlouche K, Barras A et al (2018) Reduced graphene oxide/polyethylenimine based immunosensor for the selective and sensitive electrochemical detection of uropathogenic *Escherichia coli*. Sens Actuators B Chem 260:255–263
55. Fei J, Dou W, Zhao G (2016) Amperometric immunoassay for the detection of *Salmonella pullorum* using a screen—printed carbon electrode modified with gold nanoparticle-coated reduced graphene oxide and immunomagnetic beads. Microchim Acta 183:757–764
56. Hernández R, Vallés C, Benito AM, Maser WK, Rius FX, Riu J (2014) Graphene-based potentiometric biosensor for the immediate detection of living bacteria. Biosens Bioelectron 54:553–557
57. Manzeli S, Ovchinnikov D, Pasquier D, Yazyev OV, Kis A (2017) 2D transition metal dichalcogenides. Nat Rev Mater 2(17033):1–15
58. Ahmadi M, Zahibi O, Jeon S, Yoonessi M, Dasari A, Ramakrishna S et al (2020) 2D transition metal dichalcogenide nanomaterials: advances, opportunities, and challenges in multifunctional polymer nanocomposites. J Mater Chem A 8:845–883
59. Voiry D, Mohite A, Chhowalla M (2015) Phase engineering of transition metal dichalcogenides. Chem Soc Rev 44:2702–2712
60. Chhowalla M, Shin HS, Eda G, Li LJ, Loh KP, Zhang H (2013) The chemistry of two-dimensional layered transition metal dichalcogenide nanosheets. Nat Chem 5:263–275
61. Pumera M, Sofer Z, Ambrosi A (2014) Layered transition metal dichalcogenides for electrochemical energy generation and storage. J Mater Chem A 2:8981–8987
62. Tyagi D, Wang H, Huang W, Hu L, Tang Y, Guo Z et al (2020) Recent advances in two-dimensional-material-based sensing technology toward health and environmental monitoring applications. Nanoscale 12:3535–3559
63. Li B, Zhong WH (2011) Review on polymer/graphite nanoplatelet nanocomposites. J Mater Sci 46:5595–5614
64. Tan C, Zhang H (2015) Two-dimensional transition metal dichalcogenide nanosheet-based composites. Chem Soc Rev 44:2713–2731
65. Lu Q, Yu Y, Ma Q, Chen B, Zhang H (2016) 2D transition-metal-dichalcogenide-nanosheet based composites for photocatalytic and electrocatalytic hydrogen evolution reactions. Adv Mater 28(10):1917–1933
66. Yang T, Yang R, Chen H, Nan F, Ge T, Jiao K (2015) Electrocatalytic activity of molybdenum disulfide nanosheets enhanced by self-doped polyaniline for highly sensitive and synergistic determination of adenine and guanine. ACS Appl Mater Interfaces 7:2867–2872
67. Kukkar M, Tuteja SK, Sharma AL, Kumar V, Paul AK, Kim KH et al (2016) A new electrolytic synthesis method for few-layered $MoS_2$ nanosheets and their robust biointerfacing with reduced antibodies. ACS Appl Mater Interfaces 8:16555–16563
68. Eng SK, Pusparajah P, Mutalib NS, Ser HL, Chan KG, Lee LH (2015) *Salmonella*: a review on pathogenesis, epidemiology and antibiotic resistance. Front Life Sci 8:284–293
69. Mishra A, Narang J, Pundir CS, Pilloton R, Khanuja M (2018) Morphology-preferable $MoSe_2$ nanobrooms as a sensing platform for highly selective apta-capturing of *Salmonella* bacteria. ACS Omega 3:13020–13027
70. Partida-Martinez LP, Hertweck C (2005) Pathogenic fungus harbours endosymbiotic bacteria for toxin production. Nature 437:884–888
71. Peng G, Li X, Cui F, Qiu Q, Chen X, Huang H (2018) Aflatoxin B1 electrochemical aptasensor based on tetrahedral DNA nanostructures functionalized three dimensionally ordered macroporous $MoS_2$-AuNPs film. ACS Appl Mater Interfaces 10:17551–17559
72. Pfohl-Leszkowicz A, Manderville RA (2007) Ochratoxin A: an overview on toxicity and carcinogenicity in animals and humans. Mol Nutr Food Res 51:61–99
73. Wang Y, Ning G, Bi H, Wu Y, Liu G, Zhao Y (2018) A novel ratiometric electrochemical assay for ochratoxin A coupling Au nanoparticles decorated $MoS_2$ nanosheets with aptamer. Electrochim Acta 285:120–127
74. Jiang K, Nie D, Huang Q, Fan K, Tang Z, Wu Y, Han Z (2019) Thin-layer $MoS_2$ and thionin composite-based electrochemical sensing platform for rapid and sensitive detection of zearalenone in human biofluids. Biosens Bioelectron 130:322–329

75. Pang P, Teng X, Chen M, Zhang Y, Wang H, Yang C et al (2018) Ultrasensitive enzyme-free electrochemical immunosensor for microcystin-LR using molybdenum disulfide/gold nanoclusters nanocomposites as platform and Au@Pt core-shell nanoparticles as signal enhancer. Sens Actuators B 266:400–407
76. Naguib M, Mochalin VN, Barsoum MW, Gogotsi Y (2014) MXenes: a new family of two-dimensional materials. Adv Mater 26:992–1005
77. Anasori B, Xie Y, Beidaghi M, Lu J, Hosler BC, Hultman L et al (2015) Two dimensional, ordered, double transition metals carbides (MXenes). ACS Nano 9:9507–9516
78. Sinha A, Dhanjai ZH, Huang Y, Lu X, Chen J et al (2018) MXene: an emerging material for sensing and biosensing. TrAC Trends Anal Chem 105:424–435
79. Nagarajan V, Chandiramouli R (2020) Dimethyl and ethyl methyl ether adsorption studies on β-antimonene nanosheets—a first-principles study. Mol Simul 46:1354–1361
80. Rasool K, Helal M, Ali A, Ren CE, Gogotsi Y, Mahmoud KA (2016) Antibacterial activity of $Ti_3C_2T_x$ MXene. ACS Nano 10:3674–3684
81. Zhang Y, Wang L, Zhang N, Zhou Z (2018) Adsorptive environmental applications of MXene nanomaterials: a review. RSC Adv 8:19895–19905
82. Khan R, Andreescu S (2020) MXenes-based bioanalytical sensors: design, characterisation, and applications. Sensors 20:5434–5443
83. Kalambate PK, Gadhari NS, Li X, Rao Z, Navale ST, Shen W (2019) Recent advances in MXene-based electrochemical sensors and biosensors. TrAC Trends Anal Chem 120:115643–115659
84. Wang H, Li H, Huang Y, Xiong M, Wang F, Li C (2019) A label-free electrochemical biosensor for highly sensitive detection of gliotoxin based on DNA nanostructure/MXene nanocomplexes. Biosens Bioelectron 142:111531–111538
85. Brown GD, Denning DW, Gow NAR, Levitz SM, Netea MG, White TC (2012) Hidden killers: human fungal infections. Sci Transl Med 4:165rv13
86. Liu H, Neal AT, Zhu Z, Luo Z, Xu X, Tomanek D, Ye PD (2014) Phosphorene: an unexplored 2D semiconductor with a high hole mobility. ACS Nano 8:4033–4041
87. Li L, Yu Y, Ye GJ, Ge Q, Ou X, Wu H et al (2014) Black phosphorus field-effect transistors. Nat Nanotechnol 9:372–377
88. Rodin AS, Carvalho A, Castro Neto AH (2014) Strain-induced gap modification in black phosphorus. Phys Rev Lett 112:176801
89. Gusmao R, Sofer Z, Pumera M (2017) Black phosphorus rediscovered: from bulk material to monolayers. Angew Chem Int Ed 56:8052–8072
90. Cartz L, Srinivasa SR, Riedner RJ, Jorgensen JD, Worlton TG (1979) Effect of pressure on bonding in black phosphorus. J Chem Phys 71:1718–1721
91. Tran V, Soklaski R, Liang Y, Yang L (2014) Layer-controlled band gap and anisotropic excitons in few-layer black phosphorus. Phys Rev B Condens Mater Phys 89:235319
92. Hussain T, Kaewmaraya T, Chakraborty S, Ahuja RJ (2016) Defect and substitution-induced silicene sensor to probe toxic gases. Phys Chem C 120:25256–25262
93. Zhang CD, Lian JC, Yi W, Jiang YH, Liu LW, Hu H et al (2009) Surface structures of black phosphorus investigated with scanning tunneling microscopy. J Phys Chem C 113:18823–18826
94. Abbas AN, Liu B, Chen L, Ma Y, Cong S, Aroonyadet N et al (2015) Black phosphorus gas sensors. ACS Nano 9:5618–5624
95. Kou L, Frauenheim T, Chen C (2014) Phosphorene as a superior gas sensor: selective adsorption and distinct I–V response. J Phys Chem Lett 5:2675–2681
96. Kistanov AA, Cai Y, Zhou K, Dmitriev SV, Zhang YW (2016) Large electronic anisotropy and enhanced chemical activity of highly rippled phosphorene. J Phys Chem C 120:6876–6884
97. Meng Z, Stolz RM, Mendecki L, Mirica KA (2019) Electrically-transduced chemical sensors on two-dimensional nanomaterials. Chem Rev 119:478–598
98. Xiang Y, Camarada MB, Wen Y, Wu H, Chen J, Li M, Liao X (2018) Simple voltammetric analyses of ochratoxin A in food samples using highly-stable and anti-fouling black phosphorene nanosensor. Electrochim Acta 282:490–498

99. Pfohl-Leszkowicz A, Manderville RA (2007) Ochratoxin A: an overview on toxicity and carcinogenicity in animals and humans. Mol Nutr Food Res 51(1):61–99
100. Oliveira SCB, Diculescu VC, Palleschi G, Compagnonec D, Oliveira-Bretta AM (2007) Electrochemical oxidation of ochratoxin A at a glassy carbon electrode and in situ evaluation of the interaction with deoxyribonucleic acid using an electrochemical deoxyribonucleic acid-biosensor. Anal Chim Acta 588:283–291
101. Ramalingam S, Chand R, Singh CB, Singh A (2019) Phosphorene-gold nanocomposite based microfluidic aptasensor for the detection of okadaic acid. Biosens Bioelectron 135:14–21
102. Li J, Chen X, Yang Z, Liu X, Zhang X (2021) Highly anisotropic gas sensing of atom-thin borophene: a first-principles study. J Mater Chem C 9:1069–1076
103. Hussain T, Chakraborty S, Ahuja R (2013) Metal-functionalized silicene for efficient hydrogen storage. ChemPhysChem 14:3463–3466
104. Tang Q, Zhou Z (2013) Graphene-analogous low-dimensional materials. Prog Mater Sci 58:1244–1315
105. Voon LCLY, Guzmán-Verri GG (2014) Is silicene the next graphene? MRS Bull 39:366–373
106. Bianco E, Butler S, Jiang S, Restrepo OD, Windl W, Goldberger JE (2013) Stability and exfoliation of germanane: a germanium graphane analogue. ACS Nano 7:4414–4421
107. Monshi MM, Aghaei SM, Calizo I (2017) Doping and defect-induced germanene: a superior media for sensing $H_2S$, $SO_2$, and $CO_2$ gas molecules. Surf Sci 665:96–102
108. Hussain T, Vovusha H, Kaewmaraya T, Amornkitbamrung V, Ahuja R (2018) Adsorption characteristics of DNA nucleobases, aromatic amino acids and heterocyclic molecules on silicene and germanene monolayers. Sens Actuators B Chem 255:2713–2720
109. Han WQ (2010) Anisotropic hexagonal boron nitride nanomaterials: synthesis and applications. Nanotechnol Life Sci 3:411–461
110. Arenal R, Lopez-Bezanilla A (2015) Boron nitride materials: an overview from 0D to 3D (nano)structures. Wiley Interdiscip Rev Comput Mol Sci 5:299–309
111. Chen X, Wu P, Rousseas M et al (2009) Boron nitride nanotubes are noncytotoxic and can be functionalized for interaction with proteins and cells. J Am Chem Soc 131:890–891
112. Balmain WH (1842) Remarks on the formation of compounds of boron and silicon with nitrogen and certain metals. Prakt Chem 27:422–430
113. Wood GL, Janik JF, Pruss EA et al (2006) Aerosol synthesis of spherical morphology boron nitride powders from organoborate precursors. Chem Mater 18:1434–1442
114. Lian G, Zhang X, Zhu L, Tan M et al (2010) A facile solid state reaction route towards nearly monodisperse hexagonal boron nitride nanoparticles. J Mater Chem 20:3736–3742
115. Yang G, Zhang D, Wang C et al (2019) A novel nanocomposite membrane combining BN nanosheets and GO for effective removal of antibiotic in water. Nanomaterials 9:386–398
116. Chao Y, Zhu W, Chen J et al (2014) Development of novel graphene-like layered hexagonal boron nitride for adsorptive removal of antibiotic gatifloxacin from aqueous solution. Green Chem Lett Rev 7:330–336
117. Liu D, Lei WW, Qin S et al (2016) Superior adsorption of pharmaceutical molecules by highly porous BN nanosheets. Phys Chem Phys 18:84–88
118. Bando CZY, Tang C, Golberg D (2005) Immobilization of proteins on boron nitride nanotubes. J Am Chem Soc 127:17144–17145
119. Lei W, Liu D, Chen Y (2015) Highly crumpled boron nitride nanosheets as adsorbents: scalable solvent-less production. Adv Mater Interfaces 2:1400529
120. Mannix AJ, Zhang Z, Guisinger NP et al (2018) Borophene as a prototype for synthetic 2D materials development. Nat Nanotechnol 13:444–450
121. Mannix AJ, Zhou XF, Kiraly B et al (2015) Synthesis of borophenes: anisotropic, two-dimensional boron polymorphs. Science 350:1513–1516
122. Nagarajan V, Chandiramouli R (2017) Borophene nanosheet molecular device for detection of ethanol—a first-principles study. Comput Theor Chem 1105:52
123. Shahbazi AK, Ansari G (2016) B36 borophene as an electronic sensor for formaldehyde: quantum chemical analysis. Phys Lett A 380:2664

124. Omidvar A (2017) Borophene: a novel boron sheet with a hexagonal vacancy offering high sensitivity for hydrogen cyanide detection. Comput Theor Chem 1115:179
125. Chandiramouli R, Nagarajan V (2017) Borospherene nanostructure as CO and NO sensor—a first-principles study. Vacuum 142:13
126. Kim HS, Kim YH (2015) Recent progress in atomistic simulation of electrical current DNA sequencing. Biosens Bioelectron 69:186–198
127. Das A, Sood AK, Maiti PK et al (2008) Binding of nucleobases with single-walled carbon nanotubes: theory and experiment. Chem Phys Lett 453:266–273
128. Garg P, Choudhuri I, Mahata A, Pathak B (2017) Bandgap opening in stanene induced by patterned B-N doping. Phys Chem Phys 19(5):3660–3669
129. Zhu F, Chen W, Xu Y, Gao C, Guan D, Liu C, Qian D, Zhang SC, Jia J (2015) Epitaxial growth of two-dimensional stanene. Nat Mater 14:1020–1025
130. Liao M, Zang Y, Guan Z, Li H, Gong Y, Zhu K et al (2018) Superconductivity in few-layer stanene. Nat Phys 14:344–348
131. Gao J, Zhang G, Zhang YW (2016) Exploring Ag(111) substrate for epitaxially growing monolayer stanene: a first-principles study. Sci Rep 6:29107
132. Nigam S, Gupta S, Banyai D, Pandey R, Majumder C (2015) Evidence of a graphene-like Sn-sheet on an Au(111) substrate: electronic structure and transport properties from first principles calculations. Phys Chem Phys 17:6705–6712
133. Vovusha H, Hussain T, Sajjad M, Lee H, Kartonb A, Ahuja R, Schwingenschlögl U (2019) Sensitivity enhancement of stanene towards toxic $SO_2$ and $H_2S$. Appl Surf Sci 495:143622
134. Ares P, Aguilar-Galindo F, Rodríguez-San-Miguel D, Aldave DA, Díaz-Tendero S, Alcamí M et al (2016) Mechanical isolation of highly stable antimonene under ambient conditions. Adv Mater 28:6332–6336
135. Zhang S, Yan Z, Li Y, Chen Z, Zeng H (2015) Atomically thin arsenene and antimonene: semimetal semiconductor and indirect direct band-gap transitions. Angew Chem 127:3155–3158
136. Meng RS, Cai M, Jiang JK, Liang QH, Sun X, Yang Q, Tan CJ, Chen XP (2017) First principles investigation of small molecules adsorption on antimonene. IEEE Electron Device Lett 38:134–137
137. Wang DW, Yang AJ, Chu JF, Lv PL, Yang L, Wang XH, Rong MH (2017) Antimonene: a promising candidate for acetone sensors with high selectivity and sensitivity. IEEE Sens 1–3
138. Chlazanas A, Tsirka K, Paipetis AS, Prodromidis MI (2020) 2D bismuthene/graphene modified electrodes for the ultra-sensitive stripping voltammetric determination of lead and cadmium. Electrochim Acta 336:135726
139. Jyothi MS, Nagarajan V, Chandiramouli R (2020) Benzyl alcohol and 2-methyldecalin vapor adsorption studies on β-bismuthene sheets—a DFT outlook. Chem Phys Lett 755:137819
140. Snehh P, Nagarajan V, Chandiramouli R (2018) Novel bismuthene nanotubes to detect $NH_3$, $NO_2$ and $PH_3$ gas molecules—a first-principles insight. Chem Phys Lett 712:102–111
141. Qiao J, Pan Y, Yang F, Wang C, Chai Y, Ji W (2018) Few-layer tellurium: one-dimensional-like layered elementary semiconductor with striking physical properties. Sci Bull 63:159–168
142. Yan J, Zhang X, Pan Y, Li J, Shi B, Liu S et al (2018) Monolayer tellurene–metal contacts. J Mater Chem C 6:6153–6163
143. Cui H, Zheng K, Tao L, Yu J, Zhu X, Li X, Chen X (2019) Monolayer tellurene-based gas sensor to detect SF6 decompositions: a first-principles study. IEEE Electron Device Lett 40:1522–1525
144. Wang L, Lin Z, Du Y, Guo H, Zheng K, Yu J, Chen X, Lang L (2021) Properties-enhanced gas sensor based on Cu-doped tellurene monolayer to detect acetone molecule: a first-principles study. Mol Phys. https://doi.org/10.1080/00268976.2020.1864490
145. Guo H, Zheng K, Cui H, Yu J, Tao L-Q, Li X, Liao C, Xie L, Chen X (2020) Tellurene based biosensor for detecting DNA/RNA nucleobases and amino acids: a theoretical insight. Appl Surf Sci 532:147451

# Chapter 9
# Newly Emerged 2D Mesoporous Silica Nanoparticles: Role in Target-Setting Biomedicines


**Prateek Srivastava, Sumit Kumar Hira, and Partha Pratim Manna**

## 1 Introduction

A smart nanosystem behaves as a nanodevice which ameliorates the drug pharmacokinetics and its biodistribution [1]. The physicochemical behavior of several drugs remains unsupportive having less water solubility and fewer dissolution rates which magnify in altered bioavailability and thereby lessens the treatment efficacy. The contemporary administration routes of water-insoluble drugs require organic solvents, mingling further with the catabolic steps of the blood elements which can degrade the therapeutic peptide or proteins during injections. National Institute of Health (NIH) has approved certain chemotherapeutic drugs like Doxorubicin, Cisplatin, 5-Fluorouracil, 6-Mercaptopurine which are also featured in the World health organization's list of essential medicines for medicaments of cancer malignancies. Despite the application of drugs to subdue the tumor growth, the non-specific nature of many drugs could lead to deleterious off-target side effects with reduced therapeutic efficacy. Thus, in order to magnify the solubility, stability, and tuning its outcome toward the effector/inflamed sites, various nanosystem delivery mechanisms have been laid out as a nanomedicine device for treating various ailments [2]. The term nanomedicine manifests the biological/medical implementation of the nanomaterials for improved diagnosis and therapy against diseases, and thereby improving

P. Srivastava · P. P. Manna (✉)
Immunobiology Laboratory, Department of Zoology, Banaras Hindu University, Varanasi, India
e-mail: pp_manna@yahoo.com

P. Srivastava
e-mail: prateekbhu.chem77@gmail.com

S. K. Hira
Cellular Immunology Laboratory, Department of Zoology, The University of Burdwan, Burdwan, India
e-mail: sumit.hira2008@gmail.com



Z. Khanam et al. (eds.), *2D Nanomaterials for Energy and Environmental Sustainability*,
Materials Horizons: From Nature to Nanomaterials,
https://doi.org/10.1007/978-981-16-8538-5_9

the wellbeing of patients. These nanoscale materials bring in the multifaceted modifications pertaining to tether/attach specific ligand targeted for the drug delivery and imaging in the biological system [3]. For remedial benefits of nanomedicine in the cancer therapy, the US Food and Drug Administration (FDA) has approved some of them in clinical trial like Doxil, Abraxane, and Lipoplatin. Indeed, the results for their application are superior than free drug administration and further open several key parameters which need to be highlighted like enclose of the drug, release of impetuous drug escaping from reticuloendothelial system (RES) during circulations, cytotoxicity of the engineered nanomaterials, and cost-effectivity of the nanocarriers [4].

Many efforts were made for the use of unique biocompatible and biodegradable inorganic nanomaterials which offer great versatility for the expansion of advanced drug delivery system. Inorganic 2D nanomaterials are considered as the thinnest nanomaterials because they were composed of only few sheets (nanoscale/macroscale dimension level). They have layered structure which is held by weak van der Waals molecular interactions. Two-dimensional nanomaterials like graphene offer brilliant molecular binding with the hydrophobic drugs via supramolecular stacking and hydrophobic interactions because of special $sp^2$ bond of carbon atoms. Since then, new 2D materials have been emerged including transition metal dichalcogenides ($MoS_2$, $TiS_2$), graphene, bismuth, tellurium, etc., having varying energy band, electrical properties, used in the energy storage, photoelectronics, and water splitting devices. The brilliant aspects of 2D material include photodynamic and heat conversion properties and have gained many advantages in the medical fields, like therapy, sensing, targeting, and imaging. The development and appreciation of the smart drug delivery system have created numerous opportunities and some inevitable drawbacks in treatment schedule for cancer. The most obvious demerit is the low drug loading capacity which reduces the efficacy during multi-mode treatment. However, 2D materials offer plentiful performance in drug loading. Owing to their lamellar structure, 2D nanomaterial ensures ambient surface area for maximum drug loading.

Among various inorganic 2D nanomaterials, mesoporous silica nanoparticles (MSNs) work as an excellent candidate for an efficacious delivery system, which presents brilliant biocompatibility, functional groups employment, convenient pore size, large storage capability for drugs, and vast surface area to accommodate desired chemical modifications [5]. Silica in its amorphous (pyrogenic) form is currently used in cosmetics and distinctive care products, additives in pharmaceutical and nutraceutical industries and made it a safe and harmless agent certified by FDA [6]. Further, Wiesner group received FDA safety approval for the build out of the "Cornell Dots" (core–shell silica nanoparticles) and the clinical first phase trial was successful [7]. The silica nanomaterials became the most promising inorganic nanosystem for biomedical applications. MSNs offer generous surface area and pore volumes which are crucial parameters for substantial drug loading. The cargo inside the MSN such as enzymes, drug molecules, therapeutic peptides, and oligonucleotides can be fastidiously encapsulated and protected from the harsh environments including stomach before entering the target site. Further, the liberation of loaded guest molecules from

MSNs can be fine-tuned to the internal and external signal inputs which augment the drug arm loading at the targeted area, thus bettering the overall therapeutic outcome. The loading can be performed in normal phosphate buffer saline (PBS) and thus exclude toxic organic solvents for drug loading. MSNs could act as an inorganic support floorboard for the fabrication and evolution of various cap systems which can be switched off/on via internal or external stimuli [8]. Thus, MSNs may have increased opportunity for application in the precinct of nanomedicine including drug delivery, targeting, and diagnosis on account of their modular design characteristics [9]. Another aspect of silica inorganic nanomaterials in bioengineering process is to generate 2D nanostructures which offer excellent platforms for many potential applications. Among the best 2D functional nanocomposites, 2D graphene sheet serves as a template for the assembly or coating other 2D silica-based nanomaterials. Besides that, versatile chemical properties can be doped on silica surfaces in order to achieve multiple applications [10–12]. The present chapter discusses the role of emerging 2D MSNs in target-setting biomedicines. The different synthesis approaches along with the mechanism of drug delivery using MSN have been presented in detail.

## *1.1 Focus on Nanopharmaceuticals*

For the materials science advancement in nanoscale platform, NIH encourages nanoscience-related research and development in the year 2000 under the National Nanotechnology Initiative (NNI) program. The program aims to study, design, and explore novel nanomaterials which may contribute significant progress in health science-related research [13]. The term nanomedicine emerged by blending nanomaterial science with medicine following the wisdom of nanotechnology. Later, people in the pharmaceutical field adopted the nanoscience terminology as "nanopharmaceuticals." Nanopharmaceuticals are the deployment of the nanosized materials for the transportation of drug/cargo of interest [14]. The colloidal system is a nanosystem, explored as delivery agent 40 years ago. Certain examples include the encapsulation of the anthracyclines (liposome) in 1970s [15] (Table 1). The entrapped drug manifests shoot-up in anti-tumor effect with reduced cardiotoxicity. Yet, suitability and performance of the construct faced several hurdles to purge the malignant cells. There are some key features which are essential to generate nanodevice for the cancer therapy: (a) high drug concentration at the tumor site, (b) loading capabilities, (c) stimuli-responsive release, (d) stability of the drug from hydrolysis during circulation, (e) congeniality and biodegradability, and (f) easily reproducible synthesis of the nanocarrier [16]. Thus, it is critically important to pick up a nanocarrier which inherits the above-mentioned important parameters.

**Table 1** Examples of approved cancer nanomedicines undergoing clinical trial

| Nature of the nanoparticle | Name | Cancer target | Status | References |
|---|---|---|---|---|
| Liposome | Doxil | Sarcoma | Approved | [17] |
| Liposome | Marqibo | Leukemia | Approved | [18] |
| Liposome | Lipoplatin | Pancreatic/head/malignant pleural effusion | Phase I | [19] |
| Paclitaxel in 20–50 nm micelles | Genexol® | Passive targeting via EPR effect | South Korea 2001 breast and pancreatic cancer (IV) | [20] |
| Paclitaxel covalently linked to polyglutamate nanoparticles | Opaxio® | Passive targeting via EPR effect | FDA 2012 glioblastoma | [21] |
| Albumin conjugated paclitaxel | Abraxane® | Passive targeting via EPR effect | FDA 2005 breast cancer | [22] |

*Source* Author

## 2 Fabrication Methods of Nanoparticles

Nanostructures can be synthesized by two ways: one is the bottom-up and other is top-down approach. In the bottom-up process, the particles are formed atom by atom while the top-down process involves the exodus or re-clustering of atoms to create the desired structure [23]. In the bottom-up system, atom, molecules behave as constituent blocks for the formation of complex nanostructure materials. Further, in the bottom-up approach, the nanosized structure can be finely tuned by altering the dimensions of building blocks which can control their organization and assembly. Hence, the bottom-up approach is highly controlled for complex chemical synthesis. Among the different bottom-up approaches, sol–gel process is helpful in terms of obtaining high chemical homogeneity, managing the size, and morphology at moderate temperatures executed in aqueous solution [24]. The sol–gel process consists of hydrolysis and condensation of a metal alkoxide (liquid precursor) to a solid. The protocols for the sol–gel synthesis involve three steps: first, hydrolysis of metal oxide, followed by the condensation between themselves and bring out water molecules generating gel structures, and finally, the drying process [25] (Scheme 1). The whole procedure can be set out by distinct steps (Scheme 1): formation of steady solution of precursors (the sol); the sol reaction in basic medium at around 80 °C producing a porous network (the gel); bridged, rigid, surrounded by a continuous liquid phase via gelation; drying (removal of liquid from the gel network); densification; and breakdown of the gel at high temperature [26].

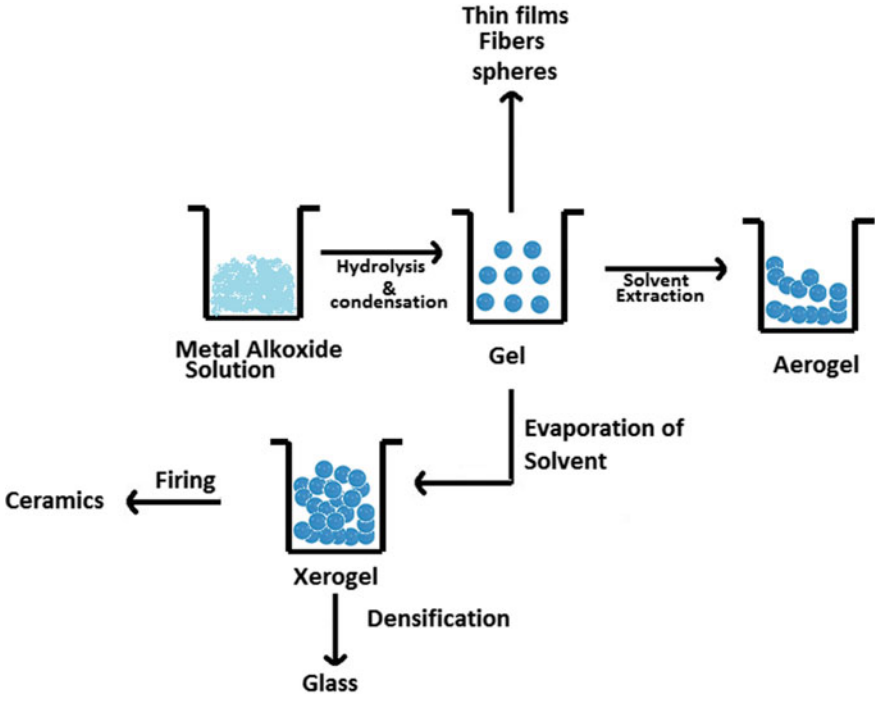


**Scheme 1** Schematic view of sol–gel processing. *Source* Author

## *2.1 Synthesis of MSN*

Ordered mesoporous materials can be synthesized with various pore dimensions via utilization of specific surfactant and framework compositions. In the early 1990s Mobil Oil Company first synthesized mesoporous silica, utilizing the cationic surfactants as fabricating agents through which inorganic material can be deposited undergoing hydrolysis and condensation via sol–gel approach, creating a mesoscopically ordered hybrid inorganic material [27, 28]. After thermal calcinations or chemical extraction, the porous construct of inorganic silica materials was obtained. The shaping of mesoporous materials was supervised by two crucial parameters, first (a) casting of surfactant molecules to develop the micelle structure and secondly, (b) potential of the inorganic oxide to undergo hydrolysis and condensation to bring out thermally stable structure. Synthesis of mesoporous materials may involve a self-assembly process, similar to the biological condition. Four major components required for the assembly of silica nanoparticles includes the silicon source, surfactants, solvent, and the base catalysis. The self-assembled liquid–crystal arrays of surfactants direct the generation of MSN material. In the liquid–crystal templating mechanism (LCT), when the surfactant was dissolved in the aqueous solution it generates a liquid crystal. However, above the critical micelle concentration (CMC),

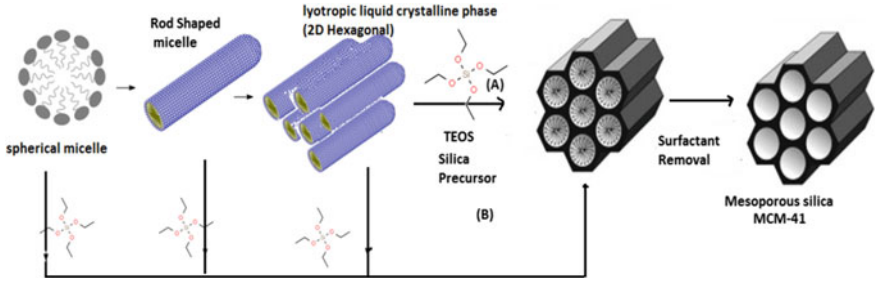


**Fig. 1** Development of mesoporous silica by structure-directing agents: **a** true liquid–crystal template mechanism, **b** cooperative liquid–crystal template mechanism. *Source* Author

they form a micelle structure. The shape and size of the micelle depend upon the surfactant type, pH, surfactant concentration, and temperature [29, 30]. In experimental setup, the micelles aggregates to form supramolecular structure containing hexagonal, cubic, or laminar geometry which determines the mesoporous framework structure [31]. An alternative route was also proposed including allied connections between surfactant and the silica precursor for generating the final mesoporous ordered material. MSN materials can also be generated when the surfactant concentration is below CMC and present at lyotropic liquid-crystalline phase which acts as a cooperative congregate of surfactant and tetraethyl orthosilicate (TEOS) [32]. In a typical synthesis procedure, the surfactant-silica precursor interactions are optimized under basic reaction condition. The silica precursors like tetramethyl orthosilicate (TMOS) or tetraethyl orthosilicate (TEOS) are normally added in the basic reaction mixture consisting of cationic surfactant cetyltrimethylammonium bromide (CTAB) at around 60–80 °C (Fig. 1). The organization framework in MSN can be regulated by the surfactant which was demonstrated by Stucky research group, utilizing the block-copolymer surfactants [33]. Further, by altering the hydrocarbon chain length of the surfactant molecules, the controllable pore size in MSN structure can be generated ranging from 2 to 30 nm [34]. The most familiar representatives of this class are MCM-41 possessing 2D-hexagonal *p6mm* structure, MCM-48 with 3D-bicontinuous cubic *Ia3d* structure and MCM-50 with lamellar *p2* structure [35] (Fig. 2). According to IUPAC, the porous materials, inherit the pore diameter ranging from 2 to 50 nm, are termed as mesoporous material. Our work underpins on the generation of mesoporous MCM-41 class of materials with well-defined pore size distribution, large surface area ($\geq$700 $m^2$/g), and pore diameter ranging from 1.5 to 10 nm.

## *2.2 Reaction Kinetics and Template Removal*

The silica source and cationic surfactant interaction are the non-covalent interactions including electrostatic and hydrogen-bonding among the head groups of surfactant

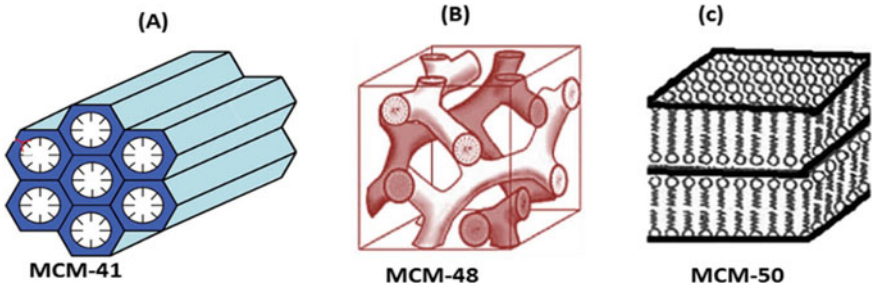


**Fig. 2** Various structures of M41S materials: **a** MCM-41 (2D hexagonal with space group p6mm), **b** MCM-48 (cubic shape with space group Ia3d), and **c** MCM-50 (lamellar form with space group p2). *Source* Author

and silica precursor without phase separation. Most commonly used silica precursors are alkoxysilanes, e.g., tetramethyl orthosilicate (TMOS), tetraethyl orthosilicate (TEOS), tetrapropyl orthosilicate (TPOS), and tetrabutyl orthosilicate (TBOS). Different alkoxysilanes, particularly the branched, bulkier precursors exhibit reduced hydrolysis rate, caused by the steric barrier and result in larger particle size [24]. Therefore, it is the basic condition which is generally adjusted to generate negatively charged particles to avoid inter-particle aggregation. pH of the reaction mixture regulates the MSN size, and lowering in pH increases the particle size [36]. The isoelectric point of silica is 2, so raising pH from 6.0 to 9.0 could result in speedy condensation rates with fast association and growth of silica–surfactant nuclei [37]. Further, the initial silicate and surfactant concentrations can be modulated for alteration in size of the silica nanoparticles under diluted condition [38]. After the completion of the reaction, the template was removed from the silica network to yield the porous network structures. Majority of the conventional method used for template removal is calcination. In this process, the silica nanoparticles are subjected to heat with heating rates of 1 °C/min up to at least 550 °C, followed by isothermal heating for 4–8 h [39]. However, this process influences the morphological framework of the silica nanoparticles including surface area, pore size, and pore capacity. The heat treatment could bring in contraction of silica structure which perhaps the fast magnitude of condensation of silica network and may affect particle aggregation/agglomeration in aqueous media [39]. An alternative template extraction method includes acid treatment, liquid extraction, and supercritical fluid extraction, rooted in the synthesis employed. The silica nanomaterials which are synthesized in basic condition, an ion exchange process involving acids or cationic proton donors is essential to break the non-covalent interactions between negatively charged silica network and the cationic surfactant head groups. Other extraction methodology for MCM-41 type materials involves drawing out using ethanolic solution of ammonium nitrate or acidic ethanol.

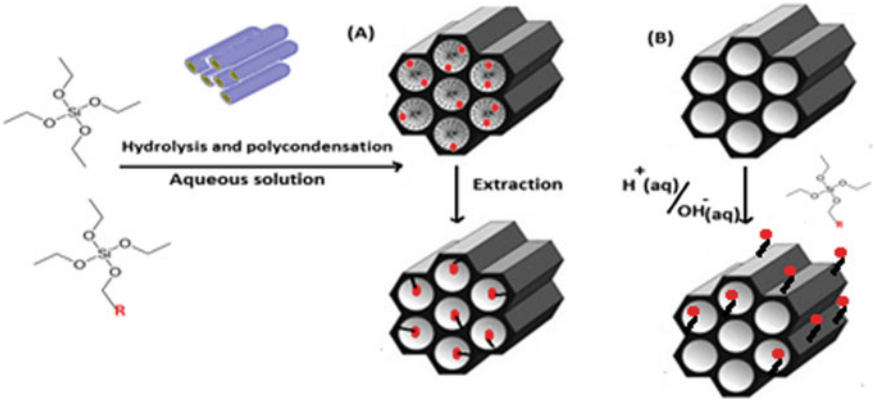


**Fig. 3** Functionalization procedures of MSN by **a** co-condensation method and **b** post-synthesis grafting method. *Source* Author

## *2.3 Surface Functionalization of MSN*

The notable advantages of using MSN material as delivery vehicle are the proficiency to incorporate desired functional groups employment. Beneficial aspect of MSN includes three functional domains—the silica framework, external particle surface, and interior pore surfaces [40]. MSN provides a broad range of flexibility to modify surfaces which generates wide varieties of silica-based hybrid materials that possess specific functions for the delivery of drug. Commonly used organic precursors are organotrialkoxysilanes [$(R'O)_3SiR$] or organotrichlorosilanes [$Cl_3SiR$]. There are two popular classical pathways for the surface functionalization. In one method, fusion of organosilanes with silica precursors results in the synthesis of MSN materials ("co-condensation"). The other pathway is to produce unfunctionalized MSN materials first and later transform their surfaces with organosilanes ("grafting") [41] (Fig. 3).

## *2.4 Surfaces Functionalization by Co-condensation Method*

Co-condensation is the direct process where the organosilanes are condensed besides the silica precursors during the production of silica nanoparticles. This leads to homogenous allocation of the organic groups to the mesostructure. Lin and coworkers proposed that varying organosilanes, associates with the surfactant through non-covalent bonds could result changes in the structural morphology. They showed that the organosilanes with hydrophobic group interact with hydrophobic tail of the surfactant molecules, stabilize the creation of long cylinder micelles, and manifest rod-shaped silica [42]. Contrarily, the hydrophobic organosilanes inhibit the

micelle growth and results in spherical shaped particles. Thus, by using two organosilanes with converse head group properties in varying ratios, the surface functionality and the particle architecture of MSN can be tuned with co-condensation method [43]. To preserve the structural parameters like pore and long-extend pore ordering, the proportion of organosilanes incorporated following co-condensation approach should not surpass 25% of the surface, assigned to the modification in condensation rates among organosilanes and silica precursors (Fig. 3a). Multiple efforts were made to incorporate various organic functional groups into the porous samples through direct synthesis method in order to augment the hybridization effectiveness. Recently, Xie et al. developed periodic mesoporous silica, functionalized with organic precursor via co-condensation using (R'O)3Si-H and (R'O)3Si-R type terminal trialkoxyorganosilanes [44]. By using this synthetic route, they have obtained materials with higher co-condensation having organic precursor. There are some other methods which could offer the organic functionality to be incorporated either on the pore surface or on the walls [45].

## *2.5 Surface Functionalization by Post-synthesis Grafting Method*

Post-synthetic tempering of mesoporous material is usually carried out after the removal of surfactant via annexation of functional moiety on the exterior by chemical conjugation (grafting), surface polymerization or by adsorption of the functional groups [46]. In adjoining method, vast majority of the functionalization occur between free silanol and the organic precursors. Majority of the open silanol groups were present around the lateral surface and at the orifices, which heads to the gathering of organic precursors on that specific area. Since organic grafting mostly occurs at the lateral surface, it pertains better with pore structure against the co-condensed material. However, the extent of functionalization by post-grafting procedure is low compared with the co-condensation method because of the restricted number in free surface silanol groups. There are reports which indicated that the functional groups are preferentially affixed to the outer/external surface or the pore opening since free silanol groups are most accessible there than the inner pore surface which suffers from lower diffusion rates of organic precursors [47] (Fig. 3b). The surface functionalization over the silica nanoparticles plays a pivotal role in biological and catalysis process. The active targeting ligands like folic acid or hyaluronic acid can be attached over the silica nanoparticles thus offering better drug entrapments inside the cancer cells via receptor-mediated endocytosis. Further, some studies suggest amination (charge) over the silica nanoparticles offers better uptake in cancer cells. The surface-functionalized drug molecule or the PEGylation can help in better circulation time and also offers zero premature release in the bloodstream. Functionalization (like –COOH, $–NH_2$, –SH, $=CH_2$, etc.) over the silica offers a vast range of chemical reactions. This can have diverse functions like development of novel cap system to

entrap the drug inside and inherit specific linker which could be melted down when met with suitable environment like pH or enzymes.

## 3 Biological Performance of MSN

### *3.1 Cellular Interaction and Uptake of MSN*

The lipid bilayer system not only furnishes integrity to the cells but also plays significant roles in cellular signaling events and molecular associations with the biomolecules including nanoparticles. Nanoparticles entail to interweave the cell membrane barrier to dispatch the cargo of interest. The physicochemical possessions of nanoparticles, like its size, shape, outer surface charge, hydrophobicity/hydrophilicity and surface chemistry or functionality could affect the endocytosis behavior of MSN [48, 49]. This relationship links the biological properties with the surface physicochemical nature of nanoparticles and contributes a keystone feature in nanomedicine. Comprehending physicochemical nature of these transported particle, various types of endocytosis pathways following internalization, cargo properties, etc., may tune the cellular uptake mechanism pathways [50]. Recently, MSNs were used as a carrier system for the transport of chromobodies inside the living cells for real-time visualization [51].

### *3.2 Effects of MSN Size*

The particle size is a critical parameter which determine the success of a delivery platform against desired tumor sites. Nanosized particles mimics with various biomolecules or viruses in terms of size and other properties which can be endocytosed in similar fashion. This molecular uptake can be energy-dependent or via recruiting caveolin- or clathrin-coated pits or other pathways, independent of these proteins. Lim et al. observed a brisk and elevated intracellular uptake of smaller MSN compared with the larger ones [47, 52]. This effect was further corroborated by Mou and coworkers which showed an optimal size of 50 nm MSN manifests the highest cellular uptake [36]. Mou and coworkers have developed MSN with varying sizes (between 30 and 280 nm) and point out that particle size was correlated to uptake studies as the largest size represents least uptake by HeLa cells. Also, noticeable endocytosis efficiencies were observed with spherical- and tubular-shaped MSNs. These investigations permitted researchers to regulate the rate of drug delivery accurately (Fig. 4). Not long ago, CT imaging and mathematical modeling helped in better understanding of the route, MSN size, biodistribution, and removal kinetics in rat model of pharmacokinetics study [53].

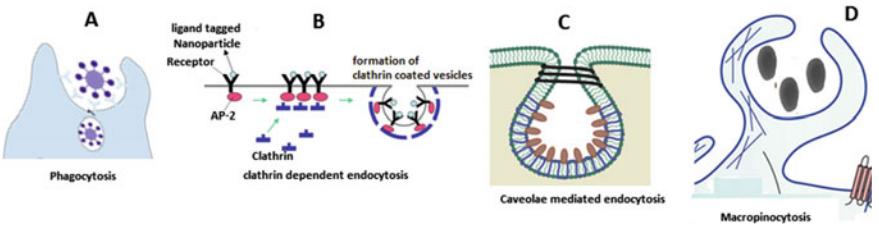


**Fig. 4** Cellular internalization pathways for the nanoparticles: **a** larger nanoparticles were internalized via phagocytosis. Smaller particles are internalized through various mechanisms, such as **b** clathrin-mediated endocytosis, **c** caveolae-mediated endocytosis, and **d** macropinocytosis-dependent pathways. *Source* Author

## *3.3 Effects of MSN Surface Charge*

Surface charge of the nanoparticles governs its molecular incitement with the cell. Usually, the cellular uptake is elevated with the positive charged nanoparticles; however, charge consistency and hydrophobicity of the particles are also significant [54, 55]. Different studies demonstrated the surface charge-dependent uptake mechanisms, but still no general procedure has been identified. Furthermore, positively charged nanosystems have the property of endosomal escape when internalized inside the cells [56]. However, neutrally and negatively charged nanoparticles prefer lysosomal co-localization. A plausible explanation for this phenomenon states that excessive positive charges on the nanoparticles cause proton pumping into the endosome with ingress of chloride ions to conserve the neutral charge, which results in increasing ionic strength within the endosome. This later condition manifests osmotic swelling and physical fracture of the endosomal membrane, an event termed as "proton-sponge" effect resulting in runoff the nanoparticles [57]. This behavior brings in cytoplasmic emplacement of positively charged nanoparticles and enhances drug accumulation throughout the nucleus. Slowing et al., have revealed that surface functionalities govern the uptake of MSN in HeLa cells with positive zeta-potentials which can be taken up more contrast to their counterparts with negative zeta-potential, owing to exorbitant electrostatic affinity to negatively charged cell membranes [58] (Fig. 5). The functional group charges on the MSN surface could affect release and encapsulation efficiency of the drug which also affects cell response [59].

## *3.4 Effect of MSN Hydrophobicity and Surface Properties*

Another crucial criterion for biomedical application of the nanoparticles is its surface hydrophobicity. Nanoparticles require hydrophilicity for stable dispersion in aqueous environment which also prevents opsonization after intravenous administration. However, hydrophobicity of the nanoparticles also encourages cellular uptake. Under in vitro condition, nanoparticles surface comes in direct association with the cell

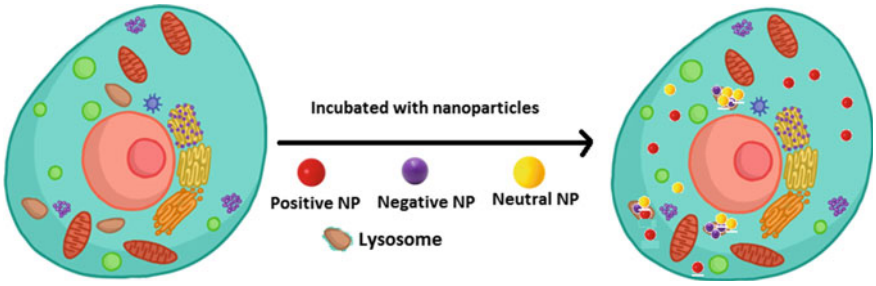


**Fig. 5** Different charges on nanoparticles affect cellular uptake and intracellular distribution. *Source* Author

membrane which bears alkyl lipids and cholesterol, imparting a partially hydrophobic character. Thus, hydrophobic nanoparticles manifest upregulated cellular uptake, compared with the hydrophilic particles. The surface of nanoparticles is important for modification through electrostatic or hydrophilic/hydrophobic interactions. Shastri and co-workers have illustrated that stabilizing both lipophilicity and charge attributes lipid in high specificity toward the endothelial cells [60]. Recently, Desai and her group have shown the difference in release profiles of hydrophobic and the hydrophilic drugs in 2D and 3D cultures [61].

## 4 Biocompatibility and Biodistribution

In order to become a good drug delivery platform, an ideal nanocarrier should have properties like efficient biodistribution, biocompatibility, and clearance from the cellular systems [16]. The critical challenges for a nanocarrier are distribution of drug to the appropriate locations with lesser after-effects compared to conventional therapies. This also includes in vivo biodistribution for maximum benefits plus excretion of vehicle like MSN. The studies suggest that MSN accumulates mainly in liver, kidney, and urinary bladder following intravenous injection and partially excreted through the renal route [62]. However, the biodistribution of MSN allying the tumor and healthy mice is somewhat different as the MSN passively gathered in tumor, owing to leaky blood vessel (EPR effect) and influence the overall biodistribution. Hyeon and coworkers employed the florescent PEGylated MSNs (<100 nm size) and observed their accretion in tumor cells after intravenous administration which is responsible for the EPR effect [63]. At a dose below 200 mg $kg^{-1}$, no toxic effect was perceived in experimental study and thus makes MSN a safe nanocarrier for drug delivery. In their next study, the same group observed that when the PEGylated MSNs (70 nm size) were passively targeted to xeno-implanted MCF-7 tumor, some percentage of MSN was accumulated in the liver, lungs, and spleen due to phagocytosis by mononuclear cells [64]. Similarly, results recorded by Lu et al. have shown biocompatibility and biodistribution of MSN in human cancer xenografts and

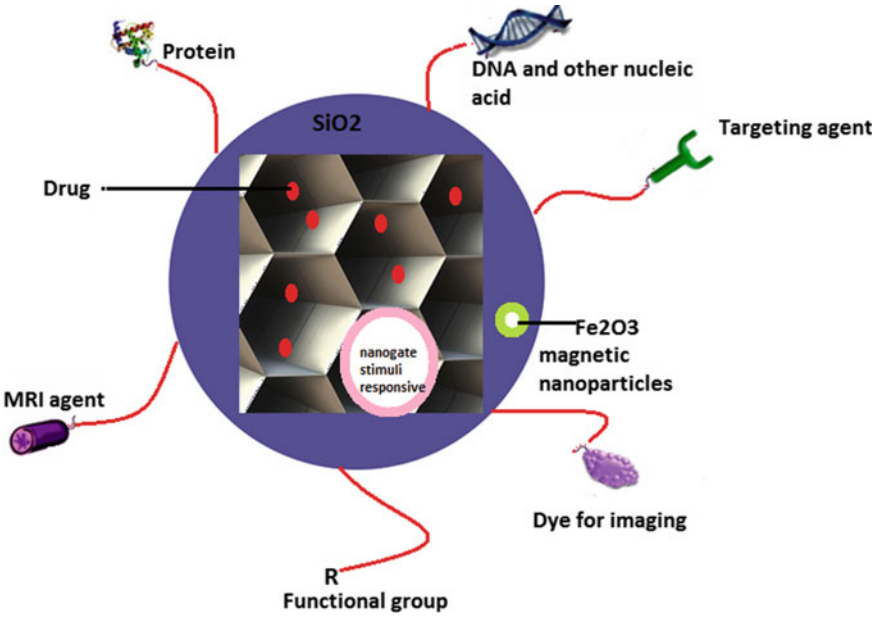


**Fig. 6** MSN as nanomedical multifunctional nanoplatforms. *Source* Author

observed that MSNs are well-tolerated up to 100 mg $kg^{-1}$ dose and favored its accumulation in tumor sites [65]. The surface modifications with protein, lipid bilayers, and polymers over the MSN via electrostatic interactions with Si–OH (outer surface) were reported to eliminate toxicity during in vivo studies [66]. Such physicochemical factors (described above) and functional group over MSN impart effect on blood circulation time, biodistribution, and biocompatibility of administered drug. Therefore, detailed guidance on distinct surface functionalization, size, charge, etc., still needs further investigation (Fig. 6).

## *4.1 Toxicity of Nanomaterials*

Mesoporous silica nanomaterial when enters the body may come in close contact with the immunocompetent cells and thereby induces immunotoxicity. The molecular association of silica nanoparticles with the immune system manifests in varying outcomes, mostly related to the morphologies and the characteristic of the construct. The major effector cells like monocytes/macrophages and polymorphonuclear leukocytes are involved in close encounter with the silica nanoparticles [67]. These particles can be phagocytosed by the dendritic cells, macrophages (antigen-presenting cells), or stimulate lymphocytes. The uptake of silica by these cells can be manifested by the damage of the cell membrane, inducing apoptosis, and necrosis [68]. Further, the

interaction can also influence the signaling pathways within the immune cells. These nanoparticles influenced signaling events can be demonstrated by proinflammatory responses, reactive oxygen species (ROS) generation, etc. Silica nanoparticles are an important candidate for application in biomedical experiments owing to their properties like large surface area, pore size, pore volume, and easy functional group employment. There are reports which indicate that the amorphous silica offers better safety features compared with the crystalline silica. During in vivo study, the silica nanoparticles were observed in the lymphocytic infiltration, which induces granuloma and hydropic degeneration in hepatocytes. When accumulated in spleen it reduces the activation and proliferation of B and T cells. Some studies also suggest that antibody levels of IgG and IgM increase which can cause histological changes [69]. The main reason is the oxidative stress that generates immunotoxicity especially the MAPK and NADPH oxidase pathways. The silica nanoparticle also induces toxic mechanisms by autophagy dysfunction.

## 5 Barriers for Drug Delivery

In order to augment the therapeutic effectiveness, the nanodelivery system must accumulate in the target cells in optimal concentration. However, the route taken by a nanocarrier to the tumor sites is hindered by the physiological and biochemical barriers. The physiological barriers for oral drug delivery include intestinal epithelium, which is highly absorptive and is built with villi, covered with enterocytes, goblet cells, and mucus layer [70]. When the drug-loaded nanocarrier was intravenously administered, it requires to overcome other obstacles and modulate other physiological barriers such as opsonization, abrogation of reticuloendothelial system, tumor microenvironment, and evasion from endosomal and lysosomal compartments [71]. After the intravenous administration, nanoparticles undergo opsonization, involving adsorption of serum albumin, apolipoproteins, complement factors and immunoglobulins onto the surface, and uptake by inhabitant macrophages [72]. This heads to non-specific dispersal of the nanotherapeutics to healthy organs like spleen and liver. Nanocarriers are passively accumulated in the tumor cells owing to leaky tumor vasculature and poor lymphatic drainage with enhanced resident time [73]. However, numerous barriers still exist, which hampers the nanoparticle's efficient extravasation. These incorporate the tumor interstitium barrier, physiological elements such as low pH, low oxygenation, very dense extracellular matrix (various architectural proteins) and raised interstitial fluid pressure in the tumor microenvironment [74]. Further, the cell membrane of tumor cells and intracellular organelles represent extra barriers for the nanoparticles to conquer for effective intracellular delivery of the cargo. For therapy in brain diseases, blood–brain barrier (BBB) behaves as diffusion barrier, made up of tight junctions, which excludes influx of elements from blood to brain [75]. Thus, to weather the storm, nanoparticle design should possess the aptness to encapsulate and protect drugs in addition to deliver them in a temporally or spatially controlled manner.

## 6 Endosomal Escape

Endocytosis is a vital mechanism for uptake and internalization of biological constituents, such as DNA, siRNA, and proteins. Following endocytosis, these biomolecules are escorted to the lysosome and are disintegrated by specific enzymes. Thus, another intracellular barrier for the nanocarrier to release drug inside the cytoplasm is the endosomal entrapment. Hence, different approaches were adopted to promote endosomal escape and assure cytosolic drug availability [76]. For example, bacteria and viruses use different penetrating pathways to escape the endosomal pathway. For carrier-mediated delivery, different approaches can be employed to ensure this escape mechanism like pore generation using different peptides, polyethylenimine (PEI) buffering effects and amalgamation with the lipid bilayer of endosomes [77]. Of late, the MSNs were decorated with self-immolative linker attached to polyvalent peptides which confer potency to deliver the nanoparticles in the cytoplasm via endosomal escape [78].

## 7 MSN for On-Demand Drug Release

As mentioned earlier, the proficiency of functional group employment, enormous surface area, pore size, large loading capacity and the superb biocompatibility makes MSNs an ideal candidate for delivery system. On-demand stimuli-responsive drug delivery systems (DDS) are convenient approach to reach drugs in spatial, temporal, and dosage-managed fashions. Stimuli-responsive system could deliver on-board cargo in site-selective and controlled release pattern upon encountering triggering agents [79]. Thus, the stimuli-responsive systems are progressive and surpass persistent drug release platforms. Among the distinct nanosystems, mesoporous silica provides the prospect to introduce a cap/gate-like assemblies over the porous framework to design the nanosystem for on-demand drug delivery. Fabrication and performance of such system inherit two subunits: first a porous silica support system for fill up with drug of interest and second zipping the pores reversibly by biological elements or supramolecular entities which can govern the movement of cargo from the pores.

In recent time, many investigators have made significant progress for the expansion of MSN-based drug delivery procedure with stimuli-responsive release properties [80]. The intracellular drug delivery by number of regulating mechanisms over the stimuli-responsive MSN has been postulated and confirmed their feasibility with accurate location and timing. The triggers or stimuli release mechanism, built on internal or external inputs, requires a pathway for application. Internal stimuli are unique and specific with the targeted pathological condition like upregulated glutathione level in cancer which permits the DDS to respond to the desired area and release its cargo in a self-regulated fashion. External inputs such as non-ionizing radiation [81], temperature [82], magnetic field, and ultrasounds [83] are noninvasive

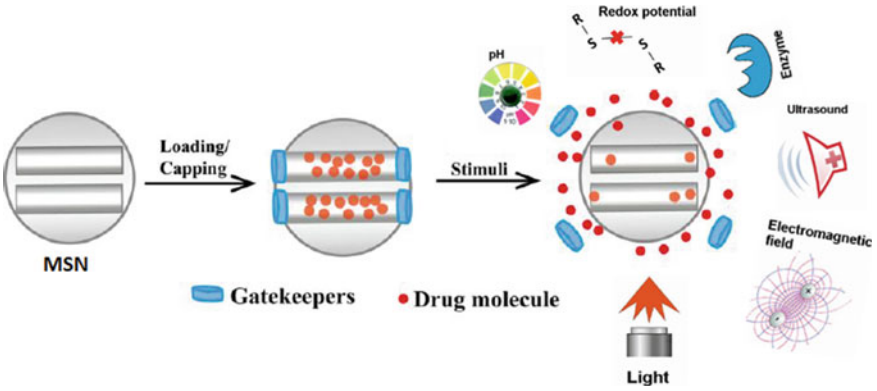


**Fig. 7** Schematic representation of various gate opening mechanisms in mesoporous silica nanocarrier. *Source* Author

and easy to perform techniques so that it could assist in localize drug release and optimize its efficiency. Examples of triggers include pH [84], light [81], redox potential [85], temperature [82], enzymes [86], etc. Operational aspects of these triggering stimuli were also presented in works, generated from our laboratory (Fig. 7).

## 8 Targeted Delivery Approach of MSN

Cell-specific targeting approach provides a basis that spontaneously distinguishes the place of action to the diseased organ and thus reduces both drug administration dosage and the side effects of the drug. The targeting module can be bifurcated into two parts, passive and active targeting [87]. Both targeting designs are applied to intensify drug bioavailability to the neoplastic cells.

### *8.1 Passive Routes*

Passive accumulation of MSN at the tumor site is attributed by EPR effect, a hypothesis predicated by Matsumura and Maeda in 1986 [88]. The tumor vasculature has increased permeability because of large gaps between the endothelial cells; hence, tumor vessels are more permeable to nanoparticles than the well-defined vasculature observed in the normal tissue [89]. Effectiveness of EPR effect can be transpired with the particle size, surface charge, or hydrophobicity. Tamanoi and coworkers illustrated that the fluorescently labeled MSNs were preferentially migrated and located in tumor site of mice following intravenous injection [65].

## 8.2 Surface Decoration with Tumor Directed Ligands

Active targeting involves the attachment of specific targeting ligands/biomolecules over the nanoparticle surface whose receptors are unique to, or upregulated in dysplastic and pathologic tissues. Targeted with specific ligand enhances the efficacy and reduces the toxicity of therapeutic agents. Anchoring a biological targeting moiety toward nanoparticle surface manifests enhanced internalization of the nanoparticles in targeted sites which contains overexpressed receptors [90]. Active targeting strategy does not intensify the tumor localization rather it accelerates the particle attachment and uptake through receptor-mediated endocytosis [91]. Certain efforts have demonstrated the nimble effect of the ligands for escalated cellular uptake when adhered to the nanoparticle surface. One such ligand is folic acid [92], whose receptors (folate receptor) are overexpressed in many different types of human neoplasia including breast, endometrial, ovarian, colorectal, and lung. Folic acid-tagged MSN (FA-MSN) upregulates cellular uptake by HeLa cells [93]. Besides that, other small nutrient biomolecules such as mannose [94] also function in similar fashion, resulted in improved uptake of MSN by MCF-7 breast cancer cells. Another targeting ligand, the RGD peptide, abbreviation for arginine–glycine–aspartic acid also shown to interact with overexpressed $\alpha_v\beta_3$ integrin receptor in metastatic cancers.

## 8.3 Enzyme-Responsive Drug Release

We have designed a novel methodology to deliver doxorubicin using biomolecules of known specificity. One such interaction in biological world is the dynamic interaction between bovine serum albumin (BSA) and bilirubin [95]. Bilirubin was attached over the nanoparticle's (MSNP-NH2) surface through an amide bond. Bilirubin is a potent antioxidant and shows strong anti-tumor effect besides inheriting strong molecular interactions with BSA molecules. Availing protein–ligand interaction for covering the pores, we have employed bilirubin-BSA complex as anew capping agent in protease-responsive drug release from MSN. Bilirubin-BSA complex was designed and explored as a biocompatible cap system with the protease-responsive pore opening for treatment against colon carcinoma. Bilirubin was tagged to the amine-terminated silica nanoparticles which were filled with doxorubicin (DOX), and the pores were sealed via molecular interactions between BSA and Bilirubin. DOX loaded MSN shows good colloidal stability and offers impressive tumoricidal property. Doxorubicin is a key drug of NCI-approved chemotherapeutic regimen R-CHOP. Doxorubicin hydrochloride (trade name Adriamycin) normally acts as a topoisomerase II poison [96]. Besides that, doxorubicin also induces cellular response like the adduct formation with DNA. The adduct formation occurs in association with endogenous formaldehyde and forms an activated Schiff base creating aminal (N–C–N) linkages with the exocyclic amino group of guanine residues [97]. Doxorubicin-loaded nano-formulation (MSNP-BR-BSA) significantly affects human (HCT-116)

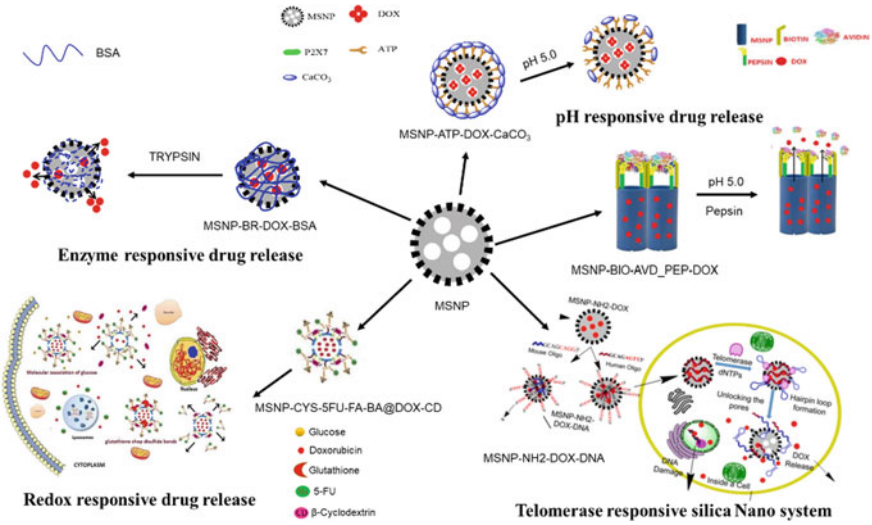


**Fig. 8** Targeted delivery of chemotherapeutic drugs from silica nanoparticle employing various platforms. *Source* Author

and murine (MC-38) colon carcinoma cells by inhibiting the amplification of cell number and inducing apoptosis (Fig. 8).

In our next study, we focused on upregulated enzymes associated with cancer malignancies as therapeutic target. Cancer cells are manifested with uncontrolled and rigorous cell division, obliged with actively functional telomerase enzyme. Telomerase enzyme is absent in the normal somatic cells which cause ageing effects as the cell undergo cycles of division. Search for novel triggering strategies specific to cancer prompted us to design telomerase-specific oligomer consisting of murine telomerase complementary repeat sequences and the telomerase-specific primer sequences. These specific oligonucleotide sequences sealed the pores of DOX-loaded aminated MSN via electrostatic interactions. Telomerase enzyme elongates the oligonucleotide sequences which resulted in the formation of rigid hairpin structure which subsequently leaves the MSN surface and release DOX from the pores [98]. Treatment of telomerase-responsive Dalton's lymphoma (DL) bearing mice with the newly fabricated oligo-wrapped nanoprobe, specific to mouse telomerase, significantly augmented the life span and improved the histopathological parameters. Besides that, treatment with this new probe-induced dramatic reduction in tumor foci across the tissue section in spleen and liver. Treatment with this nano-probe also restored the normal tissue architecture of deep vascularized organs and prevents metastasis (Fig. 8).

More than 80% of all cancers are solid tumors that grow as a lump of tissue in particular organ, or gland. The common sites are breast, lung, prostate, and colon, and other examples include brain, uterus, pancreas, skin, and liver. Examples of solid tumors are sarcomas, carcinomas, and lymphomas. Nanocarrier, when target the

solid tumor, the activity was hampered by the existence of tough extracellular matrix (ECM) which is fabricated by the architectural proteins, thus reducing the overall therapeutic efficacy. Further, poor and heterogeneously developed vascular network in solid tumor limits the oxygen supply and other crucial nutrients which lead to generation of acidic metabolites. Pepsin is a protease which is idle at physiological pH and becomes vibrant in acidic condition. Low pH in the tumor microenvironment can be an ideal condition for the pepsin activity. The pepsin biomolecules were attached to the doxorubicin-loaded mesoporous silica nanoparticles [99]. Pepsin decorated MSN demonstrated an enhanced diffusion inside the tumor mass. The tumor cells (extracted from the inner cores) over the HOPG surface manifest approximately three times more silica content compared with the non-protease attached nanoconstruct. Thus, this design enhances drug biodistribution homogenously throughout the length and breadth of the solid tumor (Fig. 8).

## *8.4 pH-Responsive Drug Release*

Chemoresistance is a phenomenon by virtue of which cancer cells reduces the killing efficiency of a particular drug. Cancer cells develop multidrug resistance receptor proteins (P-glycoprotein 1) which can pump drug outside the neoplastic cells and thus reduces desired therapeutic potential of the nanoconstruct. One way to reckon with this problem is receptor-mediated targeting. ATP is a biomolecule which has the tendency to bind the P2X7 receptors, expressed in transformed cells. These receptors are non-specific ion channels which could guide the influx of the biomolecules or nanoparticles, functionalized with ATP [100]. Further, the influx of ions like calcium brings alteration in cancer cells biomechanics leading to necrosis, membrane blebbing, and apoptosis. Based on these keystone information's, MSNs were garnished with ATP molecules and loaded with doxorubicin inside the pores. However, the design pertains to some pitfalls like the hasty drug release during circulation. There are reports where ATP acts as a stabilizer in generating the amorphous calcium carbonate nanoparticles. Thus, ATP molecules provided the organic phosphorous source for efficient calcium carbonate mediated biomineralization over the silica surface which seals the pores. The formed nanohybrid material was stable at physiological pH; however, when it encountered low pH in tumor microenvironment, calcium carbonate was leached out the surface, thus unmasking the ATP to clenched P2X7 receptor. This novel formulation augments the cellular uptake and demonstrated significant anti-tumor function against DL and doxorubicin-resistant DL cells (DLR) with large-scale growth inhibition and induction of apoptosis (Fig. 8).

### *8.5 Redox-Responsive Drug Release*

In another study, we have adopted a combination drug approach using clinically active drugs with non-overlapping toxicity contributed by incorporating varying triggering mechanisms leading to synergistic or additive effects. We employed MSN as an effective delivery platform for 5-fluoro-2-deoxyuridine (5FUdr) and doxorubicin against DL. The construct was made by attaching cysteine molecules via S–S bonds which inherit glutathione sensitivity [101]. Both the amine and carboxyl group terminated MSN-Cysteine offer the site for 5FUdr attachment via ester bond and folic acid (FA) to the amine groups. DOX was loaded inside, and the pores were sealed by using boronic ester bond using beta-cyclodextrin. FA selectively accumulates drug at the vicinity of tumor cells, and the particles can deliver both the drugs when met with respective triggering agent. This multifunctional nanoconstruct was designed for triple stimuli-responsive drug release that inherits sensitivity toward low pH, glucose molecules, and glutathione enzyme (Fig. 8).

## 9 Conclusions and Future Prospects

Two-dimensional nanomaterials are now important components in cutting edge applied research at the interface of environmental and biological interactions. Current development in this field enabled application of biomedical and environment technologies in improving human health. Extensive diversity of 2D nanomaterials with reference to their chemical and physical forms could offer numerous opportunities for researchers in broad areas of interest. However, it also poses substantial challenges for any comprehensive assessment in health effects. Studies on 2D nanomaterials come in various forms like nanosheets (sheet-like silicates), large lateral dimension (41 mm) sheets with variable effects in application. The key issue for the application of these 2D nanomaterials is affiliated to their long-term bio-persistence which is also closely related to the toxicity. This includes adverse biological responses via cell membrane compromisation and damage, phagocytosis by cells, impaired lung clearance, and lysosomal damages. These effects are critical which could be overcome by designing new thin sheet structures, interacting with the membranes, and subcellular organelles. In order to eliminate these serious limitations, high-priority research areas are required to be selected which may include several issues like release and exposure kinetics, phase transformation in medium and cellular response to chemical and physical forms. Besides that, other critical issues like degradation, bio-persistence, safety associated aspects for nanosheets and its by-product needs to be considered. Development of analytical and in-silico methods to ascertain the dissolution, transformation, and redox reactions of wide spectrum 2D nanomaterials in cellular environment are also significantly important. Clearly, maximum emphasis should be given to inevitable inflammatory reactions following absorption of the sheet-shaped silica materials in in vivo settings. Exposure to such materials could initiate plethora of

activities including phagocytosis, translocation to membrane, and interference in lung clearance, etc. It is highly probable that these biological nanosheets could be game changer in future medicine and offer significant opportunities for future research for the realization of its potential application. On a precautionary note, emerging 2D nanomaterial research requires better engineering methodology and control for fabrication and synthesis which could limit the exposure and avoid toxicity. These issues plus other concerns are required to be addressed for safe and beneficial application of 2D nanomaterials.

## References

1. Allen TM, Cullis PR (2004) Drug delivery systems: entering the mainstream. Science 303(5665):1818
2. Wagner V et al (2006) The emerging nanomedicine landscape. Nat Biotechnol 24(10):1211–1217
3. Riehemann K et al (2009) Nanomedicine—challenge and perspectives. Angew Chem Int Ed 48(5):872–897
4. Sanhai WR et al (2008) Seven challenges for nanomedicine. Nat Nanotechnol 3(5):242–244
5. Spomenka S et al (2011) Silica materials in drug delivery applications. Curr Drug Discov Technol 8(3):250–268
6. Patel AR et al (2015) Fumed silica-based organogels and 'aqueous-organic' bigels. RSC Adv 5(13):9703–9708
7. Benezra M et al (2011) Multimodal silica nanoparticles are effective cancer-targeted probes in a model of human melanoma. J Clin Investig 121(7):2768–2780
8. Aznar E et al (2016) Gated materials for on-command release of guest molecules. Chem Rev 116(2):561–718
9. Bharti C et al (2015) Mesoporous silica nanoparticles in target drug delivery system: a review
10. Xue Y et al (2016) A simple and controllable graphene-templated approach to synthesise 2D silica-based nanomaterials using water-in-oil microemulsions. Chem Commun 52(3):575–578
11. Saxena V et al (2018) Edible oil nanoemulsion: an organic nanoantibiotic as a potential biomolecule delivery vehicle. Int J Polym Mater Polym Biomater 67(7):410–419
12. Fopase R et al (2020) Lipopeptide and essential oil based nanoemulsion for controlled drug delivery. Polym Plast Technol Mater 59(18):2076–2086
13. Seigneuric R et al (2010) From nanotechnology to nanomedicine: applications to cancer research. Curr Mol Med 10(7):640–652
14. Rivera Gil P et al (2010) Nanopharmacy: inorganic nanoscale devices as vectors and active compounds. Pharmacol Res 62(2):115–125
15. Muggia FM (2001) Liposomal encapsulated anthracyclines: new therapeutic horizons. Curr Oncol Rep 3(2):156–162
16. Wicki A et al (2015) Nanomedicine in cancer therapy: challenges, opportunities, and clinical applications. J Control Release 200:138–157
17. Skubitz KM (2003) Phase II trial of pegylated-liposomal doxorubicin (Doxil™) in sarcoma. Cancer Invest 21(2):167–176
18. Zhigaltsev IV et al (2005) Liposome-encapsulated vincristine, vinblastine and vinorelbine: a comparative study of drug loading and retention. J Control Release 104(1):103–111
19. Stathopoulos GP, Boulikas T (2012) Lipoplatin formulation review article. J Drug Deliv 2012:581363

20. Werner ME et al (2013) Preclinical evaluation of genexol-PM, a nanoparticle formulation of paclitaxel, as a novel radiosensitizer for the treatment of non-small cell lung cancer. Int J Radiat Oncol Biol Phys 86(3):463–468
21. Ma P, Mumper RJ (2013) Paclitaxel nano-delivery systems: a comprehensive review. J Nanomed Nanotechnol 4(2):1000164–1000264
22. Gradishar WJ (2006) Albumin-bound paclitaxel: a next-generation taxane. Expert Opin Pharmacother 7(8):1041–1053
23. Zhang X, Sun C, Fang N (2004) Manufacturing at nanoscale: top-down, bottom-up and system engineering. J Nanopart Res 6(1):125–130
24. Brinker CJ, Scherer GW (1990) Particulate sols and gels, chap 4. In: Brinker CJ, Scherer GW (eds) Sol-gel science. Academic Press, San Diego, pp 234–301
25. Hench LL, West JK (1990) The sol-gel process. Chem Rev 90(1):33–72
26. Holmberg K, Jönsson B, Kronberg B, Lindman B (2002) Physicochemical properties of surfactants and polymers containing oxyethylene groups. In: Jönsson B, Holmberg K, Kronberg B, Lindman B (eds) Surfactants and polymers in aqueous solution. Wiley
27. Kresge CT et al (1992) Ordered mesoporous molecular sieves synthesized by a liquid-crystal template mechanism. Nature 359(6397):710–712
28. Ullattil SG, Periyat P (2017) Sol-gel synthesis of titanium dioxide. In: Pillai SC, Hehir S (eds) Sol-gel materials for energy, environment and electronic applications. Springer International Publishing, Cham, pp 271–283
29. Hoffmann F et al (2006) Silica-based mesoporous organic-inorganic hybrid materials. Angew Chem Int Ed 45(20):3216–3251
30. Wan Y, Zhao (2007) On the controllable soft-templating approach to mesoporous silicates. Chem Rev 107(7):2821–2860
31. Ould-Ely T, Bawazer LA, Morse DE (2011) 2.201—bio-inspired silica nanomaterials for biomedical applications. In: Ducheyne P (ed) Comprehensive biomaterials. Elsevier, Oxford, pp 1–16
32. Cai Q et al (1999) The preparation of highly ordered MCM-41 with extremely low surfactant concentration. Microporous Mesoporous Mater 32(1):1–15
33. Huo Q et al (1995) Mesostructure design with gemini surfactants: supercage formation in a three-dimensional hexagonal array. Science 268(5215):1324
34. Beck JS et al (1992) A new family of mesoporous molecular sieves prepared with liquid crystal templates. J Am Chem Soc 114(27):10834–10843
35. Schumacher K et al (2000) Characterization of MCM-48 materials. Langmuir 16(10):4648–4654
36. Lu F et al (2009) Size effect on cell uptake in well-suspended, uniform mesoporous silica nanoparticles. Small 5(12):1408–1413
37. Wu S-H, Mou C-Y, Lin H-P (2013) Synthesis of mesoporous silica nanoparticles. Chem Soc Rev 42(9):3862–3875
38. Nooney RI et al (2002) Synthesis of nanoscale mesoporous silica spheres with controlled particle size. Chem Mater 14(11):4721–4728
39. Hitz S, Prins R (1997) Influence of template extraction on structure, activity, and stability of MCM-41 catalysts. J Catal 168(2):194–206
40. Angelos S et al (2007) Mesostructured silica supports for functional materials and molecular machines. Adv Funct Mater 17(14):2261–2271
41. Kim CO, Cho SJ, Park JW (2003) Hyperbranching polymerization of aziridine on silica solid substrates leading to a surface of highly dense reactive amine groups. J Colloid Interface Sci 260(2):374–378
42. Huh S et al (2003) Organic functionalization and morphology control of mesoporous silicas via a co-condensation synthesis method. Chem Mater 15(22):4247–4256
43. Huh S et al (2003) Tuning of particle morphology and pore properties in mesoporous silicas with multiple organic functional groups. Chem Commun 18:2364–2365
44. Xie F et al (2018) A highly organic functionalized three-connected periodic mesoporous silica by co-condensation with hydridosilica. Microporous Mesoporous Mater 266:177–182

45. Zhou D et al (2015) One-step DGC assembly and structural characterization of a hairy particle zeolite-like organic–inorganic hybrid as an efficient modifiable catalytic material. Dalton Trans 44(33):14732–14740
46. Stein A, Melde BJ, Schroden RC (2000) Hybrid inorganic-organic mesoporous silicates—nanoscopic reactors coming of age. Adv Mater 12(19):1403–1419
47. Lim MH, Stein A (1999) Comparative studies of grafting and direct syntheses of inorganic−organic hybrid mesoporous materials. Chem Mater 11(11):3285–3295
48. Albanese A, Tang PS, Chan WCW (2012) The effect of nanoparticle size, shape, and surface chemistry on biological systems. Annu Rev Biomed Eng 14(1):1–16
49. Hoffmann F, Fröba M (2011) Vitalising porous inorganic silica networks with organic functions—PMOs and related hybrid materials. Chem Soc Rev 40(2):608–620
50. Verma A, Stellacci F (2010) Effect of surface properties on nanoparticle-cell interactions. Small 6(1):12–21
51. Chiu H-Y et al (2016) Intracellular chromobody delivery by mesoporous silica nanoparticles for antigen targeting and visualization in real time. Sci Rep 6(1):25019
52. Trewyn BG et al (2008) Biocompatible mesoporous silica nanoparticles with different morphologies for animal cell membrane penetration. Chem Eng J 137(1):23–29
53. Dogra P et al (2018) Establishing the effects of mesoporous silica nanoparticle properties on in vivo disposition using imaging-based pharmacokinetics. Nat Commun 9(1):4551
54. Hillaireau H, Couvreur P (2009) Nanocarriers' entry into the cell: relevance to drug delivery. Cell Mol Life Sci 66(17):2873–2896
55. Yue Z-G et al (2011) Surface charge affects cellular uptake and intracellular trafficking of chitosan-based nanoparticles. Biomacromolecules 12(7):2440–2446
56. Duan X, Li Y (2013) Physicochemical characteristics of nanoparticles affect circulation, biodistribution, cellular internalization, and trafficking. Small 9(9–10):1521–1532
57. Varkouhi AK et al (2011) Endosomal escape pathways for delivery of biologicals. J Control Release 151(3):220–228
58. Slowing I, Trewyn BG, Lin VSY (2006) Effect of surface functionalization of MCM-41-type mesoporous silica nanoparticles on the endocytosis by human cancer cells. J Am Chem Soc 128(46):14792–14793
59. Shahabi S et al (2015) Modulation of silica nanoparticle uptake into human osteoblast cells by variation of the ratio of amino and sulfonate surface groups: effects of serum. ACS Appl Mater Interfaces 7(25):13821–13833
60. Samadi Moghaddam M, Heiny M, Shastri VP (2015) Enhanced cellular uptake of nanoparticles by increasing the hydrophobicity of poly(lactic acid) through copolymerization with cell-membrane-lipid components. Chem Commun 51(78):14605–14608
61. Desai D et al (2018) Factors affecting intracellular delivery and release of hydrophilic versus hydrophobic cargo from mesoporous silica nanoparticles on 2D and 3D cell cultures. Pharmaceutics 10(4):237
62. He Q et al (2011) In vivo biodistribution and urinary excretion of mesoporous silica nanoparticles: effects of particle size and PEGylation. Small 7(2):271–280
63. Kim J et al (2008) Multifunctional uniform nanoparticles composed of a magnetite nanocrystal core and a mesoporous silica shell for magnetic resonance and fluorescence imaging and for drug delivery. Angew Chem Int Ed 47(44):8438–8441
64. Lee JE et al (2010) Uniform mesoporous dye-doped silica nanoparticles decorated with multiple magnetite nanocrystals for simultaneous enhanced magnetic resonance imaging, fluorescence imaging, and drug delivery. J Am Chem Soc 132(2):552–557
65. Lu J et al (2010) Biocompatibility, biodistribution, and drug-delivery efficiency of mesoporous silica nanoparticles for cancer therapy in animals. Small 6(16):1794–1805
66. Tarn D et al (2013) Mesoporous silica nanoparticle nanocarriers: biofunctionality and biocompatibility. Acc Chem Res 46(3):792–801
67. Tang L, Cheng J (2013) Nonporous silica nanoparticles for nanomedicine application. Nano Today 8(3):290–312

68. Kim B, Kim H, Yu IJ (2014) Assessment of nanoparticle exposure in nanosilica handling process: including characteristics of nanoparticles leaking from a vacuum cleaner. Ind Health 52(2):152–162
69. Chen L et al (2018) The toxicity of silica nanoparticles to the immune system. Nanomedicine 13(15):1939–1962
70. Kiptoo P, Calcagno AM, Siahaan TJ (2016) Physiological, biochemical, and chemical barriers to oral drug delivery: principles and applications, chap 2, pp 19–34
71. Blanco E, Shen H, Ferrari M (2015) Principles of nanoparticle design for overcoming biological barriers to drug delivery. Nat Biotechnol 33(9):941–951
72. Jain RK (1999) Understanding barriers to drug delivery: high resolution in vivo imaging is key. Clin Cancer Res 5(7):1605
73. Greish K (2010) Enhanced permeability and retention (EPR) effect for anticancer nanomedicine drug targeting. In: Grobmyer SR, Moudgil BM (eds) Cancer nanotechnology: methods and protocols. Humana Press, Totowa, NJ, pp 25–37
74. Sriraman SK, Aryasomayajula B, Torchilin VP (2014) Barriers to drug delivery in solid tumors. Tissue Barriers 2(3):e29528
75. Ballabh P, Braun A, Nedergaard M (2004) The blood–brain barrier: an overview: structure, regulation, and clinical implications. Neurobiol Dis 16(1):1–13
76. Kou L et al (2013) The endocytosis and intracellular fate of nanomedicines: implication for rational design. Asian J Pharm Sci 8(1):1–10
77. Dominska M, Dykxhoorn DM (2010) Breaking down the barriers: siRNA delivery and endosome escape. J Cell Sci 123(8):1183
78. Gisbert-Garzarán M et al (2021) Designing mesoporous silica nanoparticles to overcome biological barriers by incorporating targeting and endosomal escape. ACS Appl Mater Interfaces 13(8):9656–9666
79. Shim MS, Kwon YJ (2012) Stimuli-responsive polymers and nanomaterials for gene delivery and imaging applications. Adv Drug Deliv Rev 64(11):1046–1059
80. Baeza A, Colilla M, Vallet-Regí M (2015) Advances in mesoporous silica nanoparticles for targeted stimuli-responsive drug delivery. Expert Opin Drug Deliv 12(2):319–337
81. Mal NK, Fujiwara M, Tanaka Y (2003) Photocontrolled reversible release of guest molecules from coumarin-modified mesoporous silica. Nature 421(6921):350–353
82. Gu X et al (2013) Temperature-responsive drug delivery systems based on polyaspartamides with isopropylamine pendant groups. Soft Matter 9(30):7267–7273
83. Guo W et al (2014) P(EO-co-LLA) functionalized $Fe_3O_4$@$mSiO_2$ nanocomposites for thermo/pH responsive drug controlled release and hyperthermia. Dalton Trans 43(48):18056–18065
84. Zeng Z et al (2017) pH-responsive nanoparticles based on ibuprofen prodrug as drug carriers for inhibition of primary tumor growth and metastasis. J Mater Chem B 5(33):6860–6868
85. Tan S, Wang G (2017) Redox-responsive and pH-sensitive nanoparticles enhanced stability and anticancer ability of erlotinib to treat lung cancer in vivo. Drug Des Dev Ther 11:3519–3529
86. de la Rica R, Aili D, Stevens MM (2012) Enzyme-responsive nanoparticles for drug release and diagnostics. Adv Drug Deliv Rev 64(11):967–978
87. Torchilin VP (2010) Passive and active drug targeting: drug delivery to tumors as an example. In: Schäfer-Korting M (ed) Drug delivery. Springer Berlin Heidelberg, Berlin, Heidelberg, pp 3–53
88. Matsumura Y, Maeda H (1986) A new concept for macromolecular therapeutics in cancer chemotherapy: mechanism of tumoritropic accumulation of proteins and the antitumor agent smancs. Cancer Res 46(12 Part 1):6387
89. Gerlowski LE, Jain RK (1986) Microvascular permeability of normal and neoplastic tissues. Microvasc Res 31(3):288–305
90. Ruoslahti E, Bhatia SN, Sailor MJ (2010) Targeting of drugs and nanoparticles to tumors. J Cell Biol 188(6):759–768

91. Pirollo KF, Chang EH (2008) Does a targeting ligand influence nanoparticle tumor localization or uptake? Trends Biotechnol 26(10):552–558
92. Guo R et al (2012) The intracellular controlled release from bioresponsive mesoporous silica with folate as both targeting and capping agent. Nanoscale 4(11):3577–3583
93. Rosenholm JM et al (2009) Targeting of porous hybrid silica nanoparticles to cancer cells. ACS Nano 3(1):197–206
94. Brevet D et al (2009) Mannose-targeted mesoporous silica nanoparticles for photodynamic therapy. Chem Commun 12:1475–1477
95. Srivastava P et al (2017) Protease-responsive targeted delivery of doxorubicin from bilirubin-BSA-capped mesoporous silica nanoparticles against colon cancer. ACS Biomater Sci Eng 3(12):3376–3385
96. Cutts SM, Phillips DR (1995) Use of oligonucleotides to define the site of interstrand cross-links induced by Adriamycin. Nucleic Acids Res 23(13):2450–2456
97. Zeman SM, Phillips DR, Crothers DM (1998) Characterization of covalent Adriamycin-DNA adducts. Proc Natl Acad Sci 95(20):11561
98. Srivastava P et al (2018) Telomerase responsive delivery of doxorubicin from mesoporous silica nanoparticles in multiple malignancies: therapeutic efficacies against experimental aggressive murine lymphoma. Bioconjug Chem 29(6):2107–2119
99. Srivastava P et al (2018) Pepsin assisted doxorubicin delivery from mesoporous silica nanoparticles downsizes solid tumor volume and enhances therapeutic efficacy in experimental murine lymphoma. ACS Appl Bio Mater 1(6):2133–2140
100. Srivastava P et al (2018) ATP-decorated mesoporous silica for biomineralization of calcium carbonate and P2 purinergic receptor-mediated antitumor activity against aggressive lymphoma. ACS Appl Mater Interfaces 10(8):6917–6929
101. Srivastava P et al (2020) Studies on interaction potency model based on drug synergy and therapeutic potential of triple stimuli-responsive delivery of doxorubicin and 5-fluoro-2-deoxyuridine against lymphoma using disulfide-bridged cysteine over mesoporous silica nanoparticles. J Mater Chem B 8(7):1411–1421

# Chapter 10
# Futuristic 2D Nanomaterial Composites Agro-Formulations for Sustainable Agriculture


**Poonam Gogoi Konwar**

## 1 Introduction

Global hunger is on the rise impacting 9.9% people around the world which means 811 million people go hungry every single day. There are 161 million people categorized as undernourished severely influenced by the change in climate and the current Covid-19 pandemic situation. Ironically, 39% are overweight and 13% are obese out of the world's adult population in 2016 as per World Health Organization (WHO). Evidently, there is more than enough food to feed the world's population but there is not a uniform distribution of food around the world. Many reasons could be responsible, for instance, overpopulation, poverty, increased cost of living and climate changes. A significant change in dietary patterns is also a reason which seems to be associated with environmental and societal instabilities due to incompetent/insufficient policies in the sector of agriculture and environment. Traditional agricultural breeding practices are not capable to deal with the changing climatic conditions, plants succumbing to unknown diseases and other related issues. In this situation, primary objective of all the brilliant minds is the development of agriculture in an imperishable manner and at the same time to do away with the current situation. A growing movement towards sustainable agriculture that integrates three aspects; environment, economy and social equity offers innovative alternatives to protect the ecosystem in the long run. One such alternative is the use of nanotechnology for the advancement of agriculture and food industry.

Nanomaterials (NMs) and their formulations are designed to cope with the enormous agricultural challenges such as abrupt climate change, soil fertility decline, infestation by pests and weeds, disease eruption, lack of nutrients as well as low post-harvest nutritional value of agricultural products [1, 2]. Nanotechnology-based approaches bring incredible nanotools with the capacity to rapidly diagnose plant

P. G. Konwar (✉)
Department of Soil Science, Assam Agricultural University, Jorhat, Assam 785013, India
e-mail: poonam.csk@gmail.com



Z. Khanam et al. (eds.), *2D Nanomaterials for Energy and Environmental Sustainability*,
Materials Horizons: From Nature to Nanomaterials,
https://doi.org/10.1007/978-981-16-8538-5_10

diseases, enhance nutrient absorption in plants and fight the changing climate among others. The common practice of using different NMs as nanofertilizers and nanopesticides for crop development is very well documented in literature [3–7]. Nanomediated sensors for identification and detection of diseases and agrochemical residues in plants and to monitor the quality of agricultural soil have also gained popularity in recent times. Genetic engineers are also very fascinated with this novel technique for developing nanodevices for evolving genetically modified plants having distinctive and improved characteristics [8]. Naturally, NMs have been present on earth since a billion years in its native state having particular characteristics, however, due to unintentional anthropogenic involvement at various levels, it acquired some changes in its basic nature and properties resulting in the evolution of incidental NMs, which got distributed worldwide. In recent advances, mindful approaches to achieve a better understanding of their nature and formulating them for specific applications to achieve maximum benefits have led to the development of engineered NMs [9]. The utilization of wide palette of engineered NMs in site specific delivery of fertilizers and pesticides, effective detection of plant diseases, minimum usage of inputs, reducing loss and contamination of the ecosystem has led to the revolutionalizing agriculture and food industry [10]. Consequently, the repertoire of NMs has brought about a paradigm shift associated with the way the scientific world has conceived the future of nanoscience in agriculture.

One billionth of a metre, as derived from Greek word ‘dwarf’ is a nanometre. Owing to its smaller size, NMs have very large surface area to volume ratio and thus are highly reactive [11]. The NMs in form of nanoparticles (NPs), nanowires (NWs), nanotubes (NTs), nanosheets (NSs), nanoplatelets (NPts) and nanocomposites (NCs) are known to boost the overall efficacy by contributing quick response, superior sensitivity and stronger limit of detection on account of novel physicochemical, electrical and chemical properties [12]. 2D NMs, at the forefront of nanotechnology, can be incorporated into agricultural formulations in different forms like nanoflakes/nanosheets, nanowalls, nanodisks/nanopaltelets and layered materials forming junctions [13]. Their existing achievements have manifested important significance as a plant growth stimulator and component of fertilizers [14] thereby improving agricultural productivity resulting in revolutionization of the precision farming techniques and sustainable agriculture development [15]; in nanoencapsulation for smart and slow delivery systems [16]; as an antibacterial and antifungal agent [17] demonstrating its potential application in food packaging [18, 19]; improvement of soil quality by acting as nanocarriers for micro-and macronutrients [20–22]; in water treatment and ultrafiltration [23]; for pesticide and insecticide quantitation [24] and as biosensors for sensing, monitoring, quantification and restoration of biotic and abiotic stresses for in-situ soil application [25–28]. These advancements of 2D NMs are credited to their extraordinary properties like high surface area, small size, excellent variety in surface functionalization and high reactivity [29, 30].

However, it is easily debatable that the application of NMs in the field agrochemical-formulations for a sustainable agriculture is very limited and scattered. This chapter aims to bring together the research done in this regard to shed a light on the potential of 2D NMs and composites in the field of agriculture.

## 2 Preparation of 2D NMs-based agro-formulations

The methods of green synthesis are believed to safeguard the application of 2D NMs in the field of agriculture. Greener tools and techniques for the synthesis of NMs and their release with active components at different target sites have resulted in better soil health, effective control of pest and weed and improved nutrient uptake and crop nutrition [31]. Different approaches of top-down and bottom-up methods of synthesis involve additional step of surface functionalization to improve their properties, stability, cargo loading and biocompatibility. The preparation strategies of various types of 2D NMs- based formulations that are popularly used for agricultural applications are discussed here.

### *2.1 Graphene*

Graphene is a 2D packed honeycomb like lattice of single or multiple layers of C-atoms which is considered as one of the most versatile 2D NMs. It has outstanding range of properties, viz., chemical, electrical, thermal, optical, mechanical and structural [32]. Additionally, graphene can be derived into different forms by tuning its size and surface chemistry such as graphene oxide (GO), reduced GO (rGO), multi-layered graphene (MLG) and graphene flakes.

Hummer's or modified Hummer's method is the most common for the preparation of GO which involves oxidation followed by exfoliation of natural graphite powder [20]. A common practice of packing agrochemicals onto GO through π-π interactions is known to increase its performance. This can be simply achieved by mixing of all ingredients to form solution followed by separation and washing step. A functionalized GO/Fe composite was synthesized as a carrier of phosphate ions to enhance nutrient delivery in plants. A homogenized solution of GO was prepared by sonication in deionized water and then vigorously mixing with a solution of $FeCl_3$ in 1:1 mass ratio. Overnight drying of the supernatant obtained from the centrifugation process resulted in GO–Fe nanocomposite which was physically loaded with potassium dihydrogen phosphate ($KH_2PO_4$). In comparison to commercial monoammonium phosphate (MAP) fertilizer, the application of GO–Fe nanocomposite loaded with phosphate has shown slower release of phosphate ions [16].

Polymer coatings are found to improve porosity and flexibility of GO NMs. Poly-dopamine (PDA) and chitosan are some of the commonly used polymers for the purpose. Simple polymerization of PDA to prepare a coating on GO encapsulated with Hymexazol pesticide is shown by Tong et al. [33]. Most commonly used fertilizer, potassium nitrate was coated with chitosan-GO nanocomposites for enhanced porosity [22]. Furthermore, introducing oxygen-functionalized metal ions to graphene are known to increase surface area resulting in higher loading of micronutrients. For instance, Cu–GO and Zn–GO nanocomposites were prepared by the addition of $CuSO_4.5H_2O$ and $ZnSO_4.7H_2O$ salts in GO solution, respectively, and were

used as solid fertilizers with their pH maintained at 4.5 and 6. In another method, a coating of $KNO_3$ pellets with GO films through ion-mediated thermal reduction method produced $K^+$ ions encapsulated rGO films with reduced toxicity [34].

## 2.2 Transition Metal Dichalcogenides (TMDs)

TMDs consist of hexagonal layers of transition metal atoms (M) that are sandwiched between chalcogen atoms (X) in a $MX_2$ stoichiometry [35]. There are 40 different types of TMDs owing to the various combinations of transition metal (Ti, W, Hf, Nb, Re, Mo, Ta, etc.) and chalcogen (S, Se or Te). TMDs have implemented their applications in many important agricultural studies such as detection of fenitrothion and pesticide residues in plants and their parts, nitrogen fixing in the soil and regulating physiological and biochemical behaviours in rice.

The method of synthesis for TMDs is very similar to graphene which includes mechanical cleavage, chemical vapour deposition (CVD) and chemical synthesis. Ultra-thin TMD nanosheets with strong absorption and fluorescence in the visible region were prepared by using a simple kitchen-blender to exfoliate $MoSe_2$, $MoS_2$, $WSe_2$ and $WS_2$. These TMD nanosheets were used as a label-free and highly sensitive colorimetric sensor for the detection of single strand DNA based on van der Waal's interaction between them in dispersed state [36]. Another example is the use of Vanadium selenide as an electrochemical sensor in agriculture ($V_2Se_9$) which was prepared by a facile hydrothermal process and ultrasonic treatment with rGO [37]. There are also examples of the use of polymers such as poly (ethylene glycol) diacrylate (PEG) with TMDs to prepare composite nanocarriers for the loading of agri-active component [38].

## 2.3 MXenes

MXenes with a typical formula of $M_2X$, $M_3X_2$ and $M_4X_3$ are considered as one of the biggest families of 2D NMs [39]. They have layered structures stacked with thick sheets of transition metal nitrides, carbides or carbonitrides contributing to their unique combination of ceramic and metallic properties. This achieved by selectively removing aluminium from MAX which are basically layered ternary carbides, $M_{n+1}AX_n$ ($n = 1, 2$ or 3), where M refers to early d-block transition metals (Ti, V, Cr, Nb, etc.), A refers to main group 3 and 14 elements (Al, Si, Sn, In, etc.) and X refers to either C or N atoms [35]. The transition metal carbides and nitrides are known to provide amazing metallic conductive characteristic to MXenes with additional advantages, for instance, high ion transport, low diffusion barrier properties, large surface area and hydrophilicity. For instance, the use $Ti_3C_2$ nanocarrier for the efficient delivery of pesticide, avermectin (AV). HF (40%) etching of MAX phase

bulk $Ti_3AlC_2$ powder followed by ultrasonic exfoliation resulted in $Ti_3C_2$ nanocarrier which was then loaded with. AV@$Ti_3C_2$ exhibited excellent water solubility, photostability with a pH responsive release of AV with enhanced anti-pest activity [40].

Mxene-polymer nanocomposites offer excellent conductivity, affordability and mechanical flexibility with surface functionalities for multiple applications [41]. One such example is their state-of-the-art preparation as a sensor for ammonia which involves 3-stage process. Stage 1 is the synthesis of MXenes through techniques such as selective etching, CVD, chemical transformations [42]. Stage 2 is the synthesis of MXenes nanocomposites through in-situ or ex-situ approaches, wherein in-situ involves synthesis of both precursor or one precursor (Mxene) in the presence of other (polymers) and ex-situ involves blending together pre-synthesized precursors [42]. Stage 3 is the fabrication of chemiresistor by fabrication of a sensing film over a substrate through techniques such as electrospinning, drop-casting, inkjet printing and dip-coating. The substrate could be a glass, indium-tin-oxide (ITO), polyethylene terephthalate (PET), etc. [43].

## 3 Applications of 2D NMs in Agriculture

Nano-based technologies aim at improving the efficiency and availability of all essential agrochemical and biological agents to regulate the releasing concentration of agro-active ingredients. It also aids in slow degradation by increasing their stability which increase their shelf life, consequently, achieving sustainable agriculture. NPs have a large surface area which facilitates quick and higher loading attachment of agro-active ingredients [35]. 2D NMs and their nanocomposites have attracted their application in such process of absorption, encapsulation and controlled delivery of agrochemical which are shown in Fig. 1.

In this section, the different roles of 2D NMs and their nanocomposites in promoting sustainable agricultural practices are discussed in detail.

### *3.1 Boosting Seed Germination, Seedling Growth and Plant Development*

2D NMs regulate the productivity of food crop plants as well as the industrial plants. Interestingly, the impact of graphene during the initial stages of the plant (germination and seedling development) is dependent upon the size and concentration of the nanomaterial. Graphene exhibited a positive effect on germination of tomato seeds, reason being its ability to penetrate seed husk facilitating water uptake resulting in speedy germination and higher percentage of germination rates [44]. A remarkable improvement in the number and surface area of leaves, increased root length and

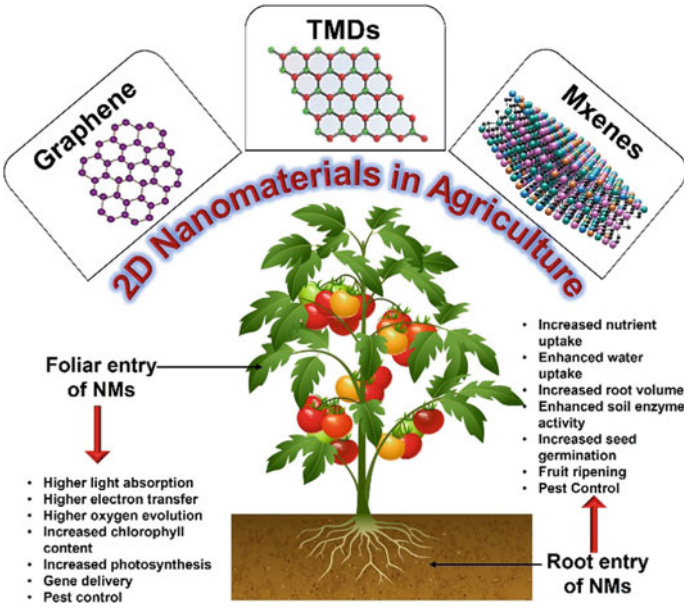


**Fig. 1** Different modes of entry and roles of 2D NMs in plants

rate of formation of flower buds has been observed simply by the application of graphene oxide to the culture medium of *Arabidopsis thaliana.* In the same way, graphene oxide increased the perimeter, contrived the ripeness and sugar content in watermelon. We believe that graphene oxide may be used as a strategy for enabling the acceleration of both plant growth and the fruit ripening process [20]. GO assisted in expediting the germination of spinach and chive plants when applied at the rate of 50, 200 $\mu g\ mL^{-1}$ and 50 $\mu g\ mL^{-1}$, respectively, due to its ability to absorb water more efficiently [45]. The spray application of graphene nanosheets in solanaceous crops such as eggplants and pepper @ 0.1, 0.2 and 0.3 GNS g $L^{-1}$ triggered the activities of enzymes, viz., ascorbate peroxidase, catalase, glutathione peroxidase and glutathione-S-transferase, thereby enhancing their overall physiological traits and yield parameters [46]. Similarly, in cotton and *Catharanthus*, soil application of graphene resulted in enhanced seed germination, better pollination, early flower production, increased flower bud number, and improved tolerance to salt and water deficit stress [47]. Therefore, graphene-based 2D nanocomposites have great potential in the field of crop improvement through enhanced plant growth and faster process of fruit ripening.

As the plant grows, its response towards graphene becomes highly dependent on concentration, length of exposure and the plant type as well. When applied at appropriate concentration, it facilitates growth and development in plant, and at higher levels, it impedes it. Low concentration (25–50 mg $L^{-1}$) of graphene on seedling growth of afforestation species such as *Larix olgensis* had a positive impact showing

an increased root, stem and leaf biomass. A higher concentration (100–500 mg $L^{-1}$), however, was found to reduce all these enhancements over a period of time. Also, the seedling survival rates followed a decrease trend with an increase in graphene concentration due to oxidative stress created at different stages in the seedlings [48]. Silver decorated graphene oxide (Ag-GO) administered radish plants appeared to have a better root elongation and improved shoot growth, whereas in alfalfa and cucumber the treatment inhibited the same [49]. A delayed seed germination, growth of radicle and plumule, length of root and stem, fresh weight of above and below ground parts, adventitious roots were observed at higher concentrations (5 mg/L) of graphene as compared to lower ones (100 and 200 mg/L) in rice seedlings [50]. However, the same treatment in tomato was adequate in inducting their growth. A 285% and 30% increase in the fresh weight of root and shoot system, respectively, was obtained. Similarly, in the dry weight 128% increase for shoot system and 480% for the root system was obtained [51].

Another parameter of 2D NMs that can affect the production and quality, and impact different molecular pathways in plants is their particle size and surface chemistry. Graphene oxide (GO), reduced GO (rGO) and GO quantum dots (GOQDs) can be translocated from the stems of wheat to grains resulting in the formation of large aggregates of graphene nanoparticles. These NMs caused a decrease in the concentration of prolamin, globulin, amylopectin and amylose and contents by 11–25%, 8–28%, 23–37% and 5–34%, respectively. A decrease in the levels of minerals with a 19–36% increase in the concentration of soluble sugar in wheat grains was reported. rGO cause a more downregulated levels of proteins possessing nutrient reservoir activity in comparison to GO. The decrease in the concentration of mineral element in presence of rGO and GOQD was much higher than as detected with GO which could be due to calmodulin upregulation facilitated by ABC transporters. GOQD and rGO were found to change the metabolomic and proteomic profiles more effectively than GO. This clearly suggests that the small size and low oxidation content in a graphene nanocomposite is more detrimental to the quality of grain [52].

## *3.2 Nurturing Plant Nutrition*

The use of fertilizers is a very common practice to increase the productivity of crops. Fertilizers provide the ultimate food to the developing crops and thus, it is a major challenge to maintain the quality and efficacy of these fertilizers. Also, different coating materials such as sulphur and polymers are extensively used, however, the severe lack of controlled release of agro-ingredients is a major issue that also hampers the soil pH. An alternative to conventional fertilizers, nanofertilizers have been designed with an aim to slowly deploy nutrients into plants and to increase their nutrient efficiency through binding to nano-adsorbents. The use of nanotechnology where nanoparticles are encapsulated with the nutrients can provide the necessary thrust to develop advanced revolution for improving agricultural production in a

sustainable manner. Notably, NMs based application of agricultural inputs (fertilizers, pesticides and herbicides) are known to increase their efficiency by delivering a desirably slow release of large quantity of macro- and micronutrients to the soil and plants, and therefore, enhances the crop productivity and at the same time ensures a minimum usage of the inputs delivering lower cost of cultivation and less wastage as compared to that of commercial fertilizer granules. With a single or multiple coating of NMs, a controlled nutrient release can be achieved, although the role of coating material and the applied method are critical. Broadly, there are three major categories into which nanofertilizers are divided; nanoscale fertilizers which are NMs containing the nutrients, nanoscale coatings which are NMs coated on the conventional fertilizers and nanoscale additives which are the conventional fertilizers containing some nanoscale additives. The first ever record of GO-based as a slow-release fertilizer was an enhanced uptake of micronutrients, Zn and Cu in the form of Zn–GO and Cu–GO nanofertilizers by the plants [53]. Graphene and GO were used as additives in the fertilizer monoammonium phosphate (MAP) to study their effect on its physical properties. Sheets of graphene and GO were co-granulated in a very dose (0.05–0.5%) with MAP. 0.5% graphene sheet co-granulation (MAP-GN) resulted in 18 times higher mechanical strength. On the other hand, same % addition of GO in MAP (MAP-GO) resulted in a lesser 8 times improvement. There was also an improved resistance in MAP granules to abrasion (> 70%) and to impact resistance (> 75%). There was also enhancement in physical properties on heating MAP-GO at 50 °C which otherwise dried in the ambient conditions. These exciting advantages of graphene and GO as additives was attributed to their nano-matrix as a superior filler, larger specific area, and most importantly, their wrinkled 2D nanostructure that contributes to the great ability of adhesion or interloacking. These findings confirmed the potential use of graphene or GO in making fertilizers that are physical more stable in a soil environment [54].

Graphene and its derivatives have been employed as coating agent for the release of NPK fertilizers, but lack from controlled release, porosity, and flexibility [16]. A chitosan polymer-based GO nanocomposite was prepared by a cross-linking reaction between the amino groups of chitosan and epoxy group of GO. This GO/chitosan nanocomposite showed increase in the mechanical strength of coating with a controlled release of agro-active ingredients for a week [22]. Remarkably, such nanocomposites can be synthesized with green methods on a very large scale at reasonable costs. As encapsulation exhibits a biphasic dissolution behaviour, it can enhance the uptake of Zn and Cu compared to soluble fertilizers that are commercially available [18].

In recent years, several new composites have been designed by using graphene and GO to enhance the mechanical properties of reinforcement materials such as polymers, alloys and metalloids, fertilizer granules and cementitious materials. Such an improvement in mechanical properties due to graphene is attributed to its high Young's modulus, high surface area and high intrinsic strength. However, there are several other parameters that can also influence the mechanical properties of the final nanocomposites. The physiochemical properties and concentration along with the chemical interactions of graphene-based nanomaterials with the matrix can also

influence the mechanical properties of composites [28]. GO modified polyacrylate polymers were used as an excellent coating material with improved mechanical strength due to a crosslinked network between them that rendered controlled release of fertilizers and increased water resistance. For instance, a reduction from 87.25 to 59.71% in the cumulative nutrient release for 28 days was obtained. A delayed release in urea was also shown at 0.3% addition of GO that improved the coating strength. This study has great advantage in delivery water-borne controlled release of fertilizers through GO-polymer nanocomposites [55].

In a pesticide carrier system, it is necessary to achieve their effective use without any loss. One example of that is the synthesis of GO and poly-dopamine (PDA) nanocomposite as a stimuli-responsive adhesive. GO with a PDA layer resulted in higher loading capacity of hymexazol (Hy) with a NIR laser- and pH-dependent release. A stimulate rain-wash experiment on adhesion-performance revealed that Hy-GO@PDA had more stable persistence and more residual Hy with a concentrated surfactant as compared to Hy solution only. It also showed an inhibited bioactivity for *Fusarium oxysporum* f. sp. *Cucumeberium.* GO@PDA has the potential to be successfully used as a pesticide carrier resolving issues of low-utilization and wash-off, in particular with water-soluble pesticides [56].

## *3.3 Diagnosing and Controlling Biotic Stresses (Pest and Diseases)*

An interesting advancement in the use of nanoparticle happened as a pesticide agent which could be an alternative to chemically synthesized pesticides [57]. Graphene-based NMs are cheap and easily produced at large scale, thus can be a great and safe alternative to ditch the traditional use of pesticides and nematicides. Moreover, they can act as good additives for soil. Inoculation of root-rot pathogens, viz., *Meloidogyne incognita* and *Macrophomina haseolina*, and their subsequent application in lentil plant with GO at 250 ppm and 125 ppm caused a significant reduction in root noduling, nematode multiplication and root-rot index as compared to the non-inoculated treatments. The total dry matter weight of the lentil plant was also more than the untreated ones [58]. There was a reduction in number of nematode galls (94%) and total egg mass (99%) by treating it with rGO in tomato plant. Also, a treatment of rGO in soil infested with *Meloidogyne incognita*, ensured a higher mortality rate of the nematode against the traditional nematicide [51].

The antimicrobial properties possessed by graphene, GO and rGO against many multi-resistant bacterial, fungal and nematicidal phytopathogens act as a powerful tool in controlling various crop diseases [59, 60]. In this regard, GO and rGO has better antimicrobial properties than graphene. GO and rGO have the capacity of deactivating bacterial cell by causing oxidative stress and disrupting phosholipid cell membrane. An improved antibacterial activity against *MRSA* and *E. coli* was seen in an injectable hydrogel incorporated with GO due to high conductivity and

photothermal activity. A very low concentration of GO @ 250 μg/mL inhibited and suppressed the bacterial infection in rice caused by *Xanthomonas oryzae* pv. *oryzae* with mortality rate of 94.48% by inducing severe oxidative damage in the bacterial cells and thereby, showcasing its superior lethal efficacy as compared to bactericide bismerthiazol. The unique and extreme sharp edges of GO can injure the cell membrane of a bacteria rendering it as a valuable antibacterial agent against pathogens with multidrug resistance [61]. However, the antimicrobial activity of graphene, GO and rGO is somewhat controversial. A study showed no such inheritance of antibacterial properties in graphene and credited its reported behaviours as a result of impurities.

At varying concentrations, graphene and its oxides (GO and rGO) have the ability to check the fungal populations by curbing the mycellar growth, inhibiting spore formation and crimping the biomass [62]. Combination of nanocomposites also have profound detrimental effects on spores and hyphae of these fungal pathogens and thus, pose as a strong antifungal agent to curb the heavy yield losses in agriculture. For instance, silver NPs nanocomposites are used against *Fusarium graminearum* for controlling leaf spot disease in plants [63, 64], GO–$Fe_3O_4$ nanocomposite, when applied to the leaf discs in grapes plants, helped in controlling the downy mildew disease caused due to *Plasmopara viticola* by inhibiting their spore formation [65, 66], rGO-CuO nanocomposites caused cell death of the fungal pathogen by creating various pits and pores in the cell membranes. 1 mg/L of the nanocomposite was sufficient to reduce the *Fusarium* wilt, reduce the severity of root-rot diseases below 5% in tomato and pepper without causing any phytotoxicity for ~ 70 days. Usually, 2.5 g/L of Kocide is used to get ~ 30% reduction in disease in both the plants [67].

Transition metal dichalcogenides (TMDs) are also known to damage the cell membrane by releasing reactive oxygen species (ROS). Some recent studies on $MoS_2$ and $WS_2$ have shown them to be non-toxic and used as antimicrobials. $MoS_2$ generates superoxide anions that slips through the membrane and bind to the peptide backbones. $WS_2$, on the other hand, can rupture the cell membrane [68]. Various other 2D NMs have the potential to be used as antimicrobial agent but is limited by the research. An antibacterial activity against gram-positive and gram-negative bacteria was demonstrated in MXenes NSs, viz., $Ti_3C_2T_x$ and indium (III) selenide ($In_2Se_3$). The sharp edges of NSs help in cellular degradation and the photothermal activity of $In_2Se_3$ increases the efficacy of antimicrobial activity [68]. An interesting use of clay nanosheets as a non-toxic and biodegradable NM is achieved in the topical RNAi delivery to achieve protection against the plant viruses [62]. The global crop production is severely hit by deadly viral pathogens [69–71], among which begomovirus species stand as one of the most prominent pant viruses. The incorporation of 2D NMs for such a viral-pathogen eradication can change the way we manage crop production in the world.

### 3.4 Combating Abiotic Stresses (Salinity and Drought)

Abiotic stresses such as salinity, drought, heat, flooding, freezing, nutrient deficiency, ultraviolet radiation, etc. have posed a major threat to agro-ecosystem by negatively altering the morphological, biochemical, physiological and cellular aspects of plants, thereby hampering crop growth and production. Abiotic stresses are known to cause oxidative stress in plants [72] resulting in cell damage. In field conditions, plants are exposed to various combinations of stress such as drought and salinity, salinity and heat etc. accelerating the intensity and severity of different stresses. There is a strong relation between drought, greenhouse emissions and the climate changes which is leading to an increase in arid land mass causing severe damages to agriculture [73]. Therefore, mitigation of these stresses by implementing modern technologies like nano-based techniques is the need of the hour [74]. NMs help in minimizing the damage through enhancing their defence mechanisms by involving antioxidant enzymes such as superoxide dismutase, peroxidase and catalase [75], supplying more efficient and less toxic fertilizers, etc. However, NMs at higher concentration can cause toxicity [14, 76] aggravating the accumulation of free radicals and reactive species of oxygen and nitrogen leading to a damage in the structure of nucleic acids, proteins and cell membrane resulting in oxidative injury in plants [77]. The damage is caused by inducing malondialdehyde, hydrogen peroxide and proline contents and decrease in antioxidant enzyme activity resulting in post-harvest yield reduction [78]. Therefore, it is essential to maintain a balanced application of NMs at different stages of plant growth.

An improved tolerance towards salinity stress was observed after the foliar application of GO by the pearl millet (*Pennisetum glaucum* L.), a fodder plant as a result of modifying its biophysical and morphological traits. Furthermore, modified GO when applied at 20 mg $L^{-1}$, a higher growth and yield in its green and dry form was achieved suggesting a boost in photosynthetic efficiency, chlorophyll content, total protein content and thus, biomass accumulation of the fodder plant [79]. It was observed that GO alleviated the damage caused due to salinity and also improved the morphological, physiological and biochemical characteristics of Milk thistle, a herbal plant [80]. Improved germination rate was also observed in Sorghum and Switch grass, bioenergy crops, under salt stress conditions when treated with graphene [81]. GO consists of hydrophilic oxygen-containing groups acting as an effective water retention agent and thus, prevents evaporation of soil water [82]. Therefore, under drought condition, a higher photosynthesis rate, lignin biosynthesis, increased activity by antioxidant enzymes, lowered residual toxicity by reactive oxygen species and glyoxylate and dicarboxylate metabolism were observed in *Paeonia ostii*, a hardy shrub [83]. Moreover, a prolonged exposure of GO brought about an increase in flowering and plant survival rate in *Catharanthus*, an ornamental plant and total fibre production in case of cotton plant by subduing the harmful effects of severe drought conditions [47].

Interestingly, 2D metal nanosheets and graphene NMs can act as nanoenzyme by mimicking activities of various enzymes, such as catalase, superoxide dismutase, peroxidase and oxidase [84]. Therefore, there is a high probability of engineering 2D NMs exhibiting antioxidant activities by preparing 2D NMs filled with different molecular antioxidants, for instance, flavonoids, carotenoids and vitamins, and 2D nanocomposites possessing radical scavenging like properties [85]. These approaches will reduce the oxidative stress and also increase the tolerance towards different kinds of stress in plants.

### *3.5 Sensing and Restoring the Ecosystem*

The rapid pressure on agriculture to meet the food supply demand of the ever-increasing population has posed a severe threat of environmental pollution in the form of contaminations caused by inorganic or organic compounds, heavy metal residue, soil degradation, poisonous gases etc. [86]. The extensive usage of chemical fertilizers and pesticides over the last six decades has resulted in heavy contamination of soil and water which ultimately harm the other members of the food chain [87]. The introduction of nanotechnology in the field of monitoring, sensing, catalyzing, imaging and prevention has been very promising in dealing with the emerging damage to the ecosystem owing to their distinctive novel material properties. viz., large surface to volume ratio, excellent chemical strength, easy functionalization, high thermal and mechanical stability, great electrical conductivity and mass production [88, 89].

NMs have enormous potential in augmenting the productivity of crops through deployment of genetic materials and drug molecules into the intracellular levels of plants [90–92]. The specific use of 2D NMs can be beneficial in tackling food insecurity through managing soil and water quality which will minimize the dependence on pesticides and fertilizers. Also, biosensors could become valuable for the integrated management of pest in crops and livestock by constant monitoring and/or early detection of any diseases to avoid potential outbreaks [93]. The very first step towards that would be to monitor the toxic chemical hazards present in the environment. Scientists have developed different sensors having unique characteristics, particular target and specific mode of operation such as phenols/phenoxy acids [94], halogenated pesticides [95] and inorganic substances, e.g. Hg [96]. Graphene-based nanocomposites are often used in the detection of nitrate and nitrite in water. Graphen/MWCNTs/FeNPs nanocomposites were developed by combining graphene with metal nanocomposites to develop glassy carbon electrode (GCE) for facilitating nitrate and nitrite ions detection in water [97]. Similarly, GO nanosheets and poly (3,4-ethylenedioxythiophene) (PEDOT) nanofibers were together fabricated to appraise the level of nitrate in the soil by immobilizing the nitrate reductase enzymes [98]. An array of GO-based nanocomposites was administered for electrochemical sensing of major environmental pollutants, viz., 4-Nitrophenol, TNP, TNT, HQ, APh and o-NPh [99]. GO-based nanocomposite was able to detect thallium

ions in cereals [100], which is detrimental for human health. Similarly, AuNPs-rGO composite formed from L-cysteine, gold nanoparticles and reduced graphene oxide was used for the determination of $Cu^{2+}$ ions in the soil samples [101].

Graphene nanocomposite based sensors have played a promising role in ultrasensitive detection of phytohormones [102, 103], flavonoids [104, 105], growth regulators [106, 107] and pesticides/herbicides in soil [108, 109], fruits [110] and vegetables [111]. A fabricated sensing film based on self-assemblage of phosphotungstic acid-GO nanohybrid on graphite electrode was able to detect minute concentration of plant hormone methyl jasmonate [112]. Similarly, sensor made up of platinum NP and loaded with graphene nanosheet was used to detect Oxalic acid (OA) is naturally present in plants, fruits and vegetables [113]. A graphene-based magnetic nanocomposite was found to be successful in detecting and extracting seven types of triazole fungicides (tebuconazole, paclobutrazol, diniconazole, triadimefon, myclobutanil, hexaconazole and propiconazole) in cucumber, cabbage and tomato [114].

Poly(safranine T)-rGO nanocomposite based disposable electrochemical sensor was able to detect indole 3-acetic acid (IAA) hormones even in low levels in plant leaves [115]. Graphene nanosheets were fabricated as sensors to quantify quercetin in onion and apple [116]. A graphene nanosheets hydroxyapatite modified glassy carbon electrodes can detect concentrations of flavonoid luteolin in peanut hulls [117]. Graphene-like tungsten disulphide ($WS_2$) nanosheets on poly(3,4-ethoxylenedioxythiophene) (PEDOT), a porous and conductive polymer was developed to detect concentration of quercetin in lotus leaves [118]. Excitingly, a chemiresistance-based hybrid gas sensor prepared from hybrid films of polyaniline (PANI)/$Ti_3C_2T_x$ was found to be capable to monitor the volatilization of ammonia in the agricultural fields [119]. A nanocomposite designed from graphene ribbon and AgNPs were found effective in the detection of organophosphorus pesticide methyl parathion in fruits and vegetables [120]. There are also photocatalysts based on $WO_3$ nanosheets/nanorods and grafts of α-CD, β-CD and γ-CD on the nanocomposites of $MoS_2$/g-$C_3N_4$ (CDs/$MoS_2$/g-$C_3N_4$) which can be used for the removal of toxic pesticides such as bromacil, chlorfenvinphos [121] and glyphosate from agricultural runoff, respectively [122]. The performance and multitude of functionalities designed for the nanosystems essentially rely on numerous parameters like sensitivity, specificity, facile operation, precision and detection limit.

## 4 Future Challenges and Conclusion

In recent years, research and innovations revolving around nanotechnology have emerged as a powerful potential tool in combating the major issues of hunger among the rising population Nano-based agricultural strategies improve food production in a sustainable manner without causing any harm to the limited natural resources. Bowing to the outstanding properties governed by 2D NMs, it is now possible to improve rate of seed germination, achieve great seedling and enhanced crop performance and growth. This can be successfully achieved by providing slow and target

oriented delivery of macro- and micronutrients to the developing plants enhancing their uptake and absorption for proper utilization. At the same time, 2D NMs enhanced pesticides, herbicides and nematicides achieve better protection, improved tolerance against biotic as well as abiotic stress with less residual effects. These nanoformulations also ensure a reduced loss of agricultural inputs and thus minimizing the cost of production. When 2D NMs are combined with any other material, the formulation will have more space for the reactions because of higher surface area providing energy storage or generation more efficiently. The smart packaging technique in the form of nanofilms aids in minimizing post-harvest loss of perishable food items such as flowers, fruits and vegetables during storage and transportation by protracting their shelf life. Researchers believe that NM might help in harvesting energy from the environment from various sources; however, it will require developing new NM and notions. Therefore, 2D NMs possess limitless potential that can achieve the goal of food sustainability for the future generations. While nanotechnologies can offer several innovative prospects, their use in food and agriculture fields has raised issues related to environment, safety, human health, ethics and regulations. Some associated factors such as toxicity of NMs, production cost and stability criteria in external environments require serious and thorough investigations. Keeping in mind that a substantial amount of research is already being conducted, it may be anticipated that society and environment will significantly benefit from 2D NMs driven technology advancement in the near future.

## References

1. Singh RP, Handa R, Manchanda G (2021) Nanoparticles in sustainable agriculture: an emerging opportunity. J Control Release 329:1234–1248
2. Myers SS, Smith MR, Guth S, Golden CD, Vaitla B, Mueller ND, Dangour AD, Huybers P (2017) Climate change and global food systems: potential impacts on food security and undernutrition. Annu Rev Public Health 38(1):259–277
3. Rehmanullah MZ, Inayat N, Majeed A (2020) Application of nanoparticles in agriculture as fertilizers and pesticides: challenges and opportunities. In: Rakshit A, Singh H, Singh U, Fraceto L (eds) New frontiers in stress management for durable agriculture. Springer, Singapore, pp 281–293. https://doi.org/10.1007/978-981-15-1322-017
4. Khan MR, Fatima FM (2017) Application of nano-fertilizers and nanopesicides for improvements in crop production and protection. Nanosci Plant-Soil Syst:405–427
5. Sekhon BS (2014) Nanotechnology in agri-food production: an overview. Nanotechnol Sci Appl 7:31
6. Fawzy ZF, Haggag WM (2020) Smart fertilizers and pesticides VIA nanotechnology for agricultural sustainability. J Biogeneric Sci Res 3(1)
7. Shang Y, Hasan M, Ahammed GJ, Li M, Yin H, Zhou J (2019) Applications of nanotechnology in plant growth and crop protection: a review. Molecules 24(14):2558
8. Servin A, Elmer W, Mukherjee A, De la Torre-Roche R, Hamdi H, White JC, Bindraban P, Dimkpa C (2015) A review of the use of engineered nanomaterials to suppress plant disease and enhance crop yield. J Nanopart Res 17(2):92
9. Hochella MF, Mogk DW, Ranville J, Allen IC, Luther GW, Marr LC, McGrail BP, Murayama M, Qafoku NP, Rosso KM (2019) Natural, incidental, and engineered nanomaterials and their impacts on the earth system. Science 363(6434)

10. Ghidan AY, Antary TMA (2019) Applications of nanotechnology in agriculture
11. Prasad R, Bhattacharyya A, Nguyen QD (2017) Nanotechnology in sustainable agriculture: recent developments, challenges, and perspectives. Front Microbiol 8:1014
12. Mittal D, Kaur G, Singh P, Yadav K, Azmal Ali A (2020) Nanoparticle-based sustainable agriculture and food science: recent advances and future outlook. Front Nanotechnol 2:579954
13. Shaw ZL, Kuriakose S, Cheeseman S (2021) Antipathogenic properties and applications of low-dimensional materials. Nat Commun 12:3897
14. Zaytseva O, Neumann G (2016) Carbon nanomaterials: Production, impacton plant development, agricultural and environmental applications. Chem Biological Technol Agric 3:17
15. Cheng HN, Klasson KT, Asakura T, Wu Q (2016) Nanotechnology in agriculture. Nanotechnol Delivering Promise 2(12):233–242
16. Andelkovic IB, Kabiri S, Tavakkoli E, Kirby JK, McLaughlin MJ, Losic D (2018). Graphene oxide-Fe(III) composite containing phosphate—a novel slow release fertilizer for improved agriculture management. J Clean Prod 185(III):97–104
17. Wang Z, Wu A, Ciacchi LC, Wei G (2018) Recent advances in Nanoporous membranes for water purification. Nanomaterials 8(65)
18. Kabiri S, Degryse F, Tran DN, da Silva RC, McLaughlin MJ, Losic D (2017) Graphene oxide: a new carrier for slow release of plant micronutrients. ACS Appl Mater Interfaces 9(49):43325–43335
19. Sundramoorthy AK, Vignesh Kumar TH, Gunasekaran S (2018) Graphene-basednanosensors and smart food packaging systems for food safety and quality monitoring food. Graphene Bioelectron:267–306
20. Park S, Choi KS, Kim S, Gwon Y, Kim J (2020) Graphene oxide-assisted promotion of plant growth and stability. Nanomaterials 10(4):758
21. Wang X, Xie H, Wang Z, He K, Jing D (2019) Graphene oxide as a multifunctional synergist of insecticides against lepidopteran insect. Environ Sci Nano 6(1):75–84
22. Li T, Gao B, Tong Z, Yang Y, Li Y (2019) Chitosan and graphene oxide nanocomposites as coatings for controlled-release fertilizer. Water Air Soil Pollut 230(7):146. https://doi.org/10.1007/s11270-019-4173-2
23. Homaeigohar S, Elbahri M (2017) Graphene membranes for water desalination. NPG Asia Mater 9:427. https://doi.org/10.1038/am.2017.135
24. Hou D, He H, Huang P, Zhang G, Loaiciga H (2013) Detection of water-quality contamination events based on multi-sensor fusion using an extended Dempster-Shafer method. Meas Sci Technol 24(055801):18
25. Zhao F, Yao Y, Jiang C, Shao Y, Barceló D, Ying Y, Ping J (2020) Self-reduction bimetallic nanoparticles on ultrathin MXene nanosheets as functional platform for pesticide sensing. J Hazard Mater 384:121358. https://doi.org/10.1016/j.jhazmat.2019.121358
26. Tu X, Gao F, Ma X, Zou J, Yu Y, Li M, Qu F, Huang X, Lu L (2020) Mxene/carbon nanohorn/β-cyclodextrin-Metal-organic frameworks as high-performance electrochemical sensing platform for sensitive detection of carbendazim pesticide. J Hazardous Mater:122776
27. Tang S, Liu T, Dang Q, Zhou X, Li X, Yang T, Luo Y, Sharman E, Jiang J (2020) Synergistic effect of surface-terminated oxygen vacancy and single-atom catalysts on defective MXenes for efficient nitrogen fixation. J Phys Chem Lett 11(13):5051–5058. https://doi.org/10.1021/acs.jpclett.0c01415
28. Wu W, Wan M, Fei Q, Tian Y, Song S, Shen H, Shen J (2021) PDA@$Ti_3C_2Tx$ as a novel carrier for pesticide delivery and its application in plant protection: NIR-responsive controlled release and sustained antipest activity. Pest management science n/a (n/a). https://doi.org/10.1002/ps.6538
29. Achari GA, Kowshik M (2018) Recent developments on nanotechnology in agriculture: plant mineral nutrition, health, and interactions with soil microflora. J Agric Food Chem 66(33):8647–8661. https://doi.org/10.1021/acs.jafc.8b00691
30. Zahedi SM, Karimi M, Teixeira da Silva JA (2020) The use of nanotechnology to increase quality and yield of fruit crops. J Sci Food Agric 100(1):25–31

31. Fojtu M, Teo W Z, Pumera M (2017) Environmental impact and potential health risks of 2D nanomaterials. Environ Sci Nano 4(8):1617–1633
32. Rao CEE, Sood AE, Subrahmanyam KE, Govindaraj A (2009) Graphene: the new two-dimensional nanomaterial. Angew Chem Int Edn 48(42):7752–7777
33. Tong Y, Shao L, Li X, Lu J, Sun H, Xiang S, Zhang Z, Wu Y, Wu X (2018) Adhesive and stimulus-responsive polydopamine-coated graphene oxide system for pesticide-loss control. J Agric Food Chem 66(11):2616–2622
34. Zhang M, Gao B, Chen J, Li Y, Creamer AE, Chen H (2014) Slow-release fertilizer encapsulated by graphene oxide films. Chem Eng J 255:107–113
35. Bhimanapati GR, Lin Z, Meunier V, Jung Y, Cha J, Das S, Xiao D, Son Y, Strano MS, Cooper VR (2015) Recent advances in two-dimensional materials beyond graphene. ACS Nano 9(12):11509–11539
36. Lan L, Yao Y, Ping J, Ying Y (2019) Ultrathin transition-metal dichalcogenide nanosheet-based colorimetric sensor for sensitive and label-free detection of DNA. Sens Actuators Chem 290:565–572
37. Hwa KY, Ganguly A, Santhan A, Sharma TSK (2021) Vanadium selenide decorated reduced graphene oxide nanocomposite: a co-active catalyst for the detection of 2, 4, 6-trichlorophenol. Chemosphere 282:130874
38. Hao L, Gong L, Chen L, Guan M, Zhou H, Qiu S, Wen H, Chen H, Zhou X, Akbulut M (2020) Composite pesticide nanocarriers involving functionalized boron nitride nanoplatelets for pH-responsive release and enhanced UV stability. Chem Eng J 396:125233
39. Gogotsi Y, Anasori B (2019) The rise of MXenes. ACS Nano 13(8):8491–8494
40. Song S, Jiang X, Shen H, Wu W, Shi Q, Wan M, Zhang J, Mo H, Shen J (2021) MXene ($Ti_3C_2$) based pesticide delivery system for sustained release and enhanced pest control. ACS Appl Bio Mater 4(9):6912–6923
41. Chaudhary V, Gautam A, Mishra YK, Kaushik A (2021) Emerging MXene–polymer hybrid nanocomposites for high-performance ammonia sensing and monitoring. Nanomaterials 11(10):2496
42. Carey M, Barsoum M (2021) MXene polymer nanocomposites: a review. Mater Today Adv 9:100120
43. Riazi H, Taghizadeh G, Soroush M (2021) MXene-based nanocomposite sensors. ACS Omega 6:11103–11112
44. Zhang M, Gao B, Chen J, Li Y (2015) Effects of graphene on seed germination and seedling growth. J Nanopart Res 17(2):1–8
45. He Y, Hu R, Zhong Y, Zhao X, Chen Q, Zhu H (2018) Graphene oxide as a water transporter promoting germination of plants in soil. Nano Res 11(4):1928–1937
46. Younes N, Dawood MF, Wardany A (2019) Biosafety assessment of graphene nanosheets on leaf ultrastructure, physiological and yield traits of *Capsicum annuum* L. and *Solanum melongena* L. Chemosphere 228:318–327
47. Pandey K, Anas M, Hicks VK, Green MJ, Khodakovskaya MV (2019) Improvement of commercially valuable traits of industrial crops by application of carbon-based nanomaterials. Sci Rep 9(1):1–14
48. Song J, Cao K, Duan C, Luo N, Cui X (2020) Effects of graphene on *Larix olgensis* seedlings and soil properties of haplic cambisols in Northeast China. Forests 11(3):258
49. Kim MJ, Kim W, Chung H (2020) Effects of silver-graphene oxide on seed germination and early growth of crop species. Peer J 8:e8387
50. Samadi S, Lajayer BA, Moghiseh E, Rodríguez-Couto S (2020) Effect of carbon nanomaterials on cell toxicity, biomass production, nutritional and active compound accumulation in plants. Environ Technol Innov
51. Gareeb RY, Elnouby MS, Hasan MA, Ticu S, Popa A, Bungau S, Hafez EE (2019) New trend for using the reduced graphene oxide as effective and eco-friendly nematicide. Mater Plast 56(1)
52. Li X, Mu L, Li D, Ouyang S, He C, Hu X (2018) Effects of the size and oxidation of graphene oxide on crop quality and specific molecular pathways. Carbon 140:352–361

53. Marchiol L, Iafisco M, Fellet G, Adamiano A (2020) Nanotechnology support the next agricultural revolution: perspectives to enhancement of nutrient use efficiency. Adv Agron 161:27–116
54. Kabiri S, Baird R, Tran DN, Andelkovic I, McLaughlin MJ, Losic D (2018) Cogranulation of low rates of graphene and graphene oxide with macronutrient fertilizers remarkably improves their physical properties. ACS Sustain Chem Eng 6(1):1299–1309
55. Shahryari Z, Yeganeh M, Gheisari K, Ramezanzadeh B (2021) A brief review of the graphene oxide-based polymer nanocomposite coatings: preparation, characterization, and properties. J Coat Technol Res 7:1–25
56. Camara MC, Campos EV, Monteiro RA, do Espirito Santo Pereira A, de Freitas Proença PL, Fraceto LF (2019) Development of stimuli-responsive nano-based pesticides: emerging opportunities for agriculture. J Nanobiotechnol 17(1):1–9
57. Ramezani M, Ramezani F, Gerami M (2019) Nanoparticles in pest incidences and plant disease control. In: Nanotechnology for agriculture: crop production and protection. Springer, Singapore, pp 233–272
58. Guroo J, Khan M, Ahmad A, Azam A, Siddiqui Z (2016) Management of meloidogyne incognita and *Macrophomina phaseolina* by graphene oxide on *Lens culinaris*. Acta Phytopathol Entomol Hungarica 51(1):43–56
59. Chen J, Peng H, Wang X, Shao F, Yuan Z, Han H (2014) Graphene oxide exhibits broad-spectrum antimicrobial activity against bacterial phytopathogens and fungal conidia by intertwining and membrane perturbation. Nanoscale 6(3):1879–1889. https://doi.org/10.1039/C3NR04941H
60. Hajong M, Devi NO, Debbarma M, Majumder D (2019) Nanotechnology: an emerging tool for management of biotic stresses in plants. In: Plant nanobionics. Springer, Cham, pp. 299–335
61. Chen J, Wang X, Han H (2013) A new function of graphene oxide emerges: inactivating phytopathogenic bacterium *Xanthomonas oryzae* pv *Oryzae*. J Nanopart Res 15(5):1658. https://doi.org/10.1007/s11051-013-1658-6
62. Mitter N, Worrall EA, Robinson KE, Li P, Jain RG, Taochy C, Fletcher SJ, Carroll BJ, Lu GM, Xu ZP (2017) Clay nanosheets for topical delivery of RNAi for sustained protection against plant viruses. Nat Plants 3(2):1–10
63. Zhou X, Sun H, Bai X (2020) Two-dimensional transition metal dichalcogenides: synthesis, biomedical applications and biosafety evaluation. Front Bioeng Biotechnol 8:236
64. Chen J, Sun L, Cheng Y, Lu Z, Shao K, Li T, Hu C, Han H (2016) Graphene oxide-silver nanocomposite: novel agricultural antifungal agent against *Fusarium graminearum* for crop disease prevention. ACS Appl Mater Interfaces 8(36):24057–24070
65. Lan L, Yao Y, Ping J, Ying Y (2019) Ultrathin transition-metal dichalcogenide nanosheet-based colorimetric sensor for sensitive and label-free detection of DNA. Sens Actuat B Chem 290:565–572
66. Wang X, Cai A, Wen X, Jing D, Qi H, Yuan H (2017) Graphene oxide-$Fe_3O_4$ nanocomposites as high-performance antifungal agents against *Plasmopara viticola*. Sci China Mater 60(3):258–268
67. El-Abeid SE, Ahmed Y, Daròs J-A, Mohamed MA (2020) Reduced Graphene oxide nanosheet-decorated copper oxide nanoparticles: a potent antifungal nanocomposite against fusarium root rot and wilt diseases of tomato and pepper plants. Nanomaterials 10(5):1001
68. Shaw ZL, Kuriakose S, Cheeseman S, Dickey MD, Genzer J, Christofferson AJ, Crawford RJ, McConville CF, Chapman J, Truong VK, Elbourne A (2021) Antipathogenic properties and applications of low-dimensional materials. Nat Commun 12(1):1–9
69. Verma S, Saxena S (2017) Dissecting papaya leaf curl disease (PLCD) complex and assessing its potential for siRNA based targeting. Int J Plant Environ 3(02):17–29
70. Verma S, Saxena S (2018) In-silico investigation of betasatellite complexity in papaya leaf curl disease complex. Int J Plant Environ 4(02):41–49
71. Verma S (2019) An insight into the approaches to target begomoviruses: RNAi perspective. Int J Plant Environ 5(03)

72. Servin AD, White JC (2016) Nanotechnology in agriculture: next steps for understanding engineered nanoparticle exposure and risk. Nano Impact 1:9–12
73. Elsakhawy T, Omara AE, Alshaal T, El-Ramady H (2018) Nanomaterials and plant abiotic stress in agroecosystems. Environ Biodiv Soil Secur 2:73–94
74. Mali SC, Raj S, Trivedi R (2020) Nanotechnology a novel approach to enhance crop productivity. Biochem Biophys Rep 24:100821
75. Raina N, Sharma P, Slathia PS, Thakur R, Raina V, Slathia G, Rani N, Sharma S, Bhagat P, Manhas R, Pathak AK (2021) Use of nanomaterials in plants to coup with abiotic stress conditions. Nanobiotechnology. Springer, Cham, pp 527–559
76. Saharan V, Kumaraswamy RV, Choudhary RC, Kumari S, Pal A, Raliya R, Biswas P (2016) Cu-chitosan nanoparticle mediated sustainable approach to enhance seedling growth in maize by mobilizing reserved food. J Agric Food Chem 64(31):6148–6155
77. Khan MA, Khan S, Khan A, Alam M (2017) Soil contamination with cadmium, consequences and remediation using organic amendments. Sci Total Environ 601:1591–1605
78. Wani SH, Kumar V, Shriram V, Sah SK (2014) Phytohormones and their metabolic engineering for abiotic stress tolerance in crop plants. Crop J 4(3):162–176
79. Mahmoud NE, Abdelhameed RM (2021) Superiority of modified graphene oxide for enhancing the growth, yield, and antioxidant potential of pearl millet (*Pennisetum glaucum* L.) under salt stress. Plant Stress 2:100025
80. Safikhan S, Chaichi MR, Khoshbakht K, Amini A, Motesharezadeh B (2018) Application of nanomaterial graphene oxide on biochemical traits of Milk thistle (*Silybum marianum* L.) under salinity stress. Australian J Crop Sci 12
81. Pandey K, Lahiani MH, Hicks VK, Hudson MK, Green MJ, Khodakovskaya M (2018) Effects of carbon-based nanomaterials on seed germination, biomass accumulation and salt stress response of bioenergy crops. PloS one 13(8):e0202274
82. Sharma G, Thakur B, Naushad M, Kumar A, Stadler FJ, Alfadul SM, Mola GT (2018) Applications of nanocomposite hydrogels for biomedical engineering and environmental protection. Environ Chem Lett 16(1):113–146
83. Zhao D, Fang Z, Tang Y, Tao J (2020) Graphene oxide as an effective soil water retention agent can confer drought stress tolerance to *Paeonia ostii* without toxicity. Environ Sci Technol 54(13):8269–8279
84. Cai S, Fu Z, Xiao W, Xiong Y, Wang C, Yang R (2020) Zero-dimensional/two-dimensional Au x Pd100–x nanocomposites with enhanced nanozyme catalysis for sensitive glucose detection. ACS Appl Mater Interfaces 12(10):11616–11624
85. Muráth S, Alsharif NB, Sáringer S, Katana B, Somosi Z, Szilagyi I (2020) Antioxidant materials based on 2D nanostructures: a review on recent progresses. Curr Comput-Aided Drug Des 10(3):14879
86. Su S, Chen S, Fan C (2018) Recent advances in two-dimensional nanomaterials-based electrochemical sensors for environmental analysis. Green Energy Environ 3(2):97–106
87. Baruah S, Dutta J (2009) Nanotechnology applications in pollution sensing and degradation in agriculture: a review. Environ Chem Lett 7:191–204. https://doi.org/10.1007/s10311-009-0228-8
88. Chhowalla M, Shin HS, Eda G, Li LJ, Loh KP, Zhang H (2013) The chemistry of two-dimensional layered transition metal dichalcogenide nanosheets. Nat Chem 5:263–275. https://doi.org/10.1038/nchem.1589
89. Xu M, Liang T, Shi M, Chen H (2013) Graphene like two-dimensional materials. Chem Rev 113(5):3766–3798. https://doi.org/10.1021/cr300263a
90. Kuzma J (2007) Moving forward responsibly: oversight for the nanotechnology-biology interface. J Nanopart Res 9:165–182
91. Scott NR (2007) Nanoscience in veterinary medicine. Vet Res Commun 31(1):139–144
92. Maysinger D (2007) Nanoparticles and cells: good companions and doomed partnerships. Org Biomol Chem 5(15):2335–2342
93. Griesche C, Baeumner AJ (2020) Biosensors to support sustainable agriculture and food safety. TrAC Trends Analyt Chem 128:115906

94. Munteanu FD, Lindgren A, Emneus J, Gorton L, Ruzgas T, Csoregi E, Ciucu A, Van Huystee RB, Gazaryan IG, Lagrimini LM (1998) Bioelectrochemical monitoring of phenols and aromatic amines in flow injection using novel plant peroxidases. Anal Chem 70(13):2596–2600
95. Oroszlan P, Duveneck GL, Ehrat M, Widmer HM (1993) Fiber-optic atrazine immunosensor. Sens Actuat B Chem 11(1–3):301–305
96. Pirvutoiu S, Surugiu I, Dey ES, Ciucu A, Magearu V, Danielsson B (2001) Flow injection analysis of mercury (II) based on enzyme inhibition and thermometric detection. Analyst 126(9):1612–1616
97. Mani V, Wu TY, Chen SM (2014) Iron nanoparticles decorated graphene-multiwalled carbon nanotubes nanocomposite-modified glassy carbon electrode for the sensitive determination of nitrite. J Solid State Electrochem 18(4):1015–1023
98. Ali MA, Jiang H, Mahal NK, Weber RJ, Kumar R, Castellano MJ, Dong L (2017) Microfluidic impedimetric sensor for soil nitrate detection using graphene oxide and conductive nanofibers enabled sensing interface. Sens Actuat B Chem 239:1289–1299
99. Prabakaran E, Pillay K (2021) Electrochemical detection of 4-nitrophenol by using graphene based nanocomposite modified glassy carbon electrodes: a mini review. Nanoarchitectonics 19:61–87
100. Yiwei X, Wen Z, Xiaowei H, Jiyong S, Xiaobo Z, Yanxiao L, Xueping C, Tahir HE, Zhihua L (2018) A self-assembled L-cysteine and electrodeposited gold nanoparticles-reduced graphene oxide modified electrode for adsorptive stripping determination of copper. Electroanalysis 30(1):194–203
101. Tseliou F, Avgeropoulos A, Falaras P, Prodromidis MI (2017) Low dimensional $Bi_2Te_3$-graphene oxide hybrid film-modified electrodes for ultra-sensitive stripping voltammetric detection of Pb (II) and Cd (II). Electrochim Acta 231:230–237
102. Li N, Chen J, Shi YP (2016) Magnetic reduced graphene oxide functionalized with β-cyclodextrin as magnetic solid-phase extraction adsorbents for the determination of phytohormones in tomatoes coupled with high performance liquid chromatography. J Chromatogr 1441:24–33
103. Gan T, Hu S (2011) Electrochemical sensors based on graphene materials. Microchim Acta 175(1–2):1
104. Liu CW, Chien MW, Su CY, Chen HY, Li LJ, Lai CC (2012) Analysis of flavonoids by graphene-based surface-assisted laser desorption/ionization time-of-flight mass spectrometry. Analyst 137(24):5809–5816
105. Hu J, Zhang Z (2020) Application of electrochemical sensors based on carbon nanomaterials for detection of flavonoids. Nanomaterials 10(10)
106. Chen JY, Cao SR, Xi CX, Chen Y, Li XL, Zhang L, Wang GM, Chen YL, Chen ZQ (2020) A novel magnetic β-cyclodextrin modified graphene oxide adsorbent with high recognition capability for 5 plant growth regulators. Food Chem 239:911–919
107. Chen X, Yuan Y, Yan H, Shen S (2021) Selective, sensitive, and miniaturized analytical method based on molecularly imprinted graphene oxide composites for the determination of naphthalene-derived plant growth regulators in apples. Food Chem 349:128982
108. Kumar V, Vaid K, Bansal SA, Kim KH (2020) Nanomaterial-based immunosensors for ultrasensitive detection of pesticides/herbicides: current status and perspectives. Biosens Bioelectron 165:112382
109. Sipa K, Brycht M, Leniart A, Nosal-Wiercińska A, Skrzypek S (2018) Improved electroanalytical characteristics for the determination of pesticide metobromuron in the presence of nanomaterials. Anal Chim Acta 1030:61–69
110. Srimathi U, Nagarajan V, Chandiramouli R (2018) Adsorption studies of volatile organic compounds on germanene nanotube emitted from banana fruit for quality assessment—a density functional application. J Mol Graph Model 82:129–136
111. Hou X, Yu H, Yan S, Xiao J, Sun M, Wu W (2020) Cationic polyelectrolyte/graphene oxide as an efficient sorbent for the extraction and analysis of trace acidic herbicides in vegetables. J Chromatogr A:460884

112. Gan T, Hu C, Chen Z, Hu S (2010) Fabrication and application of a novel plant hormone sensor for the determination of methyl jasmonate based on self-assembling of phosphotungstic acid–graphene oxide nanohybrid on graphite electrode. Sens Actuat B Chem 151(1):8–14
113. Chen X, Cai Z, Huang Z, Oyama M, Jiang Y, Chen X (2013) Non-enzymatic oxalic acid sensor using platinum nanoparticles modified on graphene nanosheets. Nanoscale 5(13):5779–5783
114. Wang L, Zang X, Chang Q, Zhang G, Wang C, Wang Z (2014) Determination of triazole fungicides in vegetable samples by magnetic solid-phase extraction with graphene-coated magnetic nanocomposite as adsorbent followed by gas chromatography—mass spectrometry detection. Food Anal Methods 7(2):318–325
115. Gan T, Hu C, Chen Z, Hu S (2011) A disposable electrochemical sensor for the determination of indole-3-acetic acid based on poly(safranine T)-reduced graphene oxide nanocomposite. Talanta 85(1):310–316. https://doi.org/10.1016/j.talanta.2011.03.070
116. Saber-Tehrani M, Pourhabib A, Husain SW, Arvand M (2013) Electrochemical behavior and voltammetric determination of quercetin in foods by graphene nanosheets modified electrode. Anal Bioanal Electrochem 5(1):1
117. Pang P, Liu Y, Zhang Y, Gao Y, Hu Q (2014) Electrochemical determination of luteolin in peanut hulls using graphene and hydroxyapatite nanocomposite modified electrode. Sens Actuat B Chem 194:397–403
118. Li Y, Niu J, Xue T, Duan X, Tian Q, Wen Y, Lu X, Xu J, Lai L, Chang Y (2020) Multi-functional porous nanohybrid based on graphene-like tungsten disulfide on poly (3, 4-ethoxylenedioxythiophene) for supercapacitor and electrochemical nanosensing of quercetin. J Electrochem Soc 167(4):047512
119. Li X, Xu J, Jiang Y, He Z, Liu B, Xie H, Li H, Li Z, Wang Y, Tai H (2020) Toward agricultural ammonia volatilization monitoring: a flexible polyaniline/$Ti_3C_2Tx$ hybrid sensitive films based gas sensor. Sens Actuat B Chem 316:128144. https://doi.org/10.1016/j.snb.2020.128144
120. Govindasamy M, Mani V, Chen S-M, Chen T-W, Sundramoorthy AK (2017) Methyl parathion detection in vegetables and fruits using silver@ graphene nanoribbons nanocomposite modified screen printed electrode. Sci Rep 7:46471
121. Roselló-Márquez G, Fernández-Domene RM, Sánchez-Tovar R, García-Carrión S, Lucas-Granados B, Garcia-Anton J (2019) Photoelectrocatalyzed degradation of a pesticides mixture solution (chlorfenvinphos and bromacil) by $WO_3$ nanosheets. Sci Total Environ 674:88–95
122. Wu Z, He X, Xue Y, Yang X, Li Y, Li Q, Yu B (2020) Cyclodextrins grafted $MoS_2$/g-$C_3N_4$ as high-performance photocatalysts for the removal of glyphosate and Cr (VI) from simulated agricultural runoff. Chem Eng J:125747

# Chapter 11
# Fate of 2D Nanomaterials and Their Toxic Effects on the Environment and Human Health


**Achyut Konwar, Jayanta Sarmah Boruah, Kabyashree Phukan, and Sazzadur Rahman**

## 1 Introduction

The importance of nanomaterials has increased tremendously in the market with people consuming them every day. It was noted that about 1814 nanomaterial-containing products have been used by consumers till March 2015 which keep on increasing manifolds. One-third of those materials belong to personal care items related to health and fitness. [1] Among different groups of nanomaterials, two-dimensional (2D) nanomaterials are gaining much focus for their versatile use in sensing, [2, 3] drug delivery, [4] energy storage, [5–7] water purification, [8] catalysis, synthesis of nanocomposites, [9] etc. Graphene, graphene oxide, nanoclay, black phosphorus and transition metal dichalcogenides (TMDs) are the most commonly used 2D nanomaterials. Because of their wide industrial applications, their impact on the environment and evaluation of toxicity causing risk to biodiversity, living organism, including human have become major concerns for the environmental safety (Fig. 1). It is found that globally about 66,000 metric tons of engineered nanomaterials (ENMs) are released into the surface water. [10] Therefore, it has become

A. Konwar (✉)
Central Institute of Plastic Engineering and Technology, Institute of Plastic Technology, Bhubaneswar, B/25, CNIC, Patia, Bhubaneswar, Odisha 751024, India
e-mail: achyutkonwar88@gmail.com

J. S. Boruah · K. Phukan · S. Rahman
Material Nanochemistry Laboratory, Institute of Advanced Study in Science and Technology, Guwahati 781035, India
e-mail: chem.jayanta2013@gmail.com

K. Phukan
e-mail: kabyashreephukan06@gmail.com

S. Rahman
e-mail: srahman.ngn1994@gmail.com



Z. Khanam et al. (eds.), *2D Nanomaterials for Energy and Environmental Sustainability*,
Materials Horizons: From Nature to Nanomaterials,
https://doi.org/10.1007/978-981-16-8538-5_11

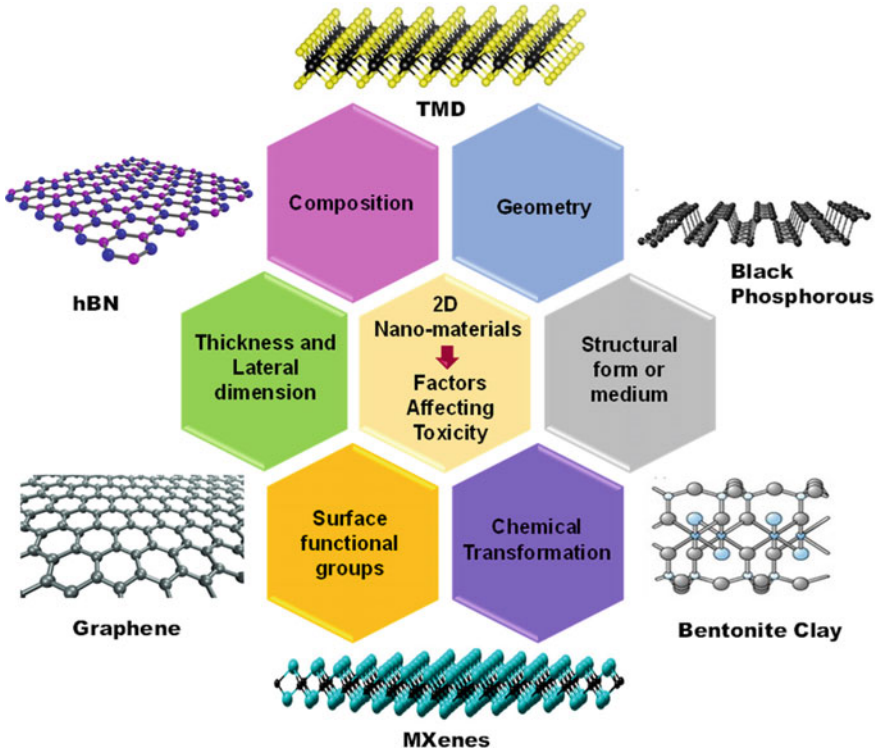


**Fig. 1** Chart showing various factors that govern the toxicity of 2D nanomaterials

utmost importance to evaluate their interaction mechanism with the environment and biological samples to get a clear understanding of their level of toxicity.

This chapter brings out the toxicological effect of common as well as most recently developed 2D nanomaterials. It includes a detailed review on the toxicological study of different 2D nanomaterials carried out by various research groups. A discussion on the probable mechanism of toxicity of 2D nanomaterials causing adversity to environment and human health and some possible measures of remediation is also included.

## 2 Fate of Nanomaterials in the Environment and Human Body

Nanomaterials can enter the environment through any natural and/or manmade pathways [11]. Apart from the natural phenomenon like volcanic activities, weathering, soil erosion, forest fires, clay minerals and dust storms, the nanomaterials could enter into the environment through various human activities such as automobile traffic,

burning fossil fuels and mining/demolition [11, 12]. The fate of nanomaterials in the environment is controlled by the physicochemical properties as well as their ability to interact with other pollutants. The major concern is related to the engineered nanomaterials. These are a group of nanomaterials intentionally produced in large quantities for various applications and can directly encounter human beings through different consumer products [13]. These engineered nanomaterials produced in industries or laboratories ultimately find their easiest way to the environment through waste systems. Degradation of nanoparticle (NP) incorporated products also causes the release of nanomaterials. Once discharged, the nanomaterials accumulate into different matrices of the environment, viz. air, water and soil (Fig. 2) [14].

Atmospheric nanomaterials exposed to sunlight and UV radiation at a significantly higher degree compared to the nanomaterials released into the other components of environment. This exposure is likely to cause various physio-chemical changes of the nanomaterial [15]. They may also change in size by interacting with other volatile

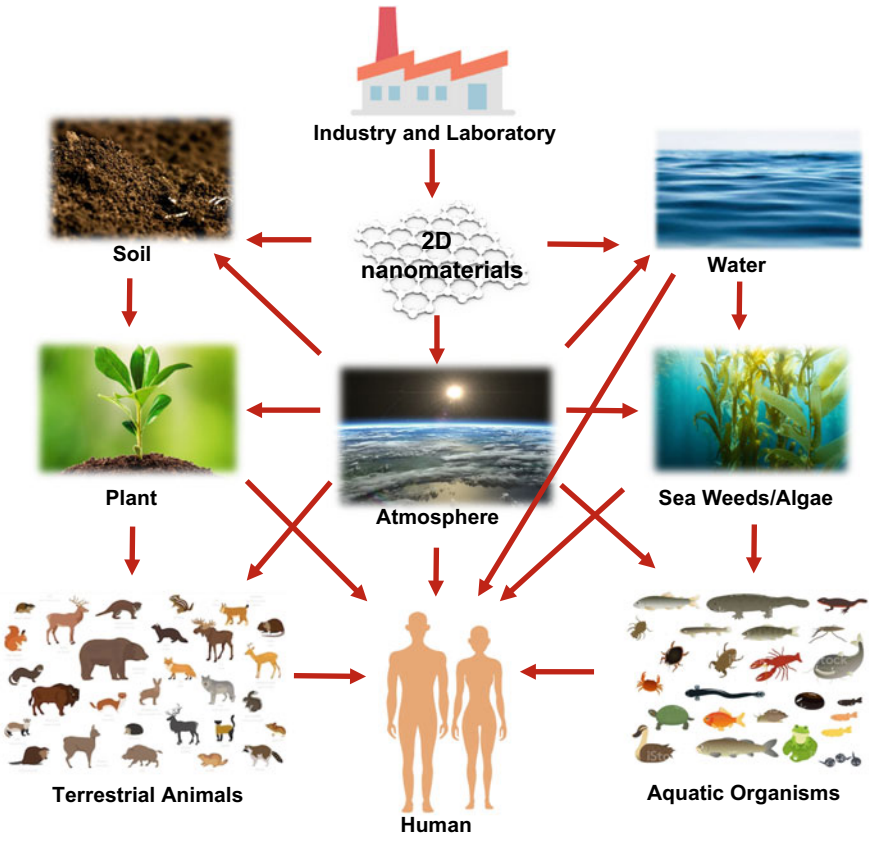


**Fig. 2** Scheme of possible pathways of 2D nanomaterials in ecosystems

compounds present in the atmosphere. Gravitational settling of the nanomaterials from the atmosphere depends upon their size and density [16, 17].

Similarly, various processes, for example, aggregation, diffusion, accumulation, interaction with other components, biological degradation, etc., affect the destiny of nanomaterials in the aquatic system [18]. Aggregation of nanomaterials by interacting with other compounds or particles may cause sedimentation. The degree of aggregation generally depends on the characteristics of the particles (i.e., type, size and surface properties) and of the environmental system (i.e., pH, ionic strength and dissolved organic carbon content). Moreover, the interaction may lead to change in the nanomaterial's surface properties and reactivity [19, 20].

Several variables (e.g., nanoparticle's physical–chemical properties, characteristics of the soil and environment and interactions of nanomaterials with natural colloidal material) influence the mobility of nanomaterials released into the soil. Previous studies have also reported that plants can take up and translocate nanomaterials from the soil, which may influence germination rate and plant growth. Nanomaterials may be responsible for adverse effects on the diversity of microorganism communities present in soil [21–24].

Transformation of nanomaterials' properties after releasing into the environment makes the situation more complicated. Most studies on the effect of environment on nanomaterials are based on their short-term effects. Whereas the transformation of nanomaterials' properties is a factor of retention time as well as the components of the environment. Hence, the dynamics of the environment introduces an uncertainty toward the fate of the nanomaterials [25, 26].

## 3 Nanotoxicity: Effect of Physicochemical Properties of Nanomaterials Toward Human Health

Nanotoxicity is a moderately new branch of toxicology that addresses the gap in knowledge of toxicity induced by nanomaterials. This branch includes the basic understanding of the physicochemical effects of nanomaterials and their routes of exposure/uptake mechanisms for toxicity assessment in humans and the environment. Toxicity of nanomaterials greatly depends on their shape, size, surface and physicochemical properties. A slight variation of their properties may have a great impact on their toxicity [25–27].

There are three ways of toxicity assessment viz., in vivo, in vitro *and* in silico assay. In in vitro study, different cell lines are exposed to several potential toxic substances and left for incubation for definite time intervals. The proliferation and the cellular metabolism of these exposed cells are measured using different assays (MTT, WST-8, etc.). The MTT {3-(4,5-dimethylthiazol-2-yl)-2,5-diphenyltetrazolium bromide} is a colorimetric assay for cell's viability by measuring it's metabolic activity. It is based on the reduction of mitochondrial NADPH-dependent cellular oxidoreductase enzymes which reduce tetrazolium dye (MTT) and gives insoluble purple

color formazan. Through the process of endocytosis cells taken up MTT and after reduction by mitochondrial enzymes it is transported back to the cell surfaces in the form of needle like insoluble formazans. The water-insoluble formazan can be dissolved in cell by adding DMSO (sodium dodecyl sulfate) into the treated 96 well plate and absorbance can be measured at a wavelength 570 nm (usually between 500 and 600 nm) by a spectrophotometer [28]. There are some limitations in the application of tetrazolium salt due to low solubility of formazan. To overcome such problems, several water-soluble tetrazolium salts (WST), which include WST-1, WST-3 and WST-8 [2-(2-methoxy-4-nitrophenyl)-3-(4-nitrophenyl)-5-(2,4-disulfophenyl)-2H-tetrazolium, monosodium salt], have been synthesized. In the presence of an electron mediator, such as 1-methoxy-5-methylphenazium methylsulfate (1-mPMS), WST is readily reduced by NAD(P)H to produce a formazan product, and the absorbance can be measured in the range 430–550 nm. Similarly, WST is also colorimetric assay that shows efficacy for various qualitative and quantitative applications [29].

In in vivo technique, a small dosage of the toxic substance is administered inside the body of model animals such as mice. The cellular uptake, distribution, metabolism and removal pathway can be studied through this technique. However, compared to in vivo assessments, in vitro testing methods are fast, low cost and do not involve ethical issues of animal testing. In silico method is one of the relatively novel approaches compared to the conventional in vitro and in vivo assessment techniques. This technique is faster and cost-effective. It utilizes several theoretical models to predict the physicochemical properties of the molecules. The toxicity of any molecular compound is predicted using the available experimental data and further interpolating using mathematical models [27].

To determine the toxicity of 2D nanomaterials, many different parameters are studied such as disruption of metabolic activity, oxidative stress and cell membrane disintegration [30]. There are many in vitro tests that can be done to determine the generation of toxicity which are grouped into two categories, namely viability tests and functional assays. In cell viability test, various cellular properties such as membrane integrity, structure and mitochondrial activity can be measured by specific assays to determine cell damage caused upon exposure of cells to 2D nanomaterials [31]. For example, MTT (3-(4,5-dimethylthiazol-2-yl)-2,5-diphenyl tetrazolium bromide) and WST-8 (water-soluble tetrazolium salt) assays assess mitochondrial activity. In metabolically active cells, the colored product formazan dye gradually increases (which indicates more viable cells as the color intensity increases) with decreasing the tetrazolium reagent [32, 33]. On the other hand, functional assays give more emphasis on the mechanism of toxicity via various cellular processes. For example, comet assay [34] where cell DNA damage can be identified by the ratio of fluorescence intensity emitted from damaged DNA to intact DNA where the value measures the level of DNA damage as a result of exposure of nanomaterials [35]. The other cellular indicators namely oxidative stress where by inducing stress, cells generate more intracellular reactive oxygen species (ROS) such as hydroxyl radicals, peroxy radicals and hydrogen peroxide [36]. Quantification of amount of ROS can be done by 2′,7′-dichlorodihydrofluorescein diacetate (DCFDA) [37–39].

# 4 Toxicity Assessment of 2D Nanomaterials in Human Health

## *4.1 Toxicity of Graphene Family Nanomaterials*

Graphene is one of the most widely used 2D nanomaterials for advanced applications. Nearly, all fields (electronics to biological) are associated with graphene or its derivatives. Although it has shown its superiority in many ways, it has shown toxicity issues toward humans and environment. The variability in their toxicity level stems from lateral dimensions (size), shape, dispersity, surface structure and charge or functionalization. The exact mechanism responsible for graphene toxicity is not clear yet. Physical interactions could be one of the major causes of graphene toxicity and antimicrobial property [40]. Graphene can bind with α-helical structures of peptides and is observed to cause an abnormal stretching of the cell membrane of RAW 264.7 cells (a type of macrophage cell line) by largely adhering to the membrane surfaces at a concentration above 75 μg/mL [41, 42]. 2D nanostructure of graphene materials also can provide sharpened edges, which can act like a 'blade', causing damage to bacterial cell membranes [43]. However, such a damage to the cell wall by physical contact with graphene can be minimized by coating with different macromolecules like PEG [44].

The oxidized form of graphene, i.e., GO can lead to the generation of excessive reactive oxygen species (ROS) on interaction with cells. Increasing levels of ROS can overwhelm the activity of antioxidant enzymes, including catalase, SOD or glutathione peroxidase, thereby producing oxidative stress within the cell. It is noted that many diseases are accompanied by a high rate of oxidative stress. It was found that the cytochrome c/$H_2O_2$ system played a key role in nanotoxicity under stress. GO offers electron transfer from cytochrome c available on the surface of mitochondria to $H_2O_2$, which subsequently increases the ROS production leading to higher cytotoxicity which is not possible in normal physiological conditions [45]. This oxidative stress generation is also responsible for GO-induced acute lung injury [46]. ROS generation can be the first step in the mechanisms of carcinogenesis, aging and mutagenesis. ROS has a significant role in cellular macromolecular damage, such as membrane lipid breakdown, protein denaturation, DNA fragmentation and mitochondrial dysfunction, affecting cell metabolism and signaling [47–49]. Exposer to GO may reduce the activity of superoxide dismutase and glutathione peroxidase [50–52].

Liao and coworker investigated the impact of graphene and graphene oxide on erythrocytes and human skin fibroblasts, considering the particle size, exfoliation method and the extent of oxidation. It was noticed that treatment of smaller GO particles showed more hemolysis than that of the aggregated or larger ones. Further, modification of GO surface with chitosan eliminates the hemolytic activity of GO [51].

GO could cause mutagenesis in mice after intravenous injection of GO at a significantly lower dose compared to cyclophosphamide, a classic mutagen [53]. GO cannot

enter into the cell nucleus although it gets the opportunity to interact with DNA during mitosis [54–57]. The π-stacking interaction between the graphene carbon rings can severely deform the hydrophobic end base pairs of DNA which potentially increases the genotoxicity [58]. DNA damage not only leads to cancer development, but also increases health risk of the next generation if the mutagenic potential of GO arises in reproductive cells impacting fertility and health of the offspring [53, 59].

Intratracheal instillation or intravenous administration of graphene nanomaterials at high doses can cause significant inflammatory response including inflammatory cell infiltration, pulmonary edema and granuloma formation [46, 60]. Figure 3 shows the effect of GO with different concentration and incubation time of human erythrocytes. Here, phosphate buffer saline (PBS) was used as control. The optical microscope images in Fig. 3a, b indicate the intact of erythrocyte morphology in

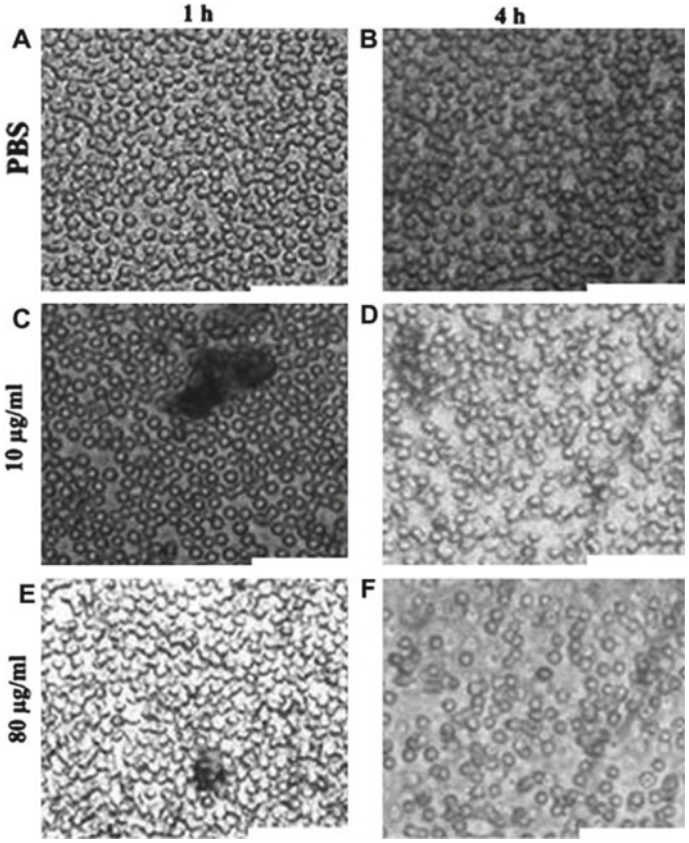


**Fig. 3** Impact of concentration and exposure time of GO on the morphological of human erythrocytes. Exposures of erythrocytes to **a** PBS for 1 h, **b** PBS for 4 h, **c** GO 10 μg $mL^{-1}$ for 1 h, **d** GO 10 μg $mL^{-1}$ for 4 h, **e** GO 80 μg $mL^{-1}$ for 1 h, **f** GO 80 μg $mL^{-1}$ for 4 h. Scale bar = 50 μm (Reprinted from 'Distribution and biocompatibility studies of graphene oxide in mice after intravenous administration', 49, [60])

PBS. However, the GO suspension ruptures the erythrocytes at higher concentration (80 μg $mL^{-1}$) with more exposure time (4 h). But lower concentration of GO (10 μg $mL^{-1}$) could not show such destruction.

A study has revealed that 21 days of subcutaneous injection of GO cause inflammation followed by a secretion of various cytokines including IL-6, IL-12, TNF-α, MCP-1 and IFN-g [61, 62]. Nanomaterials composed of graphene can elicit inflammation and tissue injury by triggering the release of whole Th1/Th2 cytokines and other chemokines which promote the engagement of circulating monocytes into the injured or damaged tissues [63, 64]. Some other graphene nanomaterials such as pristine graphene [64] and rGO [65] activate the NF-κB signaling pathway by binding to toll-like receptors (TLRs). This signaling cascade is stimulated by various pro-inflammatory cytokines such as IL-1 and TNF-α and toll-like receptors. This results in the shifting of NF-κB from cytoplasm to the nucleus and binding to IκB which acts as a transcription factor followed by the synthesis of different types of pro-inflammatory cytokines [66].

## *4.2 Toxicity of Transition Metal Dichalcogenides (TMD)*

Since 1960, people have been working on TMDs, and it was observed that based on the properties of transition metal and chalcogen, they may show insulating, semiconducting, metallic and superconducting behaviors. TMDs include inorganic compounds like $MoS_2$, $WS_2$, $MoSe_2$, $WSe_2$, $MoTe_2$, etc. Two-dimensional TMDs have emerged as promising materials for catalysis, energy storage, biosensing, photoelectronic devices, photodynamic therapy, drug and gene delivery, due to various unique mechanical, optical, electronic and chemical properties. The increasing applications of 2D TMDs have increased their environmental accumulation and the possibilities of human exposures [67–69]. Like graphene, the toxicity of TMDs varies depending on the particle shape, size and surface chemistry. It is noted that the toxicological characteristic of TMDs is still not well-explored.

2D TMDs generally have low toxicity in their bulk form. The toxicity of these materials has, however, been shown to be influenced by the parameters used in the production processes such as exfoliation conditions, as well as defect density and chemical composition [70]. Consequently, it is still difficult to draw conclusions about the toxicity of the entire class of 2D TMDs. In vitro cell viability assays such as MTT and WST-8 assays, which measure cellular reduction, have been used for assessing the toxicity of semiconducting 2D TMDs such as $MoS_2$, $WS_2$ and $WSe_2$ [71]. It is observed that while $MoS_2$ and $MoSe_2$ did not show appreciable toxicity to lung cancer cells, $WSe_2$ induced significant toxicity, although its toxicity was lower than that observed for graphene oxide and graphene. It is also observed that decreasing the number of layers in 2D $MoS_2$ can increase the toxicity, which is attributed to the enhanced surface area, defects and edges [70]. Some other studies using human pulmonary epithelial cells demonstrate a low health risk of 2D $WS_2$ and $MoS_2$ [72]. Cell viability measurement for 2D TMDs without surface modification,

carried out by Teo et al., showed a big difference between $MoS_2$, $WS_2$ and $WSe_2$ nanosheets. The degree of cytotoxicity can be ranked in the order of $WS_2 < MoS_2 < WSe_2$. The higher toxicity of $WSe_2$ can be attributed to the Se. Chalcogens mainly being located at the exterior of each 2D TMDs layer can have more interaction with cells compared to the transition metal [71].

In addition to chemical composition, surface modification also influences in vitro cytotoxicity of 2D TMDs. Chitosan-functionalized $MoS_2$ and PEGylated $WS_2$ exhibited negligible cytotoxicity while testing with different kinds of human cells [73, 74]. Thickness is also another factor playing a critical role in 2D TMDs induced toxicity. The effect of exposure to human lung cells with $MoS_2$ nanosheets of three different thicknesses by different exfoliation methods was compared. Tert-butyllithium and n-butyllithium exfoliated $MoS_2$ nanosheets were found to be more cytotoxic than methyllithium exfoliated $MoS_2$. Tert-butyllithium and n-butyllithium provided more efficient exfoliation than methyllithium reducing the final thickness of $MoS_2$. Hence, smaller the nanosheet thickness, stronger their cytotoxic influence [70]. The increase in active edge sites and surface area caused by thickness reduction might contribute to the increased cytotoxicity [75].

2D TMDs also exhibit antimicrobial activity. Unlike graphene, 2D TMDs cannot disrupt the cell membrane by cutting like a blade with sharp edges. The mechanism of antimicrobial activity of $MoS_2$ was studied against *E. coli,* and it was observed that killing ability was higher for the exfoliated nanosheets. The exfoliated $MoS_2$ could kill more than 90% of the total bacterial cells, while the unexfoliated one could kill only 40%. Cell death occurs due to both ROS generation as well as ROS independent oxidative stress [76, 77].

## *4.3 Toxicity of Phosphorene*

2D black phosphorus or phosphorene has attracted researchers for its promising properties like high carrier mobility and tunable electronic band gap making it a suitable candidate for various applications in optoelectronics, biosensing, nanoelectronics, rechargeable batteries, photocatalysis, and biomedical imaging. Phosphorene shows low toxicity, good biocompatibility, and biodegradability. A very few reports are available on the toxicity study of phosphorene. However, the application of phosphorene is not entirely safe [78].

Latiff et al. investigated the cytotoxicity effects of layered black phosphorus (BP) against human lung epithelial cells using WST-8 and MTT assays. Black phosphorous exhibited a dose-dependent response on A549 cells with a toxicity level intermediate between graphene oxide and TMDs such as $WS_2$ and $MoS_2$ [78]. Lee and his coworkers fabricated black phosphorus-based nanodots using an exfoliation method. These BP-Nanodots were stable in aqueous medium [79]. After in vitro cytotoxicity assessment in CHO-K1, HeLa and COS-7 cell lines, no or little cytotoxic effect was observed for HeLa, COS-7 cells at 1.0 mg $mL^{-1}$ concentration of nanodots and only 10% cell death for CHO-K1 cells at 3.0 mg $mL^{-1}$ of nanodots.

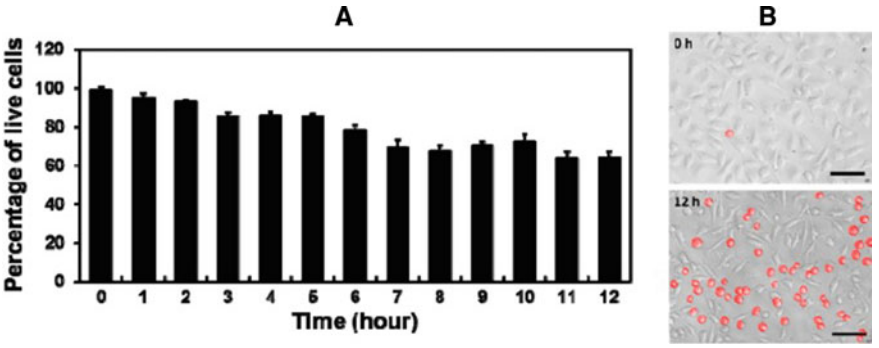


**Fig. 4** Treatment of L-929 cells with BP (10 μg/mL) for 12 h. **a** Percentage of live cells present after exposed to BP, **b** optical microscope images of L-929 fibroblasts in the presence of BP at 0 and 12 h. The scale bars = 100 μm ([80] Reproduced from the Ref. under CC BY 4.0 licensing from the MDPI publisher) https://creativecommons.org/licenses/by/4.0/

Song et al. investigated the cytotoxicity of black phosphorus nanosheets (BPNSs) by subjecting with different fibroblast cell lines, viz. NIH3T3, nHDF and HT1080. A dose and time-dependent cytotoxicity was observed for all the cell lines. The investigation revealed that the nanosheets were more toxic to cancerous HT1080 cells when compared to their toxic response to normal cells. Cytotoxic effects of layered BPs are proven to be because of both oxidative stress-mediated enzyme activity reduction and membrane disruption. Notably, layered BPs did not show significant toxicity at concentrations below 4 μg/mL [80]. But, at higher concentration (10 μg/mL), it was found to induce apoptosis of L-929 fibroblast cells on keeping exposed for longer time (12 h) as shown in Fig. 4. The percentage of live cells got reduced consequently (Fig. 4a), and the quantity of apoptotic cells (red colored) increased with time (Fig. 4b).

## *4.4 Toxicity of MXenes*

MXenes, a dynamic class of 2D nanostructures consisting of early transition metal carbides, nitrides and carbonitrides, can tune their crystal structure to apply in multiple fields [81]. It has a general formula, $M_{n+1}X_nT_z$, where M is an early transition metal, X is carbon and/or nitrogen, n = 1, 2, or 3; $T_z$ stands for the surface terminal functional groups (e.g., –OH, = O, –F) [82]. Since its discovery in 2011, its use has been rapidly expanded to cover tremendous applications [83]. Development of many theoretical and experimental results on it comes to a pose while discussing its safety measures as no such in-depth study has been taken place so far. The available literature discusses mostly the toxicity of Ti-based Mxenes. It is observed that the toxicity of MXenes is also influenced by their stoichiometry (i.e., $Ti_2C$ or $Ti_3C_2$).

An investigation by Rasool et al. [84] indicated that $Ti_3C_2$ MXene exhibited bactericidal properties against *Escherichia coli* and *Bacillus subtilis* strains, while the study of Jastrzębska et al. [85] showed the lack of toxicity of $Ti_2C$ MXene toward *Staphylococcus aureus*, *Bacillus sp.* and *Sarcina bacteria.*

Another study of Jastrzębska et al. [86] revealed varying toxicity levels of $Ti_3C_2$ MXenes for different cell lines. They also found that the toxicity was higher for cancerous cells compared to that for normal cells. The mechanism of action is assumed to be ROS-induced oxidative stress, which varies for varying cell lines. Furthermore, another report showed the possibility to 'tune' the cytotoxicity of the $Ti_3C_2T_z$ flakes using simple, inexpensive, post-delamination treatments, such as ultrasonication or mild thermal oxidation. Sonication of $Ti_3C_2T_z$ flakes or sonication followed by mild oxidation in the water at 60 °C could change their toxic effect selectively toward cancer cells as compared to non-malignant ones. Post-treatment methods sufficiently change the surface properties of the $Ti_3C_2T_z$ flakes, which significantly influence their toxicity. The most important features responsible for the toxicological properties are related to the presence of transition metal oxides $M_xO_y$ and lithium atoms on the surface [87].

## *4.5 Toxicity of Hexagonal Boron Nitrides (hBN)*

Hexagonal boron nitride (hBN) has a crystalline structure similar to graphite, except that the carbon atoms are replaced by boron and nitrogen atoms. hBN has self-lubricating ability and is used in many different applications like cosmetics, as additive in plastics and ceramics, lances, coatings, paints, etc. [88] hBN also has the potential to be used in different biomedical applications. Hence, it is important to have a knowledge about their toxicological effect. However, a very few reports are available on the toxicity study of hBN. Boron nitride (BN) does not show any toxicity at a low concentration although it has some adverse effects at a higher concentration. The size of BN nanomaterials is another factor governing its toxicology. For example, in vivo study of hBN nanoparticles having 30–60 nm radius and 1.6 nm thickness did not show any physiological change when injected into mice. The concentration used in this study was 20 μg/mL [89]. BN nanoparticles having a size 100–250 nm with concentration 30 μg/mL showed a negative effect on the viability/metabolism of osteoblast cells [90]. hBN with 75 nm size at doses 250 μg/mL even did not show any significant change in the cell morphology [91]. However, PEG-coated BN nanoparticle having a size 20 nm at a concentration 300 μg/mL was found to have some toxic effect upon in vivo testing in mice [91–93]. Investigation by Kar et al. demonstrated no significant changes in any important acute hematological or biochemical function at low doses after 24 h of intravenous injection of different doses of hBN NPs. At higher doses, i.e., 1600 and 3200 μg/kg, some adverse effects were observed. Histological detections also indicated that 1600 and 3200 μg/kg hBN NPs treatment could induce significant damage in the liver, kidney, heart, spleen and pancreas. The results of the study show that hBN NPs of 121 nm diameter could be

promising for biomedical applications where low doses between 50 and 800 μg/kg are not toxic [94].

## 4.6 Toxicity of Silicene and Germanene

Silicene and germanene are allotropes of silicon and germanium, respectively. Both silicene and germanene are 2D materials in a honeycomb structure similar to graphene [95]. Unlike **g**raphene which has a planar like structure, both silicene and germanene have buckled sheets type arrangements. They exhibit almost similar properties to graphene, but there is some restriction in their application in electronics due to the presence of negligible bandgap. Also, both silicene and germanene are thermodynamically less stable. Hence, to improve their stability and to increase their bandgap, different modifications have been carried out. The reported modified silicene and germanenes are siloxene ($Si_6H_3(OH)_3$), germanane ($Ge_6H_6$) or methylgermanane ($Ge_6(CH_3)_6$), etc. [96]. Modified forms of silicene and germanene are also formed during their synthesis. These materials have a high potential to be used in different fields of application. Germanane is reported to show photocatalytic properties which can generate hydrogen through water splitting and can hydrolyze ammonia-boron or borazine complex [97]. Methylgermanane has been reported as photocatalysts for the generation of hydrogen and also used as a fluorescence marker on nanographene-platinum microrobots [98].

Before large-scale usage of new materials, it is crucial to study their toxicity. As of now, only one report is available on the toxicology study of silicene and germanene derivatives. Toxicity of siloxene, germanane and methylgermanane was studied on the cell lines obtained from various parts of a human body, such as lung carcinoma (A549), breast carcinoma (MCF7), kidney (HEK293) and liver carcinoma (HepG2) cell. The cytotoxicity was assessed by exposing an increasing concentration of the respective material to the cell followed by evaluating the cell viability by cell counting kit8 (CCK8). The result obtained from this study revealed that siloxene has less toxicity toward all cell lines. Germanane and methylgermanane were found to show dose-dependent toxicity on cells. Germanane was found to be more toxic than methylgermanane, particularly in low concentrations (6.25 and 12.5 $\mu g\ mL^{-1}$). Furthermore, both germanane and methylgermanane were more toxic toward liver cells and more compatible toward breast cells [99].

## 4.7 Toxicity of 2D Ceramic Nanomaterials

Nanoclays are layered silicates that form platelets with nanosized thickness stacked together by van der Waals forces. Among many ceramic materials available in the market, 2D ceramic nanomaterials have a significance in terms of its widespread use.

Nanoclay is one of the most popular members of this family with tunable characteristics. Naturally occurring nanoclays, such as montmorillonite, bentonite, kaolin, and halloysite, have been employed in many industrial applications such as nanosized fillers, as fillers for polymer composites, anticorrosion and flame-retardant protective coatings. Nanoclay–polymer composites have potential for many biomedical applications, antimicrobial coatings, drug delivery, bone healing implants, paper-mimicking sheets, pesticide carriers, cosmetic formulations, etc. [100].

An investigation by Marina Kryuchkova et al., using a protozoan model organism *P. caudatum*, revealed lower cytotoxicity of some most popularly used nanoclays compared to a similar sized silica or graphene oxide nanomaterial. Different types of nanoclays were used, and the order of safety was found as halloysite > kaolin > montmorillonite > silica > bentonite > graphene oxide, where halloysite was found to be the safest against the used protozoan model. However, this study was carried out using a high concentration of nanomaterials (up to 10 mg $mL^{-1}$) [100]. Lordan et al. [101] determined the cytotoxicity of two different nanoclays: the unmodified nanoclay, Cloisite $Na^{+®}$ and the organically modified nanoclay, Cloisite 93A®, in human hepatoma HepG2 cells. Their study showed a high level of toxicity by both these nanoclay inducing necrosis, an acute form of cell death. High amount of ROS generation was observed in the presence of Cloisite $Na^{+®}$ which was the cause of damage to the cell membrane. Both the nanoclays showed a dose-dependent toxicity starting from 1 to 1000 μg/mL. However, contradictory results were also found for similar studies. A study carried out by Maisanaba et al. did not find any toxicological effect by Cloisite $Na^{+®}$ although organoclay Cloisite 30B® showed some toxicity against hepatic cell line HepG2 [102]. Nanoclays in their natural form are aggregated and stacked together due to the electrostatic interaction and van der Waals force to form cluster. Different types of organic modifiers are used to modify the surface properties of the nanoclay which helps to have good compatibility with the matrix in a composite. Tertiary ammonium cation-based modifiers are generally used for modification of nanoclay through an ion-exchange method. These organic modifiers are primarily responsible for enhanced toxicity of organoclays. Janer et al. in their study observed that after the removal of organic modifiers by washing with methanol or ethanol, the toxicity of organoclays decreases. [103] The most widely used nanoclay, i.e., montmorillonite (MMT) in its pristine form shows toxicity only at high doses and on long-time exposure. When tested against normal human intestinal cells, the cell membrane damage was observed at MMT concentration 1000 μg/mL and exposure time of 48–72 h. Significant ROS generation was also found in the cells incubated with above 50 μg/mL MMT after 48–72 h; however, it did not produce ROS within 24 h at practical biological concentration of below 500 μg/mL. MMT could be absorbed into the body within 2 h, but it did not significantly accumulate in any specific organ [104]. Since MMT is widely tested by researchers as a component in drug delivery vessels, a detailed study of its toxicological properties is very important.

## 5 Effect of 2D Nanomaterials in the Environment

Apart from the toxicological effect on human health, 2D nanomaterials also have serious environmental effects. After their release from industries, laboratories or consumer products, nanomaterials are mostly accumulated in water bodies, so there is a great chance of serious environmental damage to aquatic organisms, which is yet to be extensively evaluated. Hu and his coworkers analyzed the effect of graphene oxide (GO) on the green microalgae *Chlorella Vulgaris*, after administration of GO [39]. Their study revealed enveloping of algal cells by GO nanosheets forming blister-like nanostructures. GO could damage cell organelles especially via plasmolysis and an increase in the starch grain number after entering into the cells. Reduction of cell division was also observed along with the aggregation of chromatin and damage to the chloroplast structure. GO also inhibited cell growth, enhanced ROS generation and disrupted antioxidant enzymes. Furthermore, GO penetration into the cell caused metabolic disturbances linked to key biological processes. Similarly, the growth of *Triticum Aestivum* was inhibited as a result of graphene absorption [105]. Thus, it has been proved that graphene has a negative impact on the growth and/or alteration of photosynthesis resulting in a disproportion of nutrient homeostasis depicted through a decrease in the shoot biomass, number of root hairs, reduced PSII activity and chlorophyll content. The phytotoxicity has been evaluated on *C. Vulgaris* by incorporating GO with carboxyl single-walled carbon nanotubes (C-SWCNTs), where even at a concentration of 1 $mgL^{-1}$ DNA replication gets inhibited [106]. Begum and her colleagues [107] investigated the GO effects in terrestrial plants such as tomato, red spinach and cabbage. They found that after 20 days exposure to GO, particles accumulated on the surface of the roots at a concentration of 1000 $mgL^{-1}$ causing cell death and injury to the leaves. The phytotoxic effect varies with concentration, time and also the plant species. Although GO has many adverse effects on plant cells, an investigation by Ming Zhang revealed that GO at a concentration level 40 $\mu g\ mL^{-1}$ could promote the germination of tomato seeds by increasing their water absorption capability. However, the seedling growth was hampered by the presence of GO, indicated by a lower accumulation of biomass. Lower seedling growth may hamper the growth of the plant in its later stages [108]. Similarly, a positive effect on germination and growth of rice has been seen at a concentration of 5 $\mu g\ mL^{-1}$. Although it shows inhibitory effects at a concentration of 50 $\mu g\ mL^{-1}$ [109]. Another formulation of sulfonated graphene NPs stimulated growth (plant height, root, and shoot biomass) at a low concentration (50 mg $L^{-1}$) in maize seedlings, and on the other hand, at a high dosage (500 mg $L^{-1}$), it exhibited a strong inhibitory effect through $Ca^{2+}$ signaling and possessed ROS production and lipid peroxidation [29]. Similarly, at a high dosage of GO (2000 mg $L^{-1}$), wheat seed shows germination but with a slight reduction in root elongation. However, in such concentration of GO, the chromosomal aberrations and mitotic abnormalities increase which stipulate the clastogenic and aneugenic effect of GO in wheat root meristem [110]. The toxicity of particles depends upon the environmental air conditions. After exposure to

abiotic factors such as sunlight, water, humidity etc., their physicochemical properties changes and ultimately reduces the toxicological effect of GO [111]. Incorporation of 2D nanomaterials into water, soil and air ultimately affects the food chain. GO shows serious toxic effects beyond a concentration of 1.2 mg $L^{-1}$ in *Phanerocheate chrysosporium*, a white-rot fungus [112]. Toxicity of GO has also been seen in aquatic environment. In *Euglena Gracilis,* the growth inhibits at a concentration of GO exceeding 2.5 $mgL^{-1}$ which might be due to the coating of cell membrane by GO resulting in a decrease in light utilization [113]. Planktonic *Crustacean Daphnia magna* plays a chief role in the freshwater food chain. Carbon-14 tracking was used to investigate the toxicity of GO in the planktonic organism, where graphene was found nearly about 1% of the mass at a maximum concentration of 250 $\mu g\ L^{-1}$ for 24 h [114]. Further graphene was found in the brood pouch of gravid organisms where a few-layer graphene (FLG) with horseradish peroxidase was introduced to prevent the gathering of graphene [115]. As compared to the unmodified particles, modified FLG shows reduced toxicity. To reduce the toxicity in zebrafish, humic acid (HA) is incorporated to modify GO surface [116]. Thus, surface modification or coating may help to reduce the adverse environmental effects of GO. Direct administration of GO often causes harmful effects in living organisms. At concentrations of 0.01–100 mg $L^{-1}$, GO found to be hardly attached to the chorion surface that hinders the oxygen supply by blocking the pores. This hypoxic chorionic environment results in delayed hatching, ischemia, and malformation of the embryo. On the other hand, an incorporation of HA causes detachment of GO from the chorion results in a marked increase in physiological oxygen concentration leading to healthy embryos. Another positive effect of inducing HA is that it enhances negative charge on the surface of the material which minimizes contact of particles with the embryo. Whereas, free GO causes alteration in protein secondary structures from which the chorionic sac is made of. The level of toxicity also depends on the environment. Zebra fish in cultured water secretes various small organic molecules, proteins, mucopolysaccharides and nucleotides. These biological secretions along with the GO nanosheets (GOBS) cause extensive cell deaths [115]. The probable mechanism of toxicity is the tight adhesion of GOBS on embryonic surfaces attributed to the increase in the functional group on GO surfaces. This phenomenon ultimately inhibits oxygen and ion exchange causing a metabolic imbalance in the cell. Apart from GO nanosheets, black phosphorus nanosheets (BPNSs) also show some toxic effect on environmental organisms. Depending upon the concentration, the toxicity of BPNSs varies. The 120 h exposure of BPNSs stimulates the growth of *Chlorella vulgaris* (*C. vulgaris*) at 1 $mgL^{-1}$, and on the other hand, at high concentrations (5 and 10 $mgL^{-1}$), BPNSs retard the growth. Studies revealed that BPNSs caused a remarkable reduction of antioxidant agents such as glutathione (GSH) and glutathione disulfide (GSSG) in *C. Vulgaris.* Higher concentration of BPNSs leads to an increase amount of reactive oxygen species (ROS), and reduced superoxide dismutase results in high oxidative stress which is accompanied by the gentle release of dissolved phosphate ions, including $PO_2^{3-}$, $PO_3^{3-}$ and $PO_4^{3-}$ and causes disturbance in the growth of *C. vulgaris* [117]. Likewise, natural and modified nanoclays also exhibited some toxic effects in aquatic organisms. Robinson et al. [118] investigated the role of natural nanoclay

and found that it inhibited the growth and reproduction rate of *Daphnia Magna* by clotting the gut [118]. Another study by Blake [119] reported that nanoclays in an aggregated form present in solution show nominal toxic effects on *D. magna*, due to rapid settlement of sediment which minimizes the exposure time or interaction time to nanoclays in the water [119]. The toxicity of GO was also revealed in the zebrafish model [120]. The effect of GO on head skeleton and cardiac function of zebrafish is shown in Fig. 5. It was observed that the head skeleton formation in zebrafish decreased when treated with GO (Fig. 5b) compared to control (Fig. 5a) as indicated in the red box. Similarly, erythrocyte detection in the cardiac section of zebrafish in the presence of GO (Fig. 5d) was reduced significantly by 87.18% compared to control (Fig. 5c). The quantity of erythrocyte is the indication of the cardiac output in zebrafish embryos.

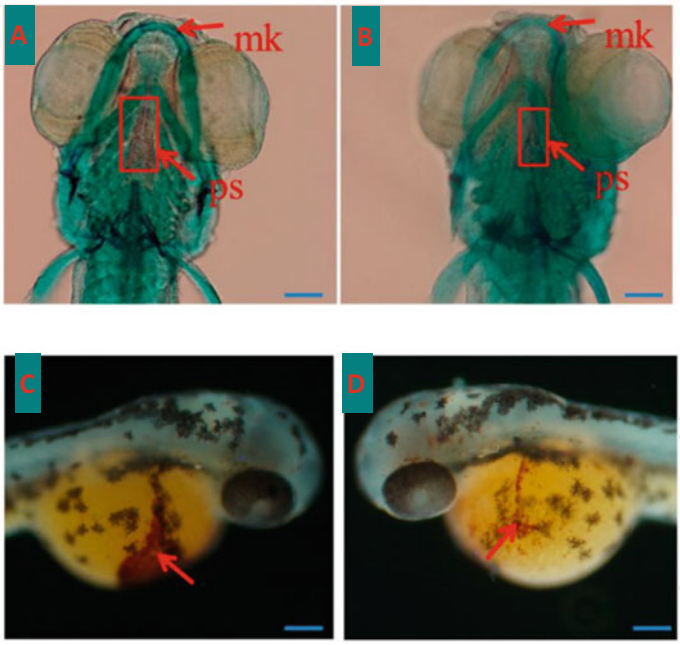


**Fig. 5** Study on skeletal and cardiac development of zebrafish larvae treated with GO. Head skeleton of zebrafish larvae stained with alcian blue/alizarin red S at 7 dpf (days post fertilization) as **a** control, absence of GO, **b** 100 μg/L GO. Erythrocyte number (as cardiac output) in zebrafish embryos at 48 hpf (hour post fertilization) in, **c** control, absence of GO and **d** 100 μg/L GO. The scale bar = 20 μm. mk = Meckel's cartilage; ps = parasphenoid (Reprinted with permission from {Ref. [121]}. Copyright {2017} American Chemical Society)

## 6 Precautionary Measures for Handling of 2D Nanomaterials

2D nanomaterials are emerging advanced materials for future technologies. Their applications and production are increasing progressively. In the future, there is a high chance of new members to add in this family. Therefore, it is of utmost importance to take necessary precautionary measures for handling and use of such nanomaterials to avoid a toxic environment and nature's imbalance. Realizing the underlying risk of nanomaterials because of their growing applications, different precautionary guidelines have been started on industrial as well as research level. Different regulatory bodies across the globe have been formed to underline the safety issue of nanomaterials. Mainly, World Health Organization (WHO), Organization for Economic Co-operation and Development (OECD) and the International Organization for Standardization (ISO) are some of the international organizations which have been involved to issue various standard guidelines to be applicable for the safe use of nanomaterials considering all the possible impact and risk assessment. Till 2017, OECD published 58 relevant reports, and ISO provided 55 standards based on the health and safety issues of nanomaterials including safe handling in the workplace, coordination with the WHO recommendations [121–123]. The basic framework of guidelines is summarized below [27].

i. Before going for a large-scale production of new nanomaterials, a thorough study on their toxicological effect must be carried out.
ii. The risk factor should be minimized with a proper approach. For example, a surface functionalization or coating generally helps to reduce their toxic effect. However, sometimes this approach may affect the most required property of a nanomaterial. It is reported that GO after coating with polyethylene glycol (PEG) exhibits lower toxicity compared to the pristine one.
iii. Proper analysis of a tolerable exposure limit of a particular nanomaterial in the environment and hence control of their production and application.
iv. Spreading awareness about nanomaterial toxicity among public and a proper management of waste of nanomaterial-based products.
v. Proper surveillance of exposure level of nanomaterial in the environment.
vi. Proper protocol should be employed to prevent exposure and any accident.
vii. Workers or employees of nanomaterial production industry or laboratory should have proper training.

## 7 Conclusions

Discovery of most of the 2D nanomaterials is very recent, and hence, toxicology of this family of nanomaterials is not well studied. Except for graphene or graphene oxide, reports on toxicological study of other nanomaterials are very few. The actual mechanism of toxicity of these nanomaterials is also not very clear. Few contradictory

results have also been observed in studies carried out by different groups. Hence, an uncertainty rules on their exposure limit in the environment. Moreover, the most challenging part is that the exposure limit varies for different organisms. Although in some cases, these nanomaterials show a positive effect, but in other cases, at the same concentration, they show adverse effects. Until and unless we have detailed information about their toxicity, we must limit the production and application of nanomaterials.

## References


1. Vance ME, Kuiken T, Vejerano EP, McGinnis SP, Hochella MF, Rejeski D, Hull MS (2015) Nanotechnology in the real world: redeveloping the nanomaterial consumer products inventory. Beilstein J Nanotechnol 6:1769–1780
2. Kannan PK, Late DJ, Morgan H, Rout CS (2015) Recent developments in 2D layered inorganic nanomaterials for sensing. Nanoscale 7:13293–13312
3. Zhu CZ, Du D, Lin YH (2017) Graphene-like 2D nanomaterial-based biointerfaces for biosensing applications. Biosens Bioelectron 89:43–55
4. Wang L, Xiong QR, Xiao F, Duan HW (2017) 2D nanomaterials based electrochemical biosensors for cancer diagnosis. Biosens Bioelectron 89:136–151
5. Wang QH, Kalantar-Zadeh K, Kis A, Coleman JN, Strano MS (2012) Electronics and optoelectronics of two-dimensional transition metal dichalcogenides. Nat Nanotechnol 7:699–712
6. Cao XH, Tan CL, Zhang X, Zhao W, Zhang H (2016) Solution-processed two-dimensional metal dichalcogenide-based nanomaterials for energy storage and conversion. Adv Mater 28:6167–6196
7. Liu B, Zhang JG, Shen GZ (2016) Pursuing two-dimensional nanomaterials for flexible lithium-ion batteries. Nano Today 11:82–97
8. Cao Y, Li XB (2014) Adsorption of graphene for the removal of inorganic pollutants in water purification: a review. Adsorption 20:713–727
9. Zhu YW, Murali S, Cai WW, Li XS, Suk JW, Potts JR, Ruoff RS (2010) Graphene and graphene oxide: synthesis, properties, and applications. Adv Mater 22:3906–3924
10. Keller AA, Lazareva A (2013) Predicted releases of engineered nanomaterials: from global to regional to local. Environ Sci Technol Lett 2013:65–70
11. Smita S, Gupta SK, Bartonova A, Dusinska M, Gutleb AC, Rahman Q (2012) Nanoparticles in the environment: assessment using the causal diagram approach. Environ Health 11:1–13
12. John AC, Küpper M, Manders-Groot AMM, Debray B, Lacome JM, Kuhlbusch TAJ (2017) Emissions and possible environmental implication of engineered nanomaterials (ENMs) in the atmosphere. Atmosphere 8(5):84
13. Kumar A, Kumar P, Anandan A, Fernandes TF, Ayoko GA, Biskos G (2014) Engineered nanomaterials: knowledge gaps in fate, exposure, toxicity, and future directions. J Nanomater 130198.https://doi.org/10.1155/2014/130198
14. Iavicoli I, Leso V, Ricciardi W, Hodson LL, Hoover MD (2014) Opportunities and challenges of nanotechnology in the green economy. Environ Health 13:78–84
15. Mitrano DM, Motellier S, Clavaguera S, Nowack B (2015) Review of nanomaterial aging and transformations through the life cycle of nano-enhanced products. Environ Int 77:132–147
16. Soni D, Naoghare PK, Saravanadevi S, Pandey RA (2015) Release, transport and toxicity of engineered nanoparticles. Rev Environ Contam Toxicol 234:1–47
17. Hermann A, Diesner MO, Abel J, Hawthorne C, Grebmann A (2014) Assessment of impacts of a European register of products containing nanomaterials. Federal Environment Agency (Umweltbundesamt), Germany, ISSN 1862-4804, Report No. (UBA-FB) 001907/E

18. Vale G, Mehennaoui K, Cambier S, Libralato G, Jomini S, Domingos RF (2016) Manufactured nanoparticles in the aquatic environment-biochemical responses on freshwater organisms: a critical overview. Aquat Toxicol 170:162–174
19. Rocha TL, Gomes T, Sousa VS, Mestre NC, Bebianno MJ (2015) Ecotoxicological impact of engineered nanomaterials in bivalve mollusks: an overview. Mar Environ Res 111:74–88
20. Baker TJ, Tyler CR, Galloway TS (2014) Impacts of metal and metal oxide nanoparticles on marine organisms. Environ Pollut 186:257–271
21. Jafar G, Hamzeh G (2013) Ecotoxicity of nanomaterials in soil. Ann Biol Res 4:86–92
22. Khodakovskaya M, Dervishi E, Mahmood M, Xu Y, Li Z, Watanabe F, Biris AS (2009) Carbon nanotubes are able to penetrate plant seed coat and dramatically affect seed germination and plant growth. ACS Nano 3(10):3221–3227
23. Hong J, Peralta-Videa JR, Rico C (2014) Evidence of translocation and physiological impacts of foliar applied $CeO_2$ nanoparticles on cucumber (*Cucumis sativus*) plants. Environ Sci Technol 48(8):4376–4385
24. Ge Y, Schime JP, Holden PA (2011) Evidence for negative effects of $TiO_2$ and ZnO nanoparticles on soil bacterial communities. Environ Sci Technol 45(4):1659–1664
25. Kabira E, Kumarb V, Kimc KH, Yipd ACK, Sohn JR (2018) Environmental impacts of nanomaterials. J Environ Manage 225:261–271
26. Fojtů M, Teo WZ, Pumera M (2017) Environmental impact and potential health risks of 2D nanomaterials. Environ Sci Nano 4:1617–1633
27. Ganguly P, Breen A, Pillai SC (2018) Toxicity of nanomaterials: exposure, pathways, assessment, and recent advances. ACS Biomater Sci Eng 4:2237–2275
28. Kuete V, Karaosmanoğlu O, Sivas H (2017) Anticancer activities of african medicinal spices and vegetables. Medicinal spices and vegetables from Africa. Academic Press, pp 271–297. ISBN 9780128092866. https://doi.org/10.1016/B978-0-12-809286-6.00010-8
29. Chamchoy K, Pakotiprapha D, Pumirat P, Leartsakulpanich U, Boonyuen U (2019) Application of WST-8 based colorimetric NAD(P)H detection for quantitative dehydrogenase assays. BMC Biochem 20:4. https://doi.org/10.1186/s12858-019-0108-1
30. Gunsolus IL, Haynes CL (2016) Analytical aspects of nanotoxicology. Anal Chem 88:451–479
31. Marquis BJ, Love SA, Braun KL, Haynes CL (2009) Analytical methods to assess nanoparticle toxicity. Analyst 134:425–439
32. Ishiyama M, Miyazono Y, Shiga M, Sasamoto K (2000) Water-soluble tetrazolium salt compounds. US Pat. 6063587
33. Mosmann T (1983) Rapid colorimetric assay for cellular growth and survival: application to proliferation and cytotoxicity assays. J Immunol Methods 65:55–63
34. Love SA, Maurer-Jones MA, Thompson JW, Lin YS, Haynes CL (2012) Assessing nanoparticle toxicity. Annu Rev Anal Chem 5:181–205
35. Collins AR (2004) The comet assay for DNA damage and repair. Mol Biotechnol 26:249–261
36. Pulskamp K, Diabaté S, Krug HF (2007) Carbon nanotubes show no sign of acute toxicity but induce intracellular reactive oxygen species in dependence on contaminants. Toxicol Lett 168:58–74
37. Zhang Y, Ali SF, Dervishi E, Xu Y, Li Z, Casciano D, Biris AS (2010) Cytotoxicity effects of graphene and single-wall carbon nanotubes in neural phaeochromocytoma-derived PC12 cells. ACS Nano 4:3181–3186
38. Horváth L, Magrez A, Burghard M, Kern K, Forró L, Schwaller B (2013) Evaluation of the toxicity of graphene derivativeson cells of the lung luminal surface. Carbon 64:45–60
39. Hu XG, Lu KC, Mu L, Kang J, Zhou QX (2014) Interactions between graphene oxide and plant cells: regulation of cell morphology, uptake, organelle damage, oxidative effects and metabolic disorders. Carbon 80:665–676
40. Guo X, Mei N (2014) Assessment of the toxic potential of graphene family nanomaterials. J Food Drug Anal 22:105–115
41. Zboril R, Marsalek B, Ou L, Song B, Liang H, Liu J, Feng X, Deng B, Sun T, Shao L (2016) Toxicity of graphene-family nanoparticles: a general review of the origins and mechanisms. Part Fibre Toxicol 13:57

42. Sasidharan A, Panchakarla LS, Sadanandan AR, Ashokan A, Chandran P, Girish CM et al (2012) Hemocompatibility and macrophage response of pristine and functionalized graphene. Small 8(8):1251–1263
43. Malina T, Marsalkova E, Hola E, Tucek J, Scheibe M (2019) Toxicity of graphene oxide against algae and cyanobacteria: nanoblade-morphology-induced mechanical injury and self protection mechanism. Carbon 155:386–396
44. Seabra AB, Paula AJ, Lima RD, Alves OL, Duran N (2014) Nanotoxicity of graphene and graphene oxide. Chem Res Toxicol 27:159–168
45. Zhang WD, Wang C, Li ZJ, Lu Z, Li Y, Yin JJ, Zhou YT, Gao XF, Fang Y, Nie GJ, Zhao YL (2012) Unraveling stress-induced toxicity properties of graphene oxide and the underlying mechanism. Adv Mater 24:5391–5397
46. Li B, Yang J, Huang Q, Zhang Y, Peng C, Zhang Y et al (2013) Biodistribution and pulmonary toxicity of intratracheally instilled graphene oxide in mice. NPG Asia Mater 5:e44
47. Waiwijit U, Kandhavivorn W, Oonkhanond B, Lomas T, Phokaratkul D, Wisitsoraat A et al (2014) Cytotoxicity assessment of MDA-MB-231 breast cancer cells on screen-printed graphene-carbon paste substrate. Colloids Surf B Biointerf 113:190–197
48. Chong Y, Ma Y, Shen H, Tu X, Zhou X, Xu J et al (2014) The in vitro and in vivo toxicity of graphene quantum dots. Biomaterials 35(19):5041–5048
49. Chen M, Yin J, Liang Y, Yuan S, Wang F, Song M et al (2016) Oxidative stress and immunotoxicity induced by graphene oxide in zebrafish. Aqua Toxicol 174:54–60
50. Zhang Y, Ali SF, Dervishi E, Xu Y, Li Z, Casciano D et al (2010) Cytotoxicity effects of graphene and single-wall carbon nanotubes in neural phaeochromocytoma-derived PC12 cells. ACS Nano 4(6):3181–3186
51. Liao KH, Lin YS, Macosko CW, Haynes CL (2011) Cytotoxicity of graphene oxide and graphene in human erythrocytes and skin fibroblasts. ACS Appl Mater Interfaces 3(7):2607–2615
52. Chang Y, Yang ST, Liu JH, Dong E, Wang Y, Cao A et al (2011) In vitro toxicity evaluation of graphene oxide on A549 cells. Toxicol Lett 200(3):201–210
53. Liu Y, Luo Y, Wu J, Wang Y, Yang X, Yang R et al (2013) Graphene oxide can induce in vitro and in vivo mutagenesis. Sci Rep 3:3469
54. Wang D, Zhu L, Chen JF, Dai L (2015) Can graphene quantum dots cause DNA damage in cells? Nanoscale 7(21):9894–9901
55. Ren H, Wang C, Zhang J, Zhou X, Xu D, Zheng J et al (2010) DNA cleavage system of nanosized graphene oxide sheets and copper ions. ACS Nano 4(12):7169–7174
56. Magdolenova Z, Collins A, Kumar A, Dhawan A, Stone V, Dusinska M (2014) Mechanisms of genotoxicity. A review of in vitro and in vivo studies with engineered nanoparticles. Nanotoxicology 8(3):233–278
57. Golbamaki N, Rasulev B, Cassano A, Robinson RLM, Benfenati E, Leszczynski J et al (2015) Genotoxicity of metal oxide nanomaterials: review of recent data and discussion of possible mechanisms. Nanoscale 7(6):2154–2198
58. Zhao X (2011) Self-assembly of DNA segments on graphene and carbon nanotube arrays in aqueous solution: a molecular simulation study. J Phys Chem C 115(14):6181–6189
59. Ciccia A, Elledge SJ (2010) The DNA damage response: making it safe to play with knives. Mol Cell 40(2):179–204
60. Zhang X, Yin J, Peng C, Hu W, Zhu Z, Li W et al (2011) Distribution and biocompatibility studies of graphene oxide in mice after intravenous administration. Carbon 49(3):986–995
61. Yue H, Wei W, Yue Z, Wang B, Luo N, Gao Y et al (2012) The role of the lateral dimension of graphene oxide in the regulation of cellular responses. Biomaterials 33(16):4013–4021
62. Chen GY, Yang HJ, Lu CH, Chao YC, Hwang SM, Chen CL et al (2012) Simultaneous induction of autophagy and toll-like receptor signaling pathways by graphene oxide. Biomaterials 33(27):6559–6569
63. Reshma SC, Syama S, Mohanan PV (2016) Nano-biointeractions of PEGylated and bare reduced graphene oxide on lung alveolar epithelial cells: a comparative in vitro study. Colloids Surf B Biointerf 140:104–116

64. Zhou H, Zhao K, Li W, Yang N, Liu Y, Chen C et al (2012) The interactions between pristine graphene and macrophages and the production of cytokines/chemokines via TLR- and NF-kappaB-related signaling pathways. Biomaterials 33(29):6933–6942
65. Chatterjee N, Eom HJ, Choi J (2014) A systems toxicology approach to the surface functionality control of graphene-cell interactions. Biomaterials 35:1109–1127
66. Lawrence T (2009) The nuclear factor NF-kappa B pathway in inflammation. Cold Spring Harb Perspect Biol 1: a001651
67. Ataca A, Şahin H, Ciraci S (2012) Stable, single-layer $MX_2$ transition-metal oxides and dichalcogenides in a honeycomb-like structure. J Phys Chem C 116:8983–8999
68. Sipos B, Kusmartseva AF, Akrap A, Berger H, Forro L, Tutis E (2008) From mott state to superconductivity in 1T-$TaS_2$. Nat Mater 7:960–965
69. Neto AHC (2001) Charge density wave, superconductivity, and anomalous metallic behavior in 2D transition metal dichalcogenides. Phys Rev Lett 86:4382–4385
70. Chng EL, Sofer Z, Pumera M (2014) $MoS_2$ exhibits stronger toxicity with increased exfoliation. Nanoscale 6:14412–14418
71. Teo WZ, Chng ELK, Sofer Z, Pumera M (2014) Cytotoxicity of exfoliated transition-metal dichalcogenides ($MoS_2$, $WS_2$, and $WSe_2$) is lower than that of graphene and its analogues. Chem Eur J 20:9627
72. Corazzari I, Deorsola F, Gulino G, Aldieri E, Bensaid S, Turci F, Fino D (2014) Hazard assessment of W and Mo sulphide nanomaterials for automotive use. J Nanopart Res 16:2401
73. Yin W, Yan L, Yu J, Tian G, Zhou L, Zheng X et al (2014) High-throughput synthesis of single-layer $MoS_2$ nanosheets as a near-infrared photothermal triggered drug delivery for effective cancer therapy. ACS Nano 8:6922–6933
74. Liu T, Wang C, Gu X, Gong H, Cheng L, Shi X, Feng L, Sun B, Liu Z (2014) Drug delivery with PEGylated $MoS_2$ nano-sheets for combined photothermal and chemotherapy of cancer. Adv Mater 26:3433–3440
75. Zhou X, Sun H, Bai X (2020) Two-dimensional transition metal dichalcogenides: synthesis, biomedical applications and biosafety evaluation. Front Bioeng Biotechnol. https://doi.org/10.3389/fbioe.2020.00236
76. Yang X, Li J, Liang T, Ma C, Zhang Y, Chen H, Hanagata N, Su H, Xu M (2014) Antibacterial activity of two-dimensional $MoS_2$ sheets. Nanoscale 6:10126–10133
77. Liu S, Zeng TH, Hofmann M, Burcombe E, Wei J, Jiang R, Kong J, Chen Y (2011) Antibacterial activity of graphite, graphite oxide, graphene oxide, and reduced graphene oxide: membrane and oxidative stress. ACS Nano 5(9):6971–6980
78. Latiff NM, Teo WZ, Sofer Z, Fisher AC, Pumera M (2015) The Cytotoxicity of layered black phosphorus. Chem Eur J 21:13991–13995
79. Lee HU, Park SY, Lee SC, Choi S, Seo S, Kim H, Won J et al (2016) Black phosphorus (BP) nanodots for potential biomedical applications. Small 12:214–219
80. Song SN, Shin YC, Lee HU, Kim B, Han DW, Lim D (2018) Dose- and time-dependent cytotoxicity of layered black phosphorus in fibroblastic cells. Nanomaterials 8(6):408
81. Jian-Feng Z, Hui-Yang C, Hong-Bing W (2017) Research progress of novel two-dimensional material MXene. J Inorg Mater 32:561
82. Verger L, Xu C, Natu V, Cheng HM, Ren W, Barsoum MW (2019) Overview of the synthesis of MXenes and other ultrathin 2D transition metal carbides and nitrides. Curr Opin Solid State Mater Sci 23:149–163
83. Naguib M, Mashtalir O, Carle J, Presser V, Lu J, Hultman L, Gogotsi Y, Barsoum MW (2012) Two-dimensional transition metal carbides. ACS Nano 6(2):1322–1331
84. Rasool K, Helal M, Ali A, Ren CE, Gogotsi Y, Mahmoud KA (2016) Antibacterial activity of $Ti_3C_2T_x$ MXene. ACS Nano 10(3):3674–3684
85. Jastrzębska A, Karwowska E, Basiak D, Zawada A, Ziemkowska W, Wojciechowski T, Jakubowska D, Olszyna A (2017) Biological activity and bio-sorption properties of the $Ti_2C$ studied by means of zeta potential and SEM. Int J Electrochem Sci 12:2159–2172
86. Jastrzębska AM, Szuplewska A, Wojciechowski T, Chudy M, Ziemkowska W, Chlubny L, Rozmysłowska A, Olszyna A (2017) In vitro studies on cytotoxicity of delaminated $Ti_3C_2$ MXene. J Hazard Mater 339:1–8

87. Jastrzębska AM, Szuplewska A, Rozmysłowska-Wojciechowska A, Chudy M, Olszyna A, Birowska M, Popielski M, Majewski JA, Scheibe B, Natu V, Barsoum MW (2020) On tuning the cytotoxicity of $Ti_3C_2$ (MXene) flakes to cancerous and benign cells by post-delamination surface modifications. 2D Mater 7:025018
88. Shinde PV, Saxena M, Singh MK (2019) Recent developments in graphene-based two-dimensional heterostructures for sensing applications. Woodhead Publishing Series, pp 407–436. https://doi.org/10.1016/B978-0-08-102577-2.00004-X
89. Lu T, Wang L, Jiang Y, Liu Q, Huang C (2016) Hexagonal boron nitride nanoplates as emerging biological nanovectors and their potential applications in biomedicine. J Mater Chem B 4:6103–6110
90. Rasel MAI, Li T, Nguyen TD, Singh S, Zhou Y, Xiao Y, Gu YT (2015) Biophysical response of living cells to boron nitride nanoparticles: uptake mechanism and bio-mechanical characterization. J Nanopart Res 17:441
91. Singh B, Kaur G, Singh P, Singh K, Kumar B et al (2016) Nanostructured boron nitride with high water dispersibility for boron neutron capture therapy. Sci Rep 6:35535
92. Liu B, Qi W, Tian L, Li Z, Miao G, An W et al (2015) In vivo biodistribution and toxicity of highly soluble PEG-coated boron nitride in mice. Nanoscale Res Lett 10(1):478
93. An W, Han B, Li K, Akhtar S, Zhang Y, Zhang X et al (2017) The protective study about alleviation of simvastatin on the damages of PEG-BNs in mice. Environ Toxicol Pharmacol 53:64–73
94. Kar F, Hacıoğlu C, Göncü Y, et al. (2020) In vivo assessment of the effect of hexagonal boron nitride nanoparticles on biochemical, histopathological, oxidant and antioxidant status. J Cluster Sci. https://doi.org/10.1007/s10876-020-01811-w
95. Cahangirov S, Topsakal M, Aktürk E, Sahin H, Ciraci S (2009) Two- and one-dimensional honeycomb structures of silicon and germanium. Phys Rev Lett 102:236804
96. Rosli NF, Rohaizad N, Sturala J, Fisher AC, Webster RD, Pumera M (2020) Siloxene, germanane, and methylgermanane: functionalized 2D materials of group 14 for electrochemical applications. Adv Funct Mater 30:1910186
97. Liua Z, Daia Y, Zheng Z, Huang B (2019) Covalently-terminated germanane GeH and $GeCH_3$ for hydrogen generation from catalytic hydrolysis of ammonia borane under visible light irradiation. Catal Commun 118:46–50
98. Liu Z, Wang Z, Sun Q, Dai Y, Huang B (2019) Methyl-terminated germanane $GeCH_3$ synthesized by solvothermal method with improved photocatalytic properties. Appl Surf Sci 467–468:881–888
99. Sahu SC, Hayes AW (2017) Toxicity of nanomaterials found inhuman environment: a literature review. Toxicol Res Appl 1(1–13)
100. Kryuchkova M, Danilushkina A, Lvovab Y, Fakhrullin R (2016) Evaluation of toxicity of nanoclays and graphene oxide in vivo: a *Paramecium caudatum* study. Environ Sci Nano 3:442
101. Lordan S, Kennedy JE, Higginbotham CL (2011) Cytotoxic effects induced by unmodified and organically modified nanoclays in the human hepatic HepG2 cell line. J Appl Toxicol 31:27–35
102. Maisanaba S, Puerto M, Pichardo S, Jordá M, Moreno FG, Aucejo S, Jos A (2013) In vitro toxicological assessment of clays for their use in food packaging applications. Food Chem Toxicol 57:266–275
103. Janer G, Fernández-Rosas E, Molino EM, González-Gálvez D, Vilar G, López-Iglesias C, Ermini V, Vázquez-Campos S (2014) In vitro toxicity of functionalised nanoclays is mainly driven by the presence of organic modifiers. Nanotoxicology 8(3):279–294
104. Baek M, Lee J, Choi S (2012) Toxicological effects of a cationic clay, montmorillonite in vitro and in vivo. Mol Cell Toxicol 8:95–101
105. Zhang P, Zhang RR, Fang XZ, Song TQ, Cai XD, Liu HJ, Du ST (2016) Toxic effects of graphene on the growth and nutritional levels of wheat (*Triticum aestivum* L.): short- and long-term exposure studies. J Hazard Mater 317:543–551

106. Hu XG, Ouyang SH, Mu L, An J, Zhou Q (2015) Effects of graphene oxide and oxidized carbon nanotubes on the cellular division, microstructure, uptake, oxidative stress, and metabolic profiles. Environ Sci Technol 49:10825–10833
107. Begurn P, Ikhtiari R, Fugetsu B (2011) Graphene phytotoxicity in the seedling stage of cabbage, tomato, red spinach, and lettuce. Carbon 49:3907–3919
108. Zhang M, Gao B, Chen JJ, Li YC (2015) Effects of graphene on seed germination and seedling growth. J Nanopart Res 17:8
109. Liu SJ, Wei HM, Li ZY, Li S, Yan H, He Y, Tian ZH (2015) Effects of graphene on germination and seedling morphology in rice. J Nanosci Nanotechnol 15:2695–2701
110. Vochita G, Opric L, Gherghel D, Mihai CT, Boukherrou R, Lobiu A (2019) Graphene oxide effects in early ontogenetic stages of *Triticum aestivum* L. seedlings. Ecotoxic Environ Safe 181:345–352
111. Hu XG, Zhou M, Zhou QX (2015) Ambient water and visible-light irradiation drive changes in graphene morphology, structure, surface chemistry, aggregation, and toxicity. Environ Sci Technol 49:3410–3418
112. Xie JR, Ming Z, Li HL, Yang H, Yu BW et al (2016) Toxicity of graphene oxide to white rot fungus *Phanerochaete chrysosporium.* Chemosphere 151:324–331
113. Hu CW, Wang Q, Zhao HT, Wang LZ, Guo SF, Li XL (2015) Ecotoxicological effects of graphene oxide on the protozoan *Euglena gracilis*. Chemosphere 128:184–190
114. Guo XK, Dong SP, Petersen EJ, Gao SX, Huang QG, Mao L (2013) Biological uptake and depuration of radio-labeled graphene by *Daphnia magna.* Environ Sci Technol 47:12524–12531
115. Mu L, Gao Y, Hu XG (2016) Characterization of biological secretions binding to graphene oxide in water and the specific toxicological mechanisms. Environ Sci Technol 50:8530–8537
116. Chen YM, Ren CX, Ouyang SH, Hu XG, Zhou QX (2015) Mitigation in multiple effects of graphene oxide toxicity in zebrafish embryogenesis driven by humic acid. Environ Sci Technol 49:10147–10154
117. Li P, Zeng L, Gao J, Yao L et al (2020) Perturbation of normal algal growth by black phosphorus nanosheets: the role of degradation. Environ Sci Technol Lett 7(1):35–41
118. Robinson S, Capper N, Klaine S (2010) The effects of continuous and pulsed exposures of suspended clay on the survival, growth, and reproduction of *Daphnia magna*. Environ Toxicol Chem 29:168–175
119. Blake DR (2012) Effects of layered double hydroxide nanoclays on the toxicity of copper to Daphnia magna. PhD Thesis, University of North Texas
120. Zhang X, Zhou Q, Zou W, Hu X (2017) Molecular mechanisms of developmental toxicity induced by graphene oxide at predicted environmental concentrations. Environ Sci Technol 51:7861–7871
121. WHO guidelines on protecting workers from potential risks of manufactured nanoma-terials. World Health Organization, Geneva. Licence: CC BY-NC-SA 3.0 IGO (2017)
122. Types and uses of nanomaterials, including safety aspects. Commission staff working paper. European Commission, Brussels. Brussels, 3.10.2012 SWD (2012)
123. Arduin R (2015) Brazilian scenario—sustainable nanotechnology. Sustainable Nanotechnology Organization, Venice

# Chapter 12
# Prospective on 2D Nanomaterials for Energy and Environment: Challenges, Commercial Aspect, and the Future Research Endeavor


**Zeba Khanam, Neelam Gogoi, and Divesh Narayan Srivastava**

## 1 The Rise of 2D Nanomaterials

Two-dimensional (2D) nanomaterials ignited a surge of unprecedented research interest since the discovery of a stable atomic carbon nanosheet 'graphene' in 2004 as a breakthrough in nanoscience and technology [1, 2]. The astonishing optoelectronic properties of pioneer graphene and its technological advances encouraged the scientific community to extensively explore the new 2D layered atomic crystals. Layered materials endow unique appealing features when scaled down to single or few atomically thin nanosheets. For instance, they possess large specific surface area which significantly increases their physical and chemical reactivity and influences the 2D wave function through quantum confinement effects. Modification in the bandgap structure with layer thickness occurs upon 2D confinement [1–3]. Henceforth, these ultrathin 2D nanomaterials present unique mechanical, electrical, photonic, magnetic, and catalytic properties that differ from those of their bulk counterparts. Due to their outstanding attributes, viz tailored surface chemistry, highly exposed active edge sites, greater flexibility, more versatility, biocompatibility, better functionality, excellent mechanical strength, etc., 2D nanomaterials

Z. Khanam (✉)
School of Materials Science and Engineering, Harbin Institute of Technology, Shenzhen 518055, China
e-mail: zbkhnm@gmail.com

N. Gogoi
School of Life and Environmental Sciences, School of Chemistry, University of Sydney, Sydney, NSW 2006, Australia
e-mail: neelam.gogoi@sydney.edu.au

D. N. Srivastava
Analytical and Environmental Science Division & CIF, CSIR-Central Salt & Marine Chemicals Research Institute, Bhavnagar, Gujarat 364002, India
e-mail: dnsrivastava@csmcri.res.in



Z. Khanam et al. (eds.), *2D Nanomaterials for Energy and Environmental Sustainability*,
Materials Horizons: From Nature to Nanomaterials,
https://doi.org/10.1007/978-981-16-8538-5_12

could be promising for diversified applications from electronics, energy, environment to biomedicines, and agriculture [1–4].

A plethora of 2D nanomaterials have been designed and developed through top-down exfoliation from bulk crystals or bottom-up approaches from small molecule precursors [1–5]. Interestingly, the library of 2D nanomaterials is expanding enormously and featuring more than 150 exotic members so far. In general, 2D nanomaterials are categorized as metals, semi-metals, superconductors, semiconductors, or insulators depending on their atomically thin structural configurations and varied chemical compositions [1–7]. These include-

- Transition metal dichalcogenides (TMDs) such as $MoS_2$, $WS_2$, $MoSe_2$, and $WSe_2$.
- Transition metal halides (TMHs) such as $PbI_2$, and $MgBr_2$.
- Transition metal oxides (TMOs) such as $MnO_2$, and $MoO_3$.
- Transition metal carbides/nitrides (MXenes) such as $Ti_3C_2T_x$.
- Mono-elemental 2D analogs (Xenes) such as
  - group III elements-borophene,
  - group IV elements-graphene, silicene, germanene, and stanene,
  - group V elements-phosphorene, arsenene, antimonene, and bismuthene,
  - group VI elements-selenene and tellurene.
- 2D nitrides—such as hexagonal boron nitride (h-BN, also known as "white graphene") and graphitic carbon nitride (g-$C_3N_4$).
- Layered perovskites—such as Oxide pervoskites-$K_2Ln_2Ti_3O_{10}$, $RbLnTa_2O_7$, etc., and Halide perovskites—$Cs_2PbI_2Cl_2$, etc.,
- Layered double hydroxides (LDHs), Silicates or aluminosilicates or 2D nanoclay,
- 2D Metal organic frameworks (MOF), 2D Covalent organic frameworks (COF) and 2D polypeptoid
- Metallenes—such as 2D iron, 2D copper, 2D rhodium, 2D platinum, and 2D gold nanosheets.

A brief overview on the rapidly emerging 2D nanomaterials along with their properties and various synthetic approaches has been already addressed in Chap. 1. The present chapter outlines the key technological challenges of 2D nanomaterials for energy and environmental applications. In addition, the future developments, prospects, and opportunities that could be offered are also discussed.

## 2 Challenges Associated with the Production Methods

Layered structures are characterized by strong in-plane bonds but weak interlayer bonding. This allows them to be isolated into individual atomically thin nanosheets. The micromechanical cleavage using "Scotch-tape" was originally used to prepare highly crystalline graphene from bulk layered graphite crystals [8, 9]. Since then,

there are probably a dozen methods that have been developed to prepare 2D nanomaterials with desired structure composition (thickness and size), quality (crystal phase, defect, and surface property), and optimized optical/electronic properties [8–14].

Major approaches for the state-of-the-art production are-

- *Top-down*: This approach includes mechanical force-assisted cleavage and liquid exfoliation such as oxidation-assisted liquid exfoliation, ion exchange-assisted liquid exfoliation, ion intercalation-assisted liquid exfoliation, and selective etching-assisted liquid exfoliation [2, 5, 8–12].
- *Bottom-up*: This approach includes chemical vapor deposition method (CVD), wet-chemical synthesis (hydrothermal or solvothermal), and epitaxial growth synthesis [12–16].

According to remarkable advancements in recent years, exfoliation approaches have become popular as one of the mainstream methods for the preparation of solution-processable 2D nanomaterials with advantages of straightforward and cost effectiveness. 2D nanomaterials are obtained in the form of dispersions that can be used directly [5, 8–12]. On the other hand, CVD can produce high-purity 2D nanomaterials with controlled thickness and size [15, 16]. Even though a variety of preparation strategies continues to emerge, several challenges remain unaddressed. Therefore, the following critical points should be carefully considered for the future studies-

1. ***Sustainable production***: Significant progress is needed to advance the sustainable and scalable synthesis of 2D nanomaterials. Efforts must be dedicated to push the limits to high structural integrity, high phase purity, and precise functionalization. For the application-driven researches, the majorly concerned areas are scalability and production costs while providing a balance between ease of fabrication and final material quality with tailoring of on-demand properties [8–11, 17]. The lack of an explicit understanding of the structural design-application mechanism adds up to the continued list of challenges. Unfortunately, exfoliation methods suffer from some drawbacks such as poor throughput and low yield, rendering it difficult to produce 2D nanosheets in bulk quantities. The applied mechanical force in exfoliation process determines not only the production rate, but also the quantity and purity of resulting 2D nanomaterials. For example, the pioneer mechanical cleavage (Scotch-tape adhesion) approach is not scalable though it can easily produce high-quality monolayers. Similarly, liquid-phase exfoliation (using ultrasonic waves, shear forces, or electrochemical exfoliation) is associated with long processing times, limited production yield, low throughputs, and induced oxidation. However, the modified Hummer's method (chemical oxidation) is readily scalable, but the products are found to be heavily defective. The exfoliation process involves many factors, such as applied mechanical forces, type of exfoliants/intercalants/stabilizers and their feeding concentrations, power supplies, and several other operational conditions. The development of new exfoliation strategies depended on the tedious cycle of trial and error. Therefore, systematic studies on the regulation of these parameters are

extremely critical. The combination of two or more methods, such as electrochemical exfoliation with shear mixing, ball milling, or thermal shock could be a better alternative to boost the production yield and to further reduce the nanosheet thickness. It shall focus on the technical innovation such as continuous feed, nonstop production, automatic separation, purification, and recycling [8–11]. On the other hand, the bottom-up approaches (for instance, CVD) involve complex and costly procedures requiring high temperatures and high vacuum conditions along with difficulties in transferring the product onto target substrates that may introduce residues or defects into the 2D structure [8–11, 15, 16]. These drawbacks limit the processing of 2D nanomaterials beyond laboratory scale. Hence, a significant understanding is required to drift this research domain toward the development of novel, efficient, economic protocols for upscaling the production of 2D nanomaterials with better control over desired product characteristics.

2. ***Pursuit of greener approaches***: To further advance research in this field, an environmentally benign method for the scalable production of 2D nanomaterials would be worthwhile and will open new avenues for commercial implementation. The conventional material synthesis approaches are dominated by the excessive use of toxic chemicals and harsh conditions posing serious health and environmental concerns. Research advances must promote the concepts of green chemistry and sustainability both in academia and industry. Substituting toxic chemicals with supercritical fluids, biocompatible materials, etc., can assure a greener way of preparing 2D nanomaterials [10, 11, 18–20].
3. ***Controlling Defects and morphology***: There is still much to learn about controlling defects, understanding the impact of substrate, developing means for controlled doping and controlled morphology, which underpin future research [3]. The undesired alteration of pristine properties of 2D nanomaterials, due to inevitable oxidation or insufficient intercalation or surface defects, during preparation is a serious issue. The multiple physio-chemical reactions during synthesis may lead to inhomogeneous oxygen content, defect density, and surface functionalities [5, 8]. In order to prevent the destruction of 2D lattice, a proper selection of starting materials such as solvents or exfoliants or other processing conditions along with their easy removal post-processing is essential. Another hurdle is to achieve 2D nanomaterials with controlled sizes and layer thicknesses. The effective preparation strategies giving more control over morphology and surface modification without compromising the inherent properties are required to advance the development of 2D nanomaterials for practical applications [5, 8–11].
4. ***Sorting and Separation***: Looking ahead, the generic approaches produce 2D nanomaterials with a wide distribution of layer numbers and lateral sizes. It is yet another difficult task to further sort and separate the product according to its lateral dimensions and thicknesses. Also, it is extremely difficult to transfer the obtained product to target substrates. Therefore, significant progress is required for well-constructed separation and transfer techniques [5, 9–11].

5. ***Storage and Stability***: The storage and stability requirements of prepared products is another roadblock on the way to commercialization [18]. For example, MXenes require sub-zero temperatures for their storage. It is extremely important to develop an effective method for long-term storage of 2D nanomaterials without undergoing oxidation or irreversible aggregation at ambient conditions.
6. ***Computational Modelling and Theoretical predictions***: There is an urgent necessity for steadfast computational methods to address the gap between theoretical predictions and experimental confirmations. Material's informatics combining computational, statistical, and machine learning approaches should be adopted to predict and establish practical design rules for accelerating the creation of next-generation 2D nanomaterials with new compositions and properties [1, 3, 19]. These data-driven approaches can then be integrated to the resulting data sets to develop an understanding of the underlying structure–property–performance relationships [19, 21–23]. Furthermore, the collaboration between characterization techniques and theoretical modeling will be beneficial for an in-depth understanding of the fundamental mechanism and providing a comprehensive perspective on materials' structure and function [3, 8]. This is a challenging direction but would make breakthrough in the nanoscience research.

## 3 2D Nanomaterials for Sustainable Future

The emergence of numerous 2D nanomaterials puts forward a giant step toward the development of sustainable technologies in the field of energy and environment. The cutting-edge attributes of 2D nanomaterials, in particular (a) in-plane electroconductivity with charge density waves, (b) asymmetric out-of-plane flexibility, (c) reduction/oxidation ability with gap tunability, and (d) exceptional large surface area with superior chemical reactivity, hold extensive implications in different fields [4], for instance:

- Energy storage and conversion,
- Photocatalytic degradation,
- Adsorption removal,
- Desalination and membrane filtration,
- Detection and sensing,
- Drug delivery and healthcare applications,
- Agricultural practices.

In spite of the substantial research garnered so far, there are still many topical and foreknown challenges and future directions which need to be considered to facilitate the commercial application of 2D nanomaterials.

### 3.1 Energy Storage and Conversion: Challenges and the Future

2D nanomaterials certainly show a great potential as next-generation electrode materials for huge application in energy. As suggested, high specific surface area, varied surface functionality, reversible transport of ion and mass, and good mechanical robustness are proven to be crucial foe systems of energy storage and conversion [4, 24, 25]. The recent progress on various 2D nanomaterials for solar cells, electrochemical water splitting, piezo and thermoelectric devices, batteries, and supercapacitors is discussed in Chaps. 2 and 3, respectively. There are still many opportunities to explore and expand the research in this field, like creation of porous structures, effects of functional groups, intercalation of ions, new hybrid device configuration, etc. [24–26], as summarized below-

1. ***Restacking and porous structure***: 2D nanomaterials have acquired importance as electrochemically active electrode materials for energy storage devices, for instance, supercapacitors and batteries [6]. As known, the specific capacitance of device depends on the surface area of active electrode material. Due to the tendency of 2D nanomaterials to irreversibly aggregate and restack, it may significantly decrease their surface area, and ion diffusion rate thereby may reduce their charge-storage capacity. Therefore, in order to exploit the full potential of 2D nanomaterials in energy storage, the research should focus to prevent restacking of 2D nanosheets and maximize the accessible surface area. One way to achieve this is to increase the active sites or enlarge the interlayer space through intercalation with guest molecules [27, 28]. The inclusion of conductive interlayer spacers may create adequate interlayer separations by introducing additional electron-conductive pathways. This promotes an easy access and swift transport of ions resulting in a better electrochemical performance of 2D nanomaterial-based electrodes [25]. Furthermore, the aggregation of 2D nanosheets can be prevented by fabricating porous microstructures that can also stimulate pathways for efficient charge transport. The porous microstructure opens 2D channels and effectively shortens the diffusion paths of ions [27, 28]. It can provide more sites for charge storage along with maintaining structure stability during charge–discharge cycles [6].
2. ***Doping, tunable functionality, and Hybrid configurations***: For further improving the electrochemical performance, approaches like defect/vacancy creation, heteroatom doping, heterostructure construction, and surface/interface modification could provide excellent opportunities [28]. 2D transition metal compounds, such as TMDs, TMOs, and TMHs, are being widely studied as active faradaic materials in electrochemical energy storage devices due to their large theoretical capacities, compatibility with electrolytes, and chemical stability. They show multiple oxidation states where the charge storage mainly arises from the pseudo-capacitance caused by rich redox reactions on their surfaces [28]. For instance, $MoS_2$ exhibits large pseudo-capacitance due to varied oxidation states of Mo (+2 to + 6), while electrical double layer

(EDL) capacitance occurs due to its stacked-sheet-like structure [6]. However, the inherently poor electronic conductivity, low-rate capability, poor cycling stability, and large structural changes during metal-ion insertion/extraction along with high cost of manufacture are major challenges that require further investigation to commercially exploit these materials [29]. On the other hand, non-faradaic materials like graphene or phosphorene-based electrodes mainly store charge through the formation of EDL, exhibiting high power density but low specific capacitance. Combining pseudocapacitive-type materials (TMOs or TMHs) with EDL capacitive-type material (say graphene) is a viable approach to overcome limitations of each component, generating hybrid electrodes with enhanced performance. Further, these impediments can be overcome by implanting vacancies or defects/holes, doping with additional metallic elements, and/or integrating with a conductive matrix [28]. For instance, introducing redox pseudo-capacitances by heterogeneous atomic doping of redox quinone/hydroquinone molecules into the EDL capacitive-type phosphorene or graphene could be an alternative choice [26]. Next, compositing or hybridizing TMDs and MXenes with different materials, such as conductive polymers, or other transition metal compounds like TMOs, or 2D nitrides, needs more attention. Besides, systematic investigations on the interfacial interactions of various 2D nanomaterials with other polymeric materials should be explored. Such polymer 2D nanocomposites are expected to accelerate the electrons/ions conduction at electrode–electrolyte interface, achieving high-performance energy storage devices. A detailed electrochemical characterization of such composites will provide important insights that will contribute to future electrochemical applications of 2D nanomaterials [24, 25]. Furthermore, the emerging conductive organic frameworks—MOFs and COFs with stacked p-conjugated 2D layers, controllable pore size, high specific surface area, tunable porous structure, and surface functionality are also appealing electrode materials for future energy devices. The high porosity from organic molecular assembly is beneficial to generate EDL capacitance, and the heteroatoms (B, N, O, and S) on the precise locations of frameworks may exhibit redox activity for the pseudo-capacitance [28]. Apart from this, the intercalation of various cations (Li, Na, K, Al) into the 2D nanomaterial interlayers (graphene, phosphorene, MXenes, etc.) could show promising potential for hybrid battery-capacitor devices or metal-ion capacitors [25, 30, 31]. The device configuration involving the hybrid/composite electrodes or the asymmetric assembly design in which positive and negative electrodes consisting of different active materials (specifically, pseudocapacitive-type electrode at one side and EDL capacitive-type electrode at the other) shows superior overall performance. Hence, designing new hybrid device configurations with high specific capacitances and wide electrochemical voltage windows represents an interesting future research direction [28].

3. ***Fabrication technologies***: The energy application of 2D nanomaterials is mainly hindered by the lack of feasible electrode fabrication technologies [28]. In addition to it, the potential problems associated with 2D nanomaterials synthesis

such as low production yield, uncontrolled morphology, inductive defects, and arbitrary functionalities overshadow their real performance. For instance, an acid-free synthesis of MXenes is a key challenge to leverage their intrinsic performance as electrode materials [24]. In general, the electrode material can be directly synthesized on the patterned current collectors using CVD, laser scribing, pyrolysis, and electrolytic deposition, or the electrodes can be fabricated using existing 2D nanomaterials dispersions/powders by means of inkjet printing, drop casting, spin coating, spray coating, layer-by-layer assembly, electrophoretic deposition, vacuum filtration, painting, filling, and rolled-up technologies [28]. A deeper understanding of different techniques or their combination is needed to realize the commercial value of energy devices.

4. ***Properties and Performance relationships***: As observed in literature, synergistic effects account for enhanced performances of energy device, but the rational factors responsible for it are still unexplored. To leverage the optimum performances, understanding the interface relationships that govern the physiochemical properties of 2D nanomaterials is critically important. How do the interface atoms adjust their orientation, crystalline structure, and layer number to exhibit high synergistic effects are the unresolved issues [24]. Few studies suggested that vertically orient 2D nanomaterials directly grown on interdigital current collectors could be advantageous to attaining low interfacial resistance and expediting the ion transport [28]. Besides, the layer number/thickness may play a decisive role in the performance. The scientist community must find the most appropriate layer number/thickness of 2D nanomaterials for high-performance energy storage/conversion devices. There are rarely any studies engaged in regulating the orientations or layer thickness of 2D nanomaterials and their corresponding electrocatalytic, electrochemical, piezo, or thermoelectric behaviors [26]. Moreover, the principles of interface chemistry and the binding mechanism of 2D nanomaterials with interacting materials influencing the overall performance should be explored. Detailed advanced studies integrated with in-situ characterizations and data mining techniques are required to unravel the fundamentals of 2D interfaces parameters to leverage the best materials performance [24].
6. ***Novel electrolytes***: Apart from electrode optimization, the electrolyte compatibility is also of paramount interest in electrochemical energy storage devices. The aqueous/non-aqueous electrolytes known so far are becoming obsolete with newly emerged 2D nanomaterials due to their superior surface chemistries and physio-chemical properties. Hence, a parallel effort is needed to design safe, compatible electrolytes such as polymer electrolytes together with the fabrication of novel 2D nanomaterials-based electrodes. To this, the electrode–electrolyte interfacial reactions occurring during electrochemical tests require a deeper investigation [24–33].
7. ***Stability***: The intrinsic instability issues of 2D nanomaterials may further hamper their applications. For instance, MXenes electrodes are susceptible to oxidize in varied electrolytes which may cause decay in capacitance and increase in internal resistance during electrochemical cycling stability tests

[24]. 2D nanomaterial-based electrodes often encounter degradation or structural collapse under ambient conditions, and thus, an inert atmosphere is mostly preferred for device assembling. This is one of the major limitations in manufacturing 2D nanomaterial-based energy devices that should be analyzed seriously. The plausible strategies to alleviate the stability issues could be surface modification or coatings or proper encapsulation of 2D nanomaterials while preserving their electrochemical entity [24, 26, 28]. For instance, in-situ deposition of a proper passivated layer on the electrode surface could suppress the reactive activities and forbid the volume change during cycling. Another possible way would be creating 2D nanomaterials heterostructures through layer-by-layer assembly that can instigate strong synergistic effects to improve the stability performances [26].

8. ***Other unexplored materials***: Energy-related investigations can be expanded to predict and discover novel 2D nanomaterials. Catalysts based on 2D nanomaterials such as $MoS_2$ and CN show high catalytic activity, particularly toward HER; however, their semiconducting nature limits the charge transfer capabilities. In addition, the catalytic active sites are mostly confined to the edges with catalytically inert in-plane atoms in these 2D nanomaterials. Theoretical analysis demonstrated that MXenes could be exceptional candidates for electrochemical water splitting, but very few experimental evidences is presented. 2D nanomaterials based on earth-abundant elements with superior electrocatalytic activities and electrochemical properties are always in huge demand. The prospects of newly discovered elemental 2D nanomaterials (such as silicene, germanene, and tellurene) toward OER, HER, EDL, or pseudo-capacitive processes are mostly unidentified [25, 28].

## *3.2 Treatment and Removal of Pollutants: Challenges and the Future*

2D nanomaterials and their functional composites are gaining tremendous research attention in treatment and monitoring of environmental contaminants due to their ultrafast processing and ultrahigh treatment efficiency. Through control over their structural morphology and highly anisotropic physicochemical properties, 2D nanomaterials have preceded the innovation and advancement of smart treatment systems equipped with remarkable catalytic, adsorptive, filtration, and sensing performance [21]. They have been used as an ultrafast visible light photocatalyst, high-efficiency absorbents, filtration membranes, and sensing platforms for removing environmental pollutants, including dyes, heavy metals ions, antibiotics, and even toxic gases. We outlined the recent progress of 2D nanomaterials in environmental remediation applications, starting with photocatalysis in Chap. 4, adsorption in Chap. 5, desalination and membrane filtration in Chap. 6, with the extension to electrochemical sensors for detecting toxic gases, water pollutants, and other biological contaminants in Chaps. 7 and 8, respectively. The rich chemical diversity of 2D nanomaterials offers myriad

opportunities in treatment and removal technologies; however, for achieving best performance, prediction of their complex physicochemical response is quite challenging. In spite of immense advancements at laboratory scale, to date only few have paved the way to market [21]. This chapter seeks to highlight the practical barriers and challenges allied with industrial implementation of 2D nanomaterials and the future directions needed to be prioritized in respective treatment technologies, as discussed below.

(a) **Photocatalytic degradation of organic contaminants**

Photocatalytic technology is a promising sustainable approach for environmental remediation. Typically, it involves the use of semiconductors as a photocatalyst to initiate the photoreactions under suitable light irradiation to degrade recalcitrant organic pollutants with minimal energy input, low operating cost and operable under ambient conditions (including pressure and temperature) [34, 35]. During the photocatalytic reaction, the free electrons get excited to conduction band (CB) while leaving holes in valence band (VB), and such electron–hole pairs take part in photocatalytic applications which can include water splitting, $CO_2$ reduction, and degradation of pollutants. 2D nanomaterials and their composites are considered as promising candidates as photocatalysts providing crucial features such as diverse host–guest species, large specific surface areas, surface-rich active sites, and porous structures. Many 2D nanomaterials including graphene, phosphorene, metal oxides, carbon nitride, MXenes, and TMDs have been evaluated as photocatalysts or co-catalysts. [21]. These 2D nanomaterial-based photocatalysts still have certain bottlenecks to move from experimental to industrial level [36].

1. ***Hybrid Photocatalysts***: The redox potentials of photogenerated electron–hole pairs rely upon the 2D bandgap structure; hence, it should be carefully adjusted for the development of effective photocatalysts. Several strategies such as hetero-structuring, size controlling, and element doping could be exploited to modulate the bandgap structure of 2D nanosheets in the desired wavelength range [21]. For instance, an atomic level investigation should be made on the variation of electronic structure in MXenes after metal doping to enhance the photocatalytic process. Engineering 2D nanomaterial hybrids or heterostructures with superior redox capability, improved interfacial arrangements, enhanced photon adsorption and charge-carrier transportation could produce efficient and broad-spectrum photocatalysts [34]. Thus, an extensive research effort should be devoted to design efficacious hybrid 2D nanomaterials photocatalysts in order to extend their commercial applications [36].
2. ***Uncontrolled aggregation and Recombination***: The photocatalytic performance is greatly affected due to undesirable aggregation of 2D nanomaterials which reduce their specific surface area. Also, the excited photogenerated charge carriers lack stability and are easy to recombine, which usually leads to low conversion efficiency. The stirring of the reaction mixture may prevent aggregation, but not accessible in practice. The judicious design of particle interaction, surface engineering of photocatalysts like self-assembly, or the charge hopping,

and wise selection of ligands could be promising approaches to mitigate these issues [21].

3. ***Effectiveness of light irradiation***: Photocatalysis often suffers low conversion efficacy of light irradiation mainly during degradation of persistent organic pollutants. There are rare reports signifying the potent strategies to enhance the usage of light energy [36].
4. ***Practical implementation***: Photocatalytic degradation is mostly performed in a model solution, while real aqueous environment is more complex. For decontaminating pollutants in rivers, lakes, or oceans, the photocatalytic performances are unignorably influenced by several environmental factors such as ionic strength, pH, and interference of other entities. A systematic investigation should be performed to discern these factors to exploit the practical implementation of 2D nanomaterial photocatalysts [36].
5. ***Recycling and toxicity***: Reportedly, 2D nanomaterial photocatalysts are unable to satisfy the demand of repetitive usage, and at the same time, their residual contamination can impose severe environmental and human health risks. Hence, it is imperative to readily and fully separate the 2D nanomaterial photocatalysts for ideal recycling as well as purifying the aqueous system completely. This could be probably resolved by hybridizing them with magnetic nanoparticles or loading on to the porous materials, or creating macroscopic 3D architecture assembly. Moreover, some of the intermediates generating during photocatalytic degradation are more harmful than the original contaminant which should be precisely studied. Few reports acclaimed that applying hybrid photocatalysts could prevent the generation of toxic intermediates [36]. Overall, it is extremely important to thoroughly investigate 2D nanomaterial photocatalysts for any toxic impacts to the environment and human health.
6. ***Stability***: The instability issue of 2D nanomaterials may hinder their technological applications in environmental remediation. The comprehensive knowledge of their oxidation in various solvent systems, subsequent lattice change of 2D nanomaterials, and their long-term stability requires in-depth analysis [34].

(b) **Adsorption of toxic gases and water pollutants**

Adsorption-based removal of pollutants like heavy metal ions, organic dyes, and toxic volatile compounds is another promising method for environmental mitigation due to its minimal capital expense and simplicity [21]. 2D nanomaterials manifest exceptionally higher adsorptive capacity and selectivity as compared to other dimensional regime materials. With the attributes of large surface area, abundant-active sites, and rapid mass transport, 2D nanomaterials bestow high levels of surface/interface interactions, favorable for adsorption which is essentially an interfacial process [21, 37]. The plausible mechanisms of selective adsorptions or interactions are hydrogen bonding, π-π stacking, ion/ligand exchange, hydrophobic interaction, Lewis acid/base, and electrostatic interaction [21]. In spite of the impressive promises of 2D nanomaterials as the new-found generation of adsorbents for the treatment and removal of pollutants, there exist numerous challenges and baffling matters to be further inspected [37].

1. ***Production***: Low yield and high material cost of adsorbents based on 2D nanomaterials limit an industrial-scale production. Henceforth, the exploration of cost-effective, environmentally-benign and upscale methods is of great significance. More research should direct toward hybrid 2D nanomaterials that have the potential for the advancement of remediation technologies for environment [34, 37].
2. ***Aggregation***: The inevitable aggregation of 2D nanomaterials in aqueous medium may reduce the specific surface area and adsorption active sites thereby lowering their adsorptive capacity [37]. For the development of high-performance 2D nanomaterials adsorbents, the rate of terminal sedimentation must be prudently considered, because fast sedimentation can lead to the removal of adsorbents prior to an effective decontamination process, while an ultra-slow sedimentation may contribute to the recovery cost in the separation process of used adsorbents from the wastewater. The judicious design to understand surface interactions and nanosheet behavior in aqueous phase is also important. Besides the colloidal stability of 2D nanomaterials, adsorbents are crucial for their practical application in offshore conditions or lakes wherein homogeneous stirring is inaccessible [21].
3. ***Mechanism studies***: 2D nanomaterials possess a very diverse chemical and physical attributes. Therefore, there is a need to precisely understand different molecular levels and tuning of their surface chemistries to have a better control over their adsorption behaviors [21]. Several factors including nature of pollutants, solution/gas chemistry, and adsorbent characteristics such as distribution of functional groups, porosity, and even defects density have significant influence on the adsorption process [35, 37]. These must be explored in detail using experimental as well as computational methods to completely understand the adsorptive removal mechanism.
4. ***Secondary contamination and separation***: Recycling of 2D nanomaterials adsorbents after adsorption process is a daunting challenge. Although magnetic separation, centrifugation, and membrane filtration could be employed, they are not feasible at an industrial scale. Moreover, inadequate separation may pose a risk of secondary contamination and toxicity to environment and human health, and therefore, it requires comprehensive investigations [37].
5. ***Stability***: The lack of stability is another critical concern that influences the overall lifespan of 2D nanomaterials adsorbents and severely restricts their practical applications. The future work should consider on reinforcing 2D nanomaterials adsorbents for their successful utilization in aqueous environment [34, 37].

### (c) Desalination and membrane filtration

Over the years, desalination and membrane filtration have been established as most potential technology for water remediation [35]. Filtration membranes can provide a physical barrier that is designed to separate the pollutants from wastewater depending upon their size or permeability [21]. The membrane separation process can be categorized into microfiltration, nanofiltration, ultrafiltration, and reverse osmosis. The

process of desalination and membrane filtration is advantageous in terms of high removal efficiency, ease of cleaning, minimal usage of toxic chemicals, and negligible carbon footprint contribution [35]. In recent times, 2D nanomaterials have shown extremely high capabilities as efficient functional membranes for application in desalination and membrane filtration. However, there are still many challenges that should be tackled to extensively make use of their remarkable properties in desalination and membrane filtration [18].

1. ***Permeability and selectivity***: The development of efficient functional membranes with high selectivity and permeability faces great challenges due to the typical trade-off that exists between selectivity and permeability. As membrane thickness is inversely proportional to permeability, designing 2D nanomaterial-based membranes with controlled atomically thin structure can allow the selective molecules to pass through [21]. Theoretical studies such as density functional theory (DFT) could be used to predict superior features of different 2D nanomaterials for their possible application in water desalination and membrane filtration [18]. Proper experimentation is required to develop next-generation 2D nanomaterial-based functional membranes that can maintain quite high permeation without sacrificing separation selectivity [18, 21].
2. ***Fouling***: Fouling is a common issue associated with filtration membranes. It prevents their long-term operation due to high energy consumption and reduced water recovery from the desalination processes. To alleviate the fouling/biofouling phenomenon, incorporation of other antibacterial nanomaterials (such as silver nanoparticles) into 2D nanomaterial-based functional membranes seems to be a beneficial approach that ensures easy inactivation of bacterial growth. Additionally, self-repair and self-cleaning designs may facilitate the use of 2D nanomaterial membranes for practical applications in water desalination and membrane filtration [21].
3. ***Water flux***: The control of water flux is correlated directly to the material flake size. Hence, experimental and theoretical approaches are extremely necessary to perceive an optimum flux rate accompanied with a high salt rejection rate and further revealing the underlying mechanism [34].
4. ***Fabrication and Stability***: More research should be directed toward the scalable fabrication of 2D nanomaterial membranes with long-term stability [21]. These membranes prone to swell or collapse easily, causing ion rejection and thereby may result in poor separation selectivity. Engineering of interlayers by tuning of d-spacing of nanosheets can prevent swelling and/or structural collapse of the membranes [34].

(d) **Detection and sensing of contaminants**

The sensing techniques offer advanced environmental monitoring that can quantitatively determine the effectiveness of treatment. 2D nanomaterials are very well-suited for sensing applications, as their high surface-to-volume ratio, an extremely high density of active surface sites, and atomic thinness contribute to a strong response

toward external stimuli [21]. Additionally, 2D nanomaterials have a broad optical spectrum with tunable band structure and favorable electronic properties. These amazing properties make 2D nanomaterials a strong candidate suitable for designing of a range of sensor modalities. They mainly include fluorescent sensors, colorimetric sensors, field-effect transistor sensors, and electrochemical sensors [2, 12, 21, 38–40]. Among them, many studies are reported for electrochemical sensors that have extreme potential to detect the amount of target analytes per unit area with a rapid response and recovery, and low power consumptions [38–40]. Typically, electrochemical sensing of pollutants relies on the principle of detecting electrodes capable of producing a measurable electrical signal as a response to electrochemical adsorption or reaction with an analyte. The sensing probe–analyte interactions are either non-covalent (electrostatic force) or covalent linkages that mainly depends upon the nature of pollutant. The pollutants, if present, can induce a change in potential, current, capacitance, or resistance, which can be easily recorded and analyzed [21]. With great progresses made in this flourishing field, broader prospects with more breakthroughs in 2D nanomaterials-based sensing applications are expected. It still needs in-depth examination to understand the interactions between newly emerged 2D nanomaterials sensing platforms and target analytes to further realize their commercial use.

1. ***Fabrication***: The critical challenge in developing any 2D nanomaterial-based sensors is lack of controlled synthesis of 2D nanomaterials with desired morphological characteristics and surface chemistries. Nevertheless, the production rate, quantity, and quality of 2D nanomaterials are limited with existing methods. For instance, the existing 2D nanomaterials' synthesis via CVD method involving high-temperature processing is incompatible with flexible polymeric substrates and is typically grown on a metal substrate which is then transferred on target polymeric substrates. However, such transfer methods end up creating wrinkles and/or defects, making the device fabrication extremely challenging. Achieving uniformity in material properties is necessary for their implementation in industries beyond fundamental science research. Therefore, a smart research objective should be either cost-effective scalable synthesis with ease of transfer methods or enabling the low-temperature yet direct synthesis onto the final substrate to avoid transfer step [2, 12, 21, 38–40].
2. ***Selectivity and sensitivity***: Fabricating a reliable, robust, and more functional sensing probe interface is an interesting research direction. Nevertheless, each 2D nanomaterial has its own peculiar characteristics and shortcomings that could affect the sensing performance. Moreover, the synthesis process or the precursors used may also introduce impurities which could influence the performances of 2D nanomaterials as sensing signal probes. Research should be emphasized toward resolving the issues of lower detection limit, poor selectivity, instability, complicated separation, and unwanted impurities/contamination that could degrade the sensor performances [41]. This can be partly tackled by regulating the properties of 2D nanomaterials and their composites in a desirable and controlled manner. Proper tailoring or altering the surface chemistries of

2D nanomaterials through functionalization or defect engineering like creating heterostructures/composites or hybridization with other materials and molecular/chemical doping will offer more room to design the signal probes with selective recognition of specific pollutant and high sensitivity [12]. For instance, metal dopants can improve the detection limit and enhance the selectivity as they facilitate better interaction between modified sensing probes and the target analyte due to effective charge transfer [41]. Further, determining the impact of target analytes on the integral properties of 2D nanomaterials and the associated sensing mechanism will be helpful to recognize the selectivity and sensitivity relationship. An attempt should be made to unravel the recognition events occurring at the interface. Understanding of interfacial interaction mechanisms of 2D nanomaterial-based sensing probe with environmental pollutants is crucial to maximize the sensor performance. Considerable research effort should be made toward combination of theoretical data (e.g., DFT calculation) and experimental analysis to develop the improved sensing probes [12, 41].

3. ***Stability***: Another challenge of 2D nanomaterial-based sensors is to maintain their long-term stability. Their tendency of aggregation, oxidation/decomposition, or structural collapse during storage and application or reaction is duly responsible for relatively low chemical and physical stability. Structural deformities arising during synthesis of 2D nanomaterials can affect their electronic properties and hence influencing their sensing performance. Stabilizing these 2D nanomaterials during the synthesis process is equally important as their storage in ambient conditions. Moreover, the performance of sensors may degrade over a short period of time while interacting with complex environment/media in practice leading to structural disfigurements, material decay, and thermal hazards. Surface functionalization, doping of other elements, and polymer coating can improve their stability to a great extent. Nevertheless, the stability issue should be solved without sabotaging the sensitivity and selectivity of the device which needs in-depth investigation [41].
4. ***Toxicity***: A parallel attempt should begin for understanding various interactions of 2D nanomaterials with biological or environmental entities to facilitate their applications in these domains ensuring human health and environment safety [42]. It is extremely crucial that 2D nanomaterials do not introduce new impurities and maintain their chemical stability while comes in contact with testing media/environment [43]. Studies on the assessment of potential toxic effects and long-term safety of 2D nanomaterial sensing platforms are still limited. Modifying surface properties of 2D nanomaterials could remarkably improve their stability, recyclability, biocompatibility, and help in reducing toxicity. It is necessary to systematically investigate the impact of surface functionalization and properties of 2D nanomaterials composites on the environment, human health, and other organisms.

### 3.3 Biomedicines and Healthcare: Challenges and the Future

The amazing physio-chemical properties of 2D nanomaterials attracted researchers to realize their application in biomedical fields that mainly include drug delivery, bioimaging, antibacterial, biosensing, clinical diagnosis, tissue engineering, and other therapeutic uses [44]. We provided a thorough discussion of newly emerged 2D mesoporous silica nanomaterials applications in biomedicines in Chap. 9. Progress in this field is continuing to push forward to take advantage of these ultrathin 2D nanostructures. Herein, we present an insight on various research opportunities and critical challenges that could be explored for investigation of next-generation 2D nanomaterials with biomedical applications at their core [45].

1. ***Fabrication***: Most of the preparation strategies of 2D nanomaterial introduce impurities, involve toxic reagents, and have insufficient control over experiments and products that are highly unfeasible for their bio-medicinal use. Therefore, more efforts should be made to explore advanced, scalable, low cost, eco-friendly synthesis methods, and to manufacture tunable structure with desired properties [44]. Scalable production of 2D nanomaterials with precise control over size, surface terminations, and morphology is very crucial for clinical trials [19, 45]. Combination of superior opto-electro-magnetic properties together with the ease of surface functionalization would open new directions in clinical diagnosis and therapy. Noting that hybridization of 2D nanomaterials will not only result in combination of advantages but also a combination of drawbacks, which is a problem worth considering [44].
2. ***Biocompatibility and safety***: For real-life biomedical applications, the safety assessment of 2D nanomaterials which includes their biocompatibility, cellular uptake mechanisms, cell toxicity, and intracellular or in vivo metabolic pathways is an important prospect [46]. There are a few reports demonstrating the short-term in vitro biocompatibility of 2D nanomaterials, but the long-term in vivo biosafety of targeted tissues and organs are almost unknown [19]. It is known that the cytotoxicity is majorly influenced by nanomaterial properties such as synthesis method, surface chemistry, and morphology. [45]. A systematic study on the effect of 2D nanomaterials and their various composites on the environment and human health with a clear mechanistic reason for toxicity is not well-reported [43]. Hence, research efforts should be put into the investigation of long-term safety, toxicology, biocompatibility, pharmacokinetics, and biodistribution of 2D nanomaterials [44]. The toxicity of 2D nanomaterials to vital systems like nervous system, reproductive system, and immune system should be critically assessed in small as well as large animal models [19, 44].
3. ***Mechanism***: The understanding of different mechanisms involved in various healthcare applications such as drug delivery, cancer treatment, or disease detection should be thoroughly investigated with the help of computational modeling and theoretical studies [44].
4. ***Possible developments***: 2D nanomaterials can offer overarching opportunities in developing advanced, smart, compatible healthcare devices. 2D nanoplatforms

could be integrated into textiles for quick monitoring of health and fitness. 2D electronic tattoos as a part of virtual/augmented reality systems can efficiently monitor and respond to user's state of motion/physiology. 2D nanomaterial-based sensors for in vitro diagnostics of nucleic acids could enable highly sensitive, label-free, rapid, and early detection of various diseases [45]. Furthermore, advancement and realization of many such nanotechnologies hinge upon smart academic research collaborated with budding industrial partners. More applications of 2D nanomaterials could be explored in biomedical fields such as acoustic dynamics therapy, acoustic power bio-implants, or acoustic sensing [44, 47]. 2D nanomaterials have the potential to serve as the next-generation technology in personalized health monitoring [44–46].

### *3.4 Agricultural Practices: Challenges and the Future*

The application of nano-enabled technologies in agricultural practices has undoubtedly delivered very covenant outcomes in achieving and boosting sustainable agriculture by facilitating proper and less damaging management strategies for limited natural resources for land, water, and energy. How and at what concentration nanomaterial will respond in a positive manner is firmly and critically dictated by their properties, interactions, and reactions with the plant and soil constituents. It is because of their excellent physicochemical properties that they have magical effects in farming system [48]. However, it is very important to understand that everything comes at a cost. Besides having multiple remarkable applications, the benefit of using nanotechnology is often succeeded by negative effects which can cause harm to the health of environment and human population in the long run. Investigations regarding the applications, uptake, mobility, fate, toxicity, loss, and remediation of nanoparticle is still sparse and for the most part limited to laboratory research studies only. It might take a long time to reach from laboratory to field for general farm practices. A brief discussion on potential of 2D nanomaterials in improving quality as well as quantity of agricultural produce has been made in Chap. 10. Recognizing the high influences of these 2D nanomaterials in opening new avenues in agrarian sector, this section will endeavor to address profuse innovation opportunities and different challenges before their market implementation for general use.

1. ***Residual effects in plants****:* The introduction of engineered 2D nanomaterials have helped in achieving an improved overall effect different from what caused by natural nanoparticles, but they might result in some residual effects which may cause harm to environment [49]. The risks of overuse of nanofertilizers carefully request examination before its general use in farming system for revamping dose–response equations [50]. It is necessary to develop sustainable conduct to upscale the manufacturing of environmentally-safe nanomaterials and in designing green nanoparticles for the controlled release and increased

rate in nutrient uptake [50]. The European Union is considering various regulatory guidelines to address safety issues for the use of nanomaterials in agriculture [51]. But the complexity involved in the agricultural systems such as multiple organisms (plants, humans, and pests), microbiomes (soil, plant), variability in climatic conditions, soil structures, compositions, design of NMs, and societal engagement [52] are major bottlenecks. Therefore, this field needs more thoughtful understanding about their ambiguous physical and chemical characteristics.

2. ***Toxicity in human and animals***: The rapid utilization of 2D nanomaterials in each prospect of growing food from soil to post-harvest application and food packaging is bringing their direct or indirect contact with one and all. Also, it is not known very clearly that how it gets infiltrated into the bodies of humans and animals and cause health hazards. Graphene could follow an entry route in humans through intracheal instillation [53], oral intravenous injection [54], administration [55], subcutaneous injection [56], and intraperitoneal injection [57]. There are also reports of exposure to graphene in occupational situations with potential toxicity to researchers and workers [58]. In animal or cell modules, nanomaterials exert numerous levels of toxicity with distinct administration routes [59]. Thus, NMs may have mysterious consequences and call for in-depth study and research regarding their mode of action for their standardized use.
3. ***Ease of application***: Development of handy and easy to use 2D nanomaterial-based sensors and techniques for rapid and real-time analysis of plants, soil, water, and pesticides is necessary. Also, designing 2D nanomaterial composites in a way that they can exhibit multifunctional properties such as acting as both fertilizers and pesticides will reduce the amount of used nanomaterials to a greater extent. This will consequently reduce a number of issues associated with nanomaterials in agriculture [60].
4. ***Incomplete knowledge***: Although experts have the opinion that 2D nanomaterials in agriculture are safe but scientific gaps are still needed to be filled in by conducting thorough assessments on the impact of life cycle of the 2D nanomaterial on environment and human health. Extensive studies are urgently required to increase the awareness of their mechanism, toxicity, impacts, and build-up strategies to assess and deal with any risks that they may arise [61].
5. ***Societal issues***: Nanoscience has an ambiguous outlook in agriculture due to the fear of the unknown generated in public from, for example, unconstructive response toward genetically modified (GM) crops, lack of serious legislation and regulatory guidelines, and new-fangled nanotechnologies. A quick action to slash down the existing ragged outlines among the society and budding scientific notions is needed in order to overcome the societal barrier toward implementation of nanotechnology in real-world agriculture [62].

## 4 Commercial Aspect of 2D Nanomaterials: Highlights on Patented Research

Moving ahead, to kick in the 2D nanomaterials commercialization, the validation and standardization of proof-of-concept prototypes are critical. In recent times, a large number of patents on 2D nanomaterials have been reported in the field of energy, environment, agriculture, and biomedicines, and some of them are summarized in Table 1. Nevertheless, it still needs a sustained collaboration, data sharing, systematic frameworks, and cooperation between the academic laboratories, the suppliers, the industries, as well as the governing ministry to make their way to the market. In addition, the industry and the academic collaborators should seek to design innovative 2D nanomaterial appliances or products from the consumers' point-of-view to increase the end-user productivity.

## 5 Conclusions

In conclusion, we have briefly outlined the technological challenges, future opportunities, and commercial aspect of 2D nanomaterials in the field of energy and environment in this chapter. As realized, criteria such as high-throughput, low-cost, and controlled manufacturing of stable 2D nanomaterials with desired structural features are critical for specific applications. Furthermore, to improve the properties and performance of the 2D nanomaterials for different applications, crystal phase engineering, surface engineering including hybridization, doping and defect engineering, creating heterostructures/composites remain the topic of interest. The stability of 2D nanomaterials is also essential that should be sustained not only during their processing and storage but also in applications. Most of the 2D nanomaterials are prone to oxidize or collapse in ambient conditions or during the chemical reaction in applications which may lead to material loss, structural degradation, or secondary contamination. The fabrication routes should also make sure to minimize the use of hazardous chemicals and should not have any negative influence on ecosystems or the life forms. Therefore, biocompatibility, safety assessment, and toxicity evaluation of 2D nanomaterials have to be taken into account to avoid any possible health risks. Another promising future direction is to identify the most suitable 2D nanomaterial for a specific application. It is extremely important to build a fundamental structure-properties-performance relationship using innovative theoretical studies, data-driven approaches, and computational modelling. Current research on newly emerging members of 2D family such as MOF, COF, 2D polypeptoid, and other mono-elemental 2D nanomaterials (silicene, germanene, phosphorene, etc.) is still at their preliminary stage and should be evaluated for unexplored applications. For instance, adsorption of pollutants using phosphorene and electrochemical detection of toxic gases using TMDs are rarely reported. At last, efforts should be made toward developing an advanced multifunctional 2D nanomaterial-based devices/assemblies

**Table 1** Highlights on patents related to 2D nanomaterials/composites-based devices/products for energy, environment, agriculture, and biomedical applications

| Synthesis/fabrication/preparation methods | | |
|---|---|---|
| 2D nanomaterials | Patent | References |
| Graphene | US8226801B2<br>Mass production of pristine nano-graphene materials | [63] |
| Graphene | US20170225233A1<br>Chemical-free production of graphene reinforced inorganic matrix composites | [64] |
| Graphene | US9236197B2<br>Graphene hybrid materials, apparatuses, systems, and methods | [65] |
| Graphene | US20190292671A1<br>Metal matrix nanocomposite containing oriented graphene sheets and production process | [66] |
| Graphene | CN103700513B<br>A kind of graphene paper and its preparation method and application | [67] |
| Graphene | CN107555424A<br>A kind of preparation method of porous class graphene active carbon material and products thereof and application | [68] |
| Graphene | US8834959B2<br>Method for the preparation of doped single graphene sheets | [69] |

(continued)

**Table 1** (continued)

| Synthesis/fabrication/preparation methods | | |
|---|---|---|
| 2D nanomaterials | Patent | References |
| Graphene | CN105514450B<br>Nitrogen-doped graphene/difunctional VPO catalysts of ferronickel houghite and its preparation method and application | [70] |
| TMDs | EP2869348B1<br>Two-dimensional chalcogenide-based materials, methods of forming the same, and devices including the two-dimensional chalcogenide-based materials | [71] |
| TMDs | US20160181516A1<br>Phase transformation in transition metal dichalcogenides | [72] |
| $MoS_2$ | US20160093491A1<br>Large scale and thickness-modulated MoS2 nanosheets | [73] |
| MXenes | US10720644B2<br>Two-dimensional, ordered, double transition metals carbides having a nominal unit cell composition M′2M″nXn + 1 | [74] |
| MXenes | US9415570B2<br>Compositions comprising free-standing two-dimensional nanocrystals | [75] |

(continued)

**Table 1** (continued)

| Synthesis/fabrication/preparation methods | | |
|---|---|---|
| 2D nanomaterials | Patent | References |
| MXenes | US20200176619A1<br>Physical forms of MXene materials exhibiting novel electrical and optical characteristics | [76] |
| MXenes | CN107159286A<br>A kind of Ti3C2/TiO2The preparation method of two-dimensional material | [77] |
| MXenes | CN107117616B<br>A method of stratiform MXenes material is prepared using ternary MAX material | [78] |
| MXenes | CN107777688B<br>Preparation method of sheet-like MXene sheet material | [79] |
| Phosphorene | US9461125B2<br>Method of preparing monoatomic layer black phosphorous by irradiating ultrasound | [80] |
| Phosphorene | US10906811B2<br>Composition comprising optically and electronically active phosphorene | [81] |
| Phosphorene | US10676357B1<br>Bipolar exfoliation of black phosphorous into phosphorene | [82] |

(continued)

**Table 1** (continued)

| Synthesis/fabrication/preparation methods | | |
|---|---|---|
| 2D nanomaterials | Patent | References |
| Phosphorene | AU2021104425A4<br>Liquid-phase exfoliation method for producing black phosphorus nanoribbons or phosphorene nanoribbons | [83] |
| Phosphorene | KR20170125677A<br>Method for preparing bulk phosphorene using spark plasma sintering and bulk phosphorene prepared thereby | [84] |
| Silicene | US10600644B2<br>Mono- and multilayer silicene prepared by plasma-enhanced chemical vapor deposition | [85] |
| Tellurene | US20200247671A1<br>Substrate-free crystalline 2D nanomaterials | [86] |
| Layered perovskite | JP6270183B2<br>Organic/layered perovskite compound and method for producing organic/inorganic layered perovskite compound | [87] |
| MOF | US10201803B2<br>Polymer-metal organic framework materials and methods of using the same | [88] |
| TMDs, TMHs, phosphorene, perovskite, many other layered materials | US10309027B2<br>Method for producing dispersions of nanosheets | [89] |

(continued)

**Table 1** (continued)

| Synthesis/fabrication/preparation methods | | | |
|---|---|---|---|
| 2D nanomaterials | | Patent | References |
| *Energy storage and conversion* | | | |
| Supercapacitor | Graphene | US9017756B2<br>Continuous process for producing spacer-modified nano-graphene electrodes for supercapacitors | [90] |
| Supercapacitor | Graphene | US9053870B2<br>Supercapacitor with a mesoporous nano-graphene electrode | [91] |
| Supercapacitor | Graphene | US20090092747A1<br>Process for producing nano-scaled graphene platelet nanocomposite electrodes for supercapacitors | [92] |
| Supercapacitor | Graphene | WO2018013254A1<br>Supercritical fluid production of graphene-based supercapacitor electrode from coke or coal | [93] |
| Batteries | Graphene | JP2019522868A<br>Chemical-free production of graphene-filled electrode active material particles for battery applications | [[94] |
| Batteries | Graphene | US11081691B2<br>Carbon nanotubes—graphene hybrid structures for separator-free silicon-sulfur batteries | [95] |

(continued)

**Table 1** (continued)

| Synthesis/fabrication/preparation methods | | | |
|---|---|---|---|
| 2D nanomaterials | | Patent | References |
| Fuel cells | Graphene | CN104959134B<br>A kind of Heteroatom doping porous graphene electro-catalyst and preparation and application and device | [96] |
| Thermoelectric device | Graphene | ES2660904T3<br>Thermoelectric materials and devices comprising graphene | [97] |
| Solar cells | Graphene | CN109659138A<br>A kind of hollow carbon sphere/nickel sulfide of N doping/graphene ternary active multilayer/multi-factor structure composite material and preparation method for dye-sensitized solar cells | [98] |
| Solar cells | Graphene | CN109423068A<br>Super-hydrophobic wear-resisting graphene composite coating and the solar energy heat collection pipe for applying it | [99] |
| Photovoltaic cells | Graphene | CN111541398A<br>Preparation method of functionalized graphene roll-up photovoltaic PN junction | [100] |

(continued)

**Table 1** (continued)

| Synthesis/fabrication/preparation methods | | | |
|---|---|---|---|
| 2D nanomaterials | | Patent | References |
| Photovoltaic cells | Graphene | US10839974B2<br>High optical transparent two-dimensional electronic conducting system and process for generating same | [101] |
| Photovoltaic Cells | TMDs | US20170179314A1<br>Photovoltaic cells | [102] |
| Photovoltaic devices | Graphene/TMDs | US10692977B2<br>Heterostructures and electronic devices derived therefrom | [103] |
| Solar-thermal fuel cells | TMDs/TMOs | US20120325200A1<br>Nano-templated energy storage materials | [104] |
| Supercapacitors | TMDs | US20190139713A1<br>Two-dimensional transition metal dichalcogenide micro-supercapacitors | [105] |
| Na-battery | TMDs ($MoS_2$)/graphene | US20190081320A1<br>Robust $MoS_2$/graphene composite paper based electrodes for Na + battery applications | [106] |
| Li-battery | TMDs ($MoS_2$)/graphene | CN102683648B<br>Preparation method of few-layer $MoS_2$/graphene electrochemical storage lithium composite electrode | [107] |

(continued)

**Table 1** (continued)

| Synthesis/fabrication/preparation methods | | | |
|---|---|---|---|
| 2D nanomaterials | | Patent | References |
| Li-battery | TMDs ($MoS_2$)/graphene | CN102142537B<br>Graphene/$MoS_2$ compound nanomaterial lithium ion battery electrode and preparation method thereof | [108] |
| Zn-battery | TMOs ($MnO_2$) | CN106571461A<br>Chargeable–dischargeable Zn–$MnO_2$ battery with long service life and applications thereof | [109] |
| Capacitor electrode | TMOs ($MnO_2$) | JPWO2012086697A1<br>Nanoporous ceramic composite metal | [110] |
| Ultracapacitor | $MnO_2$/porous carbon film/nickel composite | CN105551813A<br>Preparation method of $MnO_2$/porous carbon film/nickel composite material | [111] |
| Fuel cell | TMOs ($MnO_2$) | ES2683360T3<br>Reversible fuel cell and reversible fuel cell system | [112] |
| Al-battery | MXenes | US20180309125A1<br>Electrochemical systems comprising MXenes and max phase compositions and methods of using the same | [113] |

(continued)

**Table 1** (continued)

| Synthesis/fabrication/preparation methods | | | |
|---|---|---|---|
| 2D nanomaterials | | Patent | References |
| Li–S battery | MXenes | CN106450205B<br>Two-dimensional transition group metal carbon/nitride and nano-sulfur particle composite material and preparation and application thereof | [114] |
| Li-battery | MXenes | CN107706372B<br>MXene-coated composite electrode material and preparation method thereof | [115] |
| Li-battery or<br>Na-battery | MXenes | WO2021042456A1<br>Rapid preparation method for few-layer MXenes and application | [116] |
| Supercapacitor | MXene | CN109003836A<br>A kind of preparation method based on MXene flexible fabric electrode and its application in supercapacitor | [117] |
| Supercapacitor | MXene | CN106430195A<br>MXene material and preparation method and application thereof | [118] |
| Battery | MXene | CN109671949A<br>A kind of MXene-based flexible compound negative electrode material and preparation method thereof | [119] |

(continued)

**Table 1** (continued)

| Synthesis/fabrication/preparation methods | | | |
|---|---|---|---|
| 2D nanomaterials | | Patent | References |
| Semiconductor device | Phosphorene | JP6477315B2<br>Phosphorene film forming method and semiconductor device manufacturing method | [120] |
| Li-battery | Phosphorene | CN106711408B<br>Flexible lithium ion battery black phosphorus nanometer sheet-graphene composite film cathode and preparation | [121] |
| Li-battery | Silicene | US20150364754A1<br>Silicene nanocomposite anode for lithium ion battery | [122] |
| Photovoltaic cell | hBN | US9859034B2<br>Functionalized boron nitride materials and methods for their preparation and use | [123] |
| Solar cell | Layered perovskite | CN108365102B<br>Stable and efficient two-dimensional layered perovskite solar cell and preparation method thereof | [124] |
| Photovoltaic device | Layered perovskite | CA3079471C<br>Quasi two-dimensional layered perovskite material, related devices and methods for manufacturing the same | [125] |

(continued)

**Table 1** (continued)

| Synthesis/fabrication/preparation methods | | | |
|---|---|---|---|
| 2D nanomaterials | | Patent | References |
| Piezoelectric device | Layered perovskite | JP4419232B2<br>Crystalline oriented bismuth layered perovskite type porcelain composition and method for producing the same | [126] |
| OER | Layered perovskite | CN108039495B<br>Non-metal element modified layered perovskite oxide oxygen reduction electrode material | [127] |
| OER | Layered perovskite | CN108579751B<br>Layered perovskite oxide, preparation method and application thereof in oxygen evolution reaction electrocatalysis | [128] |
| Fuel cell | Layered perovskite | CN105449227A<br>Layered perovskite cathode material for fuel cell and preparation method of layered perovskite cathode material | [129] |
| Battery | LDH | JP6001198B2<br>Batteries using layered double hydroxides | [130] |
| Zn-battery | MOF | CN110492069A<br>A kind of synthetic method of Zn@metal organic framework combination electrode material | [131] |

(continued)

**Table 1** (continued)

| Synthesis/fabrication/preparation methods | | | |
|---|---|---|---|
| 2D nanomaterials | | Patent | References |
| Zn-battery | MOF | CN107887603B<br>Preparation method of metal organic framework MOF-5 as zinc ion battery positive electrode material | [132] |
| Redox battery | MOF | CN105789668B<br>The preparation method of metal organic framework materials/polymer composite proton exchange membrane | [133] |
| Solar cell | Halide perovskite<br>MOF<br>2D polymer<br>hBN<br>TMD<br>MXene | US10403708B2<br>Graded bandgap perovskite solar cell | [134] |
| *Photocatalytic degradation of pollutants* | | | |
| Organic pollutant degradation | Graphene | CN104001504A<br>Preparation method for silver and graphene co-modified $TiO_2$ nanowire and application of silver and graphene co-modified $TiO_2$ nanowire in photocatalytic degradation of pollutants in wastewater | [135] |

(continued)

**Table 1** (continued)

| Synthesis/fabrication/preparation methods | | | |
|---|---|---|---|
| 2D nanomaterials | | Patent | References |
| (rhodamine B) dye degradation | Graphene | CN103480398B<br>Micronano-structured and graphene-based composite visible light catalytic material and preparing method thereof | [136] |
| Organic pollutant degradation | Graphene | CN103691420A<br>Mesoporous niobium pentoxide/graphene compound photocatalyst prepared by one-step self-assembly method | [137] |
| Organic pollutant degradation | Graphene | CN106378158A<br>Preparation method of bismuth sulfide/titanium dioxide/graphene compound with high-catalysis degradation activity under visible light | [138] |
| Organic pollutant degradation | Graphene | CN104258857A<br>Silver chromate-graphene oxide composite photocatalytic material and preparation method thereof | [139] |
| Integrated photocatalytic-capacitive deionization of pollutant | Graphene | CN104829019A<br>Photo-electric organic wastewater co-processing method based on graphene material and device thereof | [140] |

(continued)

**Table 1** (continued)

| Synthesis/fabrication/preparation methods | | | |
|---|---|---|---|
| 2D nanomaterials | | Patent | References |
| Organic dye degradation | TMDs | CN105148947A<br>Preparation and application of $TiO_2$@$MoS_2$ composite | [141] |
| Organic dye degradation | TMDs | CN106268875A<br>A kind of $MoS_2$ for efficient degradation wastewater from dyestuff photocatalyst and preparation method thereof | [142] |
| Organic dye degradation | TMDs | CN109465037A<br>The magnetic CDs-MoS of micropollutants in a kind of degradation water2-$Fe_3O_4$. The green synthesis method of catalysis material | [143] |
| Organic dye degradation | TMDs | CN106964370B<br>A kind of oxidation silver nano-grain/molybdenum sulfide nanometer sheet heterojunction structure ultrasound near infrared light catalyst and preparation method | [144] |
| Heavy metal and dye degradation | TMDs | CN109225273A<br>A kind of copper sulfide/tungsten sulfide composite photocatalyst and preparation method thereof | [145] |

(continued)

**Table 1** (continued)

| Synthesis/fabrication/preparation methods | | | |
|---|---|---|---|
| 2D nanomaterials | | Patent | References |
| Pathogen (Bacteria, viruses) degradation | TMDs | KR20180055860A<br>Molybdenum disulfide and related substances for water treatment | [146] |
| Organic pollutant degradation | TMDs | CN108355679A<br>A kind of $Fe_3O_4/MoS_2/BiVO_4$ preparation method, product, and its application of material | [147] |
| Methylene blue dye degradation | g-$C_3N_4$ | CN103193785B<br>Graphene-like C3N4 material, as well as preparation method and use thereof | [148] |
| Organic pollutant degradation | MXenes | CN111715250B<br>Preparation method and application of supported transition metal carbide Fenton-like nano-catalyst | [149] |
| Organic pollutant degradation | MXenes | CN113134375A<br>MXene-based two-dimensional silver compound and preparation method and application thereof | [150] |
| Organic dye (rhodamine B) degradation | MXenes | CN111822028A<br>Bismuth-based photocatalytic composite film based on MXene and preparation method thereof | [151] |
| Organic dye degradation | MXenes | CN110560164A<br>Polydopamine-coated $C_3N_4$/MXene composite material and preparation method thereof | [152] |

(continued)

**Table 1** (continued)

| Synthesis/fabrication/preparation methods | | | |
|---|---|---|---|
| 2D nanomaterials | | Patent | References |
| $NH_3$, $H_2S$ and other organic pollutants degradation | MXenes | CN111545230A<br>Preparation method, product and application of nano-titanium dioxide/MXene composite membrane | [153] |
| Organic pollutant degradation | MXenes | CN109794281A<br>One kind preparing the nitrogen co-doped nano-TiO of carbon based on MXene material2 the method of photochemical catalyst | [154] |
| Synchronous adsorption of phenol and lead ions in water and photocatalytic phenol reduction | MXenes | CN112121855B<br>Preparation method of photocatalytic thiourea modified two-dimensional MXene material | [155] |
| Organic dye degradation | Phosphorene | CN106586987B<br>A kind of preparation method of the black phosphorus nanoscale twins for photocatalytic degradation of dye wastewater | [156] |
| Organic dye degradation | Phosphorene/g-$C_3N_4$ | CN108355696B<br>Black phosphorus/g-$C_3N_4$ composite visible light photocatalytic material and preparation method and application thereof | [157] |

(continued)

**Table 1** (continued)

| Synthesis/fabrication/preparation methods | | | |
|---|---|---|---|
| 2D nanomaterials | | Patent | References |
| Organic dye degradation | Phosphorene | CN112076769A<br>Spherical bismuth vanadate/black phosphorus composite photocatalyst and preparation method thereof | [158] |
| Photocatalytic treatment of toxic gases | Phosphorene-g-$C_3N_4$-MOF | CN108745404B<br>Carbon nitride film composite material based on black phosphorus/metal organic framework modification, preparation method thereof and application thereof in waste gas treatment | [159] |
| Photocatalytic treatment of toxic gases | Phosphorene | CN109529898B<br>Black phosphorus/bismuth tungstate nanocomposite and preparation method thereof and application of black phosphorus/bismuth tungstate nanocomposite in waste gas treatment | [160] |
| Bisphenol-A degradation | MOF | CN106927535B<br>Method for photocatalytic degradation of phenolic pollutants based on stable porphyrin metal organic framework material | [161] |
| Heavy metal and dye degradation | MOF | CN107617447B<br>Ag @ MOFs/$TiO_2$. Preparation method and application of photocatalyst | [162] |

(continued)

**Table 1** (continued)

| Synthesis/fabrication/preparation methods | | | |
|---|---|---|---|
| 2D nanomaterials | | Patent | References |
| Organic dye degradation | Layered double oxide | CN102151577B<br>Ag3PO4/Mg–Al layered double oxide (LDO) visible light composite photocatalyst, preparation, and application thereof | [163] |
| *Adsorption-based removal of pollutants* | | | |
| Organic pollutant adsorption | Graphene | CN103570009A<br>Graphene capable of efficiently adsorbing organic substances and regeneration method thereof | [164] |
| Groundwater remediation | Graphene | WO2018078427A1<br>Graphene-based filtering element and uses thereof | [165] |
| Non-polar contaminants such as oil adsorption | Graphene | US20210024378A1<br>Graphene reinforced polystyrene composite for separation of non-polar compounds from water | [166] |
| Gaseous contaminants adsorption | Graphene | WO2018006745A1<br>Air filtration device utilizing graphene coating, and system | [167] |
| $NH_3$ adsorption | Graphene | US10994241B1<br>Sorbent system for removing ammonia and organic compounds from a gaseous environment | [168] |

(continued)

**Table 1** (continued)

| Synthesis/fabrication/preparation methods | | | |
|---|---|---|---|
| 2D nanomaterials | | Patent | References |
| Toxic gas and water pollutants adsorption | Graphene | CN203916677U<br>A kind of water and gas dual-purpose graphene absorption and reclaim equipment | [169] |
| Heavy metals. nitrates, phosphates removal | Graphene | US20210060522A1<br>Graphene-based materials for the efficient removal of pollutants from water | [170] |
| Radioactive pollutants removal | Graphene | US20170151548A1<br>Sorption And Separation of Various Materials by Graphene Oxides | [171] |
| Pesticide removal | Graphene | CN110420619A<br>A method of recycling graphene-based adsorbent material processing pesticide sewage | [172] |
| Heavy metal, organic dye adsorption | TMDs/Graphene | US10493426B2<br>Graphene-metal chalcogenide porous material | [173] |
| Mercury adsorption | TMDs | USRE44124E1<br>Regenerable high capacity sorbent for removal of mercury from flue gas | [174] |
| Heavy metal adsorption | TMDs | US20190144305A1<br>Adsorption and removal of heavy metal ions from water by transition metal dichalcogenides | [175] |

(continued)

**Table 1** (continued)

| Synthesis/fabrication/preparation methods | | | |
|---|---|---|---|
| 2D nanomaterials | | Patent | References |
| Heavy metal adsorption | TMDs | US8070959B2<br>Chalcogenide compounds with a clay-like cation-exchange capacity and methods of use | [176] |
| Organic dye adsorption | TMDs | CN108383169A<br>A kind of preparation method and applications of ternary layered transitionmetal dichalcogenide | [177] |
| Atrazine removal | MXenes | CN113181947A<br>CuO-$Fe_2O_3$/MXene composite material for water treatment and purification and preparation method and application thereof | [178] |
| Heavy metal adsorption | MXenes | US11053138B2<br>Method of removing arsenic from a liquid | [179] |
| Heavy metal adsorption | MXenes | CN104587947A<br>Method for preparing two-dimensional nano-adsorbent titanium carbide for effectively adsorbing hexavalent chromium ions | [180] |
| Organic dye (Methylene blue) adsorption | MXenes | CN107694510B<br>Method for removing methylene blue in printing and dyeing wastewater by two-dimensional magnetic MXene | [181] |

(continued)

**Table 1** (continued)

| Synthesis/fabrication/preparation methods | | | |
|---|---|---|---|
| 2D nanomaterials | | Patent | References |
| Organic dye (Eosin Y and methylene blue) adsorption | MXenes | CN108774343A<br>Composite aerogel and preparation method thereof and composite hydrogel and preparation method thereof | [182] |
| Organic dyes, heavy metals adsorption | MXenes | CN106268610A<br>A kind of preparation method of two dimension titanium carbide adsorbing material | [183] |
| Organic dyes, heavy metals adsorption | hBN/GO | CN103480329B<br>Hexagonal boron nitride/graphene oxide composite adsorption material and preparation method thereof | [184] |
| SOx removal | Layered double hydroxide | US5114898A<br>Layered double hydroxide sorbents for the removal of SOx from flue gas and other gas streams | [185] |
| $CO_2$ adsorption | MOF | CN105056895B<br>A kind of preparation method and applications of metal organic framework mesopore silicon oxide composite | [186] |

(continued)

**Table 1** (continued)

| Synthesis/fabrication/preparation methods | | | |
|---|---|---|---|
| 2D nanomaterials | | Patent | References |
| Heavy metal adsorption | MOF | CN112973638A<br>Preparation method and application of modified MIL-125 (Ti) material for removing micro-polluted mercury in water body | [187] |
| Organic pollutant adsorption | MOF | CN105481043A<br>Method for adsorbing organic pollutants in water environment with porous carbon obtained by carbonizing metal organic framework material as adsorbent | [188] |
| Antibiotic adsorption | MOF | CN108201878B<br>Preparation method of carbon-point-modified metal organic framework adsorption material and application of carbon-point-modified metal organic framework adsorption material in treatment of water pollutants | [189] |
| *Desalination and membrane filtration* | | | |
| Desalination and membrane filtration | Graphene | US10456754B2<br>High-performance membranes for water reclamation using polymeric and nanomaterials | [190] |
| Deionization or desalination | Graphene | US9475709B2<br>Perforated graphene deionization or desalination | [191] |

(continued)

**Table 1** (continued)

| Synthesis/fabrication/preparation methods | | | |
|---|---|---|---|
| 2D nanomaterials | | Patent | References |
| Desalination | Graphene | CN108636141B<br>Preparation method of graphene desalination film | [192] |
| Desalination | Graphene | CN207361918U<br>A kind of porous graphene desalination plant | [193] |
| Desalination | Graphene | US20180333685A1<br>Method for making a polygraphene membrane for water desalination | [194] |
| Deionization | Graphene | US20130240355A1<br>Functionalization of graphene holes for deionization | [195] |
| Gas separation membrane | Graphene | US9610546B2<br>Separation membranes formed from perforated graphene and methods for use thereof | [196] |
| Integrated photovolataiv-desalination device | Graphene | CN111204828A<br>Preparation method of graphene-aluminum-based layer-by-layer assembled photovoltaic and seawater desalination device functional area | [197] |
| Integrated desalination-energy storage device | $MnO_2$ | AU2016203645B2<br>Redox desalination system for clean water production and energy storage | [198] |

(continued)

**Table 1** (continued)

| Synthesis/fabrication/preparation methods | | | |
|---|---|---|---|
| 2D nanomaterials | | Patent | References |
| Desalination | TMDs | US20190039028A1<br>porous membranes comprising nanosheets and fabrication thereof | [199] |
| Desalination | TMDs | CN110015722A<br>The preparation method of molybdenum disulfide@graphite paper integral capacitance type desalination electrode | [200] |
| Membrane filtration | TMDs | EP3140028A2<br>Stacked two-dimensional materials and methods for producing structures incorporating same | [201] |
| Adsorption of petroleum waste and desalination | MXenes | US20200254396A1<br>Precise Fabrication of Activated-Hydrophilic-Hydrophobic MXenes-based Multidimensional Nanosystems for Efficient and Prompt Water Purification from Petroleum Wastes and Desalination Process under Ambient Conditions | [202] |
| Capacitive deionization and desalination | MXenes/graphene | CN107633954B<br>graphene/MXene composite electrode material and application thereof | [203] |

(continued)

**Table 1** (continued)

| Synthesis/fabrication/preparation methods | | | |
|---|---|---|---|
| 2D nanomaterials | | Patent | References |
| Membrane filtration | MXenes | CN106178979B<br>High-performance two-dimensional stratiform Ti3C2- MXene film and preparation method thereof and the application in water process | [204] |
| Membrane filtration | MXenes | WO2018205290A1<br>MXene-based composite nanofiltration membrane and preparation method therefor | [205] |
| Desalination | MXenes | US20180169591A1<br>Two-dimensional metal carbide desalination membrane | [206] |
| Forward osmosis | MXenes | CN113398777A<br>Three-layer structure composite forward osmosis membrane with MXene drainage layer and preparation method thereof | [207] |
| Forward osmosis | MXenes | CN112473372A<br>Conductive forward osmosis membrane and preparation method thereof | [208] |
| Desalination | MXenes | CN109569319A<br>A kind of application of the two dimension self-crosslinking MXene film in ion isolation | [209] |

(continued)

**Table 1** (continued)

| Synthesis/fabrication/preparation methods | | | |
|---|---|---|---|
| 2D nanomaterials | | Patent | References |
| Desalination | MXenes | CN110342601B<br>Based on CuInSe2 seawater desalination structure of/MXene nano-composite material | [210] |
| Sea water desalination, sewage purification, water–oil separation | MXenes/GO | CN110090603A<br>A kind of MXene and graphene oxide composite aerogel and its preparation method and application | [211] |
| Photo-thermal desalination | MXenes | CN107537323B<br>MXene nanowire composite electrospun fiber membrane for photo-thermal desalination | [212] |
| Gas separation membrane, Desalination | MOF | CN111282405A<br>Modified metal organic framework nanosheet and preparation method thereof | [213] |
| Membrane filtration, desalination | MOF | EP3774001A1<br>Membranes comprising a layer of metal organic framework particles | [214] |
| *Detection and sensing of pollutants* | | | |
| Heavy metal detection | Graphene | CN105717174B<br>The electrochemical detection method of modified graphene oxide composite modified electrode trace heavy metal ion in water body is detected | [215] |

(continued)

**Table 1** (continued)

| Synthesis/fabrication/preparation methods | | | |
|---|---|---|---|
| 2D nanomaterials | | Patent | References |
| Heavy metal detection | Graphene | CN106483184A<br>Heavy metal analysis device and method based on graphene sensor | [216] |
| Heavy metal detection | Graphene | CN104391030B<br>A kind of heavy metal ion Cd built based on alginic acid functionalization graphene 2+, Pb 2+, and Cu 2+ the preparation method of sensor and application | [217] |
| Pesticide detection | Graphene | CN101995402B<br>Preparation and application of electrochemiluminescence sensor for detecting trace pesticide residue | [218] |
| Catechol, hydroquinone, and resorcinol detection | Graphene | CN102980928A<br>Tungsten sulfide-graphene electrochemical sensor as well as preparation method and application of sensor | [219] |
| Gas sensor | Graphene | CN102680527B<br>Method for preparing graphene gas sensors in batches based on nano soft lithography | [220] |
| Gas sensor | Graphene | Amperometric electrochemical gas sensing apparatus and method for measuring oxidizing gases | [221] |

(continued)

**Table 1** (continued)

| Synthesis/fabrication/preparation methods | | | |
|---|---|---|---|
| 2D nanomaterials | | Patent | References |
| Gas sensor | Graphene | US9869651B2<br>Enhanced sensitivity of graphene gas sensors using molecular doping | [222] |
| VOCs sensor | TMDs | US9063063B2<br>Low-dimensional material chemical vapor sensors | [223] |
| $NO_2$ gas sensor | TMDs | CN109825816A<br>A kind of molybdenum disulfide film gas sensitive and preparation method and application | [224] |
| Pesticide detection | MXenes | CN113390943A<br>Electrochemical sensor for detecting organophosphorus pesticide and preparation method thereof | [225] |
| Antibiotic detection | MXenes | CN109115850A<br>A kind of chemically modified electrode and the preparation method and application thereof of sensitive detection fortimicin | [226] |
| Phenol, catechol, bisphenol-A detection | MXenes | CN110057882A<br>A kind of electrochemical biological sensor and its application based on two-dimensional titanium carbon compound | [227] |

(continued)

**Table 1** (continued)

| Synthesis/fabrication/preparation methods | | | |
|---|---|---|---|
| 2D nanomaterials | | Patent | References |
| Nitroaromatic explosives detection | MXenes | CN109406611B<br>Nano-palladium/carbon nanotube-MXene composite material and application thereof in detection of nitroaromatic explosives | [228] |
| $H_2O_2$ detection | MXenes | CN109675608A<br>A kind of PB complex nanomaterial and its preparation method and application | [229] |
| Gas sensor | MXenes | WO2019124625A1<br>Chemiresistor gas sensor using MXene, and manufacturing method therefor | [230] |
| Gas sensor | MXenes | CN109799267B<br>Planar humidity and ammonia gas sensor based on alkalized organ-shaped MXene sensitive material and preparation method thereof | [231] |
| $NH_3$ gas sensor | Phosphorene | CN105116034A<br>Sensor based on black phosphorus electrode and preparation method of sensor | [232] |
| $NO_2$ gas sensor | Phosphorene | US10648959B2<br>Black phosphorus gas sensor | [233] |

(continued)

**Table 1** (continued)

| Synthesis/fabrication/preparation methods | | | |
|---|---|---|---|
| 2D nanomaterials | | Patent | References |
| Gas sensor | MOF | US10274421B2<br>Sensor devices comprising a metal organic framework material and methods of making and using the same | [234] |
| $H_2O_2$ detection | MOF | CN109270140B<br>Preparation method and application of electrochemical sensor made of high-dispersion graphene/Zn-based metal organic framework composite material | [235] |
| *Biomedical and Healthcare applications* | | | |
| Drug delivery | Graphene | US20150283239A1<br>Graphene derivative-based composition for drug delivery and preparation method thereof | [236] |
| Drug delivery | Graphene | CN104436210A<br>Malignant-tumor-resistant graphene oxide nano-drug delivery system and preparation method thereof | [237] |
| Drug delivery | Graphene | CN108379461A<br>A kind of graphene blood pressure lowering patch and preparation method thereof | [238] |
| Drug delivery | Graphene | Method of manufacturing graphene aerogels for drug delivery | [239] |

(continued)

**Table 1** (continued)

| Synthesis/fabrication/preparation methods | | | |
|---|---|---|---|
| 2D nanomaterials | | Patent | References |
| Magnetic thermal therapy, drug delivery | Graphene | CN104758930A Preparation method of in-situ gel based on magnetic graphene oxide and application thereof | [240] |
| Drug delivery | Graphene | KR101618556B1 Mesoporous silica-coated graphene oxide hybrid structure and development of drug delivery system using phase change material and drug delivery system using thereof | [241] |
| Cancer detection | Graphene | CN110819717A Graphene oxide-containing amplification system and application thereof in colorectal cancer marker detection | [242] |
| Rare cell detection | Graphene | US10935550B2 Functionalized graphene oxide system for detecting rare cells | [243] |
| Tumor cells detection | Graphene | CN108330054B Graphene chip for specific capture of circulating tumor cells in whole blood and preparation method and application thereof | [244] |
| Medicinal sterilizer and applicator | Graphene | CN110013601B Graphene pesticide applicator and pesticide application method | [245] |

(continued)

**Table 1** (continued)

| Synthesis/fabrication/preparation methods | | | |
|---|---|---|---|
| 2D nanomaterials | | Patent | References |
| Bioelectronic device | Graphene | WO2016200105A2<br>Graphene bioelectronic device, treatment and diagnosis nanoparticle, and endoscope system | [246] |
| Drug carrier | TMDs | CN103705928A<br>Single-layer MoS2 nano-chip, preparation method, and nano-drug carrier | [247] |
| CT imaging and phototherapy | TMDs | CN106512002A<br>Multifunctional nanometer hybrid integrated CT imaging and phototherapy and preparing method of multifunctional nanometer hybrid | [248] |
| Photo-thermal therapy for cancer treatment | TMDs | CN107802836B<br>Tumor targeted photo-thermal medicament, preparation method and application | [249] |
| Drug carrier, phototherapy | TMDs | CN106563130A<br>Stripping preparation method of molybdenum disulfide nanosheet and applications of molybdenum disulfide nanosheet | [250] |
| Drug carrier, phototherapy | TMDs | CN107375928A<br>A kind of preparation method and application of cancer target photo-thermal therapy nano-carrier | [251] |

(continued)

**Table 1** (continued)

| Synthesis/fabrication/preparation methods | | | |
|---|---|---|---|
| 2D nanomaterials | | Patent | References |
| Drug carrier | MXenes | CN108245682B<br>Acidity and photo-thermal response type mesoporous MXene nanosheet drug carrier and preparation method thereof | [252] |
| Cancer therapy | MXenes | CN108273058B<br>Sustained-release preparation for tumor targeted therapy and preparation method thereof | [253] |
| Drug carrier | MXenes | CN111110913A<br>Porous MXene membrane for drug loading and application thereof | [254] |
| Cancer diagnosis | MXenes | CN108159438A<br>A kind of photo-acoustic imaging contrast medium of cancer diagnosis and its preparation method and application | [255] |
| Photo-thermal therapy for cancer treatment | Phosphorene | CN106267201B<br>A kind of black phosphorus of polymer wrapped and preparation method and application | [256] |
| Photo-thermal therapy and photo-acoustic imaging for cancer treatment | Phosphorene | CN105535971B<br>A kind of black phosphorus nanoparticle and its preparation method and application with biocompatibility | [257] |

(continued)

**Table 1** (continued)

| Synthesis/fabrication/preparation methods | | | |
|---|---|---|---|
| 2D nanomaterials | | Patent | References |
| Photo-thermal therapy for cancer treatment | Phosphorene | CN106335885B<br>A kind of black phosphorus nanometer sheet and preparation method and application | [258] |
| Photo-thermal therapy for cancer treatment | Phosphorene | CN106366121B<br>Through ligand modified black phosphorus of titanium and preparation method and application | [259] |
| *Agriculture applications* | | | |
| Nano-fertilizer | Graphene | US11040918B2<br>Graphene for fertilizer applications | [260] |
| Nano-fertilizer | Graphene | US20190308916A1<br>Controlled release of fertilizer compositions and uses thereof | [261] |
| Nano-fertilizer | Graphene | CN104829340B<br>A kind of micro-capsule graphene composite material controlled release fertilizer granules and preparation method thereof | [262] |
| Nano-fertilizer | Graphene | CN111285729A<br>Carbon-based mica fertilizer, preparation method, and application thereof | [263] |

(continued)

**Table 1** (continued)

| Synthesis/fabrication/preparation methods | | | |
|---|---|---|---|
| 2D nanomaterials | | Patent | References |
| Soil restoration | Graphene | CN108085010B<br>A kind of complex repairation agent and its application for heavy metal pollution of soil | [264] |
| Medium for improving plant growth | Graphene | JP2019527057A<br>Graphene-based growth medium and method | [265] |
| Regulating compost for plant growth | Graphene | CN105891269A<br>Method for regulating lawn compost substrate and bioavailability using carbon nanomaterial | [266] |
| Nano-pesticide | Graphene | CN108684706A<br>A kind of graphene pesticide compound and preparation method thereof | [267] |
| Nano-pesticide | Graphene | CN112293419A<br>Graphene oxide-containing pesticide composition | [268] |
| Nano-pesticide | Graphene | CN108064844A<br>A kind of cyclodextrin modified graphene-houghite pesticide slow-releasing agent and preparation method thereof | [269] |
| Nano-pesticide-fertilizer | Graphene | CN106577644A<br>Medical fertilizer containing graphene nanomaterial and preparation method of medical fertilizer | [270] |
| Nano-pesticide-fertilizer | Graphene | CN104829340A<br>Microcapsule graphene composite material controlled-release pesticide-fertilizer granules and preparation method | [271] |

(continued)

**Table 1** (continued)

| Synthesis/fabrication/preparation methods | | | |
|---|---|---|---|
| 2D nanomaterials | | Patent | References |
| Nano-pesticide-fertilizer | Graphene | CN109053289A<br>A kind of compound controlled release fertilizer granules of graphene and preparation method thereof | [272] |

that are intelligent, adaptive, selective, and programmable. An example could be combining membrane separation technologies with photocatalysts that can enable photocatalytic degradation of organic foulants, alleviating the fouling issues. Next, energy storage devices could be integrated with capacitive deionization or electrochemical sensing, which would simultaneously remove the redox water pollutants and reutilize it for charge storage. It not only requires innovations in material property, but also calls for fundamental understanding of underlying physics, chemistry, and associated mechanism of these diverse and multidisciplinary processes. Nevertheless, massive efforts are still needed to gain the commercial success of these exciting materials for future sustainability.

## References

1. Khan K, Tareen AK, Aslam M, Wang R, Zhang Y, Mahmood A, Ouyang Z, Zhang H, Guo Z (2020) Recent developments in emerging two-dimensional materials and their applications. J Mater Chem C 8(2):387–440
2. Tan C, Cao X, Wu XJ, He Q, Yang J, Zhang X, Chen J, Zhao W, Han S, Nam GH, Sindoro M, Zhang H (2017) Recent advances in ultrathin two-dimensional nanomaterials. Chem Rev 117(9):6225–6331
3. Bhimanapati GR, Lin Z, Meunier V, Jung Y, Cha J, Das S, Xiao D, Son Y, Strano MS, Cooper VR, Robinson JA (2015) Recent advances in two-dimensional materials beyond graphene. ACS Nano 9(12):11509–11539
4. Jeong GH, Sasikala SP, Yun T, Lee GY, Lee WJ, Kim SO (2020) Nanoscale assembly of 2D materials for energy and environmental applications. Adv Mater 32(35):1907006
5. Le, T. H., Oh, Y., Kim, H., & Yoon, H. (2020). Exfoliation of 2D materials for energy and environmental applications. Chem Euro J 26(29):6360–6401
6. Choi W, Choudhary N, Han GH, Park J, Akinwande D, Lee YH (2017) Recent development of two-dimensional transition metal dichalcogenides and their applications. Mater Today 20(3):116–130
7. Glavin NR, Rao R, Varshney V, Bianco E, Apte A, Roy A, Ringe E, Ajayan PM (2020) Emerging applications of elemental 2D materials. Adv Mater 32(7):1904302
8. Yang S, Zhang P, Nia AS, Feng X (2020) Emerging 2D materials produced via electrochemistry. Adv Mater 32(10):1907857
9. Tao H, Zhang Y, Gao Y, Sun Z, Yan C, Texter J (2017) Scalable exfoliation and dispersion of two-dimensional materials—an update. Phys Chem Chem Phys 19(2):921–960
10. Khanam Z, Liu J, Song S (2021) High-concentration graphene dispersions prepared via exfoliation of graphite in PVA/$H_2O$ green solvent system using high-shear forces. J Nanoparticle Res 170
11. Khanam Z, Liu J, Song S (2020) Flexible graphene paper electrode prepared via polyvinyl alcohol-assisted shear-exfoliation for all-solid-state polymer supercapacitor application. Electrochimica Acta 363:137208
12. Gan X, Zhao H, Schirhagl R, Quan X (2018) Two-dimensional nanomaterial-based sensors for heavy metal ions. Microchim Acta 185(10):1–30
13. Zhang H (2015) Ultrathin two-dimensional nanomaterials. ACS Nano 9(10):9451–9469
14. Coogan Á, Gun'ko YK (2021) Solution-based "bottom-up" synthesis of group VI transition metal dichalcogenides and their applications. Mater Adv
15. Wang Q, Lei Y, Wang Y, Liu Y, Song C, Zeng J, Song Y, Duan X, Wang D, Li Y (2020) Atomic-scale engineering of chemical-vapor-deposition-grown 2D transition metal dichalcogenides for electrocatalysis. Energy Environ Sci 13(6):1593–1616

16. Jana M, Singh RN (2018) Progress in CVD synthesis of layered hexagonal boron nitride with tunable properties and their applications. Int Mater Rev 63(3):162–203
17. Ghavanini FA, Theander H (2015). Graphene feasibility study and foresight study for transport infrastructures
18. Ihsanullah I (2020) Potential of MXenes in water desalination: current status and perspectives. Nano-Micro Lett 12(1):1–20
19. Jiang X, Kuklin AV, Baev A, Ge Y, Ågren H, Zhang H, Prasad PN (2020) Two-dimensional MXenes: from morphological to optical, electric, and magnetic properties and applications. Phys Rep 848:1–58
20. Ren Y, Xu Q (2018) Building close ties between $CO_2$ and functional two-dimensional nanomaterials with green chemistry strategy. Energy Environ Mater 1(2):46–60
21. Zeng M, Chen M, Huang D, Lei S, Zhang X, Wang L, Cheng Z (2020). Engineered two-dimensional nanomaterials: an emerging paradigm for water purification and monitoring. Mater Horizons
22. Mounet N, Gibertini M, Schwaller P, Campi D, Merkys A, Marrazzo A, Sohier T, Castelli IE, Cepellotti A, Pizzi G, Marzari N (2018) Two-dimensional materials from high-throughput computational exfoliation of experimentally known compounds. Nat Nanotechnol 13(3):246–252
23. Haastrup S, Strange M, Pandey M, Deilmann T, Schmidt PS, Hinsche NF, Gjerding MN, Torelli D, Larsen PM, Riis-Jensen AC, Gath J, Thygesen KS (2018) The computational 2D materials database: high-throughput modeling and discovery of atomically thin crystals. 2D Mater 5(4):042002
24. Kumar KS, Choudhary N, Jung Y, Thomas J (2018) Recent advances in two-dimensional nanomaterials for supercapacitor electrode applications. ACS Energy Lett 3(2):482–495
25. Chaudhari NK, Jin H, Kim B, San Baek D, Joo SH, Lee K (2017) MXene: an emerging two-dimensional material for future energy conversion and storage applications. J Mater Chem A 5(47):24564–24579
26. Tao Y, Huang T, Ding C, Yu F, Tan D, Wang F, Xie Q, Yao S (2019) Few-layer phosphorene: an emerging electrode material for electrochemical energy storage. Appl Mater Today 15:18–33
27. Liu Y, Peng X (2017) Recent advances of supercapacitors based on two-dimensional materials. Appl Mater Today 8:104–115
28. Zhang P, Wang F, Yu M, Zhuang X, Feng X (2018) Two-dimensional materials for miniaturized energy storage devices: from individual devices to smart integrated systems. Chem Soc Rev 47(19):7426–7451
29. Soares DM, Mukherjee S, Singh G (2020) TMDs beyond $MoS_2$ for electrochemical energy storage. Chem Euro J 26(29):6320–6341
30. Liu J, Khanam Z, Ahmed S, Wang T, Wang H, Song S (2021) Flexible anti-freeze Zn-ion hybrid supercapacitor based on gel electrolyte with graphene electrodes. ACS Appl Mater Interfaces 13(14):16454–16468
31. Liu J, Khanam Z, Ahmed S, Wang H, Wang T, Song S (2021) A study of low-temperature solid-state supercapacitors based on Al-ion conducting polymer electrolyte and graphene electrodes. J Power Sour 488:229461
32. Liu J, Ahmed S, Khanam Z, Wang T, Song S (2020) Ionic liquid-incorporated Zn-ion conducting polymer electrolyte membranes. Polymers 12(8):1755
33. Liu J, Khanam Z, Muchakayala R, Song S (2020) Fabrication and characterization of Zn-ion conducting solid polymer electrolyte films based on PVdF-HFP/$Zn(Tf)_2$ complex system. J Mater Sci Mater Electron 31:6160–6173
34. Tunesi MM, Soomro RA, Han X, Zhu Q, Wei Y, Xu B (2021) Application of MXenes in environmental remediation technologies. Nano Convergence 8(1):1–19
35. Lam SM, Kee MW, Wong KA, Jaffari ZH, Chai HY, Sin JC (2019) A newly emerging MXene nanomaterial for environmental applications. MXenes Fundamentals Appl 51:20–60
36. Guan G, Ye E, You M, Li Z (2020) Hybridized 2D nanomaterials toward highly efficient photocatalysis for degrading pollutants: current status and future perspectives. Small 16(19):1907087

37. Zhao P, Jian M, Zhang Q, Xu R, Liu R, Zhang X, Liu H (2019) A new paradigm of ultrathin 2D nanomaterial adsorbents in aqueous media: graphene and GO, $MoS_2$, MXenes, and 2D MOFs. J Mater Chem A 7(28):16598–16621
38. Meng Z, Stolz RM, Mendecki L, Mirica KA (2019) Electrically-transduced chemical sensors based on two-dimensional nanomaterials. Chem Rev 119(1):478–598
39. Khanam Z, Gupta S, Verma A (2020) Endophytic fungi-based biosensors for environmental contaminants: a perspective. S Afr J Bot 134:401–406
40. Su S, Chen S, Fan C (2018) Recent advances in two-dimensional nanomaterials-based electrochemical sensors for environmental analysis. Green Energy Environ 3(2):97–106
41. Tyagi D, Wang H, Huang W, Hu L, Tang Y, Guo Z, Ouyang Z, Zhang H (2020) Recent advances in two-dimensional-material-based sensing technology toward health and environmental monitoring applications. Nanoscale 12(6):3535–3559
42. Wang Z, Zhu W, Qiu Y, Yi X, von dem Bussche A, Kane A, Gao H, Koski K, Hurt R (2016) Biological and environmental interactions of emerging two-dimensional nanomaterials. Chem Soc Rev 45(6):1750–1780
43. Chen J, Huang Q, Huang H, Mao L, Liu M, Zhang X, Wei Y (2020) Recent progress and advances in the environmental applications of MXene related materials. Nanoscale 12(6):3574–3592
44. Huang J, Li Z, Mao Y, Li Z (2021) Progress and biomedical applications of MXenes. Nano Select
45. Bolotsky A, Butler D, Dong C, Gerace K, Glavin NR, Muratore C, Robinson JA, Ebrahimi A (2019) Two-dimensional materials in biosensing and healthcare: from in vitro diagnostics to optogenetics and beyond. ACS Nano 13(9):9781–9810
46. Wen W, Song Y, Yan X, Zhu C, Du D, Wang S, Asiri AM, Lin Y (2018) Recent advances in emerging 2D nanomaterials for biosensing and bioimaging applications. Mater Today 21(2):164–177
47. Siddiqui A, Khan A (2019) Mechanism and optimization of acoustic power transfer systems. In: 2019 international conference on power electronics, control and automation (ICPECA). IEEE, pp 1–6
48. Khot LR, Sankaran S, Maja JM, Ehsani R, Schuster EW (2012) Applications of nanomaterials in agricultural production and crop protection: a review. Crop Prot 35:64–70
49. Aslani F, Bagheri S, Muhd Julkapli N, Juraimi AS, Hashemi FS, Baghdadi A (2014) Effects of engineered nanomaterials on plants growth: an overview. Scientific World J
50. Raliya R, Saharan V, Dimpka C, Biswas P (2018) Nanofertilizer for precision and sustainable agriculture: current state and future perspectives. J Sci Food Agric 66:6487–6503
51. Amenta V, Aschberger K, Arena M, Bouwmeester H, Moniz FB, Brandhoff P, Gottardo S, Marvin HJ, Mech A, Pesudo LQ, Rauscher H (2015) Regulatory aspects of nanotechnology in the agri/feed/food sector in EU and non-EU countries. Regul Toxicol Pharmacol 73:463–476
52. Lowry GV, Avellan A, Gilbertson LM (2019) Opportunities and challenges for nanotechnology in the agri-tech revolution. Nat Nanotechnol 6:517–522
53. Li B, Yang J, Huang Q, Zhang Y, Peng C, Zhang Y, He Y, Shi J, Li W, Hu J, Fan C (2013) Biodistribution and pulmonary toxicity of intratracheally instilled graphene oxide in mice. NPG Asia Mater 5:44–48
54. Wen KP, Chen YC, Chuang CH, Chang HY, Lee CY, Tai NH (2015) Accumulation and toxicity of intravenously-injected functionalized graphene oxide in mice. J Appl Toxicol 35:1211–1218
55. Yang K, Gong H, Shi X, Wan J, Zhang Y, Liu Z (2014) In vivo biodistribution and toxicology of functionalized nano-graphene oxide in mice after oral and intraperitoneal administration. Biomaterials 34:2787–2795
56. Yue H, Wei W, Yue Z, Wang B, Luo N, Gao Y, Ma D, Ma G, Su Z (2012) The role of the lateral dimension of graphene oxide in the regulation of cellular responses. Biomaterials 16:4013–4021
57. Kurantowicz N, Strojny B, Sawosz E, Jaworski S, Kutwin M, Grodzik M, Wierzbicki M, Lipińska L, Mitura K, Chwalibog A (2015) Biodistribution of a high dose of diamond, graphite

and graphene oxide nanoparticles after multiple intraperitoneal injections in rats. Nanoscale Res Lett 10:1–4
58. Lee JH, Han JH, Kim JH, Kim B, Bello D, Kim JK, Lee GH, Sohn EK, Lee K, Ahn K, Faustman EM, Faustman EM (2016) Exposure monitoring of graphene nanoplatelets manufacturing workplaces. Inhalation Toxicol 28:281–291
59. Ou L, Song B, Liang H, Liu J, Feng X, Deng B, Sun T, Shao L (2016) Toxicity of graphene-family nanoparticles: a general review of the origins and mechanisms. Part Fibre Toxicol 1:1–24
60. Chaudhry N, Dwivedi S, Chaudhry V, Singh A, Saquib Q, Azam A, Musarrat J (2018) Bio-inspired nanomaterials in agriculture and food: Current status, foreseen applications and challenges. Microb Pathog 123:196–200
61. Prasad R, Bhattacharyya A, Nguyen QD (2017) Nanotechnology in sustainable agriculture: recent developments, challenges, and perspectives. Front Microbiol 8:1014
62. Misra AN, Misra M, Singh R (2013) Nanotechnology in agriculture and food industry. Int J Pure Appl Sci Technol 16:1
63. https://patentimages.storage.googleapis.com/5c/51/84/743de1f7e88eb6/US8226801.pdf
64. https://patents.google.com/patent/US20170225233A1
65. https://patents.google.com/patent/US9236197B2/en?oq=US9236197B2
66. https://patents.google.com/patent/US20190292671A1/en?oq=US20190292671A1
67. https://patents.google.com/patent/CN103700513B/en?oq=CN103700513B
68. https://patents.google.com/patent/CN107555424A/en?oq=CN107555424A
69. https://patentimages.storage.googleapis.com/11/d0/c2/646c9935d934e8/US8834959.pdf
70. https://patents.google.com/patent/CN105514450B/en?oq=CN105514450B
71. https://patentimages.storage.googleapis.com/e2/1e/aa/4ed727eb4746ef/EP2869348B1.pdf
72. https://patentimages.storage.googleapis.com/94/5c/e7/ea3f44cb481da0/US20160181516A1.pdf
73. https://patentimages.storage.googleapis.com/b4/d8/f2/22dc12eff5d371/US20160093491A1.pdf
74. https://patentimages.storage.googleapis.com/73/e2/db/f3022caa6bc08c/US10720644.pdf
75. https://patentimages.storage.googleapis.com/a1/86/91/f70c1d402aa29d/US9415570.pdf
76. https://patentimages.storage.googleapis.com/08/5d/01/caf3077b6887b3/US20200176619A1.pdf
77. https://patents.google.com/patent/CN107159286A/en?oq=CN107159286A
78. https://patents.google.com/patent/CN107117616B/en?oq=CN107117616B
79. https://patents.google.com/patent/CN107777688B/en?oq=CN107777688B
80. https://patents.google.com/patent/US9461125B2/en?oq=US9461125B2
81. https://patents.google.com/patent/US10906811B2/en?oq=US10906811B2
82. https://patents.google.com/patent/US10676357B1/en?oq=US10676357B1
83. https://patents.google.com/patent/AU2021104425A4/en?oq=AU2021104425A4
84. https://patents.google.com/patent/KR20170125677A/en?oq=KR20170125677A
85. https://patents.google.com/patent/US10600644B2/en?oq=US10600644B2
86. https://patents.google.com/patent/US20200247671A1/en?oq=US20200247671A1
87. https://patents.google.com/patent/JP6270183B2/en?oq=JP6270183B2
88. https://patents.google.com/patent/US10201803B2/en?oq=US10201803B2
89. https://patents.google.com/patent/US10309027B2/en?oq=US10309027B2
90. https://patents.google.com/patent/US9017756B2/en?oq=US9017756B2
91. https://patents.google.com/patent/US9053870B2/en?oq=US9053870B2
92. https://patents.google.com/patent/US20090092747A1
93. https://patents.google.com/patent/WO2018013254A1
94. https://patents.google.com/patent/JP2019522868A
95. https://patents.google.com/patent/US11081691B2
96. https://patents.google.com/patent/CN104959134B
97. https://patents.google.com/patent/ES2660904T3
98. https://patents.google.com/patent/CN109659138A

99. https://patents.google.com/patent/CN109423068A
100. https://patents.google.com/patent/CN111541398A
101. https://patents.google.com/patent/US10839974B2/en?oq=US10839974B2
102. https://patentimages.storage.googleapis.com/bc/68/3e/caf2a7eb10575b/US20170179314A1.pdf
103. https://patentimages.storage.googleapis.com/0d/f2/a5/f7cf8458b5e87b/US10692977.pdf
104. https://patentimages.storage.googleapis.com/29/76/c3/bb3e3c577a9064/US20120325200A1.pdf
105. https://patents.google.com/patent/US20190139713A1/en?oq=US20190139713A1
106. https://patents.google.com/patent/CN103691420A
107. https://patents.google.com/patent/CN102683648B
108. https://patents.google.com/patent/CN102142537B
109. https://patents.google.com/patent/CN106571461A
110. https://patents.google.com/patent/JPWO2012086697A1/en?oq=JPWO2012086697A1
111. https://patents.google.com/patent/CN105551813A/en?oq=CN105551813A
112. https://patents.google.com/patent/ES2683360T3/en?oq=ES2683360T3
113. https://patentimages.storage.googleapis.com/34/b2/ae/c278a2c1d44ea4/US20180309125A1.pdf
114. https://patents.google.com/patent/CN106450205B/en?oq=CN106450205B
115. https://patents.google.com/patent/CN107706372B/en?oq=CN107706372B
116. https://patents.google.com/patent/WO2021042456A1/en?oq=WO2021042456A1
117. https://patents.google.com/patent/CN109003836A/en?oq=CN109003836A
118. https://patents.google.com/patent/CN106430195A/en?oq=CN106430195A
119. https://patents.google.com/patent/CN109671949A/en?oq=CN109671949A
120. https://patents.google.com/patent/JP6477315B2/en?oq=JP6477315B2
121. https://patents.google.com/patent/CN106711408B/en?oq=CN106711408B
122. https://patents.google.com/patent/US20190081320A1/en?oq=US+20190081320A1
123. https://patents.google.com/patent/US9859034B2/en?oq=US9859034B2
124. https://patents.google.com/patent/CN108365102B/en?oq=CN108365102B
125. https://patents.google.com/patent/CA3079471C/en?oq=CA3079471C
126. https://patents.google.com/patent/JP4419232B2/en?oq=JP4419232B2
127. https://patents.google.com/patent/CN108039495B/en?oq=CN108039495B
128. https://patents.google.com/patent/CN108579751B/en?oq=CN108579751B
129. https://patents.google.com/patent/CN105449227A/en?oq=CN105449227A
130. https://patents.google.com/patent/JP6001198B2/en?oq=JP6001198B2
131. https://patents.google.com/patent/CN110492069A/en?oq=CN110492069A
132. https://patents.google.com/patent/CN107887603B/en?oq=CN107887603B
133. https://patents.google.com/patent/CN105789668B/en?oq=CN105789668B
134. https://patents.google.com/patent/US10403708B2/en?oq=US10403708B2
135. https://patents.google.com/patent/CN104001504A/en?oq=CN104001504A
136. https://patents.google.com/patent/CN103480398B/en?oq=CN103480398B
137. https://patents.google.com/patent/US20150364754A1/en?oq=US20150364754A1
138. https://patents.google.com/patent/CN106378158A/en?oq=CN106378158A
139. https://patents.google.com/patent/CN104258857A/en?oq=CN104258857A
140. https://patents.google.com/patent/CN104829019A/en?oq=CN104829019A
141. https://patents.google.com/patent/CN105148947A/en?oq=CN105148947A
142. https://patents.google.com/patent/CN106268875A/en?oq=CN106268875A
143. https://patents.google.com/patent/CN109465037A/en?oq=CN109465037A
144. https://patents.google.com/patent/CN106964370B/en?oq=CN106964370B
145. https://patents.google.com/patent/CN109225273A/en?oq=CN109225273A
146. https://patents.google.com/patent/KR20180055860A/en?oq=KR20180055860A
147. https://patents.google.com/patent/CN108355679A/en?oq=CN108355679A
148. https://patents.google.com/patent/CN103193785B/en?oq=CN103193785B
149. https://patents.google.com/patent/CN111715250B/en?oq=CN111715250B

150. https://patents.google.com/patent/CN113134375A/en?oq=CN113134375A
151. https://patents.google.com/patent/CN111822028A/en?oq=CN111822028A
152. https://patents.google.com/patent/CN110560164A/en?oq=CN110560164A
153. https://patents.google.com/patent/CN111545230A/en?oq=CN111545230A
154. https://patents.google.com/patent/CN109794281A/en?oq=CN109794281A
155. https://patents.google.com/patent/CN112121855B/en?oq=CN112121855B
156. https://patents.google.com/patent/CN106586987B/en?oq=CN106586987B
157. https://patents.google.com/patent/CN108355696B/en?oq=CN108355696B
158. https://patents.google.com/patent/CN112076769A/en?oq=CN112076769A
159. https://patents.google.com/patent/CN108745404B/en?oq=CN108745404B
160. https://patents.google.com/patent/CN109529898B/en?oq=CN109529898B
161. https://patents.google.com/patent/CN106927535B/en?oq=CN106927535B
162. https://patents.google.com/patent/CN107617447B/en?oq=CN107617447B
163. https://patents.google.com/patent/CN102151577B/en?oq=CN102151577B
164. https://patents.google.com/patent/CN103570009A/en?oq=CN103570009A
165. https://patents.google.com/patent/WO2018078427A1/en?oq=WO2018078427A1
166. https://patents.google.com/patent/US20210024378A1/en?oq=US20210024378A1
167. https://patents.google.com/patent/WO2018006745A1/en?oq=WO2018006745A1
168. https://patents.google.com/patent/US10994241B1/en?oq=US10994241B1
169. https://patents.google.com/patent/CN203916677U/en?oq=CN203916677U
170. https://patents.google.com/patent/US20210060522A1/en?oq=US20210060522A1
171. https://patents.google.com/patent/US20170151548A1/en?oq=US20170151548A1
172. https://patents.google.com/patent/CN110420619A/en?oq=CN110420619A
173. https://patents.google.com/patent/US10493426B2/en?oq=US10493426B2
174. https://patents.google.com/patent/USRE44124E1/en?oq=USRE44124E1
175. https://patents.google.com/patent/US20190144305A1/en?oq=US20190144305A1
176. https://patents.google.com/patent/US8070959B2/en?oq=US8070959B2
177. https://patents.google.com/patent/CN108383169A/en?oq=CN108383169A
178. https://patents.google.com/patent/CN113181947A/en?oq=CN113181947A
179. https://patents.google.com/patent/US11053138B2/en?oq=US11053138B2
180. https://patents.google.com/patent/CN104587947A/en?oq=CN104587947A
181. https://patents.google.com/patent/CN107694510B/en?oq=CN107694510B
182. https://patents.google.com/patent/CN108774343A/en?oq=CN108774343A
183. https://patents.google.com/patent/CN106268610A/en?oq=CN106268610A
184. https://patents.google.com/patent/CN103480329B/en?oq=CN103480329B
185. https://patents.google.com/patent/US5114898A/en?oq=US5114898A
186. https://patents.google.com/patent/CN105056895B/en?oq=CN105056895B
187. https://patents.google.com/patent/CN112973638A/en?oq=CN112973638A
188. https://patents.google.com/patent/CN105481043A/en?oq=CN105481043A
189. https://patents.google.com/patent/CN108201878B/en?oq=CN108201878B
190. https://patents.google.com/patent/US9475709B2/en?oq=US9475709B2
191. https://patents.google.com/patent/US10456754B2/en?oq=US10456754B2
192. https://patents.google.com/patent/CN108636141B/en?oq=CN108636141B
193. https://patents.google.com/patent/CN207361918U/en?oq=CN207361918U
194. https://patents.google.com/patent/US20180333685A1/en?oq=US20180333685A
195. https://patents.google.com/patent/US20130240355A1/en?oq=US20130240355A1
196. https://patents.google.com/patent/US9610546B2/en?oq=US9610546B2
197. https://patents.google.com/patent/CN111204828A/en?oq=CN111204828A
198. https://patents.google.com/patent/AU2016203645B2/en?oq=AU+2016203645+B2
199. https://patents.google.com/patent/US20190039028A1/en?oq=US20190039028A1
200. https://patents.google.com/patent/CN110015722A/en?oq=CN110015722A
201. https://patents.google.com/patent/EP3140028A2/en?oq=EP3140028A2
202. https://patents.google.com/patent/US20200254396A1/en?oq=US20200254396A1
203. https://patents.google.com/patent/CN107633954B/en?oq=CN107633954B

204. https://patents.google.com/patent/CN106178979B/en?oq=CN106178979B
205. https://patents.google.com/patent/WO2018205290A1/en?oq=WO2018205290A1
206. https://patents.google.com/patent/US20180169591A1/en?oq=US20180169591A1
207. https://patents.google.com/patent/CN113398777A/en?oq=CN113398777A
208. https://patents.google.com/patent/CN112473372A/en?oq=CN112473372A
209. https://patents.google.com/patent/CN109569319A/en?oq=CN109569319A
210. https://patents.google.com/patent/CN110342601B/en?oq=CN110342601B
211. https://patents.google.com/patent/CN110090603A/en?oq=CN110090603A
212. https://patents.google.com/patent/CN107537323B/en?oq=CN107537323B
213. https://patents.google.com/patent/CN111282405A/en?oq=CN111282405A
214. https://patents.google.com/patent/EP3774001A1/en?oq=EP3774001A1
215. https://patents.google.com/patent/CN105717174B/en?oq=CN105717174B
216. https://patents.google.com/patent/CN106483184A/en?oq=CN106483184A
217. https://patents.google.com/patent/CN104391030B/en?oq=CN104391030B
218. https://patents.google.com/patent/CN101995402B/en?oq=CN101995402B
219. https://patents.google.com/patent/CN102980928A/en?oq=CN102980928A
220. https://patents.google.com/patent/CN102680527B/en?oq=CN102680527B
221. https://patents.google.com/patent/US20170016847A1/en?oq=US20170016847A1
222. https://patents.google.com/patent/US9869651B2/en?oq=US9869651B2
223. https://patents.google.com/patent/US9063063B2/en?oq=US9063063B2
224. https://patents.google.com/patent/CN109825816A/en?oq=CN109825816A
225. https://patents.google.com/patent/CN113390943A/en?oq=CN113390943A
226. https://patents.google.com/patent/CN109115850A/en?oq=CN109115850A
227. https://patents.google.com/patent/CN110057882A/en?oq=CN110057882A
228. https://patents.google.com/patent/CN109406611B/en?oq=CN109406611B
229. https://patents.google.com/patent/CN109675608A/en?oq=CN109675608A
230. https://patents.google.com/patent/WO2019124625A1/en?oq=WO2019124625A1
231. https://patents.google.com/patent/CN109799267B/en?oq=CN109799267B
232. https://patents.google.com/patent/CN105116034A/en?oq=CN105116034A
233. https://patents.google.com/patent/US10648959B2/en?oq=US10648959B2
234. https://patents.google.com/patent/US10274421B2/en?oq=US10274421B2
235. https://patents.google.com/patent/CN109270140B/en?oq=CN109270140B
236. https://patents.google.com/patent/US20150283239A1/en?oq=US20150283239A1
237. https://patents.google.com/patent/CN104436210A/en?oq=CN104436210A
238. https://patents.google.com/patent/CN108379461A/en?oq=CN108379461A
239. https://patents.google.com/patent/KR102051515B1/en?oq=KR102051515B1
240. https://patents.google.com/patent/CN104758930A/en?oq=CN104758930A
241. https://patents.google.com/patent/KR101618556B1/en?oq=KR101618556B1
242. https://patents.google.com/patent/CN110819717A/en?oq=CN110819717A
243. https://patents.google.com/patent/US10935550B2/en?oq=US10935550B2
244. https://patents.google.com/patent/CN108330054B/en?oq=CN108330054B
245. https://patents.google.com/patent/CN110013601B/en?oq=CN110013601B
246. https://patents.google.com/patent/WO2016200105A2/en?oq=WO2016200105A2
247. https://patents.google.com/patent/CN103705928A/en?oq=CN103705928A
248. https://patents.google.com/patent/CN106512002A/en?oq=CN106512002A
249. https://patents.google.com/patent/CN107802836B/en?oq=CN107802836B
250. https://patents.google.com/patent/CN106563130A/en?oq=CN106563130A
251. https://patents.google.com/patent/CN107375928A/en?oq=CN107375928A
252. https://patents.google.com/patent/CN108245682B/en?oq=CN108245682B
253. https://patents.google.com/patent/CN108273058B/en?oq=CN108273058B
254. https://patents.google.com/patent/CN111110913A/en?oq=CN111110913A
255. https://patents.google.com/patent/CN108159438A/en?oq=CN108159438A
256. https://patents.google.com/patent/CN106267201B/en?oq=CN106267201B
257. https://patents.google.com/patent/CN105535971B/en?oq=CN105535971B

258. https://patents.google.com/patent/CN106335885B/en?oq=CN106335885B
259. https://patents.google.com/patent/CN106366121B/en?oq=CN106366121B
260. https://patents.google.com/patent/US11040918B2/en?oq=US11040918B2
261. https://patents.google.com/patent/US20190308916A1/en?oq=US20190308916A1
262. https://patents.google.com/patent/CN104829340B/en?oq=CN104829340B
263. https://patents.google.com/patent/CN111285729A/en?oq=CN111285729A
264. https://patents.google.com/patent/CN108085010B/en?oq=CN108085010B
265. https://patents.google.com/patent/JP2019527057A/en?oq=JP2019527057A
266. https://patents.google.com/patent/CN105891269A/en?oq=CN105891269A
267. https://patents.google.com/patent/CN108684706A/en?oq=CN108684706A
268. https://patents.google.com/patent/CN112293419A/en?oq=CN112293419A
269. https://patents.google.com/patent/CN108064844A/en?oq=CN108064844A
270. https://patents.google.com/patent/CN106577644A/en?oq=CN106577644A
271. https://patents.google.com/patent/CN104829340A/en?oq=CN104829340A
272. https://patents.google.com/patent/CN109053289A/en?oq=CN109053289A